Trace Element Geochemistry of Volcanogenic Massive Sulfide Deposits in Archean Greenstone Belts: Implications for Metal Endowment and Geodynamic Settings

Ryley Penner

Supervisor: Dr. Mark D. Hannington

Thesis submitted to the
University of Ottawa
in partial fulfillment of the requirements
for the Master's degree in Earth Sciences

Department of Earth Sciences
Faculty of Science
University of Ottawa

Abstract

The Neoarchean greenstone belts of the Canadian Superior Province host world-class Au and base metal (Cu-Zn-Pb) massive sulfide deposits with distinct geological features, including a wide range of different host rocks and crustal settings. The range of settings is reflected in the trace metal signatures of their ores. This study examines the trace element geochemistry of pyrite from 55 different Archean volcanogenic massive sulfide (VMS) deposits in Canada to test the relationship to their host rocks, the deposit sizes and their grades. The database includes 258 samples of pyrite from 47 deposits in the Abitibi Greenstone Belt (AGB), together with 30 samples from 8 deposits in the Western Superior (Sturgeon Lake, Uchi, Benny, and Manitouwadge belts) and 45 samples from 6 deposits in the Slave Province (Hackett River, Amooga Booga, and High Lake belts). We used statistical methods to characterize the trace element geochemistry of pyrite in grab samples from the deposits, as well as larger samples representing many thousand of tonnes of ore from monthly concentrates. The study focused on pyrite mineral separates comparing samples from different deposits and different ore types within individual deposits. The analysis shows the trace element geochemistry of pyrite is a useful fingerprint of the different mineralizing systems, with trace element enrichments and depletions reflecting different source rocks, inferred temperatures of ore formation, and the scales of the hydrothermal systems. A comparison of the Abitibi samples to other deposits in the Superior Province shows distinct trace element signatures between primitive and more evolved crustal settings of different age. Similar results are found among 102 samples of pyrite from 30 deposits in Proterozoic and Phanerozoic belts across Canada.

District-scale variations in pyrite chemistry mainly reflect host rock and correlate different bulk Cu/(Cu+Zn) grade ratios of the deposits. Pyrite samples from Cu-rich deposits are enriched in Cu, Bi, Co, Ni, Se, Te and Mo; whereas pyrite samples from Zn-rich deposits are enriched in Pb, Ag, Cd, In, Ga, Sn, As, Sb, Hg and Tl. The same patterns are observed in Cu-rich versus Zn-rich zones of individual deposits. Statistical analyses reveal pyrite samples from VMS deposits in the AGB that are associated with primitive mafic-ultramafic tholeiitic rocks (e.g., Potter-Doal and Genex from Timmins, and East Sullivan and Dunraine from Val d'Or camps) are enriched in Cu (>5000 ppm), Co (>1500 ppm), Se (>4000 ppm), and Ni (>250 ppm), whereas pyrite from

deposits associated with tholeiitic to calc-alkaline felsic rocks (e.g., Abcourt-Barvue from the Amos-Barraute camp) are commonly enriched in Pb, Ag, Au, Cd, In, Sn, As, Sb, Hg, Tl (10s to 100s of ppm). These variations closely match primary trace element abundances in unaltered volcanic rocks compiled from over 4000 high-quality analyses of samples from the Superior Province. Whole-rock data for rhyolite confirm high concentrations of Pb, Ag, Bi, Te, Cd, In, Ga, Sn, Hg, and Tl compared to basalt and komatiite, which have higher Cu, Co, Ni, and Se.

The variation in trace element concentrations in pyrite is remarkably consistent for different deposits. We note that randomly sampled pyrite from almost any part of a deposit with a bulk enrichment in a particular element shows notable enrichment in that element compared to pyrite from other deposits. Pyrite from a deposit with a bulk enrichment in Te, for example (Quemont in the Noranda camp), will almost certainly contain more Te than pyrite from other Te-poor deposits. We test this observation among 47 deposits for 15 different elements.

Pyrite samples from Au-rich VMS deposits (e.g., Horne, Quemont, Bousquet #2, and Dumagami) have anomalous Au (>6 ppm) and Te (>70 ppm). Co-enrichment in other elements such as Bi, Se, In and Sn may reflect a common felsic magmatic source. Other trace element enrichments appear to reflect the scale of the hydrothermal system (e.g., depth and extent of leaching). For example, pyrite samples from several large-tonnage deposits (Kidd Creek, Horne #5 Zone, and Geco) have high Sn concentrations (from 450 to 15000 ppm) possibly reflecting the large volumes of felsic rock from which the Sn was extracted. In other deposits, co-enrichment of Sn with Bi (>100 ppm) and In (>10 ppm) suggest a magmatic contribution to the ore fluids

Principal Components Analysis (PCA) combined with hierarchal clustering confirms systematic trace element variability in pyrite from deposits with different host rocks and bulk Cu/(Cu+Zn) ratios. However, pyrite from deposits in different terranes seems to record major differences in the crustal compositions of those terranes. For example, pyrite samples from bimodal-felsic deposits show the same trace element signatures (i.e., enrichments in Ag, As, Sb, and Hg) in the AGB and in the Western Superior. In contrast, pyrite samples from deposits in the Slave craton

tend to show a distinct enrichment in Pb, U and Th that may be related to the more mature and thicker crust in the Slave compared to the AGB. Other deposit types (magmatic Cu vein deposits, orogenic Au deposits) also show dramatically different pyrite compositions. Pyrite concentrates from magmatic Cu vein deposits in Chibougamau are enriched in Cu, Co, Ni, Te, As, Sb compared to VMS in the AGB, and samples from orogenic Au deposits in Timmins and Val d'Or are enriched in Au and Mo and depleted in Pb, Bi, As, and Sb compared to VMS. These differences highlight the potential application of the trace element signatures of pyrite during exploration for different deposit types in the same region.

Trace element signatures of pyrite in grab samples compared favourably to much larger bulk samples from the same deposits (e.g., monthly concentrates and mine tailings) giving some confidence that the much smaller samples can provide a reliable first-order fingerprint of the deposits as a whole. LA-ICP-MS analyses of individual pyrite grains also agreed well with bulk analyses of pyrite over a wide range of trace element concentrations (10s to 100s of ppm).

Acknowledgements

Firstly, I would like to thank my supervisor Dr. Mark Hannington for his unrelenting support and feedback, without which this project would not have been possible. I would also like to thank David Diekrup and Marc Fassbender for lending their expertise and encouragement that kept me afloat at every step throughout the thesis. This research is a product of the Metal Earth subproject 3(b) (MERC-ME-2023-09). The Society of Economic Geologists is acknowledged for their support through a research grant.

Table of contents

List of figures

List of tables

1. Introduction

Volcanogenic massive sulfide (VMS) deposits are polymetallic accumulations of base (Zn, Cu, Pb) and precious (Au, Ag) metals and minor elements (Co, Sn, Se, Mn, Cd, In, Bi, Te, Ga) that formed on the ancient seafloor or subseafloor by the circulation and discharge of hydrothermal fluids. They are spatially, temporally and genetically linked to volcanic processes (Franklin et al., 1981, 2005; Hannington et al., 2005). A typical deposit consists of a concordant massive sulfide lens and a discordant alteration pipe hosting stockwork/stringer vein-type sulfides (Fig. 1.1: Franklin et al., 1981; Lydon, 1984). The ore-forming fluids evolved through water-rock interaction within the footwall and heating by subvolcanic intrusions that drove convection and also contributed fluid components. The deposits are characterized by sulfide assemblages of pyrite and/or pyrrhotite with lesser amounts of sphalerite, chalcopyrite and galena. They are commonly zoned, with variations in mineralogy due to sub-seafloor mixing, cooling and pH changes that also affect the distribution of trace metals in the deposits (Franklin et al., 2005).

Research at the deposit and district scale and comparisons with seafloor massive sulfide (SMS) deposits as modern analogues has provided a robust geological framework for understanding the processes responsible for ore formation (e.g., Gibson et al., 2005; Franklin et al., 2005; Galley et al., 2007; Monecke et al., 2014; Mercier-Langevin et al., 2014). A generalized deposit model has been developed that explains most of the deposit to district-scale features (Franklin, 1981; Lydon, 1984; Galley, 1993; Hannington, 2014). Barrie and Hannington (1999) classified VMS deposits according to host rock composition. This classification was modified to include additional lithostratigraphic facies (Franklin et al., 2005), especially in sedimentary-rock settings. The majority of Archean VMS deposits are classified as bimodal-mafic type, which are dominated by a mafic volcanic footwall with felsic volcanic rocks in the immediate-ore hosting environment. Bimodal-felsic type deposits are hosted by felsic volcanic dominated successions; the siliciclastic-felsic type have subequal amounts of sedimentary and felsic volcaniclastic rocks. The latter are more common among Proterozoic and Paleozoic VMS. The mafic type is represented by ophiolite sequences with minor sediments, and the pelitic-mafic type includes mostly pelite in the footwall. Black smoker vents on mid-oceanic ridges (MOR), intraoceanic to

epicontinental volcanic arcs, and in back-arc basins include examples of all of these deposit types (Galley et al., 2007; Hannington et al., 2005).

Advances in the geochemical characterization of VMS deposits and their host rocks have provided some important criteria for recognition of different deposit types during exploration (Franklin et al., 2005). Metal grades, including Au contents, vary considerably depending on the interplay of source rocks, fluid sources, and precipitation mechanisms and at scales from a single sulfide sample to whole deposits, districts, and entire greenstone belts (e.g., Hannington 2014; Monecke et al., 2016; Fuchs et al., 2019). The source rock controls are in turn influenced by crustal composition and regional geodynamics, with well-established compositional differences among deposits in different settings (Barrie and Hannington, 1999; Mercier-Langevin et al., 2011a). However, only limited geodynamic context can be gained from deposit-scale studies, especially in ancient greenstone terranes. For example, it remains uncertain whether large-scale differences in crustal fertility (e.g., preconcentrating metal in fertile crust that is subsequently leached by hydrothermal fluids) contribute most to mineral endowment, or if direct magmatic-hydrothermal processes (e.g., volatile saturation and magmatic degassing) are more important. A direct magmatic input to the hydrothermal fluid has been suggested as one of the factors accounting for deposit size and Au enrichment (e.g., Urabe 1987; Huston and Large 1989; Stanton, 1990; Large, 1992; Large et al., 1996; Yang and Scott, 1996; Barrie et al., 1999a; Hannington et al., 1999a; de Ronde et al., 2005; Dubé et al., 2007). A key question is whether different types of metal endowment can be identified at a large-scale from the trace element fingerprint of the ore-forming system (e.g., just as magmatic processes can be traced in volcanic rocks from trace elements in mafic and felsic magmas). The challenge in addressing this question is partly the lack of comprehensive trace element datasets for the deposits and their host rocks and the difficulty separating the effects of source rock controls from physicochemical controls on the ore-forming fluids. For most VMS deposits, trace element data are incomplete because bulk rock assays for production and grade control do not deliberately target individual trace elements. This has limited our ability to fingerprint different hydrothermal systems beyond their immediate host rocks and major base metal contents [e.g., Cu/(Cu+Zn) ratios]. In this study, we examine several newly compiled data sets on VMS ores and their host rocks in the Superior Province of

Canada to test whether there are systematic differences between well-endowed and less well-endowed deposits or districts that can be identified in their trace element signatures.

1.1 Thesis objectives and approach

In this project we investigate how trace element patterns in VMS deposits reflect both small- and large-scale influences including different host rocks, base/precious metal grades, and deposit sizes. The hypothesis is that trace elements, under relatively controlled conditions (e.g., in a single mineral like pyrite), are a fingerprint of physicochemical and geological processes that also determine overall metal endowment. We suggest that a limited number of samples from a single deposit or district can reflect large-scale influences such as the composition of the leached volcanic rocks and the nature of the hydrothermal fluid by analogy with isotopic systems that record fluid evolution and melt generation. We suggest that sulfide minerals in VMS-forming systems capture a geochemical fingerprint of certain labile trace elements that closely reflect the volcanic rock geochemistry and associated magmatic systems. To test this, we interrogate a comprehensive geochemical database of trace elements in Canadian Archean VMS deposits and compare the geochemistry of pyrite in the deposits to their host rocks and metal endowment. We also explore the possibility that these fingerprints can be used as exploration tools for selecting prospective VMS areas.

The steps taken included: 1) collection and sorting of published trace element data on sulfide minerals from Canadian VMS, including a comprehensive database of mineral separates prepared from grab samples (Jonasson et al., 2020); 2) QA/QC on the data set to identify the most reliable pyrite analyses, 3) further characterization of the analyzed samples by modal mineralogy; 4) description of the trace element data using univariate statistical analyses and PCA; 5) hierarchical clustering to define different classes (groups) of samples and sampled deposits; 6) comparing trace element data for pyrite from individual grab samples with data for pyrite from much larger samples (e.g., monthly mill concentrates) and whole deposits; 7) obtaining selected pyrite separates from the National Archive for more detailed study, including petrographic assessment of microinclusions; 8) comparing data from bulk analyses of pyrite with

data for individual pyrite grains by LA-ICP-MS; 9) comparing pyrite data with other data sets, including host rock geochemistry and other deposit types).

We examine the following research questions: (i) what is the geochemical variability of trace elements in pyrite from VMS deposits at a range of scales (i.e., within deposits, and between deposits, districts, regional assemblages, and greenstone belts)?; (ii) to what extent do trace element concentrations in the sampled pyrite reflect the host rock succession?; (iii) are enrichments in certain trace elements indicators of inherently enriched source rocks, possible magmatic inputs, or other processes responsible for metal endowment?; (iv) are there specific trace element signatures that show a statistically meaningful correlation with VMS deposits with high Au grades and large tonnages?

In this study, we compare 62 trace elements in pyrite mineral concentrates from 55 well-studied Archean VMS deposits in the Superior Province (Jonasson et al., 2020). The data used in this study are part of a massive compilation of geochemical analyses from a Canada-wide archive of ore samples assembled by the Geological Survey of Canada (GSC) and described in detail in Chapter 3. We used a subset of the published data from 288 massive sulfide samples from which pyrite was extracted and analyzed. Pyrite forms throughout the paragenesis of VMS deposits, including both low- and high-temperatures that can be readily distinguished by the association with co-existing phases (i.e., with chalcopyrite in high-temperature assemblages and with sphalerite in lower-temperature assemblages: Hannington, 2014). In this way, we are able to compare pyrite formed under similar conditions in different deposits. In addition to its ubiquity in hydrothermal ore-forming systems, pyrite is capable of incorporating a full range of trace metals (i.e., Cu, Zn, Pb, Ag, Au, Bi, Co, Ni, Se, Te, Cd, In, Ga, Sn, W, Mo, As, Sb, Hg, and Tl), some with well-established partitioning behaviour, that reflects both source-rock variations and conditions of mineralization (e.g., Maslennikov et al., 2009; Deditius et al., 2011; Reich et al., 2013; Monecke et al., 2016; Grant et al., 2018). The deposits in the database are variably classified as bimodal-mafic and bimodal-felsic according to Barrie and Hannington (1999) and Franklin et al. (2005) and range in size from <1 Mt to 171 Mt, with average Au grades of 0 g/t to 7.8 g/t. By focusing on deposits of the same age, we avoid unrelated correlations associated with

variations in conditions of mineralization previously identified in deposits of different age (e.g., Franklin et al., 2005). In particular, the selected deposits contrast with younger VMS systems in Paleozoic and Proterozoic terranes that are widely considered to have formed under different geodynamic and atmospheric conditions (e.g., Barrie and Hannington, 1999; Franklin et al., 2005; Galley et al, 2007; Huston et al., 2010). By studying a single mineral common to the ore assemblages of all deposits, we limit the degree of variability that otherwise would be expected from mineralogically more complex samples including significant variation due to partitioning of trace elements into different ore minerals and under different hydrothermal conditions.
The studied trace elements are all considered to be either in the pyrite mineral lattice or present as microinclusions of related minerals. Both the lattice-bound elements and the trace elements in microinclusions are considered to reflect the same conditions of mineralization and compositions of the ore-forming fluids (e.g., Cook, 1996; Large et al., 2009; Monecke et al., 2016; Grant et al., 2018). These authors conclude that, from the point of view of determining the sources of the elements, the conditions of transport in the hydrothermal fluids, and their enrichment or depletion in the deposits, it makes little difference whether they are lattice bound or present as trace minerals, except where partitioning in specific minerals plays a role (see subsequent chapters).

Using unsupervised machine learning methods, including a combination of principal components analysis and hierarchical clustering, we compare trace element geochemistry in pyrite from deposits in different settings, of different sizes, and with different mineral endowment. The machine learning focuses on a "hydrothermal suite" of elements, including precious (Au, Ag) and base metals (Cu, Pb, Zn) and select elements that are commonly present in trace concentrations in major sulfide minerals (i.e., Bi, Co, Ni, Se, Te, Cd, In, Ga, Sn, Mo, As, Sb, Hg, and Tl). Elements that consistently partition into pyrite in massive sulfide deposits and have well-established relationships to mineralization (i.e., pathfinder elements: Maslennikov et al., 2009; Patten et al. 2016; Grant et al., 2018) are examined in detail. An important question addressed in the study is how representative a single sample of pyrite from a large deposit might be in terms of trace element enrichments and depletions. We test this by comparing multiple samples of pyrite from the same deposit where source rocks and potential magmatic

contributions do not vary. We also compare pyrite samples from deposits for which the same trace elements have been determined on much larger bulk samples (e.g., monthly concentrates or pyrite tailings representing tens of thousands of tonnes of ore). Finally, we compare bulk analyses of pyrite mineral separates by dissolution ICP-MS to in-situ analyses of individual pyrite grains from the same samples using LA-ICP-MS, a commonly applied technique to assess the heterogeneity of trace element concentrations at the grain scale. We also examine the trace element signatures of pyrite in a number of other ore deposit types that contain abundant hydrothermal pyrite to understand the possible general application of pyrite geochemistry in metallogenic studies. The applied methods, including mineral balances of the trace elements, are a useful complement to geometallurgy applications in mining.

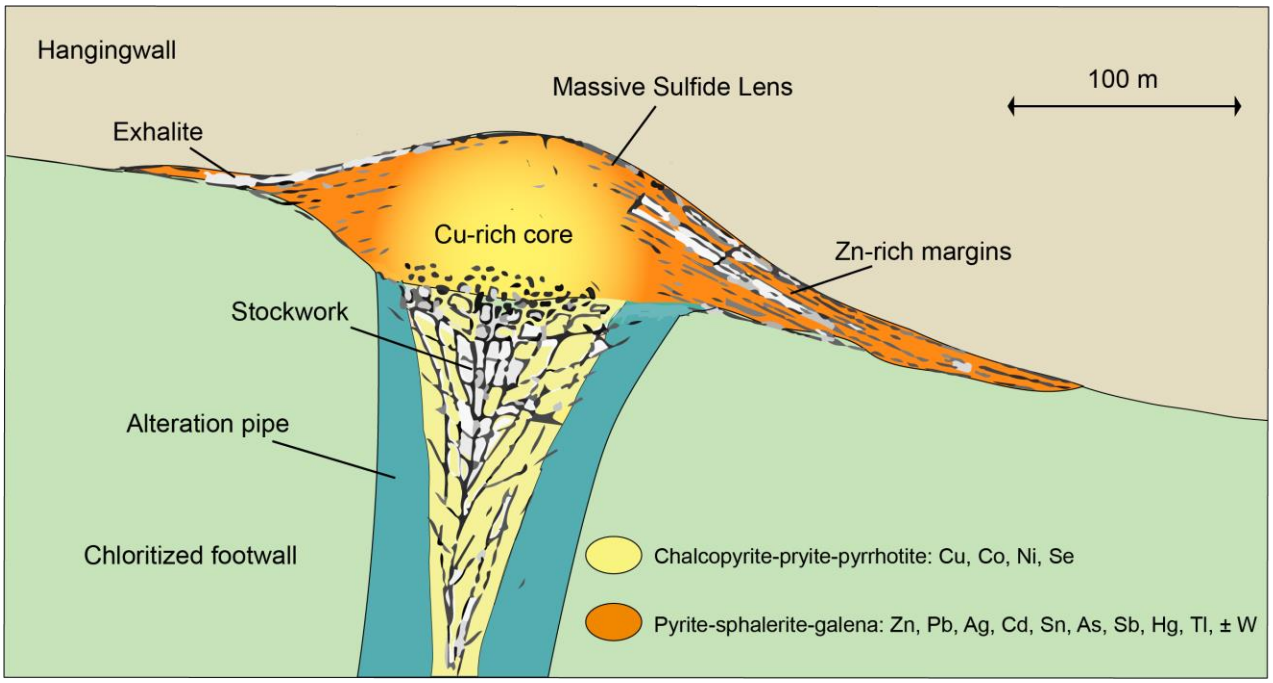

Figure 1.1 Schematic cross-section of the classic VMS deposit with a concordont massive sulfide lens overlying a discordont stockwork/stringer zone and alteration pipe (modified from Lydon, 1984). The main sulfide mineral assemblages and trace metal associations of Cu-rich and Zn-rich VMS ore are indicated (from Hannington 2014).

2. Background

2.1 Importance of VMS classification

The majority of the sampled VMS deposits in Jonasson et al. (2020) have been classified as bimodal-mafic, according to the criteria of Barrie and Hannington (1999) and Franklin et al. (2005) (Table 2.1, A.1). In addition to the lithostratigraphic classification, a range of other VMS attributes have been recognized in the database that distinguish one deposit type from another, including: ore composition (e.g., Cu-Zn-Pb ratios: Franklin et al., 1981); Au grade (Hannington et al.,1999a; Poulsen and Hannington, 1996; Sillitoe et al., 1996); tectonic setting (e.g., Sawkins, 1976. Each highlights a particular VMS-forming process or condition that is also likely to influence trace element enrichments or depletions. Some attributes are highly sensitive to ore-forming conditions, such as temperature and host rock, including the proportion of Cu-rich to Zn-rich ore from the camp-scale to individual ore zones (e.g., Gibson and Galley, 2007). Bimodal-mafic deposits, that generally have a mafic/felsic volcanic rock ratio of 3:1, are characterized by higher Cu content (Table A.1). In contrast, bimodal-felsic deposits commonly have a felsic volcaniclastic-dominated footwall (35–70%) and formed at lower temperatures and are more enriched in Pb (Franklin et al., 2005). In the Abitibi Greenstone Belt, Mercier-Langevin et al. (2015) showed a distinct provinciality of Au-rich deposits linked to upper mantle-lower crust enrichment during different episodes of volcanism in the greenstone belt. Variations in volcanic rock petrogenesis have been suggested as controlling factors for the occurrence of VMS, such as the F-classification of felsic volcanic rocks (e.g., prevalence of FIII felsic host rocks reflecting crustal thickness and depth of melting: Lesher et al., 1986, Lentz, 1998; Hart et al., 2004), and these variations in host rock composition may be important determinants of trace element assemblages of the ores.

These attributes are explored in two large compilations of global VMS tonnage and grade, prepared by Franklin et al. (2015) and Mosier et al. (2009) and modified here with additional details for the Canadian Archean deposits, including footwall compositions and trace mineralogy. A complete attributes table of the VMS deposits considered in this study is provided

in Table 2.1 and Appendix Table A.1. We compiled key information on Canadian VMS deposits from a worldwide database from Franklin et al. (2015) and a comprehensive literature review on each deposit. The table identifies a range of established deposit characteristics from Gibson et al. (1983), Lesher et al. (1986), Large (1992), Barrie and Hannington (1999), and Franklin et al. (2005) to isolate the most important factors that might influence the trace element geochemistry of pyrite. Details of the attributes table used for the classification of the deposits are discussed further in Chapter 4.

2.2 VMS deposits of the Southern Superior Province

The Superior Province is the largest exposed Archean craton in the world and hosts the vast majority of Archean Cu-Zn deposits. The different subprovinces of the Superior were assembled in the Neoarchean by plate tectonic-like processes represented by successive episodes of crustal growth and amalgamations over a length of 2000 km (e.g., Percival, 2007, 2012). The oldest crust of the Hudson Bay terrane (3800–3700 Ma) occurs in the northern and northeastern portion of the Superior Province (David et al., 2003). Protocontinental fragments (i.e., Northern Superior, North Caribou, Winnipeg River, Marmion, Minnesota River Valley, Opatica, Goudalie) of Eoarchean to Mesoarchean heritage were assembled prior to 2800 Ma (Percival, 2007). Tracts of the continental blocks are subdivided into greenstone belts interpreted to represent oceanic plateaus, volcano-plutonic arcs and analogous terranes (Thurston, 1994). The history of the greenstone belts has been summarized by, among others, Percival et al. (2007). The Neoarchean oceanic and continental margin volcanic terranes with arc affinities formed between 2750 and 2680 Ma. Widespread VMS formation in calc-alkaline sequences of rifted arc to back-arc settings occurred in the interval of 2730–2700 Ma. Younger synorogenic metasedimentary sequences separating many of the continental and oceanic terranes developed during collisional events between 2710 and 2680 and host a range of orogenic lode Au districts. Cratonization of the Superior between 2680 and 2600 Ma coincided with regional metamorphism, alkaline magmatism, and emplacement of crust-derived granites. Except for a few areas where metamorphic grades reached lower amphibolite facies, the vast majority of the volcanic rocks of the Southern Superior Province are subgreenschist.

The following sections describe the VMS deposits considered in this study. They include deposits in all of the volcanic assemblages of the AGB, except the Pacaud assemblage, as well as greenstone belts of the Wawa, Wabigoon, and Uchi Subprovinces (Fig. 2.1; Table 2.1).

2.2.1 VMS deposits of the Abitibi Greenstone Belt

The majority of the deposits considered in this study are from the Abitibi Greenstone Belt (Fig. 2.2; Table A.2). The Neoarchean Abitibi Subprovince (94,000 km^2) on the southeast side of the Superior Province is one of the most significant greenstone belts in the world in terms of its age, preservation and endowment of base and precious metals, with estimated resources totalling over 775 Mt of polymetallic ore (Mercier-Langevin et al., 2011b; Monecke et. al., 2017a). The AGB is composed of a mosaic of east-trending terranes assembled between 2750 and 2680 Ma that extends 500 km (east to west) by 350 km (north to south) in Ontario and Quebec. It is bounded by the Opatica Subprovince to the North, the Pontiac Subprovince to the southeast, and the Grenville Front tectonic zone to the east–southeast. Mafic volcanic rocks dominate the exposed portion of the AGB (90%) with felsic volcanic rocks in numerous central volcanic complexes (e.g., Goodwin and Ridler, 1970).

Six lithotectonic assemblages define the main volcanic units that are differentiated compositionally and by age (Ayer et al., 2002, 2005; Goutier and Melancon, 2007). From oldest to youngest the assemblages are the Pacaud, Deloro, Stoughton-Roquemaure, Kidd-Munro, Tisdale, and Blake River (Thurston et al., 2008). They formed during episodes of arc and back-arc related volcanism including coeval komatiitic, tholeiitic, and calc-alkalic suites formed in dominantly extensional regimes. Volcanism was especially prolific in the window of 2720-2700 Ma (Corfu, 1993) with coincident VMS endowment, especially in the Blake River and Kidd Munro assemblages (Franklin et al., 2005; Galley et al., 2007; Mercier-Langevin et al., 2011a; Dubé and Mercier-Langevin, 2020).

In addition to VMS, the volcanic rocks and synvolcanic to synorogenic sedimentary sequences host many world class orogenic lode Au deposits (>6200 t). These include the Porcupine assemblage, which was intruded by calc-alkalic plutons from 2690 to 2685 Ma (Corfu, 1993; Monecke et al., 2017a) and the Timiskaming alluvial-fluvial deposits that are coeval with alkalic magmatism between 2681 and 2676 Ma (Corfu, 1993). Crustal shortening and deformation occurred after 2669 Ma preserving large fault zones across the supracrustal Abitibi (Monecke et al., 2017a), including the Porcupine-Destor and Larder Lake-Cadillac fault systems that localized the lode Au deposits during lower crustal metamorphic and magmatic events from 2630 to 2580 Ma (Corfu, 1993; Monecke et al., 2017a).

The Pacaud assemblage (2750–2735 Ma)

The Pacaud assemblage is composed of mafic tholeiitic volcanic rocks with lesser amounts of calc-alkaline rocks (e.g., Heather and Shore, 1999 Ayer et al., 2002, van Breemen et al., 2006; Thurston et al., 2008). Outcrops of the Pacaud are relatively sparse and are mostly exposed south of Kirkland Lake and in the Swayze area in the southwest portion of the AGB, but no VMS deposits are known in this area.

The Deloro assemblage (2734–2724 Ma)

The Deloro assemblage is composed of pillowed calc-alkaline mafic flows and intermediate to felsic volcanic and volcaniclastic rocks (Pyke, 1982; Heather and Shore, 1999; Houlé et al., 2008; Thurston et al., 2008, 2012). The Deloro volcanic rocks host VMS deposits in the Matagami, Quevillon, Joutel, and Amos-Barraute camps (Fig. 2.3.a,b) as well as Chibougamau camps (not included in this study) in the NE part of the AGB. Outcrops of the Deloro are mostly present to the South of Timmins, along the Kenogamissi batholith, in the Shining Tree and Swayze areas, and at Matagami (Monecke et al., 2017a).

The Matagami district contains the bimodal-mafic Bell Allard, Isle Dieu, Mattagami Lake, Norita-Radiore A and Orchan Zn-Cu-Ag deposits and New Hosco Cu-Zn-Ag deposit. These deposits are hosted by volcanic rocks that are dominantly tholeiitic (FIIIb) rhyolite tuff and andesite-dacite flows (e.g., Gaboury and Pearson, 2008; Debreil et al., 2018). The basaltic flow

dominant footwall of Norita-Radiore A differs from the other deposits. The synvolcanic gabbro-anorthosite Bell River Complex (2724.6 +2.5/–1.9 Ma: Mortensen, 1993b) underlies all the deposits (Maier et al., 1996; Carr et al., 2008).

The Quevillon district contains the bimodal-mafic Coniagas Zn-Ag-Pb deposit with a footwall composed of an alternating succession of rhyolite-andesite lapilli tuff and massive to brecciated andesite flows (Doucet et al., 1994, 1998). Felsic host rocks to Coniagas have FIIIa affinities (Gaboury and Pearson, 2008).

The Joutel district contains the bimodal-mafic Joutel and Poirier Zn-Cu-Ag deposits with footwalls composed mainly of FIIIa rhyolite tuff and flows (Avramtechev, 1985; Gaboury and Pearson, 2008).

The bimodal-mafic Normétal Zn-Cu-Au-Ag deposit (9 Mt) in Desmeloizes Township, Quebec (Fig. 2.3.c) is underlain by FIIIa rhyolite flows, agglomerate and tuff of the Deloro Assemblage (Bertrand and Hutchison, 1973; Gaboury and Pearson, 2008).

The Amos-Barraute area is situated on the north side of the Porcupine-Destor-Manneville fault within the External or Northern Volcanic zone (2727–2714 Ma) of the AGB that includes the towns of Lasarre, Amos, and Senneterre (Gaboury and Pearson, 2008). The area is dominated by mafic flows with lesser, felsic volcanic rocks and local felsic to mafic synvolcanic plutons (Gaboury, 2006). The Amos-Barraute district contains the bimodal-mafic Abcourt-Barvue Zn-Ag, and Mogador Cu-Pb-Zn-Au deposits. Abcourt-Barvue is hosted by rhyolite tuff–agglomerate with lesser andesite and minor gabbroic sills (Drouin, 1978). The footwall rhyolite of the deposits have calc-alkaline (FII) affinities (Gaboury and Pearson, 2008).

The Stoughton-Roquemaure assemblage (2723–2720 Ma)

In the Stoughton-Roquemaure assemblage, the volcanic rocks are mainly tholeiitic massive and pillowed basalts, with lesser komatiites and minor felsic volcanic rocks (Beaudoin et al., 1987; Barrie, 1999; Ropchan et al., 2002; Thurston et al., 2008). The Stoughton-Roquemaure hosts the

Estrades VMS deposit from the Casa Berardi camp. The Stoughton-Roquemaure assemblage rocks also outcrop south of Kirkland Lake, along the Northern limits of the AGB, north of the Lyndhurst fault near the Ontario and Quebec border, but no VMS deposits are known in this area.

The Kidd-Munro assemblage (2720–2710 Ma)

In the Kidd-Munro assemblage, the volcanic rocks are dominantly mafic to intermediate tholeiitic volcanic rocks with abundant komatiite (about 10 % by area) and local rhyolite (about 5 %) (e.g., Bleeker et al., 1999; Hannington et al. 1999b; Thurston et al., 2008; Berger, 2011). The E-trending volcanic rocks extend 500 km from the Grenville province west to the Kapuskasing structural zone (Monecke et al., 2017). Notable synvolcanic ultramafic intrusive rocks in the Kidd-Munro include the 2712.4 ± 1.1 Ma Ghost Range differentiated sill (Ayer et al., 2005). Only two large VMS deposits occur in the Kidd-Munro Assemblage in Timmins (Fig. 2.3.d) including the atypical giant bimodal mafic/ultramafic Kidd Creek Cu-Zn-Pb-Ag deposit (171 Mt: Hannington et al., 2017). The immediate footwall (<500 m) of the Kidd Creek deposit is composed of FIIIb rhyolite breccia, flows and tuff (300 m thick) underlain by komatiites and minor peridotite-gabbro (e.g., Bleeker, 1999). The mafic Cu-Zn Potter and Potter-Doal deposits in the east (Fig 2.3.c) are hosted by a mafic tholeiitic succession that includes komatiitic flows of the Kidd-Munro and formed at nearly the same time as Kidd Creek (~2714 Ma) (Hannington et al., 1999b).

At Amos-Barraute, the bimodal-mafic Conigo-Jay Cu-Ag deposit is hosted entirely by rhyolite tuff of the Kidd-Munro assemblage (Chartrand, 1991).

The Tisdale assemblage (2710–2704 Ma)

In the Tisdale assemblage, the volcanic rocks are mainly tholeiitic basalts with lesser komatiites, and locally abundant calc-alkaline, intermediate to felsic volcanic rocks (e.g., Ferguson et al., 1968; Mason and Melnik, 1986; Ayer et al., 2002; Houlé and Solgadi, 2007; Bateman et al., 2008; Thurston et al., 2008). The ages and locations of VMS deposits in Val d'Or suggest that they are in the Tisdale assemblage, although rocks of the Blake River assemblage are also

present. One VMS deposit in the Casa Berardi camp (Gemini, not sampled) may also be Tisdale age. The Tisdale is mostly exposed between the Porcupine-Destor fault zone and the Larder Lake-Cadillac fault zone, in the Larder Lake area and in the Kapuskasing structural zone (Monecke et al., 2017a).

At Val d'Or, volcanic rocks of the Tisdale that host the bimodal-mafic Manitou-Barvue Cu-Zn-Ag-Au, Louvem Zn-Cu-Ag-Au and Dunraine Cu-Ag-Au deposits (Fig 2.3.e) consist mainly of tholeiitic basalt intercalated with komatiite (Chartrand, 1991; Scott et al., 2002). They include FII rhyolite tuff-agglomerate and lesser andesite-basalt that host the VMS deposits (e.g., Gaboury and Pearson, 2008). The footwall to Dunraine is spatially associated with a diorite sill (Sharpe, 1968). The host rocks for the East Sullivan Cu-Zn-Ag-Au deposit are rhyolite agglomerate, and the host rocks for the Louvicourt Cu-Zn-Ag-Au deposit are rhyolite with minor argillite units (Chartrand, 1991; Jenkins and Brown, 1999). The footwall of East Sullivan is spatially associated with an alkaline-felsic stock (Scott et al., 2002).

The Blake River assemblage (2704–2695 Ma)

The Blake River Group (BRG) is dominated by bimodal basalt, andesite, and numerous felsic (rhyodacitic to rhyolitic) centres (Jensen and Langford, 1985; Ayer et al., 2002, 2005). The exposed area of the Blake River occurs between the Porcupine-Destor fault zone in the north and the Larder Lake-Cadillac fault zone in the south. The volcanic rocks outcrop south of Matheson, west of Timmins, in the Swayze area, and in the Rouyn-Noranda area (Monecke et al., 2017a). They cover 3000 km^2 and include a volcanic sequence that is 4-7 km thick (Corfu, 1993; Pearson and Daigneault et al., 2009; Mercier et al., 2011b). The Blake River is by far the highest ore producing assemblage containing almost half of the Abitibi VMS tonnage (~375 Mt) from deposits in the Doyon-Bousquet-LaRonde (DBL), Noranda, and Kamiskotia camps (Fig. 2.3.f). Over 90% of the total tonnage of VMS-related gold in the Abitibi is from the five Au-rich deposits at DBL and Noranda (Mercier-Langevin et al., 2011b). The DBL camp contains the bimodal-mafic Bousquet #2-Dumagami Au-Ag-Cu-Zn deposit as well as the bimodal-felsic LaRonde-Penna Au-Cu-Zn-Ag and bimodal-mafic Bousquet #1 Au-Cu deposits (not sampled) that are hosted by Hébécourt (base) and Bousquet (top) formations (e.g., Dubé et al., 2014).The

footwall to the Bousquet #2-Dumagami deposit is composed of basalt overlain by calc-alkaline (FI and FII) dacitic to rhyodacitic domes and flow breccias and local thin andesitic intervals and dikes (e.g., Lafrance et al., 2003; Gaboury and Pearson, 2008; Dubé et al., 2014).

At Noranda, the deposits are all classified as bimodal-mafic, and most of the Cu-Zn deposits belong to the mine sequence of the Noranda cauldron (main camp), which is a 3000 m thick succession of basalt-andesite and subordinate high silica rhyolite flows and domes emplaced in the 3rd caldera cycle (e.g., Gibson and Galley, 2007; Monecke et al., 2017b). There are distinct differences between the lithofacies and compositions of their immediate host rocks. Ansil, Bedford, East Waite, Lac Dufault, Millenbach, Norbec, Quemont, Vauze (main camp) as well as the Aldermac Zn-Cu deposit (west camp) and Quemont Cu-Au deposit (south camp) are hosted by rhyolite flows (mafic: felsic volcanic rocks of >3:1). Amulet A-C, New Insco, Newbec, Old Waite and the Moosehead Pb-Zn deposit (main camp) are hosted by andesite flows with minor rhyolite (Gibson and Galley, 2007). Deposits formed in the 4th caldera cycle include the Delbridge and Deldona Zn-Ag-Au-Pb deposits and the Gallen Cu-Zn deposit (east camp), which are hosted by rhyolite flows (Gibson and Galley, 2007). The Horne Cu-Au deposits (H orebodies and No. 5 zone: south camp) and the Mobrun Cu-Zn deposit (north camp) are hosted by rhyolite volcaniclastic rocks outside the Noranda main camp (Kerr and Gibson, 1993). The Upper H and Lower H Horne orebodies are hosted in rhyolitic breccia (Price, 1933) and are overlain by the No.5 zone and a smaller massive pyrite replacement lens (G zone) (Sinclair, 1971, Gibson and Galley et al., 2007; Monecke et al., 2017). Felsic host rocks of all the Noranda deposits have FIIIa affinities (Gabour and Pearson, 2008).

East of Timmins, volcanic rocks of the Blake River are bimodal sequences without any ultramafic units (e.g., Barrie, 1993; Barrie and Pattison, 1999). The Kam-Kotia Cu-Zn deposit (30 km south of Kidd Creek) is the largest deposit (5 Mt), and its footwall contains rhyolite and dacite flows and lesser basalt flows (Barrie and Pattison, 1999). The Genex and Canadian Jamieson Zn-Cu deposits, also in the Kamiskotia area (Fig. 2.3.d), have footwalls containing mostly rhyolite at Canadian Jamieson and andesite-basalt with lesser rhyolite at Genex (Barrie, 1993).

2.2.2 VMS deposits of Wawa and the Western Superior Province

The Wawa subprovince includes the Manitouwadge Greenstone Belt (2720 Ma) along its northern limits adjacent to the Quetico subprovince (Williams et al., 1991). The greenstone belt consists largely of bimodal tholeiitic to transitional volcanic rocks (Lodge et al., 2015) and includes the bimodal-mafic Geco and Willecho Zn-Cu-Ag deposits of the Manitouwadge camp (Fig. 2.3.g) as well as the Willroy and Nama Creek deposits (not sampled). The Manitouwadge deposits are hosted by mafic and felsic units that have been metamorphosed to upper amphibolite facies (e.g., Zaleski and Peterson, 1995; Zaleski et al., 1999). The immediate host rocks consist of felsic volcanic rocks intercalated with banded iron formation and other sediments underlain by basalt (Zaleski and Peterson, 1995).

The Western Superior Province extends from Lake Superior in the southeast to the Phanerozoic cover in the west and north and borders the AGB to the east in the Wawa subprovince (Percival et al., 2012). The region consists of a series of west to northwest-trending belts with strike lengths of up to 1000 km. The Wabigoon subprovince situated to the west of Wawa is dominated by mafic and felsic volcanic rocks, calc-alkalic to alkalic plutons and sedimentary successions (Blackburn et al., 1991; Sanborn-Barrie and Skulski, 2005). It includes the Sturgeon Lake greenstone belt (2780–2720 Ma; Lodge et al., 2019) located 200 km NW of Thunder Bay. The Sturgeon Lake assemblage in the southern portion of the belt is dominated by mafic volcanic rocks and contains a bimodal caldera complex composed of 4500 m of volcaniclastic flows, rhyolitic tuff, basal basaltic members and pillowed to massive andesite flows, which host the bimodal-felsic Sturgeon lake, Lyon Lake, and Mattabi Zn-Cu-Ag deposits (Fig. 2.3.h) (Trowell, 1974, 1983; Blackburn et al., 1991; Morton et al., 1991, 1996). The immediate footwalls of the deposits are felsic ash flow tuffs at Sturgeon Lake, fragmental rhyolite at Lyon Lake and felsic lapilli tuff and lesser rhyolite at Mattabi that have FII affinities (Franklin et al., 1975; Morton et al. 1991; Hart et al., 2004).

The Uchi Subprovince to the north of the Wabigoon and south of the North Caribou Subprovince contains the Birch-Uchi Greenstone Belt (2740–2730 Ma) with volcanic rocks consisting of

tholeiitic basalt flows overlain by tholeiitic to calc-alkaline dacite and rhyolite (Corfu and Scott, 1993; Scott, 1996). Mafic and felsic subvolcanic intrusions and clastic sedimentary rocks are intercalated with the volcanic suites (Scott, 1996). The Birch-Uchi hosts the bimodal-felsic Zn-Cu-Ag South Bay deposit with a footwall composed of rhyolite tuff-flows with FIIIb affinities underlain by rhyodacite to dacite tuff and pillow andesite basalt (Hart et al., 2004; Pollock et al., 1972).

2.3 Other Archean VMS deposits of the Superior Province

The Benny Greenstone Belt situated in North Sudbury (Fig. 2.1), extends E-W for more than 38 km with a thickness up to 5 km and hosts the Stralak and Geneva Lake VMS deposits. The Benny Belt is comprised of a calk-alkaline to tholeiitic metavolcanic sequence composed of basalt-andesite flows, andesite-rhyolite tuff-breccia, lapilli-tuff and lesser rhyolite-dacite flows (Card and Innes, 1981). The Stralak Zn-Pb-Cu-Ag deposit has a footwall dominated by basaltic tuff and flows overlain by minor felsic volcanic rocks (Ontario Geological Survey, 1986). The bimodal-mafic Geneva Lake Zn-Pb deposit has a footwall composed of mafic volcanic rocks and lesser intermediate tuffs and breccias (Constable, 1989).

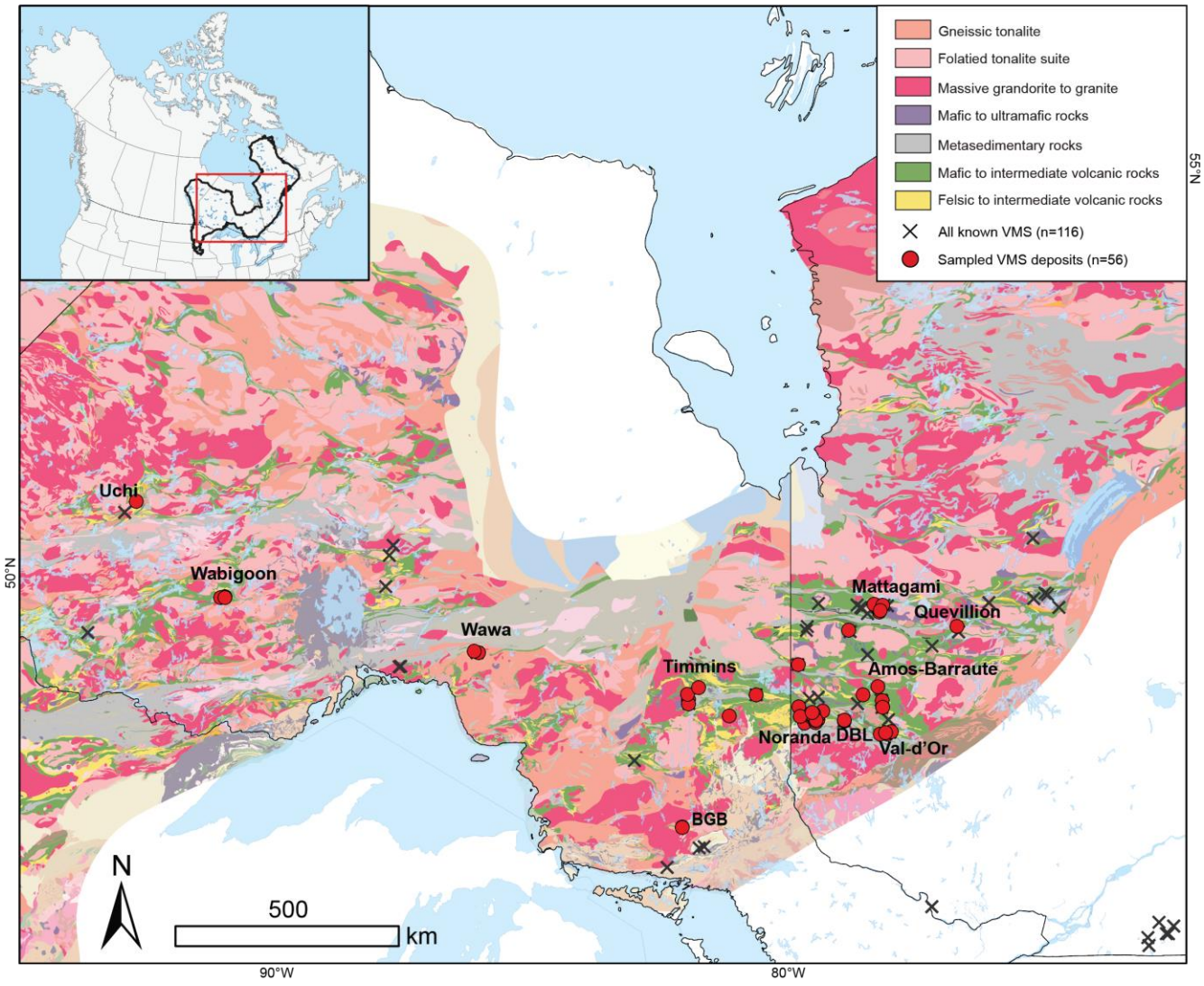

Figure 2.1 Simplified geological map of the southern Superior province (modified after Monstion et al., 2018). The locations of VMS deposits from Jonasson et al. (2020) included in this study are shown. The majority are in the Abitibi greenstone belt.

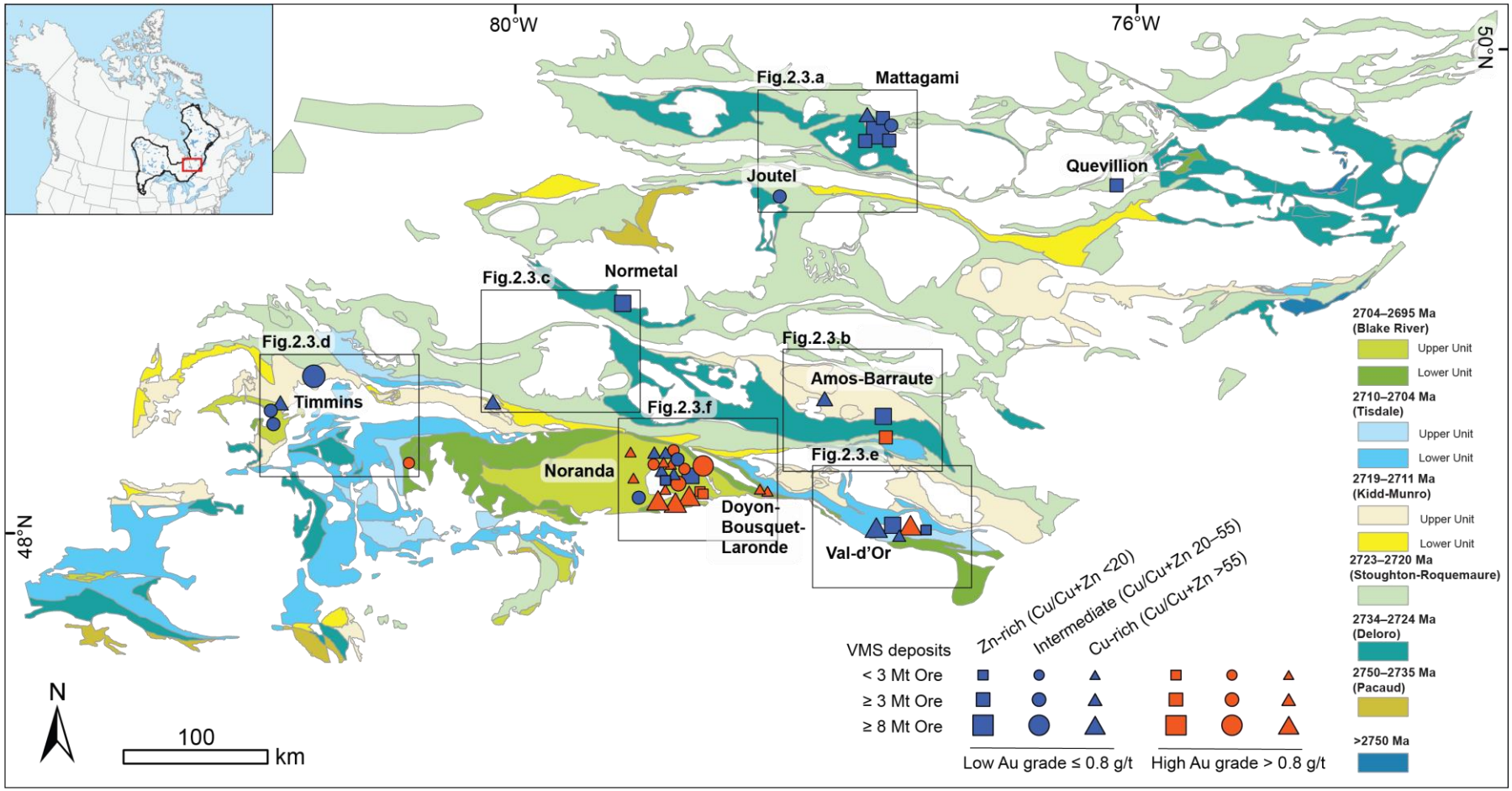

Figure 2.2 Simplified geological map of the major volcanic assemblages in the Abitibi greenstone belt (modified after Thurston et al., 2008) showing the distribution of VMS deposits in the database (Jonasson et al., 2020). Symbols represent deposits with different Cu/(Cu+Zn) grades, Au grades, and tonnages. The rectangles outline the inset maps of individual mine camps in Figure 2.3.

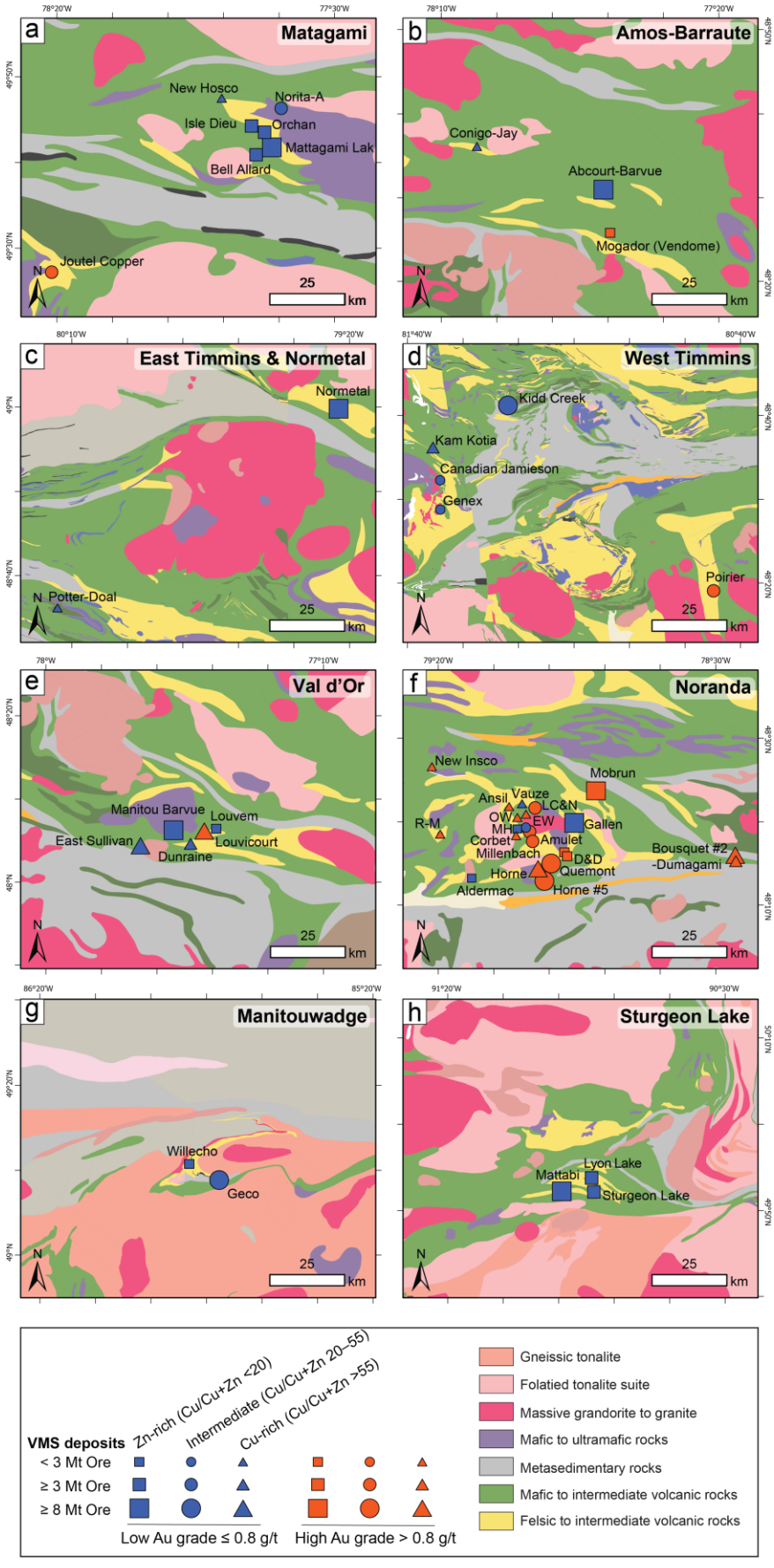
a
Matagami
New Hosco
Norita-A
Isle Dieu
Orchan
Mattagami Lak
Bell Allard
Joutel Copper
b
Amos-Barraute
Conigo-Jay
Abcourt-Barvue
Mogador (Vendome)
c
East Timmins & Normetal
Normetal
Potter-Doal
d
West Timmins
Kidd Creek
Kam Kotia
Canadian Jamieson
Genex
Poirier
e
Val d'Or
Manitou Barvue
Louvem
East Sullivan
Louvicourt
Dunraine
f
Noranda
New Insco
Mobrun
Ansil
Vauze
LC&N
OW
EW
Gallen
MH
R-M
Corbet
Amulet
Millenbach
D&D
Bousquet #2
-Dumagami
Horne
Quemont
Aldermac
Horne #5
g
Manitouwadge
Willecho
Geco
h
Sturgeon Lake
Lyon Lake
Mattabi
Sturgeon Lake
N
25
km
VMS deposits
Zn-rich (Cu/Cu+Zn <20)
Intermediate (Cu/Cu+Zn 20–55)
Cu-rich (Cu/Cu+Zn >55)
< 3 Mt Ore
≥ 3 Mt Ore
≥ 8 Mt Ore
Low Au grade ≤ 0.8 g/t
High Au grade > 0.8 g/t
Gneissic tonalite
Folatied tonalite suite
Massive grandorite to granite
Mafic to ultramafic rocks
Metasedimentary rocks
Mafic to intermediate volcanic rocks
Felsic to intermediate volcanic rocks

Figure 2.3 Geological maps of mine camps with sampled VMS deposits from Jonasson et al. (2020) included in this study (modified after Monstion et al., 2018). The majority are in the Abitibi greenstone belt. Noranda deposit name abbreviations: R-M (Robb-Montbray); OD (Old Waite); EW (East Waite); D&D (Deldona and Delbridge); MH (Moosehead); Amulet (Amulet-A and Amulet-C).

Table 2.1 Geological attributes and features of VMS deposits considered in this study (modified from Franklin et al., 2015). Map numbers correspond to VMS deposit locations in Figure 3.1.

Name	District/Camp	Assemblage	Orogen	Map #	Mtonnes Ore	Cu %	Pb %	Zn %	AU (g/t)	AG (g/t)	Cu/(Cu+Zn) *100	Ore form	Age (Ma)	No. Py Samples	Lat.	Long.
Abcourt-Barvue	Amos-Barraute	Deloro	Abitibi	1	8.3	0.1	-	3.5	-	42	1	Zn-Ag	2700	16	48.52	-77.68
Conigo-Jay	Amos-Barraute	Kidd-Munro	Abitibi	2	2.7	1.3	-	0.0	-	17	100	Cu-Ag	2715	5	48.6	-78.06
Mogador	Amos-Barraute	Deloro	Abitibi	3	0.6	0.5	-	8.1	1.18	62	6	Zn-Cu-Ag-Pb	2695	15	48.43	-77.663
Joutel Copper	Joutel	Deloro	Abitibi	4	1.7	2.2	-	3.9	-	-	36	Zn-Cu-Ag	2730	1	49.45	-78.351
Poirier	Joutel	Deloro	Abitibi	5	7.7	1.8	-	2.5	1.60	8	42	Zn-Cu-Ag	2730	4	48.32	-80.75
Bell Allard	Matagami	Deloro	Abitibi	6	3.2	1.5	-	13.8	0.76	43	10	Zn-Cu-Ag	2720	3	49.69	-77.73
Isle Dieu	Matagami	Deloro	Abitibi	7	3.0	1.0	-	17.9	0.45	82	5	Zn-Cu-Ag	2730	4	49.73	-77.74
Mattagami Lake	Matagami	Deloro	Abitibi	8	25.6	0.4	0.10	5.1	0.30	22	8	Zn-Cu-Ag	2725	3	49.72	-77.72
New Hosco	Matagami	Deloro	Abitibi	9	2.0	1.4	-	1.1	0.03	4	56	Cu-Zn-Ag	2725	3	49.79	-77.84
Norita-A	Matagami	Deloro	Abitibi	10	4.0	1.8	-	3.8	0.69	27	32	Zn-Cu-Ag	2725	2	49.78	-77.663
Orchan	Matagami	Deloro	Abitibi	11	3.5	1.2	-	8.7	0.50	37	12	Zn-Cu-Ag	2725	5	49.71	-77.71
Bousquet #2	Bousquet	Blake River	Abitibi	12	8.0	0.7	-	0.3	7.80	13	68	Pyritic Au	2698	4	48.25	-78.44
Dumagami	Bousquet	Blake River	Abitibi	13	2.1	0.7	-	0.3	7.80	13	68	Zn-Cu-Ag-Pb	2698	4	48.26	-78.442
Amulet-A	Noranda main	Blake River	Abitibi	14	4.9	5.0	-	5.2	1.43	44	49	Cu-Zn	2698	5	48.32	-79.083
Amulet-C	Noranda main	Blake River	Abitibi	15	0.6	2.2	-	8.5	0.60	87	21	Cu-Zn	2698	5	48.31	-79.068
Ansil	Noranda main	Blake River	Abitibi	16	1.6	7.2	-	0.9	1.60	27	88	Cu-Zn	2698	13	48.35	-79.117
Bedford	Noranda main	Blake River	Abitibi	17	0.2	1.5	-	-	-	-	100	Cu-Zn	2698	1	48.37	-79.2
Corbet	Noranda main	Blake River	Abitibi	18	2.8	2.9	-	1.6	1.00	21	64	Cu-Zn	2700	3	48.3	-79.1
East Waite	Noranda main	Blake River	Abitibi	19	1.5	4.1	-	3.3	1.80	31	56	Cu-Zn	2700	3	48.34	-79.077
Millenbach	Noranda main	Blake River	Abitibi	20	3.6	3.5	-	4.3	1.00	56	44	Cu-Zn	2700	1	48.3	-79.054
Moosehead	Noranda main	Blake River	Abitibi	21	0.0	0.0	-	-	-	-	0	Zn-Pb	2698	4	48.32	-79.083
Norbec & Lac Dufault	Noranda main	Blake River	Abitibi	22	4.5	2.8	-	4.8	0.91	44	37	Cu-Zn	2700	7	48.35	-79.057
Old Waite	Noranda main	Blake River	Abitibi	23	1.1	4.7	0.04	3.0	1.10	22	61	Cu-Zn	2700	4	48.34	-79.089
Quemont	Noranda main	Blake River	Abitibi	24	16.7	1.2	0.02	1.8	5.50	18	40	Cu-Au	2700	11	48.26	-79.008
Vauze	Noranda main	Blake River	Abitibi	25	0.4	2.9		0.9	0.70	24	76	Cu-Zn	2700	7	48.36	-79.081

Table 2.1 cont.

Name	District/Camp	Assemblage	Orogen	Map #	Mtonnes Ore	Cu %	Pb %	Zn %	Au (g/t)	Ag (g/t)	Cu/(Cu+Zn) *100	Ore type	Age (Ma)	No. Py Samples	Lat.	Long.
Aldermac	Noranda N-S-E-W	Blake River	Abitibi	26	2.8634	1.5	-	4.1	0.48	31	27	Zn-Cu	2698	5	48.22	-79.233
Delbridge	Noranda N-S-E-W	Blake River	Abitibi	27	0.4	0.6	-	8.6	2.40	69	6	Zn-Ag-Au-Pb	2700	2	48.27	-78.965
Deldona	Noranda N-S-E-W	Blake River	Abitibi	28	0.1	0.3	-	5.0	4.10	26	6	Zn-Ag-Au-Pb	2698	2	48.27	-78.965
Gallen	Noranda N-S-E-W	Blake River	Abitibi	29	8.1	0.1	-	3.4	0.06	2	2	Zn-Cu	2700	8	48.33	-78.953
Horne #5 Zone	Noranda N-S-E-W	Blake River	Abitibi	30	144.0	1.0	-	0.9	1.40	-	53	Cu-Au	2698	13	48.23	-79.02
Horne-H&G	Noranda N-S-E-W	Blake River	Abitibi	31	53.7	2.2	-	-	6.10	13	100	Cu-Au	2700	5	48.26	-79.012
Mobrun	Noranda N-S-E-W	Blake River	Abitibi	32	9.8	0.8	-	4.3	1.20	35	16	Zn-Cu	2698	12	48.38	-78.867
New Insco	Noranda N-S-E-W	Blake River	Abitibi	33	0.9	2.6	-	-	0.90	21	100	Cu	2700	8	48.44	-79.352
Robb Montbray	Noranda N-S-E-W	Blake River	Abitibi	34	0.1	1.7	-	0.3	4.57	-	85	Cu-Au	2698	4	48.31	-79.328
Normetal	Normetal	Deloro	Abitibi	35	9.2	0.8	2.20	5.1	0.60	50	13	Zn-Cu-Au-Ag	2727	3	49	-79.366
Coniagas	Quévillon	Deloro	Abitibi	36	0.7	-	0.70	10.7	-	182	0	Zn-Ag-Pb	2725	5	49.5	-76.17
Canadian Jamieson	Timmins	Blake River	Abitibi	37	0.7	2.4	-	4.1	0.31	30	37	Zn-Cu	2705	2	48.54	-81.57
Genex	Timmins	Blake River	Abitibi	38	1.8	0.8	-	1.6	-	-	34	Zn-Cu	2720	3	48.48	-81.57
Kam Kotia	Timmins	Blake River	Abitibi	39	5.4	1.3	-	1.2	0.26	3	53	Cu-Zn	2705	4	48.6	-81.592
Kidd Creek	Timmins	Kidd-Munro	Abitibi	40	170.9	2.3	0.22	6.2	0.01	87	27	Zn-Cu-Ag-Pb	2714	9	48.69	-81.365
Potter-Doal	Timmins	Kidd-Munro	Abitibi	41	0.0	15.2	-	4.2	-	-	79	Cu-Zn	2714	2	48.6	-80.212
Dunraine	Val d'Or	Tisdale	Abitibi	42	3.0	1.2	-	-	0.18	3	100	Cu-Ag-Au	2700	13	48.07	-77.569
East Sullivan	Val d'Or	Tisdale	Abitibi	43	15.2	1.0	-	0.5	0.27	8	67	Cu-Zn-Ag-Au	2715	3	48.07	-77.709
Louvem	Val d'Or	Tisdale	Abitibi	44	2.4	0.2	-	5.6	0.69	34	4	Zn-Cu-Ag-Au	2700	4	48.1	-77.519
Louvicourt	Val d'Or	Tisdale	Abitibi	45	19.3	3.1	-	1.7	0.83	29	65	Cu-Zn-Ag-Au	2700	8	48.1	-77.495
Manitou Barvue	Val d'Or	Tisdale	Abitibi	46	13.8	0.1	0.07	0.4	0.34	12	16	Cu-Zn-Ag-Au	2700	7	48.09	-77.61
Geneva Lake	Benny		Benny	47	0.1	0.0	3.34	9.2	-	-	0	Zn-Pb	2710	2	46.81	-81.697
Stralak	Benny		Benny	48	0.7	0.5	0.50	3.2	-	69	14	Zn-Pb-Ag-Cu	2730	3	46.8	-81.697

Table 2.1 cont.

Name	District/Camp	Assemblage	Orogen	Map #	Mtonnes Ore	Cu %	Pb %	Zn %	Au (g/t)	Ag (g/t)	Cu/(Cu+Zn) *100	Ore form	Age (Ma)	No. Py Samples	Lat.	Long.
Geco	Manitouwadge	Wawa	Wawa	49	58.4	1.9	0.15	3.5	-	50	35	Zn-Cu-Ag	2720	5	49.15	-85.792
Willecho	Manitouwadge	Wawa	Wawa	50	2.0	0.5	0.18	4.4	-	68	10	Zn-Cu-Ag	2740	4	49.18	-85.883
Lyon Lake & Creek zone	Sturgeon Lake	Wabigoon	Wabigoon	51	3.2	1.3	0.99	8.7	-	150	13	Zn-Cu-Ag	2735	3	49.89	-90.889
Mattabi	Sturgeon Lake	Wabigoon	Wabigoon	52	12.8	0.7	0.85	8.3	-	110	8	Zn-Cu-Ag	2735	7	49.88	-90.982
Sturgeon Lake	Sturgeon Lake	Wabigoon	Wabigoon	53	4.0	1.2	0.63	6.5	-	114	16	Zn-Cu-Ag	2735	4	49.88	-90.894
South Bay	Uchi	Uchi	Uchi	54	1.5	2.3	-	14.5	-	82	14		2740	2	51.11	-92.679
East Cleaver	Hackett River		Slave	55	4.6	-	0.09	6.8	0.34	160	0	Ag-Zn-Pb	2778	15	65.92	-108.46
Hackett A (Main) Zone	Hackett River		Slave	56	4.5	0.3	1.38	12.8	0.46	231	2	Ag-Zn-Pb-Cu	2778	11	65.92	-108.37
Yava Lake	Hackett River		Slave	57	1.5	0.5	0.50	3.0	2.09	103	14	Ag-Zn-Pb-Cu-Au	2778	8	65.6	-107.93
High Lake	High Lake		Slave	58	15.6	2.2	0.32	3.5	0.92	75	39	Zn-Cu-Pb-Ag	2778	3	67.38	-110.86
Gondor	Hood River		Slave	59	7.3	0.2	0.40	4.8	-	46	4	Zn-Cu-Pb-Ag	2800	5	65.56	-111.8
Hood #10	Hood River		Slave	60	3.2	3.0	-	3.5	-	34	46	Zn-Cu-Pb-Ag	2778	1	66.06	-112.75
Heninga Gemex	Keewatin		Kenoran	61	5.7	0.5	-	7.9	0.90	100	6		2695	1	61.77	-96.203

Table 2.1 cont.

Name	District/Camp	Assemblage	Orogen	Map #	Mtonnes Ore	Cu %	Pb %	Zn %	Au (g/t)	Ag (g/t)	Cu/(Cu+Zn) *100	Ore form	Age (Ma)	No. Py Samples	Lat.	Long.
Callinan	Flin Flon	Flin Flon	Trans-Hudson	62	2.6	2.0	-	5.4	1.50	21	27	Zn-Cu	1875	4	54.78	-101.88
Centennial	Flin Flon	Flin Flon	Trans-Hudson	63	2.4	1.6	-	2.2	1.51	26	41	Zn-Cu	1875	1	54.71	-101.67
Coronation	Flin Flon	Flin Flon	Trans-Hudson	64	1.3	4.3	-	0.2	2.26	6	95	Cu-Zn-Au	1875	8	54.58	-102
Flexar	Flin Flon	Flin Flon	Trans-Hudson	65	0.3	4.1	-	0.4	1.17	5	90	Cu-Zn	1875	1	54.68	-102.03
Flin Flon	Flin Flon	Flin Flon	Trans-Hudson	66	62.9	2.2	-	4.1	2.85	43	35	Zn-Cu-Au	1875	6	54.77	-101.88
North star	Flin Flon	Flin Flon	Trans-Hudson	67	0.3	5.6	-	-	0.51	2	100	Cu	1885	6	54.76	-101.57
Pinebay	Flin Flon	Flin Flon	Trans-Hudson	68	1.4	2.8	-	-	0.20	-	100	Cu	1875	4	54.77	-101.61
Schist Lake & Mandy	Flin Flon	Flin Flon	Trans-Hudson	69	2.0	4.6	0.04	7.8	1.52	41	37	Zn-Cu	1875	2	54.72	-101.83
Anderson Lake	Snow Lake	Snow Lake	Trans-Hudson	70	3.4	3.5	-	0.1	1.47	12	97	Cu	1875	7	54.86	-99.993
Chisel Lake	Snow Lake	Snow Lake	Trans-Hudson	71	7.2	0.4	1.40	10.9	1.30	37	3	Zn-Pb-Cu	1875	8	54.83	-100.12
Osborne Lake	Snow Lake	Snow Lake	Trans-Hudson	72	3.4	3.1	-	1.5	0.20	-	68	Cu-Zn	1875	2	54.95	-99.723
Photo Lake	Snow lake	Snow Lake	Trans-Hudson	73	0.7	5.6	-	6.2	5.11	20	47	Zn-Cu-Au	1875	4	54.86	-100.1
Rod	Snow Lake	Snow Lake	Trans-Hudson	74	0.7	7.2	-	3.1	0.96	-	70	Cu-Zn	1875	9	54.86	-99.919
Stall Lake	Snow Lake	Snow Lake	Trans-Hudson	75	6.5	4.4	-	0.5	1.47	12	90	Cu-Zn	1875	1	54.85	-99.44
Fox Lake	Lynn Lake		Trans-Hudson	76	10.8	1.8	-	1.8	0.17	4	51	Cu-Zn	1890	3	56.64	-101.65
Ruttan	Rusty Lake		Trans-Hudson	77	82.8	1.4	0.08	1.6	0.49	13	46	Zn-Cu	1900	3	56.46	-99.637
Sherridon	Sherridon		Trans-Hudson	78	7.0	2.8	-	3.4	0.69	31	45	Zn-Cu	1800	2	55.12	-101.09
Boylen-Koke	Labrador Trough		Trans-Hudson	79	1.1	0.7	1.03	6.9	1.03	55	9		1200	3	57.66	-69.45

Table 2.1 cont.

Name	District/Camp	Assemblage	Orogen	Map #	Mtonnes Ore	Cu %	Pb %	Zn %	AU (g/t)	AG (g/t)	Cu/(Cu+Zn) *100	Ore form	Age (Ma)	No. Py Samples	Lat.	Long.
Austin Brook	Bathurst		Appalachian	80	0.2	0.1	3.67	5.7	-	82	2	Pb-Zn-Cu-Sn	465	2	47.6	-66.045
Brunswick #12	Bathurst		Appalachian	81	229.8	0.5	3.01	7.7	0.46	91	6	Pb-Zn-Cu-Sn	465	2	47.47	-65.89
Heath Steele	Bathurst		Appalachian	82	69.9	1.0	0.89	2.7	0.54	47	27	Pb-Zn-Cu-Sn	465	2	47.29	-66.087
Key Anacon	Bathurst		Appalachian	83	2.0	0.2	2.53	6.7	0.09	81	3	Pb-Zn-Cu-Sn	465	1	47.44	-65.7
Clinton Copper	Eastern Townships		Appalachian	84	1.4	1.8	-	1.6	-	14	54		480	2	45.46	-70.908
Trinity	Eastern Townships		Appalachian	85	0.1	1.2	-	0.7	-	-	61		465	2	48.71	-77.76
Weedon	Eastern Townships		Appalachian	86	1.7	2.5	0.08	0.4	-	7	86		495	2	45.7	-71.373
Kudz Ze Kayah	Finlayson Lake		Canadian Cordillera	87	13.7	0.9	1.56	6.0	1.38	139	13		360	2	61.46	-130.61
Hart River	Hart River		Canadian Cordillera	88	1.1	1.5	0.87	3.7	1.41	50	28		1200	4	64.64	-136.82
Eskay Creek	Stewart		Canadian Cordillera	89	3.3	0.8	2.90	5.6	45.97	2224	13	Ag-Au-Zn-Pb	`	2	56.64	-130.43
Britannia	Vancouver		Canadian Cordillera	90	49.3	1.1	0.03	0.3	0.34	4	81		150	1	49.61	-123.14
Myra Falls Group (Lynx)	Vancouver Island		Canadian Cordillera	91	0.6	1.6	1.00	7.5	2.50	90	18	Zn-Cu-Ag-Au	365	3	49.54	-125.57

3. Methods

3.1 Description of the VMS mineral separate database

The data used in this study (see Appendix B) are a subset of geochemical analyses from an extensive Canada-wide archive of ore samples assembled by the Geological Survey of Canada (GSC) (Jonasson et al., 2020). The collection consists of specially prepared mineral separates from base metal sulfide deposits and occurrences across Canada, including four main deposit types: VMS, Mississippi Valley-type carbonate-hosted (MVT), sedimentary exhalative (SEDEX), and magmatic deposits (veins, mantos, skarns and porphyries). Samples were collected and processed by different GSC researchers (S.M. Roscoe, R.W. Boyle, A. Soregaroli, K.M. Dawson, W. Morgan, H.G. Ansdell, R.V. Kirkham, A.P. Sabina, J.M. Franklin, A.G. Galley, I.R. Jonasson, M.D. Hannington, D.E. Ames, and J. Peter) over a period of 50 years (1952 to 2002) and archived at the laboratories of the GSC. This study focuses on the mineral separates from ore samples of VMS deposits, with an emphasis on Archean VMS in the Abitibi subprovince (Fig. 3.1).

The sulfide samples, mainly hand specimen scale, were collected from surface outcrops at mine sites, from underground mines, and from mine dumps of past producing and producing deposits as well as exploration drill core and some concentrates and rejects (e.g., tailings) from milling operations (Jonasson et al., 2020). The preparation of samples (up to 500 g) included crushing and pulverizing in a steel shatter box (and tungsten-carbide mills in some cases), selection of a sieved fraction (between -100 and +150 mesh), superpanning to concentrate the sulfides, and cleaning with a Frantz magnetic separator, yielding final mineral separates from <100 mg up to 5 g (Jonasson et al., 2020). 97% of the samples produced separates of pyrite, pyrrhotite, chalcopyrite, sphalerite and/or galena (n=1425); and a few samples yielded separates of arsenopyrite, barite, bornite, gahnite, magnetite, dolomite, or siderite. Some incomplete mineral separations were designated as mixtures (e.g., Py/Po, Py/Sp) where the mineralogy was known (Jonasson et al., 2020).

The final database includes 2662 sulfide mineral separates from almost 200 VMS deposits with samples from nearly 2/3 of all of the deposits of this type in Canada. The samples include pyrite separates (n=452) and pyrite-dominated mixtures (n=202), chalcopyrite separates (n=311) and chalcopyrite-dominated mixtures (n=90), sphalerite separates (n=403) and sphalerite-dominated mixtures (n=193), pyrrhotite separates (n=134) and pyrrhotite-dominated mixtures (n=71), galena separates (n=59) and galena-dominated mixtures (n=18), and magnetite separates (n=14). There are 288 pyrite mineral separates from 55 different deposits in 12 mine camps of the Superior Province and 164 pyrite mineral separates from VMS deposits outside of the Superior Province. Almost all are from the AGB; 6 samples are from the Manitouwadge and Sturgeon Lake districts in the Western Superior Province and from the Uchi Subprovince.

The pyrite data from the AGB include samples from 14 deposits in the Noranda main camp (n=54 samples) and 9 deposits north, south, east, and west of the Noranda main camp (n=68 samples), 3 deposits in Amos-Barraute (n=36 samples), 7 deposits in Val d'Or (n=35 samples), 6 deposits in Mattagami (n=20 samples), and 5 deposits in Timmins (n=20 samples), including Kidd Creek (n=9 samples). Fewer samples are available from Bousquet-LaRonde (n=7 samples from Bousquet #2-Dumagami), Joutel (n=5 samples from 2 deposits), Quevillon (n=5 samples from 1 deposit), and Normetal (n=5 samples from 1 deposit).

Samples from other Archean VMS in the Western Superior and elsewhere include examples from: Sturgeon Lake (n=14 from 3 deposits), Manitouwadge (n=9 from 2 deposits), and the Uchi Belt (n=2 from the South Bay deposit); Benny Belt, Sudbury (n=5 from 2 deposits); and in the Slave Province (n= 36 from 3 deposits in Hackett River, n=6 from 2 deposits in Hood River, n=3 from 1 deposit in High Lake). Pyrite samples from younger VMS deposits include examples from: the Paleoproterozoic Trans-Hudson orogen (n=33 from 6 deposits in Snow Lake, n=31 from 9 deposits in Flin Flon, n=4 from 1 deposit in Lynn Lake, n=2 from 1 deposit in Sherridon), the Paleozoic Appalachian orogen (n=7 from 3 deposits in Bathurst, n=5 from 3 deposits in Eastern Township), and the Paleozoic–Mesozoic Canadian Cordillera (n=3 from 1 Myra Falls deposit (Lynx) on Vancouver Island, n=2 from the Eskay Creek deposit, n=2 from 1 deposit in Finlayson Lake).

3.2 Bulk analyses

The data reported in Jonasson et al. (2020) are based on bulk analyses of samples of the mineral separates that were pulverized to -200 mesh and treated by multi-acid dissolution for analysis by ICP-OES (major elements) and ICP-MS (trace elements) at the GSC in Ottawa. Additional elements were analyzed by INAA at Activation Laboratories Ltd., Ancaster, Ontario (Jonasson et al., 2020). The complete data set was acquired in 41 different submissions from 1994 to 2002. Analyses at the GSC Laboratories were performed in 1994, 1996, 1997, and 2000. Analyses at Actlabs were performed in 1999 and 2002. During this time, the analytical methods (ICP-OES, ICP-MS, and INAA) and instrumentation did not vary significantly. Results were generated for 62 elements and oxides: SiO_2, TiO_2, Al_2O_3, Fe_2O_3, MgO, CaO, Na_2O, K_2O, MnO, P_2O_5, ST (sulfur), Ag, As, Au, Ba, Be, Bi, Br, Cd, Co, Cr, Cs, Cu, Ga, Hf, Hg, In, Ir, Mo, Nb, Ni, Pb, Rb, Sb, Sc, Se, Sn, Sr, Ta, Te, Th, Tl, U, V, W, Y, Zn, Zr, La, Ce, Pr, Nd, Sm, Eu, Gd, Tb, Dy, Ho, Er, Tm, Yb, Lu. Some elements were not determined because of analytical difficulties requiring hydride generation, volatility of the elements, unresolved isotopic interferences (e.g., Ge), or the requirement for single-element methods (e.g., Re, Os, platinum-group elements). Geochemical data for elements measured by both ICP-MS and INAA (i.e., Zn, Ag, Co, Ni, Mo, Sb, U, Th, Cr, Nb, Hf, Ta, Rb, Nd, Sm, Eu, Sc, Tb, and Yb) were generally in agreement (see below). Analyses by multiple techniques (ICP and INAA) are reported as average values in this study.

3.3 LA-ICP-MS

For a selection of samples retrieved from the GSC archive, we preformed LA-ICP-MS analyses on individual pyrite grains in polished grain mounts made from the mineral separates. We chose samples from three deposits: Bousquet #2-Dumagami, Quemont, and Kidd Creek (see Section 3.5 for a description of the detailed petrography). LA-ICP-MS was performed using a Photon Machines Analyte Excite 193 nm excimer laser coupled with an Agilent 7700x ICP-MS at the University of Ottawa Laser Ablation Laboratory. The instrument tuning was optimized to provide a maximum ion transmission and low polyatomic cluster production (e.g., ThO/

Th≤0.02%; CuAr/Cu < 0.0025%) employing a hot plasma. Sample ablation was performed under He carrier gas (1.05 L/min) with Ar transport gas (0.75 L/min) added after the ablation cell. Spot analyses were performed with 30 s ablation at a laser repetition rate of 5 Hz, and a spot size of 42 um. Smaller pyrite grains from the Quemont sample were ablated with a spot size of 32 um. All analyzed spots were free of visible microinclusions at the surface (limit of visual detection ~1 μm), and the sites were visually checked post-ablation to confirm accurate placement of the laser (Fig. 3.11, 3.12). Select isotopes were monitored for potential contamination from inclusions of silicate gangue and other sulfide minerals. Fe was used as an internal standard, and GSE-1G (reference material standard from the US Geological Survey) was used for calibration of most elements. Exceptions were ^{125}Te and ^{202}Hg, for which there are no certified values in GSE-1G. For those elements, MASS1 (reference material standard from the US Geological Survey) was used for calibration. GSE does not contain any S, so a stoichiometric pyrite composition was used for the Fe and S, confirmed by EPMA analysis. GSE-1G was used for element calibration; MASS1 was used for accuracy checks. Data reduction and quantification of element concentrations was carried out using LADR v1.1.06 software. Detection limits were calculated using the standard deviation of the gas blank, the sensitivity to the mass, and the number of time slices investigated in the analysis (LADR).

In each analytical run the relationship of decreasing ^{57}Fe and ^{34}S with increasing ^{31}P was monitored (Fig. 3.13) as an indication for ablation of epoxy surrounding the pyrite grains. The increase in ^{31}P signal is caused by isobaric interference from C, O and H, probably from C released by the epoxy. 5 analyses of pyrite grains (from Quemont - 63RF48PY) were discarded due to mixed pyrite and epoxy ablation.

The following isotopes were determined to compare with the solution ICP-MS analyses: ^{65}Cu, ^{66}Zn, ^{208}Pb, ^{107}Ag, ^{197}Au, ^{209}Bi, ^{59}Co, ^{60}Ni, ^{77}Se, ^{125}Te, ^{111}Cd, ^{115}In, ^{71}Ga, ^{118}Sn, ^{182}W, ^{95}Mo, ^{51}V, ^{75}As, ^{121}Sb, ^{202}Hg, ^{205}Tl, ^{238}U, ^{232}Th, ^{53}Cr, ^{139}La, ^{140}Ce, ^{141}Pr, ^{146}Nd, ^{147}Sm, ^{153}Eu, ^{157}Gd, ^{159}Tb, ^{163}Dy, ^{165}Ho, ^{166}Er, ^{169}Tm, ^{172}, Yb, ^{175}Lu, ^{43}Ca, ^{57}Fe, ^{55}Mn, ^{31}P, ^{29}Si, ^{47}Ti, ^{34}S. We analyzed 145 pyrite grains in 5 samples of the mineral separates.

3.4 Quality assurance and control

Quality assurance for the original database was assessed by comparison of INAA and ICP-OES or ICP-MS for elements analyzed by more than one method on duplicates and splits. Of the 2662 separate analyses, 442 were by INAA only on duplicate samples or splits of samples also analyzed by ICP. Figure 3.2 shows analyses of duplicate samples that were analyzed by more than one method showing good agreement between methods. Up to 5% of the analyses for each element are below detection except for some elements such as Hg that has 15% of analyses below detection. Every step was taken in the preparation of the samples to ensure minimal contamination of mineral separates, e.g., including multiple cleaning of samples by Frantz magnetic separator (Jonasson et al., 2020). Below we assess the quality of the separates by calculation of the modal mineralogy of the samples. The number of pyrite samples analyzed from each deposit ranges from n=1 to n=16 with an average of n=5. There is generally a good balance of samples between the deposits, but some bias may be introduced in the statistical analysis by deposits or districts with fewer samples. Below, we assess the variability in trace element data for deposits with the most samples (n=>10) to determine the representativity of the original sampling. Data for certain elements, such as Cr, have been excluded owing to the probability of contamination of the samples during crushing and grinding in steel mills (Jonasson et al., 2020). We monitored specific elements vulnerable to contamination by grinding in chrome steel (Mn), high-carbon steel (Fe, Zn, Mn, Cu, Ni) or tungsten carbide (Co, Nb, W: e.g., Hickson and Juras, 1986).

For this study, all analyses were adjusted to the same measurement units (ppm for trace elements and weight percent for major elements). Values below detection limit were replaced with values equal to one-half the reported detection limit (DL). This simple substitution method is commonly used if the total number of analyses below detection limit do not exceed 25% of the results (e.g., Helsel, 1990; Davis, 2002). Approximately 30% of pyrite samples are missing analyses for some elements (in particular W, V, Hg, Ni, and Te). Most samples were not analyzed for major oxides or non-metals (SiO_2, CaO, MgO, TiO_2, Na_2O, P_2O_5, MnO, and K_2O: Table A.4). The available

data for these elements are considered separately below, but they are not included in the machine learning.

Before any statistical treatment of the data, we identified outliers for each element using log-probability plots (e.g., Reimann, 2002). The approximation to a normal distribution for each element was assessed by plotting element concentrations versus the z-score (standard deviations from the mean of a normal distribution: e.g., Williams, 1967). The trace element data for pyrite are right-skewed, due to the presence of high value outliers, and commonly approach a log-normal distribution that is typical for geochemical data (e.g., Crow and Shimizu, 1987; Rollinson, 1993). Outliers for elements such as Cu, Zn, Pb, Ag, Te, As, Hg, and U plot significantly off the normal distribution curve and were removed from the data prior to analysis. Some anomalous samples are most likely a result of sample preparation (e.g., resulting from the inability to cleanly separate multiple mineral phases). Elements with only a few analyses (e.g., n= 87 for Hg, n=34 for V, n= 17 for W) are excluded as variables in our machine learning.

3.5 Calculation of modal mineralogy

We calculated the modal mineralogy of each sample to determine the quality of the mineral separates (Fig. 3.3). We first calculated the amount of chalcopyrite, sphalerite, and galena that might be present by assuming that all Cu is in chalcopyrite ($CuFeS_2$), all Zn is in sphalerite (ZnS), and all Pb is in galena (PbS). From published LA-ICP-MS studies of pyrite (Cook, 1996; Large et al., 2009; Maslennikov et al., 2009), we expect very low concentrations of Cu, Zn and Pb in solid solution (<150 ppm, ~30 ppm, and none, respectively), and therefore any amount of Cu, Zn, and Pb in the pyrite samples is assumed to be present as discrete mineral inclusions. Modal abundances of chalcopyrite, sphalerite and galena in the samples are <8 wt% (mean of 0.9 wt%), <35 wt% (mean of 1.9 wt%), and <8 wt% (mean of 0.2 wt%), respectively. Outliers are considered to be those samples within the bottom or top 5% (2 wt% chalcopyrite, 7 wt% sphalerite, and 2 wt% galena) and these samples were rejected from further statistical analyses. The pyrite content was calculated from the amount of Fe in each sample after subtracting the amount of Fe in chalcopyrite. In the first instance, we assumed that all Fe remaining is in pyrite,

which yielded modal abundances from 38–146 wt % (mean of 82 wt%: Fig. 3.4.a). Eight samples in the database had a calculated pyrite content over 100%, most likely due to Fe-rich sphalerite that was not included in the calculation, or alternatively indicating the presence of pyrrhotite or magnetite in the samples. Given the measured Fe contents of the samples, after removal of chalcopyrite, the maximum amount of pyrrhotite is less than 20% (Fig. 3.4.b), indicating that the separates are generally clean in terms of pyrite-pyrrhotite mixtures.

We confirmed the modal mineral by inspecting a number of samples to document the quality of the mineral separations. Polished grain mounts of 5 representative samples were prepared at the University of Ottawa from pyrite mineral separates from Bousquet #2 (BSQT2-92.7L.A FE-PY and BSQT2-92.7L.B FE-PY), Dumagami (63RF299 PY), Quemont (63RF48), and Kidd Creek (2600L KIDD 07 PY). Petrographic description and mineral identification by reflected light microscopy are provided in Table A.3.a. We also performed scanning electron microscopy (SEM) with a JSM-6610 instrument equipped with an energy-dispersive X-ray spectroscopy (EDS) detector to identify trace minerals in the sample grain mounts after applying a carbon coating.

Each mount contains approximately 150–600 pyrite grains that are angular to sub-rounded and mostly fine–very fine-grained (~0.08–0.13 mm). Sample BSQT2-92.7L.A FE-PY contains pyrite grains with minor to trace amounts of sphalerite and galena as inclusions and free grains (<0.1 % by area) (Fig. 3.5.a,b; Fig. 3.6.a) in agreement with the high calculated pyrite content of 98 wt.% and a low modal abundances of other sulfides (<0.1 wt.%). Sample BSQT2-92.7L.B FE-PY contains approximately 1 wt.% of other sulfide minerals including chalcopyrite, sphalerite, and galena (Fig. 3.5c; Fig. 3.6.b). The Dumagami sample (63RF299 PY) is very clean, with only minor amounts of other sulfides (2 wt.% chalcopyrite, <0.1 wt% sphalerite and galena) among the pyrite grains or as inclusions (Fig. 3.5.d). Only one non-sulfide grain (barite, <10 μm) was detected by SEM (Fig. 3.6.c). The high Au concentration (10 ppm) in the Dumagami sample indicates electrum/free gold may be present, but none were observed in the grain mount by SEM. The Quemont sample (63RF48) contains pyrite grains with minor amounts of chalcopyrite and sphalerite as microinclusions (<1 area%) (Fig. 3.5.e). The high concentrations of Au (7 ppm) and

Te (170 ppm) in the Quemont sample reflects the likely presence of Au-tellurides inclusions, however, only inclusions of Pb-Ag telluride and selenide minerals were indicated by the EDS (<0.1 area %, <5 μm in size) (Fig. 3.6.d). The Pb-Ag-Se phases identified in the Quemont sample correspond with the high concentrations of these elements in the bulk ICP analyses of the sample (870 ppm Pb, 191 ppm Ag, 500 ppm Se). The Kidd Creek sample (2600L KIDD 07 PY) is also very clean, with only minor sphalerite (<1 area%; Fig. 3.5.f) and trace inclusions of non-sulfide minerals (cassiterite and xenotime; Fig. 3.6.e,f). In other samples, visual estimates of the amount of major mineral inclusions (chalcopyrite, sphalerite, galena) closely match the calculated modal abundances (e.g., 10% chalcopyrite, 20% sphalerite, and 5% galena, corresponding to measured concentrations of approximately 3.5 wt.% Cu, 14 wt.% Zn, and 4.5 wt.% Pb in the least pure separate, BSQT2-92.7L.B FE-PY; Fig. 3.5.b,c).

We also compared the trace element concentrations measured in the bulk samples with the observed abundance of inclusions. For example, we were able to calculate the abundance of telluride inclusions by assuming that all of the Te in the samples is present in a particular telluride phase such as calaverite, petzite, hessite, or tellurobismuthite, which are reported in the Bousquet #2-Dumagami and Quemont deposits (Table A.1). By assuming different minerals are responsible for the observed trace element concentrations in the bulk samples we performed simple mineralogical balances to apportion absolute amounts of the trace elements to different minerals. Examples of mineralogical balances and trace element accounting for the different samples are shown in Table A.3.b. For example, if we assume that all Au is present only as calaverite or free gold (or electrum) and all Te is present only as calaverite, we can calculate the proportion of the total Au that must be present in calaverite by assuming a fixed Au:Te ratio and then how much Au is left as free gold or electrum. Likewise for Ag, the total Ag concentration in the Dumagami sample (60 ppm) cannot be explained by the amount of Te as the Ag-tellurides hessite or petzite, indicating some Ag would have to be in other Ag-bearing minerals (i.e., galena or sulfosalts).

We estimate that contamination by non-sulfide minerals is unlikely to have affected the trace metal contents of the bulk samples, except by dilution. The low major oxide contents analyzed in

most samples (CaO, MgO,Na_2O and K_2O: see Appendix B) confirms minimal contamination of the samples by silicates other than quartz. Few silicate minerals were observed in the grain mounts (Fig. 3.4). The major element analyses for the least pure separate (BSQT2-92.7L.B FE-PY) suggests a maximum of 3.5 wt% dilution by silica where quartz is present, a maximum of 2 wt% dilution by carbonates, 3.3 wt% dilution by sodic minerals like albite, and 4.6 wt% dilution by manganiferous minerals like chlorite, garnet, and Fe-rich carbonates, which was checked by inspection of the samples. The very low maximum concentration of K_2O (0.06 wt%) in all the samples suggests muscovite was not concentrated during sample processing. Importantly, none of the non-sulfide trace minerals are expected to contain trace metals with the exception of cassiterite. The presence of other trace minerals in the pyrite samples, such as zircon, rutile, monazite, and xenotime is evidenced by the correlation of HFSE and REE in the pyrite samples (see section 4.3).

3.6 Assessing sample representivity

We compared different sample types to test whether the trace element concentrations of pyrite from individual grab samples are necessarily representative of the trace element geochemistry of an entire deposit. The degree to which pyrite retains a record of trace element geochemistry of the larger hydrothermal system is well established (e.g., Loftus-Hills and Solomon, 1967; Auclair and Fouquet, 1987; Huston et al., 1995; Mills, 1995; Houghton et al., 2004); however, this varies between different deposits. We compared the trace element concentrations of pyrite from individual grab samples to monthly concentrates of pyrite in tailings samples from 4 different deposits in the database (Table 3.1, A.4). The tailings represent a large bulk sample of the mined material (10s of thousands of tonnes for a monthly concentrate) from the same deposits where the grab samples were taken. In almost all cases, the trace element concentrations of pyrite from the individual grab samples correspond closely to that of pyrite from the monthly concentrates, as observed elsewhere (references).

Data from the Horne deposit show the trace element contents of pyrite mineral separates from individual grab samples are remarkably close to that of pyrite concentrates from the bulk tailings

(within 10 to 100 ppm for most elements: Fig. 3.7.a, 3.8). This is particularly so for the trace elements that are thought to be mostly lattice-bound in pyrite, such as Co (mean of 122 ppm vs. 118 ppm in the pyrite from monthly concentrate from Horne) and Au (mean of 1.26 ppm vs. 2.21 ppm in the pyrite from monthly concentrate from Horne) (Fig. 3.7.a, Fig. 3.8). The differences are well within 2 standard deviations of the mean Co concentrations for the two sample types from Horne (Table 3.1). Average concentrations of trace elements like Cd (median 40 ppm vs. 58 ppm in the pyrite from monthly concentrate from Mobrun), which is likely present in mineral inclusions in pyrite (e.g., in sphalerite) are also remarkably similar in pyrite mineral separates from grab samples of the ore and pyrite concentrates made from tailings from the same deposit. Importantly, even where there are differences between the grab samples and the monthly concentrates (e.g., mean of 13 ppm In in pyrite from grab samples versus 16 ppm In in the monthly concentrate from Horne), both sample types are enriched compared to other deposits.

We also compared trace elements in chalcopyrite mineral separates made from grab samples to monthly composites of Cu concentrates (~85% chalcopyrite). Typical Cu concentrates can contain high amounts of trace metals such as Zn, Pb, Bi, Co, Cd, As, and Sb (Mular et al., 2002). The Ag, Bi, Co, Cd, In, Mo, and Hg content of chalcopyrite mineral separates made from ore samples of 10 different deposits is compared to monthly and daily composites of Cu concentrates from the mill. Data from the 10 deposits considered in this study (Table 3.1; Horne, Lac Dufault, Isle Dieu, Orchan, Mattagami Lake, Manitou Barvue, Joutel, Poirier, Normetal, Geco) show the trace element contents of chalcopyrite from individual grab samples agree to within 10 to 100 ppm (10 % margin of error) for most elements with the concentrations in the Cu concentrates. The closest agreement is for Cu-associated elements that are mostly lattice-bound in chalcopyrite, such as In (mean of 39 ppm in chalcopyrite mineral separates from Lac Dufault vs. 42 ppm in the monthly concentrates) (Fig. 3.5). The differences are well within 2 standard deviations of the range of Ag, Bi, Co, Cd, In, Mo, and Hg concentrations in the different deposits (Table 3.1). Figure 3.9 shows the Co and Ag concentrations of chalcopyrite mineral separates versus Cu concentrates from 11 VMS deposits across Canada. The concentrations of different trace elements in chalcopyrite mineral separates from grab samples closely match those of the Cu concentrates over a wide range from 10s to 100s of ppm in the different deposits. The ranges of

concentations for different elements are clearly different from one deposit to the next, and this is well recorded in the chalcopyrite mineral separates.

We also compared trace elements in sphalerite mineral separates from grab samples of the ore with monthly composites of Zn concentrates from the same deposits (>90% sphalerite). Data from 6 deposits considered in this study (Kidd Creek, Lac Dufault, Isle Dieu, Mattagami Lake, Manitou Barvue, Normetal) show the trace element contents of sphalerite from individual grab samples are close to that of the mine concentrates (within 10 to 100 ppm for most elements), in particular for Zn-associated elements that are mostly lattice-bound in sphalerite, such as Ga (mean of 17 ppm in sphalerite mineral separates from Isle Dieu vs. 18 ppm in the monthly concentrates) (Table 3.1). The differences are well within 2 standard deviations of the range of Au, Se, Cd, Ga, Sb, and Hg concentrations in the different deposits (Table 3.1), and the ranges are clearly different from one deposit to the next. Figure 3.7.b shows the Cd content of sphalerite mineral separates from grab samples and in monthly composites of Zn concentrates from the same deposits. The close agreement spanning several orders of magnitude of Cd concentrations in the mineral separates and mine concentrates gives us confidence that the signatures of mineral separates from individual ore samples can provide a good first-order geochemical fingerprint of large tonnages of ore and perhaps an entire deposit, at least for certain lattice-bound elements.

3.7 Trace element abundances in volcanic rocks

To gain an understanding of the range of trace elements in the volcanic host rocks of the Superior Province and the AGB, we examined modern high-precision geochemical data of mafic and felsic volcanic rocks of the Superior Province (Fig. 3.14, 3.15) compiled from open-file reports of the Ontario Geological Survey and the Geological Survey of Canada (Hillary and Grunsky, 2010; Berger, 2012; Lodge and Chartrand, 2013; Ratcliffe, 2017; Gemmell and MacDonald, 2018; Gemmell and Szumylo, 2020; Hastie and Magnus, 2021; Magnus, 2021; Vice and MacDonald; 2021; Mole et al., 2021) plus an extensive compilation from Ministère des Ressources naturelles du Québec (MERN) online dataset (SIGEOM). The combined database

was sorted according to assemblage type in the AGB, and a rigorous QA/QC was performed by Fassbender et al. (2023) to eliminate any altered samples (see Appendix C).

Together, the data include analyses of 8565 samples of volcanic rocks from the AGB, the Swayze Greenstone Belt, and the Wawa, Wabigoon, Uchi, and Sachigo subprovinces (Fig. 3.14). The database includes samples analyzed for the full range of trace elements (Ag, As, Au, Ba, Be, Bi, Cd, Co, Cr, Cs, Cu, Ga, Hf, Hg, In, Mo, Nb, Ni, Pb, Rb, Sb, Sc, Se, Sn, Sr, Ta, Te, Th, Tl, U, V, W, Y, Zn, Zr, La, Ce, Pr, Nd, Sm, Eu, Gd, Tb, Dy, Ho, Er, Tm, Yb, Lu) and major elements (Fe_2O_3, SiO_2, CaO, MgO, TiO_2, Na_2O, P_2O_5, MnO, and K_2O). The samples were analyzed at different laboratories, including the GSC, the OGS Geo Labs, and several commercial labs, using primarily fusion and 4-acid dissolution followed by ICP-MS for trace elements and X-ray fluorescence spectrometry (XRF) for major elements. The results include analyses of basalt (n=5195), rhyolite (n=2828), and komatiites (n=542).

We removed 1176 samples that plotted outside the basalt and rhyolite fields of the Winchester and Floyd (1977) volcanic rock classification based on the Nb/Y vs. Zr/TiO_2 (Fig. A.1.a). Samples without major element analyses were also removed (n=121). The dataset was further filtered by removing altered samples and poor-quality analyses (Mole et al 2021). Samples identified as altered, highly metamorphosed, or near mineral occurrences/deposits from the source publication metadata were removed first. Hydrothermal alteration was then investigated using box plots of the Ishikawa alteration index (AI: Ishikawa et al., 1976) vs. chlorite-carbonate-pyrite index (CCPI and box plot: Large et al., 2001a) for mafic and felsic samples (Fig. A.1.b). Altered samples plotting outside of the least altered fields were removed (n= 2329). We also removed outliers with concentrations of trace metals corresponding to the top 5% of the data. The final dataset comprises 4322 unaltered mafic and felsic volcanic rock samples from the Superior Province.

3.8 Exploratory data analysis

We analyzed the trace element data of pyrite from 55 deposits using a variety of multivariate statistical tools. Compositional data of this type commonly exhibit closure effects that can lead to false correlations (Aitchison, 1982, 1984). This is particularly true for the major elements, but less of a problem for the trace elements. To 'open' the data so that it is normally distributed, and to remove any skewness, we performed a log-ratio transformation of the data prior to any analysis (Stanley, 2005). We used the centered log-ratio (CLR) transformation which takes the value of each element and divides it by the geometric mean of that element (Aitchison, 1982, 1984). Figure 3.10 shows the effects of the CLR transformation in a sample PCA (see below) for a subset of the pyrite data of samples VMS deposits from the AGB.

The log-transformed data were inspected by a correlation analysis. Pearson correlation coefficients were computed from each paired combination of the full suite of elements in the dataset and presented in a matrix to identify geochemical patterns. Pearson coefficients quantify the closeness to a linear relationship between variables, assuming that both variables are normally distributed (e.g., Rollinson, 1993). A lower confidence is given to the coefficients of element pairs with less data. Relationships between element pairs were also inspected in biplots, which are important for identifying outliers (e.g., strong correlations with Cu that might indicate chalcopyrite inclusions in the pyrite).

Further exploratory data analysis was carried out in the R statistical environment (R CoreTeam 2018). Plotting of results was performed in ioGAS and R. We performed principal components analysis (PCA) to identify underlying controls on the trace metal distributions. PCA is a descriptive tool that identifies linear combinations of variables (i.e., element concentrations) that account for the most variance in the data set. The identified linear combinations are represented by eigenvectors (with length or magnitude equal to 1) that are referred to as principal components (PC) (Davis, 2002; Jolliffe, 2005; Bartholomew, 2010). Eigenvalues (coefficients that correspond to the length or magnitude of the vector) represent the variance explained by each linear combination of elements or principal component. The contribution of an individual element to the total variance is described by its "loading" on the principal component. Missing data were filled using the log-ratio Expectation-Maximization algorithm (LREM)

(zCompositions package in R: Palarea-Albaladejo and Martin-Fernandez, 2015) prior to PCA. This method uses an iterative process to produce an estimate of the unknown values (22% of the dataset) by incorporating covariance information between elements (e.g., Dempster et al., 1977).

Most of the variance in all data sets is explained by the first few principal components. The first two principal components were examined in detail by plotting correlation vectors and loadings in PC1-PC2 space. Each sample point in PC1-PC2 space represents a linear combination of the loadings of Cu, Zn, Pb, Ag, Au, Bi, Co, Ni, Se, Te, Cd, In, Sn, Mo, As, Sb, and Tl for that sample on the principal components. The coordinates of the sample points projected onto the PC axes are referred to as scores.

The minimum sample size for PCA depends on the number of variables chosen for the analysis. A common practice is to aim for a sample size that is 5 times larger than the number of elements (Hatcher, 1994; Gorsuch, 1983; Comrey and Lee, 1992). In our study, PCA was performed using 17 trace metals (i.e., Cu, Zn, Pb, Ag, Au, Bi, Co, Ni, Se, Te, Cd, In, Sn, Mo, As, Sb, and Tl) from 265 pyrite samples in the CLR transformed dataset for the Superior Province deposits after removing samples above the chalcopyrite (2%), sphalerite (7%), and galena (2%) thresholds (see section 3.2, Fig. 3.2; section 4.2.1).

Some elements were also considered individually. For example, Hg was excluded from the first PCA analysis because of the limited Hg data for pyrite (n=86; ~30% missing data). However, because Hg is likely important for fingerprinting VMS deposits, a separate PCA analysis was performed just on the pyrite samples for which there are Hg analyses (n=77). The PCA was performed using the same 17 trace metals plus Hg (i.e., Cu, Zn, Pb, Ag, Au, Bi, Co, Ni, Se, Te, Cd, In, Sn, Mo, As, Sb, Tl, and Hg). The results are shown in the following chapters. PCA was also performed on 16 non-metal trace elements including the HFSE (U, Th, Zr, Nb, Hf), REE (La, Ce, Pr, Nd, Sm, Eu, Gd, Y, Dy, Yb), and Rb. These elements are not expected in the pyrite mineral structure, but they are common in other heavy minerals that were collected in the mineral separates and therefore may be useful indicators of the host rocks of the ore samples (e.g., Laflèche et al., 1992, 1998; Genna et al., 2014).

Finally, we performed cluster analysis to identify geochemically distinct groups of samples in the data set. We used unsupervised agglomerative hierarchal clustering (HC) on the first five principal components of the PCA, which account for 73% of the total variance of the data set. This method classifies different groups of sample points and maximizes the differences between the groups. We used the HCPC (Hierarchical Clustering on Principal Components) function as part of the 'FactoMineR' package in R (Husson et al., 2010), which combines three standard methods (PCA, HC, and the k-means algorithm) to determine the clusters. The analysis is unsupervised. In the first iteration, the number of clusters is determined by a hierarchal procedure that builds dendrograms (i.e., decision trees that identify the different clusters). HC first assumes individual samples form~~s~~ their own cluster, and then the distances from all other samples (statistical difference of samples points) are calculated; the samples that are closest to each other form the next level of clusters. Ward's criterion (i.e., the sum of the squared distances of sample points calculates the center of each cluster and the distance between clusters. The initial partitioning by HC is then passed through k-means clustering, which groups each sample to the nearest cluster (Hartigan and Wong, 1979). This clustering method requires a predetermined number of centroids or k-numbers, which are locations representing the centre of each cluster. The combined HC and k-means approach produces more reliable results because it uses the dendrogram to compute the right number of clusters (Husson et al., 2010).

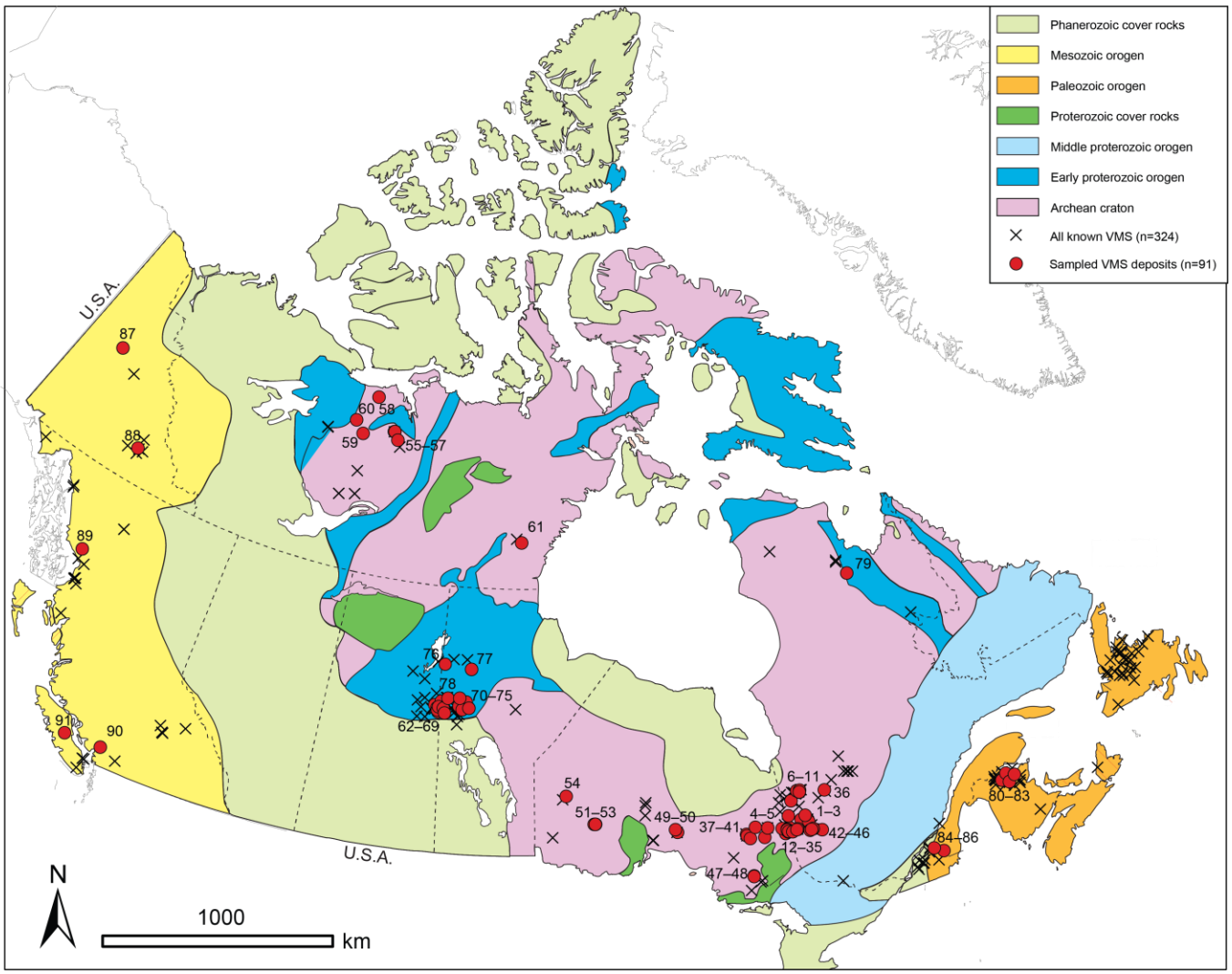

Figure 3.1 Simplified map of the major provinces and orogens of Canada, showing the locations of VMS from Franklin et al. (2015). Sampled VMS deposits with pyrite trace element analyses from Jonasson et al. (2020) are shown as red circles. Numbers correspond to the deposit numbers in Table A.1. Sampled VMS deposits include examples from all of the major VMS districts in the Superior (Abitibi and Western Superior) and Slave provinces, Churchill province (including the Trans-Hudson orogen), Appalachian orogen, and Canadian Cordillera (Northern Cordilleran orogen).

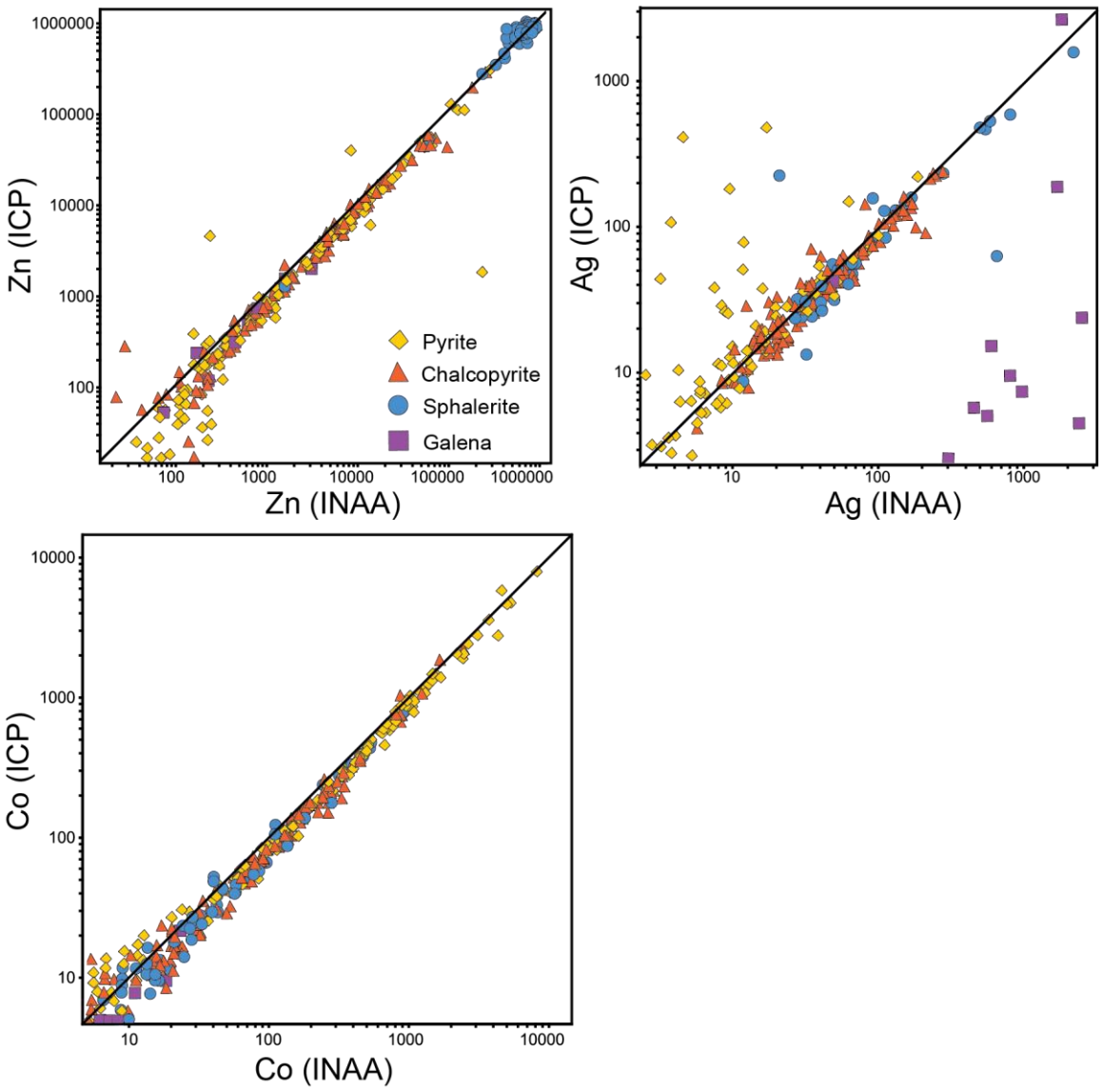

Figure 3.2 Binary plots of Zn, Ag, and Co concentration in mineral separate samples measured by both ICP and INAA. The majority of samples plot along the line y=x demonstrating a 1:1 linear relationship and the close agreement of concentrations measured by both ICP and INAA, Lattice-bound elements have higher analytical accuracy and precison than elements concentrated in inclusions as shown by Zn in sphalerite with a correlation coefficient of 0.99 and Co in pyrite with a coefficient of 0.98.

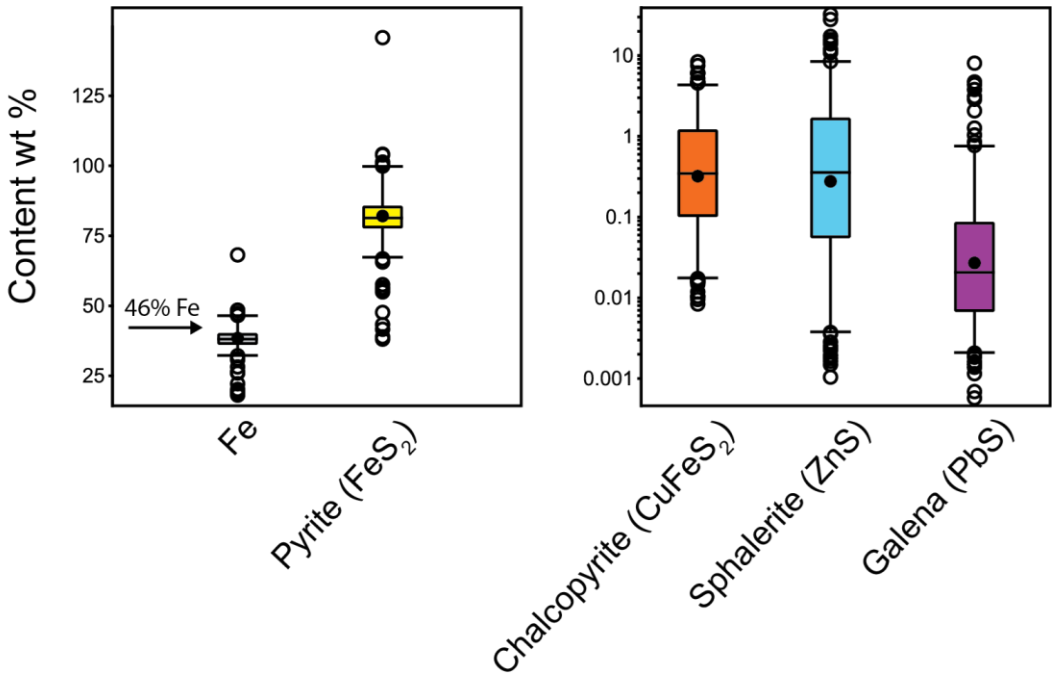

Figure 3.3 Boxplots of the calculated modal mineralogy of pyrite mineral separates from Jonasson et al. (2020). The plots show the relative abundance of major sulfide minerals in the samples. a) The calculated pyrite content of the analyzed mineral separates ranges from 38–146 wt. %, with a mean of 82 wt %). A pure pyrite sample should contain 46 wt.% Fe, indicated by the arrow. b) The calculated chalcopyrite, sphalerite, and galena contents of the samples are mostly <1 wt%). Outliers, corresponding to the top 5% of the data, were removed from the database prior to further analysis. The boxes enclose 50% of the data within the interquartile range (from Q1 to Q3). The average values (closed circle) and median (line) are shown. The lower and upper ends of the whiskers correspond to the 5th and 95th percentiles, respectively. Outliers (circles) are considered to be those samples within the bottom or top 5% (2 wt% chalcopyrite, 7 wt% sphalerite, and 2 wt% galena).

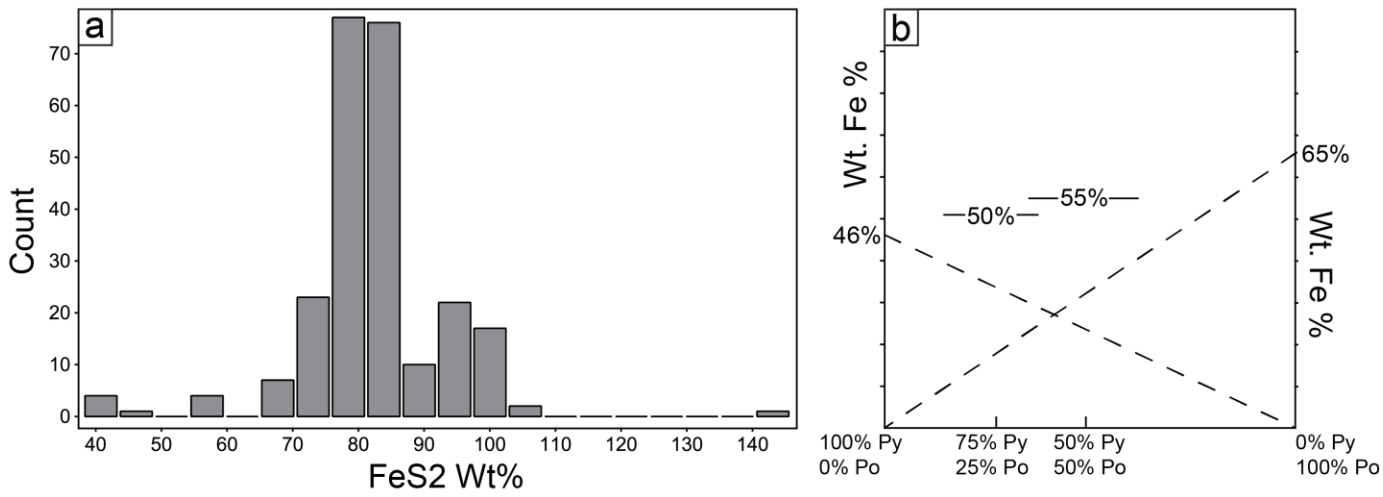

Figure 3.4 a) Histogram of calculated pyrite content of mineral separates from Jonasson et al. (2020), showing a roughly normal distribution suggesting little or no bias in the sampling or sample preparation. Pyrite contents less than 100% imply dilution by non-sulfide gangue minerals or mixtures of pyrite and other Fe-bearing minerals (e.g., pyrrhotite, magnetite, hematite). b) Possible Fe contents of different mixtures of pyrite (Py) and pyrrhotite (Po): 100% pyrite = 46 wt.% Fe; 100% pyrrhotite = 63 wt.% Fe. Any sample with more than 46 wt.% Fe (e.g., see Figure 3.2a) must include some Fe-rich pyrrhotite, assuming pyrrhotite is the only other Fe-bearing mineral in the sample. For example, The Fe content of a 50:50 mixture is: (1/2 x 46 wt.%) + (1/2 x 63 wt.%) = 55 wt.% Fe; and the Fe content of a 75:25 mixture is: (3/4 x 46 wt.%) + (1/4 x 63 wt.%) = 50 wt. % Fe.

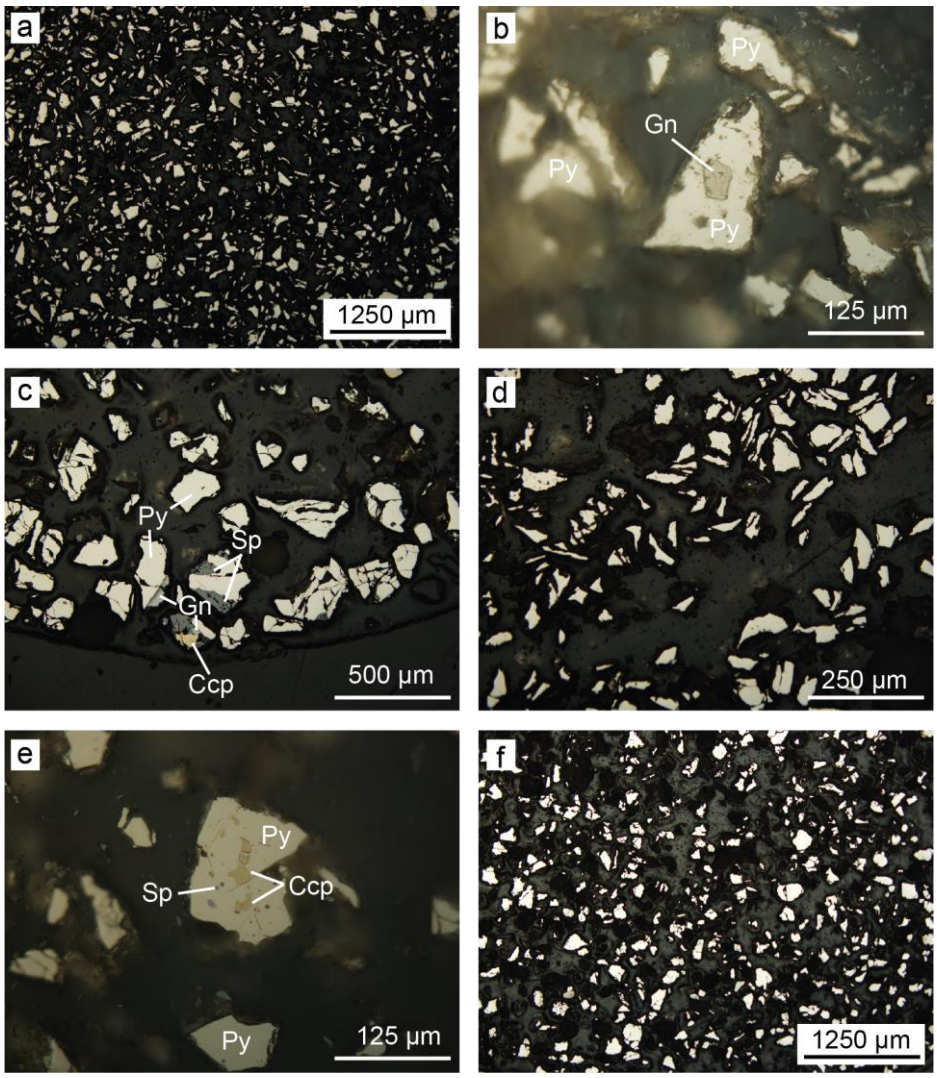

Figure 3.5 Photomicrographs in reflected plane polarized light of polished grain mounts for representative pyrite mineral separates in the database. The field of view (F.V.) in each photograph is given in parentheses. a) BSQT2-92.7L.A FE-PY (F.V. = 5 mm). b) BSQT2-92.7LA. FE-PY (F.V. = 0.5 mm). c) BSQT2-92.7LB. FE-PY (F.V. = 2 mm). d) 63RF299 PY Dumagami (F.V. = 1 mm). e) 63RF48 PY Quemont (F.V. = 0.5 mm). f) 2600L KIDD 07 PY (F.V. = 5 mm). The photomicrographs show little contamination by non-sulifdes. Only trace amounts of the other sulfide minerals (chalcopyrite, sphalerite, and galena) are observed and are well correlated with the bulk ICP-MS analytical results of the Cu, Zn and Pb. For example, based on the area % of chalcopyrite observed in the field of view in c), the calculated Cu content of the sample would be <1 wt.%, compared to 0.4 wt.% in the bulk chemical analysis of the sample.

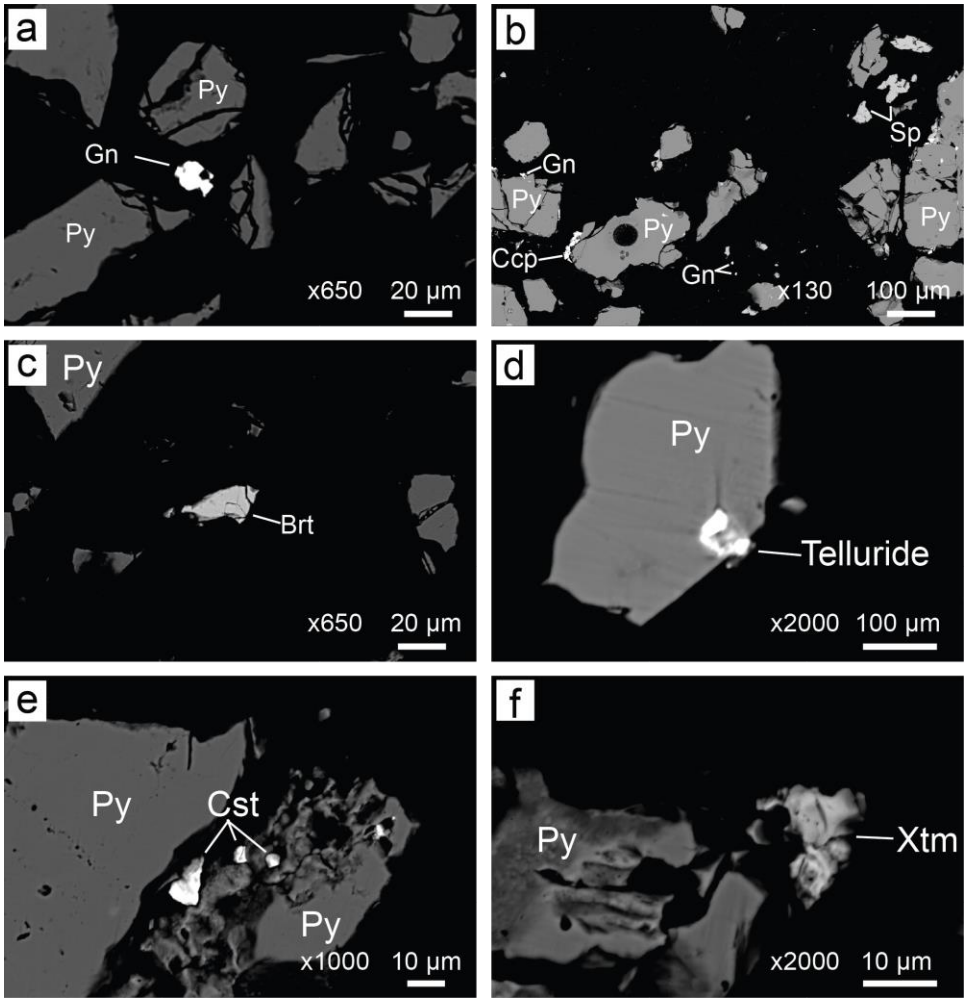

Figure 3.6 SEM backscatter electron images (20 kV) of carbon coated grain mounts for representative pyrite mineral separates in the database. A JSM-6610 SEM instrument was used. Trace mineral phases were identified by the major element peaks shown in spectra measured by the EDS detector equipped with the SEM. a) BSQT2-92.7L.A FE-PY showing a minor galena grain. b) BSQT2-92.7L.B FE-PY showing multiple grains/ inclusion of sphalerite, chalcopyrite, and galena within the pyrite separate. c) 63RF299 PY Dumagami showing a minor barite (Brt) grain; d) 63RF48 PY Quemont showing a trace Pb-Ag bearing telluride inclusion. e) 2600L KIDD 07 PY showing a trace cassiterite (Cst) inclusion. f) 2600L KIDD 07 PY showing a trace xenotime (Xtm) inclusion.

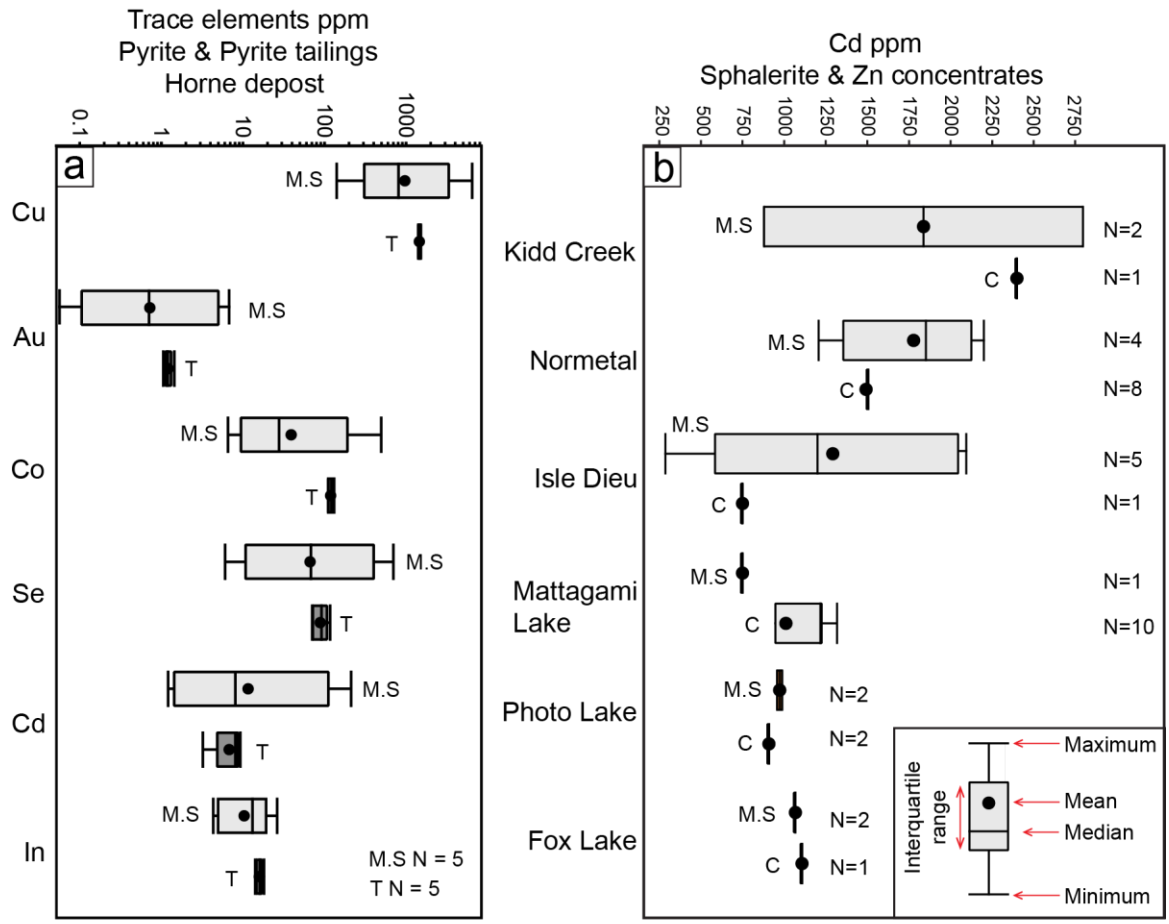

Figure 3.7 Boxplots of trace element concentrations in mineral separates from individual ore samples compared to "run of mine" daily and monthly concentrates from the same deposit. The data show the close correspondence of trace metal concentrations in individual ore samples and in the large tonnages represented by mill concentrates. a) Selected trace elements in pyrite mineral separates from individual ore samples compared to pyrite in run-of-mine tailings samples from the Horne deposit. b) Cd content of sphalerite mineral separates from individual ore samples compared to run-of-mine Zn concentrates from 6 different deposits. The boxes enclose 50% of the data within the interquartile range (from Q1 to Q3). The average values (closed circle) and median (line) are shown. The lower and upper ends of the whiskers correspond to the minimum and maximum values, respectively. Abbreviations: mineral separate samples (M.S), tailings samples (T), monthly concentrates (C), number of samples (N). The full dataset is available in Jonasson et al. (2020).

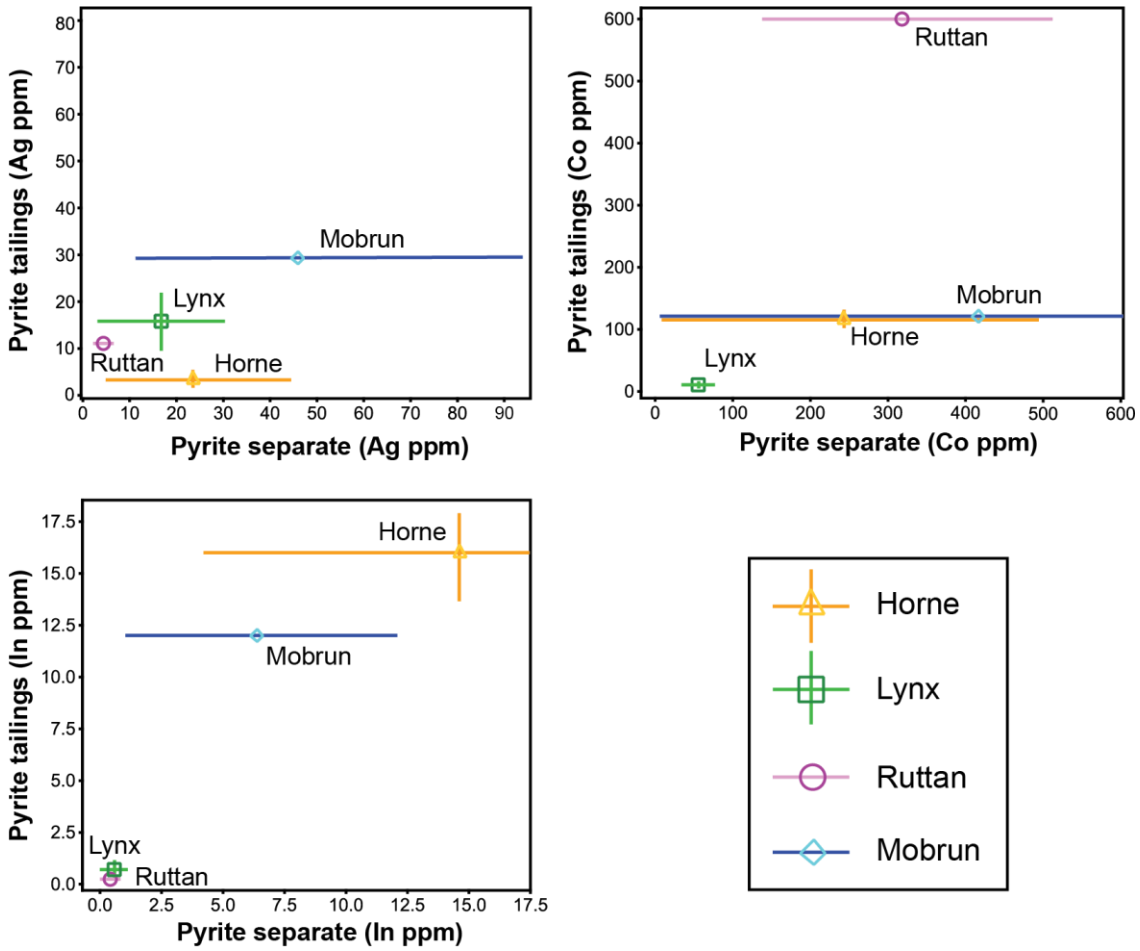

Figure 3.8 Binary plots of selected trace elements in pyrite mineral separates compared to pyrite in tailings from the same deposits. The concentration range of the samples from each deposit are indicated by lines crossing at the mean concentrations indicated by symbol. Groupings of deposits by districts are indicated by dashed circles. The full dataset is available in Jonasson et al. (2020). The trace element concentrations in the pyrite mineral separates have a larger range in concentrations than in pyrite tailings from the same deposits mainly because of the difference in the numbers of samples analyzed; but the mean concentrations are very similar.

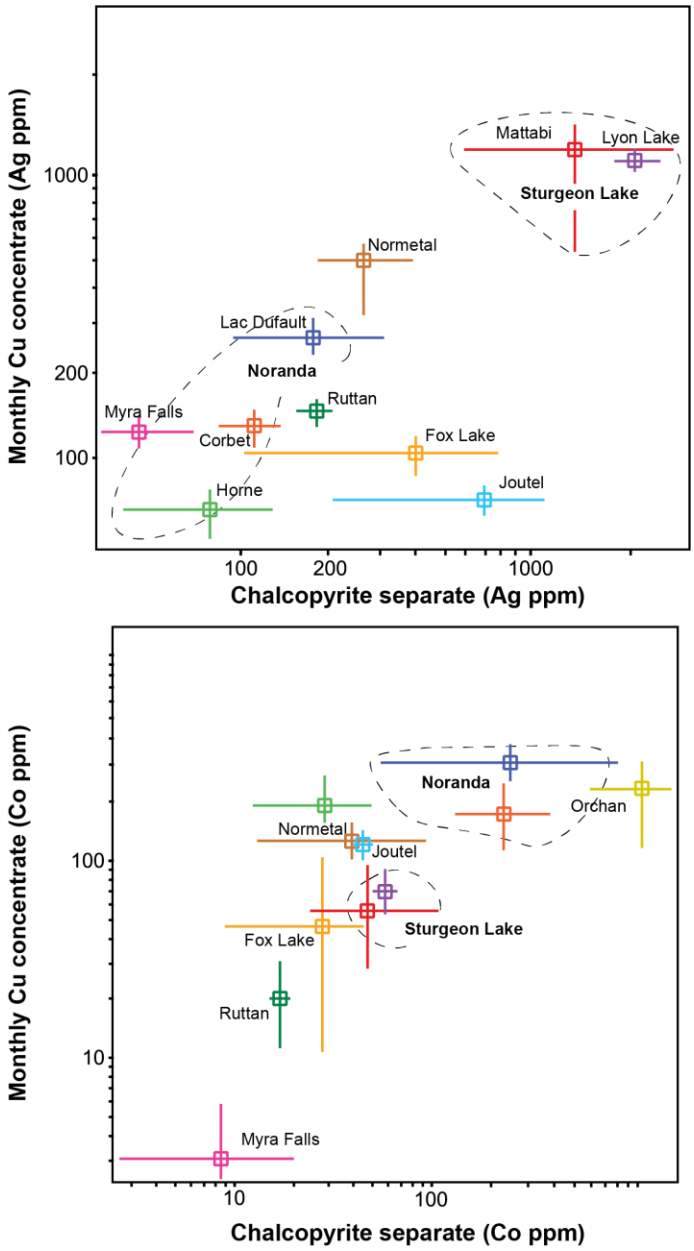

Figure 3.9 Binary plots of trace element concentrations (ppm) in chalcopyrite separates from individual ore samples of different deposits compared to run-of-mine daily and monthly bulk Cu concentrates from the same deposits. The concentration range of the samples from each deposit are indicated by lines crossing at the mean concentrations indicated by symbols. Groupings of deposits by districts are indicated by dashed circles. The full dataset is available in Jonasson et al. (2020). The Ag and Co concentrations of chalcopyrite in individual ore samples of most deposits closely approximate the bulk Ag and Co contents of the Cu-rich ores from large-tonnage concentrates.

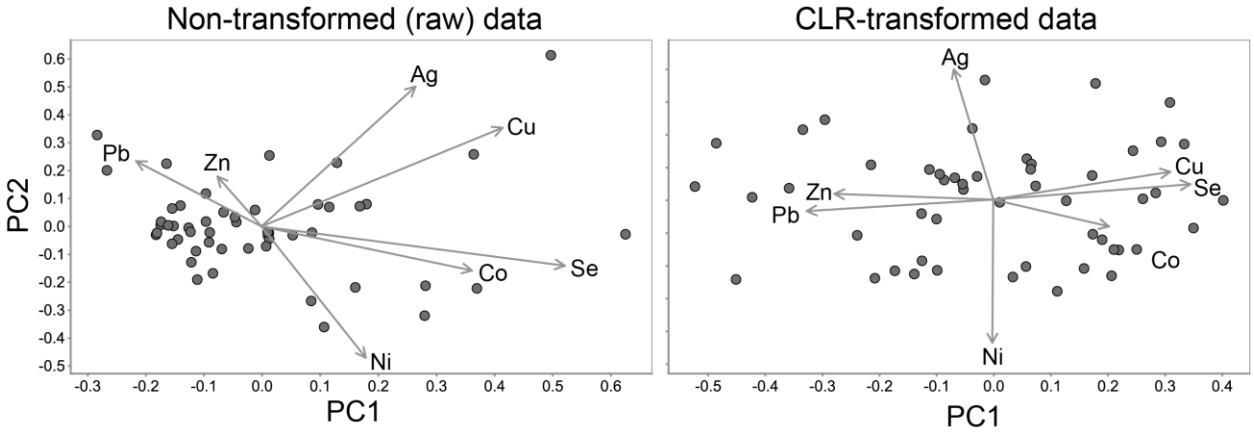

Figure 3.10 Example binary PC.1 vs. PC.2 plot with element loadings and sample scores for a subset of the pyrite data from VMS deposits in the AGB illustrating the effect of non-transformed and CLR-transformed data. Raw data (left plot) appears skewed after performing PCA, whereas the CLR transformation prior to PCA effectively normalizes (levels) the data and better distinguishes the element loadings and sample score relationships. The original dataset is available in Jonasson et al. (2020).

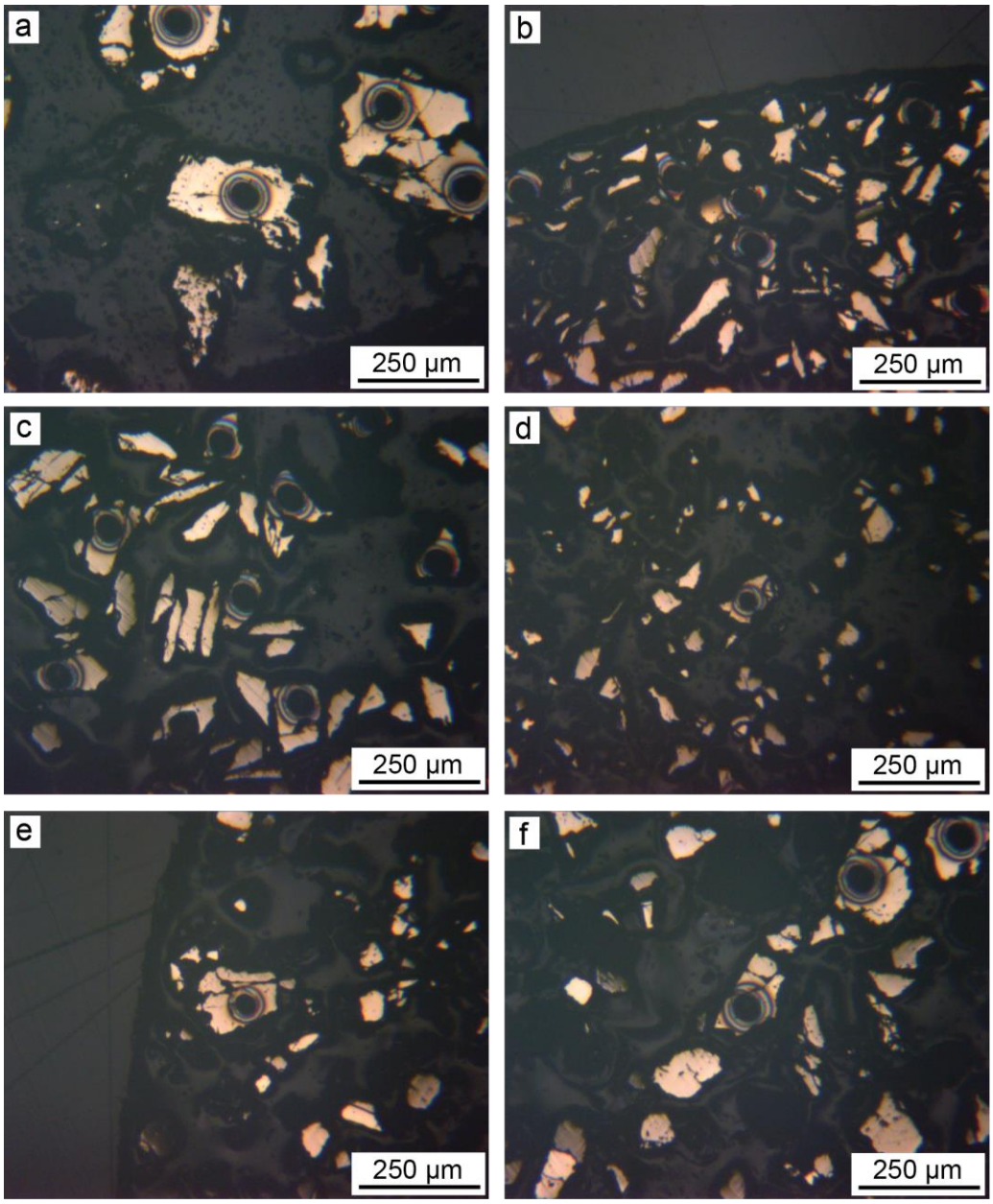

Figure 3.11 Reflected light photomicrographs of laser ablation spots in individual pyrite grains from the pyrite mineral separates analyzed in this study. a) Bousquet #2 (BSQT2-92.7L.A FE-PY); b) BSQT2-92.7L.B FE-P; c) Dumagami 63RF299 PY; d) and e) Quemont (63RF48 PY); f) Kidd Creek (2600L KIDD 07 PY). The ablation spot size was 42 um for most pyrite grains except for the Quemont sample shown in d) and e) that required a spot size of 32 um due to the smaller grains.

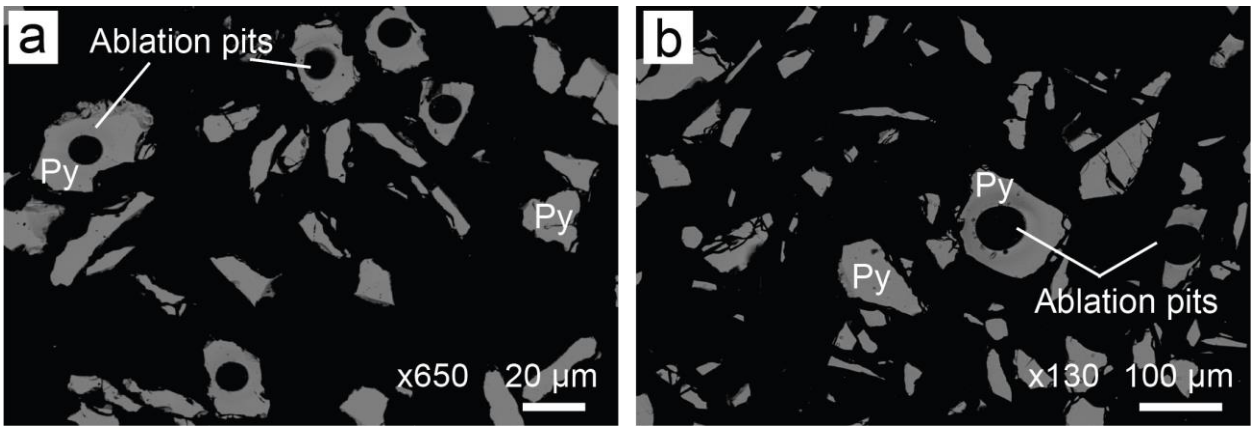

Figure 3.12 SEM backscatter electron images (20 kV) of laser ablation spots in individual pyrite grains from the pyrite mineral separates analyzed in this study. a) Bousquet #2 (BSQT2-92.7L.A FE-PY). b) 63RF299 PY Dumagami.

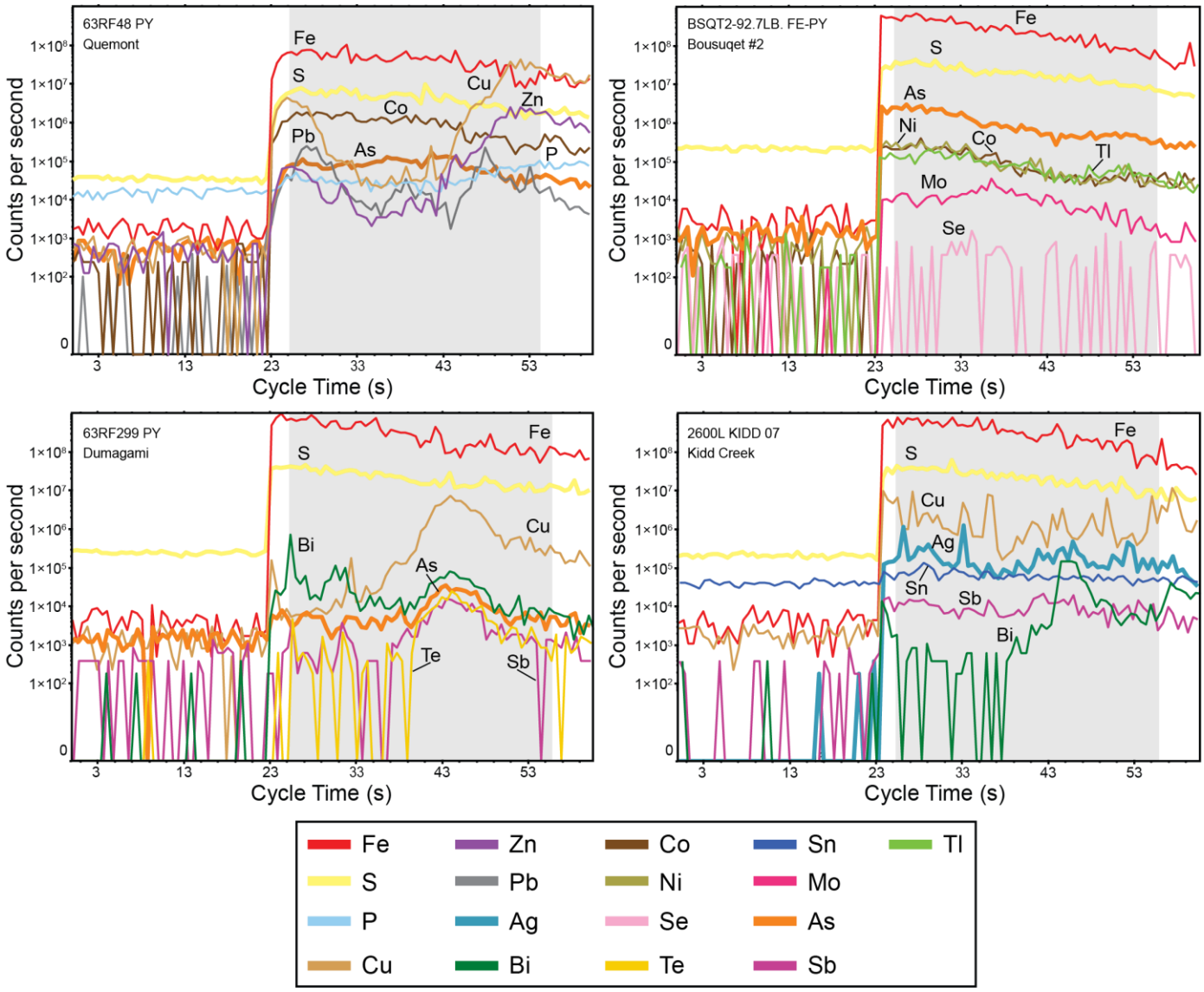

Figure 3.13 Examples of LA-ICP-MS depth profiles (time-resolved) for individual pyrite grains in pyrite mineral separate from three deposits (Bousquet #2-Dumagami, Quemont, and Kidd Creek). Smooth profiles were observed for Co, Ni, Se, Mo, As, and Tl, indicating they are lattice bound in pyrite, whereas irregular profiles with spikes for elements like Cu, Zn, Pb, Ag, Bi, Sb, and Tl likely represent microinclusions of minor and trace sulfide minerals in the pyrite grains. The grey background field in each profile outlines the portion of the LA ablation retained for analysis. In each analytical run the relationship of decreasing ^{57}Fe and ^{34}S with increasing ^{31}P was monitored as an indication of ablation of epoxy surrounding the pyrite grains (an example is shown in the profile for 63RF48PY).

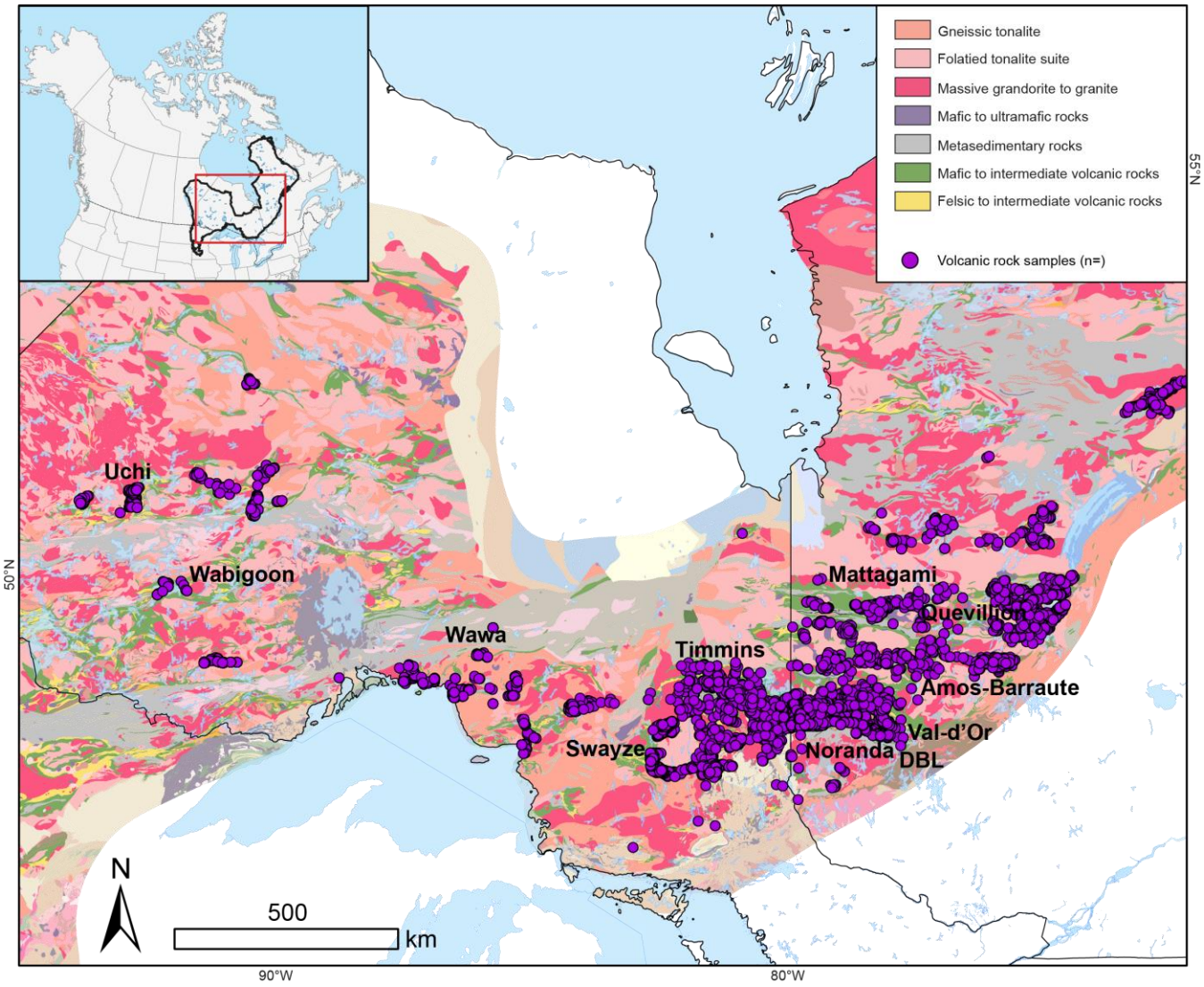

Figure 3.14 Simplified geological map of the southern Superior Province with subprovinces and greenstone belts (modified after Monstion et al., 2018) showing the locations of volcanic rock geochemical samples in the database used in this study.

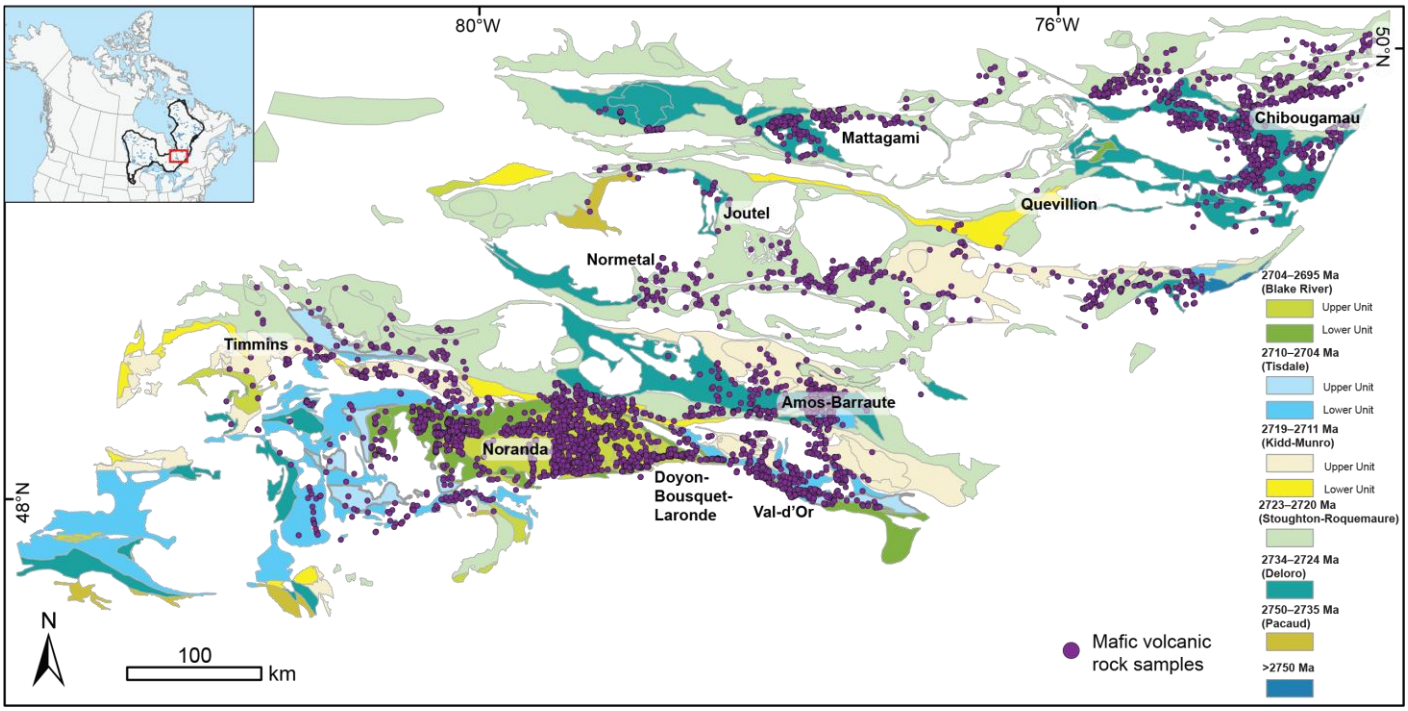

Figure 3.15 Simplified geological map of the major volcanic assemblages in the Abitibi greenstone belt (modified after Thurston et al., 2008) showing the distribution of mafic volcanic rock samples in the database (from Fassbender et al., 2023).

Table 3.1. Summary statistics of selected trace elements (ppm) in sphalerite and chalcopyrite mineral separates compared to monthly Cu/ Zn concentrates from each individual deposit. The original dataset and details of the samples are available in Jonasson et al. (2020).

Fox Lake	**Au**	**Se**	**Cd**	**Ga**	**Sb**	**Hg**	**Isle Dieu**	**Au**	**Se**	**Cd**	**Ga**	**Sb**	**Hg**
Sphalerite							**Sphalerite**						
No. Analyses	1	0	2	2	0	0	No. Analyses	3	1	5	5	5	1
Minimum	0.70	-	1100	23.0	-	-	Minimum	0.26	23.0	280	11.0	5.60	7
Maximum	0.70	-	1100	23.0	-	-	Maximum	0.41	23.0	2100	26.0	14	7
Mean	0.70	-	1100	23.0	-	-	Mean	0.34	23.0	1292	17.4	8.60	7
Standard Deviation	0	-	0	0	-	-	Standard Deviation	0	0	768	7.86	3.27	0
Zn concentrate							**Zn concentrate**						
No. Analyses	2	2	1	1	1	1	No. Analyses	2	1	1	1	2	1
Minimum	0.48	320	1100	19.0	20.0	170	Minimum	0.31	140	740	36.0	20.0	2
Maximum	0.84	323	1100	19.0	20.0	170	Maximum	0.48	140	740	36.0	36.0	2
Mean	0.66	321.5	1100	19.0	20.0	170	Mean	0.40	140	740	36.0	28.0	2
Standard Deviation	0	2.12	0	0	0	0	Standard Deviation	0	0	0	0	11.3	0

Kidd Creek	**Au**	**Se**	**Cd**	**Ga**	**Sb**	**Hg**	**Lac Dufault**	**Au**	**Se**	**Cd**	**Ga**	**Sb**	**Hg**
Sphalerite							**Sphalerite**						
No. Analyses	2	1	2	2	1	1	No. Analyses	3	3	0	0	3	1
Minimum	0.05	24.0	870	20.0	340	23.0	Minimum	0.60	94.0	-	-	3.50	10.0
Maximum	1.31	24.0	2800	49.0	340	23.0	Maximum	1.00	150	-	-	6.80	10.0
Mean	0.68	24.0	1835	34.5	340	23.0	Mean	0.78	114	-	-	5.20	10.0
Standard Deviation	0.89	0	1365	20.5	0	0	Standard Deviation	0.20	31.2	-	-	1.65	0
Zn concentrate							**Zn concentrate**						
No. Analyses	1	1	1	1	1	1	No. Analyses	5	5	5	5	2	2
Minimum	0.03	195	2400	10.0	34.0	1	Minimum	0.18	63.0	1200	15.0	3.4	18.0
Maximum	0.03	195	2400	10.0	34.0	1	Maximum	0.38	132	1300	22.0	4.6	30.0
Mean	0.03	195	2400	10.0	34.0	1	Mean	0.30	96.8	1220	17.6	4	24.0
Standard Deviation	0	0	0	0	0	0	Standard Deviation	0.07	26.8	44.7	2.70	0.85	8.49

Table 3.1 cont.

Manitou Barvue	Au	Se	Cd	Ga	Sb	Hg
Sphalerite						
No. Analyses	3	1	1	1	4	3
Minimum	0.06	9.00	3200	6.00	9.2	140
Maximum	0.27	9.00	3200	6.00	33.0	250
Mean	0.18	9.00	3200	6.00	23.6	210
Standard Deviation	0	0	0	0	10.4	60.8
Zn concentrate						
No. Analyses	6	6	5	5	3	3
Minimum	0.24	17.0	1700	3.80	120	140
Maximum	0.51	55.0	1700	5.11	220	140
Mean	0.41	29.0	1700	4.40	187	140
Standard Deviation	0	13.4	0	0.58	57.7	0

Mattagami Lake	Au	Se	Cd	Ga	Sb	Hg
Sphalerite						
No. Analyses	3	1	1	1	3	3
Minimum	0.14	870	780	31.0	5.1	3.00
Maximum	0.51	870	780	31.0	83.0	44.0
Mean	0.33	870	780	31.0	35.7	18.7
Standard Deviation	0.18	0	0	0	41.5	22.1
Zn concentrate						
No. Analyses	5	10	10	10	5	4
Minimum	0.54	152	84.0	8.8	11.0	8.00
Maximum	6.16	389	1300	31.0	137	11.0
Mean	2.84	236	991	22.68	55.8	9.75
Standard Deviation	2.91	86.0	472	7.18	61.7	1.26

Normetal	Au	Se	Cd	Ga	Sb	Hg
Sphalerite						
No. Analyses	4	3	4	4	3	4
Minimum	0.42	25.0	1200	6.00	4.50	9.00
Maximum	3.22	46.0	2200	23.0	240	71.0
Mean	1.49	34.7	1775	11.9	83.5	26.0
Standard Deviation	1.22	10.6	419	7.60	136	30.0
Zn concentrate						
No. Analyses	11	11	8	8	6	4
Minimum	0.21	34.0	1400	7.20	11.0	10.0
Maximum	0.44	51.0	1500	8.50	17.0	32.0
Mean	0.36	45.3	1488	7.70	14.3	21.0
Standard Deviation	0	5.68	35	0	2.73	12.7

Photo Lake	Au	Se	Cd	Ga	Sb	Hg
Sphalerite						
No. Analyses	2	4	2	2	4	4
Minimum	0.27	82.0	990	24.0	3.80	110
Maximum	0.31	190	1020	27.0	14.0	220
Mean	0.29	143	1005	25.5	8.40	168
Standard Deviation	0.03	55.5	21.2	2.12	5.37	60.8
Zn concentrate						
No. Analyses	2	2	2	2	2	2
Minimum	0.59	190	900	13.0	9.50	130
Maximum	0.78	230	900	17.0	10.0	150
Mean	0.68	210	900	15.0	9.75	140
Standard Deviation	0	28.3	0	2.83	0	14.1

Table 3.1 cont.

Geco	Ag	Bi	Co	Cd	In	Mo	Hg
Chalcopyrite							
No. Analyses	8	3	7	3	3	4	6
Minimum	175	6.80	2.00	39.0	58.0	1.00	2.00
Maximum	1160	680	85.0	550	400	310	10.0
Mean	422	239	24.1	240	209	83.0	5.67
Standard Deviation	328	382	30.0	273	174	152	3.39
Cu concentrate							
No. Analyses	1	1	0	1	1	1	0
Minimum	230	56.0	-	15.0	100	1.60	-
Maximum	230	56.0	-	15.0	100	1.60	-
Mean	230	56.0	-	15.0	100	1.60	-
Standard Deviation	0	0	-	0	0	0	-

Horne	Ag	Bi	Co	Cd	In	Mo	Hg
Chalcopyrite							
No. Analyses	4	2	4	2	2	2	3
Minimum	11.0	1.1	10.0	5.2	92.0	0.2	4
Maximum	96.0	60.0	228	21.0	150	16.0	23.0
Mean	53.3	30.6	82.9	13.1	121	8.1	12.7
Standard Deviation	43.0	41.6	100	11.2	41.0	11.2	9.6
Cu concentrate							
No. Analyses	5	5	5	5	5	5	4
Minimum	46.5	8.6	162	6.5	29	3.00	2.00
Maximum	76.5	15.0	261	14.0	34.0	3.60	6.00
Mean	59.0	12.1	193	9.9	31.4	3.22	3.75
Standard Deviation	11.3	2.32	38.6	3.39	1.82	0.24	1.71

Isle Dieu	Ag	Bi	Co	Cd	In	Mo	Hg
Chalcopyrite							
No. Analyses	2	2	2	2	2	2	0
Minimum	170	26.0	51	42.0	83.0	0.20	-
Maximum	425	140	133	52.0	400	7.00	-
Mean	298	83.0	92.0	47.0	242	3.60	-
Standard Deviation	180	80.6	58.0	7.07	224	4.81	-
Cu concentrate							
No. Analyses	1	1	1	1	1	1	1
Minimum	2200	69.0	150	70.0	69.0	4.10	3.00
Maximum	2200	69.0	150	70.0	69.0	4.10	3.00
Mean	2200	69.0	150	70.0	69.0	4.10	3.00
Standard Deviation	0	0	0	0	0	0	0

Joutel	Ag	Bi	Co	Cd	In	Mo	Hg
Chalcopyrite							
No. Analyses	2	2	2	2	2	2	1
Minimum	192	7.50	52.0	7.30	35.0	1.30	4.00
Maximum	1100	19.0	54.0	53.0	130	1.90	4.00
Mean	646	13.3	53.0	30.2	82.5	1.60	4.00
Standard Deviation	642	8.13	1.41	32.3	67.2	0	0
Cu concentrate							
No. Analyses	4	4	4	4	4	4	4
Minimum	64.5	26.0	105	25.0	25.0	1.50	4.00
Maximum	79.5	33.0	135.5	35.0	31.0	2.40	6.00
Mean	70.9	28.0	120	27.8	27.0	1.80	5.25
Standard Deviation	6.34	3.37	12.7	4.86	2.83	0.41	0.96

Table 3.1 cont.

Lac Dufault	Ag	Bi	Co	Cd	In	Mo	Hg
Chalcopyrite							
No. Analyses	8	7	8	7	7	3	7
Minimum	89.0	4.2	30	6.2	17.0	0.20	1.00
Maximum	345	210	807	96.0	63.0	1.00	14.0
Mean	152	46.3	236	44.6	39.0	0.63	5.29
Standard Deviation	80.7	74.7	245	33.8	13.4	0	4.86
Cu concentrate							
No. Analyses	5	5	5	5	5	5	5
Minimum	207	110	263	130	33.0	4.50	11.0
Maximum	310	150	356	200	47.0	8.30	39.0
Mean	257	130	304	164	42.2	5.77	22.6
Standard Deviation	39.5	15.8	44.6	33.6	5.45	1.52	11.8

Manitou Barvue	Ag	Bi	Co	Cd	In	Mo	Hg
Chalcopyrite							
No. Analyses	1	1	1	1	1	1	1
Minimum	643	3.50	21.0	22.0	6.60	2.60	2.00
Maximum	643	3.50	21.0	22.0	6.60	2.60	2.00
Mean	643	3.50	21.0	22.0	6.60	2.60	2.00
Standard Deviation	0	0	0	0	0	0	0
Cu concentrate							
No. Analyses	4	4	4	4	4	4	4
Minimum	140	220	55.5	30.0	13.0	120	11.0
Maximum	160	290	85.0	54.0	16.0	225	15.0
Mean	147	253	70.3	43.3	14.8	164	13.3
Standard Deviation	8.6	33.0	16.5	10.1	1.26	45.7	2.06

Normetal	Ag	Bi	Co	Cd	In	Mo	Hg
Chalcopyrite							
No. Analyses	4	4	4	4	4	3	3
Minimum	175	2.50	5.00	77.0	8.2	0.30	3.00
Maximum	330	8.30	128	89.0	39.0	0.80	4.00
Mean	273	5.93	64.4	83.0	20.2	0.57	3.33
Standard Deviation	67.4	2.45	53.7	5.48	14.4	0	0.58
Cu concentrate							
No. Analyses	7	7	7	7	7	7	7
Minimum	318	72.0	97.5	120	15.0	3.20	4.00
Maximum	557	110	139.5	170	20.0	5.40	9.00
Mean	401	84	118	146	18.1	4.30	6.43
Standard Deviation	79.5	12.7	13.0	15.1	1.95	0.94	1.90

Orchan	Ag	Bi	Co	Cd	In	Mo	Hg
Chalcopyrite							
No. Analyses	1	1	2	1	1	1	2
Minimum	507	90.0	411.5	15.0	420	3.5	1.00
Maximum	507	90.0	1920	15.0	420	3.5	10.0
Mean	507	90.0	1166	15.0	420	3.5	5.50
Standard Deviation	0	0	1067	0	0	0	6.36
Cu concentrate							
No. Analyses	5	5	5	5	5	5	0
Minimum	200	35.0	120	81.0	130	2.90	-
Maximum	510	70.0	320	160	240	8.90	-
Mean	398	56.8	224	125	166	5.74	-
Standard Deviation	121	13.1	74.4	35.5	46.2	2.16	-

Table 3.1 cont.

Horne	Au	Co	Se	Cd	In
Pyrite					
No. Analyses	5	5	4	5	5
Minimum	0.06	6.50	6.00	1.20	4.30
Maximum	6.70	491.5	691	210	26.0
Mean	2.26	122	208	55.8	12.6
Standard Deviation	2.88	208	323	89.4	8.65
Pyrite tailings					
No. Analyses	5	5	5	5	5
Minimum	1.05	110	70.0	3.20	14.0
Maximum	1.43	130	116	9.20	18.0
Mean	1.21	118	89.4	7.14	15.8
Standard Deviation	0.14	8.37	18.8	2.31	1.48

Mobrun	Au	Co	Se	Cd	In
Pyrite					
No. Analyses	8	11	8	7	8
Minimum	0.25	8.50	9.00	0.60	0.81
Maximum	3.37	835	824	130	29.0
Mean	1.57	359	278	40.1	8.30
Standard Deviation	1.19	323	247	49.9	9.28
Pyrite tailings					
No. Analyses	0	1	0	1	1
Minimum	-	125	-	58.0	12.0
Maximum	-	125	-	58.0	12.0
Mean	-	125	-	58.0	12.0
Standard Deviation	-	0	-	0	0

Myra Falls (Lynx)	Au	Co	Se	Cd	In
Pyrite					
No. Analyses	0	3	0	3	3
Minimum	-	36.0	-	1.30	0.14
Maximum	-	76.0	-	2.10	0.99
Mean	-	50.0	-	1.63	0.59
Standard Deviation	-	22.5	-	0.42	0.43
Pyrite tailings					
No. Analyses	0	2	0	2	2
Minimum	-	7.00	-	49.0	0.57
Maximum	-	8.00	-	95.0	1.00
Mean	-	7.50	-	72.0	0.78
Standard Deviation	-	0.71	-	32.5	0.30

4. Results

4.1 Deposit characteristics

In this chapter, we focus on VMS deposits in the Superior Province. Three compositional groups are identified based on Cu/(Cu+Zn) ratios: low ratios (<20; n=22), medium (20–55; n=15), and high (>55; n=17) (Fig. 4.1.a; Table 4.1.a). Deposits are further classified by Au grade, with low (<0.6 g/t; n=14), medium (0.6–1.4 g/t: n=14), high (1.6–2.4 g/t; n=4), and very high grade deposits (>4 g/t: n=6) (Fig. 4.1.a; Table 4.1.b). The most gold-rich deposits in the database (i.e., Bousquet #2-Dumagami, Horne, and Quemont) have more than 31 t of contained Au at a grade of more than 3.46 g/t (geometric mean: Mercier-Langevin et al., 2011a). We also classified the deposits according to their total tonnage, recognizing that deposit size is a potential variable when interpreting trace element enrichments and depletions (e.g., Hannington et al., 1999c). The metal budgets of the deposits have been investigated and reviewed (Barrie and Hannington, 1999), but the trace element geochemistry in relation to VMS tonnage has not been previously explored. The size of deposits is classified as small (< 3 Mt; n=28), medium (3–8 Mt; n=12), and high (8–171 Mt; n=14) (Fig. 4.1.b and Table 4.1.c). The cut-offs for the Cu-Zn ratios, Au grades, and tonnages were selected to obtain roughly equal numbers of pyrite among the different classes of deposits.

A major undertaking was to refine the host-rock classifications within the bimodal-mafic group, which is dominant in the Abitibi Greenstone Belt, including more details of the immediate footwalls compared to the original classification of Barrie and Hannington (1999). The updated compilation of Mosier et al., (1983, 2009) was used to subdivide the bimodal-mafic deposits according to the stratigraphic thicknesses and proportions of felsic to mafic rocks in the immediate footwall sequence (<1000 m). These data distinguish three classes of deposits in the broader bimodal-mafic group: a mafic-dominant subgroup with <100 m of rhyolite or a mafic: felsic ratio of more than 3:1; an intermediate subgroup with 100–500 m of rhyolite or a mafic: ratio of ~1:1); a felsic-dominant subgroup with >500 m of rhyolite or a mafic: felsic ratio of less than 1:3 (Table A.1) This analysis shows that even within a single district (e.g., Noranda) the

general bimodal-mafic class of deposits can have highly variable footwall lithologies with rhyolite dominating the footwall of some deposits (e.g., Horne and Quemont) and others having little or no rhyolite in the footwall (e.g., many deposits in the Main camp: Gibson and Galley, 2007). We show that there is a statistically meaningful relationship between the Cu-Zn ratios, Au grades, and tonnages for the largest and most gold-rich deposits (Fig. 4.1.b) and the proportion of mafic to felsic volcanic rocks within the bimodal-mafic class, and this variation is also reflected in the trace element geochemistry of the ores.

4.2 Variations of trace elements in pyrite

4.2.1 Mean concentrations and log-probability plots

A wide range of trace element concentrations are found in the pyrite samples from Archean VMS deposits in the Superior Province (Table 4.2). Mean concentrations of different elements range from 0.1 to over 10000 ppm. The highest concentrations are for the base metals Zn (mean 12200 ppm, up to 233500 ppm), Cu (mean 3180 ppm, up to 29000 ppm), and Pb (mean 1750 ppm, up to 70000 ppm), which are commonly present in discrete microinclusions of sphalerite, chalcopyrite and galena (e.g., Fig. 3.5). These elements are often found at concentrations that are well above their expected solubilities in pyrite (<2000 ppm: Large et al., 2007). In contrast, many of the trace elements are present at concentrations that likely reflect solid-solution or ultrafine microinclusions of trace minerals that cannot be distinguished from lattice-bound elements (Table 4.3). The highest mean concentrations of trace metals in pyrite mineral separates from this study are in the range of 100–1000 ppm for Ag, Co, Ni, Se, Sn and As. Significant outliers (up to 6770 ppm Ag, 11500 ppm Co, 6690 ppm Se, 15000 ppm Sn, and 44000 ppm As) are found in <5% of the samples and likely represent inclusions of many different trace minerals (see section 4.3). Mean concentrations of Bi, Te, Cd, Mo, V, Sb, Hg, Ba, Zr, Sr and Ce in the pyrite samples are in the range of 10–100 ppm, also with significant outliers (up to 870 ppm Bi, 1600 ppm Te, 960 ppm Cd, 2560 ppm Sb, and 820 ppm Hg) in <5% of samples (Table 4.2). Mean concentrations of Au, In, Ga, Tl, and W in the pyrite samples are in the range of 1–10 ppm, with significant outliers (up to 116 ppm Au and 120 ppm In) in <3% of samples. U, Th,

Nb, Hf, and Sc (so-called HFSE) are also in the range of 1–10 ppm, with significant outliers (up to 1455 ppm U and 347 ppm Th) in <3% of samples, most likely representing trace heavy minerals selectively concentrated with the pyrite during sample preparation, such as zircon. The LREE (La, Ce, Pr, Nd, Sm, Eu) + Y are present in the pyrite samples in the range of 0.1–10 ppm with significant outliers (up to 350 ppm La, 580 ppm Ce, 270 ppm Nd, and 230 ppm Y) most likely representing heavy minerals such as monazite. Concentrations of the HREE (Gd, Tb, Dy, Ho, Er, Tm, Yb, and Lu) and elements such as Ta, Be, and Cs are lower (0.1–1 ppm, close to the element detection limits).

Average concentrations for some elements are within the expected range of solubilities in pyrite: up to 10000 ppm for Co, up to 5000 ppm for Ni, up to 1000 ppm for Se, and up to 20000 ppm for As (e.g., Large et al., 2007; Cook et al., 2009; Belousov et al., 2016). Other elements, even at very low concentrations, such as Sn (<100 ppm), are still likely hosted in discrete mineral inclusions (e.g., Cook, 1996; Large et al., 2007, 2009). Reich et al. (2005) showed that lattice-bound Au in pyrite (as opposed to Au in nanoparticles) co-varies with the As content and the Au/As molar ratios are predictable ($CAu = 0.02 \times CAs + 4 \times 10–5$), which was thought to define a saturation limit in pyrite. Some studies have suggested the solid solution of trace metals in pyrite is temperature dependent. In some deposits hydrothermal pyrite formed at very high temperatures hosts the majority of trace elements in solid solution, whereas low-temperature pyrite has a much higher proportion of inclusions (Grant et al., 2018). However, recrystallization at high temperatures (e.g., during zone refining or metamorphism) can result in significant redistribution of trace elements (Maslennikov et al., 2009, Conn et al., 2019).

In Figure 4.2, we show the log-probability plots for trace elements in the pyrite mineral separates from Jonasson et al. (2020). Changes in the distribution of trace elements in pyrite, indicated by significant gaps or changes in the slopes of the probability distributions, are interpreted to indicate changes in the deportment of the trace metals, e.g., between solid solution and microinclusions. Most elements show several different populations or irregular distributions, which can reflect multiple types of trace element incorporation into pyrite as solid solutions and

lattice substitutions, surface adsorption, and trace mineral inclusions (Slack et al., 2005; Maslennikov et al., 2009; Genna and Gaboury, 2015, Dehnavi et al., 2018).

4.2.2 Variations with bulk compositions, zoning and Au grades of deposits

Binary plots showing the relationship of trace elements in the pyrite samples with bulk Cu/(Cu+Zn) grade ratios and zoning of different mine camps of the sampled deposits are shown in Figures 4.4–4.20 and discussed in section 4.3.

The Cu and Zn concentrations in the pyrite mineral separates generally reflect the bulk Cu/(Cu+Zn) ratios of the deposits but show much greater variability than the metal ratios of the deposits as a whole (Fig. 4.3). Au, Bi, Co, Ni, Se, Te, In, and Mo are positively correlated with bulk Cu/(Cu+Zn) ratios of the deposits (Fig. 4.4.a and Table 4.4, 4.6). In contrast, Pb, Ag, Cd, In, Ga, Sn, As, Sb, Hg, and Tl are negatively correlated with Cu/(Cu+Zn) of the deposits (Fig. 4.4.b, 4.5.a and Table 4.4, 4.6). The observed correlations are statistically significant at the 95% confidence level for n=265 samples, with Pearson-log coefficients for Cu with Bi, Co, Se, and In, and Zn with Pb, Cd, Ga, and Sn above the critical value of 0.423 based on a two-tailed test and 20 degrees of freedom (number of variables minus 2; Table 4.4).

Pyrite samples from Cu-rich deposits, with bulk Cu/(Cu+Zn) ratios >55 (e.g., Ansil, Corbet, East Waite, Robb-Montbray, Bousquet #2-Duamgami, Louvicourt, Dunraine; Table 4.1), have higher average concentrations Cu, Au, Bi, Co, Ni, Se, Mo, Hg, and In than pyrite samples from Cu-poor deposits. Pyrite samples from deposits with intermediate bulk Cu/(Cu+Zn) ratios (between 20 and 55) have the highest Te, Cd, and Sn (e.g., Quemont, Horne #5 Zone, Kidd Creek, and Geco; Table 4.1). Pyrite samples from Zn-rich deposits, with Cu/(Cu+Zn) ratios <20 (e.g., Abcourt-Barvue, Galen, Delbridge, Mattagami, Lake, and Mattabi; Table 4.1) have the highest Zn, Pb, Ag, W, As, Sb, and Tl (Table 4.6). These relationships are reinforced when the zoning in individual deposits is taken into account. Pyrite samples from Cu-rich ore zones of Cu-rich deposits have the highest concentrations of Au, Co, Ni, Se, and Te, and pyrite samples from Zn-rich ore zones of Zn-rich deposits have the highest concentrations of Pb, Sn, W, Sb, Tl and V

(Table 4.7). Pyrite in the Cu-rich ores of Zn-rich deposits also have the highest concentrations of Ag, Bi, and As; and pyrite in the Zn-rich ores of Cu-rich deposits have the highest concentrations of Cd and In.

Very high concentrations of certain trace metals in the pyrite separates most likely represent mineral inclusions (e.g., trace minerals such as roquesite in the case of the samples with the highest In (120 ppm). Very high concentrations of other trace metals, such as Co, in pyrite from the Cu-rich ores of Cu-rich deposits (up to 959 ppm) may be in solid solution (e.g., George et al., 2016, 2018a) or possibly as inclusions of the mineral cobaltite. In most cases, high Pb concentrations in pyrite mineral separates are interpreted to be due to inclusions of galena. To avoid comparing the trace elements in pyrite to trace elements in inclusions, we rejected samples over a certain threshold for Cu, Zn, and Pb concentrations (see section 3.2).

Pyrite samples from deposits with different bulk Au grades also have different co-enrichments of trace metals, with Au, Bi, Te, In, and Sn enriched in pyrite from the Au-rich deposits and Zn, Cd, As, and Hg enriched in pyrite from the Au-poor deposits (Table A.5). The Au concentrations in the pyrite samples also show a bimodal distribution with Au co-enriched with Bi, Se, and Te in pyrite from Cu-rich deposits and with Ag, As, Sb, and Hg in pyrite from Zn-rich deposits (Fig. 4.6; Table 4.4). Pyrite samples from the most Au-rich deposits (i.e., Horne, Quemont, and Bousquet #2-Dumagami) are significantly enriched in Te (Fig. 4.21.a). The mean Te concentration of the pyrite mineral separates from Au-rich deposits is 66 ppm, which is greater than one standard deviation from the mean for all of the pyrite samples from VMS deposits in the Superior Province (Fig. 4.21.b, 4.22.a). The positive correlation of Te concentrations in pyrite with the bulk Au grade of the sampled deposits has a Pearson coefficient of 0.45 (Fig. 4.21.c). These pyrite samples with high Te also tend to have higher concentrations of Au, Sn, and As than pyrite samples from Au-poor deposits.

A few deposits with more than 10 pyrite samples show significant variation in trace elements within the deposits (Fig. 4.23). In pyrite samples from Horne (H&G and #5 Zone), the concentrations of Se, Te, and Sn range from less than 10 ppm to 100s of ppm. However, trace

elements in pyrite from other deposits show very uniform concentrations among multiple samples (e.g., uniformly high Co concentrations between 250 to 850 ppm in pyrite from Dunraine). Sn concentrations in pyrite samples from Abcourt-Barvue, Mogador, Dunraine, and Ansil are also very consistent (10s of ppm), as are Mo concentrations in pyrite from Dunraine, Horne, and Quemont. In most cases, variations in trace element concentrations in pyrite are larger between deposits, regionally and in individual mining camps, than within individual deposits. Pyrite samples from the Cu-Zn deposits of the Noranda main camp and Cu-rich deposits from the west camp (New Insco) are enriched in Bi, Co, Ni, Se, and Sn; whereas pyrite from the Cu-Au deposits such as Horne and Quemont are enriched in Au, Se, and Te and pyrite from Zn-rich deposits like Delbridge are enriched in Pb, Ag, Au, As, Sb, Tl. The pyrite mineral separates from the giant Horne deposit include samples from Cu-rich ores in the H&G orebodies and from Zn-rich ores in Horne #5 Zone; both are enriched in Au, Te, Sn, and Hg, but the pyrite from the H&G orebodies has notably higher Bi, as noted above. These observations are summarized in Figure 4.24.a. A summary of the trace element distributions in pyrite separates grouped at different scales is shown in Table 4.9. In pyrite samples from Mogador and Amos-Barraute, the lower quartile of Pb concentrations is higher than the maximum Pb concentration in pyrite from Dunraine, and Mo concentrations in pyrite samples from Dunraine are an order of magnitude higher than the maximum Mo concentrations in samples from Mogador.

4.2.3 Variations with host rocks

We note significant trace element variations in pyrite samples from deposits with different host rocks (Table 4.8, A.6). Among the bimodal-mafic deposits of the Abitibi pyrite samples from deposits with felsic-dominated footwalls are enriched in Zn and most trace metals including Au, Bi, Se, Te, In, Sn, W, Sb, and Hg (Fig. 4.24.b; Table 4.8, A.6.b). Pyrite from deposits with intermediate mafic: felsic ratios in the footwall are enriched in elements such as Mo and Ga. Pyrite samples from deposits with mafic-dominated footwalls are enriched in Co and Ni, but also have slightly higher concentrations of Pb, Ag, Cd, and Tl than pyrite from other deposits (Table 4.8, A.6.b). Pyrite samples from deposits with intermediate and felsic-dominated footwalls have

higher Cu and As concentrations than pyrite samples from deposits with mafic-dominated footwalls.

These variations are evident in samples from deposits across the AGB (Fig.4.24; Table 4.9, A.7–9). Pyrite samples from the DBL camp are enriched in Au, Bi, and Te compared to pyrite from deposits with more primitive mafic volcanic host rocks such as in Timmins, Matagami and Val d'Or (Fig. 4.25.a and Table 4.9.a, A.8). Pyrite samples from the Val d'Or camp are generally enriched in Co, Ni, Se, Ga, Mo, and As compared to pyrite from deposits with more evolved felsic host rocks such as in the DBL. Pyrite samples from the Timmins camp in the Kidd-Munro assemblage (i.e., Kidd Creek and Potter-Doal) and Blake River (Kamiskotia area formerly assigned to the Tisdale, i.e., Canadian Jamieson, Genex, and Kam-Kotia) show variable enrichments in Co, Ni, Cd, In, Sn, and Tl (Fig. 4.25.b), with Co and Ni enriched in samples from Potter-Doal and Genex, and In, Sn, and Tl enriched in samples from Kidd Creek (Table A.9). These differences closely reflect the different footwall rocks (i.e., mafic-dominant at Potter-Doal and Genex, and intermediate to felsic-dominant at Kidd Creek). In the Deloro assemblage, pyrite samples from the Matagami camp are enriched in Co, with pyrite from some deposits containing more Bi, Se, In, and Sn (i.e., Isle Dieu, Norita-A, Orchan) and Ni (i.e., Mattagami Lake) than other deposits (Fig. 4.25.c), again reflecting the mafic: felsic host rock ratios of the deposits. Pyrite samples from the Quevillon camp are enriched in Pb, Ag, and Cd, pyrite samples from Joutel camp are enriched in Hg; and pyrite samples from the Amos-Barraute camp are enriched in Bi, As, and Sb (Fig. 4.25.d), all reflecting their felsic-dominant immediate footwalls. In the Benny greenstone belt, pyrite samples from the Geneva Lake and Stralak deposits are variably enriched in Ag, Ni, Cd, Mo, V, Sb, and Tl (Fig. 4.25.e), reflecting the variable mafic: felsic ratios of the host rocks.

Pyrite samples from deposits with geochemically different felsic host rocks, distinguished by the F classification, also show some distinct trends (Table A.6.c). The Bousquet #2-Dumagami deposits have both FI and FII rhyolite in the footwall. Their pyrite samples are enriched in Au, Bi, and Te, and depleted in Co, Ni, Se, and Sn. Some pyrite samples from Bousquet #2 have elevated U. Deposits with FII rhyolite in the footwall, including the Val d'Or, Amos Barraute

camps (and Sturgeon Lake, see below), contain pyrite that is enriched in Co, Ni, Mo, As, and Sb, and depleted in Au, Te, In, and Sn. Enrichment in As and Sb may be related to the more evolved calc-alkaline footwall rhyolite in these deposits. The Horne (H&G and #5 Zone) deposits have both FII and FIII rhyolite in the footwall, and their pyrite samples are enriched in Au, Cd, In, and Hg, which may be related to the transitional nature of the footwall rhyolite signature of these deposits. Pyrite samples from deposits with FIIIa footwall rhyolite including in Noranda, Joutel, Quévillon, and Normetal camps are enriched in Pb, Ag, Au, Ni, Se, and Te interpreted to be a tholeiitic footwall rhyolite signature. Pyrite samples from deposits with FIIIb footwall rhyolite, including Mattagami and Timmins, are enriched in Ag, In, and Sn interpreted to be a tholeiitic-high silica rhyolite signature. While there is considerable overlap between these groups, pyrite from deposits in FI-FII rhyolites is distinctly auriferous, with enrichment in (Cu) Bi, Te, and In, whereas pyrite from deposits in FIII rhyolites is more enriched in (Zn) Ag, Pb, and Sn. This is generally consistent with the interpreted origins of FI-FII rhyolites (in magmatic arcs with potentially significant magmatic volatile contributions) and FIII rhyolites (in rifted arc and back-arc settings with large-scale convective hydrothermal systems).

We isolated samples from Cu-rich ore [Cu/(Cu+Zn)x100 >35] and Cu-rich deposits [bulk Cu/(Cu+Zn) x100 grade >50] and from Zn-rich ore [Cu/(Cu+Zn)x100 <35] from Zn-rich deposits [bulk Cu/(Cu+Zn) grade <50] (Fig, 4.3.c). In the pyrite samples from Zn-rich ore and Zn-rich deposits, the pyrite samples from deposits with felsic-dominated footwalls have high concentrations of Au, Se, Sn, W, Sb, Hg, and Tl; pyrite samples from Zn-rich deposits with intermediate mafic: felsic ratios have higher concentrations of Ni, Te, and Ga; and pyrite samples from Zn-rich deposits with mafic-dominated deposits have slightly higher concentrations of Pb, Ag, Co, and Mo (Table 4.8). The pyrite samples from Cu-rich ore and Cu-rich deposits with felsic-dominated footwalls, are enriched in Au, Se, and Sn, and samples from Cu-rich deposits with mafic-dominated are enriched in Co. A number of these enrichments and depletions correspond to known enrichments and depletions in felsic versus mafic host rocks (e.g., Sn and W in felsic rocks; Ni and Co in mafic rocks: Hannington, 2014). However, certain elements are unexpectedly enriched in pyrite samples from deposits with mafic host rocks (e.g., Pb in samples from deposits with mafic-dominated host rocks).

There are some clear differences in the trace element signatures of pyrite samples from different greenstone belts and assemblages across the Superior Province (Fig. 4.26; Table A.7). In the AGB, some pyrite samples from deposits in the Deloro assemblage (e.g., Joutel, Abcourt-Barvue, Orchan) have high Mo and Hg compared to samples from deposits in the other assemblages. Pyrite samples from deposits in the Kidd-Munro assemblage (Potter-Doal, Kidd Creek) have high Co, Ni, Cd, In, and Sn, but contain less Au, Se, and Te (Fig. 4.26.a), which is interpreted to reflect the mafic-dominant host rocks of the Kidd-Munro assemblage compared to other assemblages (e.g., Blake River) and the lack of a felsic magmatic contribution to the hydrothermal systems (e.g., typical of the samples from the DBL). Pyrite samples from deposits in the Tisdale assemblage (Dunraine, East Sullivan, Louvem, Louvicourt, Manitou-Barvue) are similarly enriched in Co and Ni, as well as Se, Ga, Mo, and As, but contain less Pb, Ag, Bi, In, Sn, Sb, and Tl reflecting the dominantly mafic host rocks of the Tisdale. Pyrite samples from deposits in the BRG (Noranda and DBL) are enriched in Au, Se, Te, Cd, and In compared to deposits in other assemblages of the AGB reflecting the more evolved felsic host rocks typical of the eastern Blake River assemblage.

Pyrite samples from deposits in the Wawa, Wabigoon, and Uchi subprovinces in the western Superior are enriched in Ag, Sn, W, As, and Sb, and depleted in Au, Ni, Te, and Mo compared to pyrite from deposits in the AGB (Fig. 4.26.b; Table A.7). Pyrite samples from the Sturgeon Lake camp, in particular, are enriched in Ag, As, Sb, and Hg; whereas pyrite samples from the Manitouwadge camp (i.e., Geco) are significantly enriched in Sn reflecting the felsic-dominant footwalls of the deposits (and metasediments at Manitouwadge) that are generally more evolved than the bimodal-mafic assemblages of the AGB deposits.

4.2.4 Variations with deposit sizes

Pyrite samples from small, <8 Mt in size, typically higher grade and Cu-rich deposits tend to have high concentrations of Cu, Co, and Se (e.g., Ansil, Old Waite, East Waite, New Insco and Vauze), whereas pyrite samples from small Zn-rich deposits (e.g., Delbridge, Deldona, Geneva

Lake, and Stralak) have high concentrations of Pb, Ag, As and Sb (Table A.10). Pyrite samples from large-tonnage deposits (> 8 Mt) are commonly enriched in Sn (Fig. 4.21.a,b,c). The correlation between Sn contents of the pyrite samples and deposits size is statistically significant at the 95% confidence level for n=242 samples, with a Pearson coefficient of 0.3 (Fig. 4.21.c, Fig. 4.22.b). Pyrite samples from large deposits also tend to have elevated Ag, Au, Cd, In, As, Hg, Tl and in some cases Te (Table A.10). Pyrite samples from Manitou Barvue, Bousquet #2, and East Sullivan have the highest As concentrations among the large deposits; samples from Kidd Creek, Horne, and Mobrun have the highest In; samples from Geco, Kidd Creek and Mobrun have the highest Sn; and samples from Quemont, Bousquet #2, and Horne have the highest Te.

A potentially important question for exploration is whether the trace element signature of pyrite differs significantly between large economic massive sulfide deposits and smaller unmined mineral occurrences. A number of pyrite samples from two uneconomic mineral occurrences in the Noranda Camp (Decour-Garon and Moosehead) allow a comparison with samples from larger and higher-grade deposits. Pyrite samples from the Decouer-Garon showing, which consists of only disseminated sulfides and no massive ore, contain 110000 ppm Zn and 560 ppm Pb, and pyrite samples from the small Moosehead prospect contain an average of 6600 ppm Zn and 18000 ppm Pb (Table A.9). These Zn and Pb concentrations contrast with the average concentrations in pyrite from the nearby Noranda main camp deposits (i.e., of 8000 ppm Zn and 500 pm Pb, with total past production of >20 Mt ore) indicating the Decour-Garon and Moosehead samples are more contaminated by sphalerite and galena, respectively. However, the pyrite samples from Decour-Garon showing have uniformly low concentrations of Ag, Sn, As, and Sb compared to the much larger massive sulfide deposits. Some pyrite samples from the small Moosehead occurrence, which included mined massive sulfide, have high concentrations of Pb, Ag, Sn, Sb, and Tl, like the developed deposits of the main camp. One pyrite sample from Moosehead contains 2000 ppm Sn, similar to the highest Sn concentrations in the largest deposits, although this sample also contains 4 wt% Pb with high Sb and Tl, indicating the presence of inclusions. None of the pyrite samples from smaller occurrences show any

enrichment in magmatic-associated elements (Bi, Se, Te, and Sn), in contrast to the larger deposits.

4.3 Mineralogy of trace elements in pyrite

The presence of chalcopyrite or sphalerite inclusions in the pyrite samples from many deposits are indicated by high concentrations of Cu correlated with Co, Se, Ni, Bi, Te, and In (Fig. 4.4) or Zn and Pb correlated with Ag, Cd, Sn, As, Sb, Hg, and Tl (Fig. 4.5). The elements that are readily incorporated in the structure of pyrite as solid solutions like Ag, Co, Ni, Se, Ga, As, and Tl (e.g., Huston et al., 1995; Cook et al., 1996, 2011; Maslennikov et al., 2009) generally show a more normal distribution (continuous enrichment from low to high concentrations), whereas those elements occurring in mineral inclusions in the pyrite show large gaps in their distribution (Fig. 4.2). Importantly, many trace elements originally in solid solution in pyrite are mobilized along grain boundaries during metamorphic recrystallization of the pyrite, and consequently form discrete trace minerals in the samples (Conn et al., 2019). Regardless, the distribution of lattice-bound elements and trace elements in microinclusions are generally considered to reflect the same conditions of mineralization (e.g., compositions of the ore-forming fluids and temperature of primary mineralization: Cook, 1996; Large et al., 2009; Monecke et al., 2016; Grant et al., 2018). In cases where there has been limited remobilization, we argue that samples with high trace metals in solid solution in pyrite are enriched in those metals for the same reasons as samples with high concentrations in discrete mineral inclusions. In the following, we consider the different mineralogical controls on the distribution of trace elements in the pyrite samples (Fig. 4.8–4.19 and Table 4.2, 4.10). Many of the trace metals are present in the stoichiometric proportions of discrete minerals that are listed in Table 4.11.

Ag correlates most strongly with Pb and is likely present in many pyrite samples as inclusions of Ag-bearing galena, Pb-rich sulfosalts (e.g., samples from Manitou-Barvue, Normetal, Mattabi, Lyon Lake, South Bay, Sturgeon Lake: Fig. 4.8), or Ag-tellurides (e.g., hessite). The log-probability plot for Ag (Fig. 4.2) is irregular above the first upward data inflection , but represents a single population without significant gaps or changes in slope, which probably

reflects a homogeneous distribution of galena/ sulfosalt inclusions or nanoparticles in the pyrite samples. The strong correlation of Pb, Ag, As, and Sb in the pyrite concentrates of Delbridge, Deldona, Abcourt Barvue, Manitou Barvue, Lyon Lake, Mattabi, Geneva Lake, and Stralak (Fig. 4.9 and Table 4.4) suggests a range of different sulfosalt inclusions. Ag tends to correlate most strongly with Sb suggesting tetrahedrite is dominant, although other Sb-bearing minerals have been reported in some deposits (e.g., dyscrasite at Kidd Creek, Lac Dufault, South Bay; boulangerite at Mattabi; pearceite and proustite at Manitou Barvue: Table 4.10). Ag concentrations are positively correlated with Cu in some pyrite samples (e.g., Quemont and Gallen: Fig. 4.9 and Table 4.4) and with Zn in others (e.g., Delbridge and Geneva Lake: Fig. 4.9 and Table 4.4) and reflects the bimodal distribution of Ag in Cu- and Zn-rich massive sulfides (e.g., Hannington et al., 1999c).

Enrichment of pyrite in As in solid solution is well established in the literature (e.g., Maslennikov et al., 2009; Large et al., 2009). A significant proportion of the As in the pyrite samples is considered to be present as inclusions of arsenopyrite, or as tennantite, indicated by the correlation with Cu, Zn, Pb, Ag and Sb (Fig. 4.4, 4.5, 4.10). The observed correlation of As and Sb is statistically significant at the 95% confidence level for n=265 samples, with a Pearson-log coefficient above the critical value of 0.423 based on a two-tailed test and 20 degrees of freedom (number of variables minus 2; Table 4.4). Lower correlation coefficients with Cu, Zn, and Ag likely reflect a bimodal distribution of As in Cu- and Zn-rich ores, similar to Ag. Arsenopyrite has been documented in about 1/4 of the deposits in the dataset (Table 4.4). The Cu-As correlation in pyrite samples from deposits such as Louvicourt, East Sullivan, Kidd Creek, and Ansil (Fig. 4.27) likely indicates the presence of either arsenopyrite or cobaltite, both interpreted to have formed at higher temperatures than tennantite-tetrahedrite (cf. Hackbarth and Petersen, 1984; Hannington et al., 1999c). In the pyrite samples from Delbridge, Abcourt Barvue, Manitou Barvue, Lyon Lake, and Mattabi, the correlation of As with Zn, Pb, Ag, and Sb (Fig. 4.11) is interpreted as a lower-temperature association with Pb-, Ag-, and Sb-bearing sulfosalts.

The majority of Sb in the pyrite samples is also likely present as inclusions of tetrahedrite or other sulfosalts indicated by the correlation with Zn, Pb, Ag, As, and Hg (Fig. 4.12). Solid

solution of Sb in pyrite is generally much lower than that of As (Huston et al. 1995; Large et al., 2009; Fig. 4.2). Instead, the association of Sb with Zn in pyrite samples from Delbridge, Kidd Creek, Manitou Barvue, Geneva Lake, Lyon Lake, Mattabi, and Sturgeon Lake most likely reflects Sb-bearing trace minerals with inclusions of sphalerite; the association with Pb most likely reflects Sb-bearing trace minerals in galena and Pb-bearing sulfosalts (Fig. 4.13). Boulangerite and bournonite also have been reported in some deposits (e.g., Mattabi, Sturgeon Lake: Monecke et al., 2016). A weak correlation of Sb with Cu in our samples suggests Sb enrichment mainly at low temperatures (Hannington et al., 1999a; Monecke et al., 2016).

Hg in the pyrite samples is thought to be present in solid solution in pyrite or in sphalerite inclusions in pyrite (e.g., Jonasson and Sangster, 1975a; see also Cook et al., 2009; Maslennikov et al., 2009). Hg shows a stronger correlation with Zn than it does with Pb, Ag, As and Sb in pyrite samples from some deposits (Canadian Jamieson, Mobrun, Manitou Barvue, and Lyon Lake: Fig. 4.5 and Table 4.4) suggesting that inclusions of tetrahedrite or tennantite are unlikely hosts. Rare mercurian tennantite has been reported from Kidd Creek (Hannington et al., 1999c), but the pyrite samples in this study are not enriched in Hg (mean 1.3 ppm). Anomalous Hg with low Zn and high Te in pyrite samples from other deposits such as Horne, Horne #5 Zone, and Quemont (Fig. 4.12, 4.13) indicates the likely presence of Hg-tellurides (i.e., coloradoite: see Monecke et al., 2016). However, in general, discrete Hg-bearing minerals are rare in VMS deposits (Mosier et al., 2009).

Tl in the pyrite is considered to be mainly lattice bound (Murao and Itoh, 1992, Huston et al., 1995; Ritts, 2012). Pyrite samples with the highest concentrations of Tl are from Delbridge, Deldona, Kam-Kotia, Kidd Creek, and Mattabi (up to 27 ppm: Fig. 4.2). Strong Pb-Tl correlation in pyrite samples from Delbridge, Deldona, and Mattabi (Fig. 4.10, 4.11) suggests that minor inclusions of galena are an important host for Tl in some samples. Tl is commonly co-enriched with Sb (10–100 ppm) in the alteration haloes of Zn-rich deposits, typical of low-temperature mineralization (e.g., Smith and Huston, 1992), and this likely explains the correlation with Sb in Tl-rich pyrite in the samples considered in this study.

Electrum and free gold have been widely documented in Au-rich VMS deposits of the eastern Blake River Group and Noranda (e.g., at Dumagami, Bousquet #2, Horne H and #5 zone, Quemont, Corbet, Delbridge, and Deldona: Table 4.4; Mercier et al., 2011a). A lack of correlation between Au and As in the pyrite samples (Fig. 4.6) suggests that coupled Au-As solid solution in pyrite is not an important factor in these deposits. We suggest that much of the gold in the pyrite samples from the Superior database, including Au in solid solution, has been remobilized into free gold or electrum during metamorphism as found at the Mobrun deposit and elsewhere (e.g., Larocque et al., 1995). Highly variable correlations of Au with Cu, Pb, Ag, Bi, Se, Te, As and Sb (Fig. 4.6 and Table 4.4) suggests it may be associated with a number of different trace mineral inclusions in the pyrite concentrates, including telluride minerals in some deposits and sulfosalts in others as observed in other studies (e.g., Hannington et al., 1999a, Huston, 2000; Large et al., 2007). In the samples considered in this study, Au is strongly partitioned into Bi and Te minerals (Au-bismuthides and -tellurides) typically found in trace quantities in Cu-rich ores (see also Jonasson and Sangster, 1983). The high Au concentrations in pyrite samples from Horne, Quemont, and Bousquet #2-Dumagami correlate with Bi, Te, and Ag (Fig. 4.7) and likely reflect inclusions of calaverite, petzite, and hessite. These minerals have been reported at Bousquet #2-Dumagami, Horne (H and #5 zone), Quemont, and Old Waite; and tellurobismuthite is present at Bousquet #2-Dumagami (e.g., Tourigny et al., 1993). The Cu-Au-Bi-Te association in pyrite samples from deposits such as Robb-Montbray and Amulet-C is also consistent with tellurides as an important host. All of these minerals have been shown to concentrate Au in VMS (e.g., Maslennikov et al., 2013, Monecke et al., 2016; Goldfarb et al., 2017). The observed correlation of Au with Se and Te is statistically significant at the 95% confidence level for n=265 samples, with a Pearson-log coefficient above the critical value of 0.423 (Table 4.4). Another group of pyrite samples from Robb-Montbray, Delbridge, Normetal, Manitou-Barvue, Kam Kotia, Mattabi, and Geneva Lake with high Au concentrations (>7 ppm) and high Pb suggests a correlation with inclusions of galena or Pb-Sb-As sulfosalts (Fig. 4.6, 4.7).

Bi is concentrated in pyrite samples with high concentrations of Cu and Te from Ansil, Quemont, Horne, Bousquet #2, and Norita-A (Fig. 4.14, 4.15, 4.27). Kidd Creek contains

bismuthinite (Hannington et al., 1999c) but pyrite samples from the deposit are not enriched in Bi. Some pyrite samples from Bousquet #2, Vauze, Conigo, and Potter-Doal show a Pb-Bi correlation that may reflect Bi concentrated in Pb sulfosalt inclusions (e.g., aikinite, documented at Bousquet #2: Mosier et al., 2009).

Apart from the Au- and Ag-tellurides noted above, other Te-bearing inclusions in the pyrite samples are tellurobismuthite, coloradoite, or native Te; the solubility of Te in pyrite is considered to be negligible (Maslennikov et al., 2009; Large et al., 2009; Monecke et al., 2016). A variety of Te-bearing trace minerals have been reported at Bousquet #2-Dumagami, Horne (H and #5 zone), Quemont, Ansil, and Matagami Lake (Table 4.10), and Bi-Te, Pb-Te, Co-Te, and Ni-Te correlations (Fig. 4.14, 4.15, 4.16, 4.27 and Table 4.4) indicate the presence of tellurobismuthite, altaite, mattagamite, and melonite in samples from these deposits. The Cu-Co-Te correlation in some samples from Ansil, Quemont, Robb-Montbray, and Mattagami Lake likely indicate the presence of mattagamite (e.g., Thorpe and Harris, 1973).

Co is considered to be lattice bound in pyrite or in inclusions of Co-bearing chalcopyrite and discrete Co-bearing minerals (i.e., cobaltite). Although there is an upward inflection at 10 ppm Co in the log-probability plot for the samples considered in this study, published data on pyrite from other deposits suggest a much higher SSL (up to 5000 ppm: references; Fig. 4.2). In some samples of pyrite there is a Co-As correlation (Fig, 4.16, 4.17), most likely reflecting inclusions of cobaltite, which has been reported in many of the deposits, including Kidd Creek and Louvem (Table 4.10).

Ni is also likely lattice bound in pyrite. As for Co, although there is an upward inflection at 20 ppm Ni in the log-probability plot for the samples considered in this study, published data on pyrite from other deposits suggest a much higher SSL (up to 1000 ppm: Large et al., 2009; Fig. 4.2). Few discrete Ni-bearing phases have been reported in the deposits (Mosier et al., 2009), although some pyrite samples with anomalous Ni concentrations (e.g., from Old Waite, Potter-Doal, Isle Dieu) may contain inclusions of pentlandite. Other samples show a Ni-Te correlation (e.g., Robb-Montbray, New Insco, and Louvicourt: Fig. 4.16, 4.17) and therefore may contain

traces of melonite. Samples from Dunraine, Louvicourt, East Sullivan, Genex, and Joutel show a strong Cu-Ni correlation (Fig 4.5) indicating an association with chalcopyrite. However, many samples also show a correlation between Ni, Se, Mo, and As (from Mobrun, Old Waite, East Waite, and Genex: Fig. 4.16, 4.17), which might indicate enrichment in diagenetic pyrite (cf. Large et al., 2001b).

Se is considered to be mainly lattice bound in pyrite (e.g., Huston et al., 1995; Large et al., 2009; Genna and Gaboury, 2015) or present as inclusions of discrete selenium minerals (e.g., Jonasson and Sangster, 1975b, Monecke et al., 2016). The strong Cu-Se correlation in pyrite samples from Amulet-C, Horne, Quemont, Louvicourt, and Orchan (Fig. 4.4) probably reflects the concentration of Se in inclusions of chalcopyrite. Se-bearing covellite and digenite have been reported at Bousquet #2, Kidd Creek, and Louvem; and eucairite, klockmannite, naumannite and clausthalite at Kidd Creek (Table 4.10). In some samples of pyrite from the Orchan and Mattabi mines, Ag is correlated with Se (Fig. 4.8, 4.9) indicating the possible presence of naumannite. Samples that show a positive correlation between Se and Pb (Table 4.4) likely indicates the presence of inclusions of Se-bearing galena or clausthalite. Hannington et al. (1999c) and Huston et al. (1995) attributed the high Se in some massive sulfide deposits to represent a high-temperature magmatic input (see Chapter 5).

High concentrations of In in pyrite samples from Kidd Creek, Orchan, Horne (H and #5 Zone) and Mobrun correlate with both Cu and Zn and suggest the presence of In in chalcopyrite and sphalerite inclusions in pyrite, probably as trace roquesite (Fig. 4.4, 4.5, 4.18, 4.19). The samples from these deposits also tend to have high concentrations of Sn (Table 4.4), possibly indicating the presence of trace minerals like stannite and stannoidite, which have been reported at Bousquet#2-Dumagami, Kidd Creek, and Lac Dufault (Table 4.10). The observed correlation of In and Sn is statistically significant at the 95% confidence level for n=265 samples, with a Pearson-log coefficient above the critical value of 0.423 (Table 4.4).

Sn in the pyrite samples is probably present as inclusions of stannite, stannoidite, and cassiterite, which are abundant in the ore at Kidd Creek, South Bay, Bousquet #2-Dumagami and Lac

Dufault (Table 4.10). The correlation of Sn with Zn is stronger than its correlation with Cu (Fig. 4.4, 4.5, 4.27), indicating sphalerite likely incorporates most of the Sn-bearing mineral inclusions in the pyrite samples. However, the mixed correlations of Cu-Sn and Zn-Sn confirm a strong bimodal distribution of Sn in the ores of most of the deposits. We infer a very low limit for solid solution of Sn in pyrite (Fig. 4.2) based on other studies of trace element in pyrite (e.g., Maslennikov et al., 2009).

Cd occurs mainly in solid solution in sphalerite inclusions in the pyrite, indicated by the almost 1:1 correlation with Zn (Fig. 4.4). Correlation of Cd with In, Ga, and Sn (Table 4.4) suggest co-precipitation of these elements in sphalerite or as trace mineral inclusions in sphalerite. A few Cd-rich samples show a correlation with Se (e.g., Mobrun: Fig. 4.18. 4.19) that may reflect inclusions of the mineral cadmoselite (e.g., Monecke et al., 2016; see also Hannington et al., 1999c). Like Sn, we infer a very low limit for solid solution of Cd (Fig. 4.2) in pyrite based on other studies of the incorporation of Cd in sulfides minerals (e.g., Cook et al., 2009).

For Ga, we infer a limit of just a few ppm in solid solution in pyrite based on the first upward inflection in the log-probability distribution for the samples in this study (Fig. 4.2) and other studies of the incorporation of Ga in sulfides minerals (e.g., Cook et al., 2009). Ga is closely associated with Zn in the pyrite samples from Vauze, Manitou-Barvue, and Conigo (Fig. 4.4). High Ga concentrations can occur in sphalerite (10s to 100s of ppm), however, some Ga in the pyrite concentrates might also be present in sulfosalts or aluminosilicate gangue contaminating the samples (cf. Cook et al., 2009; Safina et al., 2018).

Traces of W in the pyrite samples likely reflect inclusions of scheelite or wolframite, which have been reported in some deposits (e.g., Kidd Creek: Hannington et al., 1999c). However, the generally low W content of the samples (<10 ppm) suggests that this is uncommon. A few W-rich pyrite samples from Kidd Creek and Geco also contain high Sn (Fig. 4.18, 4.19), most likely representing inclusions of both scheelite and cassiterite, or in rare cases possibly the unusual W-bearing sulfide minerals (e.g., Kiddcreekite, Cu_6SnWS_8: Harris et al., 1984).

Mo is present at high concentrations (50–250 ppm) in pyrite samples from Dunraine, Abcourt-Barvue, Louvicourt, and Stralak, and is thought to be mainly lattice bound in pyrite or possibly as trace inclusions of molybdenite (e.g., Monecke et al., 2016). Although there is an upward inflection at 10 ppm Mo in the log-probaility plot for the samples considered in this study (Fig. 4.2), published data on pyrite from other deposits suggest a much higher SSL (up to 50–70 ppm: Maslennikov et al., 2009). Molybdenite has been documented at Mattagami Lake and Louvem (Table 4.10), but the pyrite samples from these deposits do not show enrichment in Mo (Table A.9).

V in pyrite samples from Bousquet #2, Manitou-Barvue, New Insco, and Bell Allard (Table A. 9) is likely present in inclusions of magnetite, ilmenite, hematite, or rutile or in solid solution in pyrite or chalcopyrite. The correlation of Ti with V and Sc in pyrite samples from East Sullivan, and V with Sc in samples from East Sullivan, Manitou Barvue, Bousquet #2, and New Insco (Fig. 4.20) most likely indicate contamination by magnetite in the pyrite samples. The highest Fe content in the East Sullivan pyrite samples (56–57 wt%) further suggests significant contamination by magnetite. A correlation of U-V-Mo in some pyrite samples (Fig. 4.20) also could reflect adsorption of redox sensitive elements onto diagenetic pyrite (e.g., Wersin et al., 1994).

Total REE concentrations in the pyrite samples range from 0 to 1400 ppm. We interpret the LILE, HFSE and REE to be present in the pyrite mineral separates mainly as non-sulfide inclusions of heavy minerals, such as the REE-phosphate minerals monazite and xenotime, and other REE-bearing gangue minerals (e.g., apatite). LREE (except Eu) exhibit a near 1:1 correlation indicating inclusions of monazite in the pyrite samples (Table. 4.2). The REE data are useful indicators of the host rocks of the ore samples, but are more difficult to interpret in terms of processes responsible for the formation of the pyrite (e.g., Laflèche et al. 1992, 1998). REE are generally considered to be immobile in hydrothermal fluids, but recent work on VMS alteration systems shows that they can be highly enriched in hydrothermal fluids (Schmidt et al., 2010; Genna et al., 2014). The correlation of U with Th, Zr, Ce, and REE (Fig. 4.20) is interpreted as U in monazite or zircon that may have been concentrated in the samples during the

preparation of the pyrite separates. Th is likewise probably concentrated in monazite, indicated by the correlation with Ce and La in samples from Ansil, Manitou Barvue, Conigo, Kidd Creek, Potter-Doal, and Mattabi, with stoichiometric proportions of Ce and La consistent with monazite: (Ce, La, Nd, Th)PO_4 ; Fig. 4.20). For pyrite samples analyzed for P_2O_5, there is usually a correlation of P with Th, Ce, La, and other REEs (together with U; e.g., in pyrite samples from Dunraine and Mattabi) indicative of monazite inclusions. The strong correlation between Th, Y, and Yb, as well as the other REE, in other samples indicates xenotime is likely present (Table 4.4 and Fig. 4.20), with an almost 1:1 Y-Yb correlation. Zr shows strong correlations with Th, Hf and some REE (Nb and Nd) (Fig. 4.20) suggesting inclusions of zircon in the samples. The average concentrations of REEs (<10 ppm) are less than Zr (35 ppm: Table 4.4) in most samples. Pyrite samples from deposits with felsic-dominated footwalls have the highest Zr concentrations (Table A.6.b). Rutile is also common in the ore and alteration assemblages, for example at Kidd Creek and Louvem (Table A.1; Guha and Darling, 1972; Hannington et al., 1999c), and Ti is correlated with Cr, Zr, Ta and REE in the pyrite samples considered in this study, which may alternatively indicate titanite (Fig. 4.20; Table 4.4).

The trace element distribution among different minerals in the pyrite separates likely has been affected by metamorphic remobilization and recrystallization in some deposits. A number of LA-ICP-MS studies have demonstrated the remobilization of trace elements out of pyrite during metamorphic recrystallization (e.g., Mumin et al., 1994; Large et al., 2007, 2009; Maslennikov et al., 2009; George et al., 2018b). Samples of pyrite from deposits in the Manitouwadge and DBL camps show a number of features (Table 4.9; A.1; A.8) that are interpreted to reflect metamorphic remobilization. Conditions reached upper greenschist to amphibolite facies in these localities (Dubé and Mercier-Langevin, 2020), and pyrite samples from these higher metamorphosed deposits are variably depleted in Pb, Zn, Co, Ni, Se, Mo, Cd, Bi, In, Sn, Hg, Tl, As and Sb. Recrystallization of the pyrite is thought to have caused remobilization of trace metals to the grain boundaries of the coarsened pyrite and then loss from the grains during prograde metamorphic reactions. In the highly metamorphosed deposits, elements that are retained in the pyrite lattice (Co, Ni, Se, and As) show a poor correlation with most other elements (e.g., Cu, Zn, Pb, Ag, Au, Te, Bi) released as discrete mineral phases at the grain

boundaries (especially chalcopyrite, sphalerite, galena, tellurides, and free Au). In the Noranda camp, pyrite samples from deposits overprinted by local amphibolite facies contact metamorphism from the Lac Dufault Granodiorite (e.g., Hannington et al., 2003) are depleted in most trace metals (Amulet and Millenbach deposits: Table 4.9.c) compared to pyrite from other Noranda deposits at a lower metamorphic grade. The inconsistent or lack of depletions in pyrite from other less metamorphosed deposits suggest these metals have not been mobilized out of the pyrite and are still present in solid solution or trapped in mineral inclusions (cf. Craig et al., 1998). Trace elements in the majority of VMS deposits in the Superior Province that were only metamorphosed to greenschist facies conditions (e.g., Powell et al., 1995) are expected to show this behaviour.

Using the trace element signatures of the pyrite samples, we classified the deposits in terms of their dominant trace mineral assemblages (i.e., Bi-bearing, Se-bearing, Te-bearing, As-bearing, Sb-bearing) (Fig. 4.28). The groupings are supported by documented occurrences of the trace minerals in the deposits (Table 4.10 and Table A.1). Pyrite samples interpreted to contain abundant Sb-bearing mineral inclusions are mainly from deposits with felsic-dominated footwalls and with low Cu/Cu+Zn ratios, small tonnages, and low Au grades. Pyrite samples interpreted to contain abundant As-bearing mineral inclusions (e.g., Delbridge, Val d'Or deposits, and Timmins deposits) are from deposits with felsic and mafic footwalls with intermediate mafic: felsic ratios, low Cu/Cu+Zn ratios, and low Au grades. Pyrite samples that are interpreted to contain abundant Bi-bearing mineral inclusions are from deposits with mafic and felsic dominated footwalls, high Cu/(Cu+Zn) ratios, mid-size tonnages, and intermediate Au grades. Pyrite samples that are interpreted to contain abundant Se-bearing mineral inclusions are from deposits with variable ratios of felsic: mafic volcanic rocks in the immediate footwalls, intermediate Cu/(Cu+Zn) ratios, mid-size tonnages, and medium Au grades. Pyrite samples that are interpreted to contain abundant Te-bearing mineral inclusions are from deposits with roughly equal proportions of felsic: mafic volcanic rocks in the footwall, mostly high Cu/(Cu+Zn) ratios, large tonnages, and high Au grades. And finally, pyrite samples with low abundances of mineral inclusions of any kind are mainly from deposits with low Cu/(Cu+Zn) ratios and generally the lowest tonnages and Au grades. Most mining camps have deposits that yield pyrite with a range

of trace mineral inclusions (e.g., Noranda, Matagami, and Timmins). However, some camps have deposits that yield pyrite with very consistent trace mineral inclusions like Sturgeon Lake, Manitouwadge, and DBL (Table 4.10, A.1).

4.4 Trace elements in co-existing chalcopyrite, sphalerite and galena

Here, we compare the trace element concentrations of the pyrite to concentrates of other minerals from the same samples and deposits (Table A.11).

Trace element concentrations in chalcopyrite concentrates (n=184 from 45 deposits) are broadly similar to those of the pyrite samples reflecting varying mixtures of chalcopyrite, sphalerite and galena in the samples. Mean concentrations of Ag, Co, Se, Sn, As, and Sb are in the range of 100–1000 ppm; Bi, Ni, Te, In, Cd, and Hg are in the range of 10–100 ppm; and Au, Ga, and Tl are in the range of 1–10 ppm. Compared to the chalcopyrite samples, the pyrite concentrates from the same deposits are enriched in Pb, Ag, Au, Co, Ni, Te, Sn, As, and Tl, and depleted in Cu, Bi, Se, Cd, In, Ga, W, Mo, Sb, and Hg (Fig. 4.29, 4.30).

The concentrations of trace metals in the sphalerite mineral separates (n=242, 56 deposits) range from 0.1 to over 100 000 ppm. Mean concentrations of Cd are in the range of 1000–2000 ppm; Ag, Co, Ni, Se, Sn, As, and Sb are in the range of 100–500 ppm; Bi, Te, In, Ga, Mo, and Hg are in the range of 10–100 ppm; and Au and Tl are in the range of 1–10 ppm. Compared to the sphalerite samples, pyrite concentrates from the same deposits are enriched in Ag, Au, Bi, Co, Se, Te, Mo, and As and depleted in Cd, In, Ga, W, Sb, Hg, and Tl (Fig. 4.29, 4.30).

Trace element concentrations in mineral separates of galena (n=25, 13 deposits) differ significantly from the pyrite samples, reflecting very different mineralogical control on the partitioning of the elements. Mean concentrations of Cu, Ag, Sn, As, and Sb are in the range of 1000–10 000 ppm; Bi, Ni, Se, Te, and Cd are in the range of 100–1000 ppm; Au, Hg, and Tl are in the range of 10–100 ppm; Co, In, and Mo are in the range of 1–10 ppm; and Ga are less than 1 ppm. Galena samples have the highest concentrations of Ag, Au, Bi, Te, As, and Sb compared to

the other mineral separates, probably reflecting an abundance of Pb-rich sulfosalts and Pb-tellurides as inclusions in the galena samples (Fig. 4.22). The galena samples also have the highest concentrations of Se, Sn, Hg, and Tl, most likely reflecting solid solution in galena. Compared to the galena samples, pyrite concentrates from the same deposits are enriched in Co, In, Ga, and Mo, and depleted in Ag, Au, Bi, Te, As, Sb, and Hg (Fig. 4.29, 4.30).

4.5 Principal Components Analysis and Hierarchical Clustering

The variance explained by PC1 and PC2 from a principal components analysis of the trace element data in this study is 33% and 16%, respectively. A bar (scree) plot of the variance explained by the first 10 principal components is shown (Fig. 4.31.a.). Only the first 2 principal components explain over 10% of the variance, and are therefore, retained as significant. The remaining 8 principal components are insignificant explaining ~50% of the total variance which reflects the many different factors controlling the trace element geochemistry of the pyrite separates from source rocks to temperature and deposit zoning as well as sample preparation.

The element loadings and sample scores for the hydrothermal suite of elements are shown as two-dimensional scatterplots in PC space (PC1 versus PC2 biplots: Fig. 4.32.a) and provided in Table 4.12. The results show clear separation of the elements as described above. In the first analysis, we included data for Cu, Zn and Pb. In this case, Zn, Ag, Cd, Sn, As, Sb, and Tl have positive loadings on PC1, whereas Cu, Au, Bi, Co, Ni, Se and Te have negative loadings. Ag, As, Sb, and Tl, and Co, Ni, and Mo have positive loadings on PC2, whereas Zn, Cd, Sn, In, and Se have negative loadings, and Cu, Au, Bi, and Te have loadings near zero. When Cu, Zn, and Pb are excluded, nearly identical PC1 and PC2 scores are obtained (Fig. 4.33.a) implying that the behaviour of the trace elements relative to each other is independent of the Cu, Zn and Pb concentrations. Near zero loadings for elements like In on PC1 and only weakly positive loadings for Sn reflect the strongly bimodal distribution of these elements in both Cu-rich and Zn-rich assemblages. The weakly negative loadings for Ni and Mo on PC1 could reflect their co-enrichment in diagenetic pyrite or in pyrite from higher-temperature Cu-rich assemblages (e.g., Grant et al., 2018).

The groupings of samples on PC1 (dominated by Zn-Pb-Ag-Cd-Sn-As-Sb-Tl and Cu-Au-Bi-Co-Ni-Se-Te-Mo: Fig. 4.32.a) reflect the strongly bimodal distribution of trace elements in pyrite between Cu-rich and Zn-rich mineralization. The samples with positive scores on both PC1 and PC2 (dominated by Pb-Ag-As-Sb-Tl) reflect the influence of galena and sulfosalts inclusions. The samples with negative scores on PC1 contain Bi-, Se-, and Te-bearing mineral inclusions (Fig. 4.33.b).

Pyrite samples from different deposits have highly variable scores on PC1. Pyrite samples from Zn-rich deposits with high Sn concentrations (i.e., Kidd Creek and Isle Dieu) have positive scores on PC1 (Fig. 4.28.a). Pyrite samples from more Cu-rich deposits with high Sn and In concentrations have lower PC1 scores (i.e., Horne #5). Different pyrite samples from deposits with high Au grades may be associated with all three trace element groups identified in the PCA: Cu-Au-Co-Se-Ni-Bi-Te, Pb-As-Ag-Sb, or Zn-Sn-In-Cd (Fig. 4.33.c). Pyrite samples from the high Au grade Deldona, Delbridge, and Amulet-A deposits have positive scores on PC1 and PC2 associated with Pb-As-Ag-Sb. Samples from the Au-rich Horne, Quemont, Bousquet #2-Dumagami deposits and the Cu-rich Ansil deposit have negative scores on PC1 associated with Cu-Co-Se-Ni-Bi-Te. Some of the pyrite samples from Quemont and Horne have negative PC2 scores that reflect a strong Zn-Sn-Cd association.

A separate PCA of a smaller group of samples with Hg data (Fig. 4.33.d) shows clear separation of the elements, with Zn, Pb, Ag, Cd, In, Sn, As, Sb, and Tl having positive loadings on PC1, and Cu, Au, Bi, Co, Ni, Se, Te, and Hg having negative loadings. Pn, Ag, Bi, Co, As, Sb, Tl have positive loadings on PC2, whereas Zn, Au, Ni, Se, Te, Cd, In, Sn, and Hg have negative loadings, and Cu has a loading near zero.

Another PCA for the non-metals (i.e., U, Th, Zr, Hf, Nb, Rb, and REE; Fig. 4.33.f show HFSE, LILE, and Yb have strong positive loadings on PC1, whereas LREE (La, Ce, Nd, Pr, Sm, Eu) and HREE (Gd, Y, Dy) have negative loadings. Pr, Sm, Eu, Gd, Dy, Yb, and U and Th have low to high positive loadings on PC2, whereas Zr, Nb, and La, Ce, and Nd have negative loadings,

and Rb, Hf, and Y have loadings near zero. This behaviour corresponds with the element substitutions in different minerals collected with pyrite from deposits with different host rocks (see section 4.3). Negative loadings of the LREE on PC1 reflect concentration in inclusions of monazite in pyrite samples mainly from Zn-rich ores; the positive loadings of the HFSE on PC1 reflect concentration in inclusions of zircon, and the positive loadings of Yb on PC2 reflect concentration in inclusions of xenotime.

Hierarchical clustering of the PCA data (HCPC) identified 3 groups of samples (Fig. 4.31.b, 4.32.b). The trace elements that have the greatest influence on the defined clusters are: Cu, Au, Bi, Co, Ni, Se, Te, Mo (cluster 1); Zn, Pb, Ag, Cd, Sb, As, (cluster 2); and Se, In, and Sn (cluster 3) (Table 4.13). There is a clear separation of clusters 1 and 2 on PC1, and cluster 3 on PC2. Pyrite samples from Cu-rich deposits with a strong Cu-Au-Bi-Co-Te association, such as Dunraine Bousquet #2-Dumagami, Horne (H and #5 zone), Quemont, Robb-Montbray, Old Waite, and New Insco are mostly in cluster 1. Samples from Zn-rich deposits with a strong Ag-As-Sb-Tl association such as Deldona, Delbridge, Abcourt-Barvue, Manitou-Barvue, Sturgeon Lake, Mattabi and Kidd Creek are mostly in cluster 2. Pyrite samples from a range of other deposits (e.g., with a strong In-Sn association, such as Geco, Corbet, Mobrun, Vauze, Orchan, and Horne H&G and #5 Zone) fall in cluster 3 (Fig. 4.32.b).

In the samples belonging to Cluster 1, we conclude that Cu, Bi, and Te are incorporated mainly as inclusions of chalcopyrite; Te, Bi, and Au are also present as trace bismuthides and tellurides; and Co, Ni, Se ± Au are present as lattice-bound trace elements in pyrite. In the samples belonging to Cluster 2, Pb, Ag, Sb, ±Tl are incorporated mainly as inclusions of galena; Pb, Ag, As, Sb are also present as trace sulfosalts; and As, Sb, and Tl are lattice bound in pyrite. In the samples belonging to Cluster 3, Zn, Cd, In, Sn are incorporated mainly as inclusions of sphalerite. The same clusters are defined in the subset of pyrite samples with Hg data (Fig. 4.33.e). HCPC on the non-metals identified 3 clusters (Fig. 4.33.g: La, Ce, Pr, Sm, and Gd (cluster1); Th, Zr, Hf, Rb, Nb (cluster 2); and U, Eu, and Yb (cluster 3) (Table 4.13). The REE in cluster 1 and 3 reflect inclusions of monazite and xenotime, whereas HFSE and LILE in cluster 2 reflect inclusions of zircon.

4.6 Comparison with LA-ICP-MS of pyrite

We performed in-situ analyses of individual pyrite grains from selected mineral separates using LA-ICP-MS and compared them to the bulk analyses of the samples by dissolution ICP-MS. Laser spot analyses have been used widely to characterize pyrite and other sulfide mineral compositions (e.g., Leistel et al., 1998; Slack et al., 2005; Large et al., 2007, 2009; Cook et al., 2009; Maslennikov et al., 2009, 2013; McClenaghan et al., 2009; Lockington et al., 2014; Revan et al., 2014; Wohlgemuth-Ueberwasser et al., 2014; Genna and Gaboury, 2015; George et al., 2015; Belousov et al., 2016; Maslennikov et al., 2017; Dehnavi et al., 2018; Grant et al., 2018) and determine elements in solid solution and micro-inclusions (Table 4.14).

The results (Table A.12) show that most elements enriched in bulk samples of the pyrite are also enriched at the grain scale in individual spot analyses, even in cases where most of an element may be present as inclusions of another mineral in the pyrite samples. Similar enrichments are observed in the bulk analyses and LA-ICP-MS over a wide range of concentrations, from 10s to 100s of ppm.

The highest concentrations of trace elements in pyrite determined by LA-ICP-MS were for Cu (mean 260 ppm, up to 6100 ppm), Zn (mean 460 ppm, up to 37 000 ppm), and Pb (80 ppm, up to 3800 ppm). Table 4.15 and Figure 4.37, 4.38 show that the LA-ICP-MS analyses of pyrite grains are very similar to the bulk solution ICP-MS data for each sample, for both lattice-bound elements (i.e., Co, Ni, As) and other elements that are thought to be mainly present as microinclusions smaller than the spot size (Cu, Zn, Bi, Te, Cd, In, Sb, Tl, and U). In-situ analyses of Au and As, for example, compare remarkably well with bulk analyses of the same samples from Kidd Creek (low Au, high As) and Dumagami (high Au, low As). LA-ICP-MS and bulk ICP-MS analyses of pyrite from the Kidd Creek sample also agree very closely for Pb (within 95% or 15 ppm), Ni (within 99% or 1 ppm), Cd (within 92% or 0.2 ppm), Sb (within 95% or 1 ppm), and Tl (within 50% or 2 ppm) (Fig. 4.34; 4.35 Table 4.15. Even in cases where the absolute concentrations of the trace elements by LA and dissolution ICP-MS of the bulk

samples do not always agree, the differences between deposits are clear for both individual pyrite grains and bulk analyses (Fig. 4.34, 4.35). For example, Mo concentrations in pyrite from the Kidd Creek sample are both consistently higher than in pyrite from the other deposits whether determined by LA-ICP-MS or solution ICP-MS; pyrite from the Bousquet #2 samples has the lowest Mo and the highest U by both methods. The differences are clear for most elements (Cu, Zn, Pb, Ag, Au, Bi, Co, Ni, Se, Te, In, Mo, As, Sb, Tl, and U) except Sn, Ga, Hg, and Th, which are more variable (Fig. 4.34 and Table 4.15). Figure 4.36 illustrates the consistent trace element geochemistry of different sampling types from the scale of an entire deposit to a single sample.

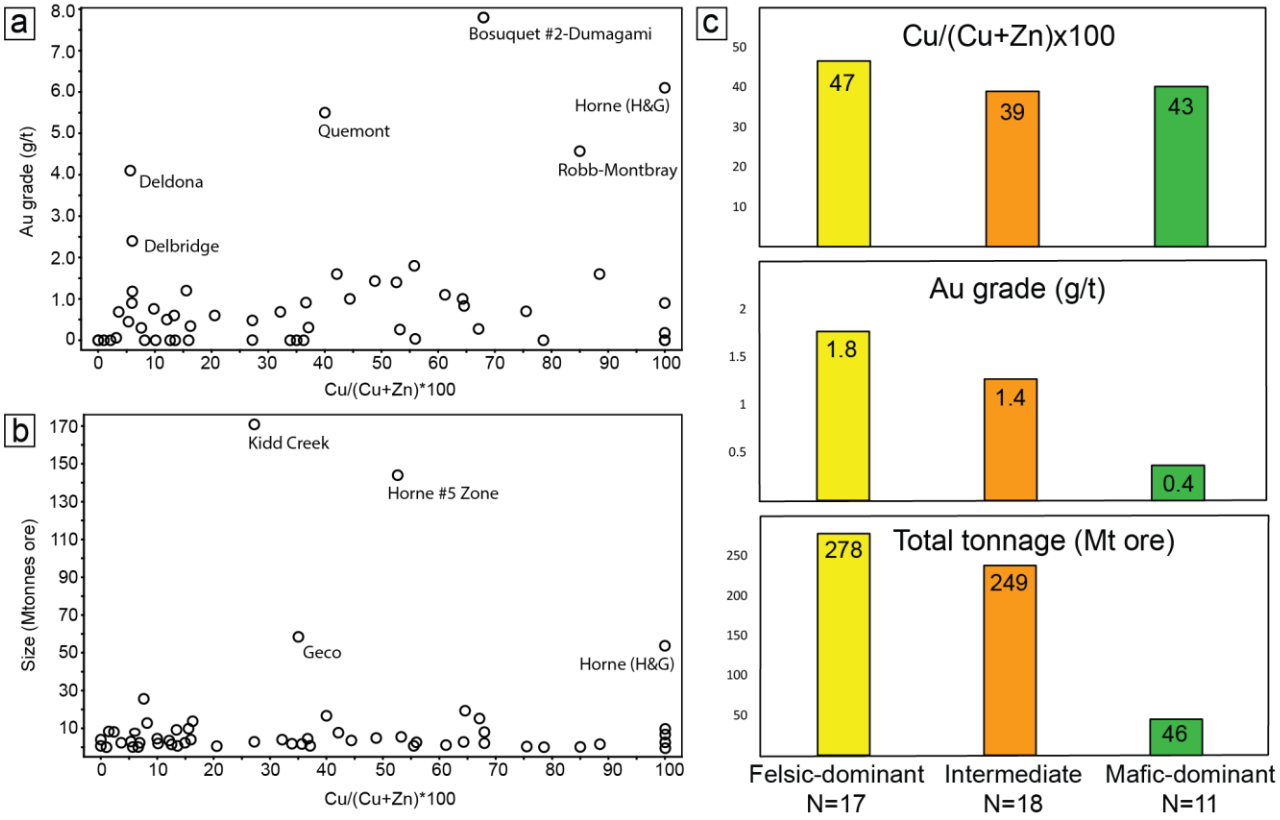

Figure 4.1 Sizes, grades, and host rocks of VMS deposits from the Superior Province. a) Biplot of Au grades of VMS deposits in the Superior versus bulk Cu/(Cu+Zn) grade ratios of the deposits (from past production and current reserves: Table 2.1) showing the range of bulk compositions (both Cu-rich and Zn-rich) among the deposits with the highest Au grades. b) Biplot of deposits sizes versus bulk Cu/(Cu+Zn) grade ratios showing the range of bulk compositions of deposits of different sizes. c) Histograms of average Cu/Cu+Zn grade ratios, average Au grades, and total ore tonnage for bimodal-mafic VMS deposits in the Abitibi Greenstone Belt classified by their immediate host rocks (this study): mafic-dominant with <100 m rhyolite or mafic: felsic volcanic rock ratios of 3:1; intermediate with 100–500 m rhyolite or mafic: felsic volcanic rock ratios of 1:1; felsic-dominant with >500 m of rhyolite or mafic: felsic volcanic rocks of 1:3; Table A.1). The felsic-dominant deposits are Cu-rich and have high Au grades and large tonnages; the deposits with more mafic host rocks are more Zn-rich, have lower Au grades and tend to be small. However, the largest and the most Au-rich deposits (Kidd Creek and Horne in a) and b) may be either Cu-rich or Zn-rich.

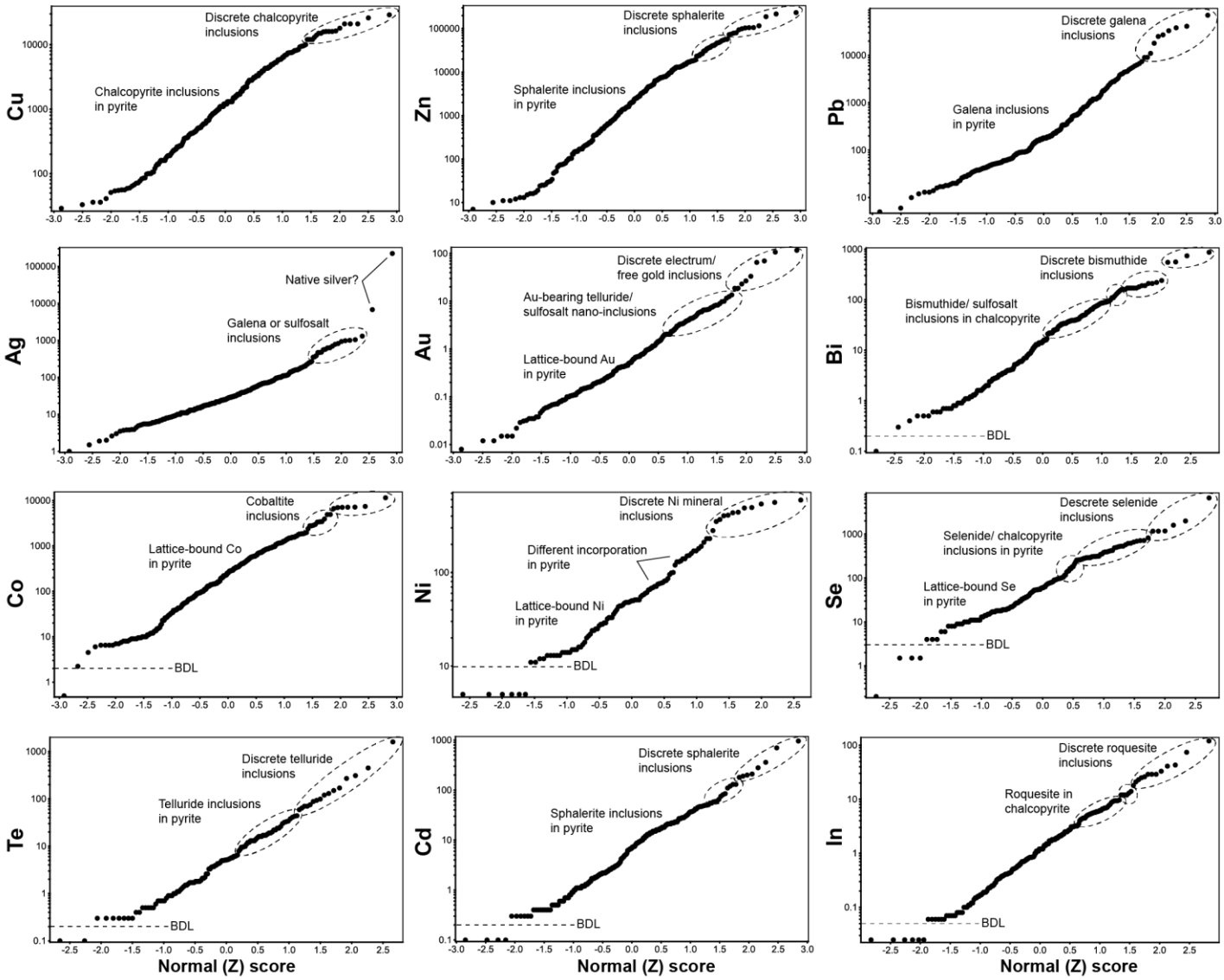
Cu
Discrete chalcopyrite inclusions
Chalcopyrite inclusions in pyrite
Zn
Discrete sphalerite inclusions
Sphalerite inclusions in pyrite
Pb
Discrete galena inclusions
Galena inclusions in pyrite
Ag
Native silver?
Galena or sulfosalt inclusions
Au
Discrete electrum/ free gold inclusions
Au-bearing telluride/ sulfosalt nano-inclusions
Lattice-bound Au in pyrite
Bi
Discrete bismuthide inclusions
Bismuthide/ sulfosalt inclusions in chalcopyrite
BDL
Co
Cobaltite inclusions
Lattice-bound Co in pyrite
BDL
Ni
Discrete Ni mineral inclusions
Different incorporation in pyrite
Lattice-bound Ni in pyrite
BDL
Se
Descrete selenide inclusions
Selenide/ chalcopyrite inclusions in pyrite
Lattice-bound Se in pyrite
BDL
Te
Discrete telluride inclusions
Telluride inclusions in pyrite
BDL
Cd
Discrete sphalerite inclusions
Sphalerite inclusions in pyrite
BDL
In
Discrete roquesite inclusions
Roquesite in chalcopyrite
BDL
Normal (Z) score
Normal (Z) score
Normal (Z) score

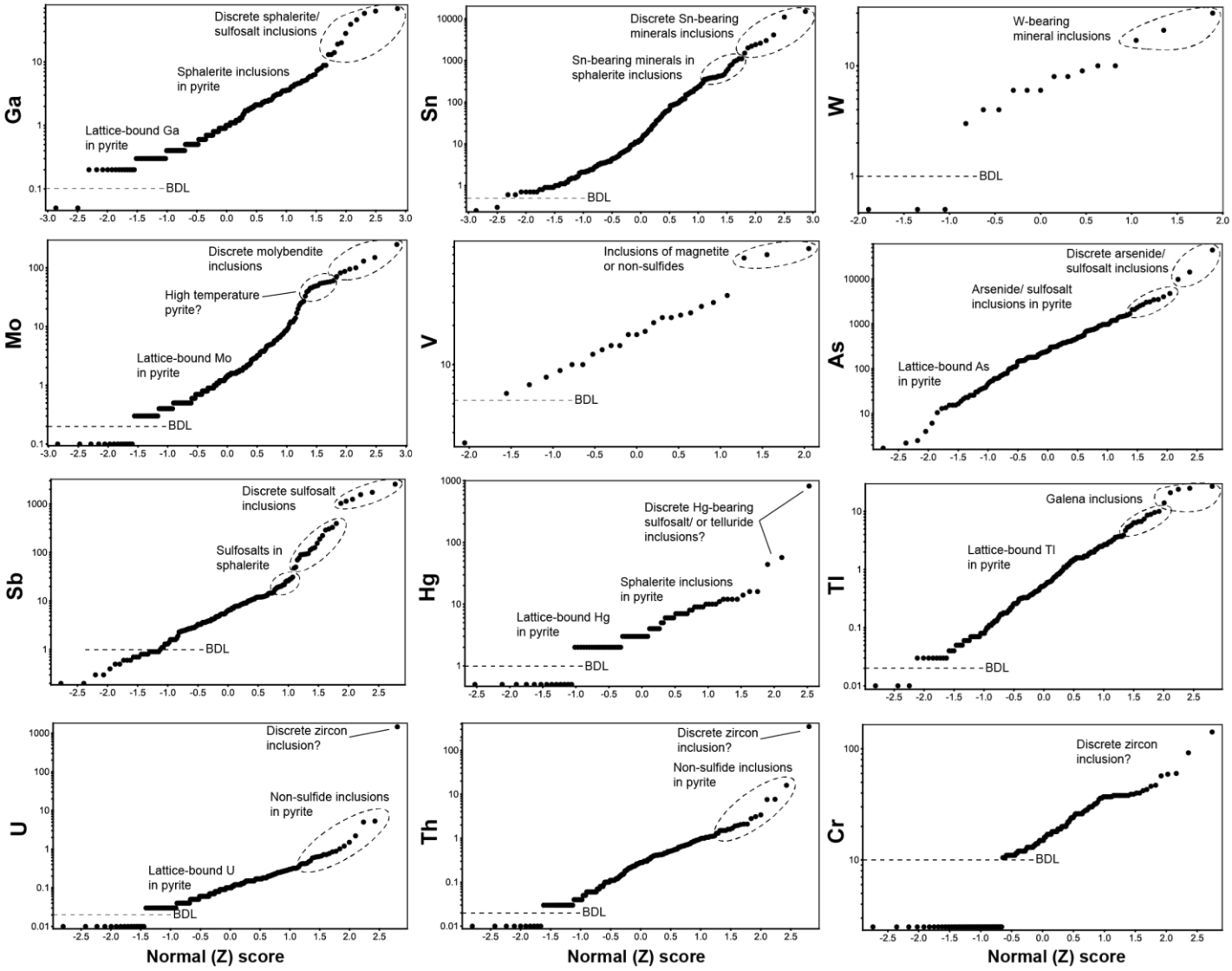

Figure 4.2 Log-probability plots of trace metal concentrations in pyrite mineral separates from VMS deposits of the Superior Province (Jonasson et al., 2020) used in this study. Only samples with more than 30% pyrite (5th percentile), and less than 2% chalcopyrite, 10% sphalerite and 2% galena (95-99th percentile) are included. Normal (continuous) distributions are shown for lattice-bound elements (Ag, Co, Ni, Se, Ga, As, and Tl). For populations with higher concentrations of the trace elements, we suggest that the trace elements are mainly hosted in mineral inclusions (e.g., Au, Bi, Te, Sn, Sb). Abbreviations: BDL (below detection limit values).

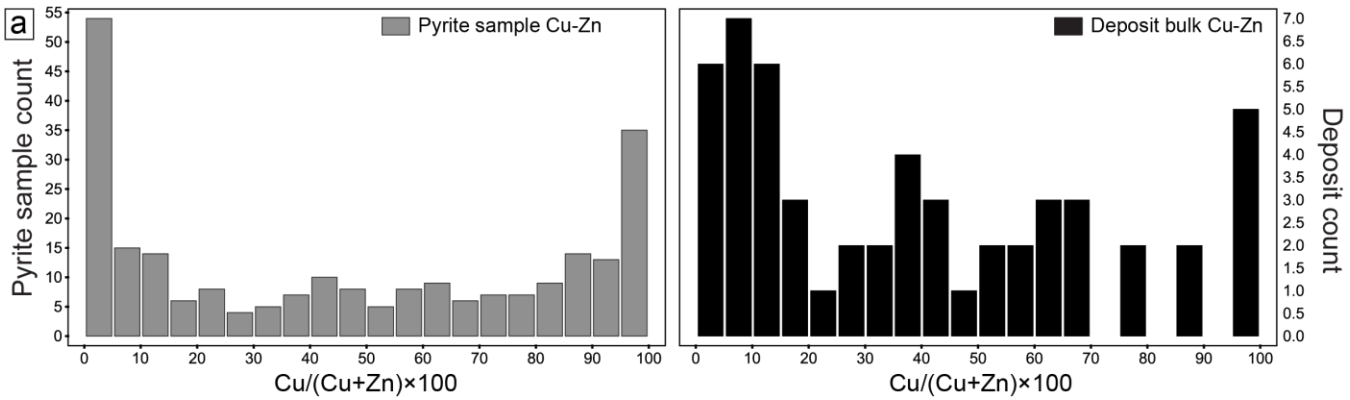
a
Pyrite sample Cu-Zn
Pyrite sample count
Cu/(Cu+Zn)×100
Deposit bulk Cu-Zn
Deposit count
Cu/(Cu+Zn)×100

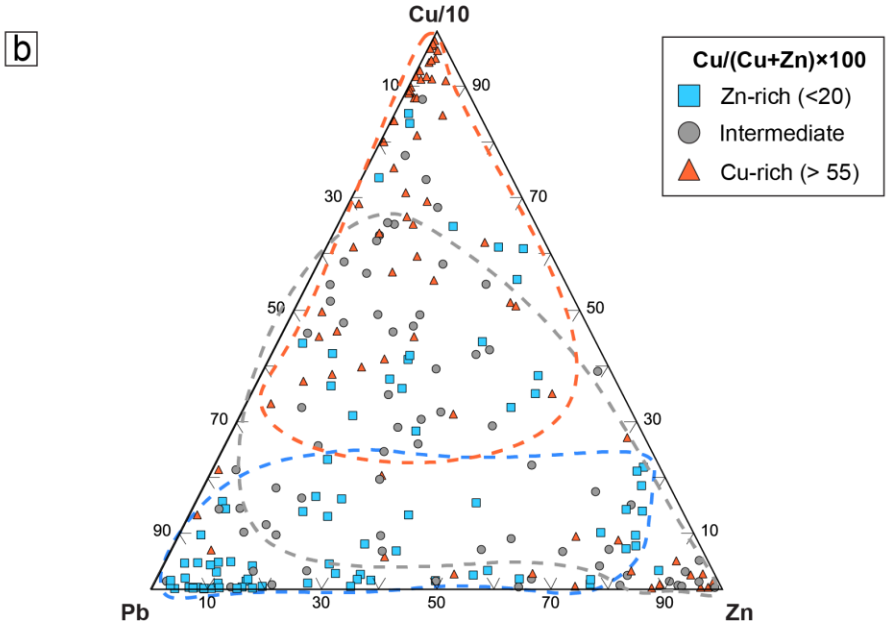
b
Cu/10
Cu/(Cu+Zn)×100
Zn-rich (<20)
Intermediate
Cu-rich (> 55)
Pb
Zn

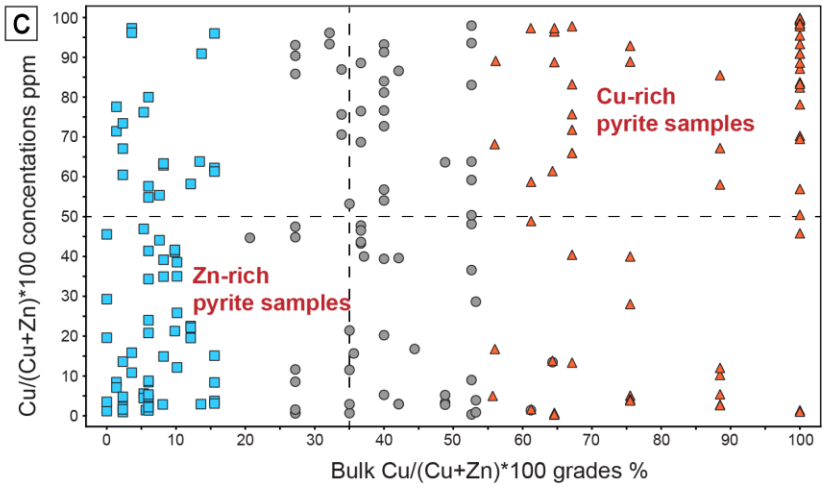
c
Cu/(Cu+Zn)*100 concentations ppm
Bulk Cu/(Cu+Zn)*100 grades %
Cu-rich
pyrite samples
Zn-rich
pyrite samples

Figure 4.3 a) Histogram showing the distribution of Cu/Cu+Zn concentration ratios (ppm) of pyrite mineral separates from Jonasson et al. (2020) compared to the bulk Cu/Cu+Zn grade ratios of the deposits. Both data sets show a similar bimodal distribution interpreted to reflect a combination of source rock controls and conditions of mineralization (e.g., temperature of formation, zone refining). b) Cu-Zn-Pb ternary plot of trace metal concentrations in pyrite samples from VMS deposits classified according to Cu/(Cu+Zn) grade ratio. The deposit classes are: Cu/(Cu+Zn) <20 (Zn-rich deposits; n=22), Cu/(Cu+Zn) =20–55 (Intermediate; n=15), and Cu/(Cu+Zn) >55 (Cu-rich deposits; n=17). The contours outline the distribution of 90% of the pyrite samples in each class. Clusters at the Cu, Zn, and Pb corners correspond to pyrite samples with chalcopyrite, sphalerite and galena inclusions. c) Binary plot of bulk Cu/(Cu+Zn) grade ratios of VMS deposits versus Cu/(Cu+Zn) concentration ratios of pyrite mineral separates from the same deposits showing the separation of samples into Cu-rich and Zn-rich populations. The classifications are: Zn-rich pyrite samples from Zn-rich deposits (Cu/Cu+Zn grade ratio <20); Cu-rich pyrite samples from Cu-rich deposits (Cu/Cu+Zn grade ratio >55); Cu-rich pyrite samples from Zn-rich deposits (Cu/Cu+Zn grade ratio <20); Zn-rich pyrite samples from Cu-rich deposits (Cu/Cu+Zn grade ratio >55); and Zn-rich pyrite samples from Zn-rich deposits (Cu/Cu+Zn grade ratio <20).

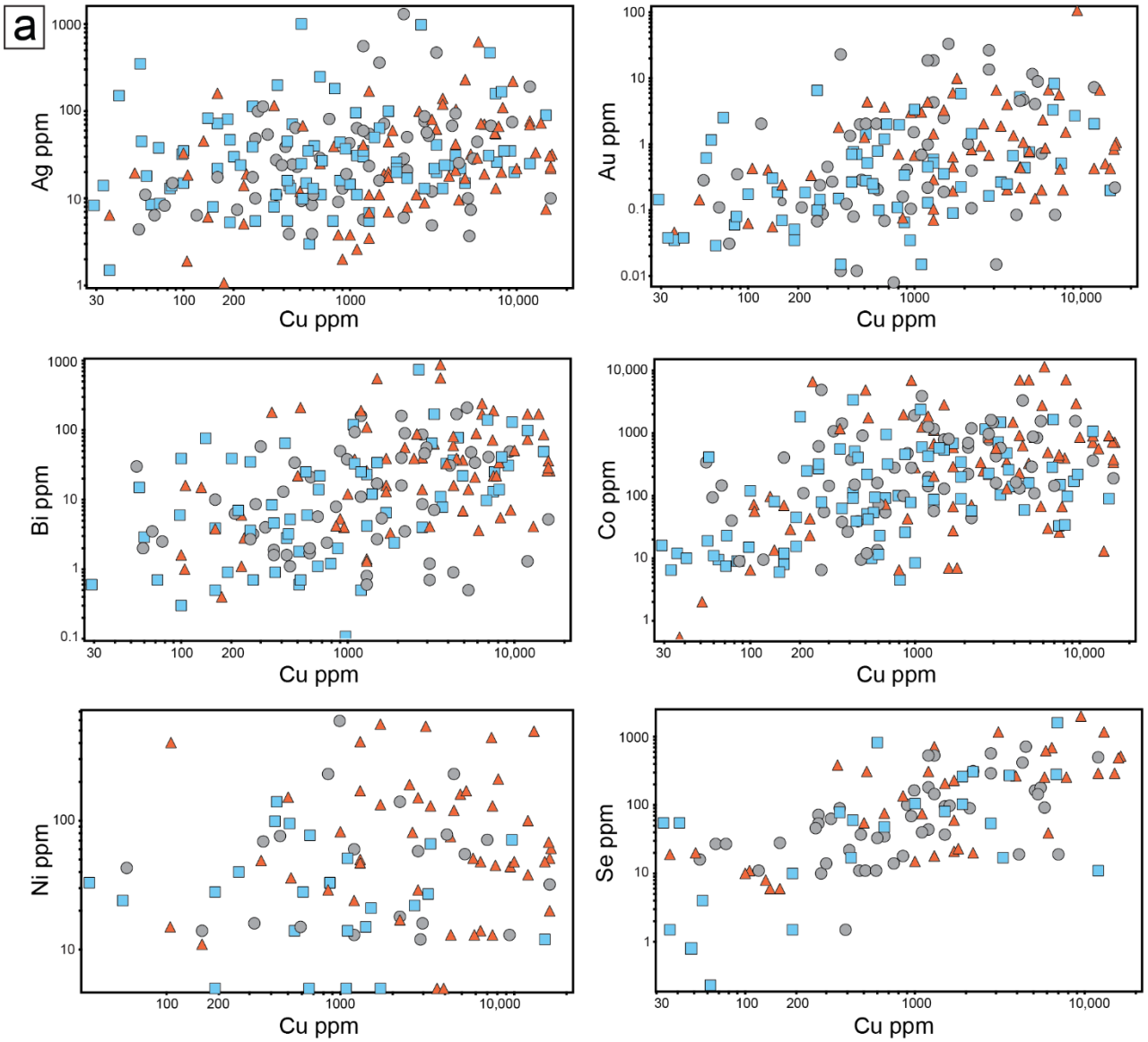
a
Ag ppm
Cu ppm
Au ppm
Cu ppm
Bi ppm
Cu ppm
Co ppm
Cu ppm
Ni ppm
Cu ppm
Se ppm
Cu ppm

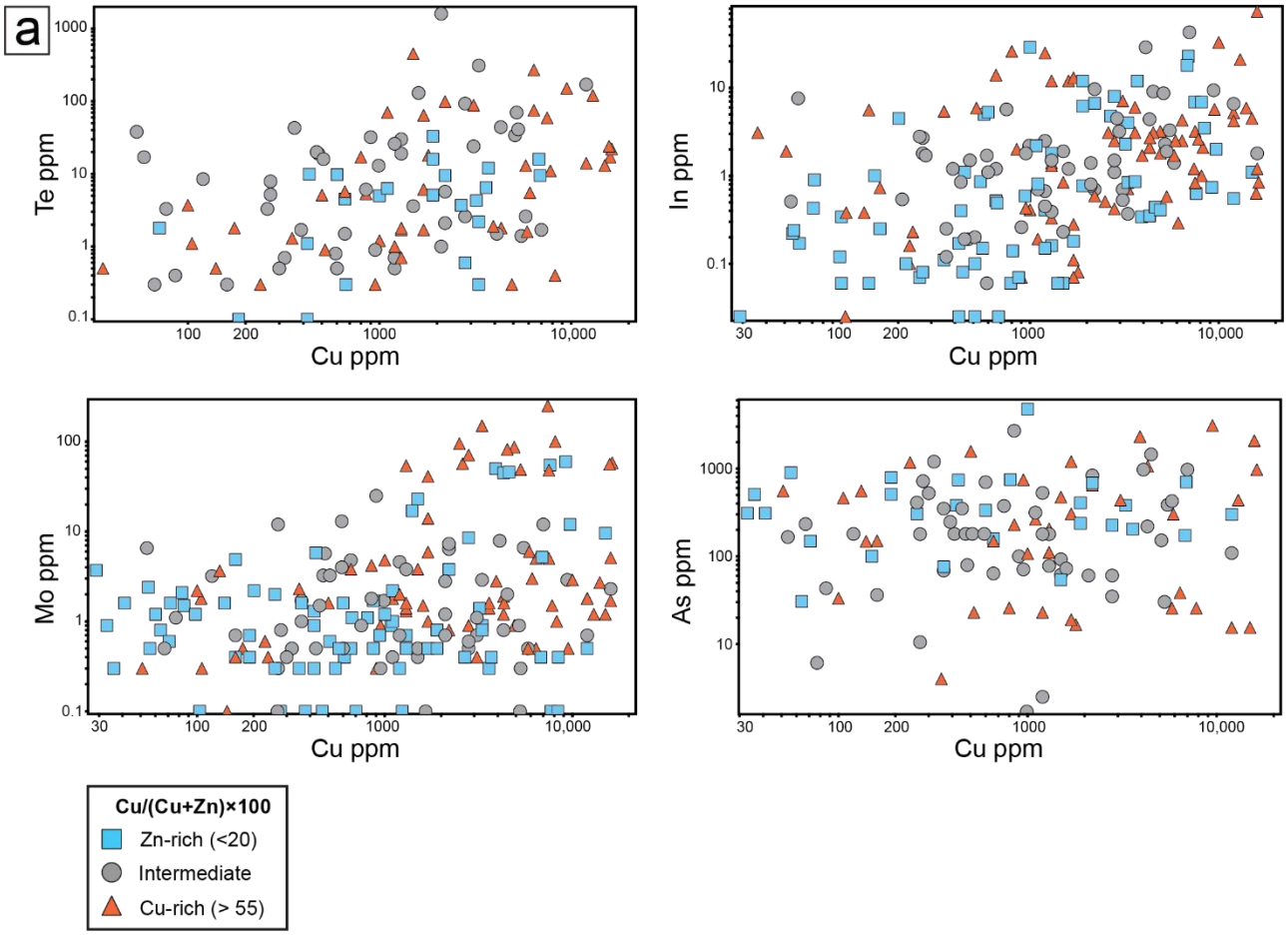

Figure 4.4 a) Binary plots of Cu versus Ag, Au, Bi, Co, Ni, Se, Te, In, Mo and As (concentrations in ppm) in pyrite samples from VMS deposits classified according to Cu/(Cu+Zn) grade ratios. The deposit classes are: Cu/(Cu+Zn) <20 (Zn-rich deposits; n=22), Cu/(Cu+Zn) = 20–55 (Intermediate; n=15), and Cu/(Cu+Zn) >55 (Cu-rich deposits; n=17). The plots in a) show Au, Bi, Co, Ni, Se, Te, In, and Mo are positively correlated with Cu in the pyrite separates and with bulk Cu/(Cu+Zn) ratios of the deposits. Ag and As show a bimodal distribution in Cu- and Zn-rich samples.

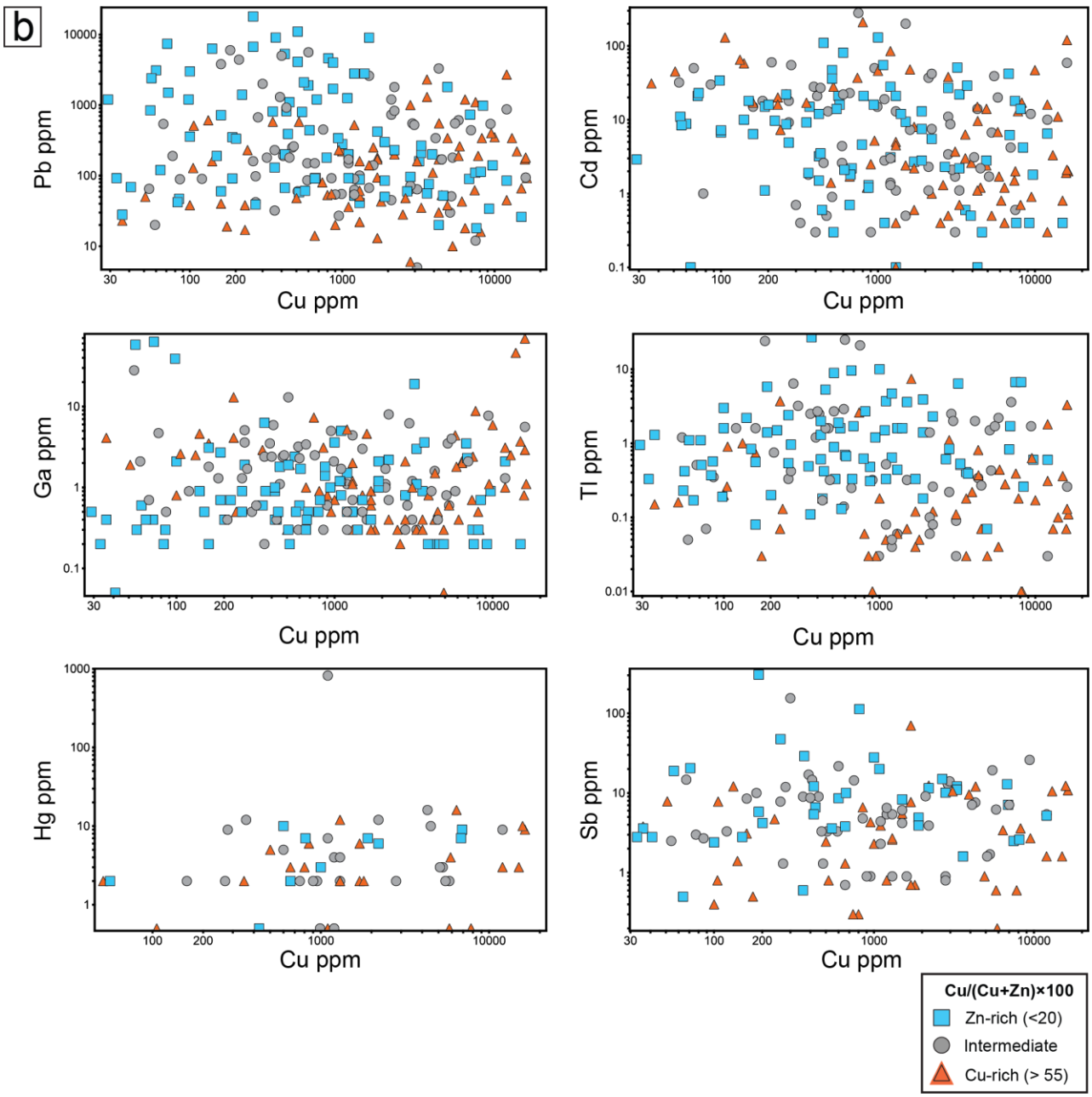

Figure 4.4 b) Binary plots of Cu versus Pb, Ga, Sn, Sb, Hg, and Tl (concentrations in ppm) in pyrite samples from VMS deposits classified according to Cu/(Cu+Zn) grade ratios of the deposits. The deposit classes are: Cu/(Cu+Zn) <20 (Zn-rich deposits; n=22), Cu/(Cu+Zn) = 20–55 (Intermediate; n=15), and Cu/(Cu+Zn) >55 (Cu-rich deposits; n=17). The plots in b) show Pb, Cd, Ga, Sb, Hg, and Tl are negatively correlated or shown no correlation with Cu in the pyrite separates and show no correlation with the bulk Cu/(Cu+Zn) ratios of the deposits.

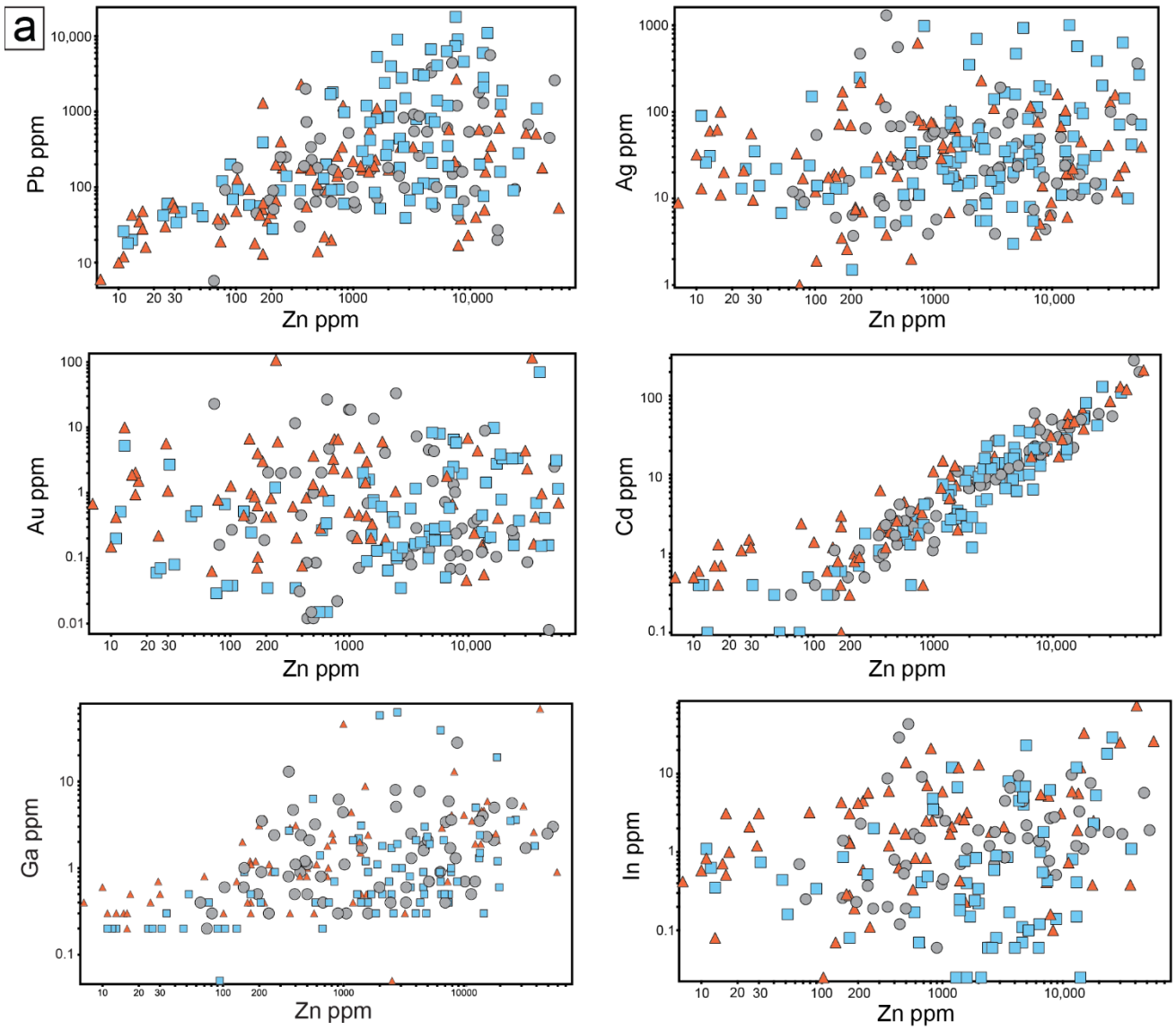
a
Pb ppm
Zn ppm
Ag ppm
Zn ppm
Au ppm
Zn ppm
Cd ppm
Zn ppm
Ga ppm
Zn ppm
In ppm
Zn ppm

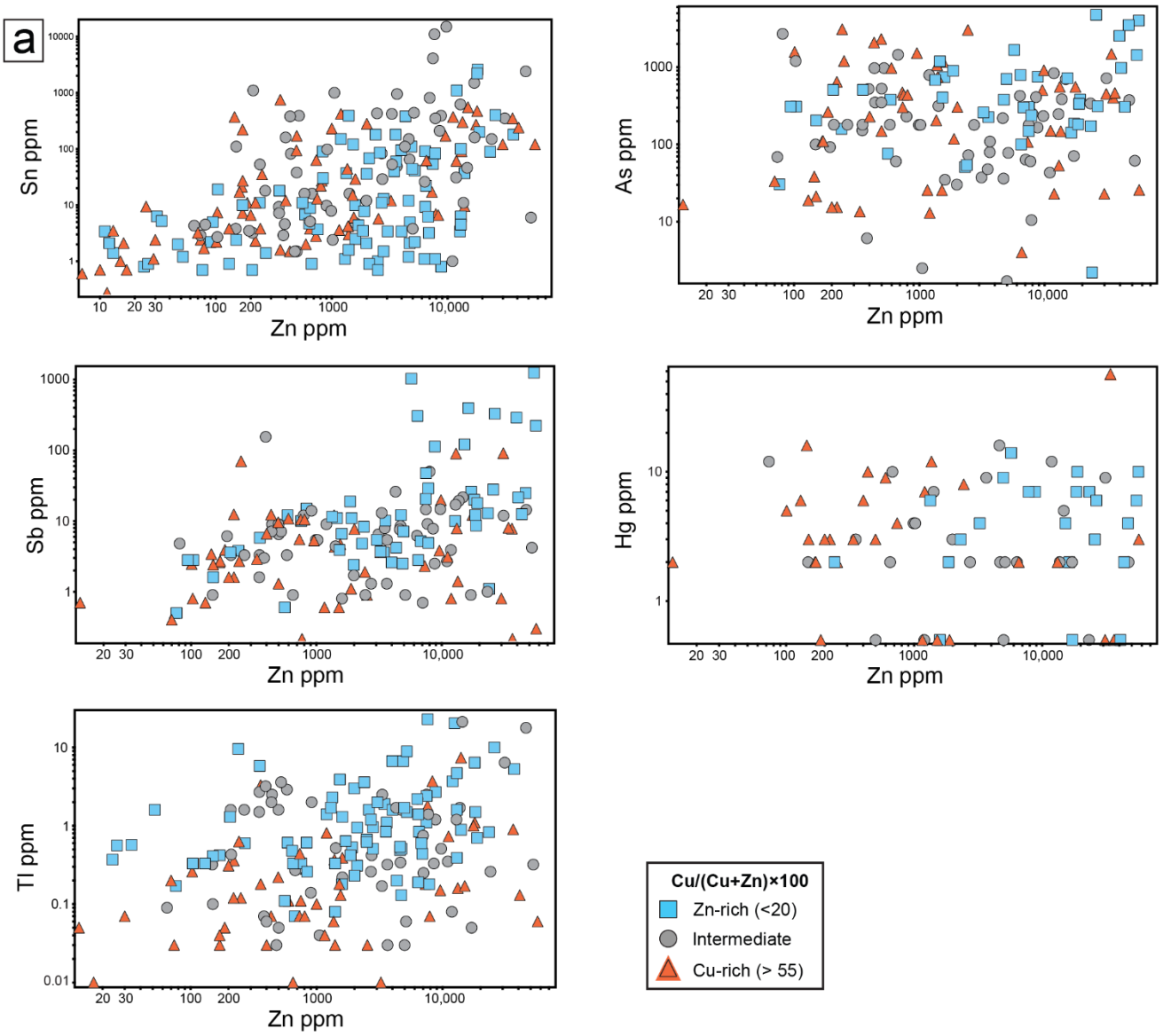

Figure 4.5 a) Binary plots of Zn versus Pb, Ag, Cd, Ga, In, Sn, As, Sb, Hg, and Tl (concentrations in ppm) in pyrite samples from VMS deposits classified according to Cu/(Cu+Zn) grade ratios of the deposits. The deposit classes are: Cu/(Cu+Zn) <20 (Zn-rich deposits; n=22), Cu/(Cu+Zn) = 20–55 (Intermediate; n=15), and Cu/(Cu+Zn) >55 (Cu-rich deposits; n=17). The plots in a) show Pb, Ag, Cd, In, Ga, Sn, As, Sb, Hg, and Tl are positively correlated with Zn in the pyrite separates and show no correlation with the bulk Cu/(Cu+Zn) ratios of the deposits.

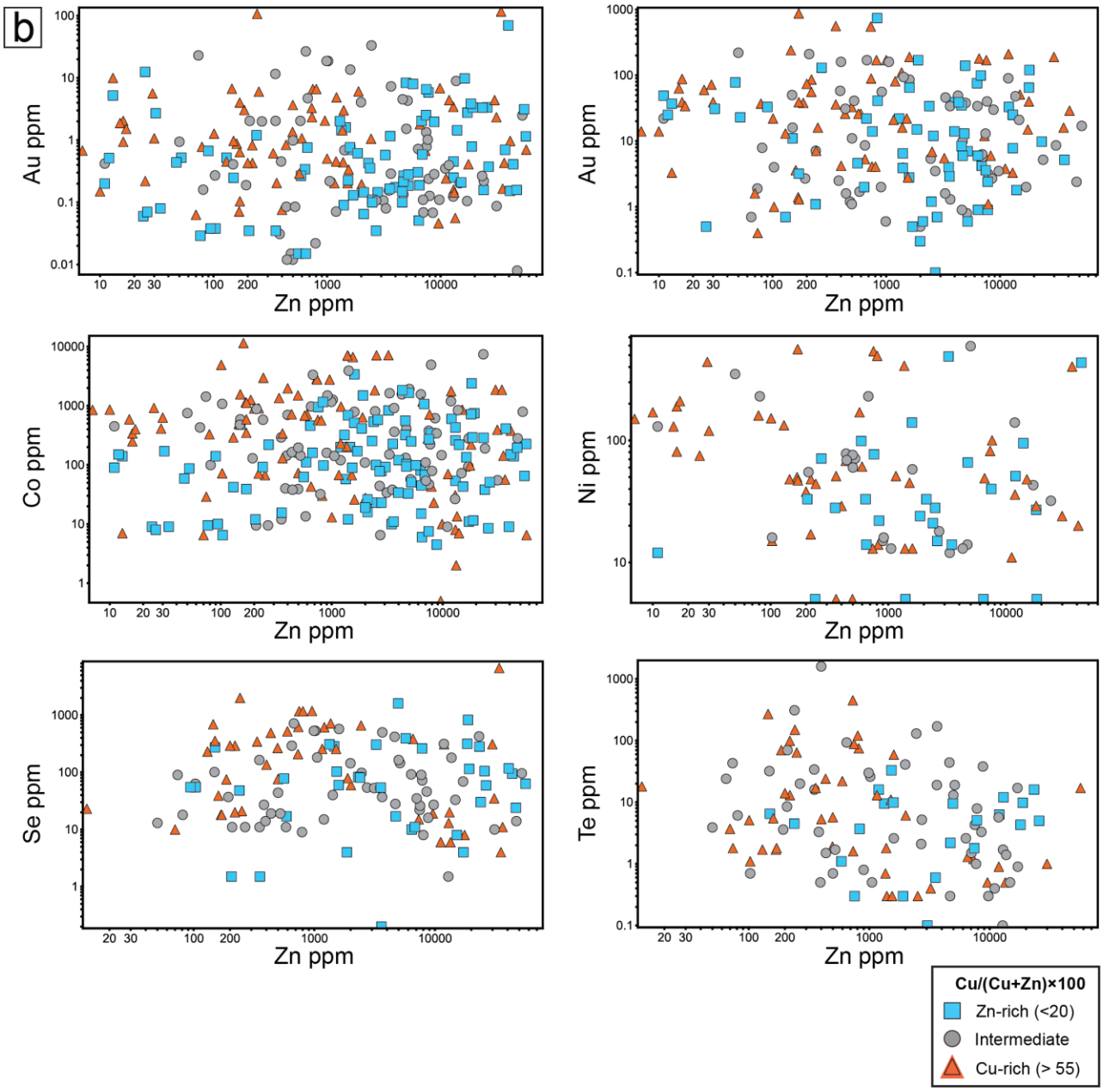

Figure 4.5 b) Binary plots of Zn versus Au, Bi, Co, Ni, Se, and Te (concentrations in ppm) in pyrite samples from VMS deposits classified according to Cu/(Cu+Zn) grade ratios of the deposits. The deposit classes are: Cu/(Cu+Zn) <20 (Zn-rich deposits; n=22), Cu/(Cu+Zn) = 20–55 (Intermediate; n=15), and Cu/(Cu+Zn) >55 (Cu-rich deposits; n=17). The plots in b) show Au, Bi, Co, Ni, Se, and Te are negatively correlated with Zn in the pyrite separates and show no correlation with the bulk Cu/(Cu+Zn) ratios of the deposits.

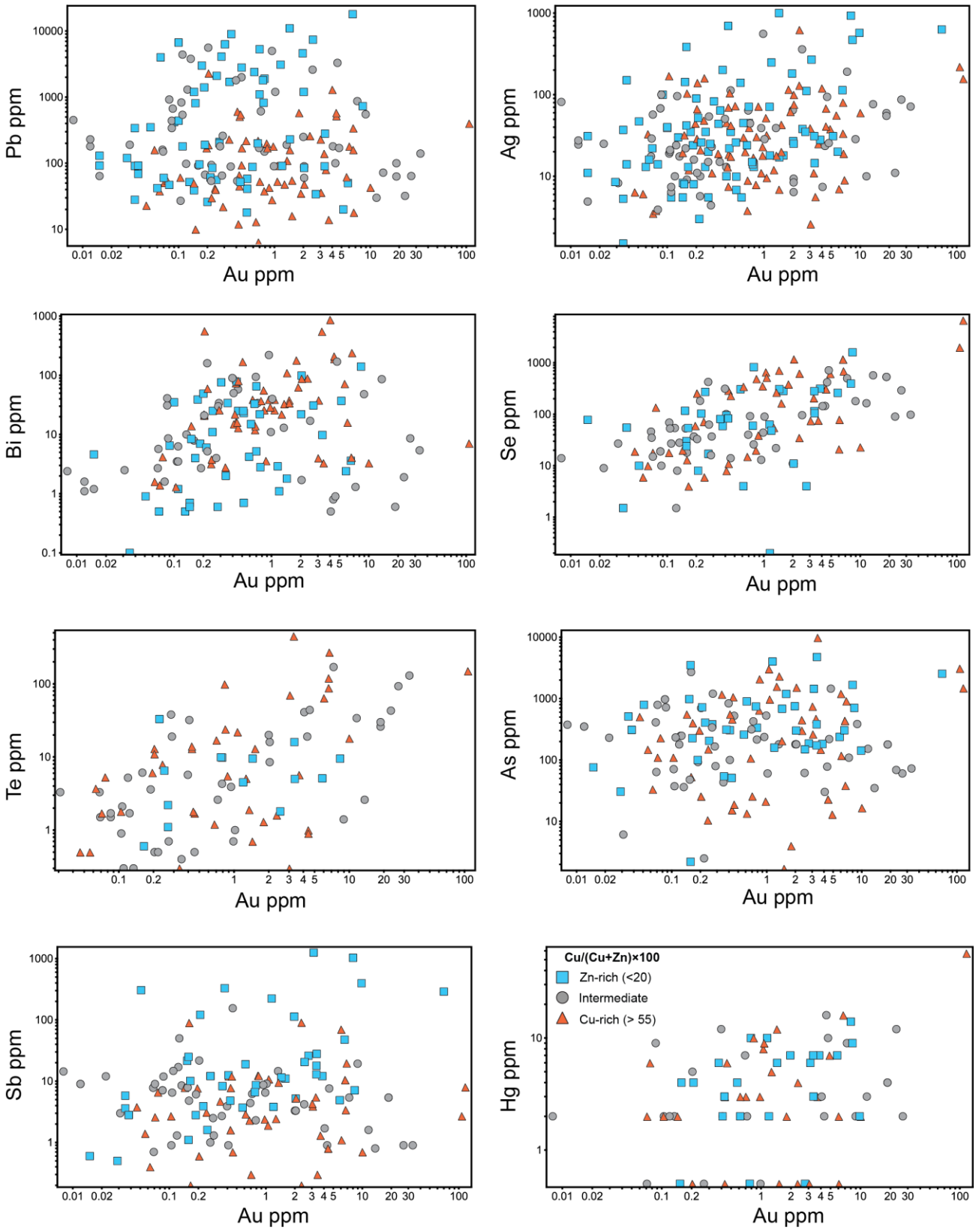
Pb ppm
Au ppm
Ag ppm
Au ppm
Bi ppm
Au ppm
Se ppm
Au ppm
Te ppm
Au ppm
As ppm
Au ppm
Sb ppm
Au ppm
Hg ppm
Au ppm
Cu/(Cu+Zn)×100
Zn-rich (<20)
Intermediate
Cu-rich (> 55)

Figure 4.6 Binary plots of Au versus Pb, Ag, Bi, Co, Se, Te, As, Sb, and Hg (concentrations in ppm) in pyrite samples from VMS deposits classified according to Cu/(Cu+Zn) grade ratio. The deposit classes are: Cu/(Cu+Zn) <20 (Zn-rich deposits; n=22), Cu/(Cu+Zn) = 20–55 (Intermediate; n=15), and Cu/(Cu+Zn) >55 (Cu-rich deposits; n=17). The Au concentrations in the pyrite samples show a bimodal distribution co-enriched with Bi, Se, and Te in the Cu-rich deposits and with Ag, As, Sb, and Hg in the Zn-rich-deposits.

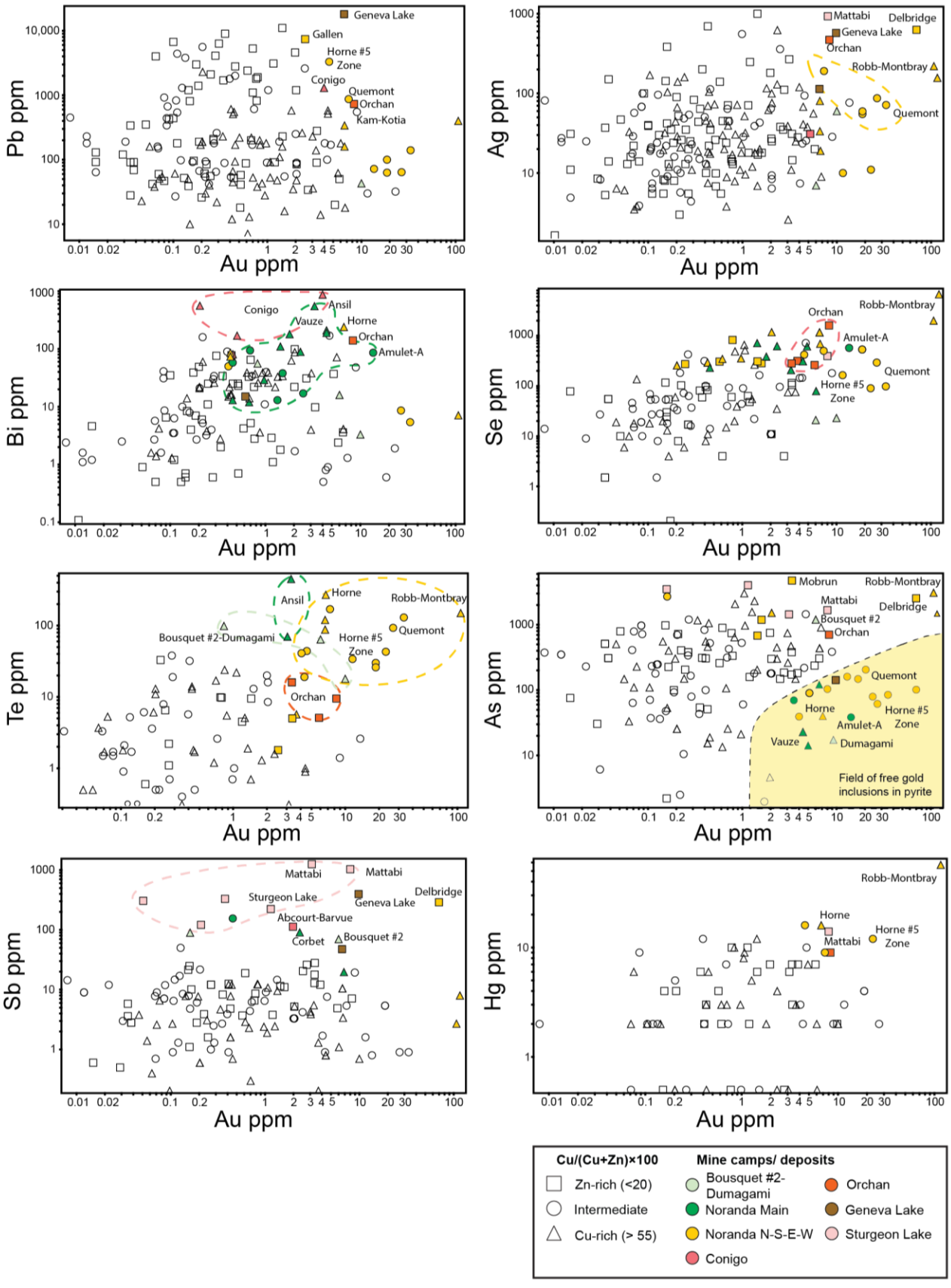
Pb ppm
Au ppm
Geneva Lake
Gallen
Horne #5
Zone
Conigo
Quemont
Orchan
Kam-Kotia
Ag ppm
Mattabi
Delbridge
Geneva Lake
Orchan
Robb-Montbray
Quemont
Bi ppm
Conigo
Ansil
Vauze
Horne
Orchan
Amulet-A
Se ppm
Orchan
Robb-Montbray
Amulet-A
Quemont
Horne #5
Zone
Te ppm
Ansil
Horne
Robb-Montbray
Quemont
Bousquet #2-Dumagami
Horne #5
Zone
Orchan
As ppm
Mobrun
Robb-Montbray
Mattabi
Delbridge
Bousquet #2
Orchan
Quemont
Horne
Horne #5
Zone
Amulet-A
Vauze
Dumagami
Field of free gold
inclusions in pyrite
Sb ppm
Mattabi
Mattabi
Sturgeon Lake
Delbridge
Geneva Lake
Abcourt-Barvue
Corbet
Bousquet #2
Hg ppm
Robb-Montbray
Horne
Horne #5
Mattabi
Zone
Cu/(Cu+Zn)×100
Zn-rich (<20)
Intermediate
Cu-rich (> 55)
Mine camps/ deposits
Bousquet #2-
Dumagami
Noranda Main
Noranda N-S-E-W
Conigo
Orchan
Geneva Lake
Sturgeon Lake

Figure 4.7 Binary plots of Au versus Pb, Ag, Bi, Co, Se, Te, As, Sb, and Hg (concentrations in ppm) in pyrite samples from VMS deposits classified by mine camp (most correlated samples). In the Au-As plot, the "Au saturation" line in pyrite is based on the Au/As molar ratio from Reich et al. (2005). A lack of correlation between Au and As in the pyrite samples is consistent with little Au present in solid solution. High Au concentrations in pyrite samples from Horne, Quemont, and Bousquet #2-Dumagami correlate with Bi-Te and Ag-Te, reflecting the presence of inclusions of calaverite, petzite, and hessite. High Au concentrations (>7 ppm) correlated with high Pb suggest the presence of inclusions of galena and/or Pb-Sb-As sulfosalts with the Au, including in samples from Robb-Montbray, Delbridge, Normetal, Manitou-Barvue, Kam Kotia, Mattabi, and Geneva Lake.

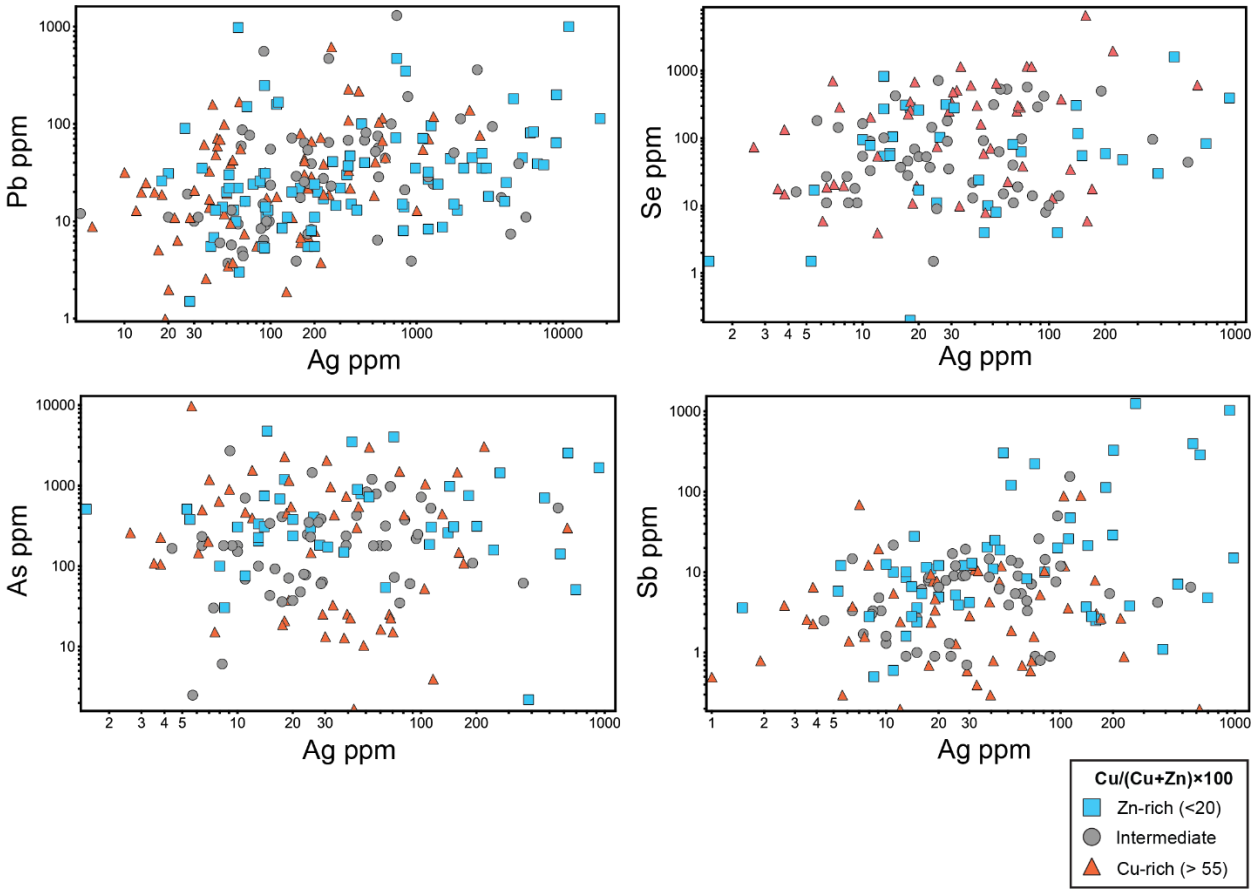

Figure 4.8 Binary plots of Ag versus Pb, Se, As, and Sb (concentrations in ppm) in pyrite samples from VMS deposits classified according to Cu/(Cu+Zn) grade ratio. The deposit classes are: Cu/(Cu+Zn) <20 (Zn-rich deposits; n=22), Cu/(Cu+Zn) = 20–55 (Intermediate; n=15), and Cu/(Cu+Zn) >55 (Cu-rich deposits; n=17). The plotted elements may be present in inclusions of sphalerite, galena or sulfosalts in pyrite (e.g., Pb and Sn), or they may be present in solid solution at lower concentrations (e.g., As).

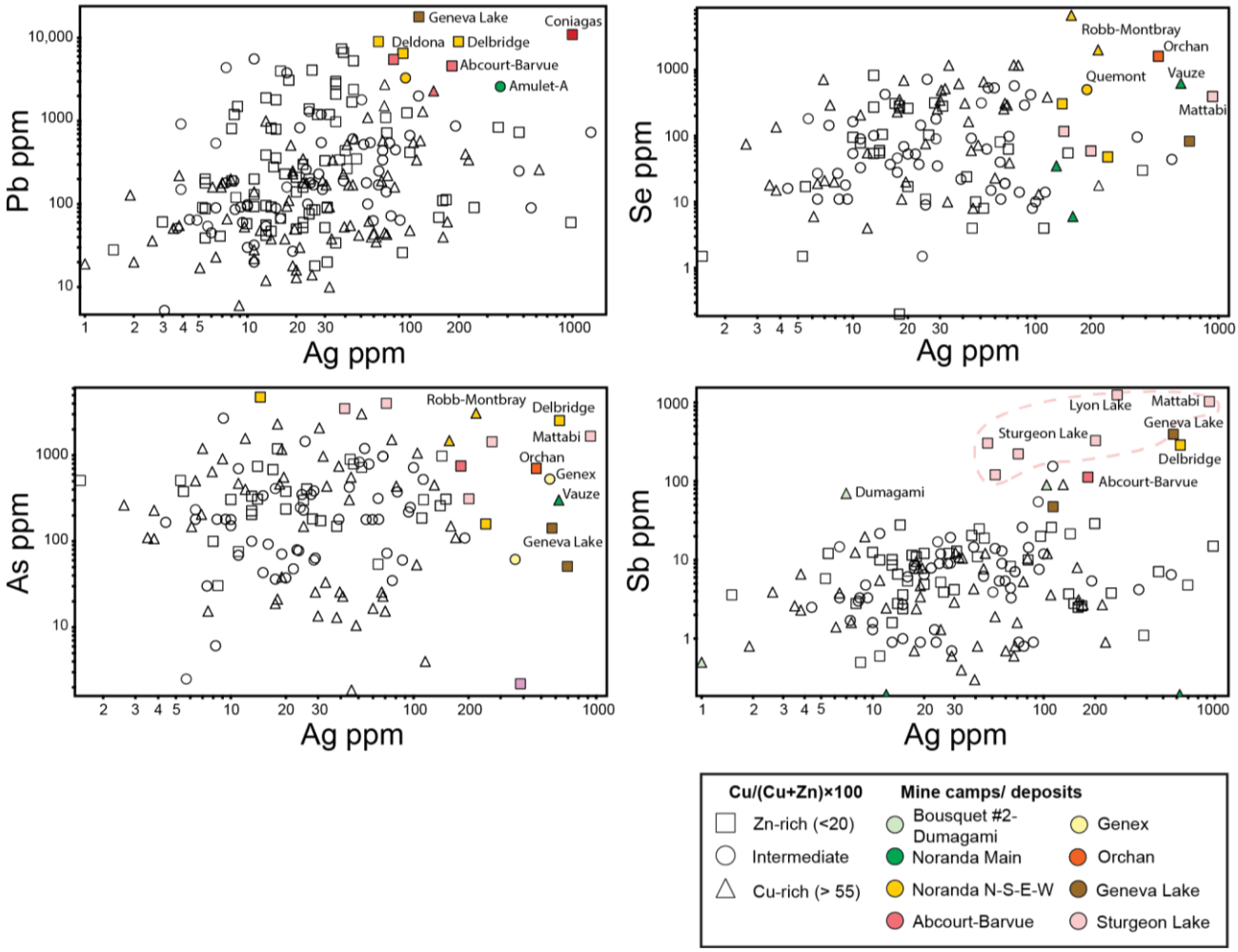

Figure 4.9 Binary plots of Ag versus Pb, Se, As, and Sb (concentrations in ppm) in pyrite samples from VMS deposits classified by mine camp (most correlated samples). Ag correlates most strongly with Pb and is likely present in many pyrite samples as Ag-bearing inclusions of galena or Pb-rich sulfosalts (e.g., samples from Manitou-Barvue, Normetal, Mattabi, Lyon Lake, South Bay, Sturgeon Lake).

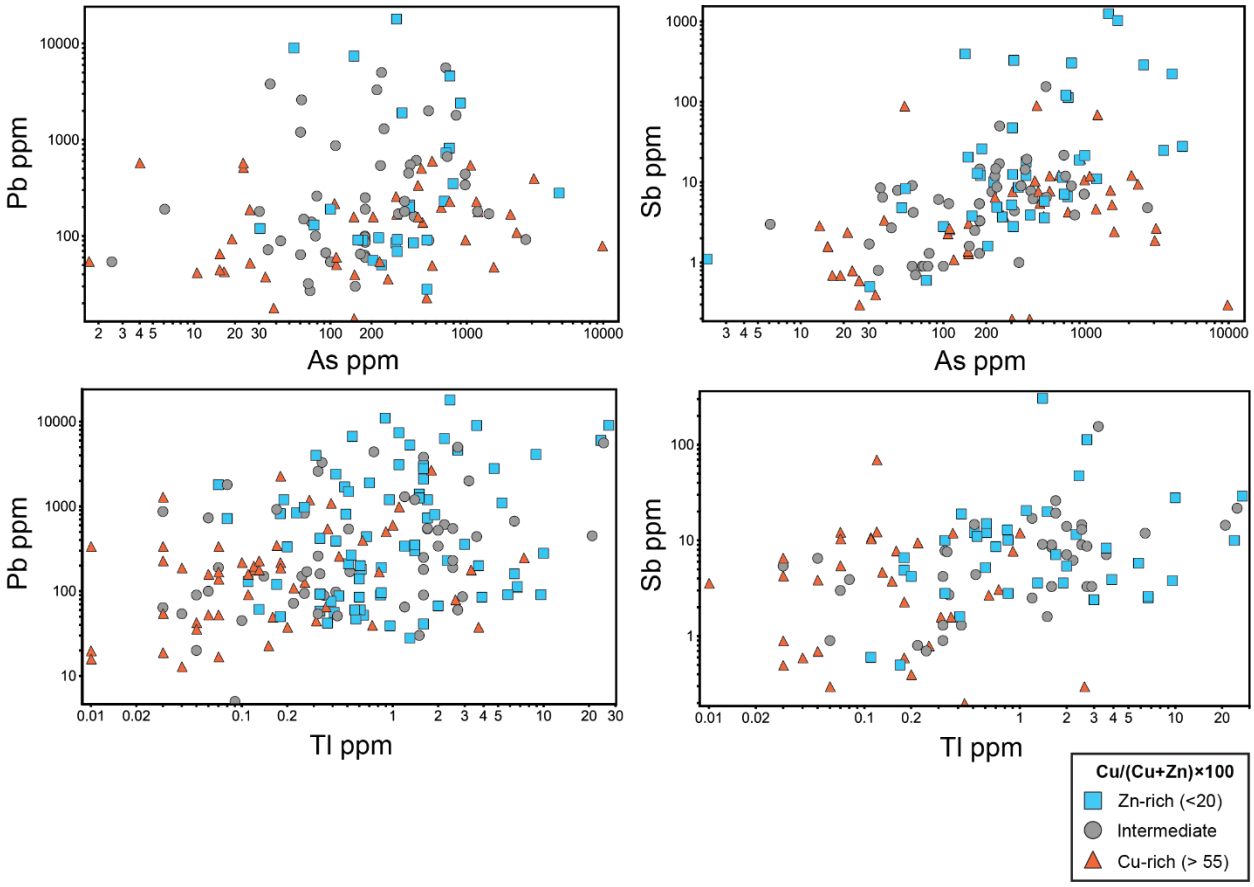

Figure 4.10 Binary plots of As and Tl versus Pb and Sb (concentrations in ppm) in pyrite samples from VMS deposits classified according to Cu/(Cu+Zn) grade ratio. The deposit classes are: Cu/(Cu+Zn) <20 (Zn-rich deposits; n=22), Cu/(Cu+Zn) = 20–55 (Intermediate; n=15), and Cu/(Cu+Zn) >55 (Cu-rich deposits; n=17). As and Tl may be present in sphalerite, galena or sulfosalts at higher concentrations and in solid solution at lower concentrations.

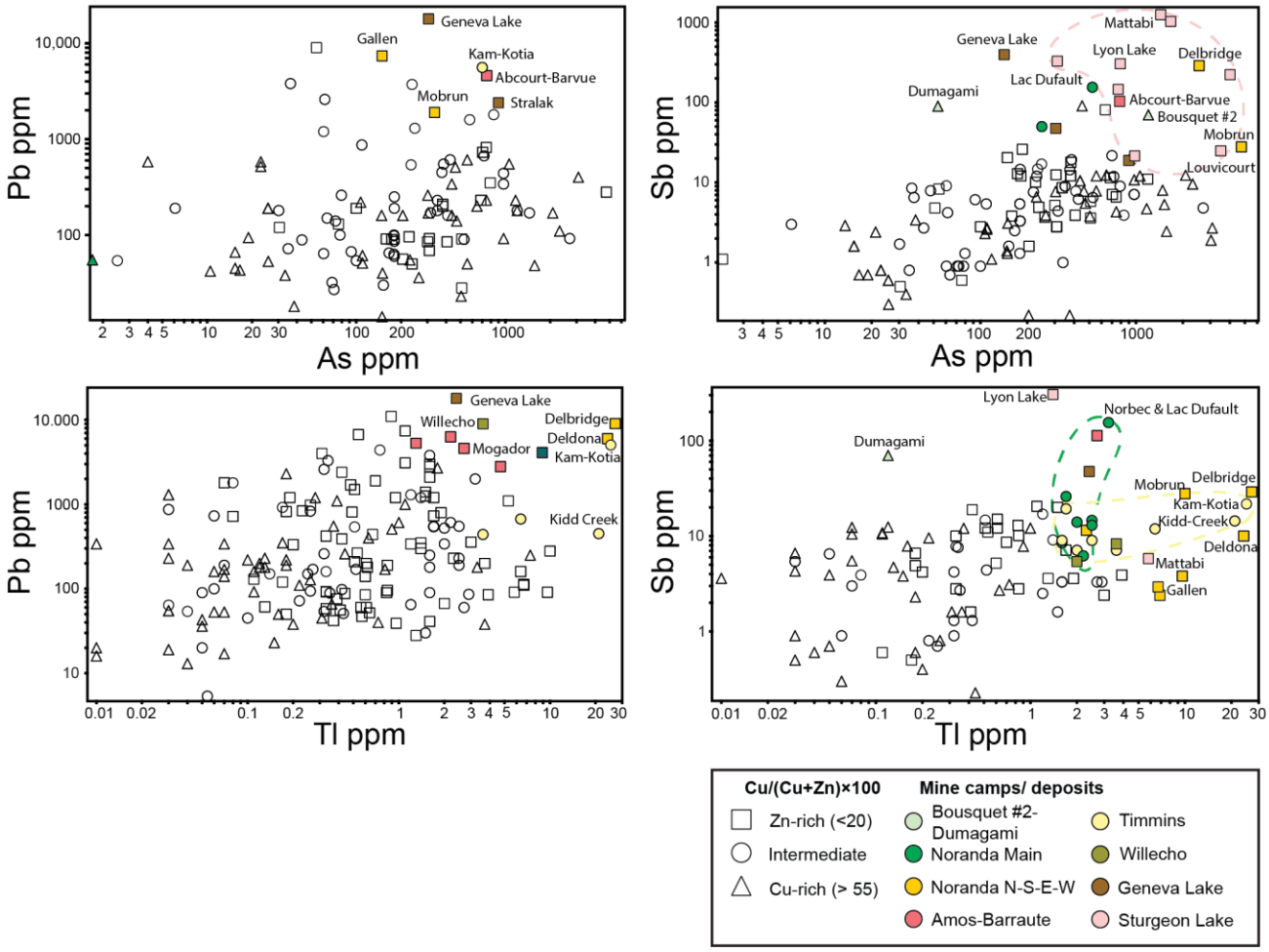

Figure 4.11 Binary plots of As and Tl versus Pb and Sb (concentrations in ppm) in pyrite samples from VMS deposits classified by mine camp (most correlated samples). As and Tl show the strongest correlations with Sb in samples from Delbridge, Mobrun, Bousquet #2 Abcourt Barvue, Manitou Barvue, Lyon Lake, and Mattabi.

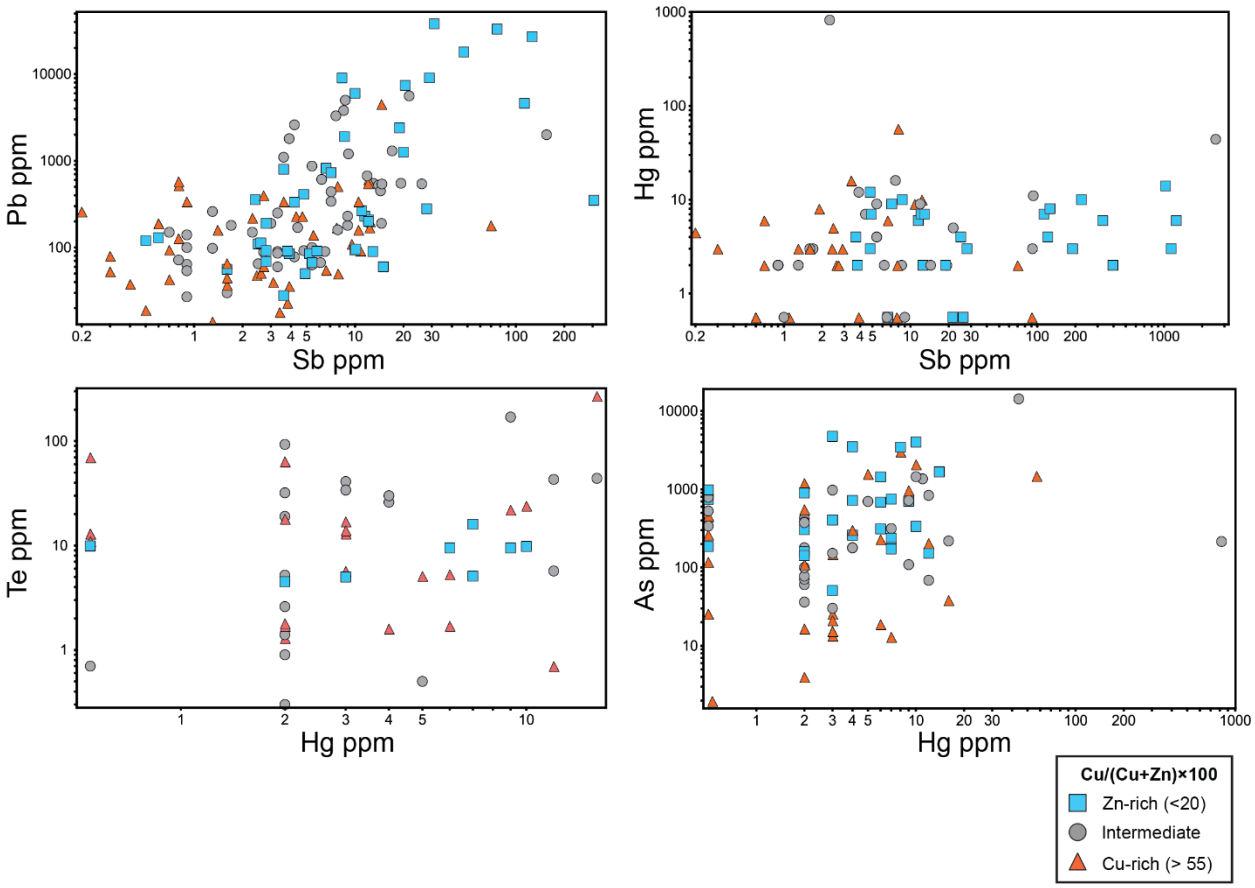

Figure 4.12 Binary plots of Sb and Hg versus Pb, Sb, and Te (concentrations in ppm) in pyrite samples from VMS deposits classified according to Cu/(Cu+Zn) grade ratio. The deposit classes are: Cu/(Cu+Zn) <20 (Zn-rich deposits; n=22), Cu/(Cu+Zn) = 20–55 (Intermediate; n=15), and Cu/(Cu+Zn) >55 (Cu-rich deposits; n=17). The strong correlation of Sb with Pb and Hg in some samples likely indicates the presence of tetrahedrite or other low-temperature sulfosalts. Hg shows a stronger correlation with Te than As in the samples suggesting Hg-tellurides are more common than Hg-bearing tennantite, which has been identified in some deposits.

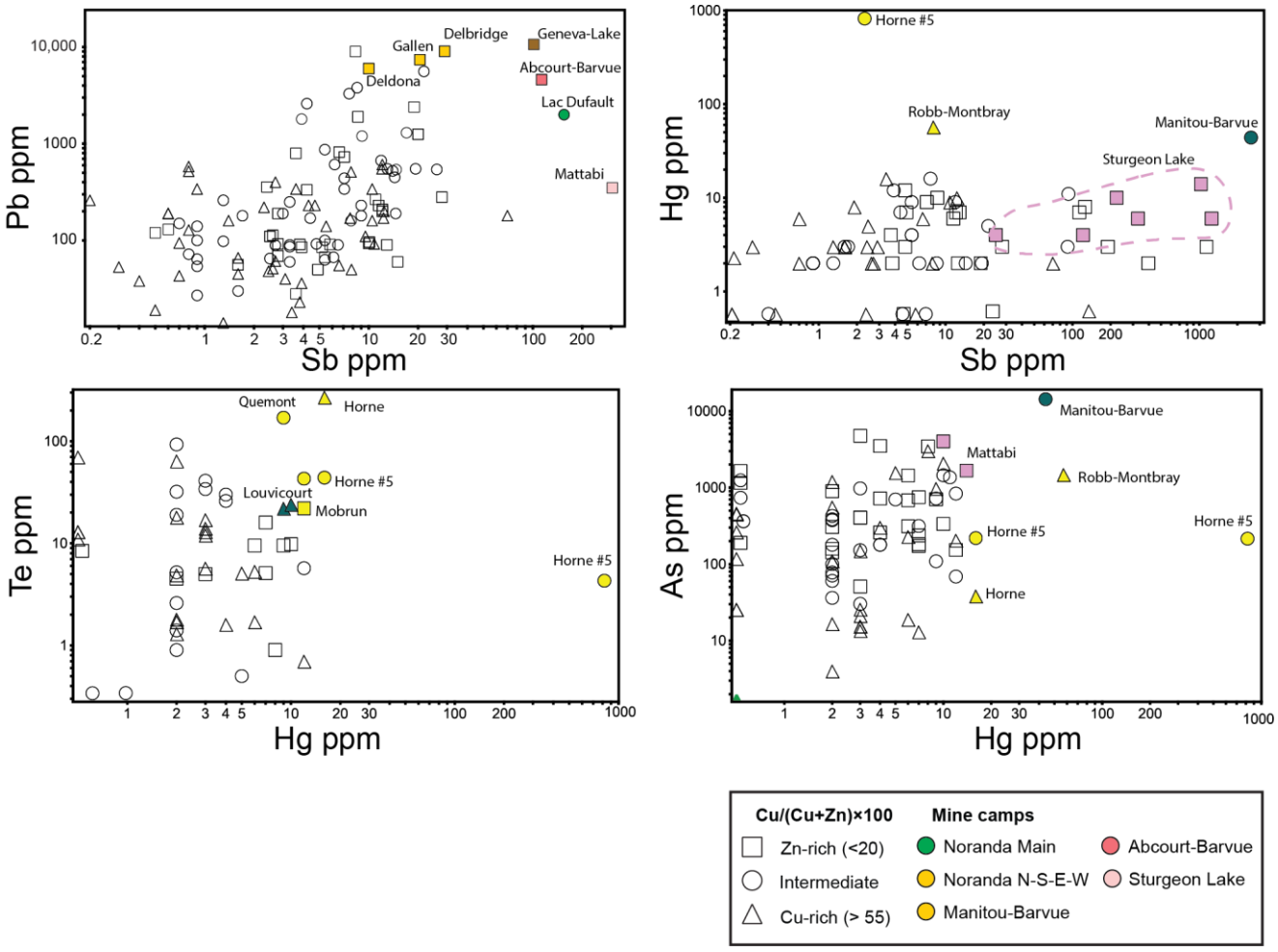

Figure 4.13 Binary plots of Sb and Hg versus Pb, Sb, and Te (concentrations in ppm) in pyrite samples from VMS deposits classified by mine camp (most correlated samples). The association of Sb with Zn in pyrite samples from Delbridge, Kidd Creek, Manitou Barvue, Geneva Lake, Lyon Lake, Mattabi, and Sturgeon Lake most likely reflects Sb-bearing trace minerals with inclusions of galena. Pyrite samples with the highest concentrations of Hg are from the Noranda camp and have some association with Te and As. Pyrite from Delbridge, Deldona, Gallen, and Lac Dufault exhibit similar element behaviour considering they are all felsic-dominated, Zn-rich deposits occurring in the highest sequence of the Noranda Cauldron (e.g., Gibson and Galley, 2007).

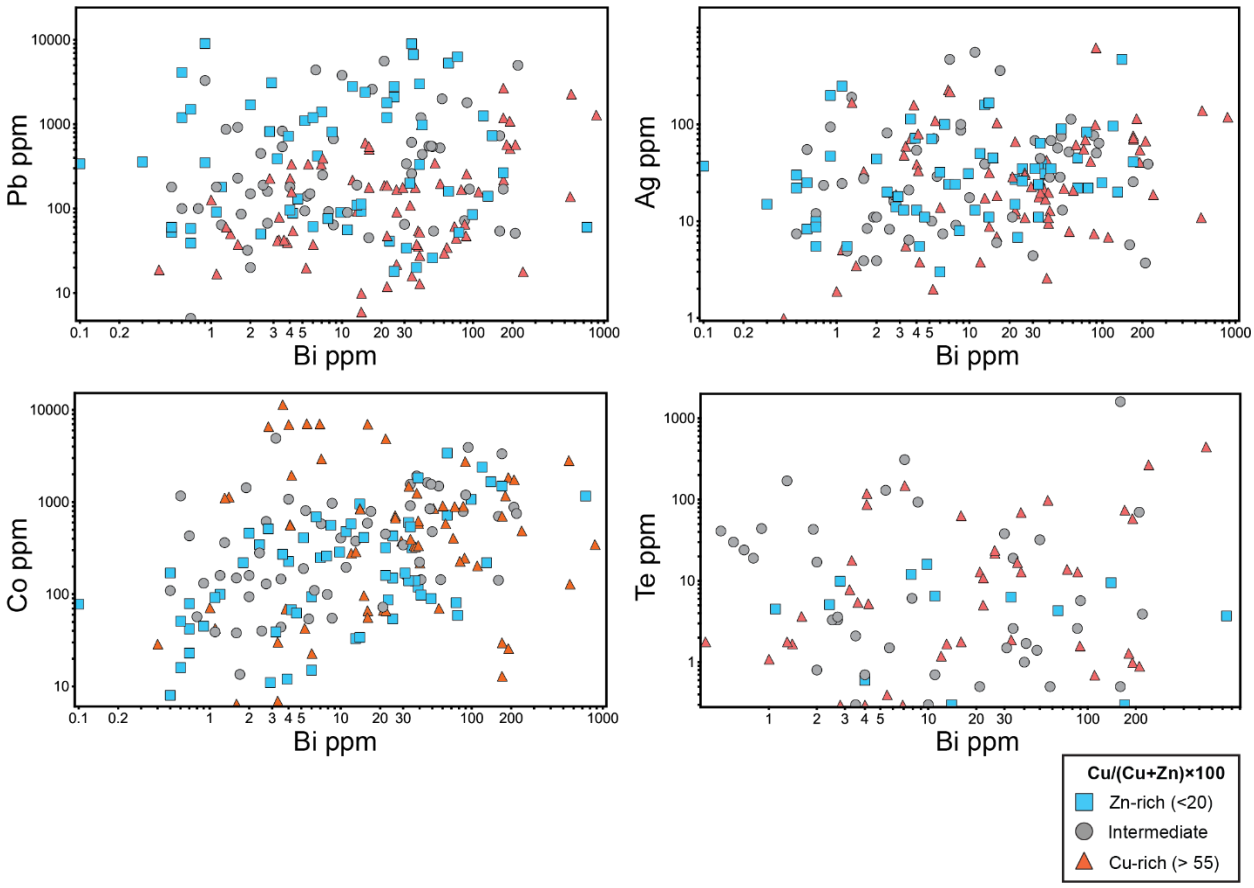

Figure 4.14 Binary plots of Bi versus Pb, Ag Co, and Te (concentrations in ppm) in pyrite samples from VMS deposits classified according to Cu/(Cu+Zn) grade ratio. The deposit classes are: Cu/(Cu+Zn) <20 (Zn-rich deposits; n=22), Cu/(Cu+Zn) = 20–55 (Intermediate; n=15), and Cu/(Cu+Zn) >55 (Cu-rich deposits; n=17). Bi shows a bimodal distribution with a Pb-Ag association (sulfosalt inclusions) and Co-Te association (chalcopyrite and tellurides).

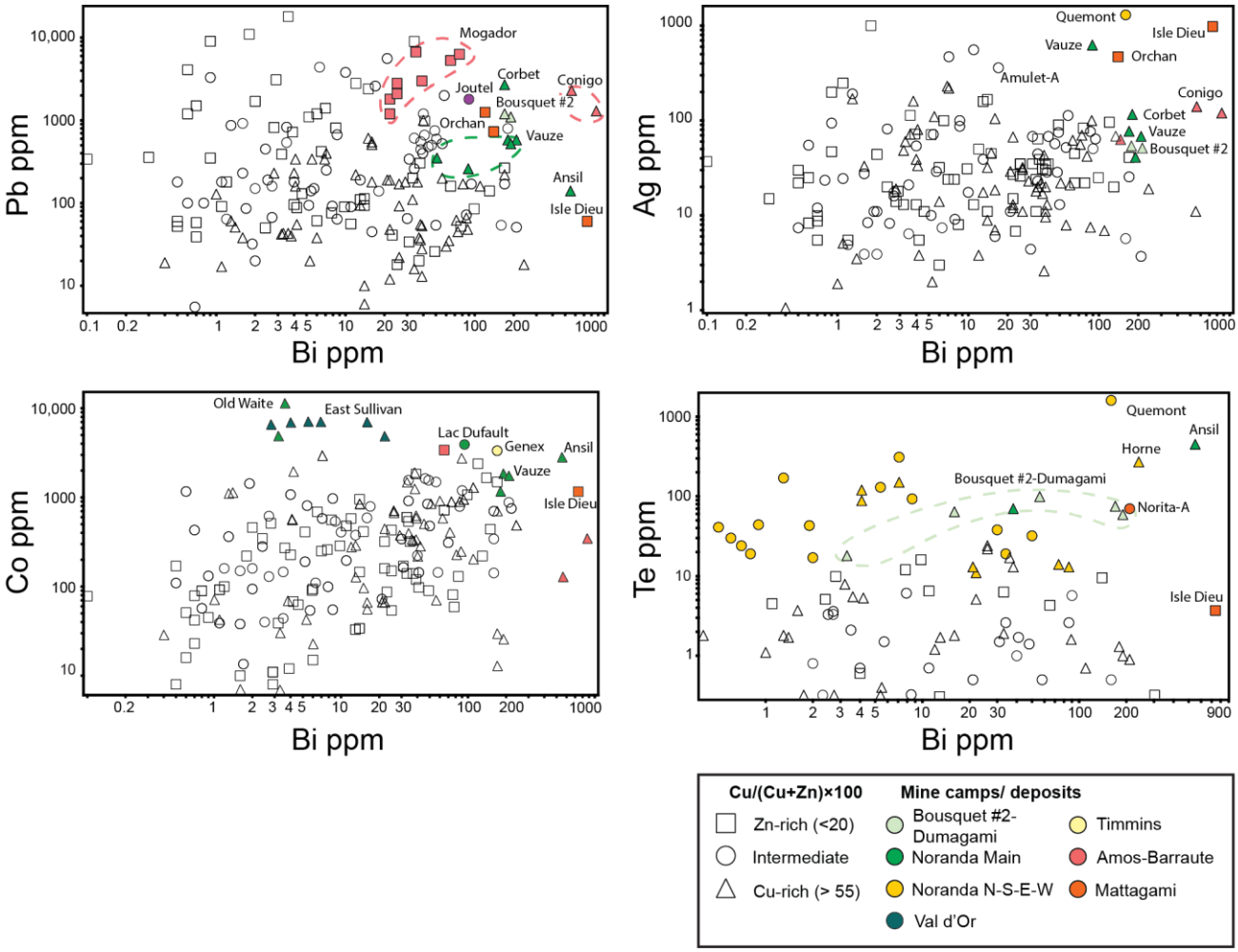

Figure 4.15 Binary plots of Bi versus Pb, Ag Co, and Te (concentrations in ppm) in pyrite samples from VMS deposits classified by mine camp (most correlated samples). Bi is mainly enriched in pyrite from Cu-rich deposits and correlated with Te in pyrite samples from Ansil, Quemont, Horne, Bousquet #2, and Norita-A. In pyrite from Zn-rich deposits, Bi is correlated with Pb-Ag in samples from Mogador, Isle Dieu, and Orchan.

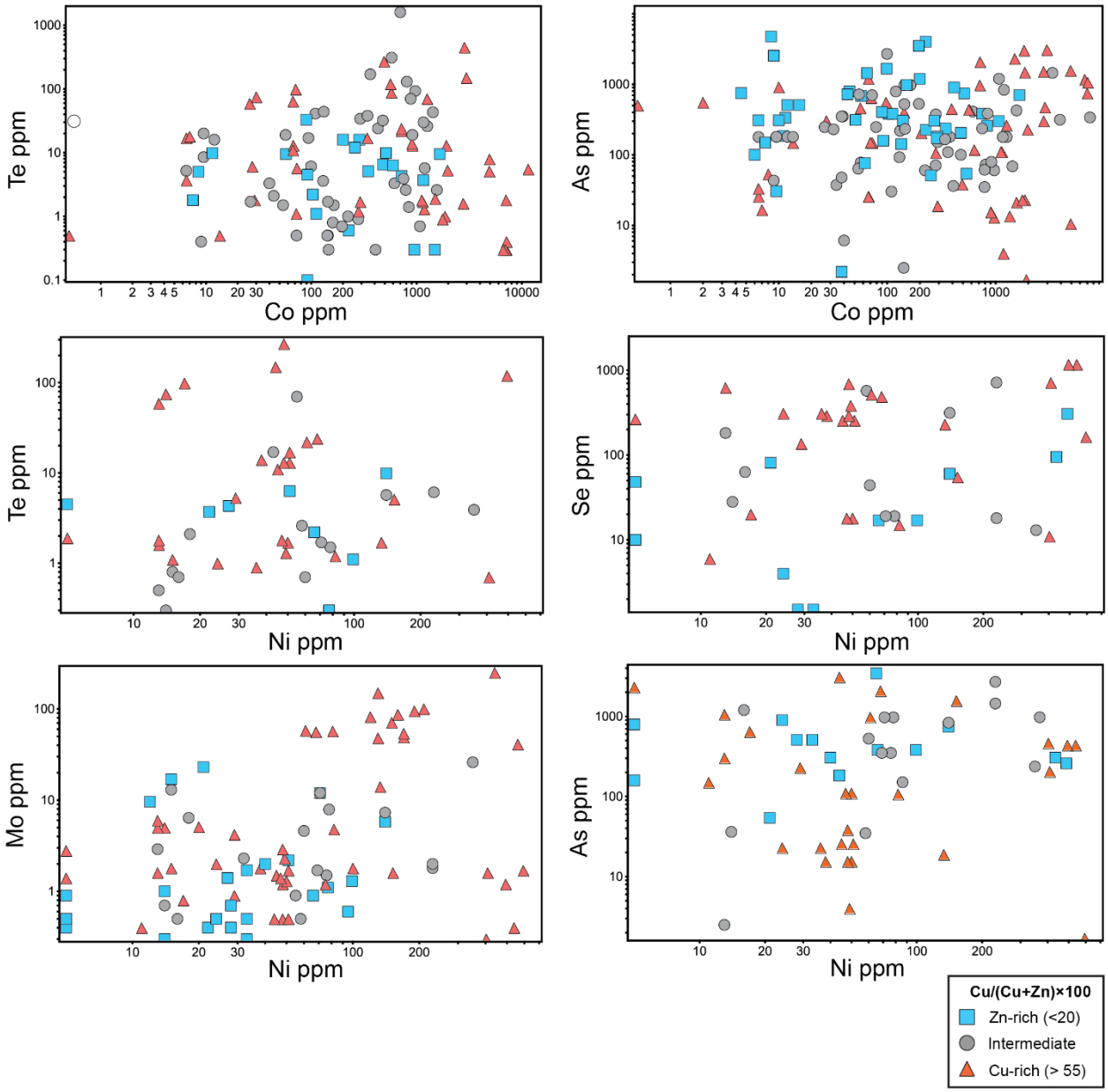

Figure 4.16 Binary plots of Co and Ni versus Se, Te, Mo and As (concentrations in ppm) in pyrite samples from VMS deposits classified according to Cu/(Cu+Zn) grade ratio. The deposit classes are: Cu/(Cu+Zn) <20 (Zn-rich deposits; n=22), Cu/(Cu+Zn) = 20–55 (Intermediate; n=15), and Cu/(Cu+Zn) >55 (Cu-rich deposits; n=17). Pyrite samples from Cu-rich deposits commonly have a strong Co-As correlation reflecting inclusions of cobaltite. The mixed correlations of Co and Ni with Te in pyrite samples from Cu-rich deposits suggest a combination of mostly lattice-bound metals together with chalcopyrite, telluride, or bismuthide inclusions.

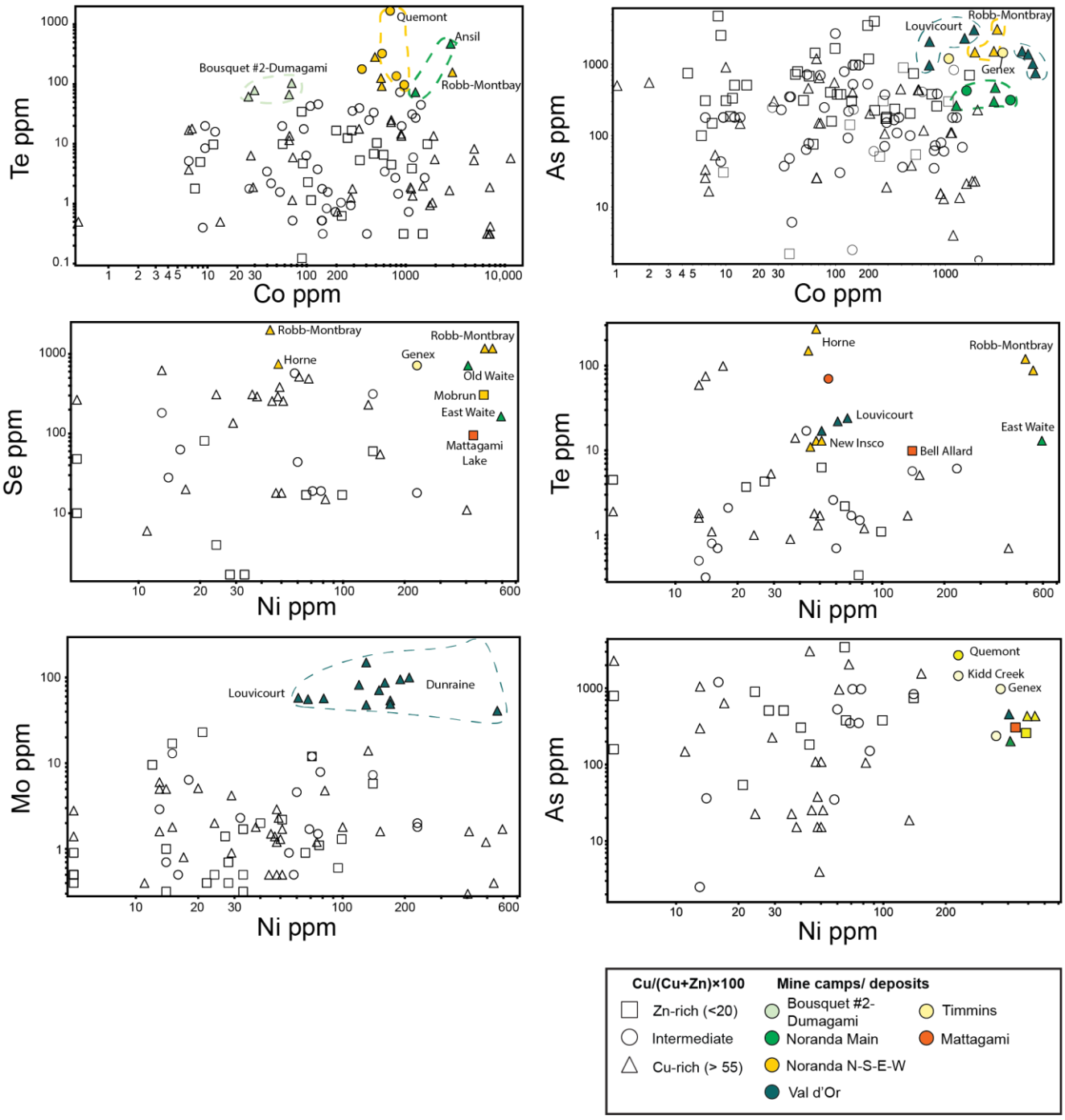
Te ppm
Co ppm
Quemont
Ansil
Bousquet #2-Dumagami
Robb-Montbay
As ppm
Co ppm
Robb-Montbray
Louvicourt
Genex
Se ppm
Ni ppm
Robb-Montbray
Horne
Genex
Old Waite
Mobrun
East Waite
Mattagami Lake
Te ppm
Ni ppm
Horne
Robb-Montbray
Louvicourt
New Insco
Bell Allard
East Waite
Mo ppm
Ni ppm
Louvicourt
Dunraine
As ppm
Ni ppm
Quemont
Kidd Creek
Genex
Cu/(Cu+Zn)×100
Zn-rich (<20)
Intermediate
Cu-rich (> 55)
Mine camps/ deposits
Bousquet #2-Dumagami
Noranda Main
Noranda N-S-E-W
Val d'Or
Timmins
Mattagami

Figure 4.17 Binary plots of Co and Ni versus Se, Te, Mo and As (concentrations in ppm) in pyrite samples from VMS deposits classified by mine camp (most correlated samples). The Cu-Co-Te correlation in some samples from Ansil, Quemont, Robb-Montbray, and Mattagami Lake may indicate the presence of mattagamite. Some pyrite samples from Robb-Montbray, New Insco, and Louvicourt show a Ni-Te correlation that may indicate traces of melonite. The correlation of Ni with Se, Mo, and As in samples from Mobrun, Old Waite, East Waite, and Genex may be related to diagenetic pyrite.

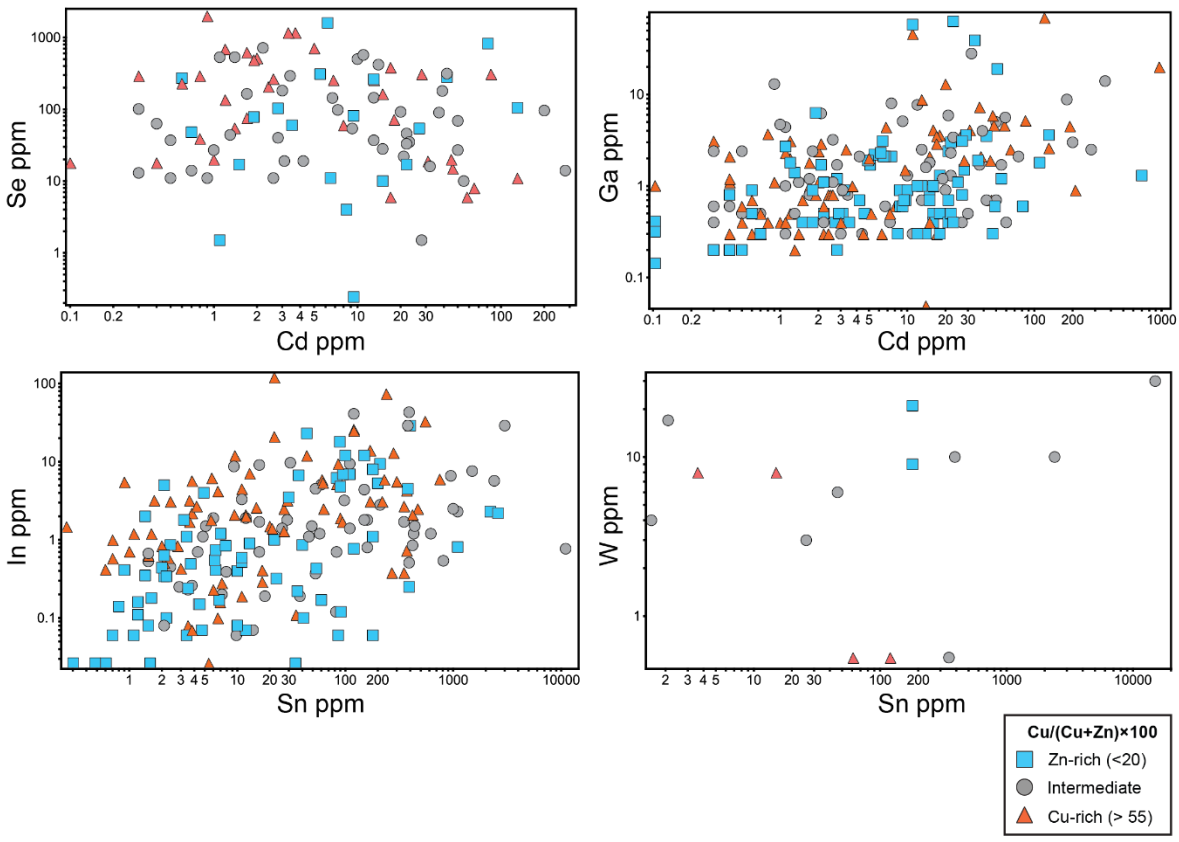

Figure 4.18 Binary plots of Cd and Sn with Se, Ga, In, and W (concentrations in ppm) in pyrite samples from VMS deposits classified according to Cu/(Cu+Zn) grade ratio. The deposit classes are: Cu/(Cu+Zn) <20 (Zn-rich deposits; n=22), Cu/(Cu+Zn) = 20–55 (Intermediate; n=15), and Cu/(Cu+Zn) >55 (Cu-rich deposits; n=17). A few samples show a Se-Cd correlation, which may indicate inclusions of cadmoselite. The correlation of Cd with Ga is interpreted to indicate co-enrichment in sphalerite inclusions. The correlation of In and Sn in samples from Cu-rich and Zn-rich deposits may indicate the presence of stannite and stannoidite inclusions. A few samples show a strong Sn-W correlation indicating inclusions of scheelite and cassiterite.

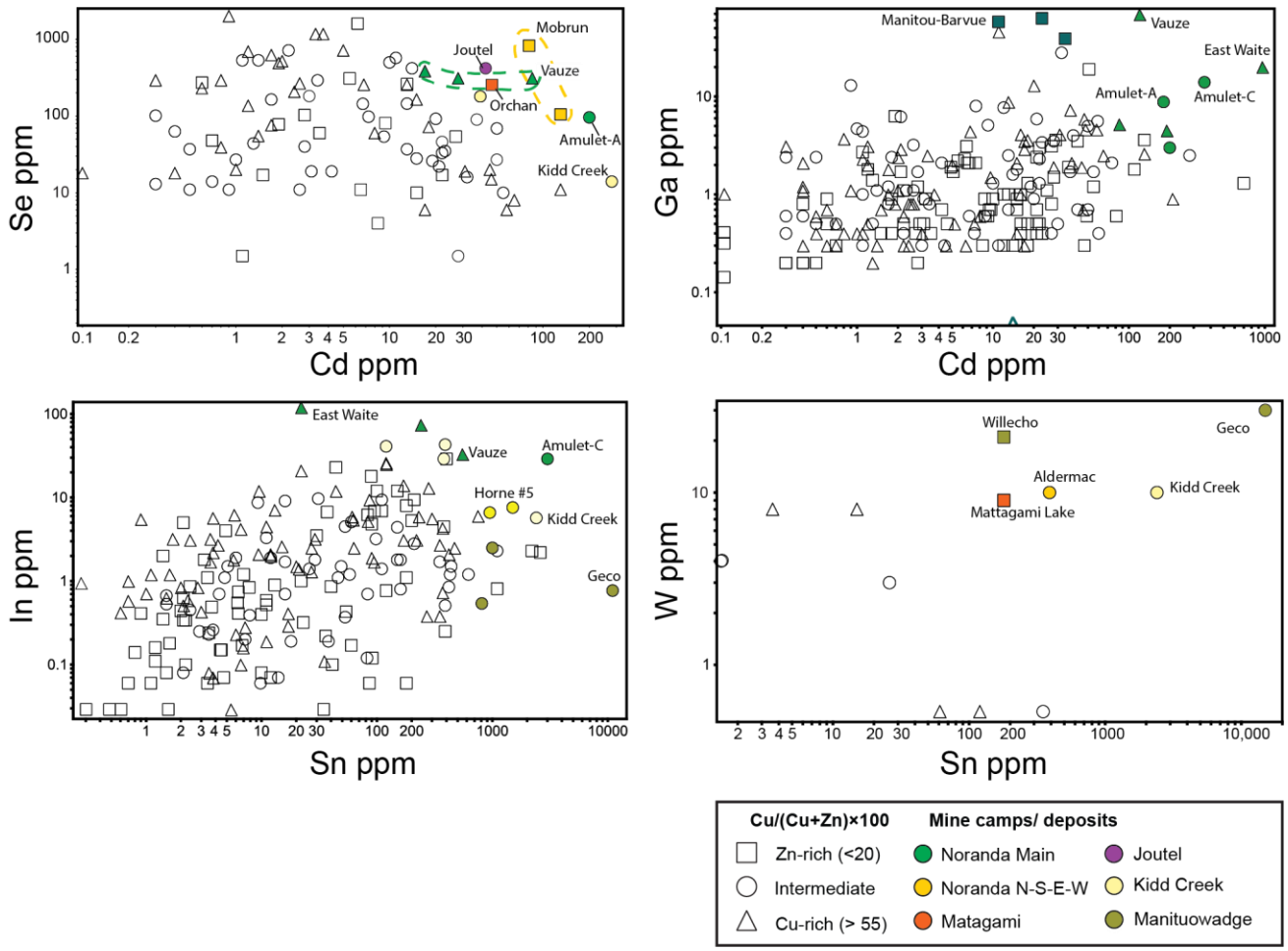

Figure 4.19 Binary plots of Cd and Sn with Se, Ga, In, and W (concentrations in ppm) in pyrite samples from VMS deposits classified by mine camp (most correlated samples). Two samples from Mobrun show a strong Se-Cd correlation likely reflecting inclusions of cadmoselite, which have been reported in the deposit. Samples from Geco, Willecho, and Kidd Creek show strong Sn-W correlations.

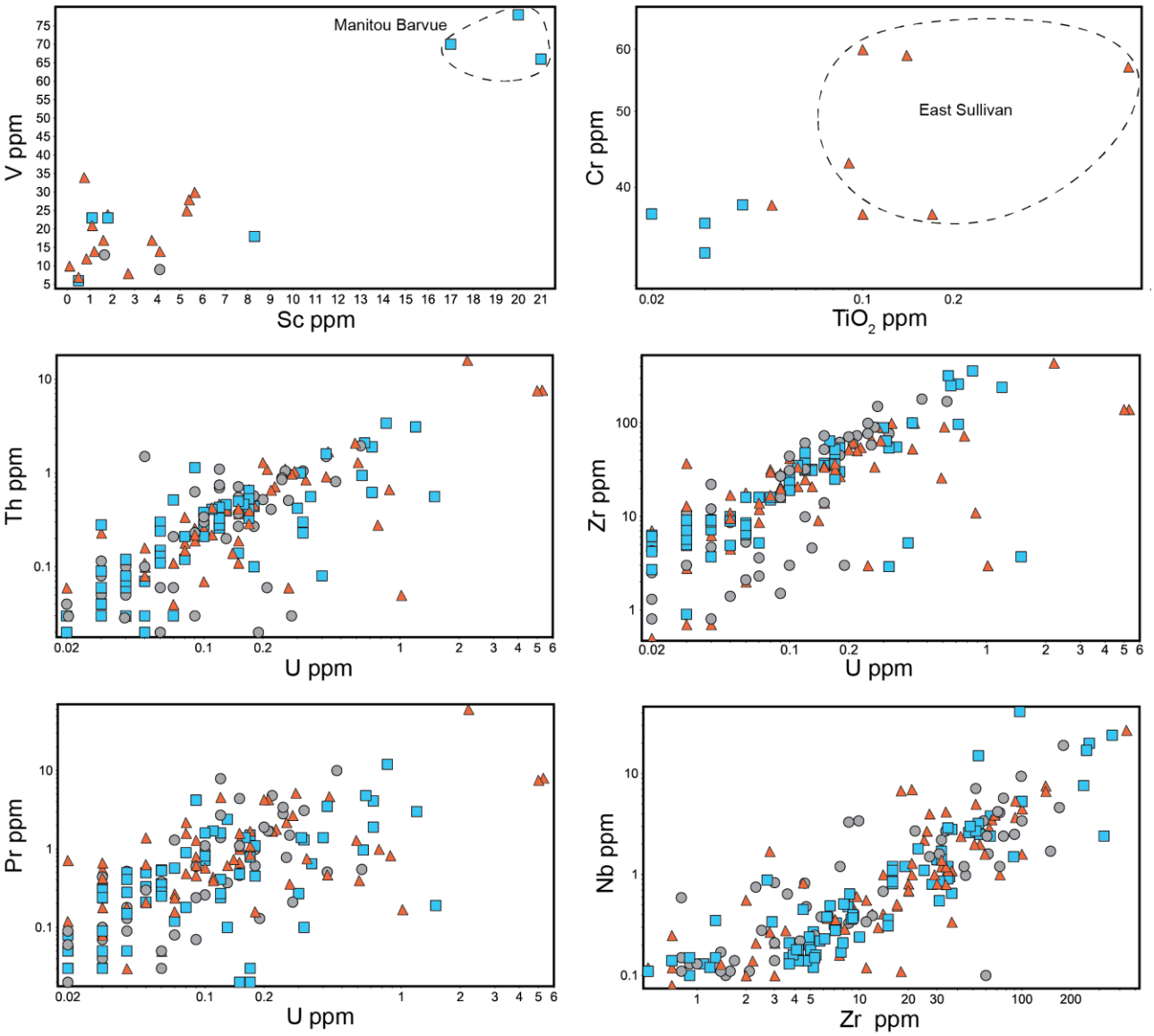
Manitou Barvue
V ppm
Sc ppm
East Sullivan
Cr ppm
TiO2 ppm
Th ppm
U ppm
Zr ppm
U ppm
Pr ppm
U ppm
Nb ppm
Zr ppm

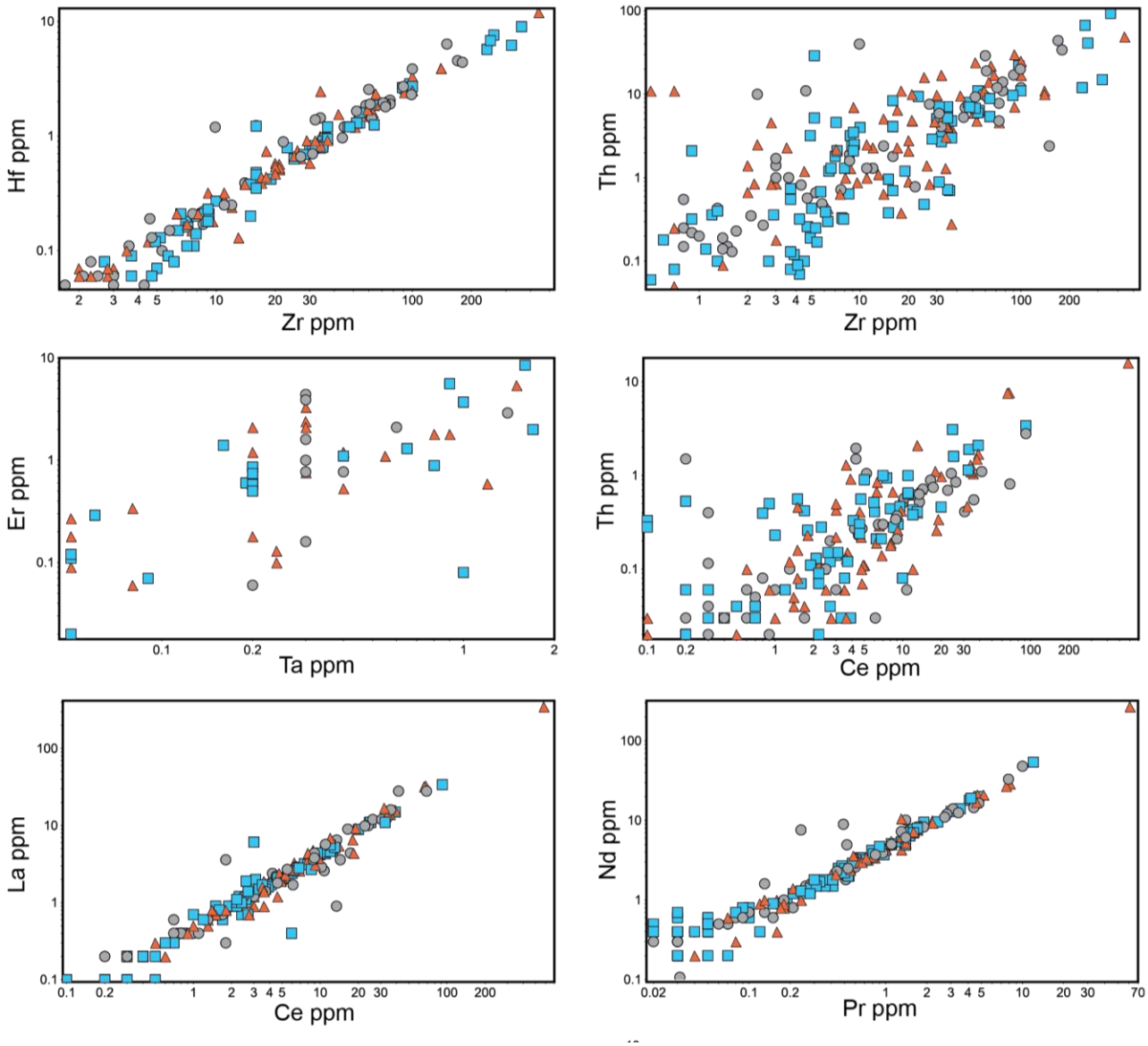
Hf ppm
Zr ppm
Th ppm
Zr ppm
Er ppm
Ta ppm
Th ppm
Ce ppm
La ppm
Ce ppm
Nd ppm
Pr ppm

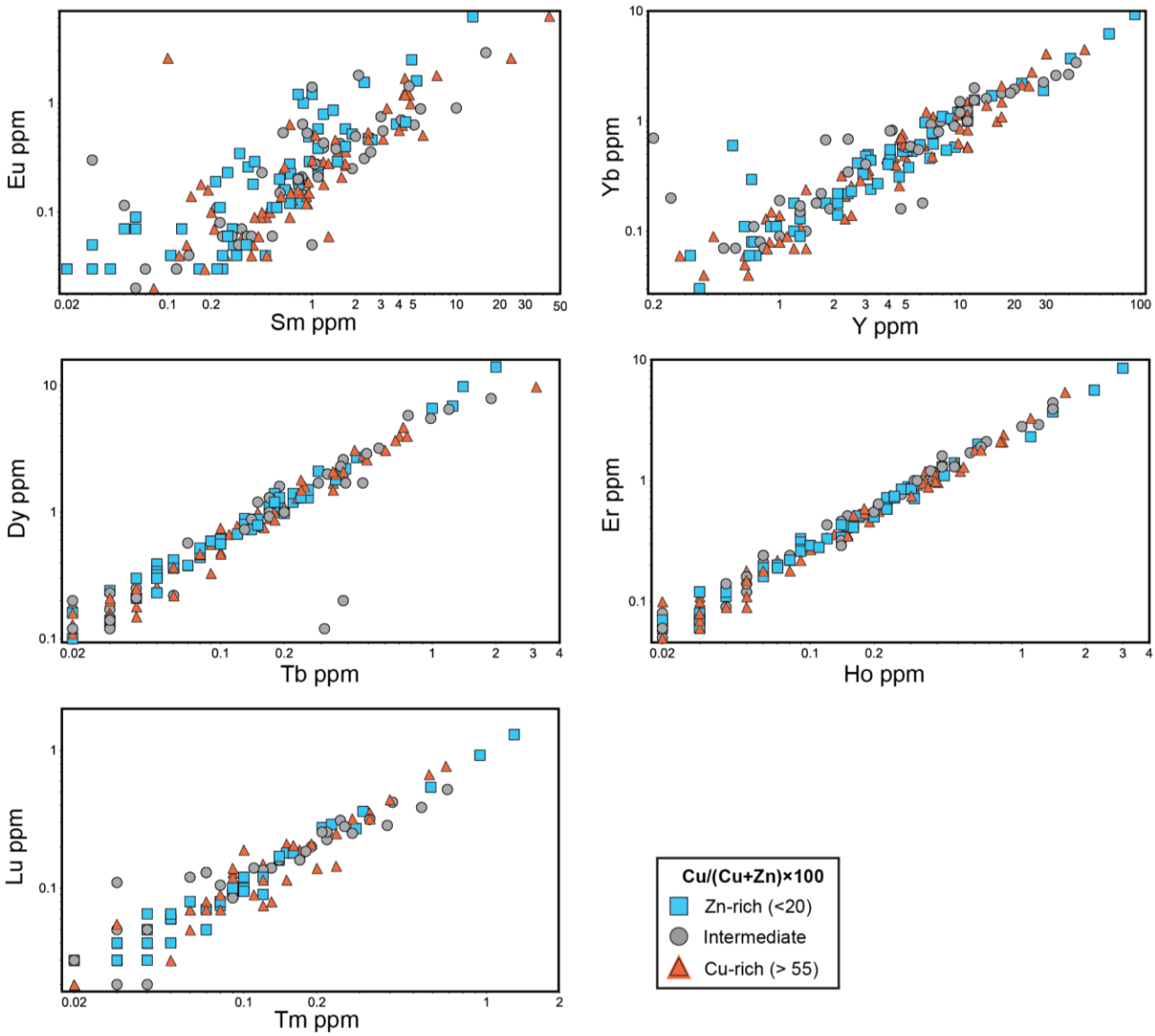

Figure 4.20 Binary plots of V, HFSE (U, Th, Nb, Hf, and Sc), LILE (Rb), and REE (La, Ce, Pr, Nd, Sm, Eu, Gd, Y, Dy, Yb) (concentrations in ppm) in pyrite samples from VMS deposits classified according to Cu/(Cu+Zn) grade ratio. The deposit classes are: Cu/(Cu+Zn) <20 (Zn-rich deposits; n=22), Cu/(Cu+Zn) = 20–55 (Intermediate; n=15), and Cu/(Cu+Zn) >55 (Cu-rich deposits; n=17). The correlation of U with Th, Zr, Ce, and REE indicates the presence of monazite in the samples. The strong correlation between Th, Y, and Yb, as well as the other REE, in other samples indicates xenotime is likely present. Zr shows strong correlations with Th, Hf and some REE (Nb and Nd). suggesting inclusions of zircon in the samples. Ti is correlated with Cr, Zr, Ta and REE indicates inclusions of rutile in the samples.

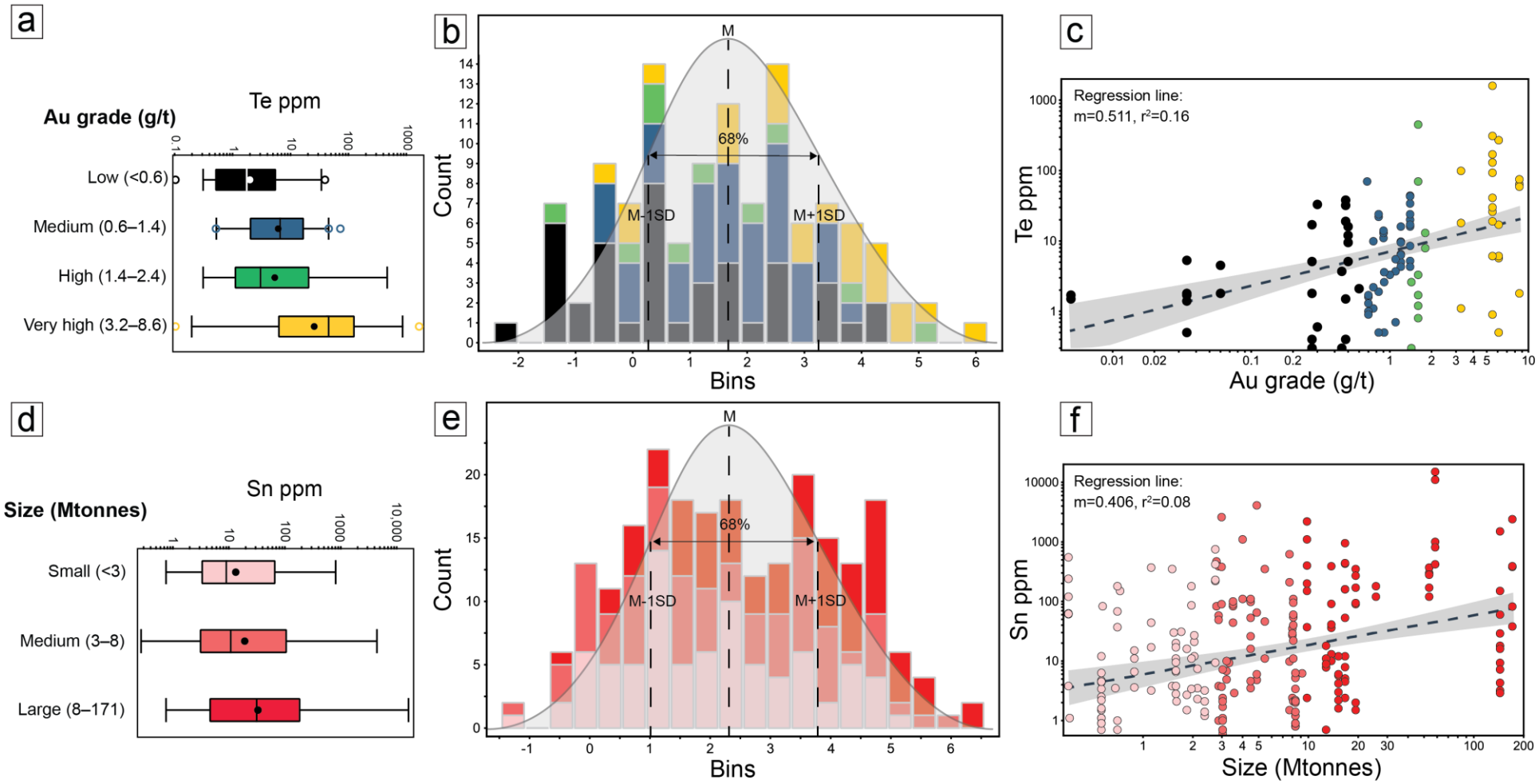
a
Au grade (g/t)
Te ppm
Low (<0.6)
Medium (0.6–1.4)
High (1.4–2.4)
Very high (3.2–8.6)
b
M
68%
M-1SD
M+1SD
Count
Bins
c
Regression line:
m=0.511, r²=0.16
Te ppm
Au grade (g/t)
d
Size (Mtonnes)
Sn ppm
Small (<3)
Medium (3–8)
Large (8–171)
e
M
68%
M-1SD
M+1SD
Count
Bins
f
Regression line:
m=0.406, r²=0.08
Sn ppm
Size (Mtonnes)

Figure 4.21 Statistical significance of observed correlations between selected trace elements in pyrite and bulk Au grades and sizes of deposits, illustrated by Sn and Te concentrations. a) Box plots showing the Te concentrations of pyrite samples from deposits with different bulk Au grades (g/t) including low (<0.6 g/t; n=14), medium (0.6–1.4 g/t: n=14), high (1.6–2.4 g/t; n=4), and very high-grade deposits (>4 g/t: n=6). Te concentrations increases with the Au grade of the sampled deposit. The box encloses 50% of the data within the interquartile range (from Q1 to Q3). The average values (open circles) and median (line) are shown. 5th and 95th percentiles are lower and upper ends of whiskers. Outliers (circles) are within the bottom or top 5% of the dataset. b) Histogram showing the log-normal distribution of Te in pyrite, coloured according to the bulk Au grade (g/t) of the deposits from a). The histogram shows 50% of the pyrite samples from the very high Au grade class have Te concentrations that are more than one standard deviation higher than the population mean. The bell-curve corresponds to a normal distribution. c) Biplot of Te concentration in pyrite versus the bulk Au grade (g/t) of the deposits from a). The regression line (dashed line) shows the goodness of fit, with the indicated 'R-squared' value and 'm' value. The Te concentrations of 111 pyrite samples have a positive correlation with the Au grades of the deposits with a Pearson coefficient of 0.4. The grey band around the regression line indicates a 95% confidence interval at a significance level of 0.05. d) Box plots showing the Sn concentrations of pyrite samples from deposits of different sizes including small (< 3 Mt; n=28), medium (3–8 Mt; n=12), and high (8–171 Mt; n=14). The average Sn concentrations of pyrite samples from large tonnage deposits are generally higher than in samples from smaller deposits. e) Histogram showing the log-normal distribution of Sn in pyrite, coloured according to the sizes of the deposits from d). The histogram shows 45% of the pyrite samples from the largest deposits have Sn concentrations that are more than one standard deviation higher than the population mean. f) Biplot of Sn concentration in pyrite versus deposit size from d). The regression line (dashed line) shows the goodness of fit, with the indicated 'R-squared' value and 'm' value. The Sn concentrations of 233 pyrite samples have a positive correlation with deposit size shown by a Pearson coefficient of 0.3. The grey band around the regression line indicates a 95% confidence interval at a significance level of 0.05.

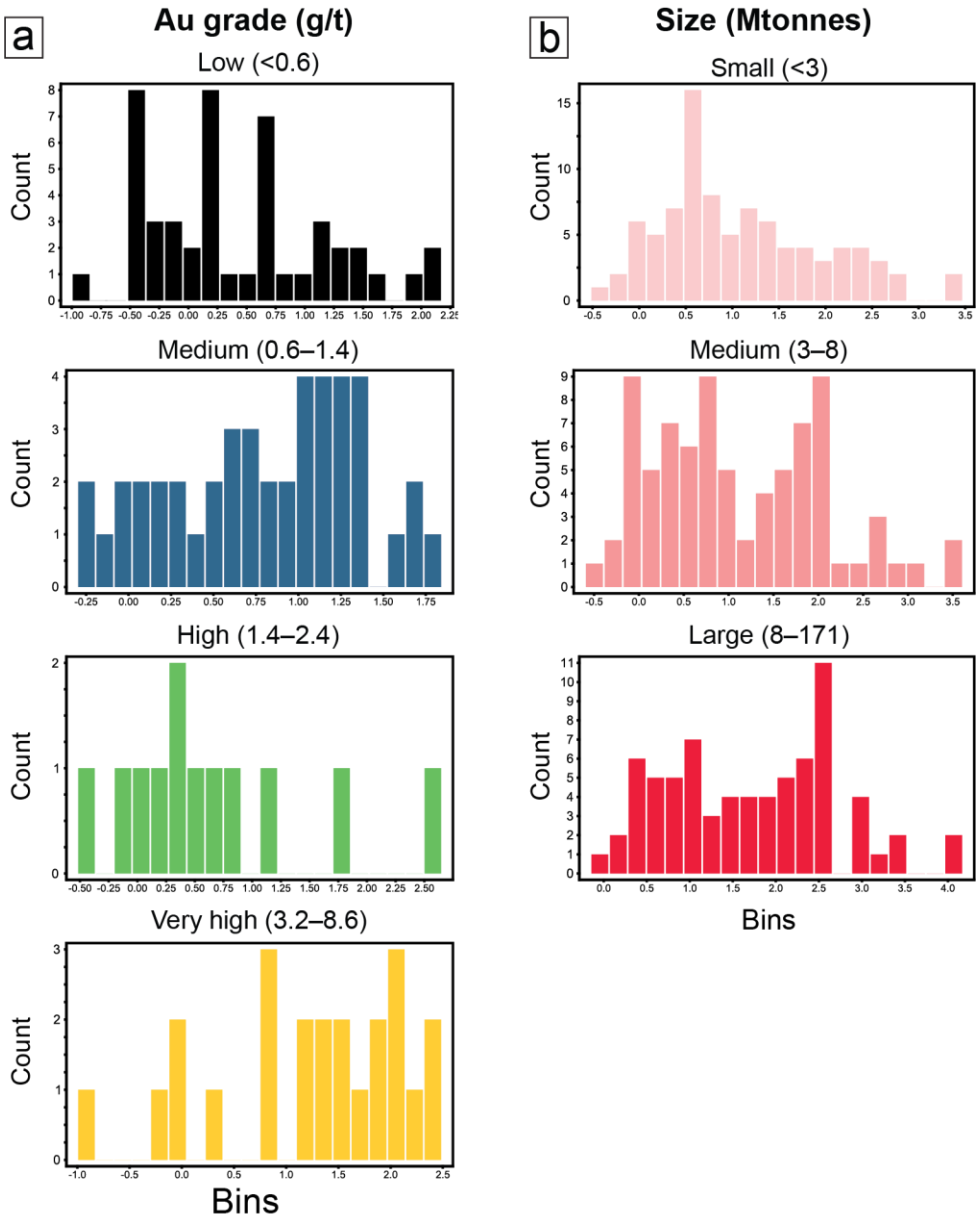

Figure 4.22 Histograms showing the log-normal distribution of Te and Sn in pyrite for the different classes of bulk Au grade (a) and deposit size (b), coloured according to the bulk Au grade (g/t) and sizes of the deposits as in Figure 4.20. Deposits with low gold grades (<0.6 g/t) have the most pyrite samples in the low Te concentration bins, whereas deposits with very high gold grades (>3.2 g/t) have the most pyrite samples in the high concentration bins. Small deposits (<3 Mtonnes) have the most pyrite samples in the low Sn concentration bins, whereas large deposits (>8 Mtonnes) have more pyrite samples in the high concentration bin.

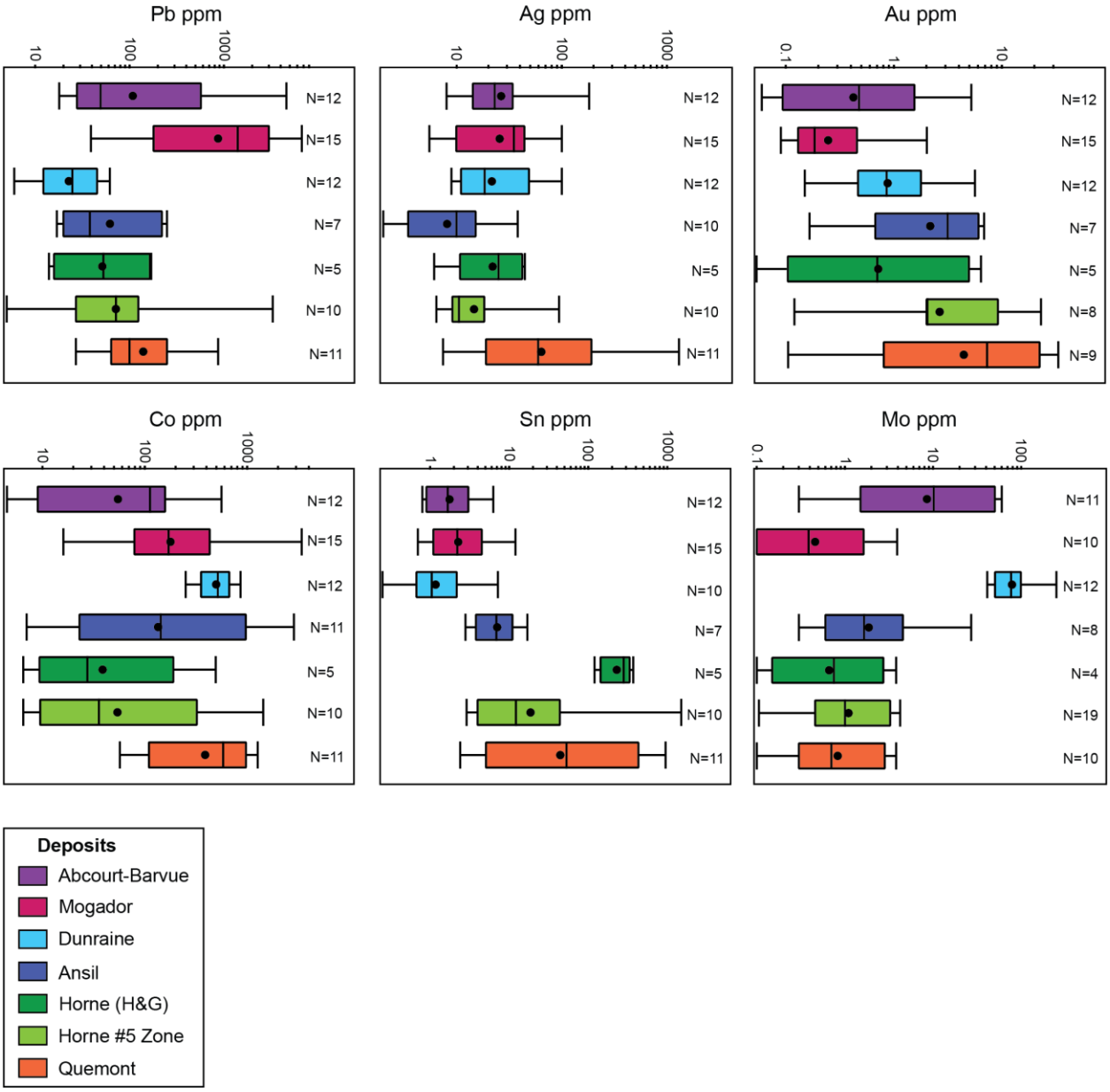
Pb ppm
10
100
1000
N=12
N=15
N=12
N=7
N=5
N=10
N=11
Ag ppm
10
100
1000
N=12
N=15
N=12
N=10
N=5
N=10
N=11
Au ppm
0.1
1
10
N=12
N=15
N=12
N=7
N=5
N=8
N=9
Co ppm
10
100
1000
N=12
N=15
N=12
N=11
N=5
N=10
N=11
Sn ppm
1
10
100
1000
N=12
N=15
N=10
N=7
N=5
N=10
N=11
Mo ppm
0.1
1
10
100
N=11
N=10
N=12
N=8
N=4
N=19
N=10
Deposits
Abcourt-Barvue
Mogador
Dunraine
Ansil
Horne (H&G)
Horne #5 Zone
Quemont

Figure 4.23 Box plots of selected trace element concentrations in pyrite samples from VMS deposits with more than 5 samples in the database. Although there are large ranges in concentrations for each deposit, there are clear differences between pyrite samples from the different deposits, reflecting differences in bulk Cu/(Cu+Zn) grade ratios of the deposits and host rocks (see text for discussion). The box encloses 50% of the data within the interquartile range (from Q1 to Q3). The average values (open circles) and median (line) are shown. 5th and 95th percentiles are lower and upper ends of whiskers. The variations in trace element concentrations in pyrite in many cases are larger between deposits than within individual deposits (i.e., little or no overlap between Q1 to Q3). Pyrite samples from the Zn-rich Mogador and Abcourt-Barvue deposits in the Amos-Barraute district have Pb concentrations that are an order of magnitude higher (>500 ppm on average) than samples from the Cu-rich Dunraine and Ansil deposits. Pyrite samples from the Quemont deposit are enriched in Ag by an order of magnitude (>100 ppm on average) compared to pyrite from the Horne (H&G and #5 zone) and Ansil deposits. Pyrite samples from the Ansil, Horne #5, and Quemont deposits tend to be enriched in Au (>5 ppm on average) compared to pyrite from the Mogador and Abcourt-Barvue deposits. Pyrite samples from the Dunraine and Quemont deposits have on average higher Co concentrations (>300 ppm on average) than pyrite from the Abcourt-Barvue and Horne deposits. Pyrite from Dunraine also has distinctly higher Mo concentrations (>80 ppm on average) than pyrite from the Amos-Barraute and Noranda deposits shown. Pyrite from the Horne (H&G and #5 zone) and Quemont deposits are enriched in Sn by 1 to 2 orders of magnitude (100–200 ppm) compared to pyrite from the other deposits.

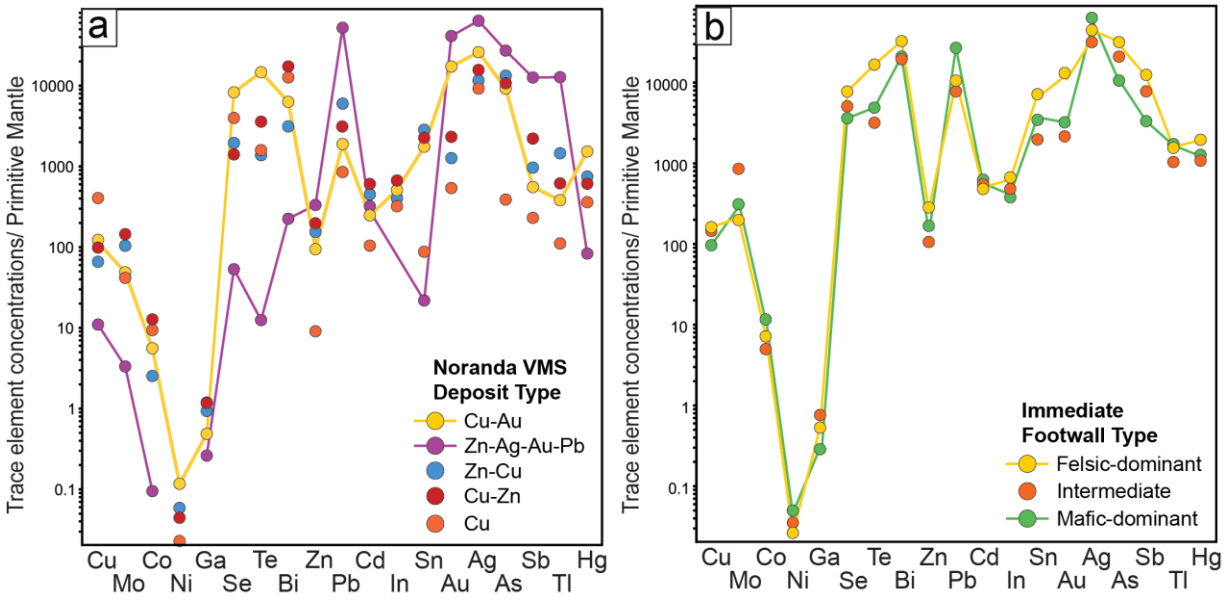

Figure 4.24 Multi-element profiles (spider diagrams) of trace element concentrations in pyrite from VMS deposits normalized to primitive mantle to match the original classification scheme of Barrie and Hannington (1999). a) Pyrite samples from all of the Noranda deposits grouped by ore type (see Table 4.6.c) The lines and coloured symbols are the mean concentrations of the trace elements in pyrite from different deposit types in the Noranda camp (Table 4.9.c). b) Pyrite samples from VMS deposits in the Superior Province classified by immediate host rocks (Table 2.1 and Table 4.8). Primitive mantle values used to normalize trace element concentrations are from Lyubetskaya and Korenaga (2007). In a) pyrite samples from the Noranda main camp Cu-Zn deposits and the west camp Cu deposit (New Insco) have variable enrichments in Bi, Co, Ni, Se, and Sn; whereas pyrite from the Cu-Au deposits like Quemont, tend to be enriched in Au, Se, and Te, and Zn-Ag-Au-Pb deposits like Delbridge are enriched in Pb, Ag, Au, As, Sb, Tl. In b) pyrite samples from felsic-dominant deposits in the Superior Province have higher Zn and most trace metals including Au, Bi, Se, Te, In, Sn, W, Sb, and Hg than mafic-dominant and intermediate deposits, whereas pyrite from mafic-dominant deposits have higher Co and Ni as well as Pb, Ag, Cd, and Tl than felsic-dominant deposits.

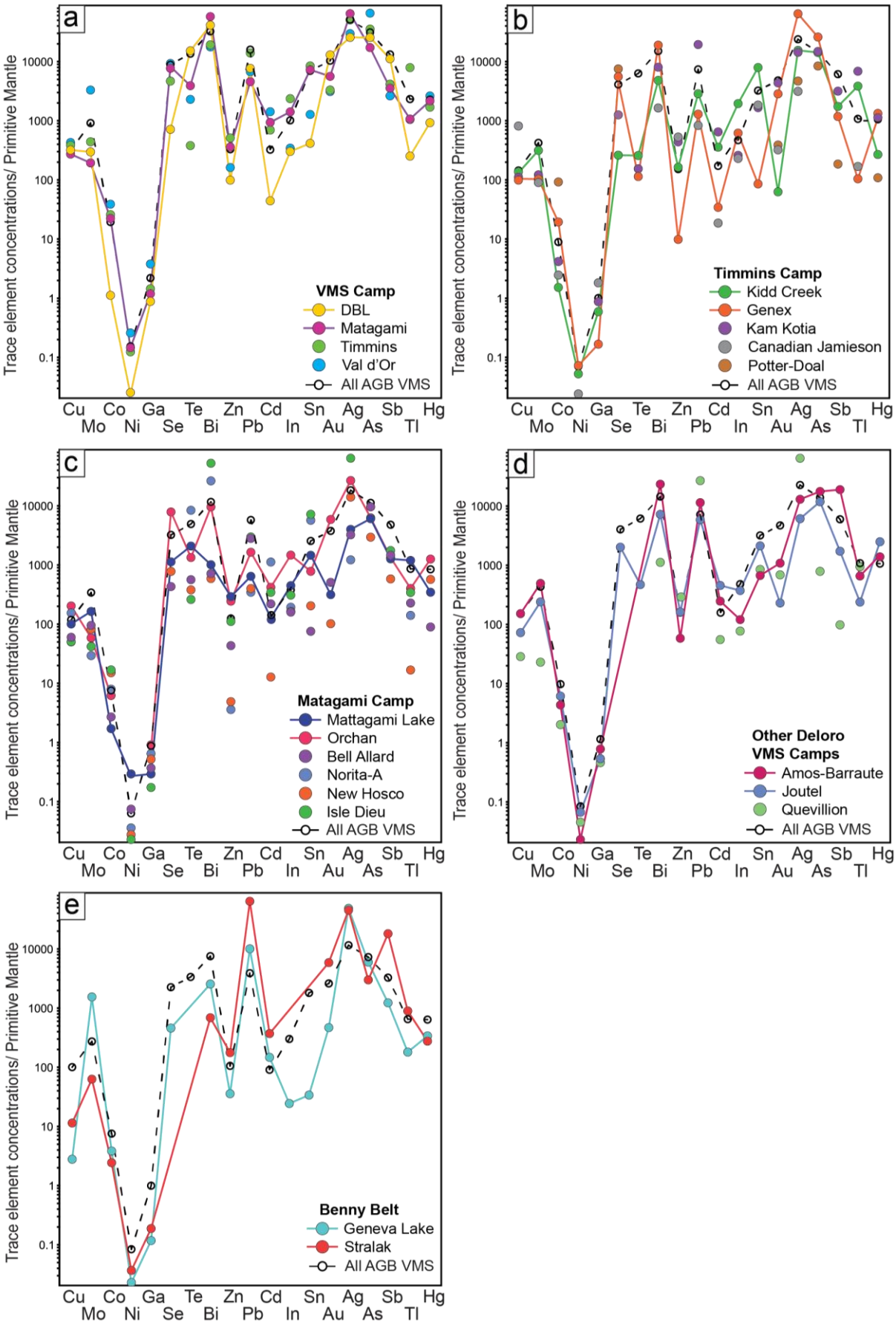
a
Trace element concentrations/ Primitive Mantle
VMS Camp
DBL
Matagami
Timmins
Val d'Or
All AGB VMS
b
Timmins Camp
Kidd Creek
Genex
Kam Kotia
Canadian Jamieson
Potter-Doal
All AGB VMS
c
Matagami Camp
Mattagami Lake
Orchan
Bell Allard
Norita-A
New Hosco
Isle Dieu
All AGB VMS
d
Other Deloro
VMS Camps
Amos-Barraute
Joutel
Quevillion
All AGB VMS
e
Benny Belt
Geneva Lake
Stralak
All AGB VMS
Cu Co Ga Te Zn Cd Sn Ag Sb Hg
Mo Ni Se Bi Pb In Au As Tl

Figure 4.25 Multi-element profiles (spider diagrams) of trace element concentrations in pyrite from VMS deposits in the Abitibi Greenstone Belt (Table 4.9.b and A.11) normalized to primitive mantle and grouped according to the different mining camps: a) DBL, Val d'Or, Timmins, and Matagami; b) Timmins; c) Matagami; d) different VMS camps in the Deloro; e) VMS deposits in the Benny Greenstone Belt. The lines and coloured symbols are the mean concentrations of the trace elements in pyrite from the camps and from selected individual deposits. The mean concentrations for all pyrite samples in the Superior Province dataset are shown by the black dashed line. Primitive mantle values used to normalize trace element concentrations are from Lyubetskaya and Korenaga (2007). In a) pyrite samples from the DBL camp are enriched in Au, Bi, and Te; pyrite from the Val d'Or camp is generally enriched in Co, Ni, Se, Ga, Mo, and As. In b) pyrite from the Timmins camp (i.e., Kidd Creek and Potter-Doal) and Blake River (Kamiskotia area, i.e., Canadian Jamieson, Genex, and Kam-Kotia) shows variable enrichments in Co, Ni, Cd, In, Sn, and Tl. In c) pyrite samples from Matagami are enriched in Co, with pyrite from some deposits containing more Bi, Se, In, and Sn (i.e., Isle Dieu, Norita-A, Orchan) and Ni (i.e., Mattagami Lake). In d) pyrite samples from Quevillon are enriched in Pb, Ag, and Cd; pyrite samples from Joutel are enriched in Hg; and pyrite samples from Amos-Barraute are enriched in Bi, As, and Sb. In e) pyrite samples from the Benny Greenstone Belt (i.e., Geneva Lake and Stralak deposits) are enriched in Ag, Ni, Cd, Mo, V, Sb, and Tl.

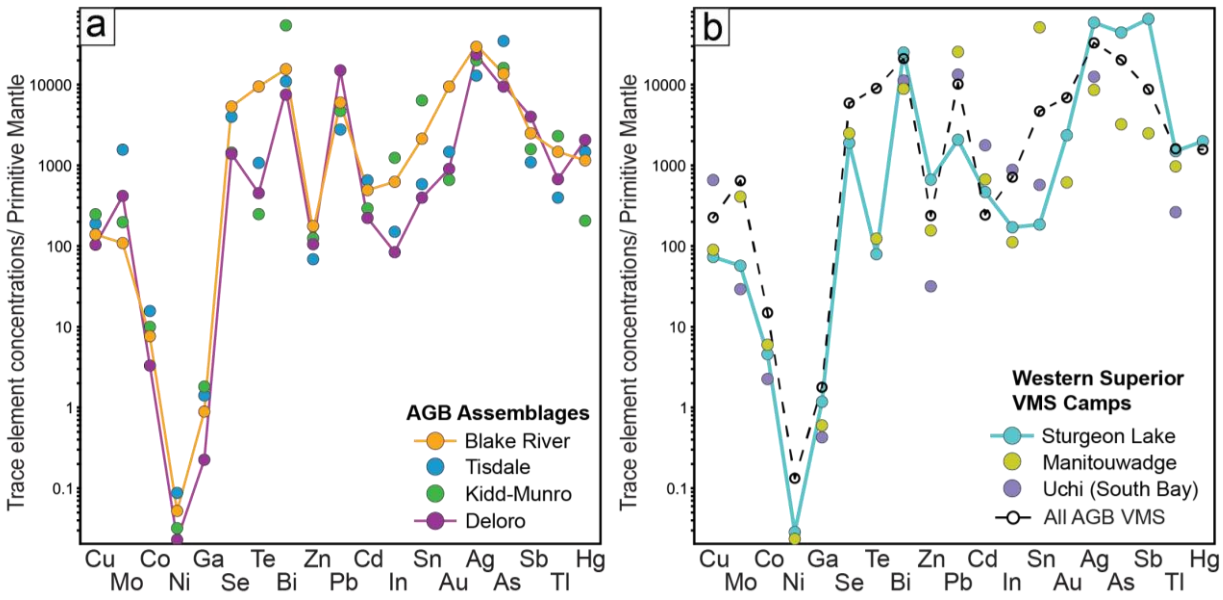

Figure 4.26 Multi-element profiles (spider diagrams) of trace element concentrations in pyrite samples from VMS deposits of the Superior Province (Table 4.9.a,b and A.11) normalized to primitive mantle and grouped according to: a) different assemblages in the AGB; b) other subprovinces including Wawa (Manitouwadge camp), Wabigoon (Sturgeon Lake camp), and Uchi (South Bay deposit). The lines and coloured symbols are the mean concentrations of the trace elements in pyrite. The mean concentrations for all pyrite samples in the Superior Province dataset are shown by the black dashed line. Primitive mantle values used to normalize trace element concentrations are from Lyubetskaya and Korenaga (2007). In a) pyrite samples from deposits in the Deloro assemblage have higher Mo and Hg and variably lower Ag, Au, Bi, Ni, Se, Te, Cd, In, Sb, Tl; samples from deposits in the Kidd-Munro assemblage (Potter-Doal, Kidd Creek) have higher Co, Ni, Cd, In, and Sn, and lower Au, Se, and Te; samples from deposits in the Tisdale have higher Co and Ni, as well as Se, Ga, Mo, and As, and are lower Pb, Ag, Bi, In, Sn, Sb, and Tl; samples from deposits in the BRG have higher Au, Se, Te, Cd, and In, and lower Pb, As, and Sb.

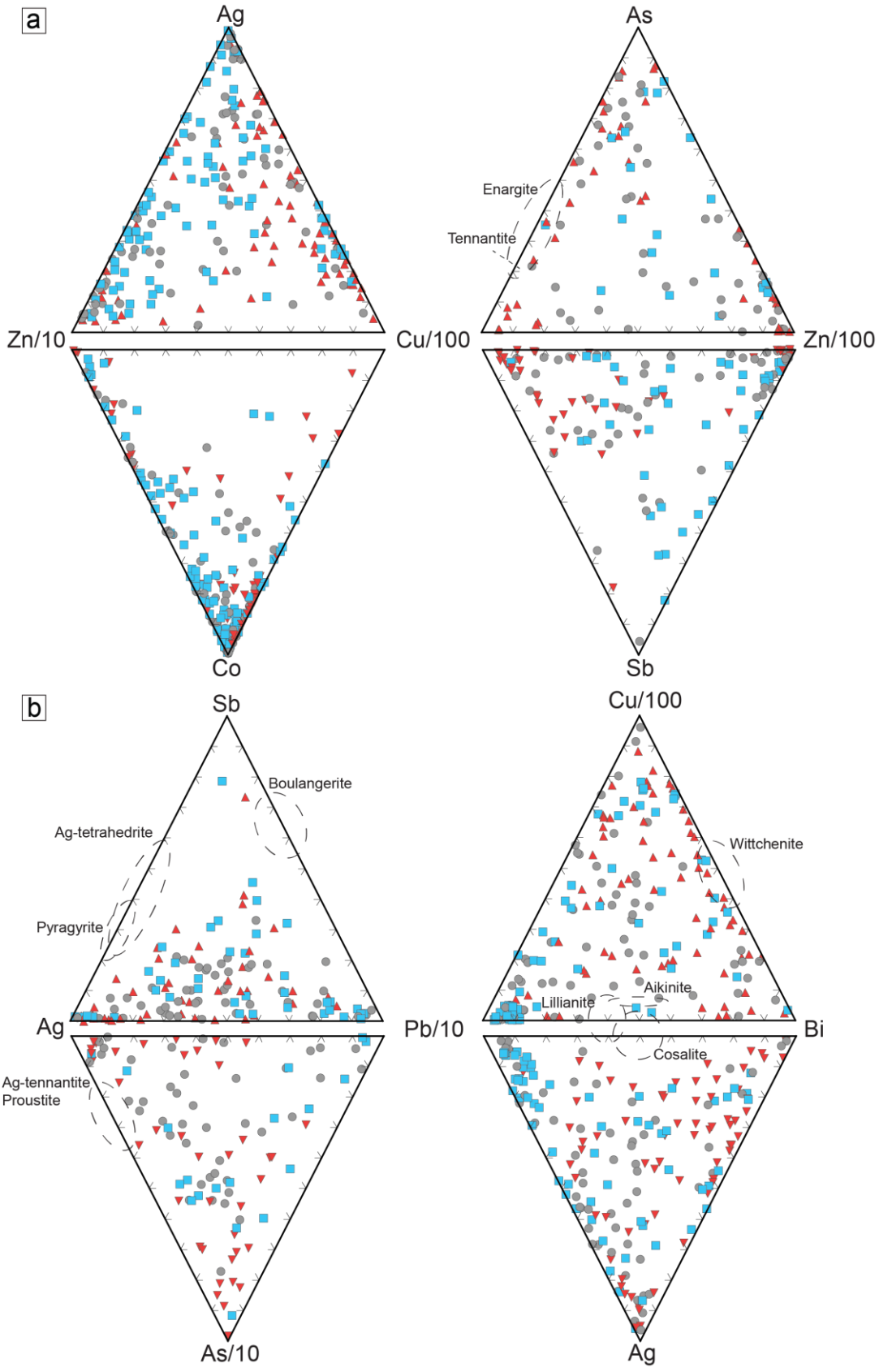
a
Ag
Zn/10
Co
Cu/100
As
Enargite
Tennantite
Zn/100
Sb
b
Sb
Boulangerite
Ag-tetrahedrite
Pyragyrite
Ag
Ag-tennantite
Proustite
As/10
Cu/100
Wittchenite
Aikinite
Lillianite
Pb/10
Bi
Cosalite
Ag

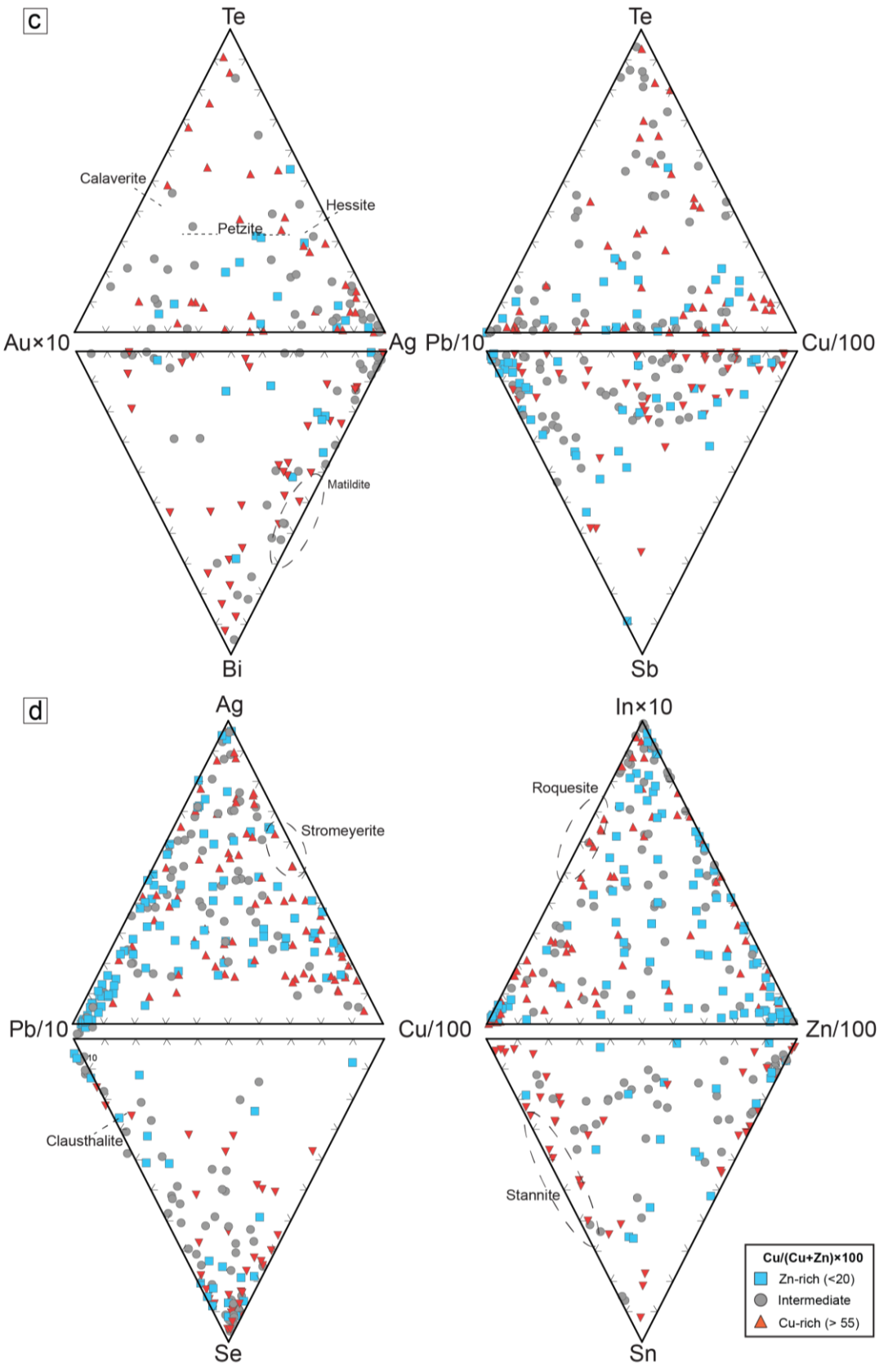
c
Te
Calaverite
Petzite
Hessite
Au×10
Ag
Matildite
Bi
Te
Pb/10
Cu/100
Sb
d
Ag
Stromeyerite
Pb/10
Clausthalite
Se
In×10
Roquesite
Cu/100
Zn/100
Stannite
Sn
Cu/(Cu+Zn)×100
Zn-rich (<20)
Intermediate
Cu-rich (> 55)

Figure 4.27 Ternary plots of trace metal concentrations (in ppm) of pyrite samples from VMS deposits classified according to Cu/(Cu+Zn) grade ratio. The deposit classes are: Cu/(Cu+Zn) <20 (Zn-rich deposits; n=22), Cu/(Cu+Zn) = 20–55 (Intermediate; n=15), and Cu/(Cu+Zn) >55 (Cu-rich deposits; n=17). a) Ag-Co-As-Sb plot on Cu and Zn, b) Ag-Bi-As-Sb on Cu and Pb c) Au-Ag-Bi-Te on Cu and Pb, d) Ag-Se-In-Sn on Cu and Pb. Trace element concentrations are in ppm. Clusters at the Cu, Zn, and Pb corners show the high proportions of pyrite samples with chalcopyrite, sphalerite and galena inclusions. Samples plotting in the Pb corner of b) indicate the presence of galena inclusions in pyrite from Zn-rich deposits (e.g., Amos-Barraute, Val d'Or, Noranda, Benny, and Manitouwadge camps). In c) pyrite samples from Cu-rich deposits cluster in the Au-Te portion of the ternary. In d) pyrite samples from Cu-rich deposits cluster in the Se-rich portion of the ternary. The Ag ternary shows the bimodal distribution between pyrite from Cu-rich deposits and Zn-Pb-rich deposits. In d), In and Sn show a similar bimodal distribution.

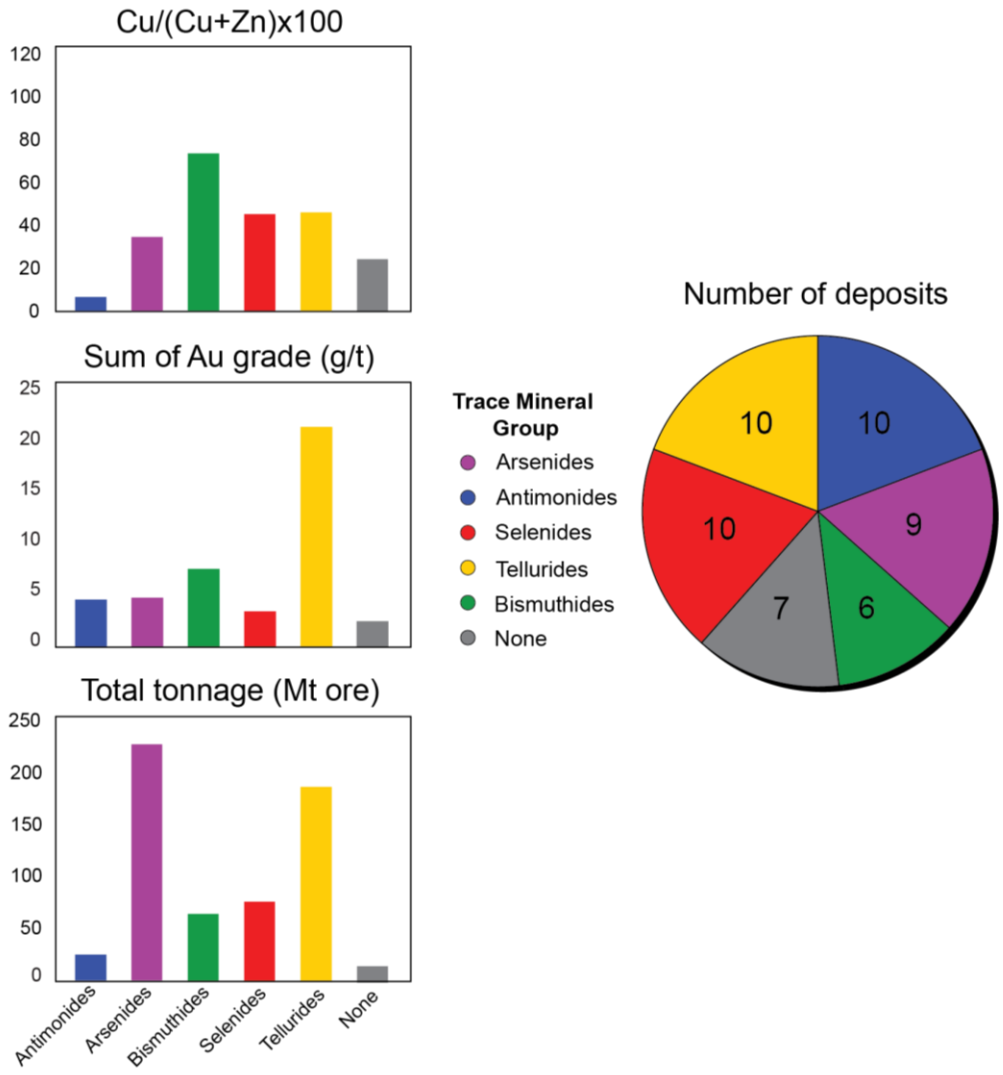

Figure 4.28 Histograms of host rocks, sizes, Au grades, and Cu-Zn grade ratios between the VMS deposits in the Superior Province classified by trace mineral groupings. Pyrite samples containing abundant Sb-bearing minerals are from deposits with mostly low Cu/Cu+Zn ratios, small tonnages, and low Au grades. Pyrite samples dominated by As-bearing minerals are from deposits with low Cu/Cu+Zn ratios, and low Au grades. Pyrite samples with abundant Bi-bearing minerals are from deposits with high Cu/(Cu+Zn) ratios, mid-size tonnages, and medium Au grades. Pyrite samples with abundant Se-bearing minerals are from deposits with intermediate Cu/(Cu+Zn) ratios, mid-size tonnages, and moderate Au grades. Pyrite samples containing abundant tellurides are from deposits with mostly high Cu/(Cu+Zn) ratios, large tonnages, and high Au grades. Pyrite samples with a low abundance of the trace minerals have low Cu/(Cu+Zn) ratios, and generally the lowest tonnages and Au grades.

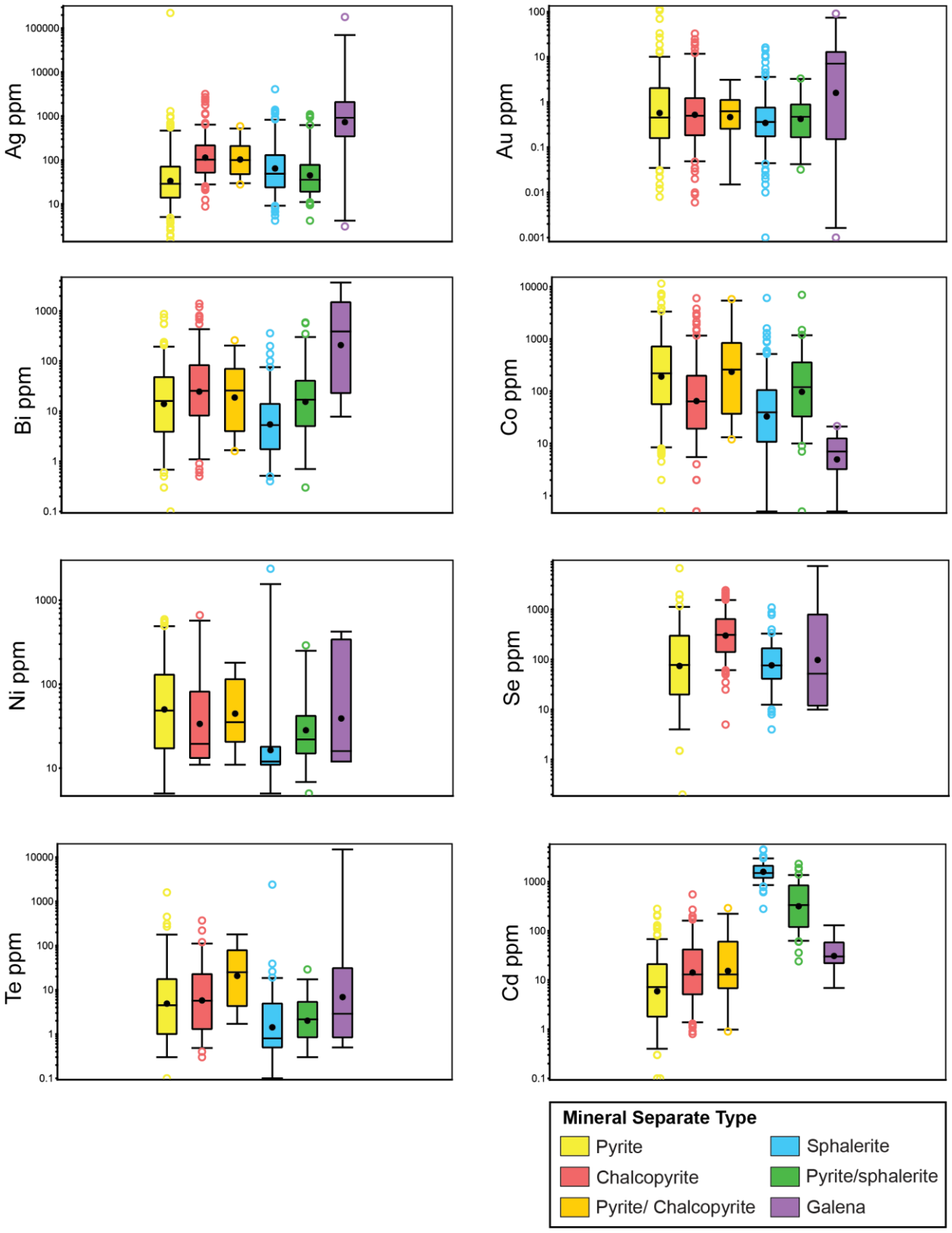
Ag ppm
Au ppm
Bi ppm
Co ppm
Ni ppm
Se ppm
Te ppm
Cd ppm
Mineral Separate Type
Pyrite
Chalcopyrite
Pyrite/ Chalcopyrite
Sphalerite
Pyrite/sphalerite
Galena

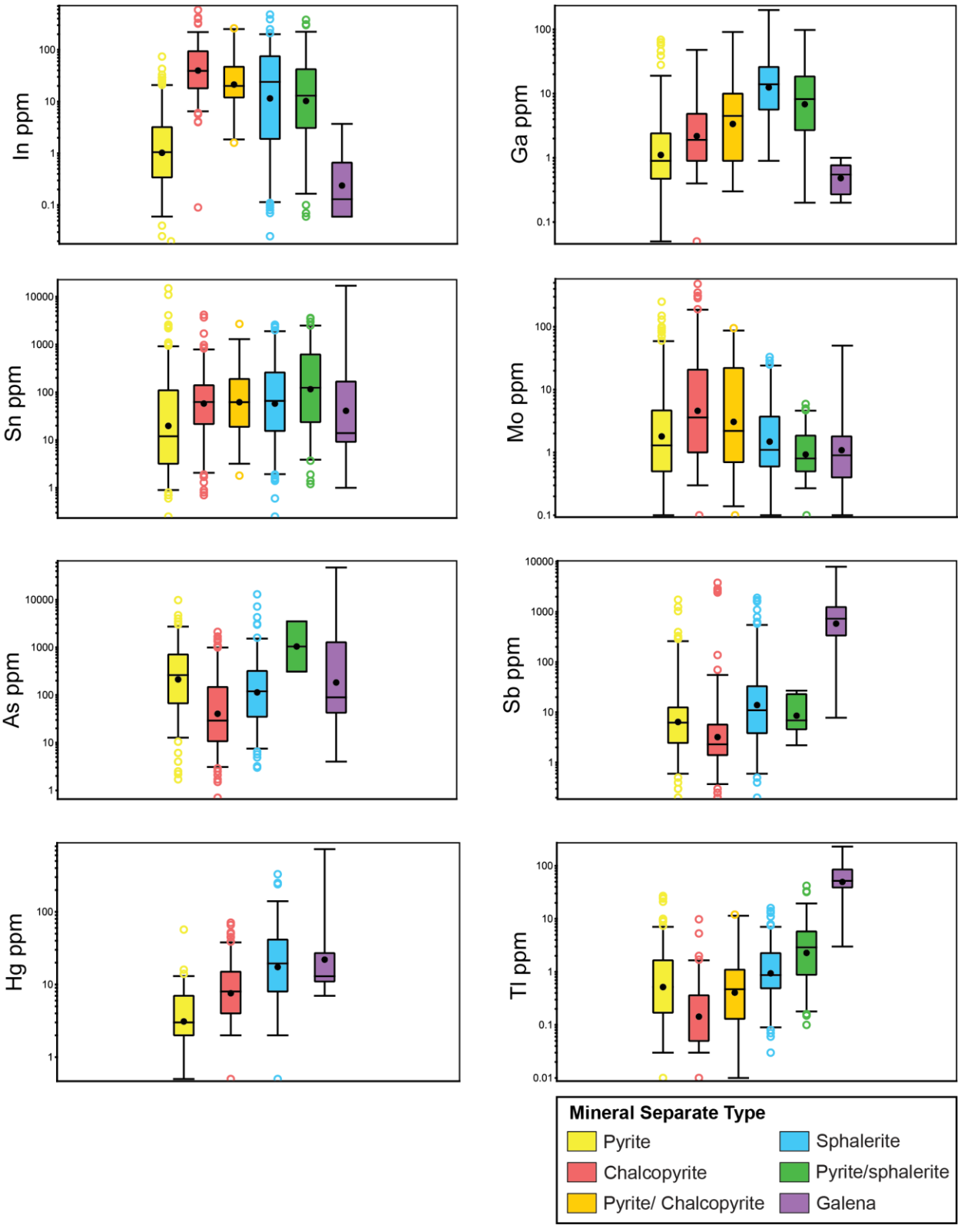
In ppm
Ga ppm
Sn ppm
Mo ppm
As ppm
Sb ppm
Hg ppm
Tl ppm
Mineral Separate Type
Pyrite
Chalcopyrite
Pyrite/ Chalcopyrite
Sphalerite
Pyrite/sphalerite
Galena

Figure 4.29 Boxplots of trace element concentrations (ppm) in different types of mineral separates (i.e., pyrite, chalcopyrite, pyrite/ chalcopyrite, sphalerite, pyrite, sphalerite galena) from VMS deposits in the Superior Province. The box encloses 50% of the data within the interquartile range (from Q1 to Q3). The average values (open circles) and median (line) are shown. 5th and 95th percentiles are lower and upper ends of whiskers.

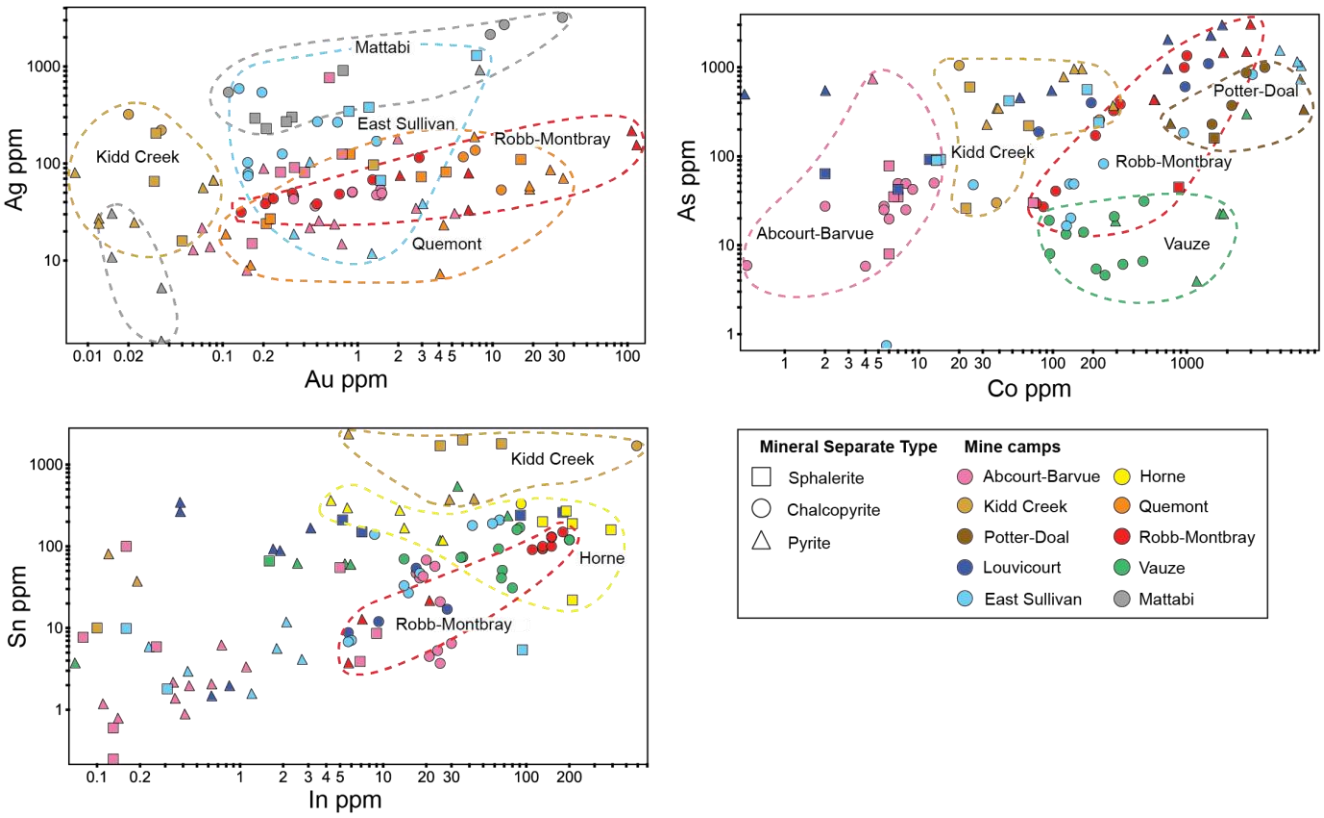

Figure 4.30 Binary plots of trace element (concentrations in ppm) in samples of different types of mineral separates (i.e., pyrite, chalcopyrite, sphalerite) from select VMS deposits. Select trace elements shown are commonly lattice bound in these minerals, or occur in trace mineral phases as inclusions in the different sample types. Samples from deposits with close distributions are outlined. The Ag-Au plot shows a range of enrichments and depletions between mineral separate types reflecting different mechanisms of incorporation for Ag and Au in the samples. The Mattabi deposit has chalcopyrite and sphalerite samples enriched in Ag, whereas pyrite samples are depleted in Ag. The Robb-Montbray deposit has pyrite samples enriched in Au and chalcopyrite samples depleted in Au. The Quemont deposit has pyrite samples with variable Au concentrations both higher and lower than chalcopyrite and sphalerite. The Co-As plot shows pyrite samples have the highest concentrations with distinct differences in distributions between the deposits except for Louvicourt and Val d'Or, which have variable Co-As concentrations in each type of mineral separate. The In-Sn plot shows sphalerite and chalcopyrite have higher concentrations than pyrite. The plots show that the variability between the deposits is generally greater than the variability between mineral separate types.

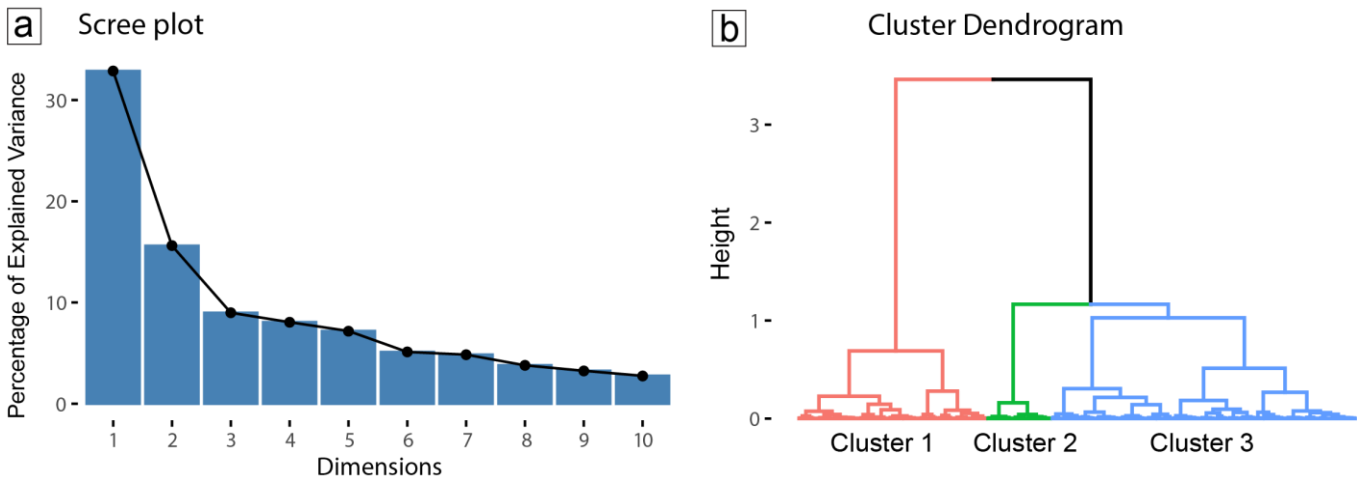

Figure 4.31 a) Scree plot of PCA results for selected trace elements in pyrite samples from VMS deposits of the Superior Province in Jonasson et al. (2020). The PCA was performed using 17 trace metals in pyrite (Cu, Zn, Pb, Ag, Au, Bi, Co, Ni, Se, Te, Cd, In, Sn, Mo, As, Sb, Tl, and Hg). The plot shows eigenvalues expressed as percentage of explained variance for each principal component (dimension) with decreasing contributions from left to right. The first two components have eigenvalues >1 (10% of variance). b) Schematic illustration of hierarchical clustering of principal components results. The number of clusters is determined by a procedure that builds dendrograms (i.e., decision trees that identify the different clusters). In the example shown, the dendrogram has three levels and three final clusters. Hierarchical clustering classifies samples into the different groups and maximizes the differences between the groups. In the method employed in this study, the analysis is unsupervised. See the text for discussion.

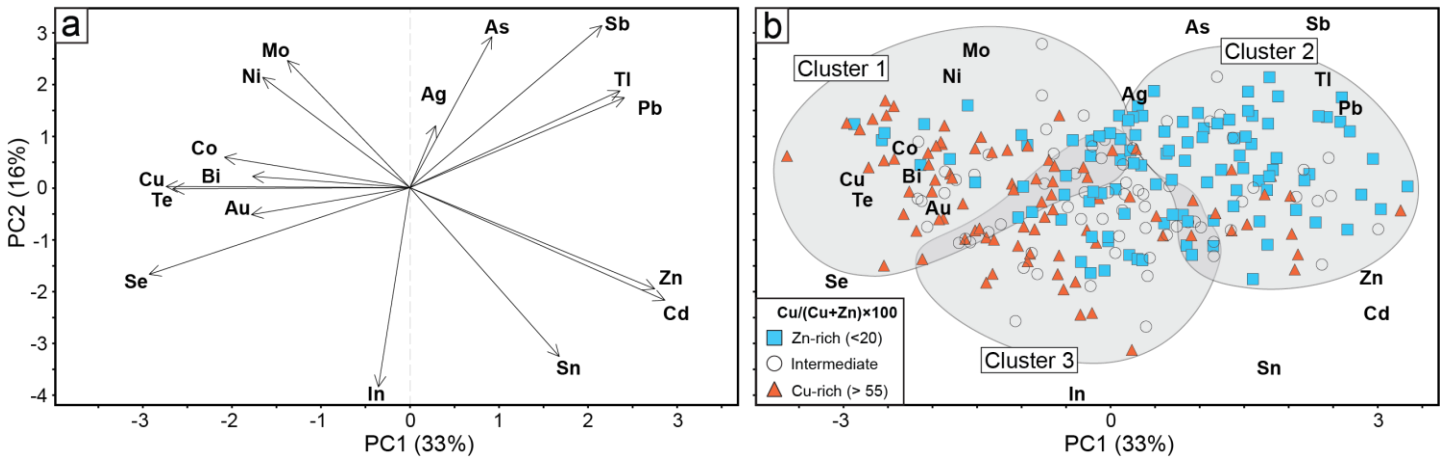

Figure 4.32 a) Loadings on PC1 and PC2 of the hydrothermal suite of trace metals (Cu, Zn, Pb, Ag, Au, Bi, Co, Ni, Se, Te, Cd, In, Sn, Mo, As, Sb, and Tl) in pyrite samples (n=265) from 55 VMS deposits in the Superior Province (Tables 2.1 and 4.1) shown as a two-dimensional scatterplot in PC space. The plotted element symbols are loadings of each element on PC1 and PC2, describing how the different elements contribute individually to the variance represented by the component. b) Results of hierarchical clustering (HCPC) of elements in pyrite samples classified according to the bulk Cu/(Cu+Zn) grade ratios of the deposits. The deposit classes are: Cu/(Cu+Zn) <20 (Zn-rich deposits; n=22), Cu/(Cu+Zn) = 20–55 (Intermediate; n=15), and Cu/(Cu+Zn) >55 (Cu-rich deposits; n=17). The plotted points for each sample are a linear combination of Cu, Zn, Pb, Ag, Au, Bi, Co, Ni, Se, Te, Cd, In, Sn, Mo, As, Sb, and Tl representing the contribution to the variance on PC1 and PC2. The trace elements that have the greatest influence on the defined clusters are: Cu, Au, Bi, Co, Ni, Se, Te, Mo (cluster 1); Zn, Pb, Ag, Cd, Sb, As, (cluster 2); and Se, In, and Sn (cluster 3) (Table 4.12). The tabulated data refer to how close individual elements are to the centre of each cluster based on Ward's Criterion (the sum of the squared distances of sample points). The variance on PC1 is interpreted to reflect a combination of the temperatures of ore formation and the compositions of the host rocks. See the text for discussion.

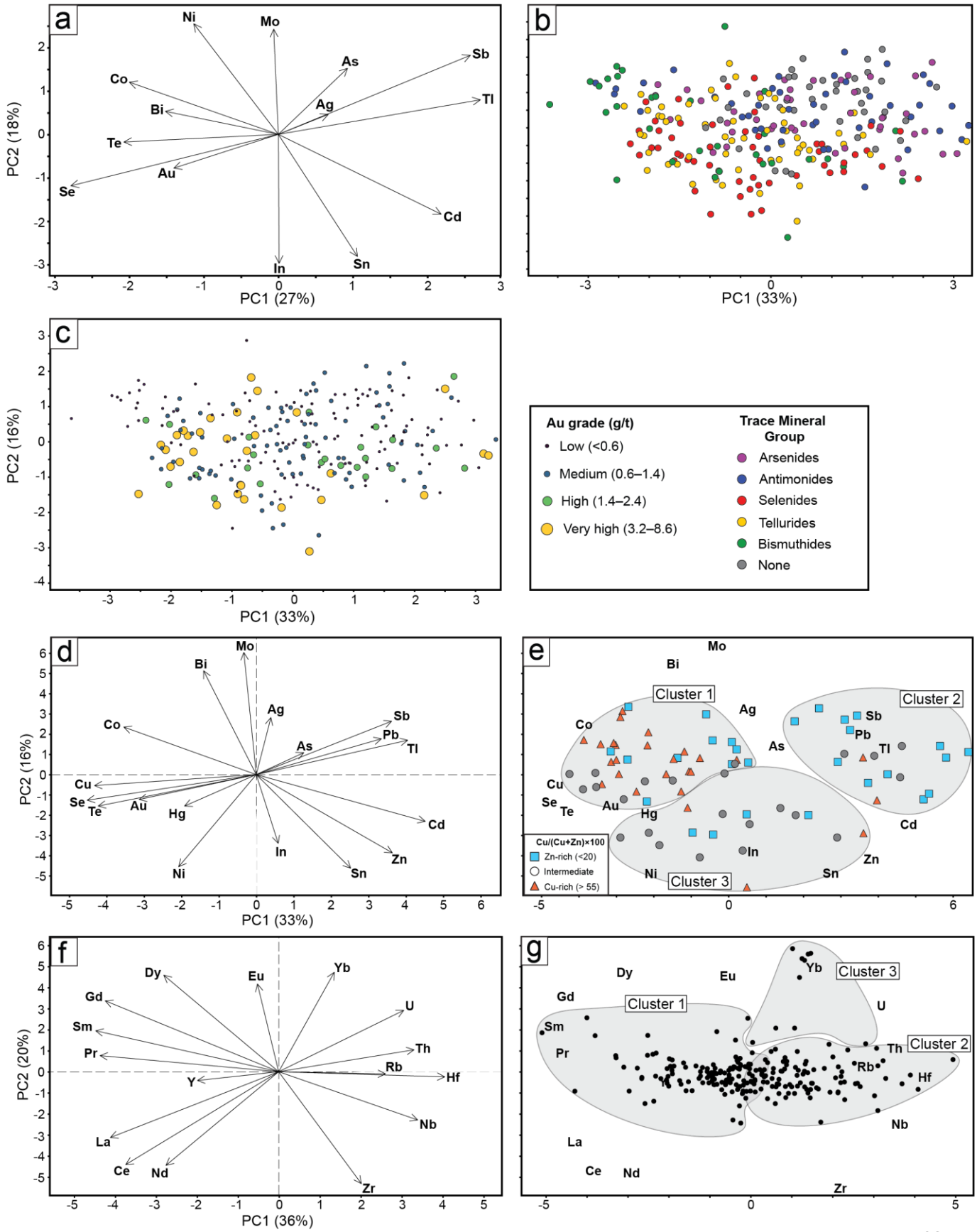
a
Ni
Mo
As
Sb
Co
Bi
Ag
Tl
Te
Au
Se
Cd
In
Sn
PC1 (27%)
PC2 (18%)
b
PC1 (33%)
c
PC1 (33%)
PC2 (16%)
Au grade (g/t)
Low (<0.6)
Medium (0.6–1.4)
High (1.4–2.4)
Very high (3.2–8.6)
Trace Mineral Group
Arsenides
Antimonides
Selenides
Tellurides
Bismuthides
None
d
Mo
Bi
Ag
Co
Sb
Pb
As
Tl
Cu
Se
Te
Au
Hg
Cd
In
Zn
Ni
Sn
PC1 (33%)
PC2 (16%)
e
Mo
Bi
Cluster 1
Cluster 2
Cluster 3
Ag
Co
Sb
Pb
As
Tl
Cu
Se
Te
Au
Hg
Cd
In
Zn
Ni
Sn
Cu/(Cu+Zn)×100
Zn-rich (<20)
Intermediate
Cu-rich (> 55)
f
Dy
Eu
Yb
Gd
U
Sm
Th
Pr
Rb
Hf
Y
Nb
La
Ce
Nd
Zr
PC1 (36%)
PC2 (20%)
g
Dy
Eu
Yb
Cluster 3
Gd
Cluster 1
U
Sm
Th
Cluster 2
Pr
Rb
Hf
Nb
La
Ce
Nd
Zr

Figure 4.33 a) Loadings on PC1 and PC2 of the hydrothermal suite of trace metals excluding Cu, Zn, and Pb in pyrite samples (n=265) from 55 VMS deposits in the Superior Province. shown as a two-dimensional scatterplot in PC space. The plotted element symbols are loadings of each element on PC1 and PC2, describing how the different elements contribute individually to the variance represented by the component. b) Pyrite sample points of the PCA in a) classified by the inferred dominant trace mineral group of each sampled deposit. c) Set of the hydrothermal suite of elements including Cu, Zn, and Pb from the PCA in Fig. 4.32.a with sample attributes representing Au grades the sampled deposits. d) Loadings and PC1 and PC2 of a subset of the hydrothermal suite of elements including Hg and excluding samples without Hg analyses. e) Results of hierarchical clustering (HCPC) of elements in pyrite samples classified according to the bulk Cu/(Cu+Zn) grade ratios of the deposits. The deposit classes are: Cu/(Cu+Zn) <20 (Zn-rich deposits; n=22), Cu/(Cu+Zn) = 20–55 (Intermediate; n=15), and Cu/(Cu+Zn) >55 (Cu-rich deposits; n=17). The plotted points for each sample are a linear combination of Cu, Zn, Pb, Ag, Au, Bi, Co, Ni, Se, Te, Cd, In, Sn, Mo, As, Sb, Hg, and Tl representing the contribution to the variance on PC1 and PC2. f) Loadings on PC1 and PC2 of HFSE (U, Th, Nb, Hf, and Sc), LILE (Rb), and REE (La, Ce, Pr, Nd, Sm, Eu, Gd, Y, Dy, Yb) in pyrite samples (n=265) from 55 VMS deposits in the Superior Province. g) Results of hierarchical clustering (HCPC) of elements in pyrite samples from the PCA in f). See the text for discussion.

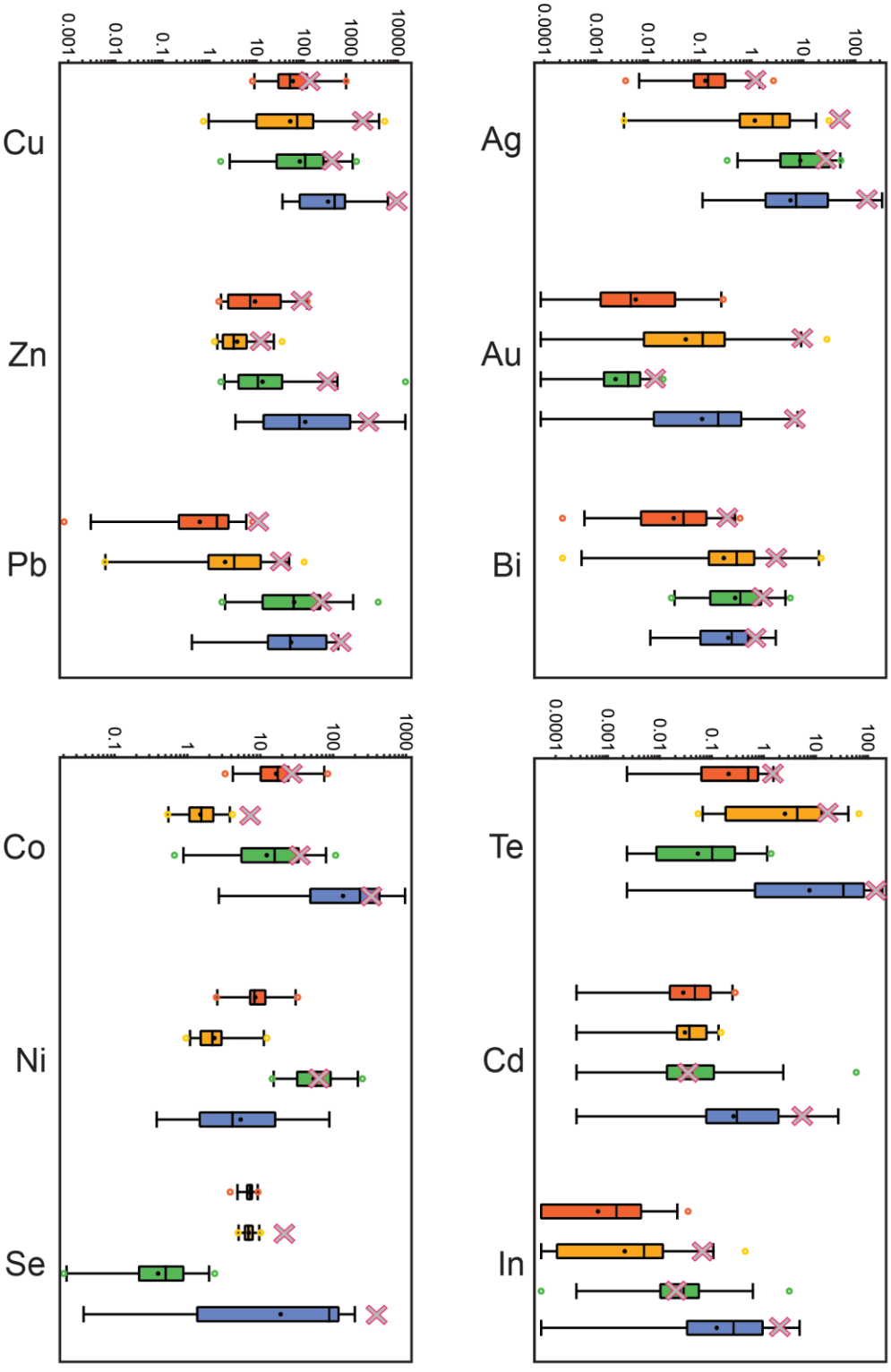
Cu
Zn
Pb
Ag
Au
Bi
Co
Ni
Se
Te
Cd
In

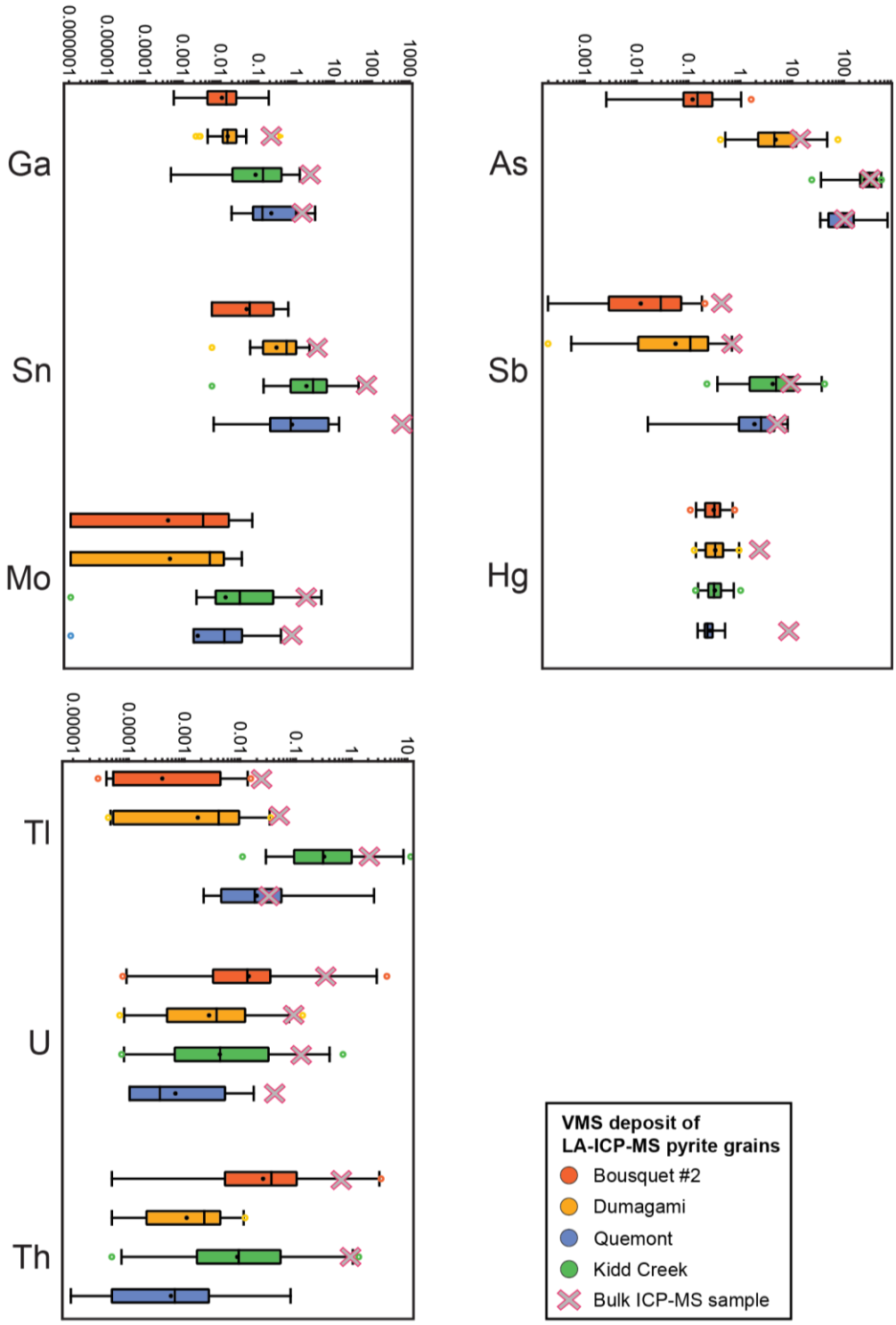
Ga
Sn
Mo
As
Sb
Hg
Tl
U
Th
VMS deposit of
LA-ICP-MS pyrite grains
Bousquet #2
Dumagami
Quemont
Kidd Creek
Bulk ICP-MS sample

Figure. 4.34 Boxplots of selected trace element concentrations in individual pyrite grains determined by LA-ICP-MS compared to bulk analyses of the pyrite concentrates by solution ICP-MS. Each box encloses 50% of the LA-ICP-MS data within the interquartile range (from Q1 to Q3). The average values (open circles) and median (line) are shown. 5th and 95th percentiles are lower and upper ends of whiskers. Outliers (circles) are within the bottom or top 5% of the dataset. The 'X' symbol corresponds to the bulk analysis of the pyrite concentrates by solution ICP-MS. The plots show that most elements enriched in bulk samples of the pyrite are also enriched at the grain scale in individual spot analyses. Both LA-ICP-MS analyses of individual pyrite grains and bulk ICP-MS analyses of the Quemont pyrite sample have the highest Cu, Zn, Pb, Ag, Au, Co, Se, and Te (e.g., compared to the Bousquet #2-Duamgami samples). Differences between the spot analyses of individual pyrite grains and the bulk analyses of the pyrite concentrates are interpreted to be mainly due to the lower detection limits of the LA-ICP-MS analyses, which are 1–3 orders of magnitude lower than the bulk ICP and INAA analyses.

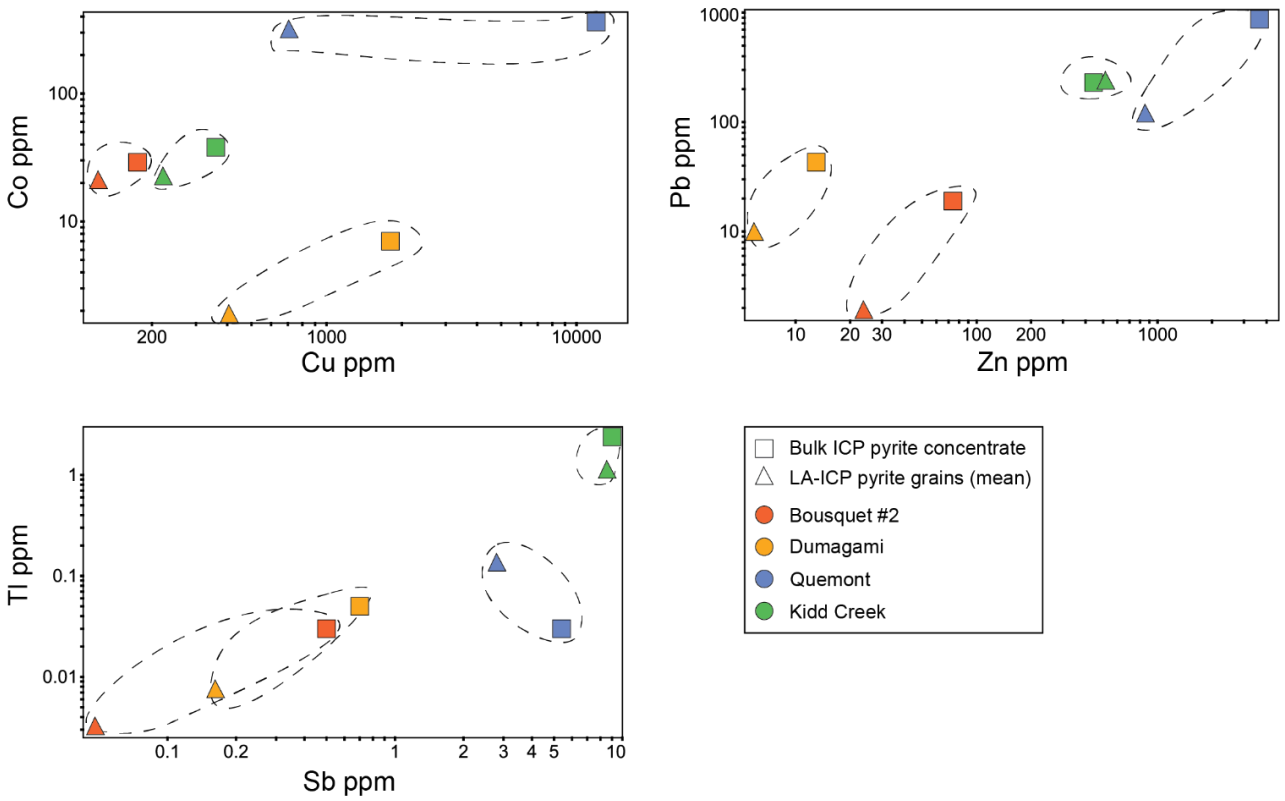

Figure 4.35 Binary plots of trace element concentrations (ppm) in individual pyrite grains determined by LA-ICP-MS (triangular symbols: averages) compared to bulk analyses of the pyrite concentrates by solution ICP-MS (squares: single analyses). There are 30 grains from the Bousquet #2 sample, 28 grains from the Dumagami sample, 24 grains from the Quemont sample, and 32 grains from the Kidd Creek sample with averaged LA-ICP-MS values. The plot illustrates the generally close similarity of trace element concentrations in individual pyrite grains and bulk samples between the different deposits. The absolute concentrations of the different elements are similar; e.g., the Kidd Creek pyrite grains analyzed by LA contain an average of 470 ppm Zn (n=32 spots on individual pyrite grains) and the bulk analysis of the pyrite concentrate contains 440 ppm. Individual pyrite grains and bulk samples of pyrite from Bousquet #2-Dumagami indicate the same low concentrations of Cu, Zn, Pb, Co, Sb, and Tl; the individual pyrite grains and bulk samples from Quemont have higher concentrations of Cu, Zn, and Pb, and the sample pairs from Kidd Creek have the highest concentrations of Zn, Pb, Sb, and Tl.

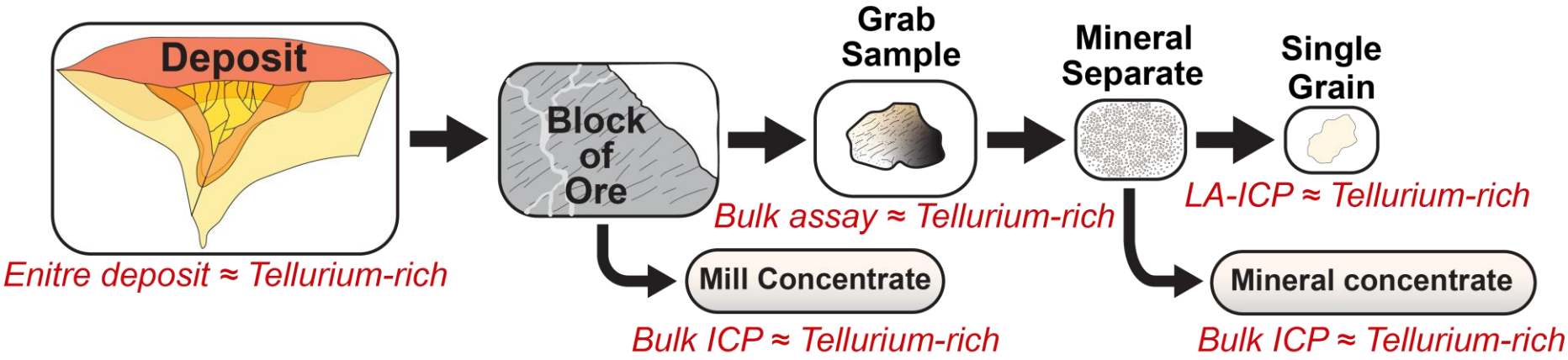

Figure 4.36 Schematic illustration of the scope of this study highlighting the relationship between different scales of sampling and sample types and showing the consistent trace element geochemistry from an entire deposit to a single sample. The data compared in this study include assays of bulk tonnage, monthly concentrates from the mill, individual grab samples, mineral separates from the grab samples, and single grains. We show that for many elements, the trace element fingerprint is the same at all scales from the deposit as a whole to an individual grab sample. A sample of ore from a deposit that is enriched in a particular element compared to another deposit, will almost always show trace enrichment of that element in all samples.

Table 4.1 Classifications of VMS deposits in the Superior Province used in this study. a) bulk Cu/(Cu+Zn) grade ratios.

Low (<20)	**Medium (20–55)**	**High (>55)**
Coniagas	Amulet-C	East Waite
Geneva Lake	Aldermac	New Hosco
Moosehead	Kidd Creek	Old Waite
Abcourt-Barvue	Norita-A	Corbet
Gallen	Genex	Louvicourt
Louvem	Geco	East Sullivan
Isle Dieu	Joutel Copper	Bousquet #2
Deldona	Norbec & Lac Dufault	Dumagami
Delbridge	Canadian Jamieson	Vauze
Mogador	Quemont	Potter-Doal
Mattagami Lake	Poirier	Robb Montbray
Mattabi	Millenbach	Ansil
Bell Allard	Amulet A	Bedford
Willecho	Horne #5 Zone	Conigo-Jay
Orchan	Kam Kotia	Dunraine
Lyon Lake		Horne-H&G
Normetal		New Insco
Stralak		
South Bay		
Mobrun		
Sturgeon Lake		
Manitou Barvue		

Table 4.1 cont. b) deposit Au grades.

Low (<0.6 g/t)	**Medium (0.6–1.4 g/t)**	**High (1.6-2.4 g/t)**	**Very high (4.1–7.8 g/t)**
Abcourt-Barvue	Norita-Radiore A	Poirier	Deldona
Conigo-Jay	Louvem	Ansil	Robb-Montbray
Geneva Lake	Vauze	East Waite	Quemont
Stralak	Bell Allard	Delbridge	Horne-H&G
Joutel Copper	Louvicourt		Bousquet #2-Dumagami
Willecho	New Insco		
Geco	Norbec & Lac Dufault		
Moosehead	Millenbach		
Bedford	Corbet		
Newbec	Old Waite		
Coniagas	Mogador		
Mattabi	Mobrun		
Lyon Lake	Horne #5 Zone		
Sturgeon Lake	Amulet-A		
Genex			
Potter-Doal			
South Bay			
Kidd Creek			
New Hosco			
Gallen			
Dunraine			
Kam Kotia			
East Sullivan			
Mattagami Lake			
Canadian Jamieson			
Manitou			
Barvue			
Isle Dieu			
Aldermac			
Orchan			
Amulet-C			
Normetal			

Table 4.1 cont. c) deposit sizes.

Small (<3 Mt)	Medium (3–8 Mt)	Large (8–171 Mt)
Moosehead	Dunraine	Gallen
Potter-Doal	Bell Allard	Abcourt-Barvue
Deldona	Lyon Lake & Creek zone	Normetal
Geneva Lake	Orchan	Mobrun
Robb Montbray	Millenbach	Mattabi
Bedford	Norita-Radiore A	Manitou Barvue
Vauze	Sturgeon Lake	East Sullivan
Delbridge	Norbec & Lac Dufault	Quemont
Mogador	Amulet A-Upper& Lower	Louvicourt
Amulet-C	Kam Kotia	Mattagami Lake
Stralak	Poirier	Horne-H&G
Coniagas	Bousquet #2	Geco
Canadian Jamieson		Horne #5 Zone
New Insco		Kidd Creek
Old Waite		
East Waite		
South Bay		
Ansil		
Joutel Copper		
Genex		
Willecho		
New Hosco		
Dumagami		
Louvem		
Conigo-Jay		
Corbet		
Aldermac		
Isle Dieu		

Sizes are total past production and current resources & reserves. Tonnage in Mtonnes.

Table 4.2 Summary statistics of bulk analyses of pyrite from VMS deposits of the Superior Province. Trace metal concentrations in ppm determined by a combination of solution ICP-MS and INAA. The original dataset and details of the samples are in Jonasson et al. (2020)

Data in ppm	**Cu**	**Zn**	**Pb**	**Ag**	**Au**	**Bi**	**Co**	**Ni**	**Se**	**Te**	**Cd**	**In**	**Ga**	**Sn**	**W**	**Mo**	**V**	**As**	**Sb**	**Hg**	**Tl**	**U**
Superior Province VMS Summary																						
N	244	287	244	286	239	203	283	109	154	127	226	211	239	242	17	226	25	171	180	87	202	196
Minimum	29.0	7.00	5.00	1.00	0.008	0.10	0.50	5.00	0.20	0.10	0.10	0.025	0.05	0.25	0.50	0.10	2.50	1.70	0.20	0.50	0.01	0.01
Maximum	29000	2E+05	70000	2E+05	117	870	11500	593	6690	1600	960	120	69.0	15000	30.0	250	78.0	44200	2560	820	27.0	1455
Mean	3204	12139	1803.0	889	3.49	50.0	678	102	230	37.4	28.3	4.54	3.13	269	8.44	9.82	23.2	929	74.0	15.1	1.79	7.65
Median	1200	2390	180.0	29.0	0.505	15.0	196	50.0	60.0	5.11	7.00	1.20	1.00	12.5	6.00	1.40	17.0	248	6.35	3.00	0.53	0.10

Elements are listed in the following order: 1) base metals; 2) precious metals; 3) Cu-associated; 4) Zn associated; 5) Pb/ sulfosalt associated; 6) U-radiogenic.

Table 4.3 Observations and interpretations of the mineralogical controls of trace element distributions in the pyrite concentrates.

	Pyrite solid solution limit (inferred)	Comments
Cu	~100 ppm	Assume all of the Cu is in chalcopyrite and convert to CuFeS2. Convert CuFeS2 to Fe and subtract from the total Fe (recalculate the amount of pyrite).
Zn	100 or 300 ppm	Assume all of the Zn is in sphalerite and calculate the modal abundance of sphalerite.
Pb	80 or 100 ppm	Assume all of the Pb is in galena and calculate the modal abundance of galena.
Ag	10 ppm (small gap). Population change below this level	Probable concentration of tetrahedrite-tennantite or galena indicated by correlation with Pb and Sb. Test correlation with stoichiometric compositions of possible silver bearing minerals.
Au	~5 ppm (upper population inflection)	Assume majority of Au is free gold/ or electrum in pyrite and to a lesser extend lattice bound or adsorbed onto pyrite surface. Possible concentration of chalcopyrite, tellurides, sulfosalts indicated by mixed correlations with Cu, Ag, Bi, Te, As and Sb of outliers.
Bi	~20 ppm. Also data gaps at 2 and 5 ppm.	Probable concentration in chalcopyrite as inclusions of tellurides, or bismuthinite indicated by correlation with Cu and Te of outliers.
Co	~2000 ppm	Assume the majority of the Co is lattice bound in pyrite or as inclusions of discrete cobalt minerals (i.e. cobaltite). Test correlation with As in subset of Co rich samples.
Ni	~250 ppm. Separate populations also at 50 and 100 ppm.	Assume the majority of the Ni is lattice bound in pyrite or as inclusions of discrete nickel minerals.
Se	~250 ppm (uppermost population change)	Assume the majority of the Se is lattice bound in pyrite or as inclusions in discrete selenium minerals. Probable concentrations in chalcopyrite or other trace minerals.
Te	~3 or 7 ppm (large gaps)	Possible concentration in tellurides, calaverite, hessite, altaite, coloradoite, or native Te indicated by correlation with Au, Ag, Bi, and Hg of outliers.
Cd	~4 ppm (small gap)	Certain concentration in sphalerite indicated by 1:1 correlation with Zn. (But some correlation in cadmium rich samples with Se)
In	~5 ppm (population change)	Probable concentration in sphalerite and chalcopyrite indicated by correlation with Zn and Cu of outliers.

Table 4.3 cont.

	Pyrite solid solution limit (inferred)	Comments
Ga	~1.5 ppm (steep population change)	Possible concentration in sphalerite indicated by slight correlation with Zn (watch for Ga-Zn interference by ICP). Test correlation with stoichiometric compositions of possible gallium bearing minerals including Ga-S and Ga bearing aluminosilicates. Possible coupled substitution of Ga and S. In solid solution in pyrite at low concentrations.
Sn	~2ppm (upper limit of first population)	Probable concentration in sphalerite and chalcopyrite as inclusions of discrete tin bearing minerals (cassiterite, mawsonite, colusite) and possibly in solid solution in chalcopyrite.
W	-	Assume the majority of W is present as inclusions of scheelite or wolframite in pyrite or sphalerite (very unlikely to be present as solid solution in pyrite or sphalerite).
Mo	~80 ppm (Uppermost population change)	Assume the majority of Mo is lattice bound in pyrite or as inclusions of molybdenite.
V	~10 ppm (first data inflection)	Assume the majority of V is present as inclusions of magnetite, ilmenite, hematite, and rutile or in solid solution in pyrite or possibly chalcopyrite.
As	~1200 ppm	Assume the majority of As is present as inclusions of arsenopyrite and tennantite-tetrahedrite (i.e. correlation with Zn, Pb, Ag and Sb of outliers) or in solid solution in pyrite or possibly sphalerite.
Sb	~15 ppm. Two higher populations	Assume the majority of Sb is present as inclusions of tennantite-tetrahedrite (i.e. correlation with Zn, Pb, Ag, As, and Hg of outliers) or in solid solution in pyrite or possibly sphalerite.
Hg	Limit uncertain due to stepped distribution. Most likely below 10 ppm.	Assume the majority of Hg is present in solid solution in sphalerite or possibly pyrite, or as inclusions of tennantite-tetrahedrite (i.e. correlation with Zn, Pb, Ag and Sb of outliers).
Tl	~ 5ppm	Assume the majority of Tl is lattice bound in pyrite or possibly sphalerite. Max values are within range of documented Tl concentrations in pyrite.
U	~0.5 ppm	Assume the majority of U is present as inclusions of discrete U bearing minerals or in solid solution in pyrite or possibly chalcopyrite and sphalerite.

The solid solution limits of element concentrations in the pyrite samples were inferred their data distributions plotted on probability curves (Fig, A.1). Limits were selected where significant gaps or changes in populations occurred in the range of concentrations documented for ICP-MS studies of pyrite from VMS

Table 4.4 Pearson correlation coefficients for log-transformed trace metal analyses of pyrite concentrates (n= 265) from VMS deposits of the Superior Province. The original dataset and details of the samples are available in Jonasson et al. (2020)

	Cu	Zn	Pb	Ag	Au	Bi	Co	Ni	Se	Te	Cd	In	Ga	Sn	W	Mo	V	As	Sb	Hg	Tl
Cu	1																				
Zn	-0.170	1																			
Pb	-0.210	**0.520**	1																		
Ag	0.230	0.210	0.380	1																	
Au	0.410	0.025	-0.002	0.300	1																
Bi	**0.440**	-0.091	0.055	0.240	0.290	1															
Co	**0.470**	-0.098	-0.051	0.130	0.320	0.370	1														
Ni	0.074	-0.190	-0.190	-0.130	0.280	0.038	0.110	1													
Se	**0.610**	-0.077	-0.100	0.160	**0.530**	0.280	**0.550**	0.180	1												
Te	0.370	-0.260	-0.200	0.100	**0.510**	0.053	0.037	0.190	0.380	1											
Cd	-0.200	**0.910**	0.420	0.085	-0.011	-0.076	-0.180	-0.130	-0.110	-0.260	1										
In	**0.460**	0.220	-0.180	0.120	0.160	0.330	0.110	-0.010	0.390	0.038	0.260	1									
Ga	0.022	**0.480**	0.092	-0.029	-0.025	0.064	-0.085	-0.160	0.015	0.098	0.400	0.260	1								
Sn	0.006	**0.510**	0.210	0.140	-0.008	0.130	-0.006	-0.320	-0.061	0.027	**0.510**	**0.460**	0.380	1							
W	-0.080	-0.410	0.110	-0.380	-0.450	-0.390	-0.210	0.410	-0.260	0.190	-0.290	**-0.570**	-0.084	0.110	1						
Mo	0.280	-0.390	-0.160	0.033	0.096	0.260	0.110	0.390	0.100	0.069	-0.270	-0.049	-0.140	-0.200	0.260	1					
V	-0.280	0.340	0.350	0.090	-0.150	-0.140	**-0.450**	**-0.520**	0.350	**0.490**	0.240	-0.008	**0.680**	0.350	0.037	-0.380	1				
As	-0.020	0.180	0.180	0.180	0.100	-0.069	-0.011	0.062	-0.091	-0.008	0.033	-0.001	-0.140	-0.068	0.150	-0.012	0.190	1			
Sb	-0.061	0.390	**0.570**	**0.490**	0.100	0.086	-0.100	-0.016	-0.200	-0.130	0.170	-0.037	-0.067	0.140	0.310	0.066	0.370	**0.550**	1		
Hg	0.140	0.110	0.150	0.098	0.290	0.062	0.010	0.004	0.270	0.074	0.006	0.250	-0.140	0.170	-0.140	-0.130	-0.160	0.270	0.210	1	
Tl	-0.140	0.340	0.420	0.200	-0.074	-0.009	-0.150	-0.270	-0.380	-0.200	0.240	-0.084	0.150	0.150	-0.085	-0.170	0.026	0.280	0.400	0.066	1

Hydrothermal suite of elements listed in the following order: 1) base metals; 2) precious metals; 3) Cu-associated; 4) Zn-associated; 5) Pb/ sulfosalt associated. Strongly correlated values highlighted in green and bold have a critical value over 0.423 at the 95% confidence level based on a two-tailed test and 20 degrees of freedom (number of variables minus 2).

Table 4.5 Pearson correlation coefficients for log-transformed HFSE and REE in pyrite concentrates (n=242) from VMS deposits of the Superior Province dataset. The original dataset and details of the samples are available in Jonasson et al. (2020)

	U	Th	Zr	Nb	Hf	Ta	Be	Rb	Sr	Cs	La	Ce	Pr	Nd	Sm	Eu	Gd	Sc	Y	Tb	Dy	Ho	Er	Tm	Yb	Lu
U	1																									
Th	**0.780**	1																								
Zr	**0.650**	**0.770**	1																							
Nb	**0.600**	**0.700**	**0.810**	1																						
Hf	**0.680**	**0.770**	**0.970**	**0.730**	1																					
Ta	**0.480**	**0.510**	**0.450**	**0.620**	**0.540**	1																				
Be	0.080	0.190	**0.490**	**0.420**	0.280	0.720	1																			
Rb	0.380	**0.480**	**0.420**	**0.420**	**0.460**	0.029	0.086	1																		
Sr	-0.190	0.320	-0.042	0.240	**0.360**	0.800	**0.970**	0.190	1																	
Cs	0.160	0.160	0.140	0.290	0.120	0.380	-0.032	0.270	0.320	1																
La	**0.620**	**0.720**	**0.660**	**0.650**	**0.670**	**0.410**	0.210	**0.410**	-0.004	0.056	1															
Ce	**0.590**	**0.730**	**0.680**	**0.670**	**0.670**	**0.410**	0.270	**0.400**	-0.039	0.140	**0.970**	1														
Pr	**0.590**	**0.710**	**0.660**	**0.650**	**0.660**	**0.490**	0.310	**0.430**	**0.450**	0.150	**0.980**	**0.970**	1													
Nd	**0.590**	**0.720**	**0.710**	**0.700**	**0.690**	**0.530**	0.320	**0.430**	0.190	0.160	**0.940**	**0.950**	**0.960**	1												
Sm	**0.580**	**0.720**	**0.670**	**0.640**	**0.690**	**0.390**	0.360	**0.410**	**0.480**	0.200	**0.940**	**0.960**	**0.970**	**0.960**	1											
Eu	**0.470**	**0.640**	**0.550**	**0.560**	**0.580**	**0.420**	**0.610**	0.310	**0.690**	0.280	**0.780**	**0.790**	**0.790**	**0.820**	**0.800**	1										
Gd	**0.570**	**0.670**	**0.670**	**0.650**	**0.690**	**0.530**	**0.490**	**0.400**	0.140	0.220	**0.910**	**0.900**	**0.930**	**0.910**	**0.960**	**0.790**	1									
Sc	**0.360**	**0.520**	**0.510**	**0.540**	**0.530**	**0.280**	-0.290	0.260	**0.590**	0.120	**0.630**	**0.640**	**0.650**	**0.670**	**0.640**	**0.550**	**0.600**	1								
Y	**0.560**	**0.650**	**0.750**	**0.720**	**0.720**	**0.520**	**0.910**	**0.420**	0.170	0.260	**0.830**	**0.840**	**0.850**	**0.850**	**0.880**	**0.710**	**0.950**	**0.570**	1							
Tb	**0.500**	**0.660**	**0.560**	**0.500**	**0.660**	**0.600**	**0.520**	0.300	**0.570**	0.310	**0.760**	**0.780**	**0.800**	**0.800**	**0.870**	**0.710**	**0.940**	**0.510**	**0.920**	1						
Dy	**0.540**	**0.690**	**0.690**	**0.660**	**0.710**	**0.570**	**0.970**	0.360	0.120	0.350	**0.830**	**0.850**	**0.870**	**0.850**	**0.910**	**0.720**	**0.970**	**0.580**	**0.980**	**0.950**	1					
Ho	**0.500**	**0.610**	**0.580**	**0.530**	**0.700**	**0.620**	**0.900**	**0.400**	**0.580**	0.360	**0.720**	**0.740**	**0.780**	**0.770**	**0.830**	**0.650**	**0.920**	**0.490**	**0.980**	**0.920**	**0.980**	1				
Er	**0.580**	**0.690**	**0.670**	**0.640**	**0.740**	**0.680**	**0.980**	0.380	**0.620**	**0.400**	**0.760**	**0.770**	**0.800**	**0.800**	**0.840**	**0.650**	**0.920**	**0.570**	**0.990**	**0.910**	**0.980**	**0.980**	1			
Tm	**0.580**	**0.660**	**0.590**	**0.590**	**0.690**	**0.550**	**0.910**	**0.390**	**0.640**	**0.410**	**0.650**	**0.640**	**0.680**	**0.660**	**0.730**	**0.610**	**0.850**	**0.340**	**0.960**	**0.900**	**0.940**	**0.970**	**0.980**	1		
Yb	**0.590**	**0.690**	**0.670**	**0.610**	**0.770**	**0.640**	**0.930**	**0.400**	**0.620**	0.360	**0.680**	**0.730**	**0.710**	**0.730**	**0.770**	**0.640**	**0.810**	**0.510**	**0.910**	**0.880**	**0.880**	**0.940**	**0.960**	**0.960**	1	
Lu	0.640	**0.700**	**0.650**	**0.650**	**0.760**	**0.640**	**0.950**	**0.390**	**0.660**	0.330	**0.620**	**0.640**	**0.610**	**0.650**	**0.680**	**0.620**	**0.710**	**0.330**	**0.830**	**0.810**	**0.800**	**0.890**	**0.890**	**0.940**	**0.980**	1

Elements are listed in the following order: U, Th, Zr, REEs. Values in bold have a critical value over 0.388 at the 95% confidence level based on a two-tailed test and 20 degrees of freedom (number of variables minus 2). Values highlighted in green (>0.8) indicate the most strongly correlated element pairs.

Table 4.6 Average trace element concentrations (ppm) of pyrite samples from VMS deposits classified by bulk Cu/(Cu+Zn) grade ratios of the deposits. The original dataset and details of the samples are available in Jonasson et al. (2020).

Data in ppm	Cu	Zn	Pb	Ag	Au	Bi	Co	Ni	Se	Te	Cd	In	Ga	Sn	W	Mo	As	Sb	Hg	Tl	U
Superior Province VMS deposit Cu/(Cu+Zn)×100																					
Low (<20)	1943	8042	1535	100	2.08	37.1	295	70.6	166	6.86	14.8	2.60	3.15	109	10.0	6.73	735	81.2	5.13	2.29	0.194
Medium (20–55)	2219	6007	619	72.6	3.40	30.9	609	63.0	128	61.6	21.9	3.46	2.57	686	9.14	3.32	341	10.5	4.79	1.93	0.133
High (>55)	4245	5812	267	53.4	4.83	74.8	1247	130	429	36.2	18.0	4.97	3.36	91.0	4.50	18.6	540	9.05	5.90	0.518	0.365

Table 4.7 Average trace element concentrations (ppm) of pyrite samples classified according to Figure 4.3.c of VMS in the Superior Province. The original dataset and details of the samples are available in Jonasson et al. (2020)

Data in ppm	Cu	Zn	Pb	Ag	Au	Bi	Co	Ni	Se	Te	Cd	In	Ga	Sn	W	Mo	As	Sb	Hg	Tl	U
Superior Province VMS deposits																					
Zn-rich pyrite samples from Zn-rich deposits	750.7	7253	3950	57.5	0.78	19.1	281	56.8	85.5	5.71	25.4	2.10	4.12	552	16.0	2.61	528	24.6	5.22	2.68	0.216
Cu-rich pyrite samples from Cu-rich deposits	4588	784	294	76.9	5.36	67.7	1068	125	318	80.1	3.75	2.80	2.15	64.3	8.00	18.3	500	6.42	5.42	0.50	0.357
Cu-rich pyrite samples from Zn-rich deposits	4071	987	250	94.8	1.16	76.1	441	49.6	268	12.7	2.96	5.23	0.83	101	4.00	10.5	591	6.13	5.00	1.56	0.152
Zn-rich pyrite samples from Cu-rich deposits	1864	13319	619	43.3	2.15	37.1	945	96.9	86.9	9.06	41.1	6.48	4.39	275	2.40	2.20	300	11.2	3.60	1.84	0.111

These data are classified in Figure 4.3.c and discussed in section 4.2.2 and in section 4.2.3.

Table 4.8 Average trace element concentrations (ppm) of Cu-rich and Zn-rich pyrite samples from VMS deposits of the Superior Province with different bulk Cu/(Cu+Zn) ratios and host rocks (felsic-dominant, intermediate, and mafic-dominant). The two groups of samples listed here are shown in Figure 4.3c. The original dataset and details of the samples are available in Jonasson et al. (2020).

Zn-rich pyrite samples from Zn-rich deposits

(Cu/Cu+Zn grade ratios <20)

Immediate host rocks	Cu	Zn	Pb	Ag	Au	Bi	Co	Ni	Se	Te	Cd	In	Ga	Sn	W	Mo	V	As	Sb	Hg	Tl	U
Felsic-dominant	540	15413	2599	104	7.52	16.8	348	79.3	482	0.70	21.4	0.55	1.19	1380	15	2.81	14.5	868	103	9.09	4.14	0.246
Intermediate	895	7315	1058	56.1	1.01	17.3	326	110	167	8.73	26.5	2.76	6.66	210	10.0	2.20	51.0	645	66.2	5.60	1.87	0.163
Mafic-dominant	718	6977	3468	146	0.68	5.52	593	39.7	87.8	1.35	25.0	2.02	1.45	57.7	9.00	12.0	-	255	13.9	2.00	1.16	0.306

Cu-rich pyrite samples from Cu-rich deposits

(Cu/Cu+Zn grade ratios >55)

Immediate host rocks	Cu	Zn	Pb	Ag	Au	Bi	Co	Ni	Se	Te	Cd	In	Ga	Sn	W	Mo	V	As	Sb	Hg	Tl	U
Felsic-dominant	4281	3257	290	122	11	89.7	1260	147	612	123	4.35	3.31	2.86	92.1	-	2.84	15.6	552	20.7	7.69	0.70	0.239
Intermediate	5294	409	163	35.8	1.49	43.9	653	115	263	26.5	2.03	1.59	1.63	14.6	8.00	45.6	23.2	714	8.44	4.08	0.25	0.565
Mafic-dominant	4783	5820	487	58.7	3.94	83.8	2148	64.0	228	56.7	5.88	2.46	0.95	83.2	-	1.55	-	133	19.6	6.33	0.74	0.202

Table 4.9 Summary of trace element signatures of pyrite samples from VMS deposits of the Superior Province grouped at different scales (assemblage/orogeny, mining districts, and individual deposits (example of the Noranda camp). See text for discussion.

a) Orogens and assemblages with pyrite data for VMS across Canada.

Assemblage/ orogen	Enrichments	Depletions
Deloro	Mo, Hg	Ag, Au, Bi, Ni, Se, Te, Cd, In, Sb, Tl
Tisdale	Co, Ni, Se, Ga, Mo, As	Pb, Ag, Bi, In, Sn, Sb, Tl
Kidd-Munro	Co, Cd, In, Sn, Ga	Au, Se, Te
Blake River	Au, Se, Te, Cd, In	Pb, As, Sb
Western Superior	Ag, Sn, W, As, Sb	Au, Ni, Te, Mo
Slave	± Pb	Au, Bi, Co, Se, Te, Sn
Trans-Hudson	As, Co, Te	Ag, Bi, Cd, In, Tl
Appalachians	Bi, In, Sn, Tl	As, Sb, Hg
Cordillera	As, Sb	Co, Ni, Cd, In, Sn

Table 4.9 cont. b) VMS camps of the Superior Province.

Camps	Enrichments	Depletions	Assemblages
Matagami	Bi, Co, Ni, Se,In, Sn	Ag, Au, Ni, Cd, In, Tl	Deloro
Joutel	Hg	Pb, Ag, Au, Bi, Te, Sb, Tl	Deloro
Quevillion	Pb, Ag, Cd	Au, Bi, Co, Ni, In, Mo, As, Sb, Tl	Deloro
Normetal	Ag, Au, Bi, As, Sb (outlier)	Pb, Se, Cd, In, Mo, Sn, Tl	Deloro
Amos-Barraute	Bi, As, Sb	Ag, Au, Ni, Cd, In, Tl	Deloro, Kidd-Munro
Timmins	Co, Ni, Cd, In, Sn, Tl	Sb, Te	Kidd-Munro, Blake River
Noranda Main	Bi, Co, Se, Te, Ga, In, Sn	Pb, Ag, Mo, As, Sb, Tl, W	Blake River
Noranda N-S-E-W	Au, Ni, Se, Te, Sn, Hg, Tl	Pb, Mo, As, Sb	Blake River
Bousquet	Au, Bi, Te	Pb, Ag, Co, Ni, Se, Sn, As, Tl	Blake River
Val d'Or	Co, Ni, Se, Ga, Mo, As	Pb, Ag, Au, Bi, Te, In, Sn, Sb, Tl	Tisdale
Uchi	None	Ag, Au, Bi, Co, Cd, Ga, Sn, Mo	Uchi
Sturgeon Lake	Ag, As, Sb, Hg	Co, Ni, Se, Te, Cd, In, Sn	Wabigoon
Manitouwadge	Pb, Cd, Sn, W	Ag, Au, Ni, Te, In, Ga, As, Sb, Tl	Wawa
Benny	Pb, Ag, Au, Mo, Sb	Cu, Zn, Bi, Ni, Se, In, Sn, Tl	Benny greenstone belt
High Lake	Bi	Ga, In, Sn, Tl	High Lake
Hackett River	Ni, Th, U, Zr	Ag, Au, Bi, Co, Se, Te, In	Hackett River
Hood River	Pb, Ag, Bi	Au, Ni,Se, Te, In, Sn, Ga, As	Amooga Booga
Flin Flon	Co, Ni, Te, Sb		Flin Flon
Snow Lake	Co, Ni, As		Snow Lake
Bathurst	Pb, Ag, Bi, In, Ga, Sn, Tl		Appalachian - Dunnage

Table 4.9 cont. c) Noranda camp.

Deposit	Enrichment	Depletion	Deposit type	Immediate host rocks	Camp
Amulet A	Ag, Cd, Sn	Te	Cu-Zn	Mafic	Noranda main
Amulet-C	Ga, Mo, Sb	Au, Bi, Te	Cu-Zn	Mafic	Noranda main
Ansil	Au, Bi, Se, Te, As	Ag	Cu-Zn	Felsic	Noranda main
Corbet	Au, Sn, Sb	Se	Cu-Zn	Mafic	Noranda main
East Waite	Co, Ni	-	Cu-Zn	Felsic	Noranda main
Millenbach	-	Au, Bi, Se, Te, Cd	Cu-Zn	Felsic	Noranda main
Newbec	Co, Ni	Ag	Cu-Zn	Mafic	Noranda main
Norbec & Lac Dufault	Bi, Co	Te	Cu-Zn	Felsic	Noranda main
Old Waite	Co, Ni, Se, Hg	Te	Cu-Zn	Mafic	Noranda main
Vauze	Ag, Bi, Co, Se, Cd, In, Sn, Ga	Te	Cu-Zn	Felsic	Noranda main
Moosehead	Pb	Au, Co	Zn-Pb	Mafic	Noranda main
New Insco	Bi, Co, Se	Au, Cd	Cu	Mafic	Noranda N-S-E-W
Quemont	Ag, Au, Ni, Se, Te	-	Cu-Au	Felsic	Noranda N-S-E-W
Robb Montbray	Ag, Au, Co, Ni, Se, Te, In, As, Hg	Bi	Cu-Au	Felsic	Noranda N-S-E-W
Horne #5 Zone	Au, Te, Sn, Hg	Bi, Cd	Cu-Au	Felsic	Noranda N-S-E-W
Horne-H&G	Au, Bi, Se, Te, Cd, In, Sn, Hg	Co	Cu-Au	Felsic	Noranda N-S-E-W
Delbridge	Pb, Ag, Au, As, Sb, Tl	Bi, Co	Zn-Ag-Au-Pb	Felsic	Noranda N-S-E-W
Deldona	Pb, Ag, Au, Tl	Co, Se, Te	Zn-Ag-Au-Pb	Felsic	Noranda N-S-E-W
Aldermac	Ga, W	Au	Zn-Cu	Felsic	Noranda N-S-E-W
Gallen	-	Co, Ni, Se, Te	Zn-Cu	Felsic	Noranda N-S-E-W
Mobrun	Ni, Se, Cd, In, Sn, As	-	Zn-Cu	Felsic	Noranda N-S-E-W

The different trace element groups are assigned to deposits according to their enrichments relative to the average concentrations of the elements in the pyrite samples from all deposits (Table A. 10–12). Groups of elements identified as 'enriched' have average concentrations above the mean for dataset. Groups of elements identified as 'depleted' have average concentrations below the median for that element in the dataset. The element assemblages for each group are ordered by: 1) base metals; 2) precious metals; 3) Cu-associated; 4) Zn-associated; 5) Pb/ sulfosalt associated.

Table 4.10 Selected trace ore minerals reported in the VMS deposits included in Jonasson et al. (2020).

	Trace mineral	Formula	Deposits
Cu			
	Chalcocite	Cu_2S	Bousquet #2 Dumagami, Kidd Creek, Norbec-Lac Dufault, Normetal, Ruttan
	Enargite	Cu_3AsS_4	Kidd Creek, Normetal, Schist Lake-Mandy
	Aikinite	$PbCuBiS_3$	Bousquet #2
	Roquesite	$CuFeS_2$	Kidd Creek
	Covellite	CuS	Bousquet #2, Dumagami, Kidd Creek, Myra Falls - Lynx, Ruttan
	Digenite	Cu_9S_5	Bousquet #2, Kidd Creek, Louvem, Myra Falls (Lynx)
	Cubanite	$CuFe_2S_3$	Coronation, Flin Flon, Hackett A Zone, Norbec-Lac Dufault, Normetal, Ruttan, Sherridon
	Renierite	$Cu_{13}Fe_2Ge_2S_{16}$	Bousquet #2
Zn			
	Gahnite	$ZnAl_2O_4$	Cornation, Hackett A Zone, Mattabi, Millenbach, Mobrun, Normetal, Sherridon
Pb			
	Anglesite	$PbSO_4$	Brunswick #12, Heath Steele
	Boulangerite	$Pb_5Sb_4S_{11}$	Brunswick #12, Chisel Lake, Eskay Creek, Kudz Ze Kayah, Mattabi, Sturgeon Lake
	Bournonite	$PbCuSbS_3$	Chisel Lake, Eskay Creek, Mattabi, Sturgeon Lake
	Jamesonite	$Pb_4FeSb_6S_{14}$	Eskay Creek
Ag			
	Native silver	Ag	Kidd Creek
	Argentite	Ag_2S	Britannia, Flin Flon, Kidd Creek, Norbec-Lac Dufault, South Bay, Willecho
	Proustite-pyrargyrite	$Ag_3(As,Sb)S_3$	Chisel Lake, Manitou Barvue
	Stephanite	Ag_5SbS_4	Hackett A Zone, Kidd Creek
	Dyscrasite	Ag_3Sb	Kidd Creek, Norbec-Lac Dufault, South Bay
	Stromeyerite	AgCuS	Dumagami, Kidd Creek, Myra Falls (Lynx)
	Sternbergite	$AgFe_2S_3$	Kidd Creek
	Mackinstryite	$(Ag, Cu)_2S$	Bousquet #2
	Acanthite	Ag_2S	Bousquet #2, Kidd Creek, Hackett A Zone
Au			
	Native gold	Au	Dumagami, Horne #5
	Electrum	Au(Ag)	Bousquet #2, Chisel Lake, Delbridge, Deldona, Eskay Creek, Flin Flon, Hackett A Zone, Horne #5, Kidd Creek, Kudz Ze Kayah, Quemont, Ruttan
	Calaverite	$AuTe_2$	Bousuqet #2, Dumagami, Horne, Old Waite, Quemont,
	Krennerite	$AuTe_2$ or Au_3AgTe_8	Corbet, Horne, Quemont
	Sylvanite	$(Au,Ag)_2Te_4$	Flin Flon, Horne, Horne #5, Quemont
	Petzite	Ag_3AuTe_2	Bousquet #2, Horne, Horne #5,

References: Price (1933), Autran et al. (1966), Sinclair (1970), Catallani et al. (1993), Hannington et al. (1999c), Mosier et al. (2009) and references therein, Dubé et al. (2014) and Grant et al. (2015).

Table 4.10 cont.

	Trace mineral	Formula	Deposits
Bi			
	Native bismuth	Bi	Ruttan
	Bismuthinite	Bi_2S_3	Heath Steele, Kidd Creek, Hackett A Zone
	Bohdanowiczite	$AgBiSe_2$	Kidd Creek
	Junoite	$Pb_3Cu_2Bi_8(S,Se)_{16}$	Kidd Creek
	Laitakarite	$Bi_4(Se,S)_3$	Kidd Creek
	Tetradymite	Bi_2Te_2S	Flin Flon, Horne, Louvem, Quemont
	Cosalite	$Pb_2Bi_2S_5$	Old Waite
	Wittchenite	Cu_3BiS_3	Bousquet #2
	Matildite	$AgBiS_2$	Hackett A Zone
	Lillianite	$Pb_3Bi_2S_6$	Hackett A Zone
	Heyrovskyite	$Pb_{10}AgBi_5S_{18}$	Hackett A Zone
Co			
	Cobaltite	CoAsS	Centennial, Heath Steele, Kidd Creek, Louvem, Rod
	Carrollite	$CuCo_2S_4$	Kidd Creek
	Cattierite	CoS_2	Kidd Creek
Ni			
	Pentlandite	$Fe,Ni)_9S_8$	Quemont
	Nickeline	NiAs	Kidd Creek
	Mackinawite	$(Fe,Ni)_9S_8$	Corbet, Millenbach, Mobrun, Lack Dufault-Norbec
Se			
	Clausthalite	PbSe	Kidd Creek, Kudz Ze Kayah
	Eucairite	CuAgSe	Kidd Creek
	Klockmannite	CuSe	Kidd Creek
	Naumannite	Ag_2Se	Kidd Creek
Te			
	Native Te	Te	Bousquet #2
	Hessite	Ag_2Te	Bousquet #2, Chisel Lake, Fox Lake, Horne, Horne #5, Mattagami Lake, Quemont, Ruttan
	Altaite	PbTe	Bousquet #2, Chisel Lake, Flin Flon, Horne, Horne #5, Mattagami Lake, Quemont
	Tellurobismuthite	Bi_2Te_3	Anderson Lake, Bousquet #2, Dumagami, Horne
	Mattagamite	$CoTe_2$	Mattagami Lake
	Melonite?	$NiTe_2$	?
	Telluroantimony	TeSb	Mattagami Lake

Table 4.10 cont.

	Trace mineral	Formula	Deposits
Cd			
	Cadmoselite	$CdSe$	Kidd Creek
In			
	Roquesite	$CuInS_2$	Kidd Creek
Ga	-	-	-
Sn			
	Cassiterite	SnO_2	
	Stannite	Cu_2FeSnS_4	Bousquet #2, Brunswick #12, Dumagami, Hackett A Zone, Horne #5, Kidd Creek, Norbec-Lac Dufault,
	Stannoidite	$Cu_6Cu_{22}(Fe_2,Zn)_3Sn_2S_{12}$	Brunswick #12, Geco, Horne #5, Kidd Creek, South Bay
	Kesterite	$Cu_2(Zn,Fe)SnS_4$	Kidd Creek
	Colusite	$Cu_{13}VAs_3S_{16}$	Bousquet #2, Kidd Creek
	Mawsonite	$Cu_6Fe_2SnS_8$	Bousquet #2, Kidd Creek
	Petrukite	$(Cu,Fe,Zn)_2(Sn,In)S_4$	Bousquet #2, Kidd Creek
W			
	Scheelite	$CaWO_4$	Horne #5, Kidd Creek
	Wolframite	$(Fe,Mn)WO_4$	Kidd Creek
	Tungstenite	WS_2	Kidd Creek
	Kiddcreekite	Cu_6SnWS_8	Kidd Creek
Mo			
	Molybdenite	MoS_2	Anderson Lake, Flexar, Horne Louvem, Mattagami Lake, Ruttan
As			
	Arsenopyrite	FeAsS	Bousquet #2, Centennial, Chisel Lake, Conigo-Jay, Coronation, Delbridge, Deldona, Flexar, Flin Flon, Fox Lake, Hackett A Zone, Heath Steel, Isle, Dieu, Kidd Creek, Kudz Ze Kayah, Lyon Lake, Manitou Barvue, Mattabi, Millenbach, Mobrun, Normetal, Osborne Lake, Rod, Schist Lake-Mandy, South Bay
	Tennantite	$(Cu,Ag,Zn,Fe)_{12}(As)_4S_{13}$	Bousquet #2, Britannia, Centennial, Chisel Lake, Flin Flon, Hackett A Zone, Hart River, Kidd Creek, Kudz Ze Kayah, Lyon Lake, Yava Manitou Barvue, Myra Falls (Lynx), South Bay
	Geocronite	$Pb_{14}(As,Sb)_6S_{23}$	Chisel Lake
	Pearceite	$(Ag,Cu)_{16}As_2S_{11}$	Manitou-Barvue
	Realgar	AsS	Eskay Creek
Sb			
	Tetrahedrite	$(Cu,Ag,Zn,Fe)_{12}(Sb)_4S_{13}$	Bousquet #2, Britannia, Centennial, Chisel Lake, Delbridge, Deldona, Eskay Creek, Flin Flon, Hackett A Zone, Hart River, Horne, Isle Dieu, Kidd Creek, Kudz Ze Kayah, Lyon Lake, Mantou Barvue, Mattabi, Myra Falls (Lynx), Normetal, Ruttan
	Freibergite	$(Ag,Cu,Fe,Zn)_{12}(Sb,As)_4S_{13}$	Eskay Creek, Heath Steel, Kidd Creek, Hackett A Zone
	Stibnite	Sb_2S_3	Eskay Creek
	Gudmundite	FeSbS	Chisel Lake, Hackett A Zone
Hg			
	Cinnabar	HgS	Eskay Creek
	Coloradoite?	HgTe	Ming (not sampled)
Tl	-	-	-

Table 4.11 Summary of deposits with samples of pyrite separates that are in stoichiometric proportion of certain trace minerals (shown in Fig. 4.26).

	Trace mineral	Deposits
Cu		
	Enargite	Mobrun, Lac Dufault, Vauze, Louvicourt, New Hosco
	Aikinite	Isle Dieu
Pb		
	Boulangerite	Bousquet #2
Ag		
	Proustite	Horne, Quemont
	Stromeyerite	Gallen, Dunraine
Au		
	Calaverite	Bousquet #2, Quemont
	Petzite	Bousquet #2, Horne #5, Mobrun, Bell Allard, New Hosco, Orchan, Louvicourt
Bi		
	Cosalite	Isle Dieu
	Wittchenite	Abcourt-Barvue, Louvem, Normetal, Dunraine, Conigo
	Matildite	Corbet, New Insco, Vauze, Dunraine, East Sullivan, Kam-Kotia, Isle Dieu, New Hosco
Te		
	Hessite	Quemont, Louvicourt, Orchan
In		
	Roquesite	Horne, Horne #5, Dunraine, New Hosco, Kidd Creek
Sn		
	Stannite	Quemont, Horne #5, Vauze, Isle Dieu, Norita-A, New Hosco
As		
	Tennantite	Horne #5, Robb-Montbray
Sb		
	Tetrahedrite	Dumagami, Ansil, Mobrun, New Hosco, Isle, Dieu, Mattagami Lake, Louvicourt, Orchan, Mattabi

Table 4.12 Results of Principal Components Analysis for three different sets of elements. Trace metals (hydrothermal suite of elements) including Cu, Zn, and Pb.

	PC1	PC2	PC3	PC4
Eigenvalues	5.59	2.65	1.53	1.37
Variance %	32.88	15.61	8.99	8.06
Cumulative %	32.88	48.49	57.47	65.53
As	0.29	0.48	0.07	0.06
Ag	0.08	0.22	0.38	-0.52
Bi	-0.50	0.06	0.01	0.14
Cd	0.78	-0.38	-0.06	0.19
Co	-0.56	0.11	0.55	0.35
In	-0.09	-0.74	-0.40	0.00
Se	-0.80	-0.34	0.18	-0.02
Sb	0.58	0.57	-0.17	-0.16
Sn	0.46	-0.62	-0.16	0.06
Te	-0.73	-0.02	-0.34	-0.33
Mo	-0.42	0.49	-0.53	0.18
Ni	-0.43	0.47	-0.18	0.53
Tl	0.65	0.34	-0.33	-0.20
Au	-0.48	-0.10	0.08	-0.62
Cu	-0.75	-0.02	0.23	0.05
Zn	0.76	-0.37	0.28	0.23
Pb	0.67	0.34	0.38	-0.06

Table 4.12 cont. Trace metals (hydrothermal suite of elements) including Cu, Zn, Pb, and Hg.

	PC1	PC2	PC3	PC4
Eigenvalues	6.24	2.81	1.98	1.35
Percent	34.65	15.60	11.00	7.52
Cumulative %	34.65	50.25	61.25	68.77
As	0.10	0.08	0.51	0.19
Ag	0.03	0.21	-0.09	0.07
Bi	-0.11	0.39	-0.29	0.05
Cd	0.34	-0.18	-0.06	-0.11
Co	-0.27	0.18	0.03	0.29
In	0.05	-0.26	-0.52	0.02
Se	-0.34	-0.10	-0.12	0.14
Sb	0.28	0.20	0.26	-0.29
Sn	0.19	-0.35	-0.18	0.13
Te	-0.32	-0.12	0.00	-0.27
Mo	-0.03	0.46	-0.08	-0.16
Ni	-0.16	-0.35	0.27	-0.28
Tl	0.31	0.13	-0.25	-0.16
Au	-0.24	-0.09	0.15	-0.51
Cu	-0.33	-0.04	0.04	0.28
Zn	0.28	-0.29	0.08	0.24
Pb	0.25	0.13	0.25	0.24
Hg	-0.15	-0.12	0.14	0.28

Table 4.12 cont. Non-metal trace elements including HFSE, LILE, and REE.

	PC1	PC2	PC3	PC4
Eigenvalues	5.79	3.13	2.39	1.08
Percent	36.18	19.55	14.91	6.77
Cumulative %	36.18	55.74	70.65	77.42
U	0.57	0.40	0.40	0.12
Th	0.61	0.14	0.46	0.27
Zr	0.37	-0.72	-0.46	0.17
Nb	0.63	-0.31	-0.09	0.02
Hf	0.75	-0.03	-0.12	0.43
Rb	0.48	-0.02	0.14	-0.77
La	-0.76	-0.42	0.27	0.07
Ce	-0.69	-0.60	0.10	0.14
Pr	-0.81	0.10	0.42	0.14
Nd	-0.51	-0.61	0.13	-0.18
Sm	-0.83	0.27	0.21	0.20
Eu	-0.10	0.57	0.40	-0.21
Gd	-0.79	0.46	-0.20	0.00
Y	-0.37	-0.06	-0.87	-0.12
Dy	-0.52	0.62	-0.53	0.05
Yb	0.25	0.64	-0.45	0.09

Table 4.13 Results of the Hierarchical Clustering on Principal Components (HCPC) analyses.

Trace metals (hydrothermal suite of elements) including Cu, Zn, and Pb.

Cluster 1	V. test	P. value	Cluster 2	V. test	P. value	Cluster 3	V. test	P. value
Te	10.18	2.52E-24	Sb	10.30	7.03E-25	In	7.16	8.15E-13
Mo	7.57	3.87E-14	Tl	10.03	1.12E-23	Se	5.56	2.67E-08
Cu	7.17	4.24E-14	Pb	9.87	5.76E-23	Sn	5.07	4.01E-07
Ni	6.64	3.11E-11	Cd	7.75	9.30E-15			
Se	6.36	2.02E-10	Zn	6.84	8.13E-12			
Au	6.26	3.76E-10	As	5.52	3.32E-08			
Co	4.66	3.11E-06	Ag	2.37	1.80E-02			
Bi	4.63	3.68E-06						

Trace metals (hydrothermal suite of elements) including Cu, Zn, Pb, and Hg.

Cluster 1	V. test	P. value	Cluster 2	V. test	P. value	Cluster 3	V. test	P. value
Co	6.06	1.33E-09	Tl	5.91	3.46E-09	Sn	4.09	5.15E-05
Cu	5.24	1.57E-07	Sb	5.83	5.43E-08	Ni	3.45	5.55E-05
Se	5.03	4.88E-07	Cd	5.54	2.99E-08	In	3.42	6.23E-04
Bi	4.78	1.72E-06	Pb	5.39	6.92E-08			
Te	4.07	4.79E-05	Zn	3.68	2.31E-04			
Au	2.71	6.76E-03						

Non-metal trace elements including HFSE, LILE, and REE.

Cluster 1	V. test	P. value	Cluster 2	V. test	P. value	Cluster 3	V. test	P. value
La	9.70	2.80E-22	Nb	8.12	4.35E-16	Eu	7.70	1.35E-14
Pr	9.36	2.06E-20	Hf	7.76	8.73E-15	U	7.15	8.59E-13
Sm	9.14	6.07E-20	Zr	5.77	7.75E-09	Yb	4.94	7.92E-07
Ce	9.05	1.37E-19	Th	5.70	1.19E-08			
Gd	8.57	9.89E-19	Rb	5.62	1.84E-08			

The elements that describe the clustering assignment of each set the most are shown. The V. test and P. values are indicated for the elements in each cluster. The V. test is the quantile of a normal distribution associated with the P. value.

Table 4.14 Summary of trace metals in common sulfide host minerals considered in this study.

Sulfide Host	Form	Trace Metals	Reference
Pyrite	Lattice-bound	Co, Se, Ni, Ga, As, Tl ± Ag ± Au, ± Hg	Beaton (1970), Large et al. (2009), Maslennikov et al. (2009)
Pyrite	Inclusions	Au	Large et al. (2009)
Chalcopyrite	Lattice-bound	Cu ± Se ± Hg	George et al. (2016, 2018b), Goldfarb et al. (2017)
Chalcopyrite	Inclusions	Ag, Bi, Se, Te, Sn, In	George et al. (2016, 2018b), Goldfarb et al. (2017)
Sphalerite	Lattice-bound	Zn, Cd, In, Ga ± As ± Hg ± Tl	Cook et al. (2009), George et al. (2016)
Sphalerite	Inclusions	Sn	Cook et al. (2009), George et al. (2016)
Galena	Lattice-bound	Pb, Ag, Se, Tl	George et al. (2016), Ford & Shawe (1989)
Galena	Inclusions	Bi, Te, As, Sb	George et al. (2016), Ford & Shawe (1989)

The "form" of the trace metal enrichment refers to different mechanisms of incorporation such as lattice substitutions, surface adsorption, and inclusion trapping

Table 4.15 Comparison of average trace element concentrations in pyrite determined by LA-ICP-MS of individual pyrite grains and by bulk analysis of pyrite concentrates from the same samples. Data in ppm. The original dataset and details of the bulk samples are available in Jonasson et al. (2020).

Sample No.	Deposit Name	Sample Type	Cu	Zn	Pb	Ag	Au	Bi	Co	Ni	Se	Te
BSQT27LPY	Bousquet #2	Bulk ICP-MS	175	74	19	1.00	-	0.40	29.0	-	-	1.80
BSQT27LPY	Bousquet #2	LA-ICP-MS	122	24	1.65	0.28	0.04	0.10	21.4	9.92	7.19	0.51
63RF299PY	Dumagami	Bulk ICP-MS	1800	13	43	60.0	9.99	3.30	7.00	-	23.0	18.0
63RF299PY	Dumagami	LA-ICP-MS	398	5.60	9.6	4.21	1.28	2.02	1.72	2.94	7.08	9.18
63RF48PY	Quemont	Bulk ICP-MS	12000	3660	870	191	7.31	1.30	363	-	500	170
63RF48PY	Quemont	LA-ICP-MS	706	853	122	23.5	0.80	0.58	323	12.5	88.3	46.3
KIDD07PY1	Kidd Creek	Bulk ICP-MS	360	443	230	27.5	0.01	1.60	38.0	69.0	-	-
KIDD07PY	Kidd Creek	LA-ICP-MS	221	469	243	17.5	0.01	1.08	22.9	68.9	0.63	0.21

Sample No.	Deposit Name	Sample Type	Cd	In	Ga	Sn	Mo	As	Sb	Hg	Tl	U	Th
BSQT27LPY	Bousquet #2	Bulk ICP-MS	-	-	-	2.40	0.50	-	0.50	-	0.03	0.18	0.46
BSQT27LPY	Bousquet #2	LA-ICP-MS	0.07	0.00	0.02	0.15	0.01	0.25	0.05	0.34	0.00	0.30	0.35
63RF299PY	Dumagami	Bulk ICP-MS	-	0.08	0.30	3.50	-	16.6	0.70	2.00	0.05	0.08	-
63RF299PY	Dumagami	LA-ICP-MS	0.05	0.02	0.03	0.66	0.01	10.00	0.16	0.38	0.01	0.01	0.00
63RF48PY	Quemont	Bulk ICP-MS	10.0	6.60	1.30	950	0.70	109	5.40	9.00	0.03	0.03	-
63RF48PY	Quemont	LA-ICP-MS	1.86	0.52	0.52	2.86	0.04	135	2.80	0.25	0.14	0.00	0.01
KIDD07PY1	Kidd Creek	Bulk ICP-MS	1.80	0.12	2.40	82.0	1.70	350	9.00	-	2.50	0.12	1.10
KIDD07PY	Kidd Creek	LA-ICP-MS	1.96	0.14	0.26	5.33	0.45	301	8.54	0.36	1.15	0.05	0.10

There are 30 grains from the Bousuqet #2 sample, 28 grains from the Dumagami sample, 24 grains from the Quemont sample, and 32 grains from the Kidd Creek sample with averaged LA-ICP-MS values

5. Discussion

5.1 Host rock controls

Clear variation in trace metal concentrations in pyrite samples from deposits with different footwall lithologies (within <1000 m: Fig. 4.24.b; Fig. 5.1.a) is evidence of the immediate host rocks being a primary control on sulfide geochemistry. Hydrothermal alteration in VMS systems typically reaches 1-2 km into the footwall, and therefore can leach metals from those rocks (e.g., Franklin et al., 2005; Hannington, 2014). Co, Ni, and Se enrichment is most common in pyrite samples from deposits with mafic or ultramafic host rocks, such as Potter-Doal, Canadian Jamieson, Genex, Old Waite, and East Waite (e.g., Fig. 4.24, 4.25 and Table 4.8, A.9). In particular, the Co and Ni enrichment in pyrite samples from deposits like Potter-Doal (Fig. 4.25.b) is most likely related to the presence of abundant komatiite in the footwall (e.g., Bleeker et al., 1999c; Berger, 2011). Pyrite samples from deposits with felsic host rocks commonly show elevated Ag, Au, In, Sn, As, Sb, Hg, and Tl, such as Delbridge, Deldona, Horne, Mattabi, and South Bay (e.g., Fig. 4.25; Table 4.8, A.9). Pyrite from the Kidd Creek deposit is additionally elevated in Cd, In, Sn, and Tl (Fig. 4.11, 4.19), were likely sourced from the local footwall rhyolite or related felsic magmas (e.g., Hannington et al., 1999b, c). These patterns are consistent with the different trace element enrichments in volcanic rocks of the AGB (discussed further below).

Pyrite samples from deposits hosted by felsic volcanic rocks show a wider range of different trace element enrichments than samples from deposits hosted by mafic rocks (Fig. 4.24.b), which suggests that other factors may be important in these deposits (e.g., direct contributions from the felsic magmas as opposed to just leaching of metals). Higher precious metal contents in pyrite from felsic-hosted deposits are common (Fig. 4.24) (e.g., Galley et al., 2007; Mercier-Langevin et al., 2011a). Pb is almost always significantly higher in pyrite samples from felsic-hosted deposits, but it can also be enriched in pyrite samples from Zn-rich deposits with mafic footwalls (Fig. 5.1.b), such as Mattagami Lake and Moosehead.

Pyrite samples from different deposits in the Noranda camp show a range of trace metal enrichments that reflect the immediate host rocks (Fig. 4.24) and their stratigraphic positions (e.g., Gibson and Watkinson, 1990; Kerr and Gibson, 1993; Gibson and Galley, 2007). Pyrite samples from deposits with rhyolite footwalls high in the stratigraphic succession, such as Delbridge and Deldona, have high Ag, As, Sb, and Tl concentrations. Pyrite samples from deposits with andesite to basalt dominating the footwalls, lower in the mine sequence, such as Vauze, Corbet, New Insco Lac Dufault, Old Waite, and Amulet, have higher Cu, Bi, Co, Ni, and Se concentrations. Compared to pyrite samples from other parts of the Superior, samples from nearly all of the BRG deposits are enriched in a range of trace metals (i.e., Cu, Co, Ni, Se, Te, and Hg; Fig. 4.25.a) that may reflect a more fertile crustal source (e.g., Mercier-Langevin et al., 2015; Dubé and Mercier-Langevin, 2020).

Pyrite samples from deposits at Val d'Or, in the Tisdale assemblage, have high concentrations of Cu, Co, Ni, Se, and Mo (Fig. 4.25.a) that were likely sourced from the dominantly tholeiitic basalt and lesser komatiite host rocks; the anomalous As and Ga may have been sourced from the more local felsic volcanic rocks (e.g., Chartrand, 1991). Pyrite samples from the East Sullivan deposit contain abundant Co, as well as As, which may have originated from deep-seated ultramafic rocks (>2–5 km: Scott et al., 2002). Elsewhere in the AGB, pyrite samples from deposits such as at Mattagami in the Deloro assemblage show some enrichment in Co, Ni, and Se (Fig. 4.25.c,d) consistent with a source in mafic intrusive rocks of the Bell River Complex or the generally more mafic rocks of the Deloro Assemblage (e.g., Ayer et al., 2002, 2005; Thurston et al., 2008). The mafic-dominated deposits of the Matagami district (i.e., Isle Dieu, Orchan, Bell Allard, and Norita A) have some of the highest Zn grades in Canadian VMS deposits, which is consistent with the higher Zn content of basalt compared to rhyolite in the Superior Province (see section 5.5).

In pyrite samples from DBL, gold enrichment is correlated with Bi-Te (Fig. 4.25.a) and U-Th, which have been interpreted to reflect crustal contamination of the arc-like melts (Mercier-Langevin et al., 2011b). As and Sb enrichment in pyrite samples from these deposits may also reflect the arc-like magmatism (e.g., Barrie et al., 1993). Au, Ni, Se, and Te enrichment in pyrite

samples from the deposits of the Noranda camp may be related to partial melting of tholeiitic basalt (Lesher et al., 1986; Lentz, 1998). Ag, In, and Sn enrichment in pyrite samples from these deposits may also reflect partial melting of the lower crust with fractionation producing high silica contents, or alternatively extreme fractional crystallization of tholeiitic mafic melt with wall rock contamination (e.g., Thurston and Fryer, 1983; Barrie et al., 1993; Lentz, 1998). These relationships are summarized in Table 4.9 and the particular variations of trace elements in different volcanic rocks of the AGB are discussed further below. Figure 5.2 shows the trend of increasing Sb concentrations in pyrite samples from VMS deposits across the Superior Province demonstrating the influence of crustal evolution on the source rocks. Sb is depleted in pyrite from deposits like Coniagas, Normetal, and New Hosco (Matagami) with primitive host rock successions, whereas Sb is enriched in pyrite from the Sturgeon Lake deposits and Bousquet #2-Dumagami with more evolved felsic host rocks (Fig. 5.2.a). This pattern of trace metals in the pyrite mineral separates is similar to the trend of $^{206}Pb/^{204}Pb$ signatures from the same deposits (Fig. 5.2.b; Thorpe, 1999).

5.2 Relationship to bulk compositions of the deposits (Cu-Zn ratio)

Although host rock is a primary control on metal enrichment, some inconsistencies, such as highly variable Se concentrations in pyrite samples from deposits hosted by the same felsic volcanic rocks, suggest that other factors influence trace metal distributions. The trace element signatures of pyrite suggest a more complex interplay of source, transport and deposition in the hydrothermal system (e.g., Fuchs et al., 2019). For example, basalt is a major source of both Cu and Zn, but in lower-temperature systems the Cu is not leached, which may account for the low Cu/(Cu+Zn) grade ratio of the Matagami deposits (Table 2.1). Low temperatures also favour transport of Pb in the hydrothermal fluids despite the rocks being generally depleted in Pb. Pb is enriched in pyrite samples from a number of Cu-rich (e.g., Potter-Doal, Kam-Kotia, Coniagas, and Amulet-A) and Zn-rich mafic-dominant deposits (e.g., Stralak, Geneva Lake, and Moosehead: Table 4.8, A.9). Figure 5.1 and Table 5.1 summarize the main geochemical controls on the enrichment or depletion of trace metals in VMS hydrothermal systems, as recorded in the pyrite samples.

High Cu grades of VMS are found among all deposit types (e.g., Barrie and Hannington, 1999), including mafic-dominated and felsic-dominated examples (Fig. 4.1.b). Cu is generally enriched in mafic volcanic rocks compared to felsic volcanic rocks due to the high Cu content of ferromagnesian minerals and the presence of minor amounts of primary igneous sulfides (e.g., Hannington, 2014). Cu is also enriched in magmatic volatiles from felsic subvolcanic intrusions underlying felsic-dominated deposits (e.g., Large, 1992, Yang and Scott, 1996, 2006; Huston et al., 2011). However, because Cu-Zn ratios are also very sensitive to the temperature of the hydrothermal systems, they can vary within a deposit, across a cluster of deposits in a single VMS district, and regionally between volcanic belts. In general, the differences in the trace element signatures of pyrite samples from different deposits are greater than the differences between pyrite samples from a single a deposit (Fig. 4.23).

In the Noranda district, pyrite samples from deposits such as Horne, New Insco, Ansil, Vauze, and New Hosco are all enriched in Cu, Bi, Co, Ni, Se, Te, In, and Mo, whereas pyrite from deposits such as Delbridge, Deldona, and Gallen are enriched in Zn, Pb, Ag, Cd, As, Sb, and Tl (Fig. 4.25.a). In this case, pyrite from deposits with very similar host rocks (e.g., Horne and Delbridge) can have very different trace element signatures. We interpret this to reflect differences in the temperature of formation of the deposits, with enrichments and depletions according to the respective solubilities of the different sulfide minerals. This manifests as different Cu/(Cu+Zn) grade ratios of the deposits as well as zoning within the deposits (e.g., in the high-temperature interiors and stockwork zones of the deposits, and the lower-temperature outer margins of the deposits). These variations are captured in the data set for deposits with larger numbers of samples (e.g., Fig. 4.3, 4.23: Ansil, Horne #5, and Abcourt-Barvue).

Pyrite samples from Cu-rich and Zn-rich ores have distinct trace metal associations that are also well known (e.g., Zachrisson, 1982; Smith and Huston, 1992; Hannington, 2014). The notable enrichments of trace metals such as Bi, Co Se, Ni, Te, In, and Mo in pyrite from Cu-rich ore are in large part controlled by the high-temperature (e.g., >300ºC) solubilities of the respective trace minerals like selenides and tellurides containing those elements. Likewise, the common enrichments of Pb, Ag, Cd, In, Ga, Sn, As, Sb, Hg, and Tl are mainly related to the lower-

temperature (e.g., <300ºC) solubilities of trace minerals like galena and sulfosalts containing those elements. Figure 4.3–4.5 and Table 4.6 show that the trace metal associations of pyrite separates correlate well with the bulk Cu/(Cu+Zn) grade ratio, and therefore the temperature of the hydrothermal system. Enrichments in elements that are strongly correlated with Cu reflect the same temperature-dependence and source-rock controls that influence chalcopyrite deposition, and enrichments in elements that are strongly correlated with Zn reflect the controls on sphalerite deposition (e.g., Cook et al., 2009; Monecke et al., 2016; George et al., 2016, 2018a). Elements that are preferentially concentrated in low-temperature pyrite (Pb, Ag, Au, Te, In, Ga, W, Mo, V, As, Sb, Hg, and Tl) are enriched in the marginal Zn-rich ore zones of the deposits, whereas elements that are preferentially concentrated in high-temperature pyrite (Co, Bi, Se, and Ni) are enriched in the Cu-rich cores of the deposits and stringer zones (e.g., Maslennikov et al., 2009; Hannington, 2014; Grant et al., 2018: Table 4.6, 4.14). Some elements, such as Ag and Sn, occur in different high- and low-temperature mineral phases (e.g., Cu-Sn sulfides as well as cassiterite) and this explains the common bimodal distribution in pyrite samples from Cu-rich and Zn-rich ores observed in this study. High concentrations of Ag occur in solid solution in pyrite and chalcopyrite at high temperature, but in galena and sulfosalts at lower temperature (cf. Huston et al., 1995).

In addition to the strong temperature dependence of the trace element distribution in the pyrite samples, the partitioning between different minerals that may occur as inclusions is also highly systematic, with partition coefficients that have been experimentally determined for many trace element substitutions (e.g., McIntire, 1963: Loftus-Hills and Solomon, 1967; Beaton, 1970; Scott and Barnes, 1971; Auclair and Fouquet, 1987; Huston et al., 1995; Cook, 1996; Cook et al., 2009; George et al., 2016; Grant et al., 2018). The partitioning is not only influenced by the availability of the cations but also by oxidation state and ionic radius of the substituting element (George et al., 2016). Elements capable of direct substitution in the pyrite lattice include divalent Co^{2+}, Mo^{2+}, and Ni^{2+} substituting for Fe^{2+}; and Se^{2-} and Te^{2-} for S^{2-} (Maslennikov et al., 2009); whereas elements such as monovalent Cu^{+} and Tl^{+}, trivalent As^{3+}, and possibly Sb^{3+} undergo coupled substitution with two Fe^{2+} ions (Huston et al., 1995). The highest Ag and Bi concentrations likely reflect coupled substitution of Ag^{+} and Bi^{3+} for Pb^{2+} in galena inclusions

(e.g., Chutas et al., 2008). However, elements with a large ionic potential (Z/r ratio) are least likely to partition into the pyrite crystal lattice and will occur in micro-inclusions of different mineral phases (e.g., Pb^{2+} in galena or Pb-bearing sulfosalts: George et al., 2016). In some cases, metal cations are also capable of adsorption onto pyrite surfaces, especially those with strong redox behaviours such as Au, Ni, Mo, V, and U (e.g., Grant et al., 2018).

5.3 Relationship to Au enrichment

Pyrite samples from auriferous VMS deposits are variably enriched in Au, Bi, Se, Te, In, and Sn or Zn, Cd, As and Hg (Table A.5), which reflect an enriched source of Au from felsic host rocks and magmas or alternatively conditions of mineralization that were favourable for gold deposition. Horne and Quemont, together with the Au-rich deposits of the DBL camp, are considered to have formed in a juvenile arc-like setting with thickened basement and significant felsic magmatic input, conditions that are thought to be favourable for precious metal enrichment (e.g., Monecke et al., 2008; Mercier-Langevin et al., 2015). The provinciality of Au-rich deposits in the BRG suggests particular geodynamic processes result in inherently enriched Au sources and fluids (Mercier-Langevin et al., 2011b; Boulerice et al., 2015). Specifically, magmatic volatiles can supply trace metals such as Au, as well as Bi, Se, Te, In, Sn, and W (Fig. 4.6, Table 4.9, 5.1: cf. Stanton, 1990; Huston et al., 2011; Berkenbosch et al. 2012). These elements are strongly partitioned into fluids during crystallization of felsic magmas (e.g., Burnham and Ohmoto, 1980; Candela and Holland, 1984; Urabe, 1985; Candela and Piccoli, 2005). Pyrite separates from Robb-Montbray, Horne, and Quemont all have high concentrations of Se, which is thought to have been enriched in volatiles with magmatic sulfur (Sharman et al., 2015). Although a magmatic source for the Se seems likely, it does not mean that the same source provided Au. For example, pyrite samples from the Genex and Joutel deposits in this study showed strong enrichment in Se, but contain virtually no Au (Table A.9). Pyrite samples from the most Au-rich deposits (i.e., Quemont, Horne, Bousquet #2, and Dumagami) are particularly enriched in Te compared to other deposits in the AGB and Superior (Fig. 4.21.a). This suggests that Te enrichment is an indicator of uniquely fertile crust and mantle, as suggested for other ore deposit types in the region (e.g., Robert et al. 2005; Sillitoe, 2008; Hronsky, et al., 2012). Several

authors have suggested that the Au endowment in the BRG is a result of enriched upper mantle/ lower crust sources (e.g., Rubingh et al., 2019; Dubé and Mercier-Langevin, 2020). These Au-rich reservoirs likely supplied a portion of the trace metals, such as Te, that are enriched in the pyrite samples. As noted above, U and Th enrichment in pyrite separates from Bousquet #2 also might reflect crustal contamination of the melts as a source of Au (Mercier-Langevin et al., 2014; Dubé and Mercier-Langevin, 2020).

In contrast to these deposits, Au-rich pyrite samples from Zn-rich ores at Delbridge and Deldona are enriched in a suite of elements normally associated with low-temperature epithermal-like systems (Fig. 4.8–4.12). Au, Ag, As, Sb, and Hg enrichment in pyrite samples from deposits with complex sulfosalt assemblages may indicate a contribution from felsic magmatic sources, or processes such as boiling that might influence Au deposition. The different influences can explain the strong bimodal distribution of Au in pyrite from both Cu- and Zn-rich deposits (Fig. 4.6; Fuchs et al., 2019). Although Au concentrations in pyrite samples commonly correlate with Cu, the Au grades of the deposits as a whole often correlate more closely with Zn (Table A.5). Magmatic fluids from arcs tend to produce high-temperature Cu-Au assemblages due to the greater concentrations in the more oxidized fluid and magmatic volatiles (Fuchs et al., 2019). However, later hydrothermal zone refining mobilizes Au at lower temperatures into Zn-rich sulfides at the cooler outer margins of the deposits.

5.4 Relationship to deposit size

We showed that pyrite samples from large-tonnage, Zn-rich deposits (>8 Mt) like Kidd Creek, Horne #5 Zone, and Geco have higher Sn contents (Fig. 4.22.b) and variable enrichments of other trace elements (Ag, Au, Cd, In, As, Hg, Tl: Table A.10) compared to pyrite from smaller Cu-rich (e.g., Robb-Montbray and Old Waite) and smaller Zn-rich deposits (e.g., Delbridge, Deldona, Stralak, and Geneva Lake). VMS deposit size is fundamentally related to the scale and the longevity of the hydrothermal system (e.g., Barrie et al., 1997; Barrie and Hannington, 1999; Hannington et al., 1999c). Long-lived hydrothermal systems tend to be low-temperature, seawater-dominated systems and produce large-tonnage Zn-rich deposits. One interpretation is

that they are Zn-rich because the thermal requirement to sustain a large but relatively low-temperature hydrothermal system would be much less than that required for a Cu-rich deposit of similar size (Hannington et al., 1999b, c). The high Sn grades are interpreted to be mainly a consequence of the long-lasting hydrothermal leaching required for the large tonnages (Hannington et al., 1999c), although others have attributed high Sn grades to direct felsic magmatic contributions (i.e., Neves Corvo in the Iberian Pyrite Belt: Huston et al., 2011; Relvas et al., 2006). However, some large deposits may also be produced by exceptionally metal-rich fluids (e.g., dominantly magmatic) forming mainly Cu-rich deposits (e.g., H orebodies at Horne and Quemont: Kerr and Gibson, 1993).Tin that is coenriched with Bi, Se, Te, and In in pyrite samples from Horne (H and #5 zone) and Mobrun (Table 4.9.c, A.9) strongly suggest a felsic magmatic source (e.g., Mercier-Langevin et al., 2011b, 2015). High Bi, Se, Sn and W concentrations from the large Geco deposit may similarly represent a magmatic input. However, the high Sn could also be related to long-lived hydrothermal leaching of the mixed volcanic and sedimentary footwall (Petersen, 1986; Hannington et al., 1999c).

5.5 Trace element abundances in volcanic rocks

Until recently, it has not been possible to compare a range of trace elements in VMS deposits to that of the host rocks owing to a lack of high precision trace element analyses of volcanic rocks. Most variations in the deposits have been interpreted in terms of conditions of mineralization or very broadly understood variations of metal enrichments in the source rocks (discussed above). Increasingly, laboratory analyses of volcanic rocks include high-precision analyses of minor and trace elements that can be compared to the deposits. Table 5.2 and Figure. 5.5, 5.6 show clear differences in the trace element distributions of the various least-altered volcanic rock compositions from the Superior Province, generally consistent with the established partitioning of trace metals between melts of different composition and the crystalizing igneous minerals (e.g., K-feldspar, plagioclase, pyroxene, olivine: Kiseeva and Wood, 2013, 2015; see below). Specifically, felsic volcanic rocks are enriched in Pb, Ag, Bi, Te, Cd, In, Ga, Sn, W, Hg, Tl, U, and Th and mafic volcanic rocks a source of Cu, Co, Ni, Se, and V (Fig. 5.5; Franklin et al., 1981; Stanton, 1994; Shikazono, 2003). Concentrations of other elements, such as As, Sb, and W

are similar between felsic and mafic rocks. We performed PCA on 256 representative volcanic rocks samples from the Superior Province containing complete analyses for the 8 select elements: Cu, Zn, Pb, Ag, Au, Co, Ni, and As and applied a CLR transformation to the data. The variance explained by PC1 and PC2 is 45% and 18%, respectively (Table A.13.a and Fig. 5.7.a), and the results show clear separation of the elements as described above. Pb, Ag, Au, and As have positive loadings on PC1, whereas Cu, Co, and Ni have negative loadings. Zn has a PC1 loading near zero, but a high positive PC2 loading compared to the other elements. The separation of the elements in the whole rock data is similar to that observed for the pyrite samples from the different massive sulfide deposits. Hierarchical clustering of the PCA data (HCPC) identified 3 main trace element associations with the different rock types (Fig. 5.7.b; Table A.13.b). The trace elements that have the greatest influence on the defined clusters are: Cu, Ni, Co (cluster 1); Zn, Pb, Ag, Au, (cluster 2); and Pb, Au, As (cluster 3). Clusters 1 and 2 correspond to the mafic and felsic volcanic samples, respectively, whereas cluster 3 may reflect more intermediate rock compositions. Controlling factors on the clustering of the volcanic rock data are considered to be the compatibility of the elements, the strongly chalcophile and siderophile behaviour of some of the metals (e.g., see Kiseeva and Wood, 2013, 2015; Kiseeva et al., 2017).

Another database compiled by Mole et al. (2021) is sorted according to assemblage type, with a subset of the data (Appendix C) focusing on mafic volcanic rocks just from the different ABG assemblages (n=5742) (Fig. 5.4). They include samples from the Pacaud (n=5), Deloro (n=961), Stoughton-Roquemaure (n=1283), Kidd-Munro (n=583), Tisdale (n=530), and Blake River Group (n=2289), and mafic volcanic rocks older than 2750 Ma (n=49). These data are compared in Fig. 5.8, 5.9 and Table 5.3. Basalt samples from the Deloro assemblage have average trace metal concentrations compared to samples from all the assemblages. Samples from Stoughton-Roquemaure have high Cu concentrations; samples from Kidd-Munro have the highest concentrations of Co, Ni, and Se; samples from Tisdale have the highest Pb, Ag, and Mo; and samples from the Upper Blake River have the lowest trace metal concentrations, but elevated U-Th. The Lower Blake River has high concentrations of Cu, Zn, and Au, and lower average concentrations of other trace metals. Mafic volcanic rocks from the Kidd-Munro assemblage

have high Co, Ni, and Se (Fig. 5.5), consistent with the primitive sources of the mafic-ultramafic melts inferred for this assemblage (Barrie et al., 1999b). In contrast, volcanic rocks from the Stoughton-Roquemaure, Tisdale, and Upper Blake River assemblages have variably high Pb, Ag, Sn, Mo, W, U, and Th (Fig. 5.8) consistent with the interpreted crustal contamination of the source melts (Ayer et al., 2002). Overall, the differences in trace element concentrations between assemblages (Fig. 5.8) are small, but may be significant in the case of source melts and differential metal endowment. The lack of trends in trace element distributions between assemblages is mainly due to the fact that assemblages are distinguished by age rather than rock type (e.g., Thurston et al., 2008).

5.6 Comparison with VMS of the Wawa, Western Superior and Slave Province

Pyrite samples from the Sturgeon Lake greenstone belt in the Wabigoon subprovince show the important control of source rock in comparison to the Abitibi. Pyrite samples from the Sturgeon Lake deposit are highly enriched in Zn, Pb, Ag, As, Sb, Hg, and Tl (Fig. 4.26.b, 5.11) which reflects the regional bimodal-felsic volcanic strata and felsic-dominant host rocks (e.g., Morton et al., 1991, 1996). The unusual metasedimentary host rocks of the Geco deposit may have been a source of Sn for the unusually Sn-rich massive sulfides (Fig. 4.26.b) (e.g., Franklin et al., 2005).

The Slave Province is an older and compositionally different Archean terrane than the Superior. It consists of plutonic suites (2.63–2.62 and 2.59–2.58 Ga), major sedimentary basins, and subordinate greenstone belts (2.73–2.66 Ga) (Fig. A.2.a; Mortensen et al., 1988; Davis and Bleeker, 1999). North trending high strain zones of lithologically distinct greenstone belts are separated into an eastern portion that is dominated by intermediate and felsic volcanic rocks, and a western portion comprised mostly of mafic volcanic and plutonic rocks (Padgham, 1985; Kusky, 1986). The VMS deposits of the Slave Province are dominantly bimodal-felsic type and occur in three volcanic belts in the eastern, west-central, and northern parts of the craton: Hackett River, Amooga Booga (formerly Hood River), and High Lake, respectively.

The 100-km long Hackett River volcanic belt in the eastern Slave is dominantly composed of calc-alkaline felsic volcanic rocks and lesser basalt, andesite, and dacite (e.g., Frith and Roscoe, 1980; Frith, 1987). It contains the bimodal-felsic Ag-Zn-Pb-Cu VMS deposits Norsemines A-Jo Zones, East Cleaver, and Yava. The footwalls to most of the deposits are rhyolite flows, rhyolite-chert tuff, and andesite (e.g., MacNeill, 1976; Frith and Roscoe, 1980; Bleeker and Hall, 2007), except at Yava, which is underlain by andesitic pillowed flows and overlain by andesitic-dacitic welded ash flow tuff-breccia (~1000 m) (Frith and Roscoe, 1980). These deposits are Zn-rich, have low-medium Au grades, and are comparable in size to the deposits of the AGB (Table 2.1). Pyrite samples from Hackett River are enriched in Pb and Au and depleted in Zn, Ag, Bi, and Te compared to pyrite samples from VMS deposits in the Superior Province, reflecting the more felsic basement in the eastern Slave (Fig. 5.10.a, 5.11; Table 4.9.b, 5.4). They are also enriched in U, Th, and Zr. Ni is enriched in pyrite samples from the Yava deposit. Elevated Th and U in pyrite samples from East Cleaver, A-Main Zone, and Yava are likely related to inclusions of zircon in the samples (Fig. A.3).

The Amooga Booga volcanic belt (~2680 Ma; formerly Hood River) in the west-central Slave Province (Fig. A.2.a) consists of mafic flows, mafic and felsic volcaniclastic rocks, and lesser calc-alkaline felsic volcanic rocks (Gebert, 1995; Jensen, 1995). The Hood River VMS deposits have low to medium Cu/(Cu+Zn) grade ratios, low Au grades, and medium sizes (Table 2.1). Data are available for pyrite from the bimodal-felsic Gondor and bimodal-mafic Hood #10 (Takijuq Lake) Zn-Cu-Pb-Ag deposits. The footwall at Hood #10 is composed of massive-brecciated dacite and rhyolite flows with lesser basalt-andesite volcanic rocks, and the footwall at Gondor is rhyolite (Bleeker and Hall 2007; Mills et al., 2016). Pyrite samples from these deposits (n=6) have high Pb and high Cu, Au, and Bi in comparison to pyrite samples from deposits elsewhere in the Slave and in the Superior (Fig. 5.10.a, 5.11; Table 4.9.b, 5.4), most likely reflecting the felsic magmatic source.

The 80-km long High Lake volcanic belt (2705–2690 Ma) in the northern part of the Slave Province (Fig. A.2.a; Henderson, 1995) is composed of bimodal intermediate-felsic and mafic volcanic rocks that host the High Lake Zn-Cu-Pb-Ag deposit (e.g., Petch, 2004). The proximal

footwall to High Lake is made up of calk-alkaline dacite-rhyolite pyroclastic rocks with minor mafic flow units (Petch, 2004). The deposit has an intermediate Cu/(Cu+Zn) grade ratio, medium Au grade (0.9 g/t) and large tonnage (~16 Mt). Pyrite samples from High Lake are enriched in Au and Bi and depleted in Sn in comparison to other deposits in the Slave and Superior (Table 4.9.b, 5.4). The high concentrations of Au and Bi suggest the pyrite samples probably contain abundant inclusions of Au-bismuthides, although Te was not analyzed.

The enrichment of Pb in pyrite samples from the Hackett River and Hood River deposits compared to pyrite from VMS deposits of the Abitibi is thought to be associated with the more evolved bimodal-felsic volcanic host successions and their emplacement in a mature continental margin setting with a thicker continental root similar to the felsic-dominated greenstone belts of the Superior Province (e.g., Sturgeon Lake: Whalen et al., 2004, Bleeker and Hall, 2007). The coupled Pb and U-Th enrichment is also consistent with a longer upper crustal history for the contained Pb (e.g., Hannington, 2014).

5.7 Comparison with younger VMS

A comparison of the geochemistry of pyrite from younger VMS deposits shows the strong influence of crustal evolution on the source rocks for the trace elements. VMS deposits occur throughout the Proterozoic and Phanerozoic orogens of Canada including the Trans-Hudson, Appalachian, and Western Cordillera. These orogens involved a more modern style of plate tectonics, including the growth and recycling of continental crust and the occurrence of mafic-pelitic and siliciclastic-felsic successions (e.g., Franklin et al., 2005; Stern, 2008; Huston et al., 2010; Pehrsson et al., 2016).

The Flin Flon-Snow Lake belt (1900–1840 Ma) within the internal zone of the Trans-Hudson orogen (Fig. A.2.b) is 250 km long and 70 km wide. It is bordered by the Kisseynew Domain in the north and overlying Phanerozoic cover to the south. The belt hosts over 30 past- and present-producing VMS deposits with total past production and reserves of over 180 million Mt (Galley et al., 2007). Pyrite mineral separates were prepared from ore samples from 15 deposits in the

Flin Flon and Snow Lake camps (Table 2.; Jonasson et al., 2020). These samples were also described in detail in Jonasson et al. (2009) 5432 Open File. Trace element enrichments in pyrite samples from the Snow Lake and Flin Flon camps are generally correlated with bulk Cu/Cu+Zn grade ratios of the deposits (Fig. A.3), but not with Au grades or deposit size.

The Flin Flon arc assemblage (>1880 Ma) consists primarily of basalt and basaltic andesite flows and breccias and lesser rhyolite flows that are generally the immediate host rocks to the VMS deposits (Syme and Bailes, 1993). The bimodal-mafic Flin Flon and Callinan deposits are hosted within mafic and heterolithic volcaniclastic rocks and mafic flows overlain by tholeiitic rhyolite complexes (e.g., Bailes and Syme, 1989; MacLachlan and Devine, 2007). The immediate host rocks to the bimodal-mafic Mandy and Schist Lake deposits consist of mafic and heterolithic volcaniclastic rocks with lesser mafic flows (DeWolfe, 2009). The Pine Bay and North Star deposits are hosted by felsic volcaniclastic rocks intruded by a dacite-rhyolite dome in the footwall (Corrigon et al., 2007). Andesitic flows host the mafic-type Flexar and Coronation deposits (e.g., Galley et al., 2007). Co and Ni are enriched in pyrite samples from the mafic-dominated Coronation deposit, similar to pyrite from mafic-dominated VMS deposits in the Superior Province (Fig. 5.10.b, 5.12; Table 4.9.b, 5.4). High Sb concentrations in some samples of pyrite from the Zn-rich Callinan and Centennial deposits indicate probable inclusions of tetrahedrite or antimonides. Tennantite and arsenopyrite also have been reported at the Centennial deposit (Aggarwal and Longstaffe, 1987) and are likely the source of As enrichment in the pyrite samples. Indium concentrations are also elevated in the pyrite samples from the Flin Flon deposits. The high Te content in pyrite from the Cu-rich Pinebay and North Star deposits and Cu-Zn-rich Flin Flon deposit is similar to Te enrichment in pyrite from deposits in the Noranda and DBL camps (Fig. 5.10.b) and reflects an abundance of telluride inclusions in the samples (Coleman et al., 1973; Price, 1973). Correlation of Te with Ag and Bi in a pyrite sample from Pinebay (Fig. A.3) suggests tellurides are present as inclusions in this sample. The Te enrichment in pyrite from deposits in the Flin Flon belt is similar to that of the Blake River Group and suggests Te may be an indicator of enhanced metal endowment in juvenile arcs.

The Snow Lake arc assemblage (>1880 Ma) consists of mafic and lesser felsic flows overlain by heterolithic volcanic facies with abundant volcaniclastic rocks that are in turn overlain by pillow basalts (Bailes and Galley, 1999). The Snow Lake VMS deposits are dominantly bimodal-mafic. The Anderson, Stall, Rod, and Osborne Cu-rich deposits are hosted within a ~2.5 km thick 'primitive arc' assemblage comprised of arc tholeiite, boninitic flows, and rhyolite that forms the immediate footwalls to the orebodies (Bailes and Galley, 1999). The Chisel Zn-rich deposit and Photo Cu-Zn-Au deposit occur within a ~3 km thick sequence consisting of mafic, intermediate, and felsic flows and volcaniclastic rocks (Bailes and Galley, 1999). Rhyolite flows are the immediate host rocks to the deposits. Pyrite samples from the small Cu-rich deposits in the lower mafic-dominated sequence of the Snow Lake camp (i.e., Anderson, Osborne, and Rod) are enriched in Co, Ni, and As (Fig. A.3), and cobaltite and arsenopyrite have been documented in the Osborne and Rod deposits (Table 2.1). Some pyrite samples from the Anderson mine are also enriched in Se and Te (Fig. 5.10.b, 5.12; Table 2.1). However, lower concentrations of elements such as Bi, In, and Sn in pyrite samples from these and other Snow Lake deposits suggest that there was not a major felsic magmatic input. Pyrite samples from the Au-rich Photo Lake deposit and the larger Zn-rich Chisel deposit in the more felsic sequence have unexpectedly low trace element contents (Table 4.9.b, 5.4), which may be due to intense metamorphic recrystallization of the ores in these deposits, whereby trace elements including Au have been remobilized out of the massive sulfide lenses (Bailes et al., 2016).

The Rusty Lake volcanic belt (1900–1800 Ma) in northern Manitoba is dominated by volcaniclastic, mafic-pelitic and siliciclastic rocks with lesser volcanic flows, mafic sills and other sediments (e.g., Baldwin, 1988). The large Ruttan Cu-Zn VMS deposit (83 Mt) is hosted within a sequence of transitional calc-alkaline to tholeiitic bimodal volcanic, volcaniclastic, and siliciclastic rocks (Ames, 1996). The immediate footwall is composed of intermediate volcanic/volcaniclastic rocks that are intercalated with the Ruttan orebodies (Barrie et al., 2005). Previous work has shown the massive sulfide ores of the Ruttan deposit to be enriched in Ag, Au, Cd, and In, and trace minerals of these elements are documented (Barrie et al., 2005; Table 2.1). Pyrite concentrates from Ruttan have low Cu and are enriched in Pb (Table 4.9.b, 5.4), similar to other deposits with metasediments in the volcanic succession (e.g., Manitouwadge:

Barrie and Hannington, 1999). The low Sn content of the pyrite samples from these more mafic-dominated deposits contrasts with the Sn enrichment found in other large-tonnage VMS in the Superior Province and younger Phanerozoic siliciclastic-type deposits (e.g., Petersen, 1986; Hannington et al., 1999c).

The Sherridon camp, situated in the Kissinew Domain north of Flin Flon hosts the Sherridon deposit in felsic to intermediate gneiss and amphibolite (Froese and Goetz, 1981). The nearby Lynn Lake belt (1890–1840 Ma) within the internal Reindeer Zone hosts the bimodal-mafic deposits of the Lynn Lake camp, including Fox Lake (Beaumont-Smith and Böhm, 2003), which has a footwall of andesite breccia (Turek et al., 1976). Pyrite samples from the Fox Lake and Sherridon deposits are depleted in most trace elements compared to samples from the Superior (Table 5.2), which may be due to the higher metamorphic grade of these deposits.

Analyses of 25 pyrite samples from other Proterozoic and Phanerozoic greenstone belts in Canada were included in Jonasson et al. (2020) from the small Zn-rich Koke deposit in the Proterozoic Labrador Trough, deposits of the Bathurst Camp in New Brunswick, the Eastern Townships of Quebec, and the Northern Cordillera (Myra Fall, Eskay Creek, the Britannia Mine and Finlayson Lake).

The Zn-Pb-Cu-Ag-Au Koke (Boylen) deposit (~1880 Ma) in the Labrador Trough is hosted within basalt and shale interbedded with banded iron formation in a pelitic-mafic volcanosedimentary sequence (Clarke and Wares, 2004). Pyrite samples from the Koke VMS deposit are slightly enriched in Pb, As, Sb, and Hg (Table 4.9.b, 5.4) in comparison to pyrite concentrates from other Canadian VMS deposits likely as a result of the pelitic-mafic host succession (e.g., Hannington, 2014).

The Ordovician Tetagouche – Exploits Zone within the peri-Gondwannan of the Appalachian orogen hosts the Bathurst camp in New Brunswick (Fig. A.2.c), which contains over 40 VMS deposits including the supergiant Brunswick #12 Zn-Pb-Cu-Ag deposit (~465 Ma) at 230 Mt (Galley et al., 2007). Bathurst VMS deposits are classified as siliciclastic-felsic with host

sequences characterized by bimodal felsic to mafic volcanics and intercalated sedimentary rocks (van Staal et al., 2003). Most of the deposits, including Brunswick #12, Heath Steele, and Austin Brook are closely associated with calc-alkaline felsic volcanic and volcaniclastic rocks occurring at the top of the Nepisiguit Falls Formation (e.g., Goodfellow and McCutcheon, 2003). The footwall successions generally consist of rhyolite porphyry overlain by rhyolite crystal tuff to dacite breccia that immediately hosts the massive sulfides interbedded with mudstone (e.g., Peter and Goodfellow, 1996). Pyrite concentrates of ore samples from the large Zn-Pb-Cu-rich deposits of the Bathurst camp have variable enrichments of Pb, Ag, Bi, In, Ga, Sn, V and Tl (Fig. 5.10.c, 5.12), although most of the samples were not analyzed for Se, Te, As, Sb, or Hg. Samples from the large Heath Steele deposit are highly enriched in Bi, In, and Sn representing a strong felsic magmatic signature (e.g., Yang and Scott, 2003). Pyrite concentrates from ore samples of the giant Brunswick #12 deposit are enriched in Pb, Ag, and Tl (Table 4.9.b, 5.4), reflecting the footwall felsic volcanic rocks and mudstone similar to pyrite from SEDEX deposits (e.g., Mukherjee and Large, 2017). Pyrite from ore samples at Brunswick #12 is also enriched in Bi, but unexpectedly depleted in Sn, despite the high Sn grades of the deposit (Goodfellow and McCutcheon, 2003). A felsic-sedimentary footwall is a common predictor of Sn enrichment among large deposits of this type (e.g., Goodfellow et al., 1993). The lack of Sn in the pyrite concentrates may be due to selective sampling of the Cu-rich vent complex that contains fewer Sn-bearing minerals compared to the bedded Pb-Zn ore (Goodfellow and McCutcheon, 2003). By contrast, magmatic fluids are thought to have contributed to Sn enrichment in other deposits similar to those in Bathurst, such as Neves Corvo in the Iberian Pyrite Belt (Yang and Scott, 2003; Huston et al., 2011). Most of the pyrite concentrates from ore samples in the Bathurst area have a high Ga content, which may be contained in inclusions of sphalerite in samples from the Zn-rich ore, or possibly Ga-bearing aluminosilicates or magnetite in samples with less Zn. Pyrite samples from the small Austin Brook deposit have the highest Ga concentrations in comparison to other Canadian VMS (Table 4.9.b, 5.4).

Pyrite samples from the small mafic-dominated VMS deposits in the Eastern Township area, Quebec, show no significant trace element enrichments, similar to pyritic ores from other

ophilite-hosted VMS deposits (e.g., Hannington, 2014). (Table 4.9.b, 5.4) that may be related to the very low MORB-like trace metal concentrations in the source rocks (Table A.14).

The Myra Falls bimodal-felsic VMS deposits (~ 365 Ma) on Vancouver Island are located in the Wrangellia terrane, a part of the Insular belt of the Canadian Cordillera (Gabriele and Yorath, 1991) (Fig. 3.1). The deposits are hosted within a succession of rhyolitic, andesitic, and basaltic volcanic and sedimentary rocks. The small Zn-rich Lynx deposit has an immediate footwall of heterolithic volcaniclastics and lesser felsic volcanic rocks, and sediments (Jones et al., 2006). Pyrite samples from this deposit are enriched in Te and Mo, and depleted in Ag, Co, In, Sn, and Tl in comparison to pyrite from other Canadian VMS (Fig. 5.10.d; Table 4.9.b, 5.4.) High-sulfidation mineral assemblages in the ores (e.g., bornite-pyrite-chalcopyrite) have been interpreted as magmatic in origin (Marshall et al., 2018), but the trace element signature of the pyrite from the Lynx deposit does not show a clear enrichment in trace metals normally associated with a direct felsic magmatic input.

The dominantly bimodal-felsic VMS deposits of the Finlayson Lake camp in the Yukon-Tanana terrane of southeastern Yukon are hosted within Devonian-Mississippian (~360–356 Ma) felsic volcanic to volcaniclastic rocks that make up the immediate footwall to the Kudz Ze Kayah Zn-Pb-Cu-Ag-Au deposit (13 Mt) deposit (e.g., Mortenson, 1992; Piercey et al., 2001; Peter et al., 2007). Pyrite concentrates of ore samples from Kudz Ze Kayah contain high Au, Se, As, and Sb in comparison to pyrite samples from other Canadian VMS (Fig. 5.10.d; Table 4.9.b, 5.4). Elevated As and Sb in pyrite samples from Kudz Ze Kayah (Fig. A.3), mainly as inclusions of tetrahedrite-tennantite and boulangerite (Peter et al., 2007), were likely sourced by leaching of the felsic volcanic and volcaniclastic rocks in the immediate footwall (Piercey et al., 2001). Se in the samples likely occurs in clausthalite (Peter et al., 2007), and Se isotope ratios indicate the elevated Se originated from the footwall rhyolite (Layton-Matthews, 2005) or by magmatic degassing from the proximal synvolcanic plutons (similar to Noranda: Sharman et al., 2015). One sample of pyrite from the Kudz Ze Kayah ore has a high Au concentration (7.4 ppm) consistent with the presence of electrum as a trace constituent of the ore (Peter et al., 2007).

The Eskay Creek Au-Ag-rich sulfide-sulfosalt deposit in the Iskut River area of the Stikine terrane is hosted by bimodal volcanic and sedimentary rocks of the Jurassic Hazelton Group (e.g., Macdonald et al., 1996). The immediate footwall to Eskay Creek is a massive to brecciated rhyolite flow unit (up to 110 m thick), with overlying carbonaceous mudstone that directly hosts the orebodies (e.g., Sherlock et al., 1999). Synvolcanic felsic intrusions crosscut the mine sequence (Bartsch, 1993). Pyrite concentrates from stringer ore in the footwall of the Eskay Creek deposit are enriched in Sb and Tl and depleted in base metals, precious metals, Bi, Co, and Sn (Fig. 5.10.d, A.3). High Sb and Tl reflect the abundant sulfosalts in the ore and the felsic-dominant source rocks (Sherlock et al., 1999). The ores are thought to have formed mainly at low-temperature and in a shallow-water environment (Sherlock et al., 1999), similar to other felsic-dominated VMS deposits in which Sb and Tl are notably enriched (e.g., Rosebery: Large et al., 2001c). Other elements in the pyrite, such as Mo and V, probably reflect adsorption onto diagenetic pyrite in the associated mudstones (cf. Large et al., 2009). Au and Ag concentrations in the pyrite samples are variable.

The trace elements in pyrite from such a wide range of deposit types show consistent enrichments and depletions, reflecting host rock and ore type, similar to the relationships observed in the AGB and confirming the ability to fingerprint large VMS-forming systems with relatively small numbers of samples. Figure 5.13 compares the chemistry of pyrite from Superior VMS hosted by different rocks types to the pyrite chemistry of deposits of all ages. The plots shows a very similar pattern overall reflecting a similar trend of relative enrichments and depletions in the volcanic rocks, regardless of age. The observed trends include high Zn and Sb in pyrite samples from bimodal felsic deposits; high Au, Se, Te, As, and Hg in pyrite samples from bimodal mafic deposits; and high Cu, Co, Ni, and Se in pyrite samples from mafic deposits (Fig. 5.13). Sediments are more common among the host rocks of the younger deposits, and generally pyrite concentrates of the ore samples from deposits in siliciclastic felsic rocks (e.g., Bathurst camp) have high average concentrations of Pb, Ag, Bi, In, Ga, Sn, Sb, and Tl (Table 5.2). Pyrite concentrates of ore samples from some younger large deposits (e.g., Ruttan and Britannia) are not consistently enriched in any trace metals, possibly reflecting the overall low metal tenor of these deposits (<2% Cu and Zn: Table 2.1).

5.8 Comparison with other hydrothermal ore deposit types

Pyrite data are also available from other deposit types, including magmatic vein Cu deposits and late-stage orogenic Au deposits in many of the same districts hosting the VMS deposits in this study (Jonasson et al., 2020; Table A.15). These data shed light on fundamental differences in the trace element signatures of diverse hydrothermal systems ranging from entirely magmatic to orogenic. The database includes pyrite samples from five Cu-Au deposits of the Chibougamau camp (n=7 samples), two orogenic Au deposits in the Val d'Or camp (n=2 samples), one orogenic Au deposit from Noranda (n=2 samples), and one orogenic Au deposit from Timiskaming (n=1 sample). The general trend of trace element enrichments is the same for all deposit types (e.g., Co, Ni, Se, Mo, V, As are enriched compared to other elements, most likely controlled by lattice-bound substitutions: Fig. 5.14). However, different enrichments and depletions are evident among the different deposit types.

The Cu-Au vein deposits of Chibougamau are in the same assemblage as the VMS deposits of the Matagami camp (n=20 samples from 6 deposits). Pyrite samples from the magmatic Cu vein deposits of Chibougamau are enriched Cu, Au, Co, Ni, Te, W, Mo, As, and Sb, and depleted in Zn, Pb, Se, Cd, In, Ga, Sn, V, and Hg compared to pyrite from the VMS (Fig 5.14; Table 5.5, A.16). Ag concentrations are similar between samples from Cu-Au veins and VMS. Co and Ni enrichment in pyrite from the Chibougamau veins were most likely sourced from the mafic Chibougamau pluton. Pyrite samples from Chibougamau magmatic deposits are also variably enriched in Bi, most likely associated with chalcopyrite inclusions containing bismuthides or tellurides. Elevated Bi and Te concentrations in some pyrite from the Chibougamau deposits are characteristic of a magmatic source. Very high W contents in one pyrite sample from the Belle deposit (420 ppm) and high Mo in samples from Opemiska may also be related to magmatic fluids from the dominantly mafic Chibougamau pluton that formed these deposits (Mathieu and Racicot, 2019).

Trace element concentrations in pyrite samples from four orogenic Au deposits in Noranda, Val d'Or, and Timiskaming are listed in Table A.17. They have similar concentrations of trace elements as pyrite from Abitibi VMS in the same with the exception of Cu, Ag, Se, Te, Cd, In, Sn, Mo, As, and Sb. Pyrite samples from the orogenic Au deposits are enriched in Au, Co, W, and Mo compared to pyrite from the VMS deposits (Fig. 5.14; Table 5.5, A.17). The high W concentration could be-from the metamorphic breakdown of W-bearing minerals in the sedimentary source rocks (Cave et al., 2015). Pyrite from the Chadbourne breccia Au deposit in Noranda has similarities to pyrite from both VMS and orogoenic Au deposits and may represent a hybrid ore-forming system (Walker and Cregheur, 1982). In general, the enrichment of trace elements in pyrite from VMS deposits compared to orogenic Au deposits reflects the polymetallic nature of VMS and the different metal sources (volcanic versus metasedimentary and plutonic host rocks). Variable salinities, composition and temperatures of the ore-forming fluids also influence the metal contents of the deposit types (e.g., Groves et al., 1998; Large et al., 2001).

5.9 Comparison of LA-ICP-MS analyses of pyrite from other VMS deposits

Abundant trace element data on pyrite from VMS deposits has been obtained by LA-ICP-MS. In Figure 5.15 and Table 5.6, we compare the LA-ICP-MS pyrite analyses from our study to other LA-ICP-MS data from the literature. The purpose is to determine how representative the data from a few deposits in the AGB is compared to published analyses from other deposits. The LA-ICP-MS data include pyrite from the Skouriotissa Cretaceous mafic deposit from the Solea Graben in Troodos, Cyprus (n=126 analyses: Keith et al., 2016); four Silurian-Ordivician siliciclastic-felsic deposits from the Bathurst camp, New Brunswick (n=460 analyses from Brunswick #6-12, Heath Steele, Key Anaconda: Dehnavi et al., 2018); seven Upper Proterozoic-Cambrian bimodal-mafic Cu+Zn±Ag±Au and four bimodal-felsic Zn+Cu±Ag±Au deposits from the Ketchikan camp, Alaska (n=13: Slack et al., 2005).

All of the pyrite data show remarkably consistent trace element enrichments and depletions with the range of values for the pyrite samples from the AGB. LA-ICP-MS analyses of pyrite from

the Skouriotissa (Troodos) deposit have higher Cu, Co, Ni, Se, Mo; lower Zn, Pb, Ag; and similar Au, Bi, Te, Cd, As, Sb compared to pyrite from the AGB deposits (Fig. 5.15). Enrichment in Cu, Co, Ni, Se, and Mo, and depletion in Zn, Pb, Ag reflects the mafic-dominant host rock source at Troodos. LA-ICP-MS analyses of pyrite from the siliciclastic-felsic Bathurst deposits have higher Zn, Pb, Ag, Bi, Co, Ni, In, Ga, Sn, As, Sb, Tl; slightly lower Cu, Au, Te; and similar Cd, Mo, Hg compared to pyrite from the AGB deposits (Fig. 5.15). Enrichment in Zn, Pb, Ag, As, Sb, Hg, Tl reflects the siliciclastic-felsic source of metals and enrichment in Bi, In, and Sn reflects a magmatic input (e.g., Goodfellow and McCutcheon, 2003; Yang and Scott, 2003). LA-ICP-MS analyses of pyrite from the bimodal-felsic Ketchikan deposits have higher Ni, Mo, As, Sb, Hg, Tl; lower Cu, Zn, Pb, Ag, Bi, Te; and similar Co, Cd, In, Sn compared to pyrite from the AGB deposits (Fig. 5.15). Pyrite from the bimodal-mafic Ketchikan deposits has higher Co; lower Cu, Zn, Pb, Ag, Bi, Te; and similar Ni, Se, Cd, In, Sn, Mo, As, Hg, and Tl compared to pyrite from the AGB deposits (Fig. 5.15). The felsic host rocks likely influence the Zn-Pb-Ag-Sb enrichment in the AGB deposits, whereas more mafic host rocks influence the Co-Ni enrichment in the Ketchikan deposits. As, Sb, Hg, and Tl enrichment in pyrite from the younger bimodal-felsic Ketchikan deposits compared to pyrite from the AGB may reflect the greater crustal contamination evidenced by Pb-isotopic signatures of the sulfides (Slack et al., 2005).

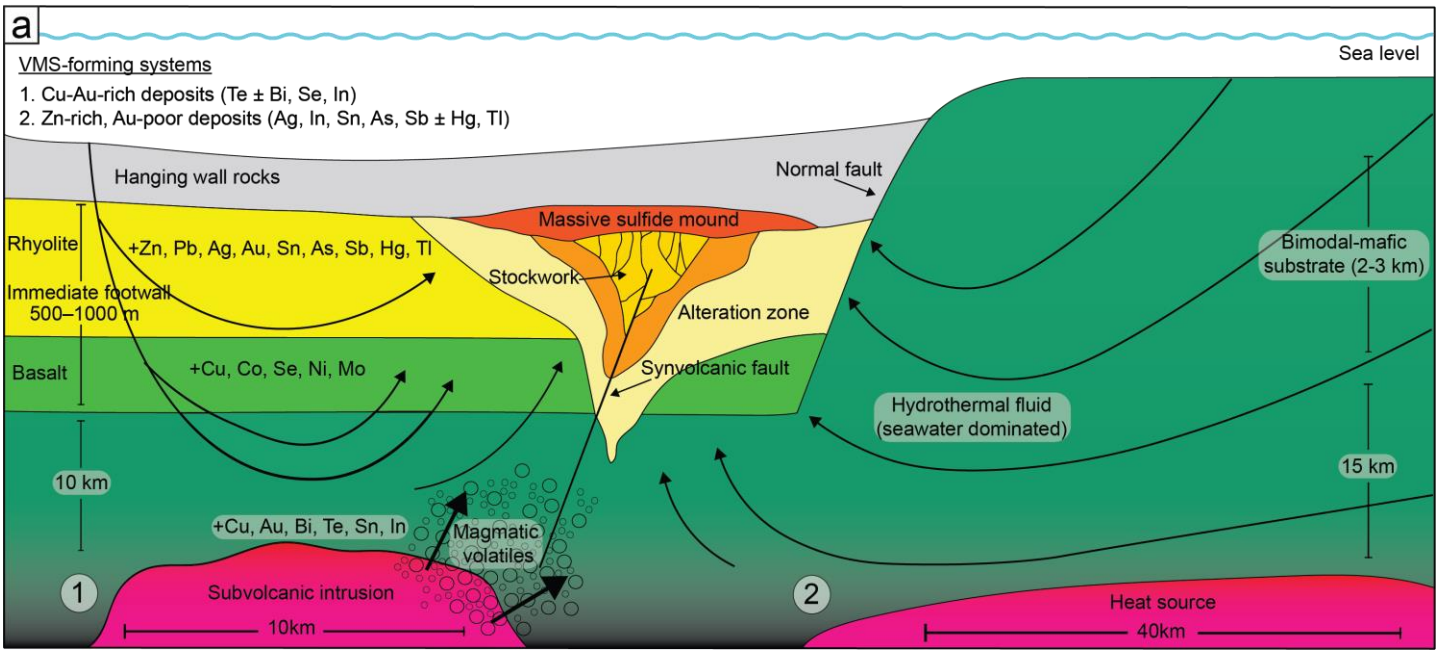
a
VMS-forming systems
1. Cu-Au-rich deposits (Te ± Bi, Se, In)
2. Zn-rich, Au-poor deposits (Ag, In, Sn, As, Sb ± Hg, Tl)
Sea level
Hanging wall rocks
Normal fault
Massive sulfide mound
Rhyolite
+Zn, Pb, Ag, Au, Sn, As, Sb, Hg, Tl
Stockwork
Alteration zone
Bimodal-mafic substrate (2-3 km)
Immediate footwall 500–1000 m
Basalt
+Cu, Co, Se, Ni, Mo
Synvolcanic fault
Hydrothermal fluid (seawater dominated)
10 km
15 km
+Cu, Au, Bi, Te, Sn, In
Magmatic volatiles
1
Subvolcanic intrusion
10km
2
Heat source
40km

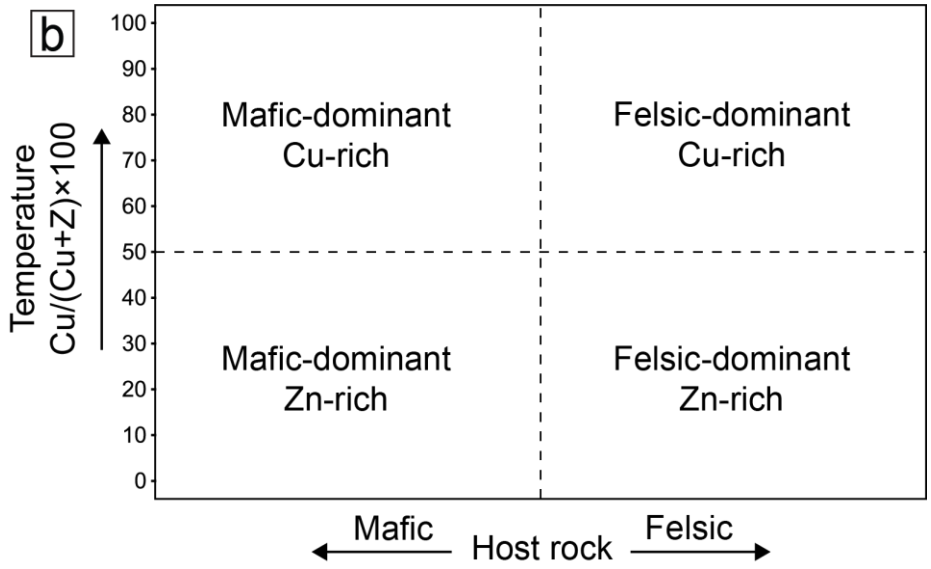
b
Temperature
Cu/(Cu+Z)×100
100
90
80
70
60
50
40
30
20
10
0
Mafic-dominant Cu-rich
Felsic-dominant Cu-rich
Mafic-dominant Zn-rich
Felsic-dominant Zn-rich
Mafic
Host rock
Felsic

Figure 5.1 a) Schematic illustration of different metal sources in VMS-forming systems. b) Diagram of the interplay between source rock and temperature in controlling the bulk composition and trace metal distribution in VMS recorded in the pyrite samples. Four groups are generally recognized: high-temperature deposits with mafic host rocks (Cu-rich); low-temperature deposits with mafic host rocks (Zn-rich); high-temperature deposits with felsic host rocks (Cu- and Zn-rich); low-temperature deposits with felsic host rocks (Zn- and Pb-rich). Temperature plays an important role in the bulk composition and metal zonation regardless of the source rock; for example, resulting in low-temperature enrichment of Pb even in mafic-hosted deposits with low Pb in the source rocks or high-temperature enrichment in elements such as Co even in felsic-hosted deposits with low Co in the source rocks.

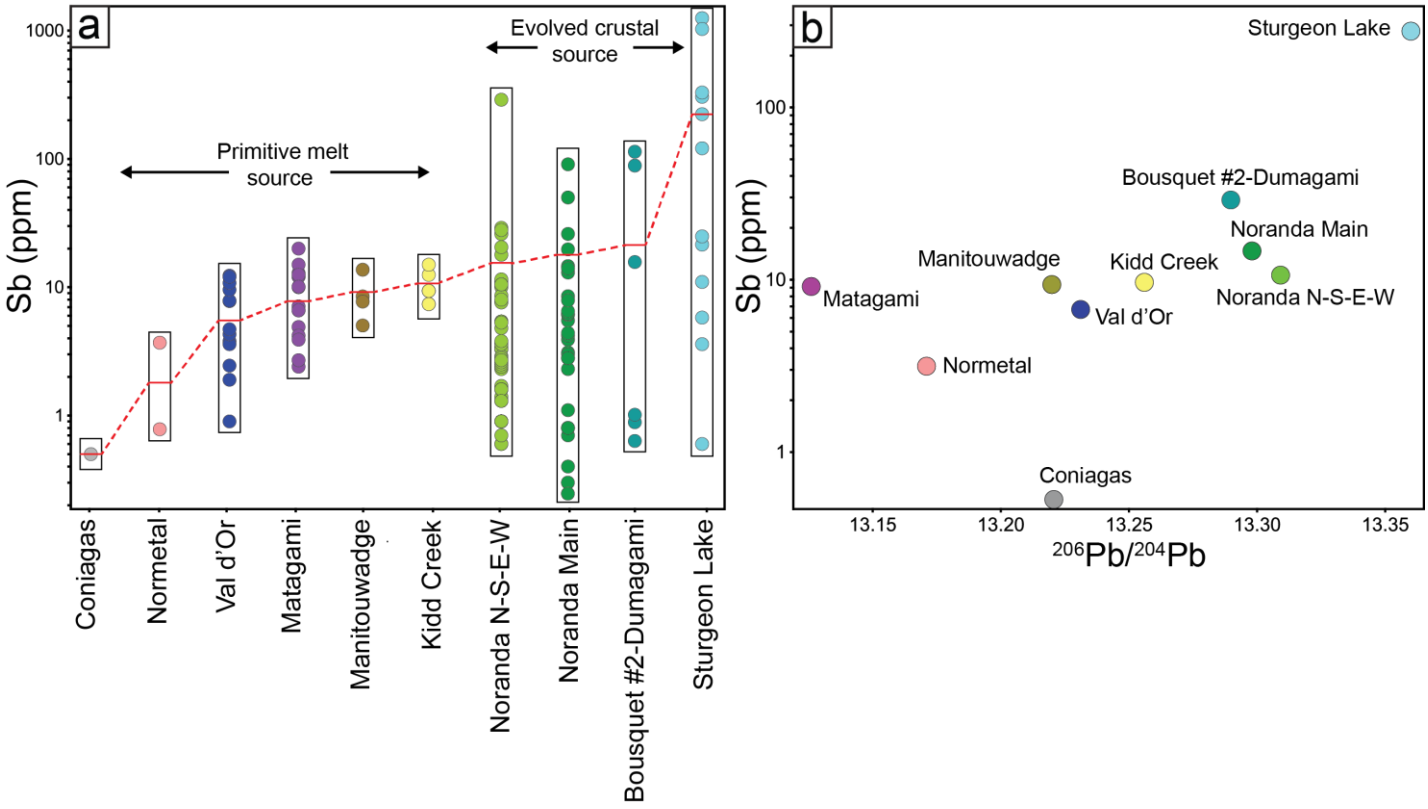

Figure 5.2 Plots of Sb in pyrite concentrates from different VMS deposits and camps in the Superior Province. a) Individual pyrite samples grouped by the sampled deposit/ camp. The boxes outline the range of concentrations and the red line in each box indicates the average concentrations in the samples from each camp/ deposit. The red dashed line connecting the boxes illustrates the increasing trend of average Sb concentrations reflecting the different compositions of host rocks and sources of melts. b) Binary plot of average Sb in pyrite vs. $^{206}Pb/^{204}Pb$ data (from Thorpe, 1999) from the same camps/ deposits. Sb concentrations in pyrite samples from these select deposits are consistent with the trend of $^{206}Pb/^{204}Pb$ signatures from the same deposits (Thorpe, 1999).

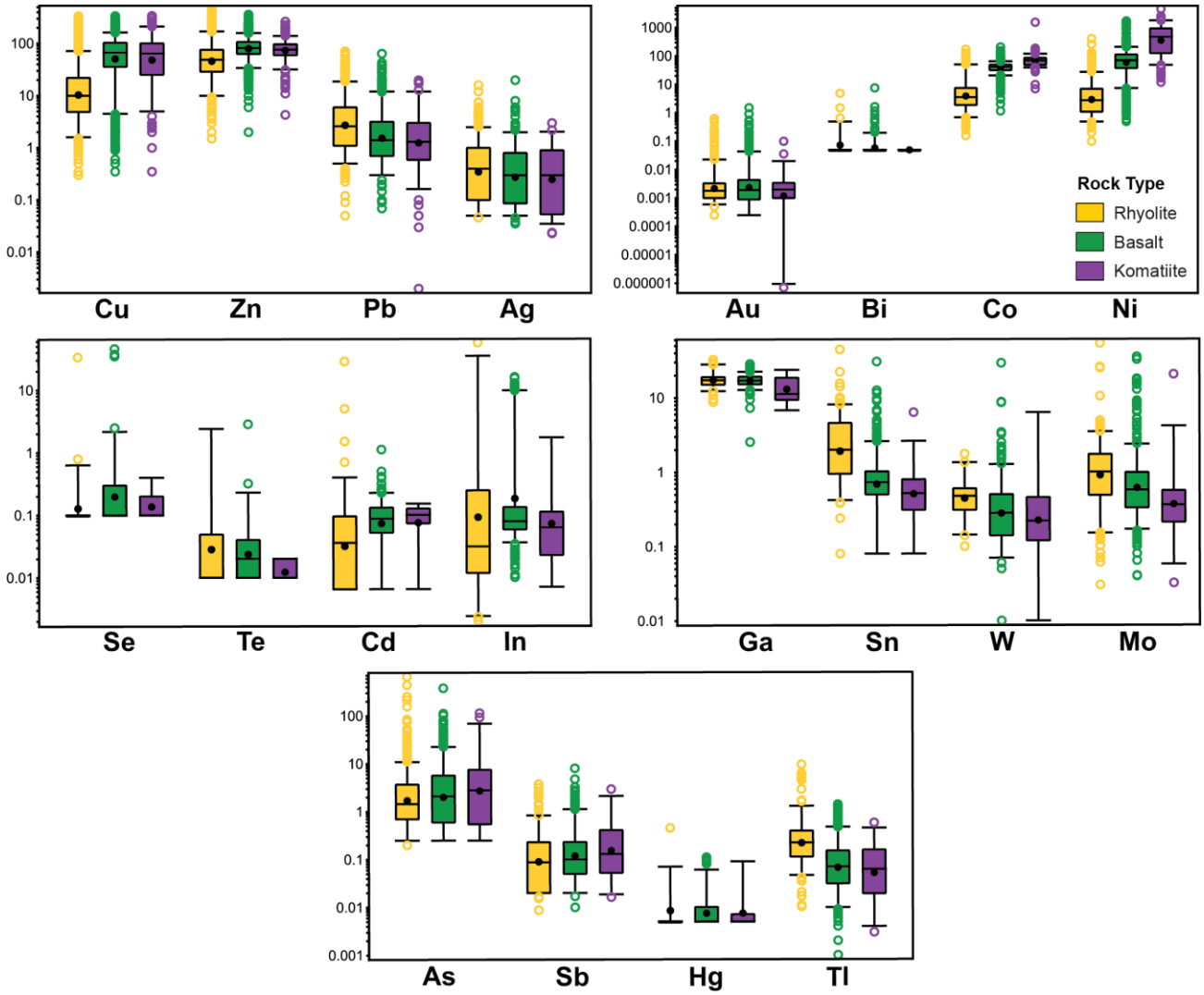

Figure 5.3 Boxplots of trace element concentrations in least altered volcanic rocks of the Superior Province. All data are in ppm (except Au is in ppb). The boxes enclose 50% of the data within the interquartile range (from Q1 to Q3). The average values (closed circle) and median (line) are shown. The lower and upper ends of the whiskers correspond to the 5th and 95th percentiles, respectively. Outliers, corresponding to the top 5% of the data, were removed from the database prior to further analysis. Elements are listed in the following order: 1) base metals; 2) precious metals; 3) Cu-associated; 4) Zn-associated; 5) Pb/ sulfosalt associated.

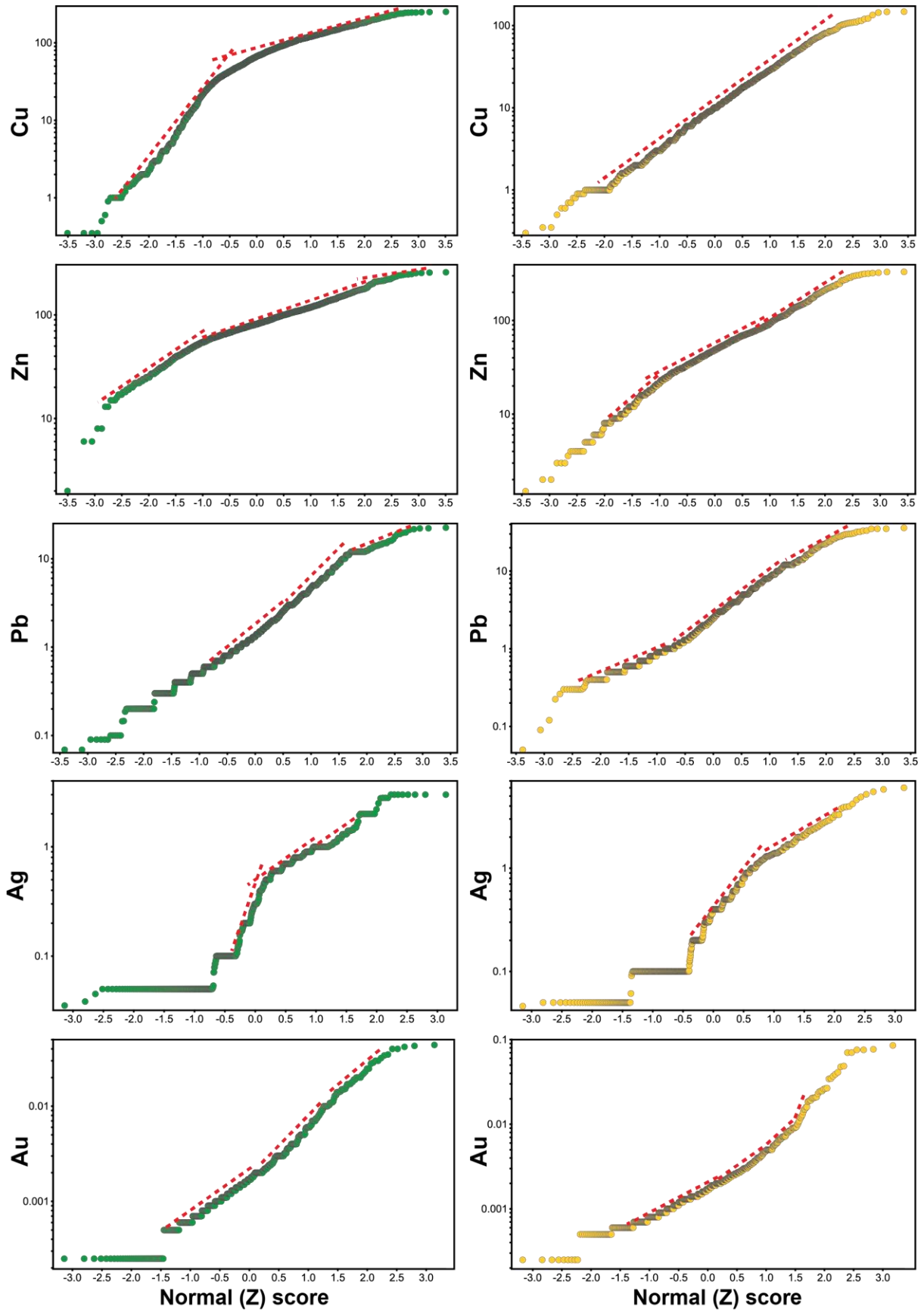
Cu
Zn
Pb
Ag
Au
Normal (Z) score
Cu
Zn
Pb
Ag
Au
Normal (Z) score

Figure 5.4 Log-probability plots of base and precious metal concentrations in different compositions of volcanic rocks. The data are from the OGS, GSC, MERN, SIGEOM, and Mole et al. (2021). All data are in ppm (except Au is in ppb). The plotted curves indicate multimodal distributions with the background concentrations interpreted to be the first significant upward inflection above the detection limit, indicated by the crossing dashed lines. The second data population above 80 ppm for Cu in mafic samples is normally distributed indicating it also represents background concentrations. Similarly, for Zn in felsic samples, the second data population likely represents background concentrations up to ~100 ppm Zn. Ag and Au data curves for both mafic and felsic samples are irregular above their detection limits suggesting very background concentrations for Ag (~0.1 ppm) and Au (~0.001 ppb).

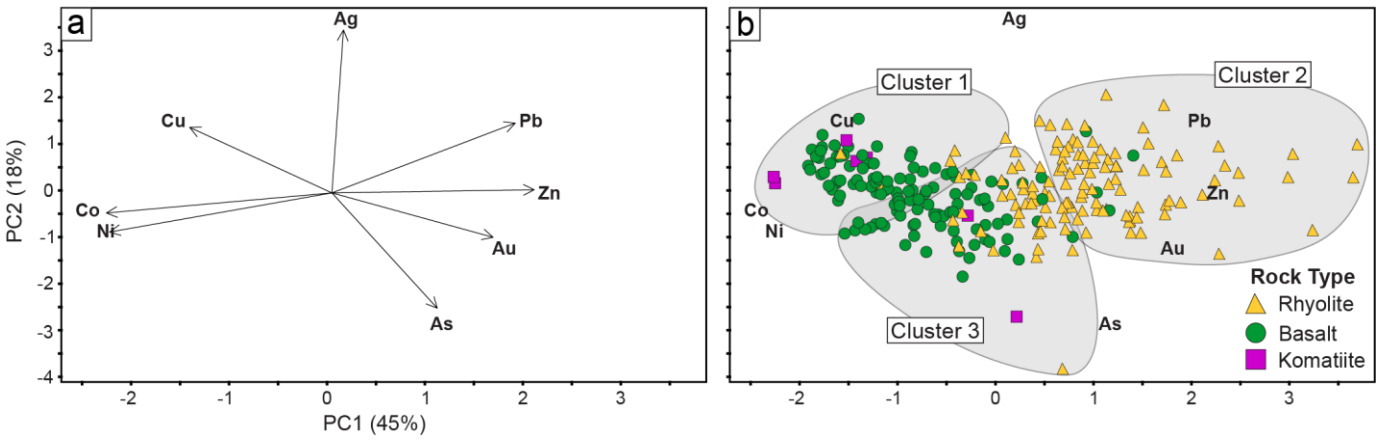

Figure 5.5 PCA plot for the filtered volcanic rock dataset from the Superior Province. a) Element loadings on PC1 and PC2 for the select trace metal set (Cu, Zn, Pb, Ag, Au, Co, Ni, As) shown on a two-dimensional scatterplot in PC space. The loadings of each element on each component describe how the different elements contribute individually to the variance represented by the component. b) Results of hierarchical clustering (HCPC) of elements and sample scores for the different rock types. The plotted points for each sample are a linear combination of Cu, Zn, Pb, Ag, Au, Co, Ni, and As. The mafic and ultramafic rocks cluster strongly with Cu, Co, and Ni (cluster 1), consistent with these elements in the deposits being sourced from the mafic-ultramafic rocks. The rhyolites cluster with the Zn-Pb-Au (cluster 2). See the text for discussion.

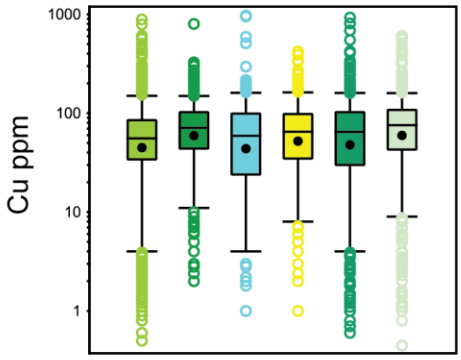
Cu ppm
1000
100
10
1

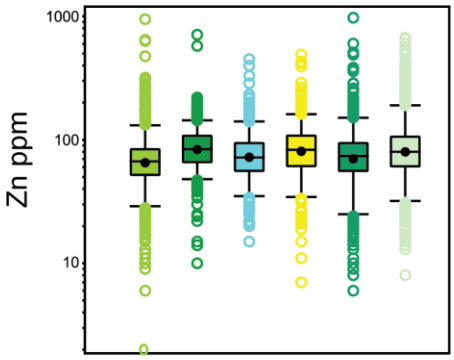
Zn ppm
1000
100
10

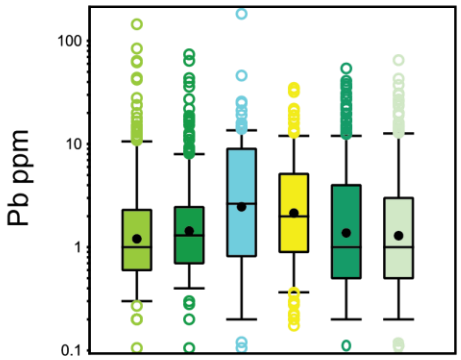
Pb ppm
100
10
1
0.1

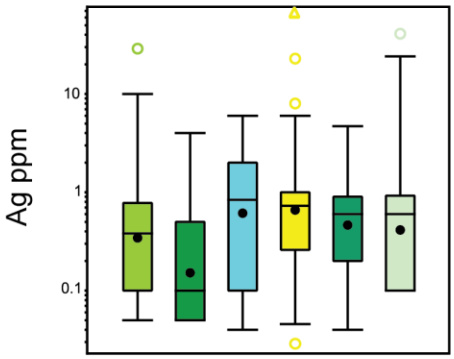
Ag ppm
10
1
0.1

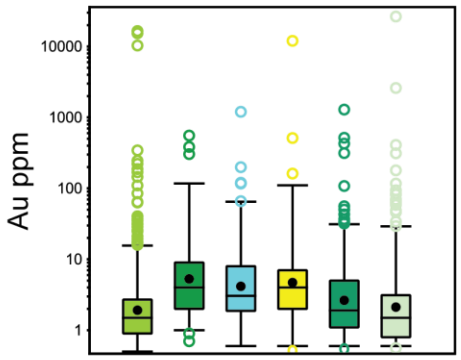
Au ppm
10000
1000
100
10
1

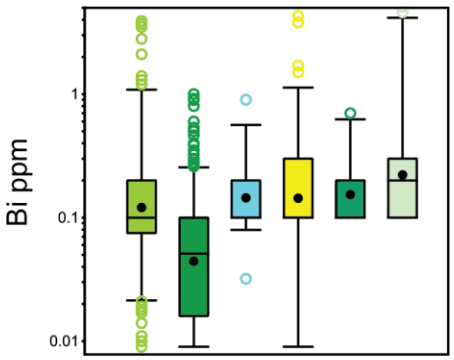
Bi ppm
1
0.1
0.01

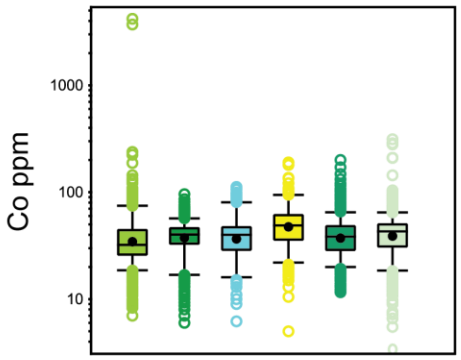
Co ppm
1000
100
10

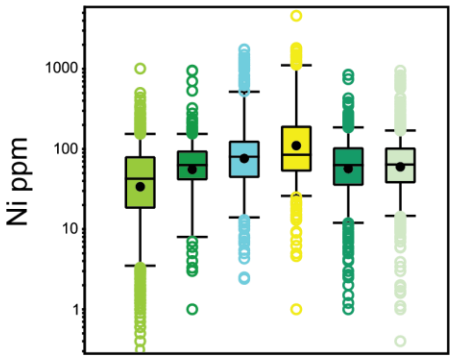
Ni ppm
1000
100
10
1

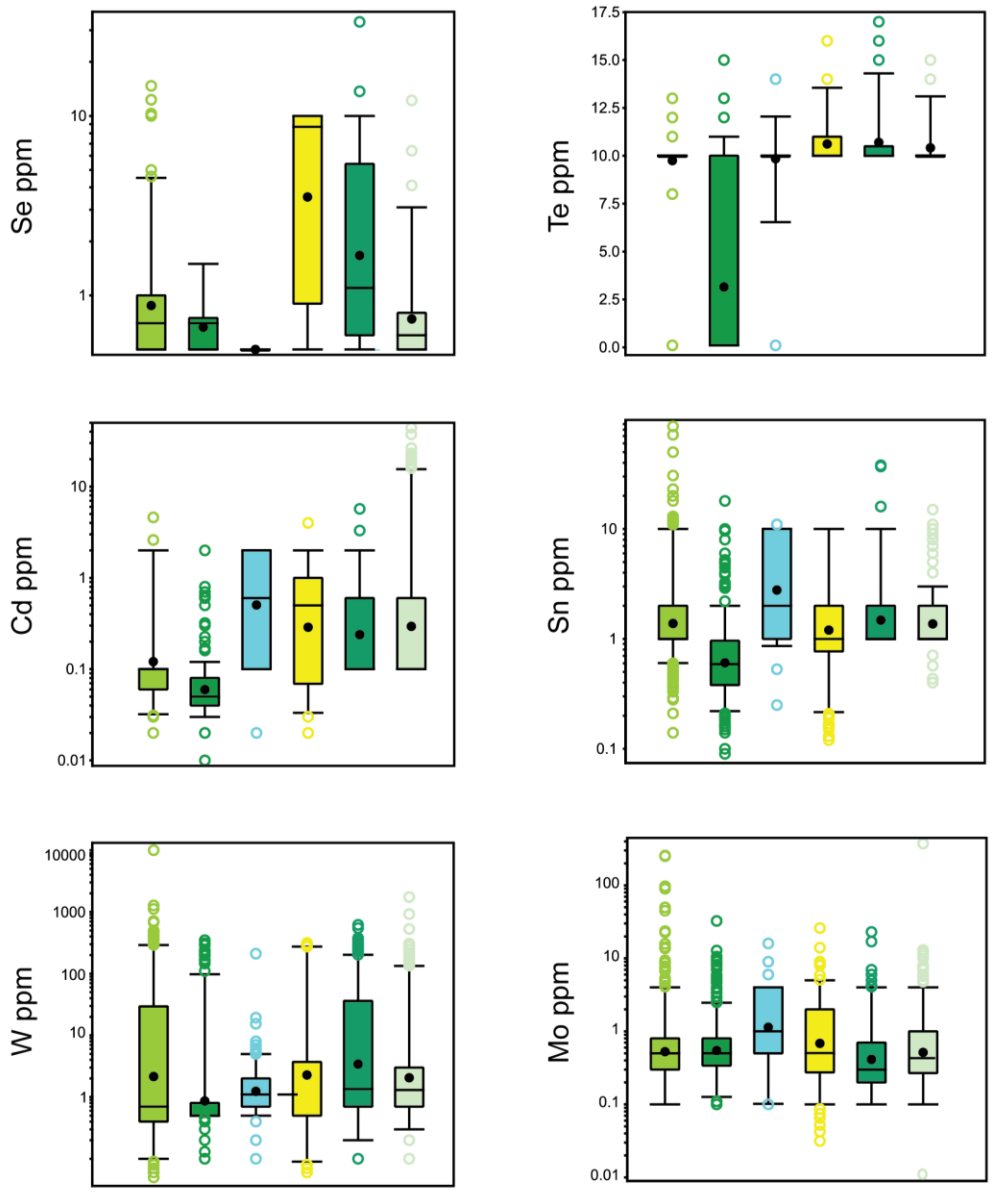
Se ppm
10
1
Te ppm
17.5
15.0
12.5
10.0
7.5
5.0
2.5
0.0
Cd ppm
10
1
0.1
0.01
Sn ppm
10
1
0.1
W ppm
10000
1000
100
10
1
Mo ppm
100
10
1
0.1
0.01

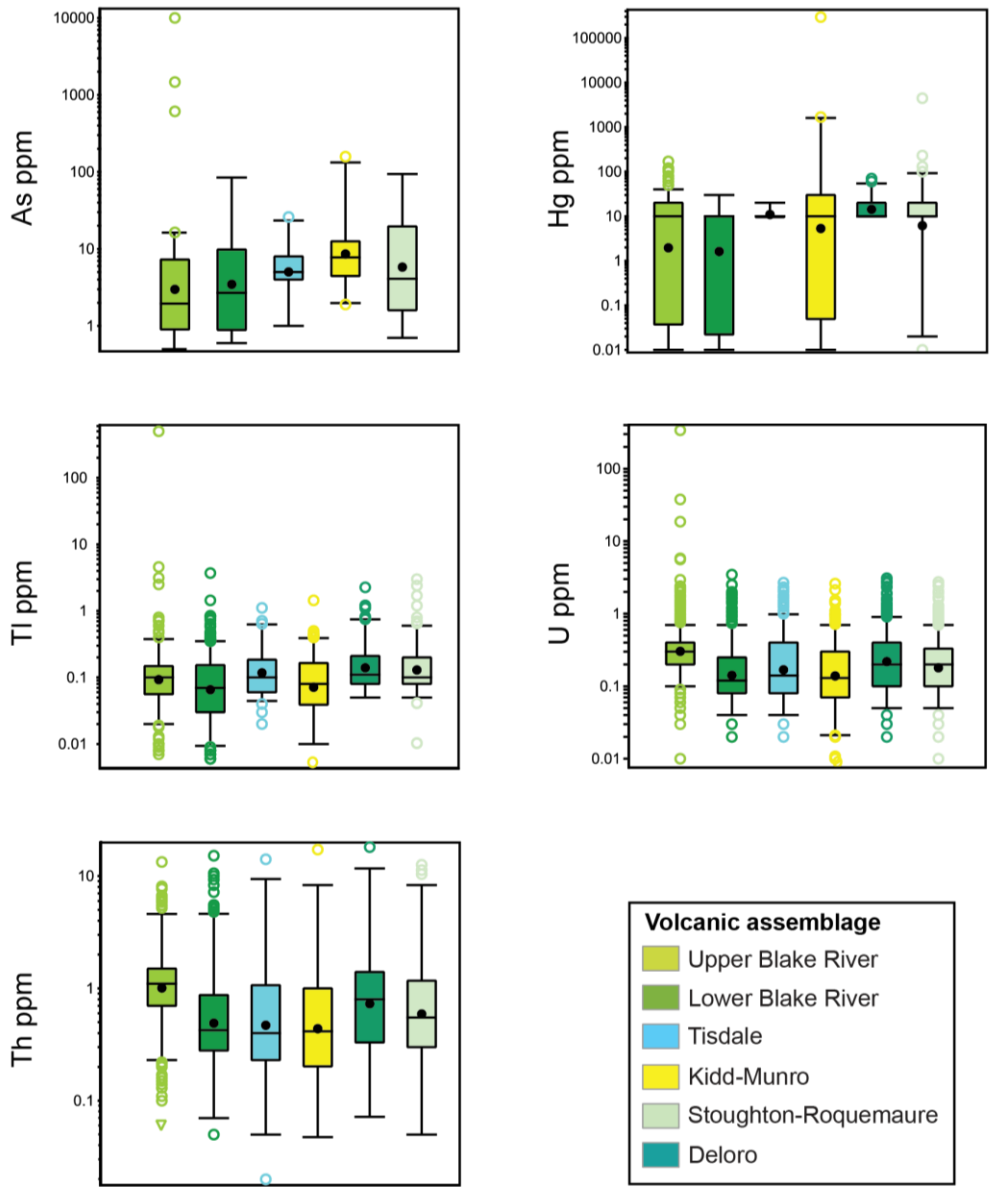

Figure 5.6 Boxplots of select trace element concentrations (Cu, Zn, Pb, Ag, Au, Co, Ni, Sn, W, Mo, As, Tl, U, Th) in mafic volcanic rocks belonging to the different assemblages of the AGB. The boxes enclose 50% of the data within the interquartile range (from Q1 to Q3). The average values (closed circle) and median (line) are shown. The lower and upper ends of the whiskers correspond to the 5th and 95th percentiles, respectively. Outliers, corresponding to the top 5% of the data, were removed from the database prior to further analysis. The mean concentrations for some assemblages are biased due to outliers such as Ag, Au, Bi, and Ni in some samples from Kidd-Munro. See text for discussion.

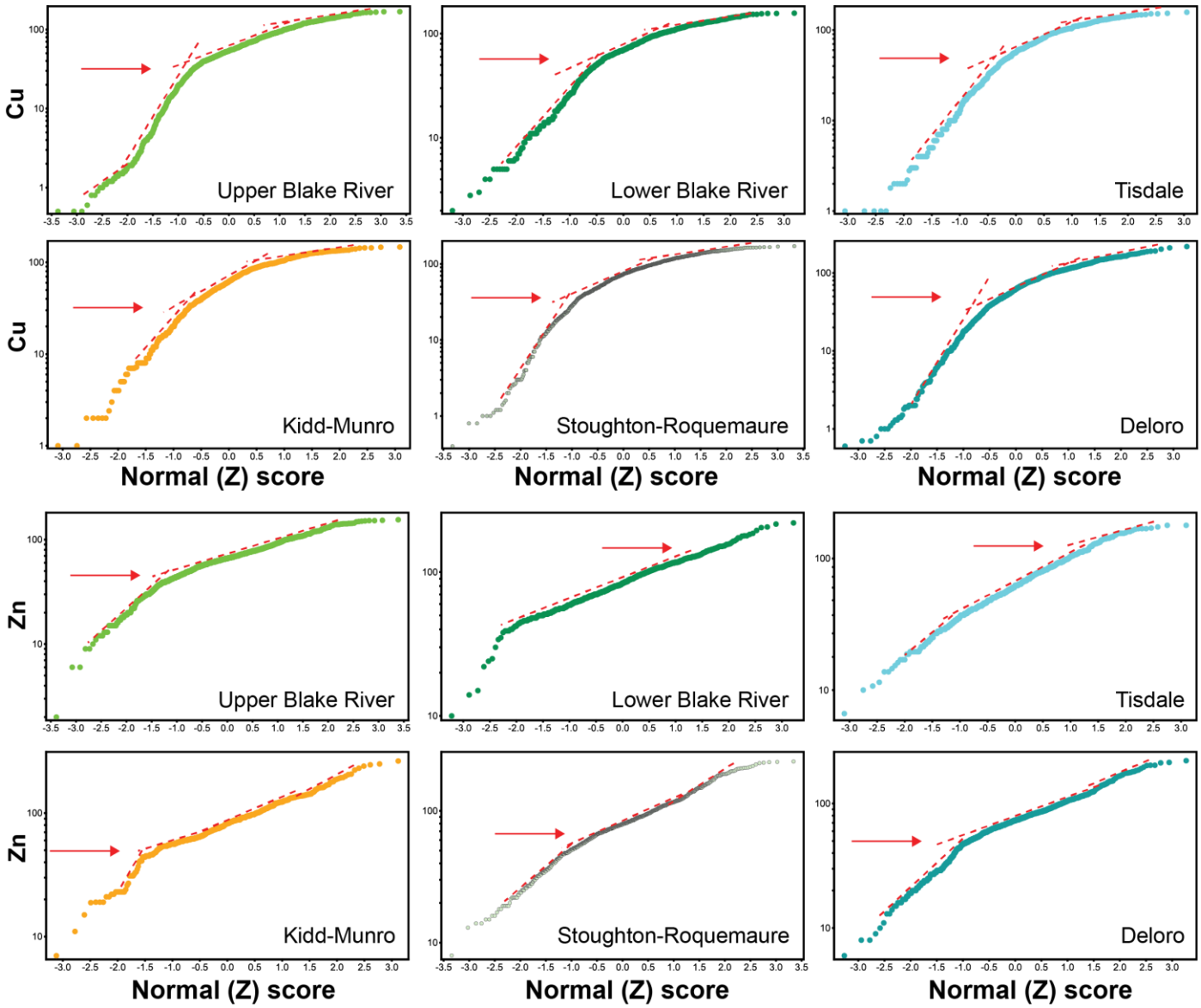
Cu
Upper Blake River
Lower Blake River
Tisdale
Kidd-Munro
Stoughton-Roquemaure
Deloro
Normal (Z) score
Zn
Upper Blake River
Lower Blake River
Tisdale
Kidd-Munro
Stoughton-Roquemaure
Deloro
Normal (Z) score

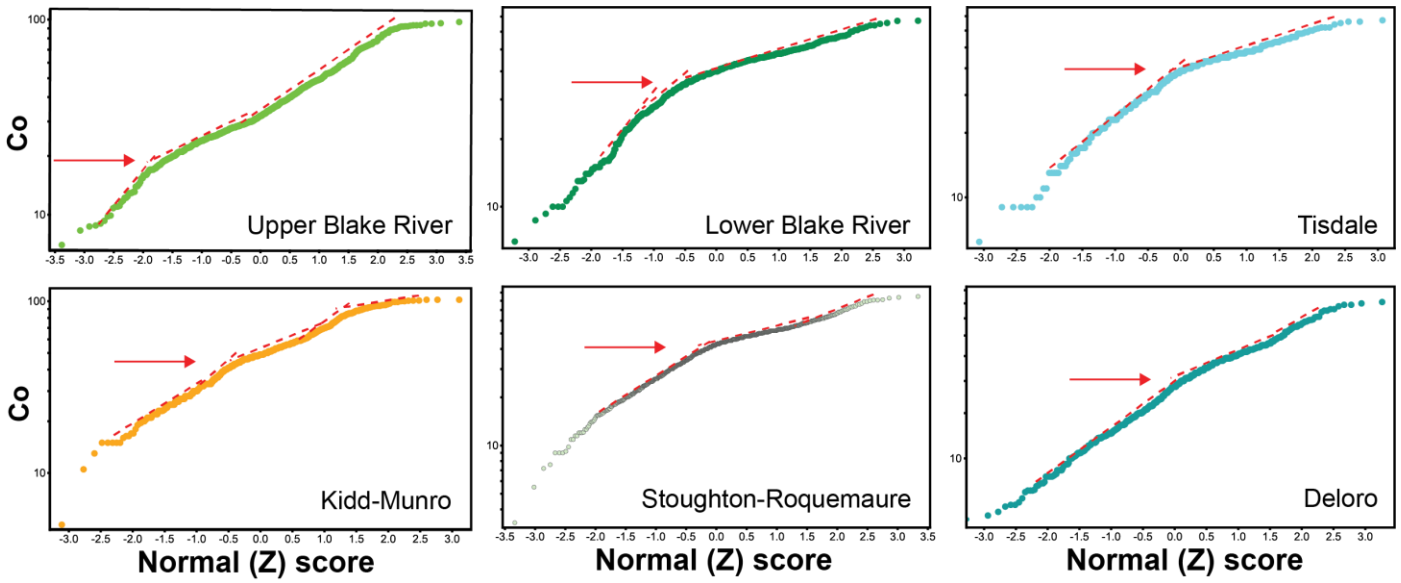

Figure 5.7 Log-probability plots of selected trace metal concentrations in mafic volcanic rocks samples from the AGB grouped by volcanic assemblage. The mafic volcanic rock data are from Fassbender et al. (2023). The plotted curves indicate multimodal distributions with the background concentrations interpreted to be the first significant upward inflection above the detection limit, indicated by the crossing dashed lines. The inferred maximum background concentrations are indicated by the red arrows. Overall, average Cu concentrations are similar between the assemblages, in the range of 55 to 75 ppm. See text for discussion. The Upper and Lower Blake River are shown to have different Cu content in the first population (up to 50 ppm in the Upper Blake River and 70 ppm in the Lower Blake River). The Zn content is also different in the Upper Blake River with two distinct populations at the inflection point of ~60 ppm and in the Lower Blake River with one continuous normal data distribution up to 100 ppm. Average Co concentrations are in the range of 30 to 45 ppm. The Upper Blake River has lower background Co indicated by the first data population up to 25 ppm, whereas the first populations in the other assemblages are up to 30 ppm and 40 ppm in Kidd-Munro.

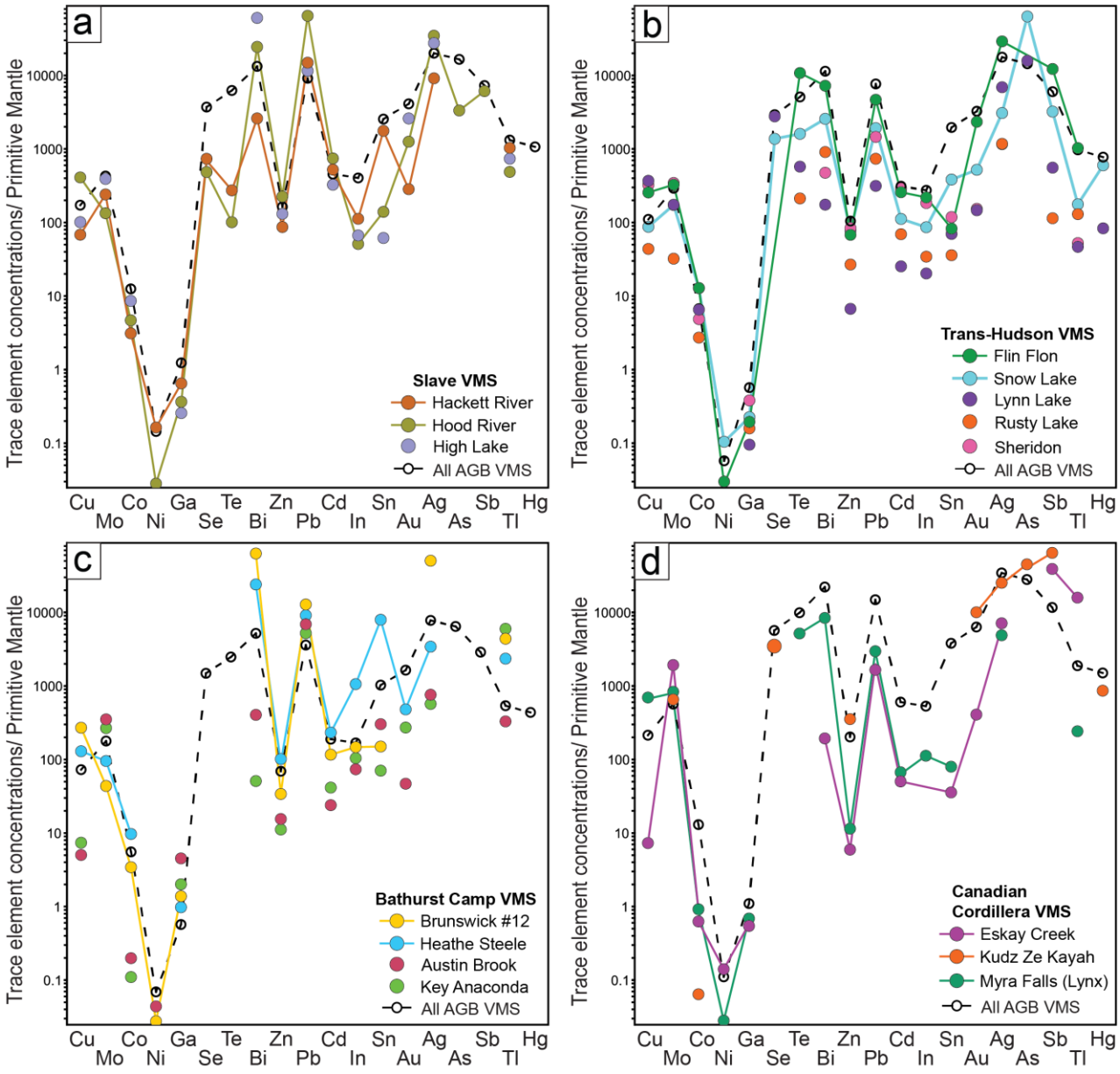

Figure 5.8 Multi-element profiles of mean trace element concentrations in pyrite samples from VMS deposits in the AGB (dashed black line) compared to other major VMS mine camps across Canada: a) Hackett River, Hood River, and High Lake camps in the Slave Province; b) Flin Flon, Snow Lake, Lynn Lake, Rusty Lake, and Sherridon in the Trans Hudson Orogen; c) Bathurst camp in the Appalachian Orogen; d) Stewart (Eskay Creek), Myra Falls (Lynx), and Finlayson Lake (Kudz Ze Kayah.) in the Canadian Cordillera. The lines and coloured symbols are the mean concentrations of the trace elements in pyrite from the camps and from selected individual deposits. Primitive mantle values used to normalize trace element concentrations are from Lyubetskaya and Korenaga (2007).

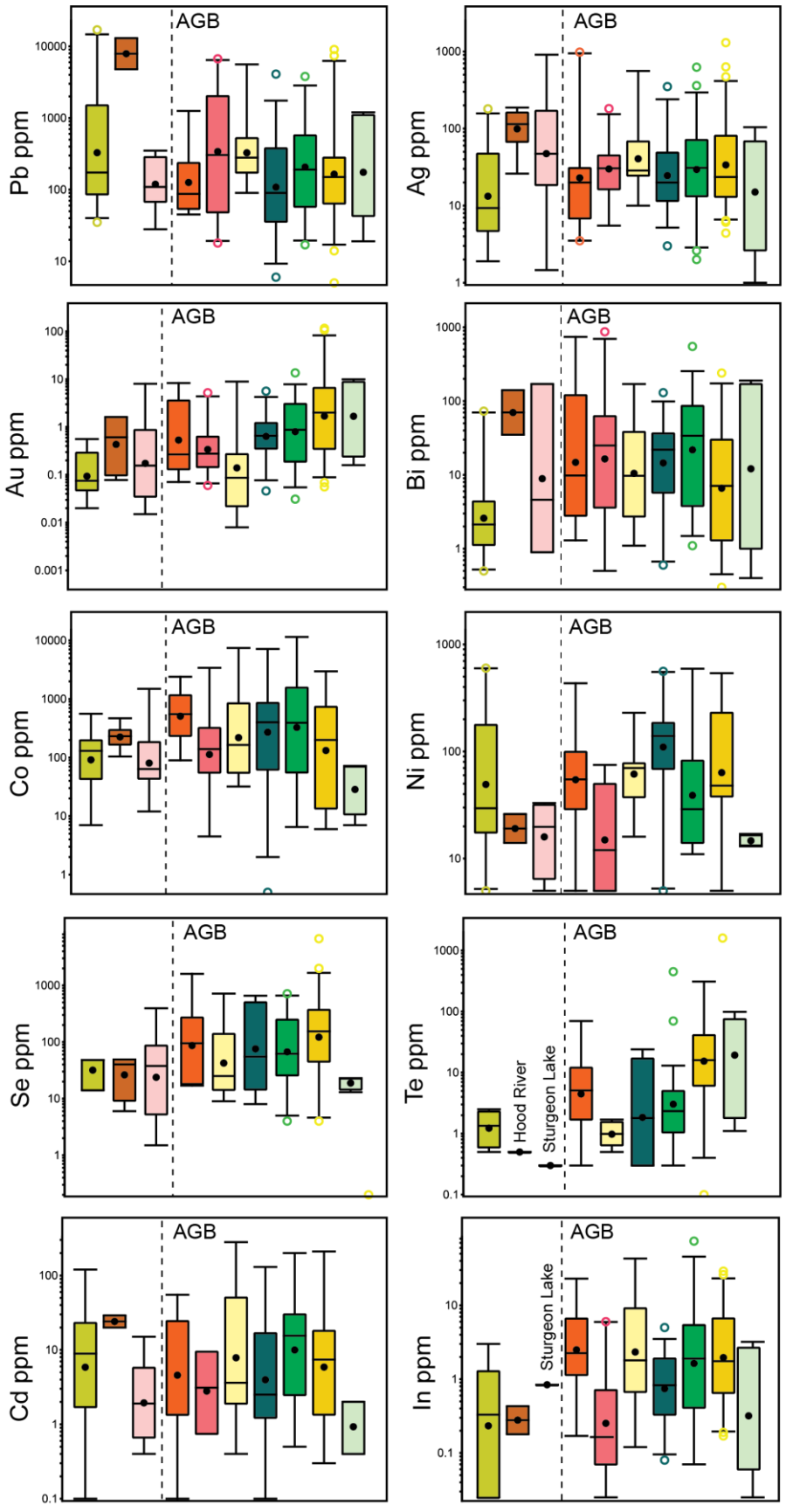
Pb ppm
AGB
Ag ppm
AGB
Au ppm
AGB
Bi ppm
AGB
Co ppm
AGB
Ni ppm
AGB
Se ppm
AGB
Te ppm
AGB
Hood River
Sturgeon Lake
Cd ppm
AGB
In ppm
AGB
Sturgeon Lake

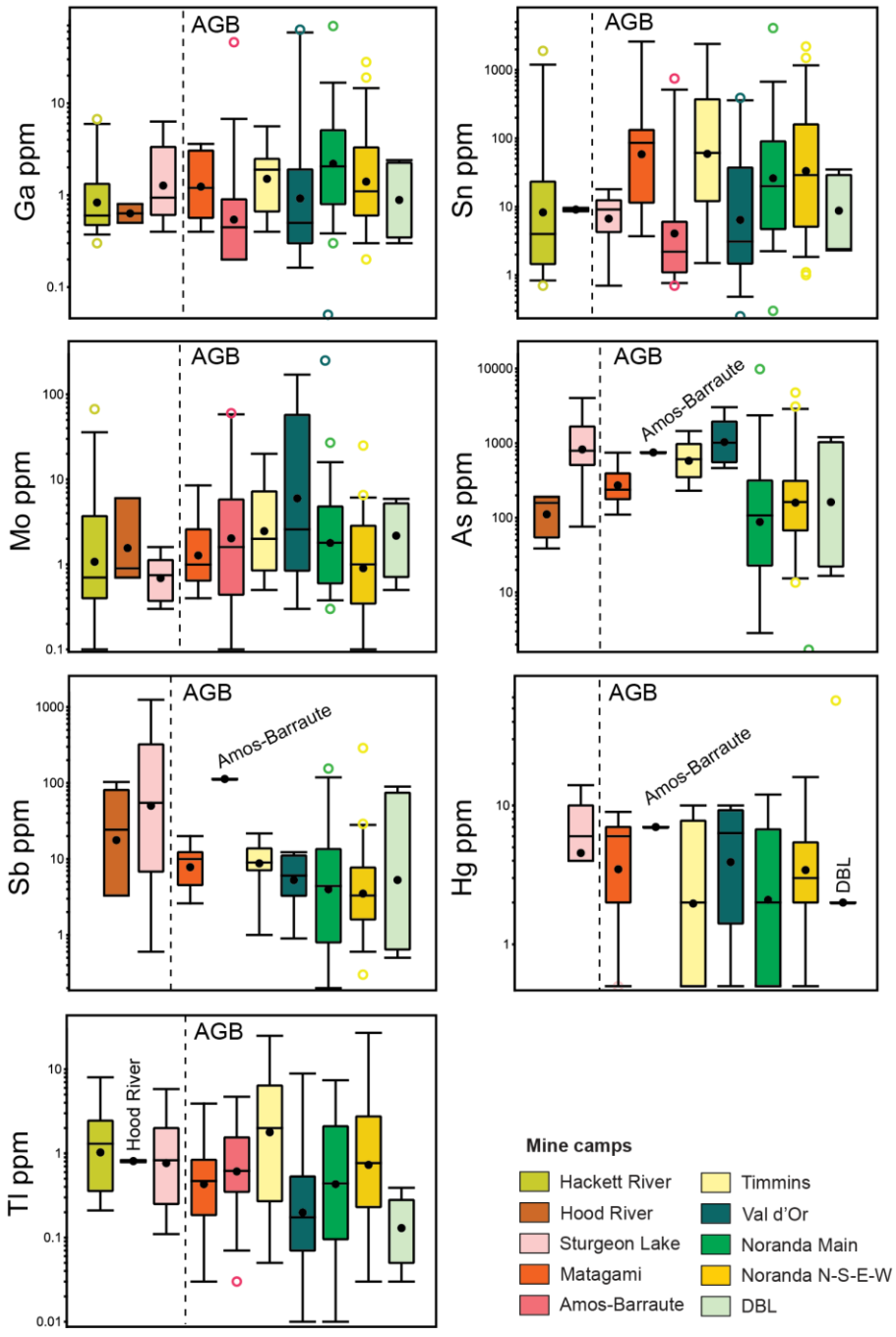
Ga ppm
AGB
Sn ppm
AGB
Mo ppm
AGB
As ppm
AGB
Amos-Barraute
Sb ppm
AGB
Amos-Barraute
Hg ppm
AGB
Amos-Barraute
DBL
Tl ppm
AGB
Hood River
Mine camps
Hackett River
Hood River
Sturgeon Lake
Matagami
Amos-Barraute
Timmins
Val d'Or
Noranda Main
Noranda N-S-E-W
DBL

Figure 5.9 Boxplots of trace element concentrations (ppm) in pyrite samples from VMS deposits in mine camps of the AGB in comparison to pyrite samples from older VMS mine camps in the Western Superior (Sturgeon Lake) and Slave Province (Hackett River and Hood River). VMS camps are ordered from oldest to youngest (left to right). The boxes enclose 50% of the data within the interquartile range (from Q1 to Q3). The average values (closed circle) and median (line) are shown. The lower and upper ends of the whiskers correspond to the 5th and 95th percentiles, respectively. Outliers, correspond to the top 5% of the data. The plots show pyrite samples from the Sturgeon Lake deposit have higher concentrations of Zn, Pb, Ag, As, Sb, Hg, and Tl. Pyrite samples from Hackett River have high Pb and Au, and low Zn, Ag, Bi, and Te compared to pyrite samples from VMS deposits in the AGB. Pyrite samples from Hood River also have high Pb as well as high Cu, Au, and Bi. See text for discussion.

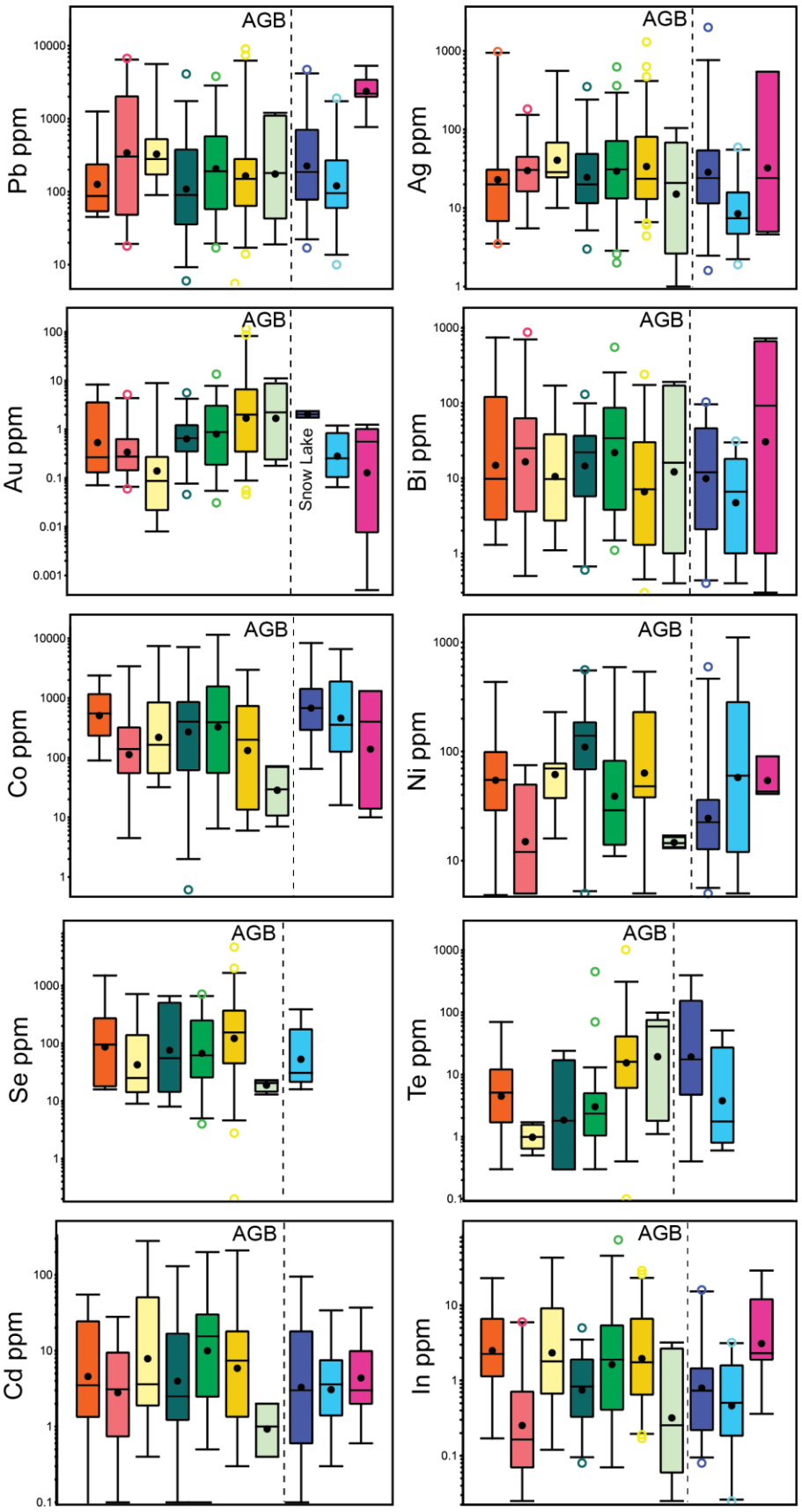
AGB
Pb ppm
Ag ppm
Au ppm
Snow Lake
Bi ppm
Co ppm
Ni ppm
Se ppm
Te ppm
Cd ppm
In ppm

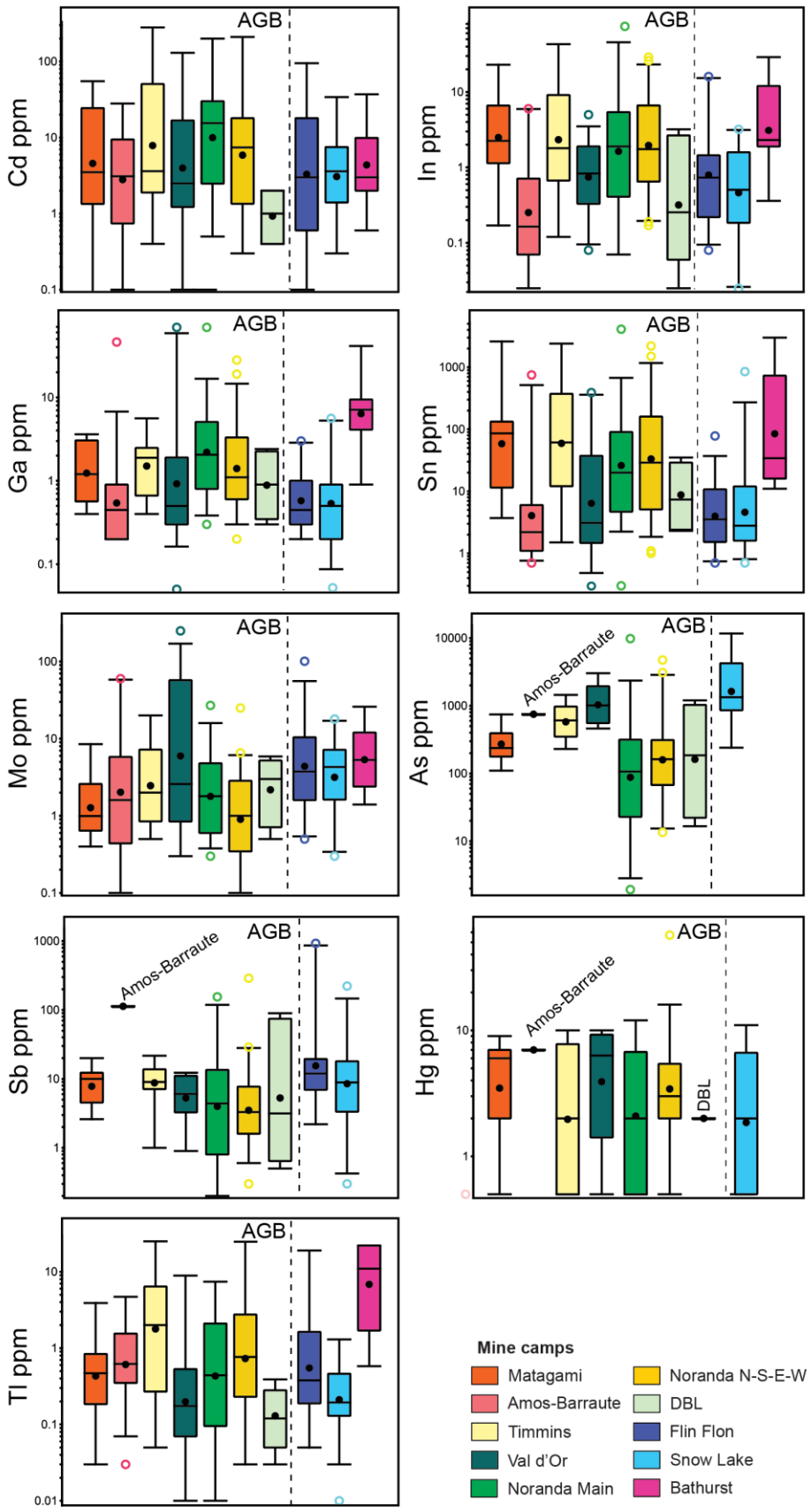
Cd ppm
In ppm
Ga ppm
Sn ppm
Mo ppm
As ppm
Sb ppm
Hg ppm
Tl ppm
AGB
Amos-Barraute
DBL
Mine camps
Matagami
Amos-Barraute
Timmins
Val d'Or
Noranda Main
Noranda N-S-E-W
DBL
Flin Flon
Snow Lake
Bathurst

Figure 5.10 Boxplots of trace element concentrations (ppm) in pyrite samples from VMS deposits in mine camps of the AGB in comparison to pyrite samples from younger VMS mine camps in the Trans-Hudson orogen (Flin Flon and Snow Lake) and Appalachian orogen (Bathurst). VMS camps are ordered from oldest to youngest (left to right). The boxes enclose 50% of the data within the interquartile range (from Q1 to Q3). The average values (closed circle) and median (line) are shown. The lower and upper ends of the whiskers correspond to the 5th and 95th percentiles, respectively. Outliers, correspond to the top 5% of the data. The plots show pyrite samples from the Flin Flon camp are variably enriched in Co-Ni, Te, In, and Sb depending on the Cu-Zn ratio of the sampled deposits. Similarly, pyrite samples from Cu-rich deposits of the Snow Lake camp have high Co-Ni, As, Se, and Te compared to average concentrations in pyrite from VMS in the AGB. Pyrite samples from Zn-Pb-Cu-rich deposits of the Bathurst camp have variable enrichments of Pb, Ag, Bi, In, Ga, Sn, and Tl. See text for discussion.

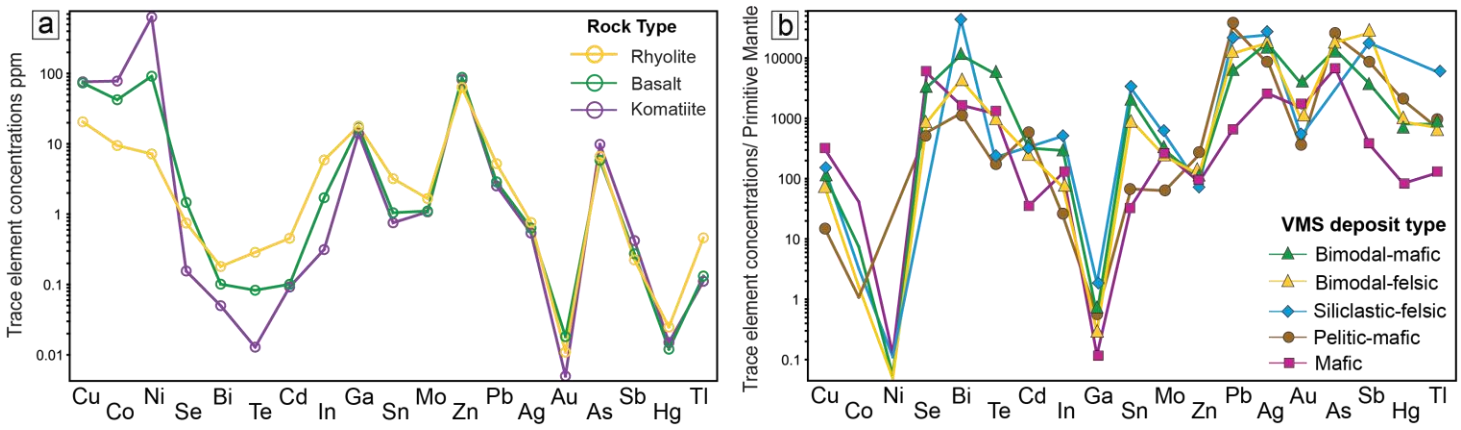

Figure 5.11 Multi element profiles (spider diagrams) of trace element concentrations in: a) least-altered volcanic rocks in the Superior Province data set; b) pyrite samples from VMS deposits across Canada classified by host rock type (Barrie and Hannington, 1999; Franklin et al., 2005). The order of the elements is according to relative enrichment in mafic versus felsic volcanic rocks then by similar chalcophile behaviour during mantle melting (need a reference for chalcophile behaviour during mantle melting). In a) rhyolite samples in the Superior province have high concentrations of Pb, Ag, Bi, Te, Cd, In, Sn, Hg, Tl, and U, whereas basalt and komatiite samples have higher concentrations of Cu, Zn, Co, Ni, and Se. In b) pyrite samples from bimodal felsic deposits have high Zn and Sb; pyrite samples from bimodal mafic deposits have high Au, Se, Te, As, and Hg; pyrite samples from mafic deposits have high Cu, Co, Ni, and Se; and pyrite samples from siliciclastic felsic deposits have high Pb, Ag, Bi, In, Ga, Sn, Sb, and Tl. Primitive mantle values used to normalize trace element concentrations of the pyrite samples are from Lyubetskaya and Korenaga (2007).

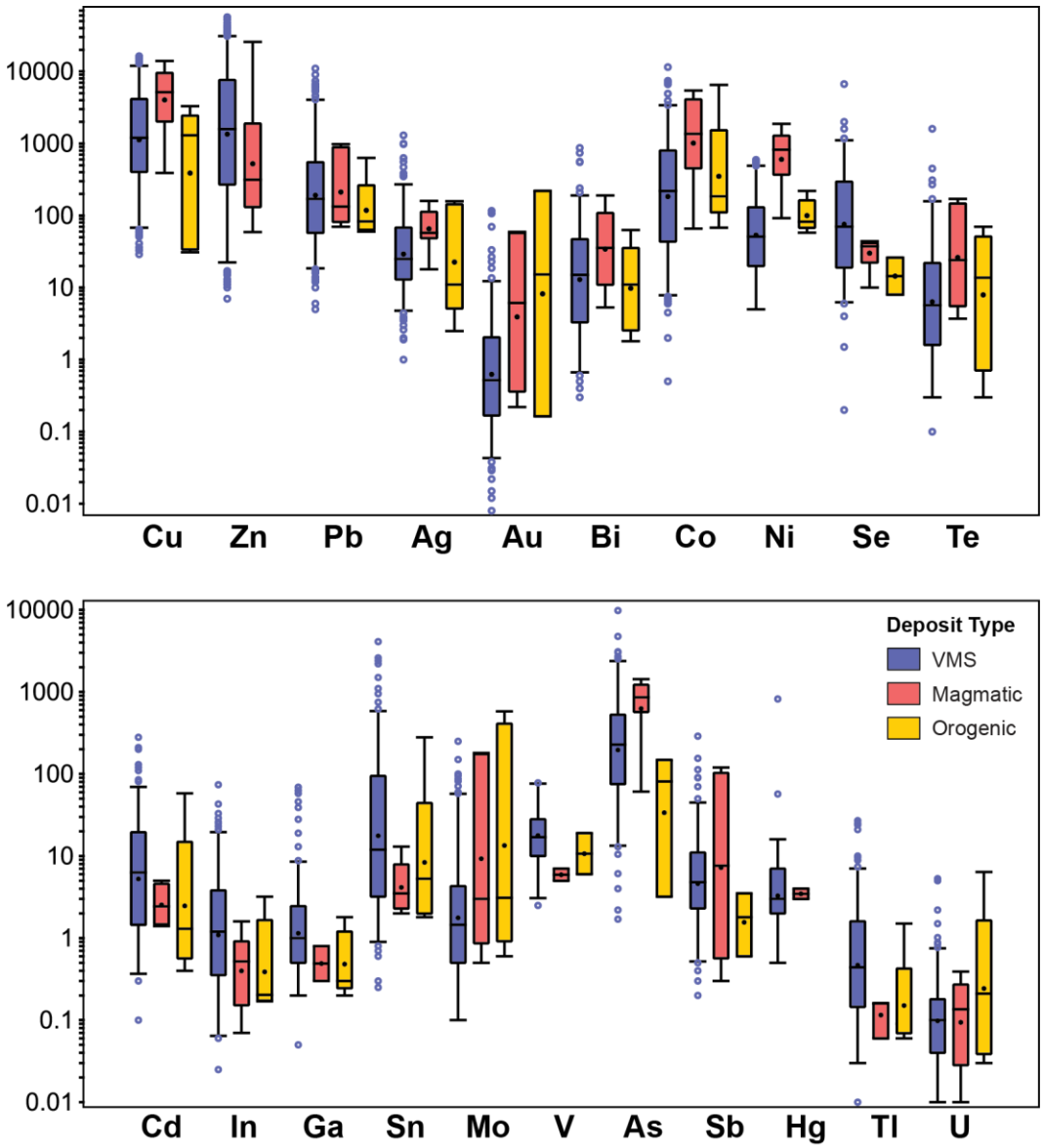

Figure 5.12 Boxplots of trace element concentrations (ppm) in pyrite samples from magmatic vein Cu deposits and orogenic Au deposits compared to pyrite samples from VMS deposits in the AGB. The boxes enclose 50% of the data within the interquartile range (from Q1 to Q3). The average values (closed circle) and median (line) are shown. The lower and upper ends of the whiskers correspond to the 5th and 95th percentiles, respectively. Outliers, correspond to the top 5% of the data. The general trend of trace element enrichments is the same for all deposit types (e.g., Co, Ni, Se, Mo, V, As are enriched compared to other elements, most likely controlled by lattice-bound substitutions). However, pyrite samples from the magmatic Cu vein deposits of Chibougamau have higher Cu, Au, Co, Ni, Te, W, Mo, As, and Sb, and lower Zn, Pb, Se, Cd, In, Ga, Sn, V, and Hg compared to Abitibi VMS. Pyrite samples from the orogenic Au deposits are enriched in Au, Co, W, Mo, and depleted in most other trace elements compared to pyrite from VMS deposits.

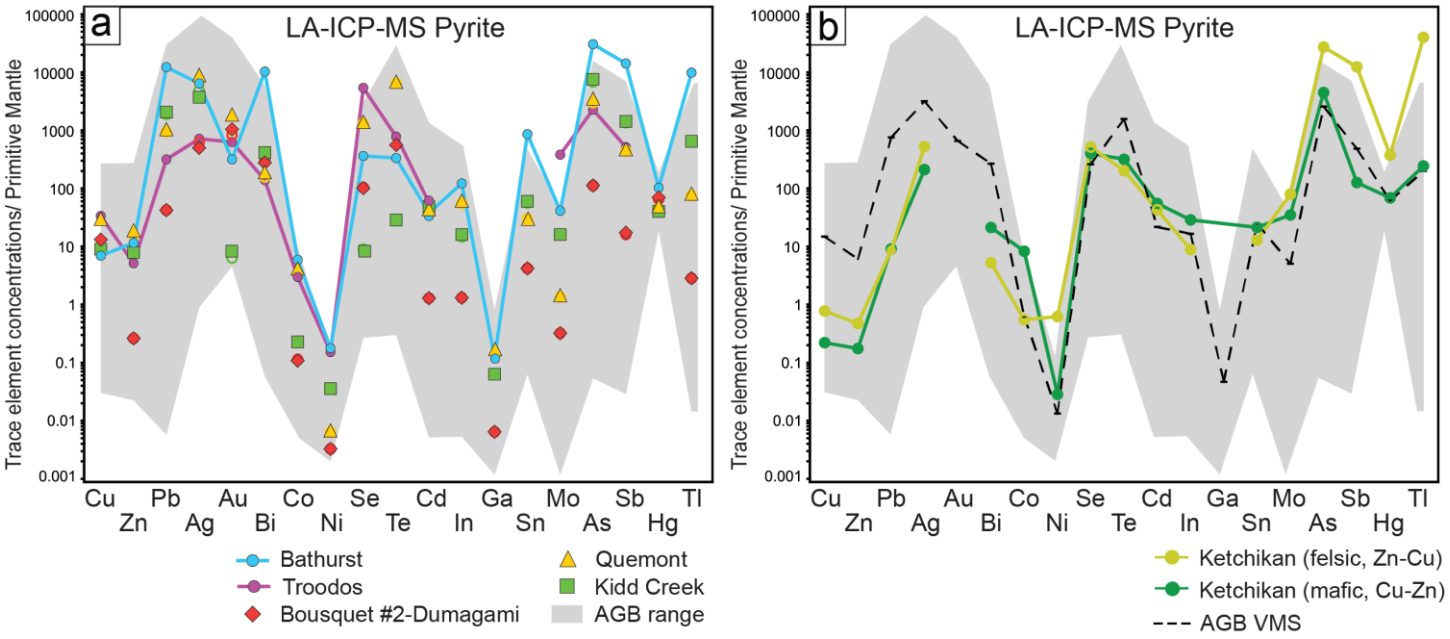

Figure 5.13 Multi-element profiles (spider diagrams) of trace element concentrations of individual pyrite grains analyzed by LA-ICP-MS from AGB VMS deposits (this study: Bousquet #2-Dumagami, Quemont, and Kidd Creek) in comparison to data from the literature (Slack et al., 2005; Keith et al., 2016; Dehnavi et al., 2018). All of the pyrite data show remarkably consistent trace element enrichments and depletions with the range of values for the pyrite samples from the AGB. LA-ICP-MS analyses of pyrite from the Skouriotissa (Troodos) have higher Cu, Co, Ni, Se, Mo; lower Zn, Pb, Ag; and similar Au, Bi, Te, Cd, As, Sb compared to pyrite from the AGB deposits. Enrichment in Cu, Co, Ni, Se, and Mo, and depletion in Zn, Pb, Ag reflect the mafic-dominant host rock. LA-ICP-MS analyses of pyrite from the siliciclastic-felsic Bathurst deposits have higher Zn, Pb, Ag, Bi, Co, Ni, In, Ga, Sn, As, Sb, Tl; slightly lower Cu, Au, Te; and similar Cd, Mo, Hg compared to pyrite from the AGB deposits. Enrichment in Zn, Pb, Ag, As, Sb, Hg, Tl reflects the siliciclastic-felsic source of metals and enrichment in Bi, In, and Sn reflects a magmatic input. LA-ICP-MS analyses of pyrite from the bimodal-felsic Ketchikan deposits have higher Ni, Mo, As, Sb, Hg, Tl; lower Cu, Zn, Pb, Ag, Bi, Te; and similar Co, Cd, In, Sn compared to pyrite from the AGB deposits. Pyrite from the bimodal-mafic Ketchikan deposits has higher Co; lower Cu, Zn, Pb, Ag, Bi, Te; and similar Ni, Se, Cd, In, Sn, Mo, As, Hg, and Tl compared to pyrite from the AGB deposits.

Table 5.1 Summary of interpreted trace element enrichments in pyrite in relation to deposit characteristics.

	Deposit characteristics							
Source rock	Zn/Pb-rich deposit	Example	Cu-Rich deposit	Example	Large tonnage	Example	High Au grade	Example
Felsic volcanic host rocks	Ag, Cd, In, Sn, As, Sb, Hg, Tl	Sturgeon Lake deposits	Au, In, Sn ±As ±Hg	Horne	Sn	Kidd Creek	Ag, Au, As, Sb, Hg, Tl	Delbridge, Deldona, Eskay Creek
Mafic volcanic host rocks	Pb, Ag	Moosehead	Co, Ni ±Se ±Mo	Potter-Doal, East Waite, East Sullivan, Coronation	-	-	-	-
Sedimentary host rocks	Pb, Ag, Sb, Tl ±As ±Hg	Koke (Boylen)	-	-	Pb, Ag, Tl	Brunswick #12	-	-
Magmatic volatile input	Sn, W	Geco	Au, Bi, Se, Te In, Sn ±Mo	Quemont	Bi, In Sn	Heath Steele	Bi, Te, Sn	Bousquet #2-Dumagami, Horne

Table 5.2 Average trace element concentrations of least-altered mafic volcanic rock samples from different assemblages of the AGB. Data are from OGS, GSC, MERN, SIGEOM, and Mole et al. (2021).All elements are in ppm (except Au are in ppb).

	No. samples	Cu	Zn	Pb	Ag	Au	Bi	Co	Ni	Se	Te	Cd	In	Sn	W	Mo	V	As	Sb	Hg	Tl	U	Th
Volcanic rocks of the Superior Province																							
Rhyolite	1789	16.3	59.4	4.59	0.68	0.004	0.077	7.51	6.23	0.10	0.019	0.051	0.03	2.87	0.55	1.05	23.4	3.06	0.24	0.006	0.28	1.20	4.88
Basalt	2341	72.1	86.3	2.60	0.52	0.004	0.050	41.3	80.7	0.19	0.028	0.089	1.75	0.85	0.48	0.68	269	2.90	0.18	0.008	0.10	0.28	0.91
Komatiite	192	64.2	72.6	0.86	0.37	0.002	0.050	69.3	522	0.10	0.015	0.076	0.033	0.52	0.13	0.31	212	3.06	0.10	0.007	0.14	0.085	0.22

Table 5.3 Average trace element concentrations of least-altered mafic volcanic rock samples from different assemblages of the AGB. Data are from Mole et al. (2021). All elements are in ppm (except Au are in ppb).

	No. samples	Cu	Zn	Pb	Ag	Au	Bi	Co	Ni	Se	Te	Cd	In	Sn	W	Mo	As	Hg	Tl	U	Th
Mafic volcanic rocks of the AGB																					
Upper Blake River	1053	57.6	68.8	1.61	0.50	2.54	0.14	32.2	58.2	0.7	9.36	0.08	0.08	1.33	3.4	0.63	2	11.9	0.11	0.34	1.18
Lower Blake River	696	71.5	88.3	2.17	0.30	8.84	0.07	38.4	71.3	0.54	1.25	0.06	0.07	0.74	0.8	0.79	8.50	12.9	0.11	0.19	0.67
Tisdale	401	61.6	76.1	3.50	1.13	7.30	0.19	36.2	87	0.50	0.10	0.12	0.03	1.33	1.72	1.19	5.83	10.8	0.12	0.24	0.81
Kidd-Munro	359	68.1	88.6	3.09	0.78	5.35	0.23	45.9	119	0.90	10.0	0.07	-	1.10	2.2	1.00	6.3	19	0.11	0.22	0.78
Stoughton-Roquemaure	1041	72.8	83.3	2.25	0.56	4.33	0.19	39.4	76.0	0.66	10.0	0.12	-	1.51	2.4	0.84	1.0	14.9	0.15	0.25	0.87
Deloro	742	65.3	73.4	2.29	0.51	3.86	0.16	37.0	73.2	0.69	10.0	0.12	-	1.42	4.3	0.58	-	16.7	0.18	0.29	1.05

Table 5.4 Average trace element concentrations (ppm) in pyrite samples from VMS deposits and occurrences in the Superior Province in comparison to the Slave Province, and in Proterozoic and younger orogens across Canada. Data are from Jonasson et al. (2021). All elements are in ppm.

Camp	Deposit	Cu	Zn	Pb	Ag	Au	Bi	Co	Ni	Se	Te	Cd	In	Ga	Sn	W	Mo	V	As	Sb	Hg	Tl	U
Amos-Barraute	Abcourt Barvue	4249	1197	642	40.1	1.07	31.5	125	12.0	-	-	3.9	0.47	0.28	2.27	-	25.0	-	750	113	7.00	0.79	0.07
	Conigo	5960	551	804	79.2	1.08	348	329	40.0	-	-	7.28	3.84	9.50	326	-	1.76	-	-	-	-	0.28	0.73
	Mogador	597	4018	2163	35.1	0.38	20.4	435	19.0	-	-	7.29	0.10	1.02	3.19	-	0.93	10.0	-	-	-	1.30	0.04
Joutel	Joutel	2200	11850	1800	50.5	0.40	90.0	1195	140	314	5.70	42.0	9.70	0.70	31.0	-	7.30	-	835	3.90	12.0	0.08	0.15
	Poirier	1085	5703	419	12.6	0.07	1.97	241	15.0	23.8	1.93	14.03	1.15	1.58	210	-	4.73	-	329	12.4	-	0.43	0.03
Normetal	Normetal	12000	15348	85	205	1.10	99	554	-	20.5	-	6.50	0.55	2.10	6.20	-	0.50	-	152	3.15	-	0.60	0.16
Quevillon	Coniagas	501	11135	3332	227	0.47	3.50	138	52.0	-	-	32.1	0.56	1.20	57.3	-	0.48	-	30.50	0.50	-	1.47	0.46
Matagami	Bell Allard	1383	2300	410	13.2	0.43	2.80	243	102	31.3	4.40	9.00	1.52	1.27	7.23	-	2.67	23.0	501	10.3	0.50	0.43	0.11
	Isle Dieu	1155	6030	435	279	-	228	1584	34.7	-	2.00	18.8	3.00	0.67	768	-	1.15	-	-	12.3	-	0.66	0.04
	Mattagami Lake	2350	16227	91	16.3	0.27	4.00	152	434	84.0	16.8	14.9	4.39	1.00	150	9.00	4.65	-	313	8.83	2.00	2.37	0.17
	New Hosco	1150	247	56	59.1	0.08	2.30	1412	42.0	57.3	2.93	0.57	1.57	1.80	20.0	-	2.30	-	150	3.97	3.33	0.03	0.36
	Norita A	3650	180	48	4.85	-	113	735	55.0	-	70.0	1.10	1.85	2.25	605	-	0.80	-	-	-	-	0.27	0.23
	Orchan	4825	13526	237	115	5.34	40.0	569	-	614	10.7	22.6	14.8	2.60	79.0	-	1.63	-	324	9.25	7.50	0.77	0.14
Timmins	Cdn. Jamieson	16000	24000	94	10.0	0.22	5.20	190	32.0	-	-	59.0	1.80	5.60	150	-	2.30	-	-	-	-	0.26	0.10
	Genex	2007	426	147	212	1.99	61.7	1537	102	274	0.70	1.30	4.89	0.50	6.73	4.00	2.37	-	1059	6.50	5.25	0.16	0.11
	Kam-Kotia	2127	19867	2273	46.5	3.08	25.9	324	-	74.3	0.95	38.7	2.03	2.67	136	3.25	2.63	-	601	17.6	5.33	11.0	0.10
	Kidd Creek	2532	7306	328	50.2	0.04	15.4	117	73.5	15.2	1.60	58.3	15.6	1.80	658	10.0	7.33	-	577	9.66	1.25	6.14	0.27
	Potter-Doal	-	23200	-	15.0	0.27	-	7420	-	425	-	-	-	-	-	-	-	-	339	1.00	0.50	-	-
Val d'Or	Dunraine	4325	81	29	30.0	1.34	40.6	532	209	-	-	1.38	1.27	0.39	1.78	-	90.3	2.50	-	-	-	0.04	0.13
	East Sullivan	5024	1510	274	76.7	1.27	13.3	5749	72.0	55.0	3.60	8.09	1.41	0.86	4.96	-	1.16	15.6	1137	4.67	5.00	0.65	0.12
	Louvem	3218	2981	83	8.83	0.44	40.8	117	71.0	-	-	9.73	2.24	0.60	1.98	-	3.43	-	-	-	-	0.69	0.19
	Louvicourt	5194	10088	223	27.8	0.67	23.2	615	134	249	12.1	39.6	1.28	1.97	140	-	17.3	10.0	1309	8.26	5.90	0.37	0.09
	Manitou Barvue	223	2995	1458	83.5	0.28	2.88	26.5	-	-	-	18.5	0.28	27.6	96.8	-	1.40	58.0	-	-	-	1.72	0.42
DBL	Bousquet #2	3944	686	625	33.5	6.02	94.1	38.0	13.5	21.0	50.0	1.20	1.94	1.80	23.4	-	4.10	29.0	1200	35.3	2.00	0.21	2.84
	Dumagami	1368	3334	124	43	3.66	20.1	39.5	16.0	18.7	39.4	1.00	0.23	0.35	4.40	-	1.30	-	238	25.9	2.00	0.14	0.24

Table 5.4 cont.

Camp	Deposit	Cu	Zn	Pb	Ag	Au	Bi	Co	Ni	Se	Te	Cd	In	Ga	Sn	W	Mo	V	As	Sb	Hg	Tl	U
Noranda Main	Amulet A	1218	16554	1666	123	4.39	31.5	592	36.0	180	1.45	61.8	1.50	2.75	1044	-	0.53	-	78.2	7.03	2.00	1.16	0.04
	Amulet-C	2200	4335	830	39.8	0.12	3.50	48.8	18.0	38.0	2.10	7.50	0.70	8.00	83.0	-	7.47	-	111	21.5	-	0.26	0.09
	Ansil	913	8350	100	11.1	3.55	88.0	524	82.0	166	174	24.6	1.91	4.06	9.70	-	4.58	8.00	1513	4.71	2.67	1.76	0.26
	Corbet	7400	18867	1850	73.3	2.33	105	441	64.5	35.0	-	27.0	3.85	1.55	277	-	1.35	-	450	90.7	0.50	1.45	0.07
	East Waite	630	6420	49	45.8	0.88	20.6	3425	593	118	10.5	16.5	2.45	2.85	177	-	6.85	13.0	6.10	-	0.50	0.03	0.15
	Millenbach	77	382	190	8.25	0.03	2.50	40.0	-	27.0	3.30	1.00	-	4.70	2.90	-	1.10	9.00	6.10	3.00	-	0.07	0.10
	Moosehead	37.0	99.0	80.5	82.3	0.04	-	8.25	-	55.0	-	-	-	0.15	12.0	-	1.25	-	309	2.80	-	0.33	-
	Norbec	5087	2838	538	61.3	-	50.3	1560	13.7	-	-	7.60	5.70	4.83	87.0	-	2.90	-	-	17.7	-	2.07	-
	Lac Dufault	2175	2088	712	59.4	0.51	47.2	1438	-	45.8	2.23	6.00	0.78	0.90	12.5	3.00	0.45	-	339	42.9	4.50	1.97	0.10
	Old Waite	1915	3186	70	68.0	0.66	29.8	2946	210	192	3.30	7.60	4.34	1.68	109	-	1.80	-	129	1.75	12.0	0.33	0.30
	Quemont	2973	3065	238	208	12.60	21.4	582	230	259	221	9.63	1.65	1.45	202	-	1.40	-	387	2.92	3.71	0.05	0.17
	Vauze	5096	15033	366	130	2.39	109	1302	46.1	371	1.30	42.8	20.8	12.5	157	0.50	5.38	-	74.1	0.63	4.00	0.25	0.13
Noranda N-S-E-W	Aldermac	436	6126	124	16.9	0.28	29.93	359	-	47.3	18.2	19.7	0.87	7.00	100	10.0	10.5	-	90.5	1.62	2.00	0.49	0.11
	Delbridge	366	23660	9047	415	69.90	0.90	9.00	-	-	-	15.0	-	0.90	1.10	-	0.10	-	2540	159	-	27.0	-
	Deldona	184	15000	5995	96.0	2.77	-	11.0	-	4.00	0.10	18.0	-	1.30	3.40	4.00	-	-	186	18.0	0.50	24.0	-
	Gallen	2145	4011	1520	83.6	1.27	6.26	27.6	9.5	24.1	3.15	12.7	2.14	0.40	49.3	-	0.41	-	136	5.46	2.00	3.87	0.10
	Horne #5	1488	2626	397	23.7	5.92	1.44	243	43.0	96.4	23.5	4.17	2.84	2.97	174	-	1.84	-	167	3.39	8.25	1.24	0.10
	Horne	1940	14581	83	26.8	2.26	240	122	48.0	208	59.9	55.8	12.6	1.82	248	-	1.35	-	133	2.82	7.33	0.06	0.05
	Mobrun	1943	10115	447	30.1	1.63	36.3	386	189	316	8.20	45.9	8.14	4.77	584	-	1.61	-	1115	11.7	5.75	3.56	0.08
	New Insco	10150	597	123	36.9	0.48	50.8	809	45.5	299	12.8	5.23	3.25	5.00	9.05	8.00	1.25	23.5	19.45	1.62	2.17	0.22	0.06
	Robb Montbray	8533	7370	300	113	47.75	5.11	1748	359	2442	119	2.63	11.3	1.53	12.9	-	0.70	-	1393	7.40	57.0	0.27	0.07
Benny	Geneva Lake	260	11895	18000	343	8.19	3.60	203	40.0	-	-	22.0	-	0.50	-	-	2.00	-	224	222	2.00	2.40	0.12
	Stralak	56	2085	2400	371	0.52	15.0	333	24.0	43.5	-	8.40	0.24	0.30	3.50	-	65.3	-	475	11.9	2.50	0.42	0.08
Manitouwadge	Geco	801	5761	1423	10.4	0.31	42.3	154	13.0	99.7	0.60	35.4	1.17	0.70	5646	30.0	0.73	-	98.6	11.9	-	0.57	0.12
	Willecho	1065	2683	3052	41.8	0.20	15.4	322	18.0	81.0	0.10	12.4	0.24	0.75	70.1	21.0	10.3	14.5	54.1	6.85	-	2.10	0.34

Table 5.4 cont.

Camp	Deposit	Cu	Zn	Pb	Ag	Au	Bi	Co	Ni	Se	Te	Cd	In	Ga	Sn	W	Mo	V	As	Sb	Hg	Tl	U
Sturgeon Lake	Lyon Lake	190	39072	350	129	1.44	0.90	112	5.00	36.5	-	15.0	-	0.70	9.30	-	0.40	-	2084	593	8.00	1.40	-
	Mattabi	997	1566	121	170	1.62	87.3	336	25.0	119	0.30	1.40	0.84	2.26	9.28	-	0.88	-	691	210	14.0	1.61	0.53
	Sturgeon Lake	-	32325	-	110	0.22	-	110	-	52.0	-	-	-	-	-	6.00	-	-	1379	124	3.63	-	-
Uchi	South Bay	8400	840	980	35.0	-	41.0	98.0	-	-	-	4.20	3.50	0.70	30.0	-	0.40	-	-	-	-	0.26	0.06
Hackett River	East Cleaver	2103	4625	2314	52.1	0.28	17.4	138	17.3	-	-	26.8	1.27	1.37	296	-	0.60	-	-	-	-	3.05	0.04
	Hackett River	102	3080	2511	19.0	0.09	1.80	121	22.7	36.7	0.50	10.8	0.08	0.66	3.81	-	9.75	-	-	-	-	0.55	0.25
	Yava	289	195	103	6.26	0.16	2.89	255	296	-	1.77	0.76	0.08	1.63	2.50	-	3.14	10.0	-	-	-	0.74	0.41
High Lake	High Lake	1567	4800	1687	92.7	1.76	230	473	-	-	-	15.2	0.34	0.63	3.80	-	7.97	-	-	-	-	0.92	0.10
Hood River	Gondor	13000	8259	4800	135	0.81	140	203	14.0	34.3	-	20.0	0.43	0.50	8.60	-	3.35	-	131	39.6	-	0.79	-
	Hood #10	960	10000	13000	26.0	-	35.0	470	26.0	-	0.50	29.0	0.18	0.80	9.60	-	0.90	-	-	-	-	0.83	0.15
Flin Flon	Callinan	6663	7771	963	539	-	2.63	2123	17.8	-	120	24.3	0.91	0.60	4.45	-	31.7	-	-	243	-	2.70	0.30
	Centennial	13100	13200	2062	39.0	-	103	65.0	-	-	0.70	46.0	1.20	3.00	13.0	-	13.0	-	-	730	-	4.30	0.46
	Coronation	6690	257	93	10.9	-	8.03	4593	244	-	9.60	0.77	0.81	0.20	4.03	-	5.60	-	-	3.17	-	0.31	0.07
	Flexar	11000	1600	100	4.80	2.37	2.50	550	-	-	-	4.80	2.60	0.80	2.10	-	15.0	-	-	-	-	0.07	0.10
	Flin Flon	6212	3663	299	98.2	1.75	11.7	640	21.8	-	106	12.4	5.38	0.48	3.60	-	7.60	-	-	10.1	-	0.54	0.91
	Northstar	7665	600	65	14.3	-	43.3	754	30.5	-	14.3	2.14	1.85	0.80	20.5	-	2.42	-	-	16.3	-	0.36	0.48
	Pinebay	7365	233	185	46.5	-	67.8	789	12.0	-	236	0.50	0.89	0.35	7.23	-	2.43	-	-	7.30	-	0.10	0.82
	Mandy	3150	16100	781	18.0	-	8.20	222	22.0	-	0.50	34.0	0.21	1.10	3.80	-	3.70	-	-	97.0	-	19.0	0.14
	Schist Lake	889	14180	4154	39.5	-	4.20	680	23.0	-	8.90	49.0	0.58	1.75	4.45	-	14.3	-	-	80.0	-	7.50	0.43
Snow Lake	Anderson Lake	4615	323	84	12.5	0.59	19.2	1507	12.0	246	38.0	1.05	0.72	0.63	3.07	-	5.98	-	1135	5.21	3.00	0.19	0.25
	Chisel Lake	752	2980	669	6.94	-	0.43	192	18.6	-	1.24	6.53	0.07	0.26	120	-	5.79	-	-	16.4	-	0.16	0.50
	Osborne Lake	1121	63	27	9.10	-	17.5	6045	-	-	17.7	0.30	0.20	0.23	1.70	-	5.70	-	-	4.15	-	0.03	0.04
	Photo Lake	689	8864	97	5.40	0.52	1.03	406	10.0	23.0	-	16.9	0.96	0.80	4.35	-	0.80	-	1430	15.1	0.50	1.02	0.03
	Rod	2433	8487	198	22.8	0.46	10.6	1628	399	72.0	1.51	3.31	1.32	2.27	10.1	-	6.71	42.3	4673	52.2	11.0	0.34	2.08
	Stall Lake	5400	250	60	5.11	0.07	6.60	140	12.0	-	-	1.50	0.99	0.40	1.60	-	1.90	-	-	-	-	-	0.01

Table 5.4 cont.

Camp	Deposit	Cu	Zn	Pb	Ag	Au	Bi	Co	Ni	Se	Te	Cd	In	Ga	Sn	W	Mo	V	As	Sb	Hg	Tl	U
Lynn Lake	Fox Lake	9233	389	45	27.7	0.13	0.70	686	-	208	4.60	1.27	0.21	0.40	7.20	-	5.23	-	791	3.90	0.50	0.09	0.49
Rusty Lake	Ruttan	1093	1557	106	4.70	-	3.63	286	-	-	1.70	3.47	0.35	0.67	3.70	-	0.97	-	-	0.80	-	0.26	0.19
Sherridon	Sherridon	8100	4870	210	4.65	0.14	1.90	510	-	-	-	14.6	1.86	1.60	12.2	-	10.4	2.50	-	-	-	0.11	0.18
Labrador Trough	Koke	375	14433	5300	38.0	0.30	4.85	114	-	44.0	1.35	28.5	0.25	2.30	6.95	-	1.90	-	1180	60.9	12.0	1.40	0.33
Bathurst	Austin Brook	152	1195	2100	5.65	0.06	2.85	19.0	90.0	-	-	1.65	1.13	22.7	53.5	-	16.2	66.0	-	-	-	1.14	0.62
	Brunswick #12	11500	2800	3400	540	-	690	420	42.0	-	-	9.20	2.40	6.25	25.0	-	1.90	-	-	-	-	19.0	0.31
	Heath Steele	5160	8100	3035	29.0	1.04	241	1300	-	-	-	19.5	20.5	4.30	1865	-	4.45	-	-	-	-	9.65	0.67
	Key Anacon	230	950	2000	5.00	0.56	0.30	10.0	-	-	-	3.00	2.00	9.40	11.0	-	12.0	14.0	-	-	-	22.0	6.10
Eastern Townships	Trinity	200	14740	1200	28.0	0.16	6.20	93.8	169	96.5	3.50	2.50	-	0.40	2.70	-	0.80	-	98.8	2.15	2.00	0.99	0.44
	Weedon	3200	7550	400	6.25	0.01	8.70	401	-	-	17.0	32.7	2.10	0.70	1.20	-	16.9	-	-	-	-	0.18	2.30
Finlayson Lake	Kudz ze Kayah	-	8900	-	62.0	4.56	-	3.50	-	135	-	-	-	-	-	3.00	9.00	-	1032	233	3.00	-	-
Hart River	Hart River	5025	596	2100	40.3	0.60	40.2	180	32.3	139	9.00	4.20	0.06	0.90	9.18	-	2.00	9.75	1100	101	-	1.01	0.75
Stewart	Eskay Creek	95	179	147	13.1	0.19	0.40	48.5	145	-	-	1.30	-	1.50	1.90	-	25.0	52.0	-	125	-	14.6	0.35
Vancouver	Brittania	2000	200	300	8.40	-	22.0	110	18.0	-	-	0.90	0.32	1.50	1.60	-	7.90	12.0	-	-	-	0.65	0.30
Vancouver Island	Myra Falls	8983	344	220	12.7	-	17.3	50.00	29.0	-	21.3	1.63	0.59	1.50	4.25	-	10.8	8.50	-	-	-	0.25	0.33

Table 5.5 Average trace element concentrations (ppm) in pyrite samples from VMS deposits in comparison to other deposit types (i.e., magmatic and orogenic Au) in the AGB.

AGB	Cu	Zn	Pb	Ag	Au	Bi	Co	Ni	Se	Te	Cd	In	Ga	Sn	W	Mo	V	As	Sb	Hg	Tl	U
VMS	2887	6139	748	70.7	3.62	50.9	760	110	264	41.6	18.0	3.83	3.23	147	6.18	9.86	23.9	548	24.1	17.2	1.73	0.23
Orogenic Au	1294	-	190	62.4	78.6	19.9	1459	112	17.0	24.9	12.9	0.95	0.68	59.3	13.0	175	12.5	77.4	1.97	-	0.37	1.42
Magmatic vein Cu	6148	4588	380	79.9	18.9	62.1	1967	833	33.2	63.0	2.90	0.61	0.53	5.18	420	71.0	6.00	836	44.1	3.50	0.13	0.17

Table 5.6 LA-ICP-MS analyses of pyrite (average values in ppm) from different VMS deposits compared to samples from the AGB.

Location	Age	Host Rock	No. of deposits	No. of analyses	Cu	Zn	Pb	Ag	Au	Bi	Co	Ni
Troodos - Skouriotissa	Late Cretaceous	Mafic	1	126	775	280	41.5	2.59	0.50	0.51	294	290
Bathurst	Middle Ordovician	Siliclastic-felsic	4	460	162	622	1561	22.9	0.25	36.5	578	338
Ketchikan	Silurian-Ordovician	Bimodal-felsic	4	4	18.8	26.7	1.17	1.93	-	0.02	55.9	1194
Ketchikan	Upper Proterozoic-Cambrian	Bimodal-mafic	7	9	5.40	9.94	1.24	0.78	-	0.08	826	56.0
AGB	Neoarchean	Bimodal-mafic	3	145	350	338	99.4	11.5	0.53	0.98	63.2	26.4

Location	Se	Te	Cd	In	Ga	Sn	Mo	As	Sb	Hg	Tl
Troodos - Skouriotissa	361	5.64	2.03	-	-	-	10.4	102	3.26	-	-
Bathurst	24.7	2.42	1.75	1.13	0.50	80.1	1.14	1,340	87.9	0.57	17.5
Ketchikan	35.6	1.50	2.01	0.09	-	1.25	2.23	1210	77.7	2.06	70.8
Ketchikan	27.7	2.34	2.58	0.27	-	2.07	0.98	202	0.82	0.385	0.45
AGB	18.0	11.4	1.02	0.16	0.19	2.41	0.14	116	3.11	0.34	0.37

6. Conclusions

Pyrite is ubiquitous in hydrothermal systems of a range of ore deposit types, and it is host to a wide range of trace elements that are sensitive to ore-forming conditions, including Ag, Au, Bi, Co, Ni, Se, Te, Cd, In, Ga, Sn, Mo, As, Sb, Hg, and Tl (e.g., Large et al., 2009; Maslennikov et al., 2009; Deditius et al., 2011; Reich et al., 2013; Genna and Gaboury et al., 2015; Grant et al., 2018). We have examined the trace element geochemistry of pyrite samples from more than 90 VMS deposits in different settings, of different sizes, and with different mineral endowment. The aim was to better understand how trace element geochemistry of sulfides in VMS ores can reflect important aspects of the mineralizing systems, such as host-rock controls, the sizes of the deposits, and endowment in economically important constituents such as Au. The findings also support previous studies (Large et al., 2009; Maslennikov et al., 2009; Genna and Gaboury et al., 2015; Belousov et al., 2016; Large et al., 2018) that have shown trace element distribution in pyrite is a useful indicator of physical and chemical controls on hydrothermal systems, including temperature and magmatic input.

The concentrations of different trace elements in pyrite are a combination of partitioning into the pyrite crystal structure and inclusions of other minerals in the pyrite (e.g., Monecke et al., 2016). The mineral inclusions reflect the same physical and chemical conditions (e.g., high and low temperatures; source rocks) that influence enrichments and depletions of elements contained in the pyrite structure. Much of the intra-deposit variation can be attributed to zone refining, with different elements partitioning into Cu-rich and Zn-rich ores, mainly as a function of temperature (Hannington, 2014). However, we also observed consistent trace element enrichments and depletions in pyrite concentrates from deposits that formed under different conditions, including large-scale variations between districts.

By examining the same mineral in every deposit, as opposed to bulk ore samples, we were able to constrain the important controls on trace element distribution between deposits and districts. In nearly every case, pyrite from deposits considered to have formed at high temperatures (e.g., with high Cu/Cu+Zn grade ratios) is enriched in a subset of Cu-Bi-Co-Ni-Se-Te-Mo. Pyrite from

lower-temperature Zn-rich ores is consistently enriched in a subset of elements from Pb-Ag-Cd-In-Ga-Sn-As-Sb-Hg-Tl. This was confirmed by PCA and hierarchical clustering of data from more than 260 samples from 55 deposits. The representativity of the samples was demonstrated by the similar Cu/Cu+Zn ratios of the pyrite samples and the bulk Cu/Cu+Zn ratios of the deposits as a whole. Trace element concentrations in individual pyrite samples also closely matched the trace element distribution in much larger bulk samples, such as pyrite tailings and monthly concentrates form the same deposit. We also observed that individual pyrite grains analyzed by LA-ICP-MS show the same trace element enrichments and depletions as the bulk samples.

The immediate hosts rocks of VMS deposits are a first-order control on the trace element enrichments and depletions in pyrite. Pyrite samples from deposits in bimodal volcanic successions in the Superior Province show trace element signatures reflecting both felsic (i.e., Ag, Au, Cd, In, Sn, As, Sb, Hg, Tl) and mafic (i.e., Co, Ni, Se, Mo) sources. The enrichments and depletions in the source rocks have been confirmed by published trace metal analyses of unaltered volcanic rocks. Basalt and komatiite are characterized by high Cu, Co, Ni, and Se, while rhyolite has higher Pb, Ag, Bi, Te, Cd, In, Ga, Sn, Hg, and Tl, which is reflected in the trace element signature of pyrite from VMS deposits with these host rocks. Similar patterns of enrichment and depletion are observed in pyrite samples from younger Proterozoic and Phanerozoic deposits. However, some data suggest larger-scale geodynamic processes are also important. U-Th and Pb enrichment in pyrite samples from VMS in the Slave craton are consistent with a thickened continental crust compared to the more primitive AGB. Similar enrichments and depletions are observed in pyrite from deposits in bimodal-felsic camps (e.g., Sturgeon Lake and Finlayson Lake). Notable enrichment in Te in pyrite from Au-rich deposits in the BRG is interpreted as a mantle signature that likely played a role in the Au endowment of the BRG relative to other assemblages of the Abitibi (Mercier-Langevin et al., 2011b, 2014). However, we found little difference in the primary trace metal contents of the volcanic rocks in different assemblages of the AGB, most likely because the assemblage divisions are based on ages rather than bulk rock composition. The different characteristics of much younger VMS

(e.g., siliciclastic-felsic host successions) are clearly reflected in the trace element signatures of the pyrite samples (e.g., Pb-Ag-In-Sn signature of Bathurst deposits).

We cannot make a direct link between pyrite chemistry as a predictor of deposit size. However, large metal tonnages are often a result of leaching of the footwall rocks in a large, long-lived hydrothermal system, commonly forming lower-temperature Zn-rich deposits that are often enriched in Sn (Hannington et al., 1999c). This is reflected in the pyrite samples from deposits such as Kidd Creek. Notable enrichments of Bi, Se, Te, In, and Sn in pyrite samples from some large Au-rich deposits (e.g., Horne, Quemont, Bousquet #2, and Dumagami) are thought to reflect a felsic magmatic contribution (Mercier-Langevin et al., 2011). Pyrite samples from large Au-poor bimodal-mafic deposits, such as Kidd Creek and Geco are enriched in Sn but lack Bi, Se, and Te. Pyrite samples from large Au-poor siliciclastic-felsic deposits, such as Brunswick #12 and Heath Steele, are enriched in Sn, Bi, and In, which suggests contributions from both large-scale hydrothermal convection and magmatic input.

Similar trace element behaviour is observed in pyrite samples from other deposit types, including magmatic Cu vein deposits and orogenic Au deposits suggesting that the trace element signatures of pyrite mineral separates may be more generally applicable as indicators of ore-forming conditions. Used in conjunction with other data (e.g., isotopic tracers: Franklin and Thorpe, 1983; Sharman et al., 2015; Laflamme et al., 2016) pyrite geochemistry can be an important tool in exploration. Vast amounts of trace element data on pyrite are becoming available from in-situ measurements by LA-ICP-MS, and the present study provides a first-order assessment of how that data might be interpreted for many different deposit types.

References

Aitchison, J., 1982, The statistical analysis of compositional data: Journal of the Royal Statistical Society: Series B (Methodological), v. 44, p. 139–160.
Aitchison, J., 1984, The statistical analysis of geochemical compositions. Journal of the International Association for Mathematical Geology, v. 16(6), p. 531–564.

Aggarwal, P.K., and Longstaffe, F.J., 1987, Oxygen-isotope geochemistry of metamorphosed, massive sulfide deposits of the Flin Flon–Snow Lake Belt, Manitoba: Contributions to Mineralogy and Petrology, v. 96, p. 314–325.

Ames, D.E., 1996, Stratigraphic and tectonic setting of the Paleoproterozoic Ruttan Cu-Zn VHMS deposit, Rusty Lake belt, Trans-Hudson Orogen: Bulletin-Geological Survey of Canada, p. 15–44.

Arevalo, R., and McDonough, W.F., 2010, Chemical variations and regional diversity observed in MORB: Chemical Geology, v. 271(1-2). p. 70–85.

Auclair, G., Fouquet, Y., and Bohn, M., 1987, Distribution of selenium in high-temperature hydrothermal sulfide deposits at 13 degrees North, East Pacific Rise: The Canadian Mineralogist, v. 25(4), p. 577–587.

Autran, A., Picot, P., and Troly, G., 1966, Étude d'une série d'échantillons de la mine orne (district de Noranda, Québec, Canada): Bureau de Recherches Géologiques et Minières—Ministère de l'Énergie et des Ressources Naturelles, GM 62415, 21 p.

Avramtechev, L., 1985, Carte géologique du Québec: Québec Ministere de I'Énergie et Des Ressources, Scale 1:500,000.

Ayalew, D. and Ishiwatari, A., 2011, Comparison of rhyolites from continental rift, continental arc and oceanic island arc: Implication for the mechanism of silicic magma generation. Island arc, v. 20(1), p. 78–93.

Ayer, J., Amelin, Y., Corfu, F., Kamo, S., Ketchum, J., Kwok, K., and Trowell, N., 2002, Evolution of the southern Abitibi greenstone belt based on U–Pb geochronology: autochthonous volcanic construction followed by plutonism, regional deformation and sedimentation: Precambrian Research, v. 115, p. 63–95.

Ayer, J., Thurston, P., Bateman, R., Dube, B., Gibson, H., Hamilton, M., Hathway, B., Hocker, S.M., Houlé, M., Hudak, G., Ispolatov, V., Lafrance, B., Lesher, M., MacDonald, P.J., Peloquin, A., Piercey, S., Reed, L.E., and Thompson, P.H, 2005, Overview of results from the greenstone

architecture project: discover Abitibi initiative: Ontario Geological Survey Open File Report, 146 p.

Bailes, A.H., Galley, A.G., Skirrow, R.G., and Young, J., 1996, Geology of the Chisel volcanic-hosted massive sulphide area, Snow Lake, Manitoba (part of 63K/16SE): Manitoba Energy and Mines, OF 95-4, Color map and marginal notes, scale 1:5,000, 1 sheet.

Bailes, A.H. and Galley, A.H., 1999, Evolution of the Paleoproterozoic Snow Lake arc assemblage and geodynamic setting for associated volcanic-hosted massive sulphide deposits, Flin Flon Belt, Manitoba, Canada: Canadian Journal of Earth Sciences, v. 36, p. 1789–1805.

Bailes, A.H., Galley, A.G., Paradis, S., and Taylor, B.E., 2016, Variations in Large Synvolcanic Alteration Zones at Snow Lake, Manitoba, Canada, with Proximity to Associated Volcanogenic Massive Sulfide Deposits: Economic Geology, v. 111(4), p. 933–962.

Baldwin, D.A., 1988, Geology of the southern part of the Rusty Lake volcanic belt; Manitoba Energy and Mines, Geological Services. Geological Report 86-1:90.

Barnes, H., and Seward, T., 1997, Geothermal systems and mercury deposits: in. Barnes H.L., ed., Geochemistry of Hydrothermal Ore Deposits, 3rd edn., p. 699–736. New York: Wiley.

Bartholomew, D.J., 2010, Principal Components Analysis: in, Peterson, P., Baker, E., and McGaw, B., ed., International Encyclopedia of Education, 3rd edn., p. 374–377. Elsevier.

Bartsch, R.D., 1993, A rhyolite flow in the upper Hazelton Group, Eskay Creek area (104B/9, 10): British Columbia Ministry of Energy, Mines and Petroleum Resources Paper 1993-1, p. 331–334.

Barrie, C.T., Ludden, J.N., and Green, T.H., 1993, Geochemistry of volcanic rocks associated with Cu-Zn and Ni-Cu deposits in the Abitibi subprovince: Economic Geology, v. 88, p. 1341–1358.

Barrie, C.T., and Hannington, M.D., 1999, Classification of volcanic-associated massive sulfide deposits based on host-rock composition: Reviews in Economic Geology, v. 8, p. 1–11.

Barrie, C.T., and Pattison, J., 1999, Fe-Ti basalts, high silica rhyolites, and the role of magmatic heat in the genesis of the Kam-Kotia volcanic-associated massive sulfide deposit, Western Abitibi Subprovince, Canada: Economic Geology Monograph 10, p. 577–599.

Barrie, C.T., Cathles, L.M., Erendi, A., Schwaiger, H., and Murray, C., 1999, Heat and Fluid Flow in Volcanic-Associated Massive Sulfide-Forming Hydrothermal Systems: Reviews in Economic Geology, v. 8, p. 201–219.

Barrie, C.T., Cousens, B.L., Hannington, M.D., Bleeker, W., Gibson, H.L., 1999. Lead and neodymium isotope systematics of the Kidd Creek Mine stratigraphic sequence and ore, Abitibi Subprovince Canada: Economic Geology Monograph 10, p. 485–510.

Barrie, C. Tucker., Taylor, C., and Ames, D.E., 2005, Geology and Metal Contents of the Ruttan volcanogenic massive sulfide deposit, northern Manitoba, Canada: Mineralium Deposita, v. 39(8), p. 795–812.

Bartholomew, D.J., 2010, Principal Components Analysis: in. Peterson et al., ed., International Encyclopedia of Education, 3rd edn., p 374-377. Elsevier Science.

Bateman, R., Ayer, J., and Dube, B., 2008, The Timmins-Porcupine Gold Camp, Ontario: Anatomy of an Archean Greenstone Belt and Ontogeny of Gold Mineralization: Economic Geology, v. 103, p.1285–1308.

Beaudoin, A., Perrault, G., and Bouchard, M., 1987, Distribution of gold, arsenic, antimony, and tungsten around the Dest-Or orebody, Noranda district, Abitibi, Quebec: Journal of Geochemical Exploration, v. 28, p. 41–70.

Beaumont-Smith, C.J. and B.C.O., 2003, Tectonic evolution and gold metallogeny of the Lynn Lake greenstone belt, Manitoba (NTS 64C10, 11, 12, 14, 15 and 16): in. Report of Activities 2003, Manitoba Industry, Trade and Mines, Manitoba Geological Survey, p. 39–49.

Berger, B.R., 2011, The Kidd-Munro episode—Volcanism and mineralization between 2720 and 2710 Ma: Ontario Geological Survey Open File Report 6258, 66 p.

Berkenbosch, H.A., de Ronde, C.E.J., Gemmell, J.B., McNeill, A.W., and Goemann, K., 2012, Mineralogy and Formation of Black Smoker Chimneys from Brothers Submarine Volcano, Kermadec Arc. Economic Geology, v. 107(8), p. 1613–1633.

Bertrand, C., and Hutchinson, R.W., 1973, Metamorphism at the Normetal mine, northwestern Quebec: Canadian Institute of Mining and Metallurgical Bulletin, v. 66(740), p. 68–76.

Bérubé, J.P., 2013, NI 43-101 Resources Evaluation For The Vendome Property: Abcourt Mines Inc, 81 p.

Bérubé, J.P., 2014, NI 43-101 Mineral Resources Report For The Abcourt-Barvue Property: Abcourt Mines Inc, 167 p.

Blackburn C.E., Johns, G.W., Ayer, J., and Davis, D.W., 1991, Wabigoon Subprovince: in. Thurston, Williams H.R, Sutcliffe R.H., Stott G. M., ed., Geology of Ontario, Ontario Geological Survey, p. 303–381.

Bleeker, W., 1999, Structure, stratigraphy, and primary setting of the Kidd Creek volcanogenic massive sulfide deposit—A semiquantitative reconstruction: Economic Geology Monograph 10, p. 71–122

Bleeker, W., and Hall, B., 2007, The Slave Craton: geological and metallogenic evolution: in. Mineral deposits of Canada: in. Goodfellow, W.D., ed., a synthesis of major deposit-types, district metallogeny, the evolution of geological provinces, and exploration methods, Geological Association of Canada, Mineral Deposits Division, Special Publication 5, p. 849–879.

Boulerice, A.R., Ross, P.S., and Mercier-Langevin., 2015, Geological and geochemical characteristics of the Waconichi Formation east of the Lemoine auriferous volcanogenic massive sulphide deposit, Abitibi greenstone belt, Quebec: in. Peter, J.M., and Mercier-Langevin, P., ed., Targeted Geoscience Initiative 4: Contributions to the Understanding of Volcanogenic Massive Sulphide Deposit Genesis and Exploration Methods Development, Open File 7853, p. 171–182.

Britton, J.M., Blackwell, J.D., and Schroeter, T.G., 1990, #21 zone deposits, Eskay Creek, northwestern British Columbia: British Columbia Ministry of Energy, Mines and Petroleum Resources. Mines and Petroleum Resources Exploration in British Columbia, p. 197–223.

Burnham, C.W., and Ohmoto, H., 1980, Late-stage processes of felsic magmatism: Mining Geology, Special Issue 8, p. 1–11.

Cabri, L.J., 1965, Phase relations in the Au-Ag-Te system and their mineralogical significance: Economic Geology, v. 60, p. 1569–1606.

Cadima, J., and Jolliffe, I.T., 1995. Loading and correlations in the interpretation of principle components: Journal of Applied Statistics, v. 22(2), p. 203–214.

Campbell, F.A., and Williams, K.L., 1968, Composition of sphalerite from Quemont mine, Quebec: Economic Geology, v. 63, p. 824–831.

Candela, P. A., and Holland, H. D., 1984, The partitioning of copper and molybdenum between silicate melts and aqueous fluids: Geochimica et Cosmochimica Acta, v. 48(2), p. 373–380.

Candela, P.A., and Piccoli, P.M., 2005, Magmatic Processes in the Development of Porphyry-Type Ore Systems: Economic Geology 100th Anniversary Volume, p. 25–38.

Carr, P.M., Cathles, L.M., and Barrie, C.T., 2008, On the size and spacing of volcanogenic massive sulfide deposits within a district with application to the Matagami district, Quebec: Economic Geology, v. 103, p. 1395–1409.

Cattalani, S., Barrett, T.J., MacLean, W.H., Hoy, L., Hubert, C., and Fox, J.S., 1993, Métallogenèse des gisements Horne et Quemont (région de Rouyn-Noranda): Ministère de l'Énergie et des Ressources du Québec, ET 90-07, 121 p.

Card, K.D., and Innes, D.G., 1981, Geology of the Benny Area District of Sudbury: Ontario Geological Survey, Report 206, 117 p.

Cave, B.J., Stepanov, A.S., Craw, D., Large, R.R., Halpin, J.A. and Thompson, J., 2015, Release of Trace Elements Through the Sub-Greenschist Facies Breakdown of Detrital Rutile to Metamorphic Titanite in the Otago Schist, New Zealand : The Canadian Mineralogist, v. 53(3), p. 379–400.

Chartrand, F., 1991, Geological setting of volcanogenic massive sulfide deposits in the central pyroclastic belt, Val D'O: in. Chartrand, F., ed., Geology and gold, rare element, and base metal mineralization of the Val D'Or area, Quebec, Society of Economic Geologists Guidebook Series v. 9, p. 75–89.

Chutas, N.I., Kress, V.C., Ghiorso, M.S., Sack, R.O., 2008. A solution model for high temperature PbS–AgSbS2–AgBiS2 galena. Am. Mineral. V. 93, p.1630–1640.

Clark, T., and Wares, R., 2004, Synthese lithotectonique et Metallogenique de l'Orogene du Nouveau-Quebec (Fosse du Labrador): Ressources Naturelles Faune et Parcs, Gouvernement Du Quebec.

Coleman, L.C., Froese, E., Hutcheon, I.E., Price, D.P., Sangster, D.F., and Stauffer, M.R., 1973, Geology and Ores of the Hanson Lake, Flin Flon and Snow Lake Areas of Saskatchewan and Manitoba: in. Simpson, F., ed., Part II: Geological Road Logs for Saskatchewan and Adjacent Areas, An Excursion Guide to the Geology of Saskatchewan, Saskatchewan Geological Society Special Publication No.1, p. 418–455.

Comrey, A.L., and Lee H.B., 1992, A first course in factor analysis: Taylor and Francis, London.

Conn, C.D., Spry, P.G., Layton-Matthews, D., Voinot, A., and Koenig, A., 2019, The effects of amphibolite facies metamorphism on the trace element composition of pyrite and pyrrhotite in the Cambrian Nairne Pyrite Member, Kanmantoo Group, South Australia: Ore Geology Reviews, v. 114, p. 103–128.

Constable, D.W., 1989, Preliminary Exploration Report On The Geneva Lake Polymetallic Deposit Hess Township, Sudbury Mining Division Ontario: For Geneva Lake Minerals Corporation.

Cook, N.J., 1996, Mineralogy of the sulphide deposits at Sulitjelma, northern Norway: Ore Geology Reviews, v. 11(5), p. 303–338.

Cook, N.J., Ciobanu, C.L., Pring, A., Skinner, W., Shimizu, M., Danyushevsky, L., Saini-Eidukat, B., and Melcher, F., 2009, Trace and minor elements in sphalerite: A LA-ICPMS study: Geochimica et Cosmochimica Acta, v. 73(16), p. 4761–4791.

Cook, N.J., Ciobanu, C.L., and Williams, T., 2011, The mineralogy and mineral chemistry of indium in sulphide deposits and implications for mineral processing. Hydrometallurgy, v. 108(3–4), p. 226–228.

Corcoran, P. L., and Dostal, J., 2001, Development of an Ancient Back-Arc Basin Overlying Continental Crust: The Archean Peltier Formation, Northwest Territories, Canada. The Journal of Geology, v. 109(3), p. 329–348.

Corfu, F., 1993. The evolution of the southern Abitibi greenstone belt in light of precise U-Pb geochronology: Economic Geology, v. 88(6), p.1323–1340.

Corfu, F., and Scott, G.M., 1993, Age and petrogenesis of two late Archean magmatic suites. northwestern Superior Province, Canada, inferred from Zircon U-Pb and Lu-Hf isotopic systematics: Journal of Petrology, v. 34, p. 817–838.

Corrigon, D., Galley, A.G., Pehrsson, S., 2007, Mineral deposits of Canada: a synthesis of major deposit-types, district metallogeny, the evolution of geological provinces, and exploration methods: in. Goodfellow, W.D., ed., Geological Association of Canada, Mineral Deposits Division, Special Publication no. 5, p. 881–902.

Corrigan, D., Pehrsson, S., Wodicka, N., and de Kemp, E., 2009, The Palaeoproterozoic Trans-Hudson orogen; a prototype of modern accretionary processes: Geological Society Special Publications, v. 327, p. 457–479.

Craig, J.R., Vokes, F.M., and Solberg, T.N., 1998, Pyrite: physical and chemical textures: Mineralium Deposita, v. 34(1), p. 82–101.

Crow, E.L., and Shimizu K., 1988, Lognormal Distributions: Theory and Applications, New York: Marcel Dekker, Inc.

David, J., Parent, M., Stevenson, R., Nadeau, P., and Godin, L., 2003, The Porpoise Cove supracrustal sequence, Inukjuak area: A unique example of Paleoarchean crust (ca. 3.8 Ga) in the Superior Province: Geological Association of Canada, Program with Abstracts.

Davis, W., and Bleeker, W., 1999, Timing of plutonism, deformation, and metamorphism in the Yellowknife Domain, Slave Province, Canada: Canadian Journal of Earth Sciences, v. 36, p. 1169–1187.

Davis, J. C., 2002, Statistics and data Analysis in Geology, 3rd ed., Wiley & Sons Ltd, 656 p.

Debriel, J.A., Ross, P.S., and Mercier-Langevin, P., 2018, The Matagami District, Abitibi Greenstone Belt, Canada: Volcanic Controls on Archean Volcanogenic Massive Sulfide Deposits Associated with Voluminous Felsic Volcanism: Economic Geology, v. 113(4), p. 891–910.

de Ronde, C.E.J., Hannington, M.D., Stoffers, P., Wright, I.C., Ditchburn, R.G., Reyes, A.G., Baker, E T., Massoth, G.J., Lupton, J.E., Walker, S.L., Greene, R.R., Soong, C.W.R., Ishibashi, J., Lebon, G.T., Bray, C.J., and Resing, J. A., 2005, Evolution of a Submarine Magmatic-Hydrothermal System: Brothers Volcano, Southern Kermadec Arc, New Zealand: Economic Geology, v. 100(6), p. 1097–1133.

Deditius, A.P., Utsunomiya, S., Reich, M., Kesler, S.E., Ewing, R.C., Hough, R., and Walshe, J., 2011, Trace metal nanoparticles in pyrite: Ore Geology Reviews, v. 42(1), p. 32–46.

Dekov, V.M., and Savelli, C., 2004, Hydrothermal activity in the SE Tyrrhenian Sea: An overview of 30 years of research: Marine Geology, v. 204, p. 161–185.

Dempster, A P., Laird, N.M., and Rubin, D.B., 1977, Maximum Likelihood from Incomplete Data Via the EM Algorithm: Journal of the Royal Statistical Society: Series B, v, 39(1), p. 1–22.

DeWolfe, Y.M., 2009, Stratigraphy and structural geology of the hangingwall to the hostrocks of the Schist Lake and Mandy volcanogenic massive sulphide deposits, Flin Flon, Manitoba (part of NTS 63K12): in. Report of Activities 2009, Manitoba Science, Innovation, Energy and Mines, Manitoba Geological Survey, p. 22–36.

Divi, S.R., Thorpe, R.I., and Franklin, J.M., 1979, Application of discriminant analysis to evaluate compositional controls of stratiform massive sulfide deposits in Canada: Journal of the International Association for Mathematical Geology, v. 11, p. 391–406.

Doucet, P., Mueller, W., and Chartrand, F., 1994, Archean, deep-marine, volcanic eruptive products associated with the Coniagas massive sulfide deposit, Quebec, Canada: Canadian Journal of Earth Science, v. 31, p. 1569–1584.

Doucet, P., Mueller, W., and Chartrand, F., 1998, Alteration and ore mineral characteristics of the Archean Coniagas massive sulfide deposit, Abitibi belt, Quebec: Canadian Journal of Earth Sciences, v. 35(6), p. 620–636.

Drouin, M., 1978, Results of Rock Geochemical Orientation Surveys in the Amos-Barraute Area N.T.S. 32C, D.

Dubé, B., Gosselin, P., Mercier-Langevin, P., Hannington, M.D., and Galley, A., 2007, Gold rich volcanogenic massive sulphide deposits: in. Goodfellow, W.D., ed., Mineral Deposits of Canada: A Synthesis of Major Deposit Types, District Metallogeny, the Evolution of Geological Provinces, and Exploration Methods, Geological Association of Canada, Mineral Deposits Division, v. 5, p. 75–94,

Dubé, B., Mercier-Langevin, P., Kjarsgaard, I., Hannington, M., Becu, V., Cote, J., Moorhead, J., Legault, M., and Bedard, N., 2014, The Bousquet 2-Dumagami World-Class Archean Au-Rich Volcanogenic Massive Sulfide Deposit, Abitibi, Quebec: Metamorphosed Submarine Advanced Argillic Alteration Footprint and Genesis: Economic Geology, v. 109(1), p. 121–166.

Dubé, B., and Mercier-Langevin, P., 2020, Gold Deposits of the Archean Abitibi Greenstone Belt, Canada: in. Sillitoe, R.H., Goldfarb, R.J., Robert, F., and Simmons, S.F., ed., Geology of the World's Major Gold Deposits and Provinces, 23rd edn., p. 669–708. SEG Special Publications.

Dong, Y. and Peng, C.Y.J., 2013. Principled missing data methods for researchers: Springer Plus, v. 2(1), p. 1–17.

Fassbender, M.L., Hannington, M., Baxter, A.T., Diekrup, D., Stewart, M., and Brandl, P.A, 2023, Geochemical signatures of mafic volcanic rocks in modern oceanic settings and implications for Archean mafic magmatism: Economic Geology, in review.

Fietzke, J., Liebetrau, V., Gunther, D., Gürs, K., Hametner, K., Zumholtz, K., Hansteen, T.H., Eisenhauer, A., 2008, An alternative data acquisition and evaluation strategy for improved isotope ratio precision using LA-MC-ICP-MS applied to stable and radiogenic strontium isotopes in carbonates: Journal of Analytical Atomic Spectrometry, v. 23, p. 955–961.

Fietzke, J., Frische, M., 2016, Experimental evaluation of elemental behavior during LAICP-MS: influences of plasma conditions and limits of plasma robustness: Journal of Analytical Atomic Spectrometry, v. 31, p. 234–244.

Ferguson, S.A., Buffam, B.S.W., Carter, O.F., Griffis, A.T., Holmes, T.C., Hurst, M.E., Jones, W.A., Lane, H.C., and Longley, C.S., 1968, Geology and ore deposits of Tisdale Township, District of Cochrane: Ontario Department of Mines Geological Report 58, 177 p.

Franklin, J.M., Kasarda, J., and Poulsen, K.H, 1975, Petrology and chemistry of the alteration zone of the Mattabi massive sulfide deposit: Economic Geology, v. 70(1), p. 63–79.

Franklin, J.M., Lydon, J.W., and Sangster, D.F., 1981, Volcanic-Associated Massive Sulfide Deposits: in. Skinner, B.J., ed., Economic Geology 75th Anniversary Volume, Society of Economic Geologists, p. 485–627.

Franklin, J.M., Gibson, H.L., Jonasson, I.R., and Galley, A.G., 2005, Volcanogenic massive sulfide deposits: Economic Geology 100th Anniversary Volume, Society of Economic Geologists, p. 523–560.

Franklin, J.M., Gibson, H.L., Jonasson, I.R., Galley, A.G., 2015, World volcanogenic massive sulphide (VMS) deposit database; Geological Survey of Canada, Open File 7776.

Frith, R. A., and Roscoe, S.M., 1980, Tectonic setting and sulphide deposits of the Hackett River belt, Slave Province: Canadian Institute of Mining and Metallurgical Bulletin, v. 73(815), p. 143–153

Frith, R.A., 1987, Precambrian geology of the Hackett River area, District of Mackenzie, N.W.T.: Geological Survey of Canada, Memoir 417, 61 p

Froese, E. and Goetz, P.A. 1981, Geology of the Sherridon Group in the vicinity of Sherridon, Manitoba: Geological Survey of Canada, Paper 80-21, 20 p.

Fuchs, S., Hannington, M.D., and Petersen, S., 2019, Divining gold in seafloor polymetallic massive sulfide systems: Mineralium Deposita, v. 54(6), p. 789–820.

Gabrielse, H., and Yorath, C.J., 1991, Tectonic Synthesis: in. Geology of the Cordilleran Orogen in Canada: Geological Survey of Canada, Geology of Canada Series no. 4, 844 p.

Gaboury, D., 2006, Geochemical approaches in the discrimination of synvolcanic intrusions as a guide for volcanogenic base metal exploration: Example from the Abitibi belt, Canada: Applied Earth Science, v. 115, p. 71–79.

Gaboury, D., and Pearson, V., 2008, Rhyolite Geochemical Signatures and Association with Volcanogenic Massive Sulfide Deposits: Examples from the Abitibi Belt, Canada: Economic Geology, v. 103(7), p. 1531–1562.

Galley, A.G., 1993, Characteristics of semi-conformable alteration zones associated with volcanogenic massive sulphide districts: Journal of Geochemical Exploration, v.48(2), p. 175–200.

Galley, A.G., Hannington, M.D., and Jonasson, I.R., 2007, Volcanogenic massive sulphide deposits: in. Goodfellow, W.D., ed., Mineral Deposits of Canada: A Synthesis of Major Deposit

Types, District Metallogeny, the Evolution of Geological Provinces, and Exploration Methods, Geological Association of Canada, Mineral Deposits Division, Special Publication 5, p. 141–161

Gebert, J.S., 1995, Archean Geology of the Hanikahimajuk Lake Area, Northern Point Lake Volcanic Belt, West-Central Slave Structural Province, District of Mackenzie, N.W.T.: NWT EGS Open File 27.

Genna, D., Gaboury, D., and Roy, G., 2014, Evolution of a volcanogenic hydrothermal system recorded by the behavior of LREE and Eu: Case study of the Key Tuffite at Bracemac–McLeod deposits, Matagami, Canada: Ore Geology Reviews, v. 63, p. 160–177.

Genna, D., and Gaboury, D., 2015, Deciphering the Hydrothermal Evolution of a VMS System by LA-ICP-MS Using Trace Elements in Pyrite: An Example from the Bracemac-McLeod Deposits, Abitibi, Canada, and Implications for Exploration. Economic Geology, v. 110(8).

George, L., Cook, N.J., and Ciobanu, C.L., 2016, Partitioning of trace elements in co-crystallized sphalerite–galena–chalcopyrite hydrothermal ores: Ore Geology Reviews, v. 77, p. 97–116.

George, L., Cook, N.J., Crowe, B.B.P., and Ciobanu, C. L., 2018a, Trace elements in hydrothermal chalcopyrite: Mineralogical Magazine, v. 82(1), p. 59–88.

George, L.L., Biagioni, C., D'Orazio, M., and Cook, N.J., 2018b, Textural and trace element evolution of pyrite during greenschist facies metamorphic recrystallization in the southern Apuan Alps (Tuscany, Italy): Influence on the formation of Tl-rich sulfosalt melt: Ore Geology Reviews, v. 102, p. 59–105.

Gibson, H.L., Watkinson, D.H., and Comba, C.D.A., 1983, Silicification; hydrothermal alteration in an Archean geothermal system within the Amulet Rhyolite Formation, Noranda, Quebec: Economic Geology, v. 78(5), p. 954–971.

Gibson, H. L., and Watkinson, D.H., 1990, Volcanogenic massive sulphide deposits of the Noranda Cauldron and Shield Volcano, Quebec: in. Rive, M., Verpaelst, P., Gagnon, Y., Lulin, L.M., Riverin, G., and Simard, A., ed., The Northwestern Quebec Polymetallic Belt: a summary of 60 years of mining exploration, v. 43 p.119–132. Canadian Institute of Mining and Metallurgy.

Gibson, H.L., Franklin, J.M., Hannington, M.D., and Piercey, S., 2005, Abitibi volcanogenic massive sulphide deposits: the spectrum on environments, modern analogs and implications for exploration: in. Program with Abstracts, Quebec Exploration 2005, 6 p.

Gibson, H., and Galley, A., 2007, Volcanogenic Massive Sulphide Deposits of the Archean, Noranda District, Quebec., Special Publication 5, Mineral Deposits Division, Geological Association of Canada, v. 5, p. 533–552.

Goutier, J., and Melançon, M., 2007, Compilation géologique de la Sousprovince de l'Abitibi (version préliminaire): Ministère des Ressources naturelles et de la Faune du Québec.

Goldfarb, R.J., Berger, B.R., George, M.J., and Seal, R.R., 2017, Tellurium: in. Critical mineral resources of the United States—Economic and environmental geology and prospects for future supply: U.S. Geological Survey Professional Paper, v. 1892, p. 1–27. U.S. Geological Survey.

Goodfellow, W.D., Lydon, J.W., and Turner, R.W., 1993. Geology and genesis of stratiform sediment-hosted (SEDEX) Zn-Pb-Ag sulphide deposits: Geological Association of Canada Special Paper 40, p. 201–251.

Goodfellow, W.D., and McCutcheon, S.R., 2003, Geologic and Genetic Attributes of Volcanic Sediment-Hosted Massive Sulfide Deposits of the Bathurst Mining Camp, Northern New Brunswick—A Synthesis: in. Massive Sulfide Deposits of the Bathurst Mining Camp, New Brunswick, and Northern Maine. Society of Economic Geologists.

Goodwin, A. M., and Ridler, R. H., 1970, The Abitibi orogenic belt: Geological Survey of Canada Paper v. 70(40), p. 1–30.

Gorsuch, R.L., 1983, Factor analysis: Lawrence Erlbaum Associates, Hillsdale NJ.

Grant, H.L.J., 2019, Trace and critical metal behaviour in seafloor massive sulfide deposits: A mineralogical and geochemical assessment: Dissertation zur Erlangung des Doktorgrades der Mathematisch-Naturwissenschaftlichen Fakultät der Christian-Albrechts-Universität zu Kiel, 550 p.

Grant, H.L.J., Hannington, M.D., Petersen, S., Frische, M., and Fuchs, S.H., 2018, Constraints on the behavior of trace elements in the actively-forming TAG deposit, Mid-Atlantic Ridge, based on LA-ICP-MS analyses of pyrite: Chemical Geology, v. 498, p. 45–71.

Grant, H.L.J., Layton-Matthews, D., and Peter, J.M., 2015, Distribution and controls on silver mineralization in the Hackett River Main zone, Nunavut, Canada: An Ag- and Pb-enriched Archean volcanogenic massive sulfide deposit: Economic Geology, v. 110, p. 943–982.

Groves, D.I., Goldfarb, R.J., Gebre-Mariam, H., Hagemann, S.G., and Robert, F., 1998, Orogenic gold deposits - a proposed classification in the context of their crustal distribution and relationship to other gold deposit types: Ore Geology Reviews, v. 13, p. 7–27.

Groves, D.I., Zhang, L. and Santosh, M., 2020, Subduction, mantle metasomatism, and gold: A dynamic and genetic conjunction: GSA Bulletin, v. 132(7-8), p. 1419–1426.

Guha, J., and Darling, R., 1972, Ore mineralogy of the Louvem copper deposit, Val d'O, Quebec: Canadian Journal of Earth Science, v. 9(12), p. 1596–1611.

Hackbarth, C.J., and Petersen, U., 1984, A fractional crystallization model for the deposition of argentian tetrahedrite: Economic Geology, v. 79(3), p. 448–460.

Hamlyn, P., Keays, R.R., Cameron, W.E., Crawford, A.J., and Waldron, H.M. 1985, Precious metals in magnesian low-Ti lavas: Implications for metallogenesis and sulfur saturation in primary magmas: Geochimica et Cosmochimica Acta, v. 49, p. 1797–1811.

Hannington, M.D., and Scott, S.D., 1989, Sulfidation equilibria as guides to gold mineralization in volcanogenic massive sulfides; evidence from sulfide mineralogy and the composition of sphalerite: Economic Geology, v. 84(7), p. 1978–1995.

Hannington, M., Herzig, P., Scott, S., Thompson, G., and Rona, P, 1991, Comparative mineralogy and geochemistry of gold-bearing sulfide deposits on the mid-ocean ridges. Marine Geology, v. 101(1), p. 217–248.

Hannington, M. D., Galle, A. G., Herzig, P. M., & Petersen, S, 1998, Comparison of the TAG mound and stockwork complex with Cyprus-type massive sulfide deposits: Proceedings of the Ocean Drilling Program, v. 158, p. 389–415.

Hannington, M.D., Poulsen, K H., Thompson, J.F.H., and Sillitoe, R. H, 1999a, Volcanogenic Gold in the Massive Sulfide Environment: in. Volcanic-Associated Massive Sulfide Deposits: Processes and Examples in Modern and Ancient Settings, Reviews in Economic Geology, v. 8, p. 325–356.

Hannington, M.D., Barrie, C.T. and Bleeker, W., 1999b, The giant Kidd Creek volcanogenic massive sulfide deposit, western Abitibi subprovince, Canada: Preface and Introduction: in. The giant Kidd Creek volcanogenic massive sulfide deposit, western Abitibi subprovince, Canada. Economic Geology Monograph (10). The Economic Geology Publishing Company, Littleton, CO, p. 1–30.

Hannington, M.D., Bleeker, W., and Kjarsgaard, I, 1999c, Sulfide Mineralogy, Geochemistry, and Ore Genesis of the Kidd Creek Deposit: Part I. North, Central, and South Orebodies: in. The giant Kidd Creek volcanogenic massive sulfide deposit, western Abitibi subprovince, Canada. Economic Geology Monograph (10). The Economic Geology Publishing Company, Littleton, CO, p. 163–224.

Hannington, M.D., Santaguida, F., Kjarsgaard, I.M., and Cathles, L.M, 2003, Regional-scale hydrothermal alteration in the Central Blake River Group, western Abitibi subprovince, Canada: implications for VMS prospectivity: Mineralium Deposita, v. 38(4), p. 392–422.

Hannington, M.D., de Ronde, C.E.J., and Petersen, S., 2005, Sea-floor tectonics and submarine hydrothermal systems: in. Hedenquist J.W., Thompson J.F.H., Goldfarb R.J., and Richards J.P., ed., Economic Geology 100th Anniversary Volume, Society of Economic Geologists, p. 111–141.

Hannington, M.D., 2014, 13.18—Volcanogenic Massive Sulfide Deposits: in. Holland, H.D., and Turekian, K.K., ed., Treatise on geochemistry, 2nd edn., p. 463–488. Elsevier, Oxford.

Hannington, M.D., Gemmell, T., and Monecke, T, 2017, The Kidd Creek Volcanogenic Massive Sulfide Deposit—An Update: in. Archean Base and Precious Metal Deposits, Southern Abitibi Greenstone Belt, Canada, Reviews in Economic Geology, v. 19, p. 81–102.

Harris, D.C., Roberts, A.C., Thorpe, R.I., Criddle, A.J., and Stanley, C.J., 1984, Kiddcreekite, a new mineral species from the Kidd Creek mine, Timmins, Ontario and from the Campbell orebody, Bisbee, Arizona: Canadian Mineralogist, v. 22, p. 227–232.

Hart, T.R., Gibson, H.L., and Lesher, C.M., 2004, Trace element geochemistry and petrogenesis of felsic volcanic rocks associated with volcanogenic massive Cu-Zn-Pb sulfide deposits: Economic Geology, v. 99, p. 1003–1013.

Hartigan, J.A., and Wong, M.A., 1979. Algorithm AS 136: A k-means clustering algorithm: Journal of the royal statistical society. series c (applied statistics), v. 28(1), p.100–108.

Hatcher, L., 1994, A step-by-step approach to using the SAS system for factor analysis and structural equation modeling: SAS Institute, Cary.

Helsel, D., 1990, Less than obvious - statistical treatment of data below the detection limit: Environmental Science & Technology, v. 24, p. 1766–1774.

Henderson, J.R., Kerswill, J.A., Henderson, M.N., Villeneuve, M., Petch, C.A., Dehls, J.F., and O'Keefe, M.D., 1995, Geology, geochronology, and metallogeny of the High Lake greenstone belt Archean Slave Structural Province, Northwest Territories: Canadian Shield/Bouclier Canadian, Geological Survey of Canada, Current Research 1995-C, p. 97–106.

Hickson, C.J., and Juras, S.J., 1986, Sample Contamination by Grinding. Canadian Mineralogist, v. 24, p. 585–589.

Hinton, G.E., and Roweis, S., 2002, Stochastic Neighbor Embedding: in. Becker, S., Thrun, S., and Obermayer, K., ed., Advances in Neural Information Processing Systems, v. 15, MIT Press.

Heather, K.B., and Shore, G.T., 1999, Geology, Swayze greenstone belt, Ontario: Geological Survey of Canada Open File 3384a, Scale 1:50,000.

Hoffe, B.H., and Lines, L.R., 1997, Comparison of 2D pre-stack and 3D post-stack migrations from the Matagami mining camp, Quebec: The University of Calgary Department of Geology and Geophysics CREWES Research Report 9, p. 1–11.

Hoffman, P.F., 1988, United plates of America, the birth of a craton: Early Proterozoic assembly and growth of Laurentia: Annual Review of Earth and Planetary Science Letters, v. 16, p. 543–603.

Hoffman, P.F., 1990, Subdivision of the Churchill Province and extent of the Trans-Hudson Orogen: in. Lewry, J.F. and Stauffer, M.R., ed., The Early Proterozoic Trans-Hudson Orogen of North America: Lithotectonic Correlations and Evolution, Geological Association of Canada; Special Paper 37, p. 15–39.

Hollings, P.N., 1998, Geochemistry of the Uchi Subprovince, Northern Superior Province: An Evaluation of the Geodynamic Evolution of the Northern Margin of the Superior Province Ocean Basin: Unpublished PhD thesis, University of Saskatchewan, 229 p.

Houghton, J. L., Shanks, W.C., and Seyfried, W. E., 2004, Massive sulfide deposition and trace element remobilization in the Middle Valley sediment-hosted hydrothermal system, northern Juan de Fuca Rdge1 1Associate editor: E. M. Ripley. Geochimica et Cosmochimica Acta, v. 68(13), p. 2863–2873.

Houlé, M.G., and Solgadi, F, 2007, Geological and mineral potential of Bartlett and Geikie townships in the Bartlett Dome, Abitibi greenstone belt: Ontario Geological Survey Open File Report 6213, p. 1–15.

Houlé, M.G., Ayer, J.A. , Baldwin, G., Berger, B.R., Dinel, E., Fowler, A.D., Moulton, B., Saumur, B.M., and Thurston, P.C., 2008, Field trip guidebook to the stratigraphy and volcanology of supracrustal assemblages hosting base metal and gold mineralization in the Abitibi greenstone belt, Timmins, Ontario: Ontario Geological Survey Open File Report 6225, 84 p.

Hronsky, J.M.A., Groves, D.I., Loucks, R.R., and Begg, G.C., 2012, A unified model for gold mineralisation in accretionary orogens and implications for regional-scale exploration targeting methods: Mineralium Deposita, v. 47(4), p. 339–358.

Hu, Z. and Gao, S., 2008, Upper crustal abundances of trace elements: a revision and update: Chemical Geology, v. 253(3-4), p.205–221.

Husson, F., Josse, J., and Pages, J., 2010, Principal component methods-hierarchical clustering-partitional clustering: why would we need to choose for visualizing data?: Applied Mathematics Department, p. 1–17.

Huston, D.L., 2000, Gold in volcanic-hosted massive sulfide deposits: distribution, genesis, and exploration: in. Hagemann, S.G. and Brown, P.E., ed., Gold in 2000, Society of Economic Geologists. p. 401–426.

Huston, D.L., and Large, R.R., 1989, A chemical model for the concentration of gold in volcanogenic massive sulphide deposits: Ore Geology Reviews, v. 4(3), p. 171–200.

Huston, D.L., Sie, S.H., Suter, G.F., Cooke, D.R., and Both, R.A., 1995, Trace elements in sulfide minerals from eastern Australian volcanic-hosted massive sulfide deposits; Part I, Proton microprobe analyses of pyrite, chalcopyrite, and sphalerite, and Part II, Selenium levels in pyrite; comparison with delta 34 S values and implications for the source of sulfur in volcanogenic hydrothermal systems: Economic Geology, v. 90(5), p. 1167–1196.

Huston, D.L., Pehrsson, S., Eglington, B.M., and Zaw, K., 2010, The geology and metallogeny of volcanic-hosted massive sulfide deposits: Variations through geologic time and with tectonic setting: Economic Geology, v. 105, p. 571–591.

Huston, D.L., Relvas, J.M., Gemmell, J.B., and Drieberg, S., 2011, The role of granites in volcanic-hosted massive sulphide ore-forming systems: an assessment of magmatic–hydrothermal contributions: Mineralium Deposita, v. 46(5–6), p. 473–507.

Hutchinson, R.W., 1973, Volcanogenic sulfide deposits and their metallogenic significance: Economic Geology, v. 68, p. 1223–1246.

Ishikawa, Y., Sawaguchi, T., Ywaya, S., and Horiuchi, M., 1976, Delineation of prospecting targets for Kuroko deposits based on modes of volcanism of underlying dacite and alteration haloes: Mining Geology, v. 26, p. 105–117.

Ingham, E.S., Cook, N.J., Cliff, J., Ciobanu, C.L. and Huddleston, A., 2014, A combined chemical, isotopic and microstructural study of pyrite from roll-front uranium deposits, Lake Eyre Basin, South Australia: Geochimica et Cosmochimica Acta, 125, p.440–465.

Jenkins, C.L., and Brown, A.C., 1999, Cadre métallogénique des gisements de sulfures massifs volcanogènes et filoniens aurifères des cantons Bourlamaque et Louvicourt, partie sud de la Sous-province de l'Abitibi: Géologie Québec Report MB, p. 99-12.

Jensen, L.S., and Langford, F.F., 1985, Geology and petrogenesis of the Archean Abitibi belt in the Kirkland Lake area, Ontario, Ontario Geological Survey Miscellaneous Paper 123, 130 p.

Jensen, J.E., 1995, Geology, geochemistry and Nd isotopic study of the Hanikahimajuk Lake area, Slave Province, NWT: MSc Thesis, University of Alberta, Edmonton, Alberta.

Jolliffe, I., 2005, Principal Component Analysis: in. Encyclopedia of Statistics in Behavioral Science. John Wiley & Sons, Ltd.

Jonasson, I.R., and Sangster, D.F., 1975a, Variations in the mercury contents of sphalerite from some Canadian sulphide deposits: Association of Exploration Geochemists, Special Publication (2), p. 313–332.

Jonasson, I.R., and Sangster, D.F., 1975b, Selenium in sulphides from some Canadian base metal deposits: Geological Survey of Canada, Paper 75-1C, p. 231–232.

Jonasson, I.R., and Sangster, D.F., 1983, A Preliminary Report On the Gold Content of Sulphide Separates From Some Canadian Base-metal Deposits: Report of Activities, Part B, p. 47–52.

Jonasson, I.R., Ames, D.E., and Galley, A.G.,2009, Sulphide ore geochemistry database for volcanogenic massive sulfide deposits of the Paleoproterozoic Flin Flon Belt and Sherridon area, Manitoba and Saskatchewan: Geological Survey of Canada, Open File 5432, 1 CD-ROM.

Jonasson, I.R., Hillary, E.M., Hannington, M.D., Mercier-Langevin, P., and Diekrup, D., 2020, Trace-element geochemistry of ore-mineral separates from selected Canadian base-metal deposits: Geological Survey of Canada, Open File 8727.

Jones, S., 2006, Petrographic, Geochemical, and Fluid Inclusion Evidence for the Origin of Siliceous Cap Rocks Above Volcanic-Hosted Massive Sulfide Deposits at Myra Falls, Vancouver Island, British Columbia, Canada: Economic Geology, v. 101(3), p. 555–584.

Juras, S.J., 1987, Geology of the polymetallic volcanogenic Battle Lake camp, with emphasis on the Price hillside, Central Vancouver Island, British Columbia, Canada: Unpublished Ph.D. Thesis, Vancouver, University of British Columbia, 278 p.

Keays, R.R., and Scott, R.B., 1976, Precious metals in ocean-ridge basalts: Implications for basalts as source rocks for gold mineralization: Economic Geology, v. 71, p. 705–720.

Keith, M., Haase, K.M., Klemd, R., Krumm, S., and Strauss, H., 2016, Systematic variations of trace element and sulfur isotopic compositions in pyrite with stratigraphic depth in the Skouriotissa volcanic-hosted massive sulfide deposit, Troodos ophiolite, Cyprus: Chemical Geology 423, p. 7–18.

Keith, M., Smith, D.J., Jenkin, G.R., Holwell, D.A. and Dye, M.D., 2018, A review of Te and Se systematics in hydrothermal pyrite from precious metal deposits: Insights into ore-forming processes: Ore Geology Reviews, 96, p. 269–282.

Kerr, D.J., and Gibson, H.L., 1993, A comparison of the Horne volcanogenic massive sulfide deposit and intracauldron deposits of the Mine Sequence, Noranda, Quebec: Economic Geology, v. 88(6), p. 1419–1442.

Kerrich, R., Goldfarb, R.J., and Richards, J.P.R., 2005, Metallogenic Provinces in an Evolving Geodynamic Framework: in. 100th Anniversary Volume of Economic Geology, Society of Economic Geologists, p. 1097–1136.

Kiseeva, E.S., and Wood, B.J., 2013, A simple model for chalcophile element partitioning between sulphide and silicate liquids with geochemical applications: Earth and Planetary Science Letters, v. 383, p.68–81.

Kiseeva, E.S., and Wood, B.J., 2015, The effects of composition and temperature on chalcophile and lithophile element partitioning into magmatic sulphides: Earth and Planetary Science Letters, v. 424, p.280–294.

Kiseeva, E.S., Fonseca, R.O., and Smythe, D.J., 2017, Chalcophile elements and sulfides in the upper mantle: Elements, v. 13(2), p.111–116.

Knuckey, M.J., 1982, Structure, metal zoning and alteration at the Millenbach deposit, Noranda, Quebec: Geological Association of Canada Special Paper 25, v. 255–295.

Kusky, T.M., 1986, Are greenstone belts in the Slave Province, NWT, allochthonous?: in de Wit, M.J., and Ashwal, L., ed., Workshop on the tectonic evolution of greenstone belts: Lunar and Planetary Institute Technical Report 86-10, p. 135–139.

Kusky, T.M., 1989, Accretion of the Archean Slave province: Geology, v. 17(1), p. 63–67.

LaFlamme, C., Martin, L., Jeon, H., Reddy, S.M., Selvaraja, V., Caruso, S., Bui, T.H., Roberts, M.P., Voute, F., Hagemann, S. and Wacey, D., 2016, In situ multiple sulfur isotope analysis by SIMS of pyrite, chalcopyrite, pyrrhotite, and pentlandite to refine magmatic ore genetic models: Chemical Geology, v. 444, p.1–15.

Laflèche, M.R., Dupuy, C., and Bougault, H., 1992, Geochemistry and petrogenesis of Archean mafic volcanic rocks of the southern Abitibi Belt, Québec. Precambrian Research, v. 57(3–4), p. 207–241.

Laflèche, M.R., Camiré, G., and Jenner, G.A., 1998, Geochemistry of post-Acadian, Carboniferous continental intraplate basalts from the Maritimes Basin, Magdalen Islands, Québec, Canada. Chemical Geology, v. 148(3–4), p. 115–136.

Lafrance, B., Moorhead, J., and Davis, D., 2003, Cadre géologique du camp minier de Doyon-Bousquet-LaRonde: Ministère des Ressources Naturelles, Québec Report ET 2002-07, 45 p.

Large, R.R., 1992, Australian volcanic-hosted massive sulfide deposits; features, styles, and genetic models. Economic Geology, v. 87(3), p. 471–510.

Large, R.R., Gemmell, J.B., Paulick, H., and Huston, D.L., 2001a, The alteration box plot: A simple approach to understanding the relationships between alteration mineralogy and lithogeochemistry associated with VHMS deposits: Economic Geology, v. 96, p. 957–971.

Large, R.R., McPhie, J., Gemmell, B., Herrmann, W., and Davidson, G.J., 2001b, The spectrum of ore deposit types, volcanic environments, alteration halos, and related exploration vectors in submarine volcanic successions: some examples from Australia: Economic Geology, v. 96, p. 913–938.

Large, R.R., Allen, R.L., Blake, M.D. and Herrmann, W., 2001c, Hydrothermal alteration and volatile element halos for the Rosebery K lens volcanic-hosted massive sulfide deposit, western Tasmania: Economic Geology, v. 96(5), p.1055–1072.

Large, R.R., Maslennikov, V., Robert, F., Danyushevsky, L., and Chang, Z., 2007, Multistage Sedimentary and Metamorphic Origin of Pyrite and Gold in the Giant Sukhoi Log Deposit, Lena Gold Province, Russia: Economic Geology, v. 102(7), p. 1233–1267.

Large, R.R, Doyle, M., Raymond, O., Cooke, D., Jones, A., and Heasman, L., 1996, Evaluation of the role of Cambrian granites in the genesis of world class VHMS deposits in Tasmania: Ore Geology Reviews 10, p. 215–230.

Large, R.R., Danyushevsky, L., Hollit, C., Maslennikov, V., Meffre, S., Gilbert, S., Bull, S., Scott, R., Emsbo, P., Thomas, H., Singh, B., and Foster, J., 2009, Gold and Trace Element Zonation in Pyrite Using a Laser Imaging Technique: Implications for the Timing of Gold in Orogenic and Carlin-Style Sediment-Hosted Deposits. Economic Geology, v. 104(5), p. 635–668.

Larocque, A.C.L., Hodgson, C.J., Cabri, L.J., and Jackman, J. A., 1995, Ion-microprobe analysis of pyrite, chalcopyrite and pyrrhotite from the Mobrun VMS deposit in northwestern Quebec; evidence for metamorphic remobilization of gold: The Canadian Mineralogist, v. 33(2), p. 373–388.

Latulippe, M., 1972, The Mattagami area: in. Allard, G.O., Duquette, G., Latulippe, M., van de Walle, M., Brown, A., Guilloux, L., and LaSalle, P., ed., Precambrian geology and mineral deposits of the Noranda-Val d'Or and Matagami-Chibougamau greenstone belts, Quebec: Montreal, Quebec, 24th International Geological Congress Guide to Excursions A41 and C41, p. 27–33.

Layton-Matthew, D., 2005, Genesis of Se in Volcanic-Hosted Massive-Sulfide Systems: Wolverine, Kudz Ze Kayah, and GP4F VMS Deposits, Finlayson Area, Yukon, Canada: Ph.D. Thesis, University of Toronto, Toronto, Ontario, 247 p.

Leistel, J.M., Marcoux, E., Deschamps, Y., Joubert, M., 1998, Antithetic behavior of gold in the volcanogenic massive sulphide deposits of the Iberian Pyrite Belt: Mineral. Deposita, v. 33, p. 82–97.

Lentz, D.R., 1998, Petrogenetic evolution of felsic volcanic sequences associated with Phanerozoic volcanic-hosted massive sulphide systems: the role of extensional geodynamics: Ore Geology Reviews, v. 12, p. 289–327.

Lesher, C.M., Goodwin, A.M., Campbell, I.H., and Gorton, M.P., 1986, Trace-element geochemistry of ore-associated and barren, felsic metavolcanic rocks in the Superior Province, Canada: Canadian Journal of Earth Sciences, v. 23, p. 222–237.

Lockington, J.A., Cook, N.J., Ciobanu, C.L., 2014, Trace and minor elements in sphalerite from metamorphosed sulphide deposits: Mineral. Mag. V. 108, p. 873–890.

Lodge, R.W.D., Gibson, H.L., Stott, G.M., Franklin, J.M., and Hudak, G.J., 2015, Geodynamic setting, crustal architecture, and VMS metallogeny of ca. 2720 Ma greenstone belt assemblages of the northern Wawa subprovince, Superior Province. <i>Canadian Journal of Earth Sciences, v. 52(3), p. 196–214.

Lodge, R.W.D., Ma, C., Etienne, M., Nelson, T.J., Chandler, M.D., and Brock, N.M·, 2019, Geologic overview and petrogenetic history of the Sturgeon Lake transect, western Wabigoon: in. Summary of Field Work and Other Activities, Ontario Geological Survey Open File Report 6360, p. 35-1–35-10.

Loftus-Hills, G., and Solomon, M., 1967, Cobalt, nickel, and selenium in sulphides as indicators of ore genesis: Mineral. Deposita, v. 2, p. 228–242.

LV, C.C, Ding, J., Liu, Y., Fu, G.Y., Qian, P., Ye, S.F., 2017 Characterization of a copper mine tailing and comprehensive recovery of Cu and S from the tailing: Journal of Residuals Science & Technology, v. 41(2), p. 125–135.

Lydon, J.W., 1984, Ore Deposit Models – 8. Volcanogenic Massive Sulphide Deposits Part I: A descriptive Model.: Geoscience Canada, v. 11(4), p. 195–202.

Lyubetskaya, T. and Korenaga, J., 2007, Chemical composition of Earth's primitive mantle and its variance: 1. Method and results: Journal of Geophysical Research: Solid Earth, v. 112(B3).

Macdonald, A J., Lewis, P.D., Thompson, J F.H., Nadaraju, G., Bartsch, R., Bridge, D.J., Rhys, D.A., Roth, T., Kaip, A., Godwin, C.I., and Sinclair, A.J., 1996, Metallogeny of an Early to Middle Jurassic arc, Iskut River area, northwestern British Columbia: Economic Geology, v. 91(6), p. 1098–1114.

MacLachlan, K., and Devine, C., 2007, Stratigraphic evidence for volcanic architecture in the Flin Flon mining camp: Implications for mineral exploration: Saskatchewan Geological Survey, Saskatchewan Ministry of Energy and Resources, Miscellaneous Report 2007-4.2, 29 p.

MacNeill, R.J., 1976, Twenty years of persistence at Bathurst Norsemines is paying off: Canadian Mining Journal, v. 97(9), p. 28–33.

Maier, W.D., Barnes, S.-J., and Pellet, T., 1996, The economic significance of the Bell River Complex, Abitibi subprovince, Quebec: Canadian Journal of Earth Sciences, v. 33, p. 967–980.

Marshall, D., Nicol, C.A., Greene, R., Sawyer, R., Stansell, A., and Easterbrook, R., 2018, Precious Metal Enrichment at the Myra Falls VMS Deposit, British Columbia, Canada: Geosciences, v. 8(11), p. 422.

Marquis, P., Hubert, C., Brown, A.C., and Rigg, D.M., 1990, An evaluation of genetic models for gold deposits of the Bousquet district, Quebec, based on their mineralogic, geochemical, and structural characteristics: Canadian Institute of Mining and Metallurgy Special Volume 43, p. 383−399.

Mason, R., and Melnik, N., 1986, The anatomy of an Archean gold system - The McIntyre-Hollinger complex at Timmins, Ontario, Canada: Gold ‘86: An International Symposium on the Geology of Gold Deposits, Toronto, Canada, 1986, Proceedings Volume, p. 40–55.

Maslennikov, V., Maslennikova, S.P., Large, R.R., and Danyushevsky, L., 2009, Study of Trace Element Zonation in Vent Chimneys from the Silurian Yaman-Kasy Volcanic-Hosted Massive Sulfide Deposit (Southern Urals, Russia) Using Laser Ablation-Inductively Coupled Plasma Mass Spectrometry (LA-ICPMS): Economic Geology, v. 104(8), p. 1111–1141.

Maslennikov, V., Maslennikova, S.P., Large, R.R., Danyushevsky, L, Herrington, R.J., and Stanley, C. J., 2013, Tellurium-bearing minerals in zoned sulfide chimneys from Cu-Zn massive sulfide deposits of the Urals, Russia. Mineralogy and Petrology, 107(1).

Mathieu, L., 2019, Detecting magmatic-derived fluids using pyrite chemistry: Example of the Chibougamau area, Abitibi Subprovince, Québec: Ore Geology Reviews, v. 114, p.103–127.

Mathieu, L. and Racicot, D., 2019, Petrogenetic study of the multiphase Chibougamau Pluton: Archaean magmas associated with Cu–Au magmato-hydrothermal systems: Minerals, v. 9(3), 174 p.

McClenaghan, S.H., Lentz, D.R., Martin, J., Diegor, W.G., 2009. Gold in the Brunswick No. 12 volcanogenic massive sulfide deposit, Bathurst Mining Camp, Canada: evidence from bulk ore analysis and laser ablation ICP-MS data on sulfide phases: Mineral. Deposita, v. 44, p. 523–557.

Mercier-Langevin, P., Dubé, B., Hannington, M.D., Davis, D.W., Lafrance, B., and Gosselin, G., 2007, The LaRonde Penna Au-rich volcanogenic massive sulfide deposit, Abitibi greenstone belt, Quebec: Part I. Geology and geochronology: Economic Geology, v. 102(4), p. 585–609.

Mercier-Langevin, P., Hannington, M.D., Dubé, B., and Bécu, V., 2011a, The gold content of volcanogenic massive sulphide deposits: Mineralium Deposita, v. 46, p. 509–539.

Mercier-Langevin, P., Goutier, J., Ross, P.S., McNicoll, V., Monecke, T., Dion, C., Dubé, B., Thurston, P., Bécu, V., Gibson, H., Hannington, M., and Galley, A., 2011b, The Blake River Group of the Abitibi Greenstone Belt and its unique VMS and gold-rich VMS endowment: Geological Survey of Canada, Open File, 6869, 61 p.

Mercier-Langevin, P., Gibson, H.L., Hannington, M.D., Goutier, J., Monecke, T., Dubé, B. and Houlé, M.G., 2014. A special issue on Archean magmatism, volcanism, and ore deposits: part 2. Volcanogenic massive sulfide deposits preface: Economic Geology, v. 109(1), p.1–9.

Mercier-Langevin, P., Hannington, M.D., Dubé, B., Piercey, S J., Peter, J.M., and Pehrsson, S.J., 2015, Precious metal enrichment processes in volcanogenic massive sulphide deposits - a summary of key features, with an emphasis on TGI-4 research contributions: Targeted geoscience initiative 4, p. 117–130.

Miesch, A.T., 1967, Methods of Computation for Estimating Geochemical Abundance: U.S. Geological Survey Professional Paper 574-B, 15 p.

Mills, R.A., 1995, Hydrothermal deposits and metalliferous sediments from TAG, 26°N Mid-Atlantic Ridge: in. Parson, L.M., Walker, C.L., and Dixon D.R., ed., Hydrothermal Vents and Processes, p. 77–86. Geological Society of London Special Publication.

Mills, H.K., Piercey, S., and Tools, T, 2016, Geology, alteration, and lithogeochemistry of the Hood volcanogenic massive sulfide (VMS) deposits, Nunavut, Canada: Mineralium Deposita, v. 51(4), p. 533–556.

Mikhlin, Y., Romanchenko, A., Likhatski, M., Karacharov, A., Erenburg, S., and Trubina, S., 2011, Understanding the initial stages of precious metals precipitation: Nanoscale metallic and sulfidic species of gold and silver on pyrite surfaces: Ore Geology Reviews, v. 42(1), p. 47–54.

Mole, D.R., Thurston, P.C., Marsh, J.H., Stern, R.A., Ayer, J.A., Martin, L.A. J., and Lu, Y.J., 2021, The formation of Neoarchean continental crust in the south-east Superior Craton by two distinct geodynamic processes: Precambrian Research, v. 356.

Monecke, T., Gibson, H.L., Dubé, B., Laurin, J., Hannington, M.D., and Martín, L., 2008, Geology and volcanic setting of the Horne deposit, Rouyn-Noranda, Quebec: initial results of a new research project: Geological Survey of Canada, Current Research, 9, 16 p.

Monecke, T., Petersen, S., and Hannington, M.D., 2014, Constraints on water depth of massive sulphide formation: evidence from modern seafloor hydrothermal systems in arc related settings: Economic Geology, v. 109, p. 2079–2101.

Monecke, T., Petersen, S., Hannington, M.D., Grant, H., and Samson, I.M., 2016, The Minor Element Endowment of Modern Sea-Floor Massive Sulfides and Comparison with Deposits Hosted in Ancient Volcanic Successions: Reviews in Economic Geology, v. 18, p. 245–306.

Monecke, T., Mercier-Langevin, P., Dubé, B., Frieman, B.M., 2017a, Geology of the Abitibi Greenstone Belt, Canada: Reviews in Economic Geology, v. 19, p. 7–49.

Monecke, T., Gibson, H.L., and Goutier, J., 2017b, Volcanogenic massive sulfide deposits of the Noranda camp: Reviews in Economic Geology, v. 19, p. 169–223.

Montsion, R., Thurston, P., Ayer, J., 2018, 1:2 000 000 Scale Geological Compilation of the Superior Craton – Version 1: Mineral Exploration Research.

Centre, Harquail School of Earth Sciences, Laurentian University Document Number MERC-ME-2018-017

Mortenson, J. K., 1987, Preliminary U-Pb zircon ages for volcanic and plutonic rocks of the Noranda-Lac Abitibi area, Abitibi subprovince, Quebec: Geological Survey of Canada Paper, 87-1A, p. 581–590.

Mortensen, J.K., and Jilson, G.A., 1985, Evolution of the Yukon-Tanana terrane: Evidence from southeastern Yukon Territory. Geology, v. 13(11), p. 806–810.

Mortensen, J.K., Thorpe, R.I. , Padgham, W.A., King, J.E., and Davis, W.J., 1988, U-Pb zircon ages for felsic volcanism in the Slave Province, N.W.T., Radiogenic Age and Isotope Studies: Report 2, 88-2, Geological Survey of Canada, p. 85–95.

Mortensen, J.K., 1992, Pre-mid-Mesozoic tectonic evolution of the Yukon-Tanana terrane, Yukon and Alaska: Tectonics, v. 11, p. 836–853.

Mortensen, J.K., 1993a, U-Pb geochronology of the eastern Abitibi subprovince: Part 2: Noranda-Kirkland Lake area: Canadian Journal of Earth Sciences, v. 30, p. 29–41.

Mortensen, J.K., 1993b, U-Pb geochronology of the eastern Abitibi subprovince. Part 1: Chibougamau-Matagami-Joutel region: Canadian Journal of Earth Sciences, v. 30, p. 11–28.

Morton, R.L., and Franklin, J.M., 1987, Two-fold classification of Archean volcanic-associated massive sulfide deposits: Economic Geology, v. 82, p. 1057–1063.

Morton, R.L., Walker, J.S., and Hudak, G.J., 1991, The early development of an Archean submarine caldera complex with emphasis on the Mattabi ash-flow tuff and its relationship to the Mattabi massive Sulfide deposit: Economic Geology, v. 86, p. 1002–1011.

Morton, R.L., Hudak, G.J., and Koopman, E., 1996, Physical volcanology, hydrothermal alteration and massive sulphide deposits of the Sturgeon Lake caldera: in. Field Trip Guidebook B3, Geological Association of Canada/Mineralogical Association of Canada Annual Meeting, Winnipeg, Manitoba, May 27–29.

Mosier, D. L., Singer, D.A., and Salem, B.B., 1983, Geologic and grade tonnage information on volcanic-hosted copper-zinc-lead massive sulfide deposits. U.S. Geological Survey Open-File Report 83-89, p. 1–78.

Mosier, D. L., Berger, V. I., and Singer, D.A., 2009, Volcanogenic massive sulfide deposits of the world; database and grade and tonnage models. U.S. Geological Survey Open-File Report 2009-1034.

Mukherjee, I., and Large, R., 2017, Application of pyrite trace element chemistry to exploration for SEDEX style Zn-Pb deposits: McArthur Basin, Northern Territory, Australia: Ore Geology Reviews, v. 81, p. 1249–1270.

Mular, A.L., Halbe, D.N. and Barratt, D.J., 2002, Mineral Processing Plant Design, Practice, and Control: Society for Mining, Metallurgy, and Exploration, v. 1.

Mumin, A.H., Scott, S.D., Somarin, A.K., and Oran, K.S., 2007, Structural Controls on Massive Sulfide Deposition and Hydrothermal Alteration in the South Sturgeon Lake Caldera, Northwestern Ontario. Exploration and Mining Geology, v. 16(1–2).

Murao, S., and Itoh, S., 1992, High thallium content in Kuroko-type ore. Journal of Geochemical Exploration, v. 43, p. 223–231.

Nelson, J., and Colpron, M., 2007, Tectonics and metallogeny of the British Columbia, Yukon and Alaskan Cordillera, 1.8 Ma to the present: in. Goodfellow, W.D., ed., Mineral deposits of Canada; A synthesis of major deposit-types, district metallogeny, the evolution of geological provinces, and exploration methods: Geological Association of Canada, Mineral Deposits Division, Special Publication no. 5, p. 755–791.

Ontario Geological Survey., 1986, Geological highway map, northern Ontario: Ontario Geological Survey Map 2506, Scale 1:1,600,000.

Padgham, W.A., 1985, Observations and speculations on supracrustal successions in the Slave Structural Province: in Ayres, L.D., Thurston, P.C., Card, K.D., and Weber, W., ed., Evolution of Archean supracrustal sequences, Geological Association of Canada Special Paper 28, p. 133–151.

Palarea-Albaladejo, J., and Martín-Fernández, J. A., 2015, zCompositions — R package for multivariate imputation of left-censored data under a compositional approach: Chemometrics and Intelligent Laboratory Systems, v. 143, p. 85–96.

Patten, C.G.C., Pitcairn, I.K., Teagle, D. A.H., and Harris, M., 2016, Mobility of Au and related elements during the hydrothermal alteration of the oceanic crust: implications for the sources of metals in VMS deposits: Mineralium Deposita, v. 51(2), p. 179–200.

Payne, J.G., Bratt, J.A., and Stone, B.G., 1980, Deformed Mesozoic volcanogenic Cu-Zn sulfide deposits in the Britannia District, British Columbia. Economic Geology, v. 75(5), p. 700–721.

Paradis, S., 1990, Stratigraphy, volcanology and geochemistry of the New Vauze-Norbec area, Central Noranda Volcanic Complex, Quebec, Canada: Unpublished Ph.D. thesis, Ottawa, Ontario, Canada, Carleton University, 453 p.

Pearson, V., and Daigneault, R., 2009, An Archean megacaldera complex: The Blake River Group, Abitibi greenstone belt: Precambrian Research, v. 168(1), p. 66–82.

Pehrsson, S., Gibson, H. L., and Gilmore, K., 2016, A Special Issue on Volcanogenic Massive Sulfide Deposits of the Trans-Hudson Orogen: Preface. Economic Geology, v. 111(4), p. 803–816.

Percival, J.A., 2007, Geology and metallogeny of the Superior province, Canada: in. Goodfellow, W.D., ed., Mineral deposits of Canada: A synthesis of major deposit-types, district metallogeny, the evolution of geological provinces, and exploration methods: Mineral Deposits Division, Geological Association of Canada, Special Publication no. 5, p. 903–928.

Percival, J. A., Skulski, T., Sanborn-Barrie, M., Stott, G.M., Leclair, A.D., Corkery, M.T., and Boily, M., 2012, Geology and tectonic evolution of the Superior Province, Canada, Tectonic styles in Canada: The Lithoprobe Perspective, Geological Association of Canada, Special Paper, 49, p. 321–378.

Petch, C.A., 2004, The Geology and Mineralization of the High Lake Volcanic-hosted Massive Sulfide Deposit, Nunavut. Exploration and Mining Geology, v. 13(1–4), p. 37–47.

Peter, J.M., and Goodfellow, W.D., 1996, Mineralogy, bulk and rare earth element geochemistry of massive sulphide-associated hydrothermal sediments of the Brunswick Horizon, Bathurst Mining Camp, New Brunswick. Canadian Journal of Earth Sciences, v. 33(2), p. 252–283.

Peter, J., Layton-Matthews, D., Piercey, S., Bradshaw, G., Paradis, S., and Boulton, A., 2007, Volcanic-hosted massive sulphide deposits of the Finlayson Lake District, Yukon, v. 5, p. 471–508.

Petersen, E.U., 1986, Tin in volcanogenic massive sulfide deposits; an example from the Geco Mine, Manitouwadge District, Ontario, Canada: Economic Geology, v. 81(2), p. 323–342.

Piercey, S. J., 2011, The setting, style, and role of magmatism in the formation of volcanogenic massive sulfide deposits: Mineralium Deposita, v. 46(5–6), p. 449–471.

Piercey, S.J., Paradis, S., Murphy, D.C., and Mortensen, J.K., 2001, Geochemistry and Paleotectonic Setting of Felsic Volcanic Rocks in the Finlayson Lake Volcanic-Hosted Massive Sulfide District, Yukon, Canada: Economic Geology, v. 96, p. 1877–1905.

Pollock, G.D., Sinclair, I.G., Warburton, A.F., and Wierzbicki, V., 1972, he Uchi orebody—A massive sulfide deposit in an Archean siliceous volcanic environment: Montreal, International Geological Congress, 24th, Sec. 4, p. 299–308.

Poulsen, K.H. and Hannington, M.D., 1996, Volcanic-associated massive sulphide gold: in. Eckstrand, O.R., Sinclair, W.D., and Thorpe, R.I., ed., Geology of Canadian Mineral Deposit Types, Geological Survey of Canada, Geology of Canada Series no. 8, p. 183–196.

Powell, W.G., Carmichael, D.M., and Hodgson, C.J.,1995, Conditions and timing of metamorphism in the southern Abitibi greenstone belt, Quebec: Canadian Journal of Earth Sciences, v. 32, p. 787–805.

Price, P., 1933, The geology and ore deposits of the Horne mine, Noranda, Quebec: Unpublished Ph.D. thesis, Montreal, Quebec, Canada, McGill University, 288 p.

Price, P., 1934, The geology and ore deposits of the Horne mine, Noranda, Quebec: The Transactions of the Canadian Institute of Mining and Metallurgy and of the Mining Society of Nova Scotia, v. 37, p. 108–140.

Price, D.P., 1973, Geology of the Flin Flon mine: in. Simpson, F., ed., An excursion guide to the geology of Saskatchewan: Saskatchewan Geological Society Special Publication no. 1, p. 433–437.

Pyke, D.R., 1982, Geology of the Timmins area, District of Cochrane. Toronto: Ontario Ministry of Natural Resources. Ontario Geological Survey Report, 219.

R Core Team 2020, R: A language and environment for statistical computing: R Foundation for Statistical Computing, Vienna, Austria. (https://www.R-project.org).

Reich, M., Kesler, S.E., Utsunomiya, S., Palenik, C.S., Chryssoulis, S.L., and Ewing, R., 2005, Solubility of gold in arsenian pyrite: Geochemica et Cosmochimica Acta, v. 69, p. 2781–2796.

Reich, M., Deditius, A., Chryssoulis, S., Li, J.W., Ma, C.Q., Parada, M.A., Barra, F., and Mittermayr, F., 2013, Pyrite as a record of hydrothermal fluid evolution in a porphyry copper system: A SIMS/EMPA trace element study: Geochimica et Cosmochimica Acta, v. 104, p. 42–62.

Reimann, C., Filzmoser, P., and Garrett, R.G., 2002, Factor analysis applied to regional geochemical data: problems and possibilities: Applied Geochemistry, v. 17(3), p. 185–206.

Relvas, J.M., Barriga, F.J., Ferreira A., Noiva, P.C., Pacheco, N., Barriga, G., 2006, Hydrothermal alteration and mineralization in the Neves-Corvo volcanic-hosted massive sulfide deposit, Portugal: I. Geology, mineralogy, and geochemistry. Economic Geology, v. 101, p. 753–790.

Revan, M.K., Genc, Y., Maslennikov, V.V., Maslennikova, S.P., Large, R.R., Danyushevsky, L.V., 2014, Mineralogy and trace-element geochemistry of sulfide minerals in hydrothermal chimneys from the Upper Cretaceous VMS deposits of the eastern Pontide orogenic belt (NE Turkey): Ore Geology Reviews, v. 63, p. 129–149.

Richards, J.P., 2009, Post-subduction porphyry Cu-Au and epithermal Au deposits: Products of remelting of subduction-modified lithosphere: Geology, v. 37, p. 247–250,

Ritts, A., 2012, Texture and composition of pyrite contained in the mudstone host of the Eskay Creek sulfide and sulfosalt deposit, British Columbia: M.Sc. Thesis, Golden, Colorado, Colorado School of Mines, 185 p.

Robert, F., Poulsen, K.H., Cassidy, K.F., and Hodgson, C.J., 2005, Gold metallogeny of the Superior and Yilgarn cratons: 100th Anniversary Volume of Economic Geology, p. 1001–1033.

Rogers, N., Staal, C., Zagorevski, A., Skulski, T., Piercey, S., and Mcnicoll, V., 2007, Timing and tectonic setting of volcanogenic massive sulphide bearing terranes within the Central Mobile Belt of the Canadian Appalachians: in. Proceedings of Exploration, v. 7, p. 1199–1205.

Rollinson, H., 1993, Using geochemical data: Longman Scientific & Technical, Essex, UK, 352 p.

Ropchan, J.R., Luinstra, B., Fowler, A D., Benn, K., Ayer, J., Berger, B., Dahn, R., Labine, R. , and Amelin, Y., 2002, Host-rock and structural controls on the nature and timing of gold mineralization at the Holloway mine, Abitibi subprovince, Ontario: Economic Geology, v. 97, p. 291–309.

Rubingh, L.R.E. and S.R.L., 2019, Regional field mapping to determine the significance of a magnatotelluric anomaly in the Blake River Group, Katrine township, Northeastern Ontario. Ontario Geological Survey Open File Report 6360, p. 1–9.

Safina, N.P., Ayupova, N.R., Belogub, E., Maslennikov, V., Blinov, I.A., Zhukov, I.G., and Artem'ev, D. A., 2018, First Find of Ga-Bearing Minerals in Ores of Ural Massive Sulfide Deposits: in. Doklady Earth Sciences, v. 480(2), p. 746–749.

Sanborn-Barrie, M., and Skulski, T., 2005, Geology, Sturgeon Lake greenstone belt, western Superior Province, Ontario (scale 1:100 000): Geological Survey of Canada, Open File 1763.

Santander, M., and Valderrama, L., 2019, Recovery of pyrite from copper tailings by flotation: Journal of Materials Research and Technology, v. 8(5), pp.4312–4317.

Sawkins, F.J., 1976, Massive sulfide deposits in relation to geotectonics: Geological Association of Canada Special Paper 14, p. 222–240.

Schmidt, K., Garbe-Schönberg, D., Bau, M., and Koschinsky, A., 2010, Rare earth element distribution in> 400 C hot hydrothermal fluids from 5 S, MAR: The role of anhydrite in controlling highly variable distribution patterns: Geochimica et Cosmochimica Acta, v. 74(14), p.4058–4077.

Scott, G.M., 1996, The Geology and Tectonic History of the Central Uchi Subprovince: Ontario Geological Survey Open File Report 5952.

Scott, C.R., Mueller, W.U., and Pilote, P., 2002, Physical volcanology, stratigraphy, and lithogeochemistry of an Archean volcanic arc: evolution from plume-related volcanism to arc rifting of SE Abitibi Greenstone Belt, Val d'Or, Canada: Precambrian Research, v. 115(1–4).

Sharman, E.R., Taylor, B.E., Minarik, W.G., Dubé, B., and Wing, B.A., 2015, Sulfur isotope and trace element data from ore sulfides in the Noranda district (Abitibi, Canada): implications for volcanogenic massive sulfide deposit genesis: Mineralium Deposita, v. 50(5), p. 591–606.

Sharpe, J. I., 1968, Louvicourt Township, Abitibi-East County: Quebec Department of Natural Resources Geology Report 135, 53 p.

Sherlock, R.L., Roth, T., Spooner, E.T.C., and Bray, C.J., 1999, Origin of the Eskay Creek precious metal-rich volcanogenic massive sulfide deposit; fluid inclusion and stable isotope evidence: Economic Geology, v. 94(6), p. 803–824.

Sillitoe, R.H., Hannington, M.D., and Thompson, J.F.H., 1996, High sulfidation deposits in the volcanogenic massive sulfide environment: Economic Geology, v. 91(1), p. 204–212.

Sillitoe, R., 2008, Special Paper: Major Gold Deposits and Belts of the North and South American Cordillera: Distribution, Tectonomagmatic Settings, and Metallogenic Considerations: Economic Geology, v. 103, p. 663–687.

Sinclair, W.D., 1970, Geology of the No. 5 Zone, Horne mine, Noranda, Quebec, Canada: Unpublished M.Sc. thesis, Madison, Wisconsin, University of Wisconsin-Madison, 69 p.

Sinclair, W. D., 1971, A Volcanic Origin for the No. 5 Zone of the Horne Mine, Noranda, Quebec: Economic Geology, v. 66(8), p. 1225–1231.

Slack, J.F., Shanks, W.C., Karl, S.M., Gemery, P.A., Bittenbender, P.E., and Ridley, W.I., 2005, Geochemical and Sulfur Isotopic Signature of Volcanogenic Massive Sulfide Deposits on Prince of Wales Island and Vicinity, Southeastern Alaska: USGS Professional Paper 1732-C, 37 p.

Smith, R.N., and Huston, D.L., 1992, Distribution and association of selected trace elements at the Rosebery deposit, Tasmania: Economic Geology, v. 87, p. 706–719.

Solomon, M., 1976, Volcanic massive sulphide deposits and their host rocks: A review and an explanation: in. K.H. , Wolf, K.H., ed., Handbook of strata-bound and stratiform ore deposits, II: Regional studies and specific deposits, p. 1307–1328. Amstedam, Elsevier.

Stanley, C.R., 2005, Numerical transformation of geochemical data: 1. Maximizing geochemical contrast to facilitate information extraction and improve data presentation: Geochemistry: Exploration, Environment, Analysis, v. 5, p. 1–11.

Stanton, R. L., 1990, Magmatic evolution and the ore type-lava type affiliations of volcanic exhalative ores., Australasian Institute of Mining and Metallurgy Monograph, v. 14, p. 101–108.

Stanton, R. L., 1994, Ore elements in arc lavas. Oxford monographs on geology and geophysics. Clarendon, New York, 404 p.

Stephens, M.B., Swinden, H.S., and Slack, J.F., 1984, Correlation of massive sulfide deposits in the Appalachian-Caledonian orogen on the basis of paleotectonic setting: Economic Geology, v. 79, no. 7, p. 1442–1478.

Swinden, H.S., and Thorpe, R.I., 1984, Variations in style of volcanism and massive sulfide deposition in Early to Middle Ordovician island-arc sequences of the Newfoundland Central Mobile Belt: Economic Geology, v. 79, no. 7, p. 1596–1619.

Stern, R. A., 1995, Paleoproterozoic (1.86-1.90 Ga) arc volcanism in the Flin Flon belt, Trans-Hudson Orogen, Canada: Contributions to Mineralogy and Petrology, v. 119, p. 117-141.

Stern, R. J., 2008, Modern-style plate tectonics began in Neoproterozoic time: An alternative interpretation of Earth's tectonic history: in. Condie, K.C., Pease, V., ed., When Did Plate Tectonics Begin on Planet Earth?: Geological Society of America, Special Paper 440, p. 265–280.

Steven, M., 1997, Geology, Petrology, and Geochemistry of the Potter Doal Cu-Zn Deposit, Kidd-Munro Assemblage, Munro Township, Ontario: MSc Thesis, McMaster University, Hamilton, Ontario.

Syme, E.C., and Bailes, A.H., 1993, Stratigraphic and Tectonic Setting of Early Proterozoic Volcanogenic Massive Sulfide Deposits, Flin Flon, Manitoba. Economic Geology, v. 88, p. 566–589.

Syme, E.C., 1999, Contrasting arc and MORB-like assemblages in the Paleoproterozoic Flin Flon Belt, Manitoba, and the role of intra-arc extension in localizing volcanic-hosted massive sulphide deposits, Canadian Journal of Earth Sciences, v. 36(11), p. 1767–1788.

Taylor, S.R. and McLennan, S.M., 1985. The continental crust: its composition and evolution.

Thurston, P.C., 1994, Archean volcanic patterns: in. Condie, K.C., ed., Archean Crustal Evolution: Developments in Precambrian Geology, 11, Elsevier, Amsterdam, p. 45-84.

Thurston, P.C., and Fryer, B.J., 1983, The geochemistry of repetitive cyclical volcanism from basalt through rhyolite in the Uchi-Confederation greenstone belt, Canada: Contributions to Mineralogy and Petrology, v. 83, p. 204–226.

Thurston, P.C., Ayer, J.A., Goutier, J., and Hamilton, M.A., 2008, Depositional gaps in Abitibi greenstone belt stratigraphy: A key to exploration for syngenetic mineralization: Economic Geology, v. 103, p. 1097–1134.

Thurston, P.C., Kamber, B.S., and Whitehouse, M., 2012, Archean cherts in banded iron formation: Insight into Neoarchean ocean chemistry and depositional processes: Precambrian Research, v. 214, p. 227–257.

Thomas, H., Large, R.R., Bull, S.W., Maslennikov, V., Berry, R.F., Fraser, R., Froud, S., and Moye, R., 2011, Pyrite and Pyrrhotite Textures and Composition in Sediments, Laminated Quartz Veins, and Reefs at Bendigo Gold Mine, Australia: Insights for Ore Genesis: Economic Geology, v. 106(1), p. 1–31.

Thorpe, R.I., and Harris, D.C., 1973, Mattagamite and tellurantimony, two new telluride minerals from Mattagami Lake mine, Matagami area, Quebec: Canadian Mineralogist, v. 12, p. 55–60.

Tourigny, G., Doucet, D., and Bourget, A., 1993, Geology of the Bousquet 2 mine: An example of a deformed, gold-bearing, polymetallic sulfide deposit: Economic Geology, v. 88, p. 1578−1597.

Trowell, N.F., 1974, Geology of the Bell Lake-Sturgeon Lake Area, Districts of Kenora and Thunder Bay: Ontario Division of Mines, Geological Report 114, 67 p.

Turek, A. , Tetley, N., and Jackson, T., 1976, A study of metal dispersion around the Fox orebody in Manitoba: Canadian Institute of Mining Bulletin , v. 69(770), p. 104–110.

Urabe, T., 1985, Aluminous granite as a source magma of hydrothermal ore deposits: An experimental study: Economic Geology, v. 80, p. 148–157.

Urabe, T, 1987, Kuroko deposit modeling based on magmatic hydrothermal theory: Mining Geology, v. 37, p. 159–176.

van Breemen, O., Heather, K.B., and Ayer, J.A., 2006, U-Pb geochronology of the Neoarchean Swayze sector of the southern Abitibi greenstone belt: Geological Survey of Canada Current Research 2006-F1, 32 p.

van Staal, C.R., Wilson, R.A., Rogers, N., Fyffe, L.R., Langton, J.P., McCutcheon, S.R., McNicoll, V·, and Ravenhurst, C.E., 2003, Geology and tectonic history of the Bathurst Supergroup, Bathurst Mining Camp, and its relationships to coeval rocks i n southwestern New Brunswick and adjacent Maine—a synthesis: Economic Geology Monograph 11, p. 37–60.

Walker, S.D., and Cregheur, P., 1982, The Chadbourne mine, Noranda, Quebec: A gold-bearing breccia: in Hodder, R.W., and Petruk, W., ed., Geology of Canadian gold deposits: The Canadian Institute of Mining and Metallurgy, Special Volume 24, p. 58–66.

Wang, Z, and Becker, H., 2015, Abundances of Ag and Cu in mantle peridotites and the implications for the behavior of chalcophile elements in the mantle: Geochimica et Cosmochimica Acta, v. 160, p. 209–226.

Wedepohl, K.H., 1995, The composition of the continental crust: Geochimica et cosmochimica Acta, v. 59(7), p.1217–1232.

Wersin, P., Hochella, M.F., Persson, P., Redden, G., Leckie, J.O., and Harris, D.W., 1994, Interaction between aqueous uranium (VI) and sulfide minerals: Spectroscopic evidence for sorption and reduction: Geochimica et Cosmochimica Acta, v. 58(13), p. 2829–2843.

Whalen, J.B., McNicoll, V.J., Galley, A., and Longstaffe, F.J., 2004, Tectonic and metallogenic importance of an Archean composite high- and low-Al tonalite suite, western Superior Province, Canada: Precambiran Research, v. 132, p. 275–301.

Wheeler, J.O., Brookfield, A.J., Gabrielse, H., Monger, J.W.H., Tipper, H.W., and Woodsowrth, G.J., 1988, Terrane map of the Canadian Cordillera: Geological Survey of Canada, Open File 1984.

Wheeler, J.O., Hoffman, P.F., Card, K.D., Davidson, A, Sanford, B.V., Okulitch, A.V., Roest, W.R., 1996, Geological Survey of Canada, "A" Series Map 1860A, 3 sheets; 1 CD-ROM.

White, W.M. and Klein, E.M., 2014, 4.13-Composition of the oceanic crust: in. Holland, H.D., and Turekian, K.K., ed., Treatise on geochemistry, 2nd edn., p.457–496. Elsevier, Oxford.

Williams, H., 1979, Appalachian Orogen in Canada: Canadian Journal of Earth Sciences, v. 16(3), p. 792–807.

Williams, H., Colman-sadd, S.P., and Swinden, H.S., 1988, Tectonic-stratigraphic subdivisions of central Newfoundland: Current Research, Part B. Geological Survey of Canada, Paper 88, p.91–98.

Williams, H.R., Stott, G.M., Heather, K.B., and Muir, T.L., 1991, Wawa Subprovince: in. Geology of Ontario, Ontario Geological Survey, Special Vol. 4, Part 1, p. 485–541.

Winchester, J.A., and Floyd, P.A., 1977\, Geochemical discrimination of different magma series and their differentiation products using immobile elements: Chemical geology, v. 20, p. 325–343.

Wise, A.S., Watters, R.L., 2012. Certificate of Analysis, Standard Reference Material 610: National Institute of Standards and Technology. http://www.nist.gov/srm.

Wohlgemuth-Ueberwasser, C.C., Ballhaus, C., Berndt, J., Stotter, V., Meisel, T., 2007, Synthesis of PGE sulfide standards for laser ablation inductively coupled plasma mass spectrometry (LA-ICP-MS): Contributions Mineral. Petrology, v. 154, p. 607–617.

Wohlgemuth-Ueberwasser, C.C., McClung, C.R., Viljoen, F., 2014, Metamorphic alteration of the massive sulfide horizon from the Salt River VMS deposit (South Africa): Ore Geology Reviews, v. 56, p. 45–52.

Yamashita, K., Creaser, R A., Jensen, J.E., and Heaman, L.M., 2000, Origin and evolution of mid- to late-Archean crust in the Hanikahimajuk Lake area, Slave Province, Canada; evidence from U–Pb geochronological, geochemical and Nd–Pb isotopic data: Precambrian Research, v. 99(3), p. 197–224.

Yang, K., and Scott, S D., 1996, Possible contribution of a metal-rich magmatic fluid to a sea-floor hydrothermal system: Nature, v.383(6599), p. 420–423.

Yang, K., and Scott, S.D., 2003, Geochemical relationships of felsic magmas to ore metals in massive sulfide deposits of the Bathurst mining camp, Iberian pyrite belt, Hokuroku district, and the Abitibi belt: Economic Geology, p. 457–478.

Yang, K., and Scott, S.D., 2006, Magmatic fluids as a source of metals in arc/back-arc hydrothermal systems: Evidence from melt inclusions and vesicles: in. Christie, D.M., Fisher, C.R., and Lee, S.M., ed., Back-Arc Spreading Systems: Geological, Biological, Chemical, and Physical Interactions. Geophysical Monograph Series, v. 166, p. 163–184. Washington, DC: American Geophysical Union.

Yukon Geological Survey, 2005, Hart River: Yukon MINFILE Record no. 116A 009.

Zachrisson, E., 1982, Spilitization, mineralization, and vertical zonation at the Stekkenjokk stratabound sulfide deposit, Scandinavian Caledonides: Institution of Mining and Metallurgy Transactions, v. 91, p. 192–199.

Zaleski, E., and Peterson, V.L., 1995, Depositional setting and deformation of massive sulfide deposits, iron formation, and associated alteration in the Manitouwadge greenstone belt, Superior Province, Ontario: Economic Geology, v. 90, p. 2244–2261.

Zaleski E., van Breemen O., and Peterson V.L., 1999, Geological evolution of the Manitouwadge greenstone belt and Wawa–Quetico subprovince boundary, Superior Province,

Ontario, constrained by U–Pb zircon dates of supracrustal and plutonic rocks: Canadian Journal of Earth Sciences, v. 36(6), p. 945–966.

A. Appendix

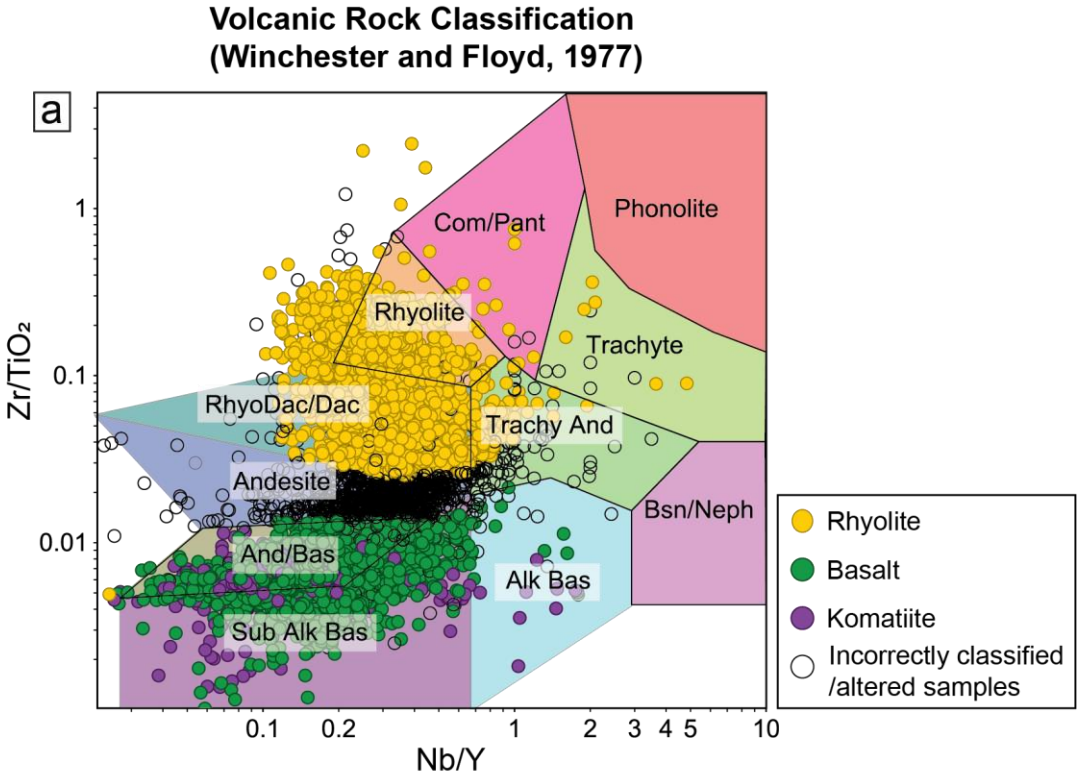
Volcanic Rock Classification
(Winchester and Floyd, 1977)
a
Com/Pant
Phonolite
Rhyolite
Trachyte
RhyoDac/Dac
Trachy And
Andesite
Bsn/Neph
And/Bas
Alk Bas
Sub Alk Bas
Zr/TiO₂
Nb/Y
Rhyolite
Basalt
Komatiite
Incorrectly classified
/altered samples

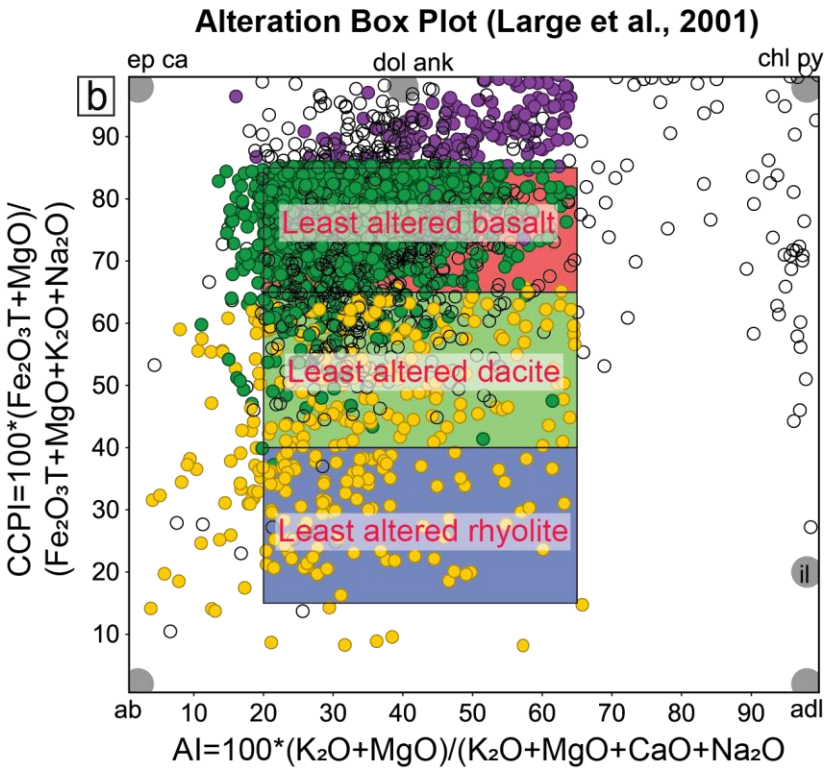
Alteration Box Plot (Large et al., 2001)
b
ep ca
dol ank
chl py
Least altered basalt
Least altered dacite
Least altered rhyolite
il
ab
adl
CCPI=100*(Fe₂O₃T+MgO)/
(Fe₂O₃T+MgO+K₂O+Na₂O)
AI=100*(K₂O+MgO)/(K₂O+MgO+CaO+Na₂O

Figure A.1 Plots used to filter volcanic rock samples from the database for quality. a) Binary plot of Nb/Y vs. Zr/Tio_2 ratios (Winchester and Floyd, 1977) of volcanic rock samples used to check classification by composition. Samples plotting in the andesite field or outside of their respective felsic and mafic fields were removed from further analysis. b) box plots of the Ishikawa alteration index (AI: Ishikawa et al., 1976) vs. chlorite-carbonate-pyrite index (CCPI and diagram: Large et al., 2001c) used to select the least-altered volcanic rocks samples from the database. All samples with an AI >65 were removed. Rhyolite samples with a CCPI > 65 were removed. Basalt samples with a CCPI >85 were removed. Abbreviations: $AI=100*(K_2O+MgO)/(K_2O+MgO+CaO+Na_2O)$, $CCPI=100*(Fe_2O_3T+MgO)/(Fe2O_3T+MgO+K_2O+Na_2O)$.

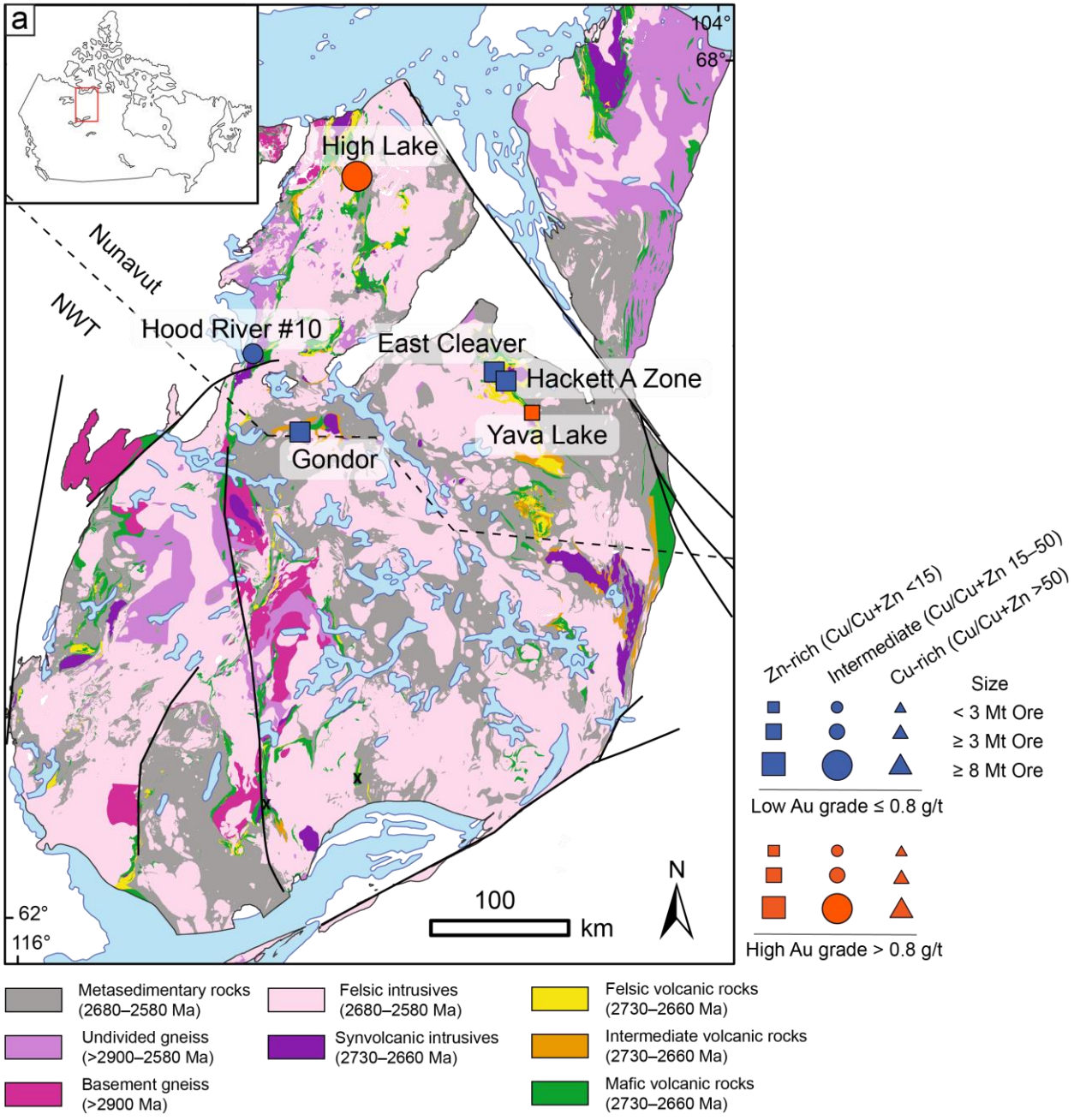
a
104°
68°
High Lake
Nunavut
NWT
Hood River #10
East Cleaver
Hackett A Zone
Yava Lake
Gondor
62°
116°
100
km
N
Zn-rich (Cu/Cu+Zn <15)
Intermediate (Cu/Cu+Zn 15–50)
Cu-rich (Cu/Cu+Zn >50)
Size
< 3 Mt Ore
≥ 3 Mt Ore
≥ 8 Mt Ore
Low Au grade ≤ 0.8 g/t
High Au grade > 0.8 g/t
Metasedimentary rocks (2680–2580 Ma)
Undivided gneiss (>2900–2580 Ma)
Basement gneiss (>2900 Ma)
Felsic intrusives (2680–2580 Ma)
Synvolcanic intrusives (2730–2660 Ma)
Felsic volcanic rocks (2730–2660 Ma)
Intermediate volcanic rocks (2730–2660 Ma)
Mafic volcanic rocks (2730–2660 Ma)

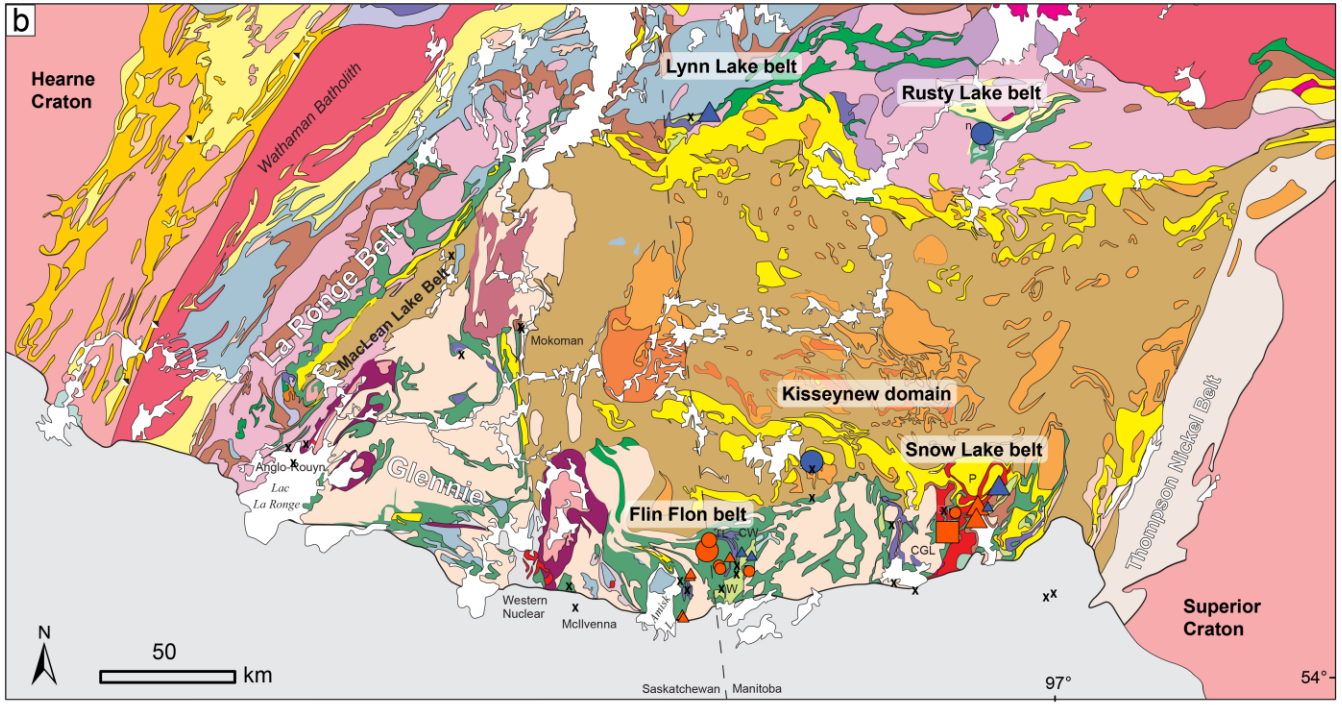

Proterozoic

POST- TRANS-HUDSON BASINS

- Phanerozoic cover
- Late- Paleoproterozoic Athabasca Basin

PROTEROZOIC PLUTONIC SUITES

Glennie and Kisseynew domains

- Ca. 1.84 Ga felsic plutonic rocks
- Ca. 1.835 Ga enderbite
- Predominantly diatexite derived from turbidites

La Ronge - Lynn Lake Domain

- 1.86-1.85 Ga Satellite intrusions
- 1.86-1.85 Ga Wathaman-Chipewyan continental arc
- Ca. 1.87 Ga Pool Lake intrusive suite; tonalite, gabbro
- 1.90-1.88 Ga juvenile and evolved arc pluton

Glennie - Flin Flon Complex

- Ca. 1.84 Ga gabbro
- 1.84-1.83 Ga late successor arc plutons
- 1.90-1.86 Ga early juvenile arc + early successor arc plutons of the Glennie-Flin Flon Complex

INTER-ARC, BACK-ARC, FORELAND BASINS

- 1.85-1.835 Ga meta-turbidite; arkose, conglomerate
- 1.88-1.86 Ga arkose, conglomerate, psammite
- ≥1.88 Ga pelites and psammites

JUVENILE VOLCANIC SEQUENCES

- 1.88-1.84 Ga intermediate to felsic rocks of the Lynn Lake and Flin Flon belts
- 1.92-1.88 Ga undivided arc, back-arc, ocean floor and ocean plateau volcanics
- (1900–1880 Ma) Calc-alkaline volcanics, arc rift basalt tholeiitic, mafic-felsic volcanics

PROTEROZOIC COVER SEQUENCE

- Wollaston Group (lower/upper sequences

Archean

La Ronge - Lynn Lake Domain

- Ca. 2.56 Ga Swan River Complex
- 2.68-2.58 Ga Peter Lake Domain orthogneis

Hearne, Superior and Sask Cratons

- Mixed Archean-Paleoproterozoic tectonite
- Reactivated Superior Craton margin and cover
- Archean felsic orthogneiss and plutonic rocks

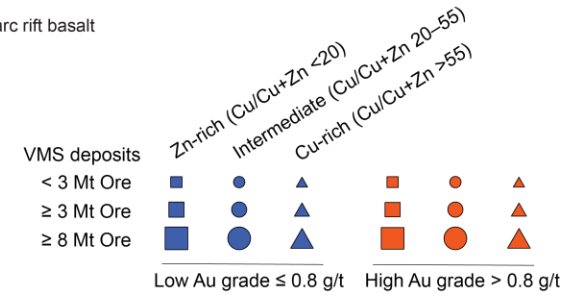

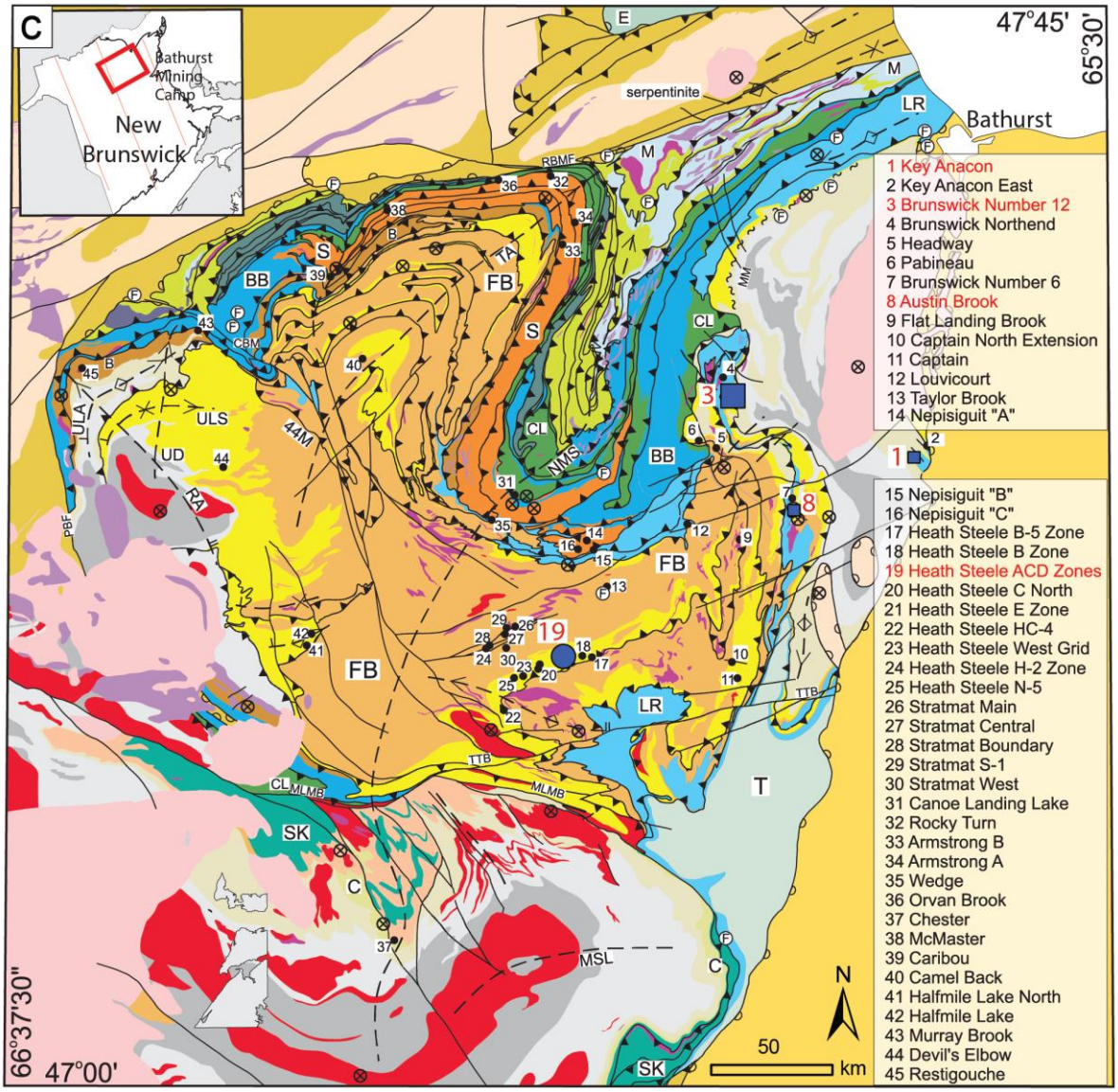

Carboniferous

- Sedimentary rocks
- Gabbro
- Granite

Upper Silurian - Devonian

- Granite
- Gabbro
- Sedimentary and volcanic rocks

Silurian

- Sedimentary and volcanic rocks

Middle Ordovician- Lower Silurian

- Blueschist nappe

Fournier Group

- Elmtree Formation (E)
- Millstream Formation (M)
- Sormany Formation

California Lake Group

- Boucher Brook Formation (BB)
- Mount Brittain Formation (B)
- Spruce Lake Formation (S)
- Canoe Landing Lake Formation (CL)

Tetagouche Group

- Tomogonops Formation (T)
- Little River Formation (LR)
- Flat Landing Brook Formation (FB)
- Nepisiguit Falls Formation

Sheephouse Brook Group

- Slacks Lake Formation (SK)
- Sevogle River Formation
- Clearwater Stream Formation (C)

Cambrian - Lower Ordovician

Miramichi Group

- Patrick Brook Formation
- Knights Brook Formation
- Chain of Rocks Formation

- fold axis
- fault
- thrust fault
- unconformity
- U-Pb zircon age
- fossil localit
- mélange

VMS deposits

- < 3 Mt Ore
- ≥ 3 Mt Ore
- ≥ 8 Mt Ore

Zn-rich (Cu/Cu+Zn <20)
Intermediate (Cu/Cu+Zn 20–55)
Cu-rich (Cu/Cu+Zn >55)

Low Au grade ≤ 0.8 g/t
High Au grade > 0.8 g/t

Figure A.2 Simplified geological maps of other VMS hosting terranes in Canada with pyrite samples represented in the database. a) The main volcanic belts of the Slave Craton (modified after Mills et al., 2016). Labeled greenstone belts are the Amooga Booga Volcanic Belt (ABVB), Hackett River Volcanic Belt (HRVB), and High Lake Volcanic Belt (HLVB) (Stubley, 2005). The locations of sampled VMS deposits with pyrite trace element analyses from Jonasson et al. (2020) are shown symbolized according to Cu(Cu+Zn) grades, Au grades, and tonnages. b) The main tectonostratigraphic units of the Reindeer zone within the Trans-Hudson orogen (THO) (Modified after Corrigon et al., 2007). The locations of sampled VMS deposits with pyrite trace element analyses from Jonasson et al. (2020) are shown symbolized according to Cu(Cu+Zn) grade ratios, Au grades, and tonnages. The majority of analyzed deposits are represented in the Flin Flon and Snow Lake belts that dominant the THO in terms of metal endowment. Pyrite samples from VMS deposits from the Kisseynew domain, Lynn Lake Belt, and Rusty Lake Belt are also examined. c) The Bathurst camp situated in northeastern New Brunswick within the Appalachian orogen (Modified after van Staal et al. 2003; Goodfellow et al., 2007). The locations of sampled VMS deposits with pyrite trace element analyses from Jonasson et al. (2020) are shown symbolized according to Cu(Cu+Zn) grade ratios, Au grades, and tonnages. Abbreviations: MLMB - Moose Lake-Mountain Brook fault; MSL - Mullin Stream Lake structure; TA - Tetagouche antiform; TTB -Tomogonops - Tozer Brook fault; UD - Upsalquitch dome; ULA - Upsalquitch Lake antiform; ULS - Upsalquitch Lake synform.

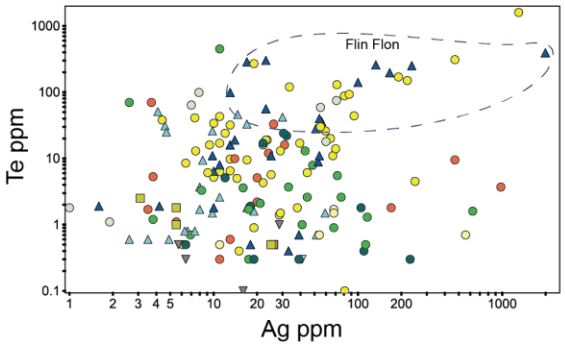
Flin Flon
Te ppm
Ag ppm

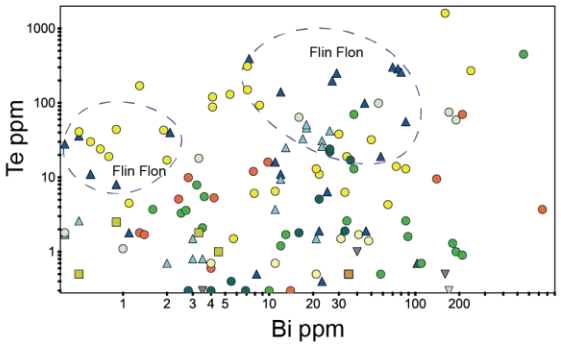
Flin Flon
Flin Flon
Te ppm
Bi ppm

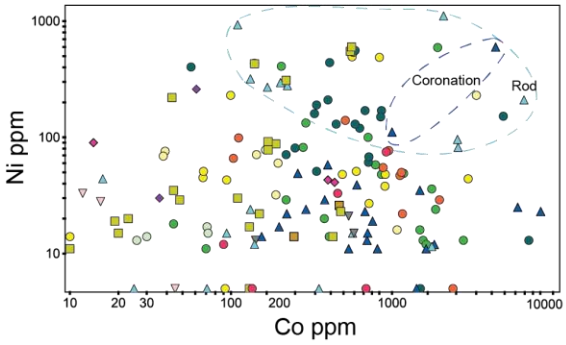
Coronation
Rod
Ni ppm
Co ppm

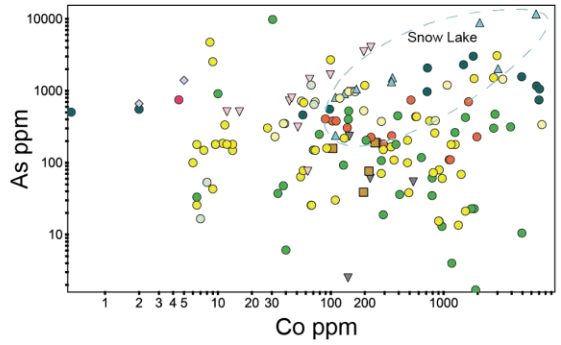
Snow Lake
As ppm
Co ppm

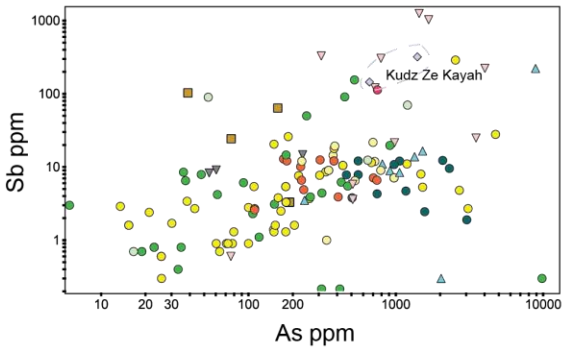
Kudz Ze Kayah
Sb ppm
As ppm

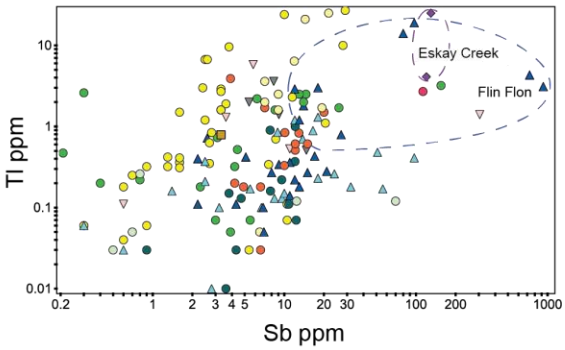
Eskay Creek
Flin Flon
Tl ppm
Sb ppm

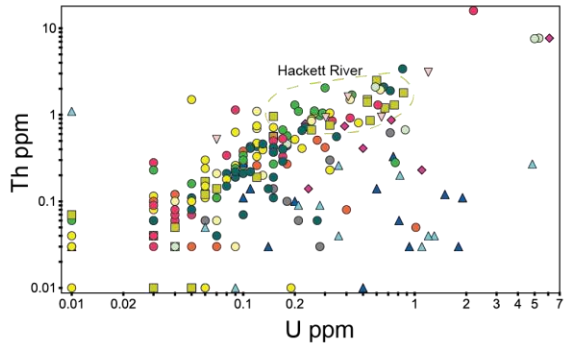
Hackett River
Th ppm
U ppm

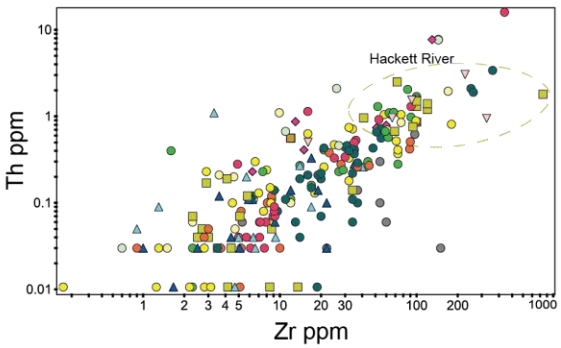
Hackett River
Th ppm
Zr ppm

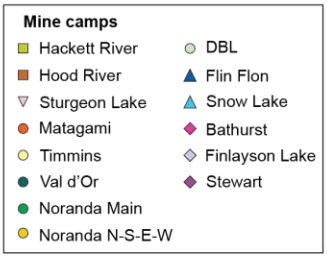
Mine camps
Hackett River
Hood River
Sturgeon Lake
Matagami
Timmins
Val d'Or
Noranda Main
Noranda N-S-E-W
DBL
Flin Flon
Snow Lake
Bathurst
Finlayson Lake
Stewart

Figure A.3 Binary plots of select trace element concentrations (ppm) in pyrite samples from VMS deposits in the Superior Province that differ from pyrite samples from VMS in the Slave Province, and in Proterozoic and younger orogens across Canada. Samples are classified by mine camps of the sampled deposits. Enriched element Abbreviations: East Sullivan (ES), Robb-Montbray (RB).

Table A.1. Classification and additional compiled information of VMS deposits with samples considered in this study. Mineral abbreviations: chalcopyrite (Cp), pyrite (Py), pyrrhotite (Po), sphalerite (Sp), galena (Gn), magnetite (Mt), arsenopyrite (Asp), marcasite (Mr).

Name	Host-Rock-Type	Refined host rock classes	FW rocks underlying ore	Metamorphic Grade	Main ore minerals	Trace ore minerals	Trace Mineral Group	Tectonic Setting	Felsic Affinity	References
Abcourt-Barvue	Bimodal-mafic	Felsic-dominant	rhyolite tuff, andesite, gabbro sills	Greenschist			Antimonides	mature epicontinental arc	FII	Drouin (1978), Bérubé (2014)
Conigo-Jay	Bimodal-mafic	Felsic-dominant	rhyolite tuff	Greenschist	Cp, Py, Po, Sp, Gn	Asp, Mt, pyrargyrite	Bismuthides	mature epicontinental arc	FII	Drouin (1978), Chartrand (1991), Divi et al. (1980), Mosier et al. (2009), Bérubé (2014)
Mogador (Vendome)	Bimodal-mafic	Intermediate	rhyolite tuff	Greenschist			None	mature epicontinental arc	FII	Bérubé (2013)
Joutel Copper	Bimodal-mafic	Felsic-dominant	rhyolite	Greenschist	Cp, Py, Po		Selenides	rifted island arc	FIIIa	Mosier et al. (2009), Legault et al. (2002)
Poirier	Bimodal-mafic	Felsic-dominant	rhyolite flow	Greenschist			Arsenides	rifted island arc	FIIIa	Mosier et al. (2009), Legault et al. (2002)
Bell Allard	Bimodal-mafic	Intermediate	rhyolite-intermediate dike (200 m), gabbro (50 m), rhyolite (50 m)	Lower Greenschist			Arsenides	oceanic rifted arc	FIIIb	Lavallière (1995), Hart (1984), Barrie et al. (1993), Lavalliére et al. (1994), Hoffe and Lines, 1997, Mosier et al. (2009), Debreil et al. (2018)
Isle Dieu	Bimodal-mafic	Intermediate	rhyolite flows (20 m), tonalite dike (>100 m)	Lower Greenschist	Cp, Py, Po, Sp, Gn	Asp, Mt, Mr, tetrahedrite	Bismuthides	oceanic rifted arc	FIIIb	Lavallière (1995), Hart (1984), Barrie et al. (1993), Lavalliére et al. (1994), Hoffe and Lines, 1997, Mosier et al. (2009), Debreil et al. (2018)
Mattagami Lake	Bimodal-mafic	Mafic-dominant	vitroclastic rhyolite (80 m), andesite flow (117 m), pillow andesite (30 m), andesite pyroclastics (5 m)	Lower Greenschist	Cp, Py, Po, Sp, Gn	Altaite, Asp, hessite, ilmenite, Mt, Mr, mattagamite, molybdenite, rhodochrosite, telluroantimony	Tellurides	oceanic rifted arc	FIIIb	Lavallière (1995), Hart (1984), Barrie et al. (1993), Lavalliére et al. (1994), Hoffe and Lines, 1997, Mosier et al. (2009), Debreil et al. (2018)
New Hosco	Bimodal-mafic	Intermediate	agglomerate-tuff, rhyolite, gabbro plug	Lower Greenschist	Cp, Py, Po, Sp	Mt, Mr,	None	oceanic rifted arc	FIIIb	
Norita-Radiore A	Bimodal-mafic	Intermediate	chert-volcaniclastics (3 m), rhyolite (60 m), tuff (60 m), rhyolite (60 m), tuff (75 m), rhyolite (30 m), tonalite (>20 m)	Lower Greenschist	Cp, Py, Po, Sp	Mt	Tellurides	oceanic rifted arc	FIIIb	Hart (1984), Piche et al. (1993), Barrie et al. (1993), Lavallière (1995), Mosier et al. (2009)
Orchan	Bimodal-mafic	Intermediate	rhyolite flow (80 m), basalt flow or gabbro (50 m), rhyolite (>20 m)	Lower Greenschist	Cp, Py, Po, Sp	Mt	Selenides	oceanic rifted arc	FIIIb	Hart (1984), Barrie et al. (1993), Lavallière (1995), Mosier et al. (2009), Debreil et al. (2018),
Bousquet #2	Bimodal-mafic	Intermediate	basalt overlain by calc-alkaline dacitic to rhyodacitic domes and flow breccias and local thin andesitic intervals and dikes (within 100 m?)	Upper greenschist-lower amphibolite	Cp, Py, Po, Sp, Gn	Asp, bornite, chalcocite, electrum, covellite, digenite, tennantite, tellurobismuthite, tetrahedrite, native tellurium, calaverite, stannite, colusite, renierite, petzite, wittchenite, alabandite, aikinite, mawsonite, altaite, mackinstryite, pretzite, acanthite, hessite	Tellurides	juvenile arc back arc	FI_FII	Tourigny et al. (1993), Lafrance (2003), Mercier-Langevin (2005), Mercier-Langevin (2007), Mosier et al. (2009), Dube et al. (2014)
Dumagami	Bimodal-mafic	Intermediate	basalt overlain by calc-alkaline dacitic to rhyodacitic domes and flow breccias and local thin andesitic intervals and dikes (within 100 m?)	Upper greenschist-lower amphibolite	Cp, Py, Po, Sp	Bornite, calaverite, chalcocite, native gold, stannite, stromeyerite, tellurobismuthite	Tellurides	juvenile arc back arc	FI_FII	Marquis et al. (1990), Lafrance (2003), Mercier-Langevin (2005), Mercier-Langevin (2007), Mosier et al. (2009), Dube et al. (2014)
Amulet A-Upper& Lower	Bimodal-mafic	Mafic-dominant	andesite flow (600 m)	Greenschist	Cp, Py, Po, Sp	Mr	Selenides	mature arc back arc	FIIIa	Kerr and Gibson (1993), Mercier-Langevin (2007), Gaboury and Pearson (2008), Mosier et al. (2009)
Amulet-C	Bimodal-mafic	Mafic-dominant	flow-mafic	Greenschist	Cp, Py, Po, Sp	Mr	Antimonides	mature arc back arc	FIIIa	Kerr and Gibson (1993), Mercier-Langevin (2007), Gaboury and Pearson (2008), Mosier et al. (2009)
Ansil	Bimodal-mafic	Felsic-dominant	rhyolite (500-700 m)	Lower Greenschist	Cp, Py, Po, Sp	Mt	Tellurides	mature arc back arc	FIIIa	Kerr and Gibson (1993), Mercier-Langevin (2007), Gaboury and Pearson (2008), Mosier et al. (2009)
Bedford	Bimodal-mafic	Intermediate	andesite flow	Greenschist	Cp, Py, Po, Sp			mature arc back arc	FIIIa	Mercier-Langevin (2007), Gaboury and Pearson (2008), Mosier et al. (2009)
Corbet	Bimodal-mafic	Mafic-dominant	chert-andesite volcaniclastic (5-20 m), andesite flow (>30 m)	Greenschist	Cp, Py, Po, Sp, Gn	Gold, krennerite, mackinawite, Mt, tetrahymite	Bismuthides	juvenile arc back arc	FIIIa	Barret et al. (1993), Kerr and Gibson (1993), Mercier-Langevin (2007), Gaboury and Pearson (2008), Mosier et al. (2009)
East Waite	Bimodal-mafic	Intermediate	rhyolite flow (300 m), andesite flow (100 m), rhyolite flow (500 m), andesite (350 m), rhyolite (300 m), andesite (300 m)	Greenschist	Cp, Py, Po, Sp	Mr	Tellurides	juvenile arc back arc	FIIIa	Mercier-Langevin (2007), Gaboury and Pearson (2008), Mosier et al. (2009)
Millenbach	Bimodal-mafic	Felsic-dominant	pillow andesite (0-60 m), tuff (0-0.3 m), rhyolite flow-flow breccia (>900 m)	Sub Greenschist	Cp, Py, Po, Sp	Asp, gahnite, mackinawite, Mt, silver	None	juvenile arc back arc	FIIIa	Mercier-Langevin (2007), Gaboury and Pearson (2008) Riverin & Hodgson (1980) Mercier-Langevin (2007), Mosier et al. (2009)
Moosehead (C Contact)	Bimodal-mafic	Mafic-dominant	Flow-mafic	Greenschist	Py, Sp, Gn		Antimonides	mature arc back arc	FIIIa	Mercier-Langevin (2007), Gaboury and Pearson (2008), Mosier et al. (2009)
Norbec & Lac Dufault	Bimodal-mafic	Felsic-dominant	rhyolite cherty tuff-rhyolite breccia (150 m), andesite flow, rhyolite (500 m),	Greenschist	Cp, Py, Po, Sp, Gn	Argentite, chalcocite, cubanite, dyscrasite, mackinawite, Mt, Mr, stannite	Antimonides	juvenile arc back arc	FIIIa	Shriver & MacLean (1992), Mercier-Langevin (2007), Gaboury and Pearson (2008), Mosier et al. (2009)
Old Waite	Bimodal-mafic	Mafic-dominant	rhyolite flow (200 m), andesite flow (150 m), rhyolite flow (600 m), andesite (350 m), rhyolite (300 m), andesite (250 m)	Greenschist	Cp, Py, Po, Sp, Gn	Calaverite, cosalite, Mr, silver	Selenides	juvenile arc back arc	FIIIa	Mercier-Langevin (2007), Gaboury and Pearson (2008), Mosier et al. (2009)

Table A.1. cont.

Name	Host-Rock-Type	Refined host rock classes	FW rocks underlying ore	Metamorphic Grade	Main ore minerals	Trace ore minerals	Trace Mineral Group	Tectonic Setting	Felsic Affinity	References
Quemont	Bimodal-mafic	Felsic-dominant	rhyolite tuff-agglomerate-rhyolite breccia- rhyolite porphyry (300 m), rhyolite (350 m)	Sub Greenschist	Cp, Py, Po, Sp	Altaite, calaverite, electrum, hessite, krennerite, Mt, Mr, pentlandite, sylvanite, tetradymite	Tellurides	juvenile arc back arc	FIIIa	Campbell and Williams (1968), Kerr and Gibson (1993), Mercier-Langevin (2007), Gaboury and Pearson (2008), Mosier et al. (2009)
Vauze	Bimodal-mafic	Felsic-dominant	rhyolite breccia-dacite flow-breccia (400 m), andesite flow (100 m), rhyolite (500 m), andesite (300 m), rhyolite (250 m), andesite (350 m)	Lower Greenschist	Cp, Py, Po, Sp	Bornite, Mt,	Selenides	juvenile arc back arc	FIIIa	Spence (1975), Kerr and Gibson (1993), Mercier-Langevin (2007), Gaboury and Pearson (2008), Mosier et al. (2009)
Aldermac	Bimodal-mafic	Intermediate	rhyolite tuff-rhyolite breccia (61-152 m), gabbro, quartz diorite	Greenschist	Cp, Py, Po, Sp	Brochantite, Mt, Mr,	Tellurides	mature arc back arc	FIIIa	Kerr and Gibson (1993), Mercier-Langevin (2007), Gaboury and Pearson (2008), Mosier et al. (2009)
Delbridge	Bimodal-mafic	Felsic-dominant	rhyolite porphyry (500 m)	Sub Greenschist	Cp, Py, Sp, Gn	Asp, electrum, silver, tetrahedrite	Arsenides	juvenile arc back arc	FIIIa	Mercier-Langevin (2007), Gaboury and Pearson (2008), Mosier et al. (2009)
Deldona	Bimodal-mafic	Felsic-dominant	rhyolite porphyry (500 m)	Greenschist	Cp, Py, Sp, Gn	Asp, electrum, silver, tetrahedrite	Antimonides	mature arc back arc	FIIIa	Mercier-Langevin (2007), Gaboury and Pearson (2008), Mosier et al. (2009)
Gallen	Bimodal-mafic	Felsic-dominant	rhyolite tuff-breecia	Sub Greenschist	Cp, Py, Po, Sp, Gn		None	juvenile arc back arc	FIIIa	Mercier-Langevin (2007), Gaboury and Pearson (2008), Mosier et al. (2009)
Horne #5 Zone	Bimodal-mafic	Felsic-dominant	rhyolite tuff-agglomerate-rhyolite breccia- rhyolite porphyry (300 m), rhyolite (350 m)	Sub Greenschist	Cp, Py, Gn	Po, Mt, Gn, stannite, ilmenite, rutile, altaite, hessite, petzite, cassiterite, electrum, native gold, scheelite, sylvanite	Tellurides	mature arc back arc	FII_FIII	Price (1933), Autran et al. (1966), Sinclair (1970), Maclean & Hoy (1991), Catallani et al. (1993), Mercier-Langevin (2007), Mosier et al. (2009), Monecke et al. (2017)
Horne-H&G	Bimodal-mafic	Felsic-dominant	rhyolite tuff-agglomerate-rhyolite breccia- rhyolite porphyry (300 m), rhyolite (350 m)	Sub Greenschist	Cp, Py, Po, Sp	Altaite, calaverite, petzite, hessite, krennerite, molybdenite, rickardite, sylvanite, tetradymite, tetrahedrite, tellurobismuthite	Bismuthides	juvenile arc back arc	FII_FIII	Price (1933, 1934), Cabri (1965), Maclean & Hoy (1991), Mercier-Langevin (2007), Mosier et al. (2009)
Mobrun	Bimodal-mafic	Intermediate	rhyolite flows (160 m), andesite pyroclastics-rhyolite pyroclastics (20 m), spherulitic rhyolite flow (120 m), andesite flows (120 m), rhyolite flows (>100 m)	Sub Greenschist	Cp, Py, Po, Sp	Asp, gahnite, mackinawite, Mt, silver,	Selenides	mature arc back arc	FII	Barret & Lafleur (1992), Mercier-Langevin (2007), Gaboury and Pearson (2008), Mosier et al. (2009)
New Insco	Bimodal-mafic	Intermediate	pillow andesite-andesite breccia (5 m), rhyolite crystal tuff-lapilli tuff-breccia (40 m), quartz-porphyry sill (10 m), diorite (>80 m)	Greenschist	Cp, Py, Po, Sp, Gn	Goethite, hematite, Mt, Mr,	Selenides	juvenile arc back arc	FIIIa	Mercier-Langevin (2007), Gaboury and Pearson (2008),
Robb Montbray (Inmont)	Bimodal-mafic	Felsic-dominant	rhyolite flow, breccia, tuff, diorite	Lower Greenschist	Cp, Py, Po		Selenides	mature arc back arc	FIIIa	Mercier-Langevin (2007), Gaboury and Pearson (2008),
Normetal	Bimodal-mafic	Felsic-dominant	rhyolite tuff (120 m), bedded tuff (30-50 m), rhyolite flows (229 m), rhyolite agglomerate (23 m), rhyolite flows (570 m)	Upper greenschist-lower amphibolite	Cp, Py, Po, Sp, Gn	Asp, azurite, bornite, chalcocite, cubanite, enargite, gahnite, Mt, malachite, Mr, tetrahedrite	Antimonides		FIIIa	Lafrance (2003), Thurston et al. (2008), Gaboury and Pearson, (2008), Mosier et al. (2009)
Coniagas	Bimodal-mafic	Mafic-dominant	rhyolite lapilli tuff (6 m), massive andesite flows-flow breccias (30 m), andesite tuff (6 m), massive andesite flow (4 m), andesite tuff (15 m), andesite lapilli tuff (>5 m)	Greenschist	Cp, Py, Po, Sp, Gn	Silver	None	intra arc bimodal-rift	FIIIa	Doucet et al. (1998), Mosier et al. (2009)
Canadian Jamieson	Bimodal-mafic	Intermediate	rhyolite flow (60 m), dacite flow (>180 m)	Greenschist	Cp, Py, Po, Sp		None	mature back arc rift basin. Associated with mantle plume.	FIIIb	Hart (1984), Barrie et al. (1993), Hathway et al. (2008), Mosier et al. (2009)
Genex	Bimodal-mafic	Mafic-dominant	rhyolite flow (15 m), andesite-basalt flows (>90 m)	Greenschist	Cp, Py, Po		Selenides	mature back arc rift basin. Associated with mantle plume.	FIIIb	Hart (1984), Barrie et al. (1993)
Kam Kotia	Bimodal-mafic	Mafic-dominant	rhyolite agglomerate (20 m), dacite flow, basalt flows	Greenschist	Cp, Py, Po, Sp, Gn		Arsenides	mature back arc rift basin. Associated with mantle plume.	FIIIb	Hart (1984), Barrie et al. (1993), Barrie and Pattison (1999), Hathway et al. (2008), Mosier et al. (2009)
Kidd Creek	Bimodal-mafic-ultramafic	Intermediate	rhyolite tuff-rhyolite flows-rhyolite breccia (280 m), komatiite-carbonate-talc rock-peridotite-gabbro (>500 m)	Lower greenschist	Cp, Py, Sp, Gn	Acanthite, argentite, Asp, azurite, bismuth, bismuthinite, bohdanowiczite, bornite, brochantite, cadmoselite, carrollite, cassiterite, cattierite, chalcocite, clausthalite,cobaltite, colusite, covellite, digenite, dyscrasite, electrum, enargite, eucairite, freibergite, junoite, kiddcreekite, kesterite, klockmannite, laitakarite, Mt, malachite, Mr, mawsonite, monazite, naumannite, nickeline, petrukite, pyrargyrite, roquesite, scheelite, native silver, stannite, stannoidite, stephanite, sternbergite, stromeyerite, tennantite, tetrahedrite, tungstenite, wolframite, petrukite	Arsenides	mature back arc rift basin. Associated with mantle plume.	FIIIb	Bleeker et al. (1999), Hannington, et al. (1999b,c), Hannington et al. (2017)
Potter-Doal	Mafic	Mafic-dominant		Lower greenschist			Bismuthides			Steven (1997), Hannington et al. (1999b)
Dunraine	Bimodal-mafic	Mafic-dominant	rhyolite tuff-dacite-trachyte-rhyolite agglomerate-andesite-basalt (450 m), dacite-trachyte-andesite-basalt flow (1200 m), rhyolite lapilli tuff (150 m), rhyodacite (>150 m)	Greenschist	Cp, Py, Sp		Bismuthides	oceanic intra arc	FII	Yergeua (2010), Scott et al. (2002), Thurston et al. (2008), Mosier et al. (2009), Monecke et al. (2017)
East Sullivan	Bimodal-mafic	Felsic-dominant	rhyolite agglomerate	Greenschist	Cp, Py, Po, Sp	Mr	Arsenides	mature epicontinental arc	FII	Jenkins & Brown (1999), Lavoie et al. (2001), Scott et al. (2002), Thurston et al. (2008), Mosier et al. (2009), Monecke et al. (2017)
Louvem	Bimodal-mafic	Intermediate	rhyolite tuff, andesite flow	Greenschist	Cp, Py, Po, Sp	Bornite, cobaltite, digenite, molybdenite, rutile, tellurides, tetradymite	Tellurides	oceanic intra arc	FII	Guha & Darling (1972), Scott et al. (2002), Thurston et al. (2008), Mosier et al. (2009), Monecke et al. (2017)
Louvicourt	Bimodal-mafic	Intermediate	rhyolite tuff-dacite breccia-tuff, sandstone-graywacke-shale, andesite	Greenschist	Cp, Py, Po, Sp		Arsenides	Siliciclastic-felsic in mature epicontinental arc	FII	Guha & Darling (1972), Tourigny (1995), Jenkins & Brown (1999), Scott et al. (2002), Thurston et al. (2008), Monecke et al. (2017)
Manitou Barvue	Bimodal-mafic	Intermediate	rhyolite tuff-agglomerate, andesite, andesite porphyry	Greenschist	Cp, Py, Sp, Gn	Asp, pearceite, proustite, pyrargyrite, tennantite, tetrahedrite	Arsenides	oceanic intra arc	FII	Gilbert (1960), Jenkins & Brown (1999), Scott et al. (2002), Thurston et al. (2008), Monecke et al. (2017)

Table A.1. cont.

Name	Host-Rock-Type	Refined host rock classes	FW rocks underlying ore	Metamorphic Grade	Main ore minerals	Trace ore minerals	Trace Mineral Group	Tectonic Setting	Felsic Affinity	References
Geco	Bimodal-mafic	Felsic-dominant	sillimanite-muscovite-quartz schist, orthoamphibole-cordierite-garnet gneiss	Upper amphibolite	Cp, Gn, Py, Po, Sp	Cassiterite, högbomite, Mt, nigerite	Selenides	oceanic arc		Zaleski and Peterson, (1995), Zaleski (1999), Mosier et al. (2009)
Willecho	Bimodal-mafic	Felsic-dominant	rhyolite_tuff	Upper amphibolite	Cp, Py, Po, Sp, Gn	Argentite, Mt, silver	None	oceanic arc		Zaleski and Peterson, (1995), Zaleski (1999)
Lyon Lake & Creek zone	Bimodal-felsic	Felsic-dominant	rhyolite tuff (0-10 m), cherty rhyolite tuff-agglomerate-graphitic shale (50 m), rhyolite agglomerates-breccias (>20 m)	Greenschist	Cp, Py, Po, Sp, Gn	Asp,Mt, tennantite, tetrahedrite	Antimonides	mature epicontinental arc	FII	Hart et al. (2004), Mosier et al. (2009)
Mattabi	Bimodal-felsic	Felsic-dominant	rhyolite flow, cherty rhyolite agglomerate-tuff (90 m)	Greenschist	Cp, Py, Sp, Gn	Asp, boulangerite, bournonite, gahnite, Mt, tennantite, tetrahedrite	Antimonides	mature epicontinental arc	FII	Hart et al. (2004), Mumin et al. (2007), Mosier et al. (2009)
Sturgeon Lake	Bimodal-felsic	Felsic-dominant	rhyolite porphyry, rhyolite tuff, basalt flows-lapilli tuff-debris flow	Greenschist	Cp, Gn, Py, Po, Sp	Boulangerite, bournonite	Antimonides	mature epicontinental arc	FII	Hart et al. (2004), Mosier et al. (2009)
South Bay	Bimodal-felsic	Felsic-dominant	rhyolite tuff-flows (1000 m)	Greenschist	Cp, Py, Sp, Gn	Argentite, Asp, cassiterite, dyscrasite, Mt, silver, tennantite		oceanic arc		Hart et al. (2004), Mosier et al. (2009)
East Cleaver	Bimodal-felsic		dacite (50 m), rhyolite tuff (10 m), calcareous tuff (50 m), rhyolite tuff (70 m)	Amphibolite		Mt, gahnite,		epicontinetal arc		Frith and Roscoe (1980), Frith (1987), Bleeker and Hall (2007), Mosier et al. (2009)
Hackett A (Main) Zone	Bimodal-felsic		rhyolite cherty tuff, rhyolite flow, andesite	Amphibolite	Cp, Py, Po, Sp, Gn	Freibergite, stephanite, electrum, stephanite, tennantite, tetrahedrite, matildite, lillianite, heyrovskyite, acanthite, stannite, bismuthinite, cubanite, native bismuth, Asp, Mt, gudmundite		epicontinetal arc		Frith and Roscoe (1980), Frith (1987), Bleeker and Hall (2007), Mosier et al. (2009), Grant et al. (2015)
Yava Lake	Bimodal-felsic		rhyolite flow, dacite welded ash flow tuff	Amphibolite		Tennantite		epicontinetal arc		Frith and Roscoe (1980), Frith (1987), Bleeker and Hall (2007), Mosier et al. (2009)
High Lake	Bimdoal-mafic		dacite pyroclastics					epicontinetal arc		Frith and Roscoe (1980), Frith (1987), Bleeker and Hall (2007), Mosier et al. (2009)
Gondor	Bimodal-felsic		felsic volcanics	Greenschist				epicontinetal arc		Frith and Roscoe (1980), Frith (1987), Bleeker and Hall (2007), Mosier et al. (2009)
Hood #10	Bimdoal-mafic		massive to brecciated dacite and rhyolite flows with minor basalt and andesite volcanic units	Greenschist				mature epicontinental arc		Frith and Roscoe (1980), Frith (1987), Bleeker and Hall (2007), Mosier et al. (2009), Mills et al. (2016)
Heninga Gemex	Bimodal-mafic		rhyolite pyroclastics					oceanic arc		Mosier et al. (2009)
Callinan	Bimodal-mafic		rhyolite quartz porphyry					juvenile arc		Bailes and Syme (1989), Syme and Bailes (1993), Stern et al. (1995), Syme et al. (1999)
Centennial	Bimodal-mafic		rhyolite volcaniclastics and flows--dacite volcaniclastics-basalt volcaniclastics (600 m), gabbro	middle greenschist	Cp, Py, Sp, Gn	Asp, cobaltite, Mt, tennantite, tetrahedrite, wurtzite		juvenile arc		Bailes and Syme (1989), Stern et al. (1995), Syme et al. (1999), Mosier et al. (2009)
Coronation	Mafic		andesite flow		Cp, Py, Po, Sp	Pl, Chisello, Mt, Gn, stannite, ilmenite, rutile, altaite, hessite, petzite, cassiterite, electrum, native gold, scheelite, sylvanite		juvenile arc		Syme et al. (1999), Galley et al. (2007), Mosier et al. (2009)
Flexar	Mafic		andesite flow	Greenschist	Cp, Py, Po, Sp	Mt, Asp, molybdenite		juvenile arc		Syme et al. (1999), Galley et al. (2007), Mosier et al. (2009)
Flin Flon	Bimodal-mafic		rhyolite-dacite porphyry (3-150 m), andesite breccia (30-350 m), andesite flow (>500 m)	lower greenschist	Cp, Py, Po, Sp, Gn	Altaite, argentite, Asp, cubanite, electrum, ilmenite, Mt, Mr, sylvanite, tennantite, tetradymite, tetrahedrite		juvenile arc		Bailes and Syme (1989), Syme and Bailes (1993), Stern et al. (1995), Syme et al. (1999), MacLachlan and Devine (2007)
North star	Bimodal-felsic		pillow basalt flow breccia-tuff	Greenschist	Cp, Py			juvenile arc		Corrigon et al. (2007), Galley et al. (2007), Mosier et al. (2009)
Pinebay	Bimodal-mafic		rhyolite tuff, andesite		Cp, Py, Po			juvenile arc		Corrigon et al. (2007), Galley et al. (2007), Mosier et al. (2009)
Schist Lake & Mandy	Bimodal-mafic		rhyolite tuff, andesite volcaniclastics, andesite flow		Cp, Py, Sp, Gn	Asp, enargite		juvenile arc		Bailes and Syme (1989), Syme and Bailes (1993), Stern et al. (1995), Syme et al. (1999), DeWolfe (2009)

Table A.1. cont.

Name	Host-Rock-Type	Refined host rock classes	FW rocks underlying ore	Metamorphic Grade	Main ore minerals	Trace ore minerals	Trace Mineral Group	Tectonic Setting	Felsic Affinity	References
Anderson Lake	Bimodal-mafic		basalt (1000 m), basalt-andesite (250 m), rhyolite volcaniclastics (3 m)	Upper amphibolite	Cp, Py, Po, Sp	Anhydrite, ilmenite, Mt, molybdenite, rutile, tellurobismuthite,		juvenile arc		Bailes et al. (1996); Bailes and Galley (1999), Mosier et al. (2009), Bailes et al. (2016)
Chisel Lake	Bimodal-mafic		rhyolite breccia-rhyolite flow-dacite tuff (50-100 m)	Lower amphibolite	Cp, Py, Po, Sp, Gn	Altaite, arsenic, Asp, bismuth, boulangerite, bournonite, electrum, geocronite, gold, gudmundite, hessite, Mr, meneghinite, proustite, pyrargyrite, silver, tennantite, tetrahedrite		juvenile arc		Bailes et al. (1996); Bailes and Galley (1999), Mosier et al. (2009), Bailes et al. (2016)
Osborne Lake	Bimodal-mafic		rhyolite tuff	Greenschist	Cp, Py, Po, Sp, Gn	Asp, Mr, rutile		juvenile arc		Bailes et al. (1996); Bailes and Galley (1999), Mosier et al. (2009), Bailes et al. (2016)
Photo Lake	Bimodal-mafic		rhyolite flows	Greenschist	Cp, Py, Po, Sp	Mt		mature arc		Bailes et al. (1996); Bailes and Galley (1999), Mosier et al. (2009), Bailes et al. (2016)
Rod	Bimodal-mafic		rhyolite tuff, basalt flows-tuff	Amphibolite	Cp, Py, Po, Sp, Gn	Asp, cobaltite		juvenile arc		Bailes et al. (1996); Bailes and Galley (1999), Mosier et al. (2009), Bailes et al. (2016)
Stall Lake	Bimodal-mafic				Cp, Py, Po, Sp	Ilmenite, Mt		juvenile arc		Bailes et al. (1996); Bailes and Galley (1999), Mosier et al. (2009), Bailes et al. (2016)
Fox Lake	Bimodal-mafic		andesite breccia (>50 m)		Cp, Py, Po, Sp, Gn	Asp, gold, hessite, ilmenite, Mt, silver				Turek et al. (1976), Mosier et al. (2009)
Ruttan	Bimodal-siliciclastic		basaltic andesite volcaniclastics-breccia (150 m), rhyolite volcaniclastics-rhyolite breccia-andesite volcaniclastics-andesite breccia-agglomerate-andesite flows-sediments (220 m), basalt-pillow basalt (350 m)	Lower amphibolite	Cp, Py, Po, Sp, Gn	Tetrahedrite, molybdenite, cubanite, native bismuth, bismuth sulfosalts, tellurbismuth, electrum, hessite, covellite, chalcocite		riftend continental arc		Ames (19996), Barrie et al. (2005), Mosier et al. (2009)
Sherridon	Bimodal-mafic		gneissoid quartzite (lithic arenite)	Amphibolite	Cp, Py, Po, Sp	Cubanite, gahnite, Mt, Mr,				Turek et al. (1976); Froese and Goetz (1981), Mosier et al. (2009)
Boylen-Koke	Pelitic-mafic							mature oceanic backarc		Clarke and Wares (2004), Mosier et al. (2009)
Austin Brook	Siliciclastic-felsic		rhyolite crystal tuff-dacite lapilli tuff-dacite breccia (200 m), sandstone-graywacke-slate, andesite-spilite	Lower greenschist	Cp, Py, Po, Sp, Gn			continental back arc	FII	Peter and Goodfellow (1996), Goodfellow and McCutcheon, (2003), van Staal et al. (2003), Franklin et al. (2005), Mercier-Langevin et al. (2007)
Brunswick #12	Siliciclastic-felsic		graphitic argillite (20 m) , rhyolite crystal tuff-dacite breccia (600 m), sediments-tuff	Lower greenschist	Cp, Py, Po, Sp, Gn	Anglesite, Asp, boulangerite, cassiterite, graphite, Mt, Mr, stannite		continental back arc	FII	Peter and Goodfellow (1996), Goodfellow and McCutcheon, (2003), van Staal et al. (2003), Franklin et al. (2005), Mercier-Langevin et al. (2007)
Heath Steele	Siliciclastic-felsic		argillite, rhyolite porphyry, rhyolite crystal tuff-dacite breccia-tuff (3000 m), graywacke-sandstone-shale, andesite-spilite	Lower greenschist	Cp, Py, Po, Sp, Gn	Anglesite, Asp, bismuth, bismuthinite, cobaltite, freibergite, Mt, Mr		continental back arc	FII	Peter and Goodfellow (1996), Goodfellow and McCutcheon, (2003), van Staal et al. (2003), Franklin et al. (2005), Mercier-Langevin et al. (2007)
Key Anacon	Siliciclastic-felsic		rhyolite tuff-slate-phyllite-quartz arenite (20 m), graywacke (60 m)	Lower greenschist	Cp, Py, Po, Sp, Gn	Asp		continental back arc	FII	Peter and Goodfellow (1996), Goodfellow and McCutcheon, (2003), van Staal et al. (2003), Franklin et al. (2005), Mercier-Langevin et al. (2007)
Clinton Copper	Bimodal-mafic		basalt, rhyolite tuff	Greenschist	Cp, Py, Po, Sp, Gn					Stephens (1984), Swinden and Thorpe (1984), Mosier et al. (2009)
Trinity (Weedon?)	Bimodal-mafic		rhyolite agglomerate-flow, dacite flow, siltstone-graywacke-pebble conglomerate-ferruginous chert	Greenschist						Stephens (1984), Swinden and Thorpe (1984), Mosier et al. (2009)
Weedon	Bimodal-felsic		andesite tuff	Greenschist	Cp, Py, Po, Sp, Gn	Bornite, cubanite, Mt, Mr,				Stephens (1984), Swinden and Thorpe (1984), Mosier et al. (2009)
Kudz Ze Kayah	Bimodal-felsic		rhyolite flows-felsic tuff-chlorite-biotite tuff (25-50 m), felsic lapilli tuff-ash tuff (10 m)	Lower greenschist	Py, Sp, Po, Gn, Cp, a	Asp, tetrahedrite-tennantite, boulangerite, electrum, clausthalite, Mt		continental back arc rift basin		Piercey et al. (2001), Peter et al. (2007), Mosier et al. (2009)
Hart River	Bimodal-mafic/Sedex?		basalt flows	Greenschist	Cp, Py, Po, Sp, Gn	Argyrodite, canfieldite, tennantite, tetrahedrite				Yukon Geological Survey (2005)
Eskay Creek	Siliciclastic-felsic		rhyolite flows-breccia (30-110 m), mudstone (3 m), volcaniclastics-andesite flows (>100 m), sandstone-limestone-argillite-andesite breccia, arenite-argillite-siltstone-volcanic congomerate	Lower greenschist	Py, Sp, Gn, barite	Boulangerite, bournonite, cinnabar, electrum, freibergite, gold, jamesonite, realgar, stibnite, tetrahedrite				Macdonald et al. (1996), Sherlock et al. (1999), Mosier et al., 2009)
Britannia	Bimodal-mafic		dacite lapilli tuff (500 m), andesite-argillite	Lower greenschist	Cp, Py, Po, Sp	Argentite, barite, bornite, clinozoisite, gold, tennantite, tetrahedrite		mature epicontinental arc		Payne et al. (1980), Mosier et al. (2009)
Myra Falls Group (Lynx)	Bimodal-felsic		rhyolite flow, andesite breccia, basalt	Greenschist	Cp, Py, Sp, Gn	Barite, bornite, covellite, digenite, stromeyerite, tennantite, tetrahedrite				Juras (1987), Gabrielse and Yorath, (1991), Jones et al. (2006), Marshall et al. (2016)

Table A.2 Spatial/ temporal/ geological organization of VMS deposits in Canada with pyrite samples in the database.

Age	Orogen	Assemblage	Camp	Deposit
Archean	AGB	Pacaud		
		Deloro	Chibougamau	
			Matagami	Mattagami Lake, New Hosco, Orchan, Bell Allard, Isle Dieu, Norita-A
			Joutel	Poirier, Joutel
			Quevillion	Coniagas
			Normetal	Normetal
			Amos-Barraute	Abcourt-Barvue, Cons. Mogador, Vendome
		Stoughton-Roquemaure		
		Kidd-Munro	Timmins	Kidd Creek, Potter-Doal
			Amos-Barraute	Conigo
		Tisdale	Val d'Or	Dunraine, East Sullivan, Louvem, Louvicourt, Manitoue-Barvue
		Blake River	Noranda (Felsic-hosted)	Aldermac, Mobrun, Horne, Horn-5, Quemont, Delbridge, Deldona
			Noranda (Mafic-hosted)	Amulet A-C, Corbet, Old Waite, Moosehead, New Insco
		DBL	Bousquet	Bousquet #2, Dumagami
			Timmins	Kam Kotia, Genex, Canadian Jamieson
	West Superior	Uchi	Uchi	South Bay
		Wabigoon	Sturgeon Lake	Mattabi, Lyon Lake, Sturgeon Lake
		Wawa	Manitouwadge	Willecho, Geco
			Sudburry, Benny Area	Stralak, Geneva Lake
	Slave		Hackett River	Hackett River (Main zone, Duck Lake), East Cleaver, Yava
			High Lake	High Lake
			Hood River	Gondor, Takijuq Lake (Hood #10)
			Kennedy Lake	
			Keewatin	Heninga Gemex, Spi Lake
			Slave	Clinton Golden
Paleoproterozoic	Trans-Hudson	Flin Flon-Snow Lake	Flin Flon	Callinan, Centennial, Coronation, Flexar, Flin Flon, Mandy, Northstar, Pinebay, Schist Lake
			Snow Lake	Anderson Lake, Chisel Lake, Osborne Lake, Photo Lake, Rod, Stall Lake
			Lynn Lake	Fox Lake
			Sherridon	Sherridon
			Rusty Lake	Ruttan
			Labrador Trough	Koke
Paleozoic	Appalachian		Eastern Township	Weedon, Clinton Copper, Trinity
			Bathurst	Austin Brook, Brunswick #12, Heathe Steele, Key Anaconda
	Cordillera		Vancouver Island	Myra Falls Group (Lynx)
			Vancouver	Brittania
			Finlayson Lake	Kudz ze Kayah
Mesozoic			Stewart	Eskay Creek

Table A.3 a) Petrographic descriptions for polished grain mounts of representative samples of pyrite concentrates from the database.

Sample	Mineral	Amount	Shape	Size (mm)	FeS_2	$CuFeS_2$	ZnS	PbS	Other trace elements
BSQT2-92.7L.A FE-PY - Bousquet #2	Pyrite	>95% (~600 grains)	Sub-angular	0.06–0.12	98	0.05	0.01	0.002	Low Ag, Bi, Te, Sb
	Sphalerite	<1%	Sub-angular	<0.02					
	Galena	<1%	Sub-angular	<0.02					
BSQT2-92.7L.B FE-PY - Bousquet #2	Pyrite	>90% (150–200 grains)	Sub-angular to sub-rounded	0.06 – 0.25					
	Sphalerite	~1%	Sub-angular	<0.1					
	Chalcopyrite	<1%	Sub-angular	<0.06					
	Galena	<0.1%	Sub-angular	<0.03					
	Light blue mineral?	<0.1%	Sub-angular	<0.01					
	Telluride	Trace	Sub-angular	<0.01					
63RF299 PY - Dumagami	Pyrite	>99% (150–200 grains)	Angular to sub-angular	0.06 – 0.20	80	0.50	0.002	0.005	High Ag (60 ppm), Au (10 ppm), Te (18 ppm)
	Silicate mineral?	Trace		<0.01					
63RF48 PY - Quemont	Pyrite	>95% (~500 grains)	Sub-angular to sub-rounded	0.06 – 0.10	79	3.50	0.50	0.10	High Ag (110 ppm), Au (7 ppm), Te (170 ppm), and Hg (9 ppm)
	Chalcopyrite	<1%	Sub-angular	~0.01					
	Sphalerite	<1%	Sub-angular	~0.01					
	Silicate mineral?	Trace	Sub-angular	<0.01					
2600L KIDD 07 PY - Kidd Creek	Pyrite	>99% (300–400 grains)	Angular to sub-angular	0.08 – 0.25	86	0.10	0.07	0.03	High As (350 ppm)

Table A.3 b) Mineral-element mass balance calculations to show the amount of Ag, Au, and Bi that may be present as telluride minerals and other trace mineral phasers in the Quemont and Bousquet #2-Dumagami samples as examples.

Pyrite sample	**ICP and INAA data**			
	Ag	Au	Bi	Te
BSQT93A2PY - Bousquet #2	7.00	6.02	16.0	64.0
BSQT2-92.7L.A FE-PY - Bousquet #2	1.00		0.40	1.80
63RF299 PY - Dumagami	60.0	10.0	3.30	18.0
63RF48 PY - Quemont	191	7.31	1.30	170
Mineral calculations	**Calaverite**			
	Ag	Au = AuTe2/2.30	Bi	AuTe2 = Te*1.77
BSQT93A2PY - Bousquet #2		49.3		113.3
BSQT2-92.7L.A FE-PY - Bousquet #2				3.19
63RF299 PY - Dumagami		13.9		31.9
63RF48 PY - Quemont		130.8		300.9
	Petzite			
	Ag = Ag3AuTe2/2.06	Au =Ag3AuTe2/3.39	Bi	Ag3AuTe2 = Te*5.23
BSQT93A2PY - Bousquet #2	162	98.7		335
BSQT2-92.7L.A FE-PY - Bousquet #2	4.57			9.41
63RF299 PY - Dumagami	45.7	27.8		94.1
63RF48 PY - Quemont	432	262		889
	Hessite			
	Ag =Ag2Te/1.59	Au	Bi	Ag2Te = Te*2.69
BSQT93A2PY - Bousquet #2	108			172
BSQT2-92.7L.A FE-PY - Bousquet #2	3.05			4.84
63RF299 PY - Dumagami	30.5			48.4
63RF48 PY - Quemont	288			457
	Tellurobismuthite			
	Ag	Au	Bi = Bi2Te3/1.92	Bi2Te3=Te*2.09
BSQT93A2PY - Bousquet #2			69.7	134
BSQT2-92.7L.A FE-PY - Bousquet #2			1.96	3.76
63RF299 PY - Dumagami			19.6	37.6
63RF48 PY - Quemont			185	355

Table A.4 Summary statistics of trace element geochemistry of monthly concentrates of pyrite in tailings samples as well as Cu concentrates and Zn concentrates from the mill. These data are used in comparison with trace elements in pyrite, chalcopyrite, and sphalerite from the same deposits to demonstrate the reliability of the mineral separate sampling method used for the database.

Data in ppm	**Cu**	**Zn**	**Pb**	**Ag**	**Au**	**Bi**	**Co**	**Ni**	**Se**	**Te**	**Cd**	**In**	**Ga**	**Sn**	**W**	**Mo**	**V**	**As**	**Sb**	**Hg**	**Tl**	**U**
Pyrite tailings																						
N	8	9	8	9	5	7	9	4	4	3	8	7	8	8	0	7	2	4	6	3	7	7
Minimum	420	360	27.0	5.11	0.06	8.80	4.00	5.00	11.0	0.10	4.20	0.06	0.30	1.90	-	0.30	6.00	3.70	1.00	3.00	0.08	0.11
Maximum	275000	520000	7700	1000	2.04	560	1070	290	130	1.4	920	43.0	17.0	3500	-	43.0	7.00	670	220	140	32.0	0.42
Mean	37394	128601	1709	229	0.67	130	303	78.75	66.0	0.73	151	9.86	3.64	718	-	9.76	6.50	280	42.45	50.33	6.01	0.23
Median	2615	6795	360	50.0	0.51	40.0	150	10.0	61.5	0.70	12.0	5.90	1.35	193	-	1.40	6.50	224	5.30	8.00	1.60	0.19
Cu concentrates																						
N	46	54	46	50	29	42	53	18	17	17	45	44	46	46	2	41	10	19	19	19	42	44
Minimum	50.0	79.0	10.0	5.11	0.03	0.60	2.00	11.0	6.00	0.60	0.50	0.03	0.30	0.90	3.00	0.30	6.00	3.00	0.60	3.00	0.01	0.01
Maximum	314000	621000	154000	13518	8.33	2100	2550	780	1600	9300	4200	120	99.0	1900	29.0	1850	190	6840	260	45.0	90.0	26.0
Mean	40457	221478	15630	479	0.71	141	267	143	210	575	782	21.0	12.1	218	16.0	70.4	42.4	482	52.4	20.9	7.09	1.40
Median	3650	31500	705	64.3	0.28	12.5	59.0	75.5	74.0	4.20	75.0	5.75	4.50	32.5	16.0	2.20	12.0	76.3	17.0	12.0	1.20	0.13
Zn concentrates																						
N	35	39	35	37	22	33	38	18	14	17	34	33	35	35	2	34	11	15	20	14	34	32
Minimum	120	239	25.0	2.80	0.00	0.50	5.00	5.00	9.00	0.30	0.40	0.03	0.30	2.70	8.00	0.30	6.00	5.00	0.20	0.50	0.03	0.01
Maximum	311000	543000	212000	2540	21.6	270	4900	218	570	145	2800	180	100	11000	13.0	180	320	390	8800	250	66.0	7.6
Mean	44258	168376	14407	201	2.17	41.4	307	49.5	232	22.6	493	25.0	13.6	486	10.5	12.4	53.4	128	481	25.1	5.02	1.05
Median	6100	19000	230	77.0	0.36	5.00	37.5	22.5	165	4.20	35.0	4.20	3.40	29.0	10.5	1.60	28.0	62.8	8.60	6.50	0.79	0.19

Table A.5 Average trace element concentrations (ppm) in pyrite samples from VMS deposits in the Superior Province classified by bulk Au grade (g/t). Data in ppm.

Au-grade	Cu	Zn	Pb	Ag	Au	Bi	Co	Ni	Se	Te	Cd	In	Ga	Sn	W	Mo	V	As	Sb	Hg	Tl	U
Low (<0.6 g/t)	3352	6222	492	72.4	1.20	40.7	1044	125	121	7.29	17.0	4.00	1.90	160	7.20	21.8	14.3	394	8.30	4.38	2.56	0.15
Medium (0.6–1.4 g/t)	2987	7231	741	46.1	1.46	42.1	702	80.3	200	12.0	17.9	4.55	3.29	142	4.20	3.63	16.5	613	47.2	5.21	1.22	0.11
High (1.6-2.4 g/t)	966	10280	1011	71.8	6.73	49.2	748	152	143	55.1	28.6	1.75	2.73	302	-	4.13	10.5	363	28.8	2.40	2.64	0.17
Very high (4.1–7.8 g/t)	2603	5873	496	113	7.60	51.1	293	56.2	180	127	20.9	4.09	1.48	149	4.00	1.93	29.0	329	11.4	4.08	2.12	0.75

Table A.6 a) Average trace element concentrations (ppm) of pyrite samples from bimodal-mafic VMS deposits in the AGB compared with VMS deposits of other host rock types (Barrie and Hannington, 1999) across Canada.

Host rock type	Cu	Zn	Pb	Ag	Au	Bi	Co	Ni	Se	Te	Cd	In	Ga	Sn	W	Mo	V	As	Sb	Hg	Tl
AGB Bimodal-mafic	2985	6045	784	68.5	3.80	46.4	734	109	276	47.2	18.5	3.70	3.42	137	4.95	10.7	24.0	580	13.0	5.42	1.85
Other Bimodal-mafic	3596	5267	997	68.8	1.23	40.9	850	96.4	163	38.0	12.5	2.18	1.00	367	20	6.12	19.4	1102	45.2	3.64	1.09
Mafic	7768	5114	95.0	10.5	1.32	6.65	4350	244	425	9.60	1.78	1.26	0.50	3.55	-	7.95	-	339	2.63	0.50	0.25
Pelitic-mafic	375	14433	5300	38.0	0.30	4.85	114	-	44	1.35	28.5	0.25	2.30	6.95	-	1.90	-	1180	60.9	12.0	1.40
Bimodal-felsic	1841	6841	1725	70.9	0.85	17.4	170	97.0	64.7	7.98	12.7	0.73	1.23	96.1	4.50	7.00	9.25	910	182	5.25	1.41
Siliciclastic-felsic	3699	4550	3380	106	0.45	175	340	221	-	1.80	16.8	5.13	7.83	326	-	15.9	61.9	-	125	-	11.8

Table A.6 b) Average trace element concentrations (ppm) of all pyrite samples from VMS deposits in the Superior Province classified by immediate footwall composition (felsic-dominant, intermediate, and mafic-dominant).

Immediate host rocks	Cu	Zn	Pb	Ag	Au	Bi	Co	Ni	Se	Te	Cd	In	Ga	Sn	W	Mo	V	As	Sb	Hg	Tl	U	Zr
Felsic-dominant	3083	7203	762	86.8	6.07	61.2	755	70.6	326	69.1	15.4	4.34	2.73	368	9.43	5.11	14.7	557	53.5	6.71	1.94	0.190	40.6
Intermediate	2800	5140	636	49.1	1.06	42.4	583	121	209	16.3	18.4	3.30	3.85	165	9.00	16.7	29.4	599	10.1	4.41	1.28	0.305	33.8
Mafic-dominant	1697	9507	1879	122	1.61	31.4	911	146	126	4.06	24.9	2.73	1.78	218	5.00	6.19	9.00	330	27.9	3.86	2.21	0.187	20.7

Table A.6 c) Average trace element concentrations (ppm) of pyrite samples from VMS deposits grouped by the F-classification of their felsic host rocks (Hart et al., 2004; Gaboury and Pearson, 2008).

	No. deposits	No. samples	Cu	Zn	Pb	Ag	Au	Bi	Co	Ni	Se	Te	Cd	In	Ga	Sn	W	Mo	V	As	Sb	Hg	Tl	U
FI-FII	2	8	2840	2010	410	38.5	4.25	62.4	38.8	14.8	19.3	45.4	1.13	1.09	3.66	15	-	3.17	29.0	479	29.0	2.00	0.18	1.72
FII	16	82	3143	5554	784	59.8	0.91	52.0	794	123	148	6.16	10.0	1.08	3.48	47	6.00	23.2	26.1	1262	131	6.21	0.96	0.219
FII-FIII	2	15	1639	6611	292	24.7	4.52	41.2	203	45.5	134	36.5	25.7	6.32	1.78	199	-	1.71	-	154	3.15	7.86	1.13	0.091
FIIIa	21	106	2847	7661	850	92.6	6.15	44.1	759	110	341	62.7	21.3	4.94	2.59	177	5.00	2.82	15.4	399	13.2	5.38	2.14	0.154
FIIIb	10	33	2891	7188	445	91.5	1.52	63.7	678	87.4	178	8.51	14.8	6.53	1.22	222	5.00	3.24	23.0	513	9.9	4.73	2.14	0.179

Table A.7 Average trace element concentrations (ppm) of pyrite samples from VMS deposits in different assemblages and greenstone belts. Data in ppm. A summary is provided of the distinguishing trace element characteristics of pyrite samples from the different regions in Table 4.9.a.

Assemblage / Orogen	Cu	Zn	Pb	Ag	Au	Bi	Co	Ni	Se	Te	Cd	In	Ga	Sn	W	Mo	V	As	Sb	Hg
Deloro	2131	5017	1589	68.1	0.62	25.5	307	45.1	80.5	2.88	11.7	0.70	0.89	32.6	-	10.0	10.0	368	21.2	9.50
Kidd-Munro	4246	5930	566	58.7	0.46	182	760	62.3	83.5	1.60	32.8	9.72	5.65	492	10.0	4.80	-	547	8.58	1.00
Tisdale	3823	3301	358	44.8	1.00	26.5	1410	167	227	6.69	13.9	1.24	5.35	47.6	-	36.3	27.2	1251	6.72	5.75
Blake River	2886	7349	659	76.4	6.26	45.7	717	101	308	56.4	21.4	4.98	3.47	170	4.5	2.71	20.5	508	13.6	5.38
Western Superior	1922	10342	754	94.5	1.22	66.2	492	64.1	152	8.72	14.9	3.80	1.43	988	16.5	2.67	17.3	681	107	5.44
Slave	1360	3903	2249	43.5	0.34	14.1	173	120	35.3	1.26	17.2	0.67	1.17	129	-	4.52	10.0	131	39.6	-
Trans-Hudson	4380	4510	617	57.0	0.77	28.0	1146	122	117	47.6	9.94	1.38	0.90	20.3	-	7.05	32.4	2605	48.1	3.88
Appalachian	4045	6338	2107	111	0.39	189	407	102	96.5	10.3	13.2	6.03	7.76	390	-	9.15	48.7	98.8	2.15	2.00
Cordillera	4923.90	1814.33	965.40	29.81	1.48	26.13	90.33	55.00	137.20	16.40	2.66	0.32	1.26	5.62	3.00	9.76	14.28	1072	145	3.00

Table A.8 Average trace element concentrations (ppm) of pyrite samples from different VMS camps in the Superior Province. Data in ppm. A summary is provided of the main differences in trace element characteristics of pyrite samples between the camps in Table 4.9.b.

Camp	Cu	Zn	Pb	Ag	Au	Bi	Co	Ni	Se	Te	Cd	In	Ga	Sn	W	Mo	V	As	Sb	Hg	Tl	U
Amos-Barraute	2805	2418	1381	43.9	0.75	80.4	302	26.0	-	-	6.23	0.89	2.07	53.3	-	11.3	10.0	750	113	7.00	1.01	0.20
Mattagami	2418	7421	242	98.2	1.82	87.5	803	93.1	229	11.5	13.2	5.16	1.65	277	9.00	2.05	23.0	322	9.14	4.72	0.77	0.18
Joutel	1308	6932	695	20.2	0.15	24.0	432	77.5	121	2.88	19.6	2.86	1.40	174	-	5.38	-	497	9.57	12.0	0.36	0.06
Quévillon	501	11135	3332	227	0.47	3.5	138	52.0	-	-	32.1	0.56	1.20	57.3	-	0.48	-	30.5	0.50	-	1.47	0.46
Normetal	12000	15348	85.0	205	1.10	99.0	554	-	20.5	-	6.50	0.55	2.10	6.20	-	0.50	-	152	3.15	-	0.60	0.16
Timmins	3422	10615	750	76.8	1.07	28.7	934	79.0	129	1.08	39.2	8.70	2.01	322	5.13	4.72	-	669	10.7	3.69	5.85	0.17
Val d'Or	3823	3301	358	44.8	1.00	26.5	1410	167	227	6.69	13.9	1.24	5.35	47.6	-	36.3	27.2	1251	6.72	5.75	0.76	0.18
Bousquet	2840	2010	410	38.5	4.25	62.4	38.8	14.8	19.3	45.4	1.13	1.08	1.22	15.2	-	3.17	29.0	479	29.0	2.00	0.18	1.72
Noranda Main	2717	8828	544	62.0	2.00	63.4	1152	88.3	164	28.7	26.0	6.77	4.92	192	1.33	3.63	10.0	495	15.5	3.67	1.24	0.18
Noranda N-S-E-W	2854	6476	715	87.2	9.89	26.2	474	144	443	74.5	18.8	4.59	2.88	187	7.50	2.03	23.5	479	10.8	6.38	2.91	0.10
Benny Greenstone	2131	8151	8320	217	3.06	16.0	225	273	43.5	1.80	30.1	0.38	3.18	3.30	-	36.1	78.3	349	117	2.33	6.74	2.34
Manitouwadge	919	4393	2147	24.3	0.28	32.2	229	16.3	95.0	0.48	25.2	0.77	0.72	3168	25.5	6.17	14.5	87.5	9.38	-	1.25	0.22
Sturgeon Lake	863	19686	160	142	1.11	58.5	205	20.0	75.6	0.30	4.12	0.84	2.00	9.28	6.00	0.80	-	1321	277	6.36	1.58	0.53
Uchi	8400	840	980	35.0	-	41.0	98.0	-	-	-	4.20	3.50	0.70	30.0	-	0.40	-	-	-	-	0.26	0.06

Table A.9 Average trace element concentrations (ppm) in pyrite samples from VMS deposits and occurrences across mine camps in the Superior Province. Data in ppm. A summary is provided of the main differences in trace element characteristics of pyrite samples between the deposits in the Noranda camp in Table 4.9.c.

Camp	Deposit	Cu	Zn	Pb	Ag	Au	Bi	Co	Ni	Se	Te	Cd	In	Ga	Sn	W	Mo	V	As	Sb	Hg	Tl	U
Amos-Barraute	Abcourt-Barvue	4249	1197	642	40.1	1.07	31.5	125	12.0	-	-	3.9	0.47	0.28	2.27	-	25.0	-	750	113	7.00	0.79	0.07
	Conigo	5960	551	804	79.2	1.08	348	329	40.0	-	-	7.28	3.84	9.50	326	-	1.76	-	-	-	-	0.28	0.73
	Mogador	597	4018	2163	35.1	0.38	20.4	435	19.0	-	-	7.29	0.10	1.02	3.19	-	0.93	10.0	-	-	-	1.30	0.04
Joutel	Joutel	2200	11850	1800	50.5	0.40	90.0	1195	140	314	5.70	42.0	9.70	0.70	31.0	-	7.30	-	835	3.90	12.0	0.08	0.15
	Poirier	1085	5703	419	12.6	0.07	1.97	241	15.0	23.8	1.93	14.03	1.15	1.58	210	-	4.73	-	329	12.4	-	0.43	0.03
Normetal	Normetal	12000	15348	85	205	1.10	99	554	-	20.5	-	6.50	0.55	2.10	6.20	-	0.50	-	152	3.15	-	0.60	0.16
Quevillon	Coniagas	501	11135	3332	227	0.47	3.50	138	52.0	-	-	32.1	0.56	1.20	57.3	-	0.48	-	30.50	0.50	-	1.47	0.46
Matagami	Bell Allard	1383	2300	410	13.2	0.43	2.80	243	102	31.3	4.40	9.00	1.52	1.27	7.23	-	2.67	23.0	501	10.3	0.50	0.43	0.11
	Isle Dieu	1155	6030	435	279	-	228	1584	34.7	-	2.00	18.8	3.00	0.67	768	-	1.15	-	-	12.3	-	0.66	0.04
	Mattagami Lake	2350	16227	91	16.3	0.27	4.00	152	434	84.0	16.8	14.9	4.39	1.00	150	9.00	4.65	-	313	8.83	2.00	2.37	0.17
	New Hosco	1150	247	56	59.1	0.08	2.30	1412	42.0	57.3	2.93	0.57	1.57	1.80	20.0	-	2.30	-	150	3.97	3.33	0.03	0.36
	Norita A	3650	180	48	4.85	-	113	735	55.0	-	70.0	1.10	1.85	2.25	605	-	0.80	-	-	-	-	0.27	0.23
	Orchan	4825	13526	237	115	5.34	40.0	569	-	614	10.7	22.6	14.8	2.60	79.0	-	1.63	-	324	9.25	7.50	0.77	0.14
Timmins	Canadian Jamieson	16000	24000	94	10.0	0.22	5.20	190	32.0	-	-	59.0	1.80	5.60	150	-	2.30	-	-	-	-	0.26	0.10
	Genex	2007	426	147	212	1.99	61.7	1537	102	274	0.70	1.30	4.89	0.50	6.73	4.00	2.37	-	1059	6.50	5.25	0.16	0.11
	Kam-Kotia	2127	19867	2273	46.5	3.08	25.9	324	-	74.3	0.95	38.7	2.03	2.67	136	3.25	2.63	-	601	17.6	5.33	11.0	0.10
	Kidd Creek	2532	7306	328	50.2	0.04	15.4	117	73.5	15.2	1.60	58.3	15.6	1.80	658	10.0	7.33	-	577	9.66	1.25	6.14	0.27
	Potter-Doal	-	23200	-	15.0	0.27	-	7420	-	425	-	-	-	-	-	-	-	-	339	1.00	0.50	-	-
Val d'Or	Dunraine	4325	81	29	30.0	1.34	40.6	532	209	-	-	1.38	1.27	0.39	1.78	-	90.3	2.50	-	-	-	0.04	0.13
	East Sullivan	5024	1510	274	76.7	1.27	13.3	5749	72.0	55.0	3.60	8.09	1.41	0.86	4.96	-	1.16	15.6	1137	4.67	5.00	0.65	0.12
	Louvem	3218	2981	83	8.83	0.44	40.8	117	71.0	-	-	9.73	2.24	0.60	1.98	-	3.43	-	-	-	-	0.69	0.19
	Louvicourt	5194	10088	223	27.8	0.67	23.2	615	134	249	12.1	39.6	1.28	1.97	140	-	17.3	10.0	1309	8.26	5.90	0.37	0.09
	Manitou Barvue	223	2995	1458	83.5	0.28	2.88	26.5	-	-	-	18.5	0.28	27.6	96.8	-	1.40	58.0	-	-	-	1.72	0.42

Table A.9 cont.

Camp	Deposit	Cu	Zn	Pb	Ag	Au	Bi	Co	Ni	Se	Te	Cd	In	Ga	Sn	W	Mo	V	As	Sb	Hg	Tl	U
DBL	Bousquet #2	3944	686	625	33.5	6.02	94.1	38.0	13.5	21.0	50.0	1.20	1.94	1.80	23.4	-	4.10	29.0	1200	35.3	2.00	0.21	2.84
	Dumagami	1368	3334	124	43	3.66	20.1	39.5	16.0	18.7	39.4	1.00	0.23	0.35	4.40	-	1.30	-	238	25.9	2.00	0.14	0.24
Noranda Main	Amulet A	1218	16554	1666	123	4.39	31.5	592	36.0	180	1.45	61.8	1.50	2.75	1044	-	0.53	-	78.2	7.03	2.00	1.16	0.04
	Amulet_C	2200	4335	830	39.8	0.12	3.50	48.8	18.0	38.0	2.10	7.50	0.70	8.00	83.0	-	7.47	-	111	21.5	-	0.26	0.09
	Ansil	913	8350	100	11.1	3.55	88.0	524	82.0	166	174	24.6	1.91	4.06	9.70	-	4.58	8.00	1513	4.71	2.67	1.76	0.26
	Corbet	7400	18867	1850	73.3	2.33	105	441	64.5	35.0	-	27.0	3.85	1.55	277	-	1.35	-	450	90.7	0.50	1.45	0.07
	East Waite	630	6420	49	45.8	0.88	20.6	3425	593	118	10.5	16.5	2.45	2.85	177	-	6.85	13.0	6.10	-	0.50	0.03	0.15
	Millenbach	77	382	190	8.25	0.03	2.50	40.0	-	27.0	3.30	1.00	-	4.70	2.90	-	1.10	9.00	6.10	3.00	-	0.07	0.10
	Moosehead	37.0	99.0	80.5	82.3	0.04	-	8.25	-	55.0	-	-	-	0.15	12.0	-	1.25	-	309	2.80	-	0.33	-
	Norbec	5087	2838	538	61.3	-	50.3	1560	13.7	-	-	7.60	5.70	4.83	87.0	-	2.90	-	-	17.7	-	2.07	-
	Lac Dufault	2175	2088	712	59.4	0.51	47.2	1438	-	45.8	2.23	6.00	0.78	0.90	12.5	3.00	0.45	-	339	42.9	4.50	1.97	0.10
	Old Waite	1915	3186	70	68.0	0.66	29.8	2946	210	192	3.30	7.60	4.34	1.68	109	-	1.80	-	129	1.75	12.0	0.33	0.30
	Quemont	2973	3065	238	208	12.60	21.4	582	230	259	221	9.63	1.65	1.45	202	-	1.40	-	387	2.92	3.71	0.05	0.17
	Vauze	5096	15033	366	130	2.39	109	1302	46.1	371	1.30	42.8	20.8	12.5	157	0.50	5.38	-	74.1	0.63	4.00	0.25	0.13
Noranda N-S-E-W	Aldermac	436	6126	124	16.9	0.28	29.93	359	-	47.3	18.2	19.7	0.87	7.00	100	10.0	10.5	-	90.5	1.62	2.00	0.49	0.11
	Delbridge	366	23660	9047	415	69.90	0.90	9.00	-	-	-	15.0	-	0.90	1.10	-	0.10	-	2540	159	-	27.0	-
	Deldona	184	15000	5995	96.0	2.77	-	11.0	-	4.00	0.10	18.0	-	1.30	3.40	4.00	-	-	186	18.0	0.50	24.0	-
	Gallen	2145	4011	1520	83.6	1.27	6.26	27.6	9.5	24.1	3.15	12.7	2.14	0.40	49.3	-	0.41	-	136	5.46	2.00	3.87	0.10
	Horne #5	1488	2626	397	23.7	5.92	1.44	243	43.0	96.4	23.5	4.17	2.84	2.97	174	-	1.84	-	167	3.39	8.25	1.24	0.10
	Horne	1940	14581	83	26.8	2.26	240	122	48.0	208	59.9	55.8	12.6	1.82	248	-	1.35	-	133	2.82	7.33	0.06	0.05
	Mobrun	1943	10115	447	30.1	1.63	36.3	386	189	316	8.20	45.9	8.14	4.77	584	-	1.61	-	1115	11.7	5.75	3.56	0.08
	New Insco	10150	597	123	36.9	0.48	50.8	809	45.5	299	12.8	5.23	3.25	5.00	9.05	8.00	1.25	23.5	19.45	1.62	2.17	0.22	0.06
	Robb Montbray	8533	7370	300	113	47.75	5.11	1748	359	2442	119	2.63	11.3	1.53	12.9	-	0.70	-	1393	7.40	57.0	0.27	0.07

Table A.10 Average trace element concentrations (ppm) in pyrite samples from VMS deposits in the Superior Province classified by ore tonnage (Mt). Data in ppm.

Size (Mtonnes)	Cu	Zn	Pb	Ag	Au	Bi	Co	Ni	Se	Te	Cd	In	Ga	Sn	W	Mo	V	As	Sb	Hg	Tl	U
Small (<3 Mt)	2498	6422	1141	84.8	1.90	73.4	785	69.2	168	23.4	16.2	3.73	3.39	102	7.13	5.01	15.3	280	15.1	3.44	1.53	0.22
Medium (3–8 Mt)	3072	9442	562	58.7	1.88	43.0	522	121	145	15.1	14.7	3.12	1.76	172	4.00	28.0	20.7	686	83.2	5.06	1.68	0.42
Large (8–171 Mt)	2750	5584	570	73.0	2.81	26.2	665	99.9	168	58.7	21.6	3.69	3.45	475	16.3	6.29	29.3	591	22.7	5.57	1.91	0.17

Table A.11 Comparison of trace element concentrations (ppm) in samples of different types of mineral separates (i.e., pyrite, chalcopyrite, pyrite/ chalcopyrite, sphalerite, pyrite, sphalerite galena) from VMS deposits in the Superior Province. Data in ppm.

Mineral	Cu	Zn	Pb	Ag	Au	Bi	Co	Ni	Se	Te	Cd	In	Ga	Sn	W	Mo	V	As	Sb	Hg	Tl	U
PY	2874	7199	928	1014	3.43	51.2	730	107	269	43.6	18.9	3.82	3.17	283	8.69	10.8	22.5	631	48.9	5.35	1.80	8.95
CP	279010	10178	260	221	2.03	95.8	268	89.9	470	24.3	36.3	72.6	4.37	208	40.0	29.4	12.7	177	99.4	11.4	0.44	1.02
SP	3223	479825	2503	177	0.89	18.6	138	126	126	33.2	1717	56.4	22.5	289	32.6	4.24	55.3	440	107	38.1	1.88	0.37
GN	678	3219	808714	8677	10.6	848	8.23	121	921	1087	38.9	0.73	0.55	1456	249	5.61	9.00	5525	1323	78.2	72.7	0.30
Py/Cp	145957	5384	381	151	0.60	45.8	912	71.1	-	50.7	21.5	40.7	8.04	99.1	-	17.0	23.5	-	-	-	1.17	0.26
Py/Sp	3730	179126	2825	113	0.75	56.9	308	47.3	2.0	3.84	516	41.5	15.1	523	-	1.34	8.06	1906	11.9	-	5.12	0.16

Table A.12 Individual trace element LA-ICP-MS analyses for the five select pyrite samples from four different VMS deposits in the AGB. Data in ppm. Negative values indicate below detection limit or not detected.

ID	Deposit name - Sample	Cu	Zn	Pb	Ag	Au	Bi	Co	Ni	Se	Te	Cd	In
s5-1	Bousquet #2 - BSQT27LPY	194	2.00	1.54	0.19	0.17	0.35	69.1	32.7	7.61	0.03	0.048	-0.002
s5-10	Bousquet #2 - BSQT27LPY	9.6	2.38	0.02	0.014	0.002	0.005	17.7	14.2	7.69	0.06	-0.025	0.008
s5-11	Bousquet #2 - BSQT27LPY	61.5	5.25	1.39	0.27	0.004	0.047	25.6	11.8	6.39	1.43	0.048	0.006
s5-12	Bousquet #2 - BSQT27LPY	10.9	3.08	0.09	0.011	0.001	0.000	8.16	10.3	7.30	0.03	0.019	0.004
s5-13	Bousquet #2 - BSQT27LPY	283	103	2.76	0.87	0.003	0.071	17.6	8.37	7.19	1.06	0.28	0.015
s5-14	Bousquet #2 - BSQT27LPY	34.4	17.3	0.30	0.019	-0.001	0.002	8.97	12.3	7.34	0.46	0.073	-0.003
s5-15	Bousquet #2 - BSQT27LPY	51.2	38.5	0.87	0.12	0.007	0.017	46.0	9.14	6.98	0.49	0.063	-0.005
s5-16	Bousquet #2 - BSQT27LPY	15.8	2.80	1.86	0.083	0.25	0.17	13.9	12.8	8.13	0.51	-0.053	0.005
s5-17	Bousquet #2 - BSQT27LPY	791	118	2.66	2.66	0.011	0.27	21.6	8.27	7.61	1.68	0.22	0.035
s5-18	Bousquet #2 - BSQT27LPY	45.9	10.1	4.62	0.14	0.29	0.40	42.7	12.8	8.07	0.73	0.12	-0.005
s5-19	Bousquet #2 - BSQT27LPY	8.1	1.57	0.00	0.004	0.001	0.002	11.8	9.17	7.91	-0.17	0.016	-0.009
s5-2	Bousquet #2 - BSQT27LPY	116	116	1.96	0.15	0.005	0.040	24.2	7.00	5.90	0.79	0.23	0.009
s5-20	Bousquet #2 - BSQT27LPY	50.8	31.1	2.51	0.26	0.012	0.051	10.3	8.01	6.15	0.17	0.11	0.012
s5-21	Bousquet #2 - BSQT27LPY	215	3.04	8.25	0.31	0.19	0.60	3.30	2.64	3.87	0.21	0.047	0.001
s5-22	Bousquet #2 - BSQT27LPY	33.8	2.61	0.06	0.10	0.000	0.004	9.62	2.50	9.31	-0.12	0.021	0.002
s5-23	Bousquet #2 - BSQT27LPY	38.6	1.91	2.88	0.21	0.040	0.17	10.9	9.42	6.23	0.27	0.005	0.002
s5-24	Bousquet #2 - BSQT27LPY	44.5	26.5	0.42	0.066	0.002	0.008	19.8	7.46	8.49	0.07	0.023	0.004
s5-25	Bousquet #2 - BSQT27LPY	50.7	11.0	0.71	0.22	0.003	0.010	20.5	7.54	7.04	0.29	0.080	-0.002
s5-26	Bousquet #2 - BSQT27LPY	13.7	2.52	1.93	0.15	0.005	0.020	11.2	8.13	7.70	0.54	0.015	0.000
s5-27	Bousquet #2 - BSQT27LPY	116	18.0	1.06	0.28	0.001	0.10	17.1	7.39	7.26	0.73	0.089	-0.009
s5-28	Bousquet #2 - BSQT27LPY	30.4	36.0	0.07	0.14	0.000	0.016	6.14	8.92	6.29	0.05	0.043	-0.010
s5-29	Bousquet #2 - BSQT27LPY	793	2.21	1.12	0.081	0.076	0.22	84.3	29.0	9.12	0.51	-0.006	-0.006
s5-3	Bousquet #2 - BSQT27LPY	50.6	2.27	0.01	0.027	0.003	0.001	5.16	3.75	7.54	-0.16	0.012	0.003
s5-30	Bousquet #2 - BSQT27LPY	63.5	3.18	2.22	0.41	0.015	0.093	27.1	7.57	6.67	0.65	0.023	0.003
s5-4	Bousquet #2 - BSQT27LPY	178	60.1	0.72	0.51	0.004	0.057	13.7	9.54	6.46	0.83	0.17	0.000
s5-5	Bousquet #2 - BSQT27LPY	84.9	29.2	2.50	0.37	-0.001	0.040	27.1	11.8	6.93	0.98	0.066	0.002
s5-6	Bousquet #2 - BSQT27LPY	18.4	3.62	0.07	0.034	0.001	0.005	18.0	7.01	7.26	0.06	0.034	0.000
s5-7	Bousquet #2 - BSQT27LPY	119	36.7	2.72	0.36	0.033	0.12	9.06	4.58	7.28	0.78	0.14	0.000
s5-8	Bousquet #2 - BSQT27LPY	25.3	2.06	1.50	0.090	0.034	0.087	23.8	7.88	7.07	0.64	0.007	0.002
s5-9	Bousquet #2 - BSQT27LPY	103	15.0	2.53	0.32	0.022	0.083	17.2	5.54	6.87	1.18	0.074	-0.001

Table A.12 cont.

ID	Deposit name - Sample	Ga	Sn	W	Mo	V	As	Sb	Hg	Tl	U	Th
s5-1	Bousquet #2 - BSQT27LPY	0.032	-0.09	0.007	-0.010	0.045	0.46	0.083	0.41	0.016	0.000	-0.001
s5-10	Bousquet #2 - BSQT27LPY	0.001	-0.02	0.001	-0.013	0.027	0.01	-0.027	0.34	-0.001	0.001	0.000
s5-11	Bousquet #2 - BSQT27LPY	0.012	0.06	0.077	0.004	0.044	0.26	0.012	0.47	-0.002	0.025	0.029
s5-12	Bousquet #2 - BSQT27LPY	0.078	0.06	-0.001	0.009	0.034	-0.06	0.000	0.22	0.003	0.009	0.10
s5-13	Bousquet #2 - BSQT27LPY	0.020	0.41	1.96	0.051	0.18	0.58	0.077	0.40	0.010	0.046	0.13
s5-14	Bousquet #2 - BSQT27LPY	0.012	0.02	0.010	0.002	0.042	0.07	0.017	0.20	0.004	0.004	0.004
s5-15	Bousquet #2 - BSQT27LPY	0.003	0.26	0.11	0.006	0.076	-0.04	0.026	0.32	-0.003	0.010	0.034
s5-16	Bousquet #2 - BSQT27LPY	0.015	-0.05	0.18	0.028	0.044	-0.01	0.14	0.25	0.012	0.16	0.38
s5-17	Bousquet #2 - BSQT27LPY	0.026	0.62	0.12	0.029	0.12	0.72	0.075	0.45	-0.001	0.032	0.046
s5-18	Bousquet #2 - BSQT27LPY	0.038	0.59	9.58	-0.004	1.08	0.26	-0.005	0.32	-0.001	4.32	3.40
s5-19	Bousquet #2 - BSQT27LPY	0.017	-0.14	-0.004	-0.009	0.024	0.07	-0.002	0.19	0.006	-0.001	0.000
s5-2	Bousquet #2 - BSQT27LPY	0.014	0.24	1.06	0.006	0.22	0.48	-0.008	0.67	-0.001	0.028	0.090
s5-20	Bousquet #2 - BSQT27LPY	0.002	0.04	0.77	0.030	0.11	0.22	0.071	0.42	0.002	0.021	0.045
s5-21	Bousquet #2 - BSQT27LPY	0.028	-0.01	0.13	0.069	0.10	0.28	0.033	0.21	0.000	0.92	2.98
s5-22	Bousquet #2 - BSQT27LPY	0.003	-0.13	0.002	0.008	0.034	0.08	0.023	0.18	-0.001	0.006	0.006
s5-23	Bousquet #2 - BSQT27LPY	0.010	0.04	0.18	0.001	0.046	0.11	0.007	0.18	-0.002	0.002	0.020
s5-24	Bousquet #2 - BSQT27LPY	-0.019	0.21	0.10	-0.005	0.089	0.11	0.040	0.29	-0.002	0.009	0.034
s5-25	Bousquet #2 - BSQT27LPY	0.025	0.01	0.10	0.003	0.089	0.29	0.023	0.32	0.003	0.013	0.034
s5-26	Bousquet #2 - BSQT27LPY	0.026	0.11	0.12	-0.005	0.021	0.10	0.049	0.24	0.005	0.004	0.008
s5-27	Bousquet #2 - BSQT27LPY	0.006	0.13	1.54	0.017	0.085	0.40	0.071	0.32	0.009	0.030	0.045
s5-28	Bousquet #2 - BSQT27LPY	0.006	0.17	0.011	-0.001	0.029	0.13	-0.002	0.17	0.004	0.001	0.001
s5-29	Bousquet #2 - BSQT27LPY	0.19	-0.10	0.090	0.005	0.032	0.09	-0.003	0.20	-0.001	1.19	1.23
s5-3	Bousquet #2 - BSQT27LPY	0.001	-0.11	0.021	0.001	0.026	0.08	0.011	0.32	0.000	0.001	0.003
s5-30	Bousquet #2 - BSQT27LPY	-0.004	-0.17	0.067	-0.010	0.060	0.08	0.036	0.11	0.004	0.014	0.037
s5-4	Bousquet #2 - BSQT27LPY	0.005	0.29	0.10	0.001	0.12	0.26	0.10	0.47	-0.005	0.016	0.036
s5-5	Bousquet #2 - BSQT27LPY	0.018	0.26	1.23	0.017	0.11	0.30	0.059	0.55	-0.010	0.013	0.041
s5-6	Bousquet #2 - BSQT27LPY	0.018	0.19	0.004	0.000	0.051	0.17	0.011	0.37	-0.001	0.000	0.004
s5-7	Bousquet #2 - BSQT27LPY	0.020	0.56	0.57	0.016	0.50	1.62	0.16	0.39	0.011	0.10	0.20
s5-8	Bousquet #2 - BSQT27LPY	0.034	-0.06	0.11	-0.007	0.060	0.13	0.21	0.36	-0.001	2.03	1.42
s5-9	Bousquet #2 - BSQT27LPY	0.009	0.25	0.49	0.006	0.080	0.23	0.060	0.78	-0.011	0.026	0.064

Table A.12 cont.

ID	Deposit name - Sample	Cu	Zn	Pb	Ag	Au	Bi	Co	Ni	Se	Te	Cd	In
s2-1	Dumagami - 63RF299PY	79.2	5.68	7.08	1.69	0.074	0.16	1.30	2.20	9.21	0.16	0.059	-0.001
s2-10	Dumagami - 63RF299PY	116	6.03	14.8	8.80	0.53	1.09	0.96	1.98	5.13	17.5	0.11	0.012
s2-11	Dumagami - 63RF299PY	173	2.15	9.57	4.90	0.28	1.00	3.45	2.57	7.48	8.53	0.038	0.017
s2-12	Dumagami - 63RF299PY	2190	34.5	9.98	5.47	0.22	22.2	1.38	4.28	6.20	8.16	0.12	0.44
s2-13	Dumagami - 63RF299PY	66.3	2.71	7.72	8.45	1.38	1.22	1.24	1.50	7.01	22.0	0.021	0.013
s2-14	Dumagami - 63RF299PY	6.65	1.75	3.12	0.59	0.20	0.17	1.70	1.30	6.72	4.30	0.032	0.006
s2-15	Dumagami - 63RF299PY	111	4.32	4.54	6.48	0.31	0.54	0.57	2.31	7.02	8.21	0.090	-0.009
s2-16	Dumagami - 63RF299PY	21.20	2.40	2.61	2.57	0.43	0.57	2.16	7.62	6.15	4.05	0.052	-0.003
s2-17	Dumagami - 63RF299PY	19.16	1.94	17.5	0.19	0.005	0.49	0.58	1.64	8.66	0.18	0.027	0.002
s2-18	Dumagami - 63RF299PY	1813	4.17	17.5	1.84	0.16	0.73	4.16	2.86	6.65	4.51	0.076	0.005
s2-19	Dumagami - 63RF299PY	5233	6.13	1.45	2.56	0.034	0.81	1.11	1.35	6.31	13.2	0.042	0.006
s2-2	Dumagami - 63RF299PY	7.22	1.72	0.44	1.25	0.11	0.095	0.86	1.48	9.04	1.71	0.014	0.005
s2-20	Dumagami - 63RF299PY	5.19	1.76	0.04	0.011	-0.003	0.011	1.58	3.03	4.98	0.10	0.013	0.002
s2-21	Dumagami - 63RF299PY	245	14.2	13.0	5.49	0.092	2.26	1.05	1.60	5.90	18.3	0.022	0.014
s2-22	Dumagami - 63RF299PY	78.9	8.25	16.4	8.48	0.055	1.14	2.18	2.21	6.37	13.4	0.079	0.000
s2-23	Dumagami - 63RF299PY	26.9	2.81	0.94	0.47	0.000	0.12	2.30	2.42	8.20	0.13	0.028	0.000
s2-24	Dumagami - 63RF299PY	23.3	2.16	2.49	3.10	0.17	0.32	0.94	2.36	7.84	3.93	0.024	-0.008
s2-25	Dumagami - 63RF299PY	132	10.7	1.29	5.50	0.57	0.50	2.61	9.91	10.1	12.1	0.056	0.010
s2-26	Dumagami - 63RF299PY	0.74	1.86	0.01	0.003	0.001	0.001	0.54	0.96	5.44	0.12	0.018	0.006
s2-27	Dumagami - 63RF299PY	7.94	1.99	0.95	0.63	0.004	0.15	2.56	1.68	5.88	0.05	-0.006	0.005
s2-28	Dumagami - 63RF299PY	58.9	1.91	102	31.3	28.6	17.8	1.74	1.27	7.86	67.5	-0.001	0.015
s2-3	Dumagami - 63RF299PY	2.17	1.27	0.03	0.009	0.000	-0.002	1.58	2.41	7.31	0.09	0.018	0.006
s2-4	Dumagami - 63RF299PY	168	10.3	5.96	2.95	0.24	1.40	1.47	1.76	7.43	4.33	0.11	0.003
s2-5	Dumagami - 63RF299PY	134	9.90	2.57	2.77	0.12	0.59	1.52	3.45	9.11	7.43	0.11	0.004
s2-6	Dumagami - 63RF299PY	89.8	5.56	3.57	8.61	2.27	0.47	1.69	1.64	7.79	9.46	0.15	0.001
s2-7	Dumagami - 63RF299PY	56.7	5.21	0.78	1.25	0.044	0.20	1.28	1.28	6.24	3.21	0.036	0.004
s2-8	Dumagami - 63RF299PY	1.02	1.74	0.01	0.003	0.001	0.002	3.27	12.4	6.48	0.20	0.035	-0.001
s2-9	Dumagami - 63RF299PY	264	3.73	22.6	2.49	0.066	2.38	2.35	2.97	5.83	24.1	0.080	0.019

Table A.12 cont.

ID	Deposit name - Sample	Ga	Sn	W	Mo	V	As	Sb	Hg	Tl	U	Th
s2-1	Dumagami - 63RF299PY	0.014	0.06	0.019	0.003	0.032	7.03	0.025	0.39	-0.008	0.001	0.002
s2-10	Dumagami - 63RF299PY	0.036	1.03	0.038	0.014	0.11	6.01	0.32	0.55	0.009	0.017	0.005
s2-11	Dumagami - 63RF299PY	0.025	0.79	0.017	0.007	0.034	9.05	0.12	0.68	0.023	0.000	0.001
s2-12	Dumagami - 63RF299PY	0.37	1.66	0.035	-0.009	0.21	2.95	0.30	0.95	0.022	0.012	0.012
s2-13	Dumagami - 63RF299PY	0.015	0.28	0.007	-0.002	0.049	8.97	0.15	0.33	0.032	0.006	-0.002
s2-14	Dumagami - 63RF299PY	0.003	-0.15	-0.001	-0.016	0.052	26.4	0.002	0.30	-0.005	0.000	-0.003
s2-15	Dumagami - 63RF299PY	0.027	1.01	0.029	0.008	0.054	2.60	0.19	0.56	0.003	0.016	0.003
s2-16	Dumagami - 63RF299PY	0.013	0.54	0.003	0.008	0.050	3.07	0.11	0.28	0.003	0.003	0.002
s2-17	Dumagami - 63RF299PY	0.005	0.13	-0.001	-0.003	0.039	1.80	0.016	0.17	0.036	0.000	0.000
s2-18	Dumagami - 63RF299PY	0.022	0.90	0.015	0.009	0.059	2.12	0.086	0.22	0.003	0.006	0.003
s2-19	Dumagami - 63RF299PY	0.022	1.22	0.037	0.001	0.10	4.34	0.34	0.33	0.013	0.027	0.003
s2-2	Dumagami - 63RF299PY	0.031	0.19	0.002	0.000	0.045	13.6	0.056	0.48	0.007	0.002	-0.001
s2-20	Dumagami - 63RF299PY	0.003	0.14	0.000	-0.006	0.037	19.9	0.003	0.16	0.001	0.002	0.011
s2-21	Dumagami - 63RF299PY	0.048	2.25	0.047	0.019	0.17	11.9	0.69	0.39	0.008	0.027	0.007
s2-22	Dumagami - 63RF299PY	0.032	0.38	0.011	0.005	0.064	76.4	0.20	0.64	0.004	0.013	0.003
s2-23	Dumagami - 63RF299PY	0.012	-0.17	0.003	0.001	0.033	1.48	-0.012	0.15	0.004	0.001	0.000
s2-24	Dumagami - 63RF299PY	0.013	0.64	0.011	-0.020	0.041	12.1	0.073	0.27	0.000	0.002	0.000
s2-25	Dumagami - 63RF299PY	0.015	0.85	0.009	-0.009	0.050	17.0	0.26	0.19	0.012	0.006	0.009
s2-26	Dumagami - 63RF299PY	0.021	0.08	0.003	0.011	0.036	0.69	0.005	0.13	0.009	0.000	-0.002
s2-27	Dumagami - 63RF299PY	-0.007	0.10	-0.002	-0.003	0.038	0.68	0.006	0.21	-0.002	0.000	0.002
s2-28	Dumagami - 63RF299PY	-0.013	1.54	0.016	0.005	0.047	25.7	0.22	0.37	0.010	0.009	0.004
s2-3	Dumagami - 63RF299PY	0.008	-0.10	0.000	0.007	0.052	0.67	0.010	0.28	-0.004	0.000	0.000
s2-4	Dumagami - 63RF299PY	0.014	0.58	0.026	0.013	0.068	2.80	0.11	0.40	0.002	0.13	0.005
s2-5	Dumagami - 63RF299PY	0.021	0.83	0.036	0.037	0.12	11.2	0.25	0.43	0.007	0.007	0.002
s2-6	Dumagami - 63RF299PY	0.012	0.98	0.021	0.034	0.13	2.52	0.20	0.95	0.000	0.009	0.004
s2-7	Dumagami - 63RF299PY	0.023	0.45	0.002	0.013	0.056	3.64	0.10	0.23	0.000	0.001	0.001
s2-8	Dumagami - 63RF299PY	0.016	0.14	0.001	0.003	0.048	0.41	0.008	0.21	-0.002	0.000	0.000
s2-9	Dumagami - 63RF299PY	0.047	1.68	0.038	0.030	0.15	4.75	0.69	0.38	0.009	0.038	0.006

Table A.12 cont.

ID	Deposit name - Sample	Cu	Zn	Pb	Ag	Au	Bi	Co	Ni	Se	Te	Cd	In
s3-1	Quemont - 63RF48PY	35.3	3.54	27.1	1.37	0.042	0.10	432	0.76	67.3	2.81	0.002	0.011
s3-10	Quemont - 63RF48PY	354	81.2	50.1	2.85	2.09	0.36	615	1.49	70.2	89.7	0.31	0.12
s3-11	Quemont - 63RF48PY	1340	2581	98.7	15.9	7.54	0.63	310	0.65	24.2	196	5.69	0.99
s3-12	Quemont - 63RF48PY	406	14.71	47.7	2.38	0.003	0.15	343	3.61	95.9	17.9	0.081	0.019
s3-13 - 32	Quemont - 63RF48PY	72.9	5.13	4.60	0.52	0.20	0.052	248	2.78	189	19.9	0.029	-0.002
s3-14	Quemont - 63RF48PY	332	11.04	60.8	1.32	1.25	0.22	652	2.99	90.5	34.9	0.093	0.18
s3-15	Quemont - 63RF48PY	3414	14298	157	333	7.78	1.56	234	9.74	88.5	168	27.0	4.89
s3-16	Quemont - 63RF48PY	6111	962	393	8.64	0.63	0.77	237	5.38	122	84.5	1.92	1.15
s3-17	Quemont - 63RF48PY	686	85.2	82.5	30.6	0.69	0.80	430	3.24	146	66.4	0.19	0.18
s3-18 - 32	Quemont - 63RF48PY	620	1574	51.8	7.27	0.21	0.36	495	3.12	125	59.9	4.53	1.91
s3-19	Quemont - 63RF48PY	386	557	111	1.63	0.77	0.24	430	9.21	131	70.7	1.34	0.17
s3-2	Quemont - 63RF48PY	385	2145	30.1	9.35	0.13	0.14	399	5.45	175	39.3	5.99	1.20
s3-20	Quemont - 63RF48PY	107	351	5.89	0.11	0.32	0.049	711	1.61	91.3	16.1	0.81	0.033
s3-21	Quemont - 63RF48PY	470	1130	324	4.71	3.72	0.86	206	1.99	199	192	2.44	0.55
s3-22	Quemont - 63RF48PY	655	469	26.4	2.12	0.59	0.22	273	1.03	76.5	21.7	0.82	0.35
s3-23	Quemont - 63RF48PY	356	49.4	142	13.4	0.96	0.64	261	2.29	119	85.9	0.16	0.12
s3-24 - 32	Quemont - 63RF48PY	72.9	21.9	301	14.7	-0.017	1.96	23.7	37.7	1.37	0.32	0.021	0.066
s3-25 - 32	Quemont - 63RF48PY	164	248	50.1	4.40	0.17	0.11	734	1.10	95.6	25.9	0.69	0.047
s3-26 - 32	Quemont - 63RF48PY	49.7	7.91	137	29.8	0.005	0.67	16.3	37.0	0.41	0.68	0.10	0.034
s3-27 - 32	Quemont - 63RF48PY	454	99.12	11.2	52.8	0.057	2.96	193	11.8	176	49.6	0.37	0.95
s3-28 - 32	Quemont - 63RF48PY	6.92	24.4	73.0	0.65	0.084	0.088	379	3.04	80.5	23.3	0.12	0.042
s3-29 - 32	Quemont - 63RF48PY	1000	65.8	136	30.3	0.013	0.10	3.68	16.0	-0.42	-0.41	0.079	0.12
s3-3 - 32	Quemont - 63RF48PY	316	14.0	17.5	5.21	0.066	0.29	48.6	10.2	92.6	12.2	0.15	0.13
s3-30 - 32	Quemont - 63RF48PY	27.1	4.57	23.8	2.30	0.063	0.29	383	1.17	86.4	11.7	0.050	0.51
s3-4	Quemont - 63RF48PY	35.2	3.62	16.6	1.88	0.006	0.42	2.71	88.8	-0.08	0.53	-0.013	0.012
s3-5	Quemont - 63RF48PY	82.3	4.11	0.42	0.13	0.004	0.011	218	62.3	0.15	-0.01	0.11	-0.012
s3-6 - 32	Quemont - 63RF48PY	178	561	19.3	0.49	0.30	0.10	285	0.38	115	44.8	1.51	0.15
s3-7 - 32	Quemont - 63RF48PY	748	75.9	401	47.1	0.23	0.99	277	3.97	102	42.2	0.27	0.35
s3-8 - 32	Quemont - 63RF48PY	980	1243	115	8.16	0.92	0.53	972	1.43	118	141	4.85	1.16
s3-9	Quemont - 63RF48PY	601	26.6	539	12.7	0.35	0.69	222	4.15	86.8	33.9	0.074	0.064

Table A.12 cont.

ID	Deposit name - Sample	Ga	Sn	W	Mo	V	As	Sb	Hg	Tl	U	Th
s3-1	Quemont - 63RF48PY	0.086	-0.04	0.003	0.002	0.059	56.6	0.78	0.23	0.002	0.001	0.001
s3-10	Quemont - 63RF48PY	0.77	0.72	0.003	0.015	0.061	46.5	2.52	0.15	0.004	0.000	-0.001
s3-11	Quemont - 63RF48PY	0.36	0.59	0.006	0.011	0.093	36.8	4.53	0.49	0.031	0.004	-0.001
s3-12	Quemont - 63RF48PY	0.052	-0.02	0.017	0.013	0.078	79.2	0.80	0.24	-0.001	0.005	0.001
s3-13 - 32	Quemont - 63RF48PY	0.46	0.12	0.006	-0.004	0.042	67.9	0.54	0.19	0.016	-0.001	0.005
s3-14	Quemont - 63RF48PY	0.13	2.07	0.022	-0.004	0.077	214	1.28	0.18	-0.004	0.002	-0.001
s3-15	Quemont - 63RF48PY	0.31	3.71	0.16	0.069	0.13	47.0	7.58	0.34	0.035	0.018	0.019
s3-16	Quemont - 63RF48PY	0.31	0.52	0.014	0.028	0.089	108	4.77	0.29	0.009	0.005	0.001
s3-17	Quemont - 63RF48PY	0.27	3.42	0.013	0.009	0.059	119	7.74	0.22	0.073	0.002	0.002
s3-18 - 32	Quemont - 63RF48PY	1.76	7.11	0.018	0.075	0.069	69.0	2.44	0.22	0.003	0.000	0.000
s3-19	Quemont - 63RF48PY	0.28	1.65	0.031	-0.003	0.063	40.9	3.75	0.15	-0.002	0.001	0.001
s3-2	Quemont - 63RF48PY	0.60	2.80	0.027	-0.006	0.071	251	1.37	0.26	0.011	0.000	0.000
s3-20	Quemont - 63RF48PY	0.37	0.02	-0.001	0.000	0.048	89.9	0.30	0.20	0.005	0.000	0.000
s3-21	Quemont - 63RF48PY	0.99	11.9	0.001	0.011	0.037	35.0	2.89	0.23	0.021	0.000	0.000
s3-22	Quemont - 63RF48PY	0.089	2.71	-0.002	0.036	0.058	133	3.68	0.21	0.014	-0.001	-0.001
s3-23	Quemont - 63RF48PY	0.049	0.38	0.018	0.014	0.053	130	4.48	0.13	0.10	0.001	0.003
s3-24 - 32	Quemont - 63RF48PY	0.13	10.5	1.55	0.20	0.093	216	8.16	0.20	0.30	-0.003	-0.005
s3-25 - 32	Quemont - 63RF48PY	0.54	-0.08	-0.002	0.021	0.060	73.2	1.07	0.20	0.018	0.001	0.002
s3-26 - 32	Quemont - 63RF48PY	0.026	5.22	1.48	0.39	0.13	96.7	6.09	0.49	0.055	0.013	0.081
s3-27 - 32	Quemont - 63RF48PY	0.13	0.33	0.016	-0.009	0.061	50.0	0.85	0.26	0.019	0.008	0.002
s3-28 - 32	Quemont - 63RF48PY	0.078	3.26	-0.002	0.012	0.047	127	0.77	0.11	0.012	-0.001	-0.001
s3-29 - 32	Quemont - 63RF48PY	1.49	12.1	0.62	0.037	5.24	130	2.46	0.37	0.20	0.000	0.002
s3-3 - 32	Quemont - 63RF48PY	0.062	0.26	0.007	-0.012	0.072	156	2.30	0.23	0.024	0.004	0.000
s3-30 - 32	Quemont - 63RF48PY	0.24	-0.22	-0.002	0.006	0.11	38.5	2.33	0.17	-0.009	0.004	0.003
s3-4	Quemont - 63RF48PY	1.57	3.55	0.071	0.007	1.96	423	4.56	0.51	2.55	-0.001	0.003
s3-5	Quemont - 63RF48PY	0.020	0.15	0.002	0.000	0.033	690	0.017	0.23	0.006	0.000	0.029
s3-6 - 32	Quemont - 63RF48PY	0.045	0.55	-0.012	0.002	0.077	122	1.14	0.29	0.055	-0.001	0.005
s3-7 - 32	Quemont - 63RF48PY	0.075	-0.06	0.030	0.002	0.068	91.5	3.41	0.21	0.005	0.006	0.001
s3-8 - 32	Quemont - 63RF48PY	3.16	9.38	0.002	0.014	0.11	47.3	4.55	0.29	0.018	-0.002	0.000
s3-9	Quemont - 63RF48PY	0.072	0.21	0.030	0.013	0.064	152	0.94	0.22	0.004	0.004	0.001

Table A.12 cont.

ID	Deposit name - Sample	Cu	Zn	Pb	Ag	Au	Bi	Co	Ni	Se	Te	Cd	In
s4-1	Kidd Creek - KIDD07PY	254	7.90	440	18.4	0.008	1.61	56.5	118.8	0.42	0.09	0.048	0.038
s4-10	Kidd Creek - KIDD07PY	3.39	1.74	13.0	1.03	0.003	0.063	1.41	40.3	0.69	-0.01	0.014	0.005
s4-11	Kidd Creek - KIDD07PY	14.4	2.70	10.8	3.83	0.008	0.079	56.8	14.6	0.19	-0.04	-0.008	0.009
s4-12	Kidd Creek - KIDD07PY	613	32.6	60.3	8.24	0.004	1.27	56.7	79.1	0.69	0.20	0.048	0.063
s4-13	Kidd Creek - KIDD07PY	24.9	4.67	150	26.3	0.005	1.65	33.9	111.0	0.02	0.01	0.079	0.11
s4-14	Kidd Creek - KIDD07PY	1.72	86.4	2.32	0.34	-0.002	0.035	1.03	70.0	1.23	0.03	0.39	0.032
s4-15	Kidd Creek - KIDD07PY	197	14.5	9.70	2.06	0.003	0.14	21.2	33.8	0.79	0.21	0.009	0.024
s4-16	Kidd Creek - KIDD07PY	36.9	14399	3804	6.21	0.006	5.62	1.95	74.1	2.38	0.46	60.2	3.10
s4-17	Kidd Creek - KIDD07PY	1318	82.5	136	53.3	0.020	1.46	27.6	65.1	0.25	1.06	0.42	0.26
s4-18	Kidd Creek - KIDD07PY	14.9	2.85	60.9	8.30	0.004	0.70	20.4	202.6	0.62	0.42	-0.027	0.006
s4-19	Kidd Creek - KIDD07PY	41.4	4.76	13.0	2.10	0.000	0.15	5.45	66.5	1.07	0.05	0.084	0.014
s4-2	Kidd Creek - KIDD07PY	38.1	3.32	1.82	0.69	-0.005	0.028	4.45	97.4	1.80	-0.01	0.022	0.017
s4-20	Kidd Creek - KIDD07PY	125	10.8	45.5	10.8	0.004	0.59	14.4	29.1	0.06	0.14	0.018	0.008
s4-21	Kidd Creek - KIDD07PY	269	14.9	179	17.2	0.012	0.63	16.5	46.6	0.40	0.12	0.037	0.075
s4-22	Kidd Creek - KIDD07PY	410	7.39	286	28.2	0.013	0.85	7.29	103.9	0.37	-0.03	0.11	0.018
s4-23	Kidd Creek - KIDD07PY	31.9	16.2	47.0	5.65	0.006	0.27	15.2	60.1	0.34	-0.19	0.006	0.018
s4-24	Kidd Creek - KIDD07PY	818	41.9	240	51.1	0.017	4.03	10.1	50.9	0.56	0.01	0.22	0.044
s4-25	Kidd Creek - KIDD07PY	25.0	3.97	10.6	0.85	-0.001	0.066	0.67	115.0	1.26	-0.14	0.019	-0.006
s4-26	Kidd Creek - KIDD07PY	987	51.3	14.0	7.68	-0.005	0.37	7.04	25.9	1.31	0.41	0.19	0.040
s4-27	Kidd Creek - KIDD07PY	46.9	2.25	13.2	3.54	-0.003	0.041	108	45.3	0.22	0.01	0.026	0.006
s4-28	Kidd Creek - KIDD07PY	113	10.3	212	29.5	0.004	0.44	33.7	32.0	0.51	0.03	0.014	0.039
s4-29	Kidd Creek - KIDD07PY	11.8	2.63	49.7	8.96	0.004	0.64	9.72	119.8	1.19	0.08	-0.010	0.007
s4-3	Kidd Creek - KIDD07PY	147	12.6	14.4	1.60	0.006	0.22	1.95	57.0	0.50	0.28	-0.006	0.020
s4-30	Kidd Creek - KIDD07PY	263	14.6	78.6	33.5	0.001	0.77	8.12	15.7	0.13	0.05	0.068	0.030
s4-31	Kidd Creek - KIDD07PY	155	4.65	228	27.3	0.001	1.27	5.81	16.9	0.26	0.00	0.021	0.035
s4-32	Kidd Creek - KIDD07PY	76.2	6.01	33.5	6.68	0.003	0.28	67.7	26.5	0.22	0.27	0.027	0.001
s4-4	Kidd Creek - KIDD07PY	58.0	3.38	374	36.4	0.011	3.50	22.5	74.2	0.18	0.17	0.11	0.031
s4-5	Kidd Creek - KIDD07PY	531	35.2	309	40.0	0.001	0.54	18.7	27.9	0.57	0.22	0.094	0.061
s4-6	Kidd Creek - KIDD07PY	206	58.1	180	34.2	0.005	1.56	33.4	34.6	0.02	0.37	0.19	0.13
s4-7	Kidd Creek - KIDD07PY	136	50.3	578	43.4	0.002	3.18	41.6	63.9	0.85	1.39	0.28	0.12
s4-8	Kidd Creek - KIDD07PY	12.5	8.64	32.8	4.06	0.007	0.34	4.70	32.3	0.89	0.22	-0.008	0.027
s4-9	Kidd Creek - KIDD07PY	99.9	15.9	160	38.6	0.005	2.28	19.1	252.9	0.11	0.32	0.055	0.028

Table A.12 cont.

ID	Deposit name - Sample	Ga	Sn	W	Mo	V	As	Sb	Hg	Tl	U	Th
s4-1	Kidd Creek - KIDD07PY	0.44	4.41	0.98	0.030	1.19	263	24.5	0.42	1.70	0.013	0.014
s4-10	Kidd Creek - KIDD07PY	0.020	-0.16	0.001	-0.006	0.046	305	1.46	0.28	0.049	0.000	0.001
s4-11	Kidd Creek - KIDD07PY	0.32	0.86	2.83	0.011	0.19	463	0.98	0.25	0.27	0.000	0.003
s4-12	Kidd Creek - KIDD07PY	0.24	7.06	0.43	0.041	0.21	342	5.00	0.39	0.44	0.036	0.25
s4-13	Kidd Creek - KIDD07PY	0.015	2.30	0.15	1.34	0.065	491	14.5	0.24	5.13	0.008	0.008
s4-14	Kidd Creek - KIDD07PY	0.016	0.14	0.003	0.007	0.024	426	0.47	0.29	0.011	0.001	0.000
s4-15	Kidd Creek - KIDD07PY	0.032	0.20	0.15	0.030	0.16	519	0.74	0.57	0.052	0.10	0.24
s4-16	Kidd Creek - KIDD07PY	0.81	2.73	0.071	0.034	0.75	150	5.32	0.49	1.05	0.046	0.057
s4-17	Kidd Creek - KIDD07PY	0.70	44.5	10.9	0.25	3.77	184	14.6	0.62	1.64	0.30	0.075
s4-18	Kidd Creek - KIDD07PY	0.55	1.02	0.044	0.003	0.99	515	10.1	0.39	0.89	0.023	0.10
s4-19	Kidd Creek - KIDD07PY	0.34	0.61	0.041	0.015	0.31	354	2.30	0.22	0.48	0.70	0.92
s4-2	Kidd Creek - KIDD07PY	0.025	0.14	0.039	0.022	0.059	206	0.23	1.02	0.057	0.004	0.004
s4-20	Kidd Creek - KIDD07PY	0.20	1.12	0.058	1.33	0.68	305	6.27	0.40	1.43	0.23	1.35
s4-21	Kidd Creek - KIDD07PY	1.25	10.6	0.96	0.25	2.14	377	4.85	0.17	0.14	-0.001	0.001
s4-22	Kidd Creek - KIDD07PY	0.000	2.94	0.42	0.008	0.029	23.9	2.06	0.20	0.053	0.002	0.001
s4-23	Kidd Creek - KIDD07PY	0.025	3.39	0.023	0.068	0.037	525	2.09	0.27	0.092	0.068	0.053
s4-24	Kidd Creek - KIDD07PY	0.063	4.37	0.16	4.64	0.55	470	42.3	0.42	7.31	0.015	0.016
s4-25	Kidd Creek - KIDD07PY	0.13	0.29	0.004	0.000	0.11	396	1.34	0.33	0.19	0.001	0.000
s4-26	Kidd Creek - KIDD07PY	0.17	0.69	0.10	0.031	0.42	241	1.74	0.52	0.31	0.015	0.009
s4-27	Kidd Creek - KIDD07PY	0.006	0.80	0.084	0.002	0.035	326	0.69	0.24	0.049	0.000	0.000
s4-28	Kidd Creek - KIDD07PY	0.021	7.55	0.69	0.18	0.25	206	4.29	0.19	0.39	0.000	0.003
s4-29	Kidd Creek - KIDD07PY	0.21	0.99	0.64	-0.004	0.22	433	9.20	0.19	0.36	0.004	0.011
s4-3	Kidd Creek - KIDD07PY	0.95	2.30	0.033	0.023	0.91	335	2.71	0.64	1.06	0.005	0.005
s4-30	Kidd Creek - KIDD07PY	0.17	5.74	1.04	0.18	1.64	71.7	8.66	0.16	0.26	0.007	0.013
s4-31	Kidd Creek - KIDD07PY	0.021	4.56	0.21	0.070	0.075	45.0	1.38	0.14	0.10	0.004	0.020
s4-32	Kidd Creek - KIDD07PY	0.020	0.36	0.92	0.052	0.19	350	5.73	0.31	0.071	0.004	0.006
s4-4	Kidd Creek - KIDD07PY	0.033	5.27	0.23	4.54	0.065	282	34.7	0.41	11.5	0.005	0.035
s4-5	Kidd Creek - KIDD07PY	0.52	9.43	0.59	0.57	4.15	222	4.56	0.45	0.19	0.069	0.053
s4-6	Kidd Creek - KIDD07PY	0.13	19.0	1.09	0.33	1.55	204	11.5	0.32	0.33	0.003	0.010
s4-7	Kidd Creek - KIDD07PY	0.14	17.9	0.92	0.28	0.81	177	22.4	0.31	0.47	-0.001	0.001
s4-8	Kidd Creek - KIDD07PY	0.66	6.60	1.32	-0.001	1.00	287	5.39	0.30	0.30	0.000	0.005
s4-9	Kidd Creek - KIDD07PY	0.002	2.85	1.46	-0.007	0.033	147	21.2	0.31	0.31	0.001	-0.001

Table A.13 a) Results of Principal Components Analysis (PCA) and element loadings of the select trace metal set (Cu, Zn, Pb, Ag, Au, Co, Ni, As) for the filtered volcanic rock data of the Superior Province.

	PC1	PC2	PC3	PC4
Eigenvalues	3.56	1.45	1.07	0.72
Variance %	44.53	18.11	13.40	9.04
Cumulative %	44.53	62.63	76.03	85.07
Ag	0.79	0.02	0.12	0.30
As	0.41	-0.60	-0.44	-0.51
Au	0.63	-0.23	0.61	0.06
Co	-0.88	-0.11	-0.08	0.25
Cu	-0.56	0.34	0.53	-0.44
Ni	-0.87	-0.21	-0.17	0.24
Pb	0.72	0.36	-0.30	0.17
Zn	0.05	0.85	-0.29	-0.16

Table A.13 b) Results of the Hierarchical Clustering on Principal Components (HCPC) analysis showing the elements that describe the clustering assignment of each set the most. The V. test and P. values are indicated for the elements in each cluster. The V. test is the quantile of a normal distribution associated with the P. value.

Cluster 1	V. test	P. value	Cluster 2	V. test	P. value	Cluster 3	V. test	P. value
Co	11.02	2.85E-28	Pb	9.82	8.95E-23	As	5.76	8.95E-23
Ni	9.98	1.83E-23	Ag	9.73	2.27E-22	Au	2.45	2.27E-22
Cu	7.73	1.09E-14	Au	6.8	1.05E-11	Pb	2.2	1.05E-11
			Zn	6.2	0.0			

Table A.14 Average trace element abundances in different rock types for comparison with concentrations in the pyrite concentrates from this study. Data are in ppm.

	Cu	Zn	Pb	Ag	Bi	Co	Ni	Se	Te	Cd	In	Ga	Sn	W	Mo	As	Sb	Hg	Tl
Average abundances in different rock types																			
UCC[1]	25.0	71.0	-	-	0.13	10.0	20.0	-	-	0.098	0.05	17.0	5.50	2.00	1.50	1.50	-	-	0.75
UCC[2]	14.0	52.0	-	-	0.123	12.0	19.0	-	-	0.102	0.061	14.0	2.50	1.40	1.40	2.00	-	-	0.75
MORB[3]	80.8	86.8	0.657	-	-	43.7	100	0.21	-	-	-	-	-	0.043	-	0.11	-	-	-
MORB[4]	70.0	80.0	0.57	0.027	0.0095	56.0	200	0.21	0.0049	0.14	0.075	0.021	1.00	0.052	0.39	0.11	0.014	0.012	0.0066

[1]Taylor and McLennan (1985).

[2] Wedepohl (1995).

[3]White and Klein (2014).

[4]Arevalo et al. (2010); and references therein.

Table A.15 Trace element geochemistry dataset of pyrite separates from ore samples of different deposit types in Canada, specifically magmatic vein Cu and orogenic Au deposits in the AGB (from Jonasson et al., 2020).

Sample No.	Deposit Name	District/ Camp	Deposit Type	Province	Cu	Zn	Pb	Ag	Au	Bi	Co	Ni	Se	Te	Cd	In	Ga
				Method	**ICP**	**ICP**	**ICP**	**ICP, INAA**	**INAA**	**ICP**	**ICP, INAA**	**INAA**	**INAA**	**ICP**	**ICP**	**ICP**	**ICP**
				Detection Limits	**10.0**	**1.00**	**1.00**	**0.5, 5**	**0.005**	**0.20**	**5, 1**	**20.0**	**3.00**	**0.20**	**0.20**	**0.05**	**0.10**
63RF600PY	Belle	Chibougama	Magmatic	QC	390	59	70.0	160	0.22	5.30	453	92.0	10.0	3.7			0.80
63RF624PY	Copper Rand (Patino)	Chibougama	Magmatic	QC	3500		86.0	113	7.98	90	5435	925	41.0	140		0.07	0.30
63RF614PY	Opemiska (Perry)	Chibougamau	Magmatic	QC	6500	172	94.0	18.0	6.14	14.0	748	822	29.0	13.0	1.40	0.33	0.60
63RF622PY	Opemiska (Perry)	Chibougamau	Magmatic	QC	8400	513	980	51.0	1.08	29.0	1610	1285	44.0	6.30	3.50	0.52	0.80
63RF630PY	Portage	Chibougamau	Magmatic	QC	14000	793	190	48.5	59.2	190	4095	460	36.0	170	5.00	1.60	0.30
63RF631PY	Portage	Chibougamau	Magmatic	QC	4100	194	860	57.5	57.3	44.0	1365	370	39.0	45.0	1.70	0.52	0.40
66RF844PY	Tache Lake (Berrigan)	Chibougamau	Magmatic	QC		25800		112	0.36		66.0	1880					
63RF540PY	Chadbourne	Noranda	Orogenic Au	QC	31.0		83.0	11.0	15.3	20.0	185	82.0	26.0	20.0	0.40		0.80
63RF602PY	Chadbourne	Noranda	Orogenic Au	QC	1800		67.0	130		11.0	6500	79.0		70.0	0.80	0.18	0.30
SP2607PY	Aumaque	Val d'Or	Orogenic Au	QC	37.0		110	2.50		63.0	180	58.0			1.30	0.23	1.80
63RF509PY	New Formaque	Val d'Or	Orogenic Au	QC	1300		630	10.5	0.16	1.80	68.0	120	8.00	0.30	3.80	0.17	0.30
63RF206PY	Cathroy-Larder	Timiskaming	Orogenic Au	ON	3300		60.0	158	220	3.60	361	220		9.40	58.0	3.20	0.20

Table A.15 cont.

Sample No.	Deposit Name	District/ Camp	Deposit Type	Province	Sn	W	Mo	V	As	Sb	Hg	Tl	U	Th	Cr	Ba	Zr
				Method	**ICP**	**INAA**	**ICP**	**ICP**	**INAA**	**ICP, INAA**	**INAA**	**ICP**	**ICP, INAA**	**ICP, INAA**	**10**	**INAA**	**ICP**
				Detection Limits	**0.50**	**1.00**	**0.20**	**5.00**	**0.50**	**1, 0.1**	**1.00**	**0.02**	**0.02, 0.5**	**0.02, 0.2**		**0.20**	**0.50**
63RF600PY	Belle	Chibougama	Magmatic	QC	13.0	420	3.00		60.9	1.30		0.06	0.39	0.83	15.0		140
63RF624PY	Copper Rand (Patino)	Chibougama	Magmatic	QC	2.00		0.50		1430		4.00		0.04		12.0		1.00
63RF614PY	Opemiska (Perry)	Chibougamau	Magmatic	QC	3.60		170	5.00	1220	44.6		0.16	0.24	0.10	12.0	20.0	23.0
63RF622PY	Opemiska (Perry)	Chibougamau	Magmatic	QC	6.70		180	7.00	570	120		0.16	0.23	0.21	12.0	40.0	64.0
63RF630PY	Portage	Chibougamau	Magmatic	QC	3.40		1.5		860	0.30			-0.02		12.0		1.10
63RF631PY	Portage	Chibougamau	Magmatic	QC	2.40				851	0.70	3.00		0.08	0.03	16.0		57.0
66RF844PY	Tache Lake (Berrigan)	Chibougamau	Magmatic	QC					859	97.6							
63RF540PY	Chadbourne	Noranda	Orogenic Au	QC	2.20	13.0	290	19.0	3.20	0.60		0.06	0.42	0.80	16.0		60.0
63RF602PY	Chadbourne	Noranda	Orogenic Au	QC	1.80		1.40					0.08	0.03		16.0		
SP2607PY	Aumaque	Val d'Or	Orogenic Au	QC	280		580	6.00				0.12	6.40	43.0			150
63RF509PY	New Formaque	Val d'Or	Orogenic Au	QC	7.00		0.60		148	3.50		1.50	0.21	0.21	12.0		9.50
63RF206PY	Cathroy-Larder	Timiskaming	Orogenic Au	ON	5.30		3.10		81.0	1.80		0.09	0.05	0.13	17.0	30.0	8.60

Samples from sulfide mineral separates in the database were analyzed by ICP-MS and INAA. Elements are listed in the following order: 1) abundance in samples and base metals; 2) precious metals; 3) Cu-associated and abundance; 4) Zn associated and abundance; 5) Pb/ sulfosalt associated; 6) U-Th - radiogenic; 7) Ba and Cr; 8) Zr and transition metals; 9) Noble gas (Br) and alkaline earth (Be); 10) Large ion lithophiles; 11) LREEs; 12) HREEs. Trace element concentrations from the geochemical analysis results are reported in ppm and include below detection limit measurements (negative). This study focuses on a subset of pyrite samples to compare trace element distributions of the different deposit types with pyrite samples from VMS.

Table A.16 a) Summary statistics of trace element concentrations (ppm) in pyrite samples from Chibougamau magmatic vein deposits in the AGB. These pyrite mineral separate data are a subset from the Jonasson et al. (2020) database.

Data in ppm	Cu	Zn	Pb	Ag	Au	Bi	Co	Ni	Se	Te	Cd	In	Ga	Sn	W	Mo	V	As	Sb	Hg	Tl	U
Chibougamau Magmatic Summary																						
Count Numeric	7	7	7	8	7	7	8	7	6	7	5	6	7	7	1	6	2	7	6	2	4	7
Minimum	390	59.0	51.0	14.0	0.22	2.40	66.0	92.0	10.0	3.70	1.40	0.07	0.30	2.00	420	0.50	5.00	60.9	0.30	3.00	0.06	0.01
Maximum	14000	25800	980	160	59.2	190	5435	1880	44.0	170	11.0	4.70	0.90	69.0	420	180	7.00	1430	120	4.00	0.16	0.39
Mean	5470	4690	333	71.7	18.9	53.5	1764	833	33.2	54.7	4.52	1.29	0.59	14.3	420	59.3	6.00	836	44.1	3.50	0.13	0.15
Median	4100	512.5	94.0	54.3	6.14	29.0	1056	822	37.5	13.0	3.50	0.52	0.60	3.60	420	2.25	6.00	859	23.0	3.50	0.15	0.08

Table A.16 b) Average trace element concentrations (ppm) in pyrite samples from Chibougamau magmatic vein deposits in comparison with Matagami VMS deposits.

Deloro	Cu	Zn	Pb	Ag	Au	Bi	Co	Ni	Se	Te	Cd	In	Ga	Sn	W	Mo	V	As	Sb	Hg	Tl	U
Chibougamau Magmatic	6148	4588	380	79.9	18.9	62.1	1967	833	33.2	63.0	2.90	0.61	0.53	5.18	420	71.0	6.00	836	44.08	3.50	0.13	0.17
Matagami VMS	2418	7421	242	98.2	1.82	87.5	803	93.1	229	11.5	13.23	5.16	1.65	276.7	9.00	2.05	23.00	322	9.14	4.72	0.77	0.18

Table A.17 a) Summary statistics of trace element concentrations (ppm) in pyrite samples from orogenic Au deposits in the AGB. These pyrite mineral separate data are a subset from the Jonasson et al. (2020) database.

Data in ppm	Cu	Zn	Pb	Ag	Au	Bi	Co	Ni	Se	Te	Cd	In	Ga	Sn	W	Mo	V	As	Sb	Hg	Tl	U
AGB Orogenic Au Summary																						
Count Numeric	5	0	5	5	3	5	5	5	2	4	5	4	5	5	1	5	2	3	3	0	5	5
Minimum	31.0	-	60.0	2.50	0.164	1.80	68.0	58.0	8.00	0.30	0.40	0.17	0.20	1.80	13.0	0.60	6.00	3.20	0.60	-	0.06	0.03
Maximum	3300	-	630	158	220	63.0	6500	220	26.0	70.0	58.0	3.20	1.80	280	13.0	580	19.00	148	3.50	-	1.50	6.40
Mean	1294	-	190	62.4	78.6	19.9	1459	112	17.0	24.9	12.9	0.95	0.68	59.3	13.0	175	12.50	77.4	1.97	-	0.37	1.42
Median	1300	-	83.0	11.0	15.3	11.0	185	82.0	17.0	14.7	1.30	0.21	0.30	5.30	13.0	3.10	12.50	81.0	1.80	-	0.09	0.21

Table A.17 b) Average trace element concentrations (ppm) in pyrite samples from orogenic Au deposits in comparison with VMS deposits in the same districts.

Val d'Or	**Cu**	**Zn**	**Pb**	**Ag**	**Au**	**Bi**	**Co**	**Ni**	**Se**	**Te**	**Cd**	**In**	**Ga**	**Sn**	**W**	**Mo**	**V**	**As**	**Sb**	**Hg**	**Tl**	**U**
Orogenic Au	669	-	370	6.50	0.16	32.4	124	89.0	8.00	0.30	2.55	0.20	1.05	144	-	290	6.00	148	3.50	-	0.81	3.31
VMS	3823	3301	358	44.8	1.00	26.5	1410	167	227	6.69	13.9	1.24	5.35	47.6	-	36.3	27.2	1251	6.72	5.75	0.76	0.18

Noranda South	**Cu**	**Zn**	**Pb**	**Ag**	**Au**	**Bi**	**Co**	**Ni**	**Se**	**Te**	**Cd**	**In**	**Ga**	**Sn**	**W**	**Mo**	**V**	**As**	**Sb**	**Hg**	**Tl**	**U**
Orogenic Au	916	-	75.0	70.5	15.3	15.5	3343	80.5	26.0	45.0	0.60	0.18	0.55	2.00	13.0	146	19.0	3.20	0.60	-	0.07	0.22
VMS	2650	6664	189	152	8.91	43.2	438	139	243	170	25.0	5.29	1.57	217	-	1.39	-	296	2.89	4.80	0.05	0.13

Appendix B Major and Trace element geochemistry database (see attached Excel file) of mineral separates from ore samples of different VMS deposits in Canada (modified from Jonasson et al., 2020). Samples from sulfide mineral separates in the database were analyzed by ICP-MS and INAA. Elements are listed in the following order: 1) abundance in samples and base metals; 2) precious metals; 3) Cu-associated and abundance; 4) Zn associated and abundance; 5) Pb/ sulfosalt associated; 6) U-Th - radiogenic; 7) Ba and Cr; 8) Zr and transition metals; 9) Noble gas (Br) and alkaline earth (Be); 10) Large ion lithophiles; 11) LREEs; 12) HREEs. Trace element concentrations from the geochemical analysis results are reported in ppm and include below detection limit measurements (negative). This study focuses on a subset of pyrite samples of Archean VMS deposits from the Superior Province that are then discussed in comparison to the pyrite data of other Archean and younger VMS in the database.

Appendix C Trace element geochemistry database (see attached Excel file) of volcanic rock samples from the Superior Province compiled from previously published datasets (Ontario Geological Survey, 2001; Hillary and Grunsky, 2010; Berger, 2012; Lodge and Chartrand, 2013; Ratcliffe, 2017; Gemmell and MacDonald, 2018; Gemmell and Szumylo, 2020; Hastie and Magnus, 2021; Magnus, 2021; Mole et al., 2021; Vice and MacDonald; 2021; Fassbender et al., 2023). A total of 3557 samples were removed in the filtering for quality process. The subset of mafic volcanic rock samples in the AGB are sorted by assemblage and were subjected to additional quality control filtering by Fassbender et al. (2023).